



ΕΘΝΙΚΟ ΜΕΤΣΟΒΙΟ ΠΟΛΥΤΕΧΝΕΙΟ
ΣΧΟΛΗ ΠΟΛΙΤΙΚΩΝ ΜΗΧΑΝΙΚΩΝ

ΜΗ ΓΡΑΜΜΙΚΗ ΣΥΜΠΕΡΙΦΟΡΑ ΚΑΙ ΣΧΕΔΙΑΣΜΟΣ
ΣΥΝΘΕΤΩΝ ΥΠΟΣΤΥΛΩΜΑΤΩΝ ΑΠΟ ΧΑΛΥΒΑ
ΥΠΟ ΑΞΟΝΙΚΗ ΚΑΙ ΕΓΚΑΡΣΙΑ ΦΟΡΤΙΣΗ

ΔΙΔΑΚΤΟΡΙΚΗ ΔΙΑΤΡΙΒΗ

ΚΩΝΣΤΑΝΤΙΝΟΥ Ε. ΚΑΛΟΧΑΙΡΕΤΗ

Διπλωματούχου Πολιτικού Μηχανικού Ε.Μ.Π.

ΕΠΙΒΛΕΠΩΝ:

Χ. Ι. ΓΑΝΤΕΣ

Καθηγητής Ε.Μ.Π.

ΑΘΗΝΑ, Ιανουάριος 2014



**NATIONAL TECHNICAL UNIVERSITY OF ATHENS
SCHOOL OF CIVIL ENGINEERING**

**NONLINEAR BEHAVIOUR AND DESIGN
OF STEEL BUILT-UP COLUMNS
UNDER AXIAL AND TRANSVERSE LOADING**

DOCTORAL THESIS OF
KONSTANTINOS E. KALOCHAIRETIS
Civil Engineering Diploma N.T.U.A.

SUPERVISOR:

C. J. GANTES
Professor N.T.U.A.

ATHENS, January 2014



**NATIONAL TECHNICAL UNIVERSITY OF ATHENS
SCHOOL OF CIVIL ENGINEERING**

**NONLINEAR BEHAVIOUR AND DESIGN
OF STEEL BUILT-UP COLUMNS
UNDER AXIAL AND TRANSVERSE LOADING**

DOCTORAL THESIS OF

KONSTANTINOS E. KALOCHAIRETIS

Civil Engineering Diploma N.T.U.A. (2007)

Master of Science in Earthquake Engineering Imperial College London (2008)

The thesis is submitted to the School of Civil Engineering
of the National Technical University of Athens
in fulfilment of the requirements for the Degree of Doctor of Philosophy

ADVISORY COMMITTEE:

1. C. J. GANTES, Professor N.T.U.A. (Supervisor)
2. G.I. IOANNIDIS, Professor N.T.U.A.
3. I. G. RAFTOYIANNIS, Associate Professor N.T.U.A.

EXAMINATION COMMITTEE:

1. C. J. GANTES, Professor N.T.U.A. (Supervisor)
2. V. K. KOUMOUSIS, Professor N.T.U.A.
3. I. VAYAS, Professor N.T.U.A.
4. V. K. KOUMOUSIS, Professor N.T.U.A.
5. E. S. MISTAKIDIS, Professor University of Thessaly
6. I. G. RAFTOYIANNIS, Associate Professor N.T.U.A.
7. T. P. AVRAAM, Assistant Professor N.T.U.A.

Athens, January 2014

© Copyright 2014 by Konstantinos E. Kalochairetis
All Rights Reserved



ΕΘΝΙΚΟ ΜΕΤΣΟΒΙΟ ΠΟΛΥΤΕΧΝΕΙΟ
ΣΧΟΛΗ ΠΟΛΙΤΙΚΩΝ ΜΗΧΑΝΙΚΩΝ

ΜΗ ΓΡΑΜΜΙΚΗ ΣΥΜΠΕΡΙΦΟΡΑ ΚΑΙ ΣΧΕΔΙΑΣΜΟΣ
ΣΥΝΘΕΤΩΝ ΥΠΟΣΤΥΛΩΜΑΤΩΝ ΑΠΟ ΧΑΛΥΒΑ
ΥΠΟ ΑΞΟΝΙΚΗ ΚΑΙ ΕΓΚΑΡΣΙΑ ΦΟΡΤΙΣΗ

ΔΙΔΑΚΤΟΡΙΚΗ ΔΙΑΤΡΙΒΗ

ΚΩΝΣΤΑΝΤΙΝΟΥ Ε. ΚΑΛΟΧΑΙΡΕΤΗ

Δίπλωμα Πολιτικού Μηχανικού Ε.Μ.Π. (2007)

Μεταπτυχιακό Δίπλωμα Αντισεισμικής Μηχανικής Imperial College London (2008)

Η διατριβή υποβλήθηκε στη Σχολή Πολιτικών Μηχανικών του Εθνικού Μετσοβίου Πολυτεχνείου
προς εκπλήρωση των προϋποθέσεων του τίτλου του Διδάκτορος Μηχανικού

ΤΡΙΜΕΛΗΣ ΣΥΜΒΟΥΛΕΥΤΙΚΗ ΕΠΙΤΡΟΠΗ:

1. Χ. Ι. ΓΑΝΤΕΣ, Καθηγητής Ε.Μ.Π. (Επιβλέπων)
2. Γ. Ι. ΙΩΑΝΝΙΔΗΣ, Καθηγητής Ε.Μ.Π.
3. Ι. Γ. ΡΑΥΤΟΓΙΑΝΝΗΣ, Αν. Καθηγητής Ε.Μ.Π.

ΕΠΤΑΜΕΛΗΣ ΕΞΕΤΑΣΤΙΚΗ ΕΠΙΤΡΟΠΗ:

1. Χ. Ι. ΓΑΝΤΕΣ, Καθηγητής Ε.Μ.Π. (Επιβλέπων)
2. Γ. Ι. ΙΩΑΝΝΙΔΗΣ, Καθηγητής Ε.Μ.Π.
3. Ι. ΒΑΓΙΑΣ, Καθηγητής Ε.Μ.Π.
4. Β. Κ. ΚΟΥΜΟΥΣΗΣ, Καθηγητής Ε.Μ.Π.
5. Ε. Σ. ΜΥΣΤΑΚΙΔΗΣ, Καθηγητής Παν. Θεσσαλίας
6. Ι. Γ. ΡΑΥΤΟΓΙΑΝΝΗΣ, Αν. Καθηγητής Ε.Μ.Π.
7. Τ. Π. ΑΒΡΑΑΜ, Επ. Καθηγητής Ε.Μ.Π.

Αθήνα, Ιανουάριος 2014

Η έγκριση της διδακτορικής διατριβής από την Ανώτατη Σχολή Πολιτικών Μηχανικών του Ε. Μ. Πολυτεχνείου δεν υποδηλώνει αποδοχή των γνώμων του συγγραφέα (Ν. 5343/1932, Άρθρο 202)

PREFACE

The research work in this thesis was carried out in the Institute of Steel Structures, School of Civil Engineering, at the National Technical University of Athens, under the supervision of Dr. Charis Gantes, Professor NTUA. Reaching the end of this work, I profoundly thank the people that contributed to its completion.

I would like to express my endless appreciation and sincere gratitude to my supervisor for his invaluable guidance and support during the course of this study. I am deeply honoured for his belief in me and for his giving me the chance to work on my PhD thesis under his supervision. His high educational level, broad scientific interests and practical experience resulted in the successful completion of this research and in his becoming a model for me as a researcher, engineer and teacher.

I also owe a debt of gratitude to Professor Georgios Ioannidis and Associate Professor Ioannis Raftoyiannis for their advice and guidance throughout the course of this research. They were willing to help whenever their opinion was asked.

I am also very thankful to Dr. Xenophon Lignos and Stilianos Katsatsidis for their precious help in performing the experimental tests. Their experience facilitated their fast and safe performance and the careful collection of the experimental results.

I also express my gratitude to Dr. Isabella Vassilopoulou who patiently guided me during the last steps of the doctoral thesis by providing me with information regarding its preparation. The quality of the presentation of this work would be lower, if it had not been for her precious help.

Special thanks are due to all members of the Institute of Steel Structures for the nice working environment which we created. In particular, I would like to thank Dr. Cyril Douthe, Dr. Athanasios Papageorgiou, Dr. Christoforos Dimopoulos, Konstantina Koulatsou, Vasileios Melissianos, Dr. Vasileios Karlos, Konstantinos Adamakos, Georgia Dougka, Danae Dimakogianni, Maria-Eleni Dasiou and Andreas Spiliopoulos.

I would also like to thank my family from the bottom of my heart for the financial support and psychological encouragement during these years. Without their priceless help, this work would not have been possible.

This PhD thesis is the outcome of a research work that lasted for many years. Therefore, I would like to mention that the maximum effort has been made in order to minimise errors and that I am the one to blame for those that may still exist.

Konstantinos E. Kalochairetis

January 2014

To my family,
for their invaluable support



Εθνικό Μετσόβιο Πολυτεχνείο
Σχολή Πολιτικών Μηχανικών
Τομέας Δομοστατικής
Εργαστήριο Μεταλλικών Κατασκευών

Διδακτορική Διατριβή Κωνσταντίνου Ε. Καλοχαιρέτη
Μη γραμμική συμπεριφορά και σχεδιασμός
σύνθετων υποστυλωμάτων από χάλυβα
υπό αξονική και εγκάρσια φόρτιση

Επιβλέπων: Δρ. Χάρης Ι. Γαντές, Καθηγητής Ε.Μ.Π.

Αθήνα, Ιανουάριος 2014

Περίληψη

Στόχος της παρούσας διδακτορικής διατριβής είναι η μελέτη της συμπεριφοράς σύνθετων υποστυλωμάτων με ράβδους δικτύωσης και τυχαίες συννοριακές συνθήκες υπό αξονική και εγκάρσια φόρτιση και η διατύπωση οδηγιών για το σχεδιασμό τους. Για την επίτευξη αυτού του στόχου ακολουθείται συνδυασμένη πειραματική, αριθμητική και αναλυτική προσέγγιση.

Αρχικά, παρουσιάζεται ο σχεδιασμός και η εκτέλεση μιας σειράς πειραματικών δοκιμών σε δέκα αμφιέριστα σύνθετα υποστυλώματα με ράβδους δικτύωσης (πέντε ομάδες με δύο ίδια υποστυλώματα στην κάθε μία για λόγους επαναληψιμότητας) με ρεαλιστικές καθολικές και τοπικές ανηγμένες λυγηρότητες. Τα δοκίμια υποβάλλονται σε αξονικά θλιπτικά φορτία και συγκεντρωμένες ακραίες ροπές προκαλούμενες λόγω εκκεντρότητας των αξονικών φορτίων. Τα αποτελέσματα για κάθε δοκίμιο παρουσιάζονται με φωτογραφίες τους για διάφορα επίπεδα φόρτισης, και δρόμους ισορροπίας με τη μορφή διαγραμμάτων φορτίου-εγκάρσιας μετακίνησης καθώς και φορτίου-παραμόρφωσης σε χαρακτηριστικές θέσεις. Η συμπεριφορά όλων των δοκιμών είναι αρχικά ελαστική, ενώ διαπιστώνεται πως σε όλες τις ομάδες η τοπική ελαστοπλαστική αστοχία ενός φατνώματος οδηγεί σε καθολική αστοχία χωρίς περιθώρια ανακατανομής της έντασης. Με βάση την τοπική συμπεριφορά των κρίσιμων φατνωμάτων καταδεικνύεται η επιρροή των αρχικών τοπικών ατελειών και των τοπικών εσωτερικών ροπών.

Στη συνέχεια, πραγματοποιείται αριθμητική προσομοίωση των πειραμάτων με τη μέθοδο πεπερασμένων στοιχείων, με στόχο τη βαθμονόμηση των αριθμητικών προσομοιωμάτων έχοντας ως βάση τα πειραματικά αποτελέσματα, ώστε να μπορούν να χρησιμοποιηθούν στη μετέπειτα πορεία της έρευνας. Για την προσομοίωση τόσο των πελμάτων όσο και των ράβδων δικτύωσης χρησιμοποιούνται αρχικά επιφανειακά πεπερασμένα στοιχεία. Προκειμένου να ληφθεί υπόψη η παρουσία παραμενουσών τάσεων λόγω θερμικής κατεργασίας η διατομή των πελμάτων χωρίζεται κατάλληλα σε τμήματα, σε κάθε ένα εκ των οποίων αποδίδεται διαφορετική ποιότητα χάλυβα. Οι καθολικές και τοπικές γεωμετρικές ατέλειες ενσωματώνονται στις αριθμητικές αναλύσεις σύμφωνα με τις πρώτες ιδιομορφές καθολικού και τοπικού λυγισμού, αντίστοιχα. Από τις αριθμητικές αναλύσεις προκύπτει πως εφόσον ληφθούν υπόψη στην ανάλυση η μη γραμμικότητα γεωμετρίας και υλικού, οι αρχικές γεωμετρικές καθολικές και τοπικές ατέλειες και οι παραμένουσες τάσεις θερμικής κατεργασίας, υπάρχει μια πολύ καλή συμφωνία μεταξύ αριθμητικών και πειραματικών αποτελεσμάτων, σε όρους μετακινήσεων, παραμορφώσεων και αντοχής. Επιπλέον, η σύγκριση των αριθμητικών προσομοιωμάτων με επιφανειακά πεπερασμένα στοιχεία με αντίστοιχα ραβδωτών πεπερασμένων στοιχείων οδηγεί στο συμπέρασμα πως η χρήση των δευτέρων μπορεί να προβλέψει ικανοποιητικά τη συμπεριφορά των σύνθετων μελών με αισθητά μικρότερο υπολογιστικό κόστος.

Στη συνέχεια, με χρήση αριθμητικών προσομοιωμάτων κυρίως ραβδωτών πεπερασμένων στοιχείων, διερευνάται η απόκριση σύνθετων υποστυλωμάτων με ράβδους δικτύωσης με καθολικές και τοπικές ατέλειες. Διαπιστώνεται ότι η αστοχία εκδηλώνεται συνήθως ως τοπική ελαστοπλαστική αστοχία του κρίσιμου φατνώματος, ή σπανιότερα ως καθολική ελαστική αστοχία. Στη δεύτερη περίπτωση η αλληλεπίδραση μεταξύ καθολικού και τοπικού λυγισμού είναι σημαντική και θα πρέπει να λαμβάνεται

υπόψη, ενώ στην πρώτη μπορεί να ενσωματωθεί έμμεσα στην τοπική αντοχή του κρίσιμου φαινομένου. Η μεγαλύτερη μείωση του φορτίου αστοχίας του ατελούς φορέα σε σχέση με τον τέλει πραγματοποιείται και στις δύο περιπτώσεις όταν τα φορτία καθολικού λυγισμού, τοπικού λυγισμού και πλήρους διαρροής ταυτίζονται, ενώ η μικρότερη όταν το κρίσιμο φορτίο καθολικού λυγισμού είναι μικρότερο από του τοπικού. Η αδυναμία της ικανοποιητικής πρόβλεψης του φορτίου αστοχίας από τις διατάξεις του Ευρωκώδικα 3 στην περίπτωση της δεύτερης μορφής αστοχίας, καθώς δε λαμβάνεται εκεί υπόψη η αλληλεπίδραση καθολικού και τοπικού λυγισμού, αποτελεί κίνητρο για τη δημιουργία μιας προσεγγιστικής αναλυτικής διαδικασίας που προβλέπει επαρκώς την απόκριση των σύνθετων μελών και στις δύο περιπτώσεις αστοχίας. Παρόλα αυτά, η πλέον συχνή μορφή αστοχίας στην πράξη είναι η πρώτη, λόγω χρήσης μελών με μικρές ως μέτριες καθολικές και τοπικές ανηγμένες λυγηρότητες και λόγω συνύπαρξης σημαντικών εγκάρσιων φορτίων, και με βάση αυτή συνεχίζεται η παρούσα έρευνα.

Εν συνεχεία, εφόσον η προσομοίωση των σύνθετων μελών με ράβδους δικτύωσης ως μελών Timoshenko κρίνεται επαρκής και αξιόπιστη, η έρευνα επικεντρώνεται στην πρόβλεψη του ελαστικού κρίσιμου φορτίου λυγισμού μελών Timoshenko με τυχαίες συνοριακές συνθήκες με τη μέθοδο του Engesser. Προτείνεται για αυτό το σκοπό ένα μητρώο ευστάθειας 3×3 που οδηγεί σε τρεις μη γραμμικές σχέσεις για αμετάθετα, μερικώς μεταθετά και μεταθετά μέλη. Εξάγονται επίσης εξισώσεις γωνιών στροφής με τη μέθοδο Engesser για μέλη Timoshenko με ημι-άκαμπτες συνδέσεις στα άκρα τους. Με βάση αυτές, υπολογίζονται στροφικές δυσκαμψίες για τα προς αντικατάσταση μέλη Timoshenko σε πλαίσια, ανάλογα με τη συνοριακή συνθήκη στο απέναντι άκρο τους και την παρουσία ή όχι αξονικής δύναμης. Η χρήση των μη γραμμικών σχέσεων και των στροφικών δυσκαμψιών συμβάλλει στον επαρκή υπολογισμό του ελαστικού κρίσιμου φορτίου λυγισμού πλαισίων που αποτελούνται από μέλη Timoshenko και από σύνθετα μέλη.

Ακολουθώντας, διερευνάται η ανάλυση 2^{ης} τάξης ατελών μελών Timoshenko με τυχαίες συνοριακές συνθήκες υπό συνδυασμό αξονικού φορτίου και συνήθων εγκάρσιων φορτίων, με στόχο να προταθούν κλειστές λύσεις για τον υπολογισμό εντατικών μεγεθών και μετακινήσεων κατά μήκος των μελών. Η ενσωμάτωση αρχικής καθολικής ατέλειας σύμφωνα με το σχήμα της 1^{ης} ιδιομορφής καθολικού λυγισμού γίνεται με χρήση προσεγγιστικού μεγεθυντικού συντελεστή που υπολογίζεται με βάση τα φορτία λυγισμού της προηγούμενης παραγράφου. Οι εγκάρσιες φορτίσεις περιλαμβάνουν ομοιόμορφα κατανομημένο φορτίο, ακραίες συγκεντρωμένες ροπές και ακραίες συγκεντρωμένες δυνάμεις και η ανάλυση υπό την επίδρασή τους πραγματοποιείται με χρήση των εξισώσεων γωνίας στροφής 2^{ης} τάξης με τη μέθοδο Engesser για μέλη Timoshenko. Η σύγκριση με αριθμητικά προσομοιώματα ραβδωτών πεπερασμένων στοιχείων οδηγεί σε πολύ ικανοποιητική συμφωνία μεταξύ τους.

Ο τερματισμός της ελαστικής ανάλυσης 2^{ης} τάξης για τον υπολογισμό του φορτίου αστοχίας τους πραγματοποιείται με χρήση μιας προτεινόμενης απλής σχέσης αλληλεπίδρασης που βασίζεται στο συμπέρασμα ότι τα σύνθετα μέλη με ράβδους δικτύωσης αστοχούν συνήθως λόγω τοπικής ελαστοπλαστικής αστοχίας. Συνεπώς, συνολικά η προτεινόμενη μέθοδος για μεμονωμένα σύνθετα μέλη με τυχαίες συνοριακές συνθήκες περιλαμβάνει την ελαστική ανάλυση 2^{ης} τάξης των ισοδύναμων μελών Timoshenko και τον τερματισμό αυτής για τον προσδιορισμό του φορτίου αστοχίας με βάση τη σχέση αλληλεπίδρασης. Η χρήση της προτεινόμενης διαδικασίας για τον υπολογισμό των μετακινήσεων και των φορτίων αστοχίας μεγάλου πλήθους σύνθετων υποστυλωμάτων με ράβδους δικτύωσης αποδεικνύεται ότι ευρίσκεται σε πολύ καλή συμφωνία με αριθμητικά αποτελέσματα που πρόκυπτουν από πλήρως μη γραμμικές αναλύσεις.

Τέλος, η προτεινόμενη μέθοδος εφαρμόζεται σε μονώροφα βιομηχανικά πλαίσια με σύνθετα υποστυλώματα υπό συμμετρικές και αντισυμμετρικές φορτίσεις. Στις εφαρμογές αυτές, η δοκός του πλαισίου αντικαθίσταται από κατάλληλα στροφικά ελατήρια, όπως αυτά εξήχθησαν για τον υπολογισμό του ελαστικού φορτίου λυγισμού πολυώροφων κατασκευών από μέλη Timoshenko, ανάλογα με το αν η φόρτιση προκαλεί παραμόρφωση μονής (αμετάθετη συμπεριφορά) ή διπλής (μεταθετή συμπεριφορά) καμπυλότητας. Ακολουθώντας απομονώνεται το δυσμενέστερο υποστυλόμενο και εφαρμόζεται η διαδικασία που περιγράφηκε στην προηγούμενη παράγραφο για μεμονωμένα σύνθετα μέλη με τυχαίες συνοριακές συνθήκες. Η εφαρμογή της προτεινόμενης μεθόδου σε μονώροφα πλαίσια με σύνθετα μέλη βρίσκεται σε ικανοποιητική συμφωνία με αριθμητικά αποτελέσματα που εξάγονται με τη χρήση πλήρως μη γραμμικών αναλύσεων. Η χρήση της σύγχρονης μελετητικής πρακτικής σχεδιασμού οδηγεί σε λιγότερο ακριβή αποτελέσματα από εκείνα της προτεινόμενης μεθόδου και σε αρκετές περιπτώσεις είναι κατά της ασφαλείας. Τέλος, με βάση αυτή τη διερεύνηση προτείνονται πρακτικοί τρόποι προσομοίωσης, ανάλυσης και ελέγχου επάρκειας των σύνθετων μελών, με στόχο τη βελτίωση της αξιοπιστίας κατά το σχεδιασμό τους σε επίπεδο μελετητικής πρακτικής.



National Technical University of Athens
School of Civil Engineering
Department of Structural Engineering
Institute of Steel Structures

Doctoral Thesis of Konstantinos E. Kalochairetis

**Nonlinear behaviour and design
of steel built-up columns
under axial and transverse loading**

Supervisor: Dr. Charis J. Gantes, Professor N.T.U.A.

Athens, January 2014

Abstract

The present doctoral thesis aims at investigating the behaviour of laced built-up beam-columns with arbitrary boundary conditions and providing practical guidance for their design. To that effect, a combined experimental, numerical and analytical approach is adopted.

Initially, the design and execution of a series of experimental tests on ten simply-supported laced built-up members (five pairs of similar columns for repeatability purposes) with realistic global and local non-dimensional slenderness is presented. The specimens are subjected to axial compressive loads and to end concentrated moments due to axial loads' eccentricity. The results for each specimen are presented with the use of photographs at various load levels, as well as with load-lateral displacement and load-strain graphs at characteristic locations. The specimens' behaviour is initially elastic, while failure in all cases is due to local elastoplastic failure of a critical panel, without beneficial effects of stress redistribution. Based on the local behaviour of the critical panels the effect of initial local imperfections and local internal bending moments is identified.

Next, numerical modelling of the experimental tests with the finite element method takes place, aiming at calibrating the numerical models based on the experimental results, so that they can then be used in the subsequent stages of research. Both chords and lacing bars are modelled with the use of shell elements. The effect of thermally induced residual stresses due to fabrication is incorporated in the chords' behavior by discretizing their cross-sections into sufficiently small shell elements, each of which has different steel yield strength. Global and local geometrical imperfections are included in the numerical analyses according to the first global and local buckling modes, respectively. It is concluded that if geometrical and material nonlinearity, initial global and local geometrical imperfections and thermally induced residual stresses due to fabrication are included in the analysis, a very good correlation between numerical and experimental results is observed, in terms of deflections, deformations and strength. Moreover, the comparison of numerical shell element models to corresponding beam element models leads to the conclusion that the use of the latter ones can predict the response of laced members in a satisfactory manner, with significantly smaller computational effort.

The behaviour of laced columns with global and local imperfections is then investigated with the use of numerical models, mainly employing beam elements. It is concluded that failure usually takes place due to local elastoplastic failure of the critical panel, or more rarely in the form of global elastic failure. In the second case, interaction between global and local buckling is important and should be taken into account, while in the first one this interaction can be incorporated indirectly in the local capacity of the critical panel. The largest reduction of collapse load of the imperfect structure when compared to the perfect one appears for both types of failure when the critical loads associated with global buckling, local buckling and yielding coincide, while the smallest reduction when the global buckling load is smaller than the local one. Because of the inability of Eurocode 3 to safely predict the collapse load corresponding to the second type of failure, as global and local buckling interaction is not accounted for, an approximate analytical procedure is

formulated, by means of which the response of laced built-up columns can be sufficiently evaluated in both cases. Nevertheless, local elastoplastic failure is much more frequent in practice, due to the use of members with small and intermediate values of global and local non-dimensional slenderness and due to the significant lateral loads, therefore, the subsequent stages of this research are based on this failure mode.

Taking advantage of the fact that modelling of laced built-up members as equivalent Timoshenko ones is found to be sufficient and reliable, the research then focuses on the calculation of the elastic critical buckling load of Timoshenko members with arbitrary boundary conditions according to Engesser's method. To that effect, a 3x3 stability matrix that leads to three nonlinear equations for braced, partially-braced and unbraced members is proposed. In addition, slope-deflection equations for Timoshenko members with semi-rigid connections at their ends based on Engesser's method are derived. Based on them, a complete set of rotational stiffness coefficients for the replacement of Timoshenko members in frames, depending on the boundary condition at their far end and the eventual presence of axial force, is calculated. The use of the nonlinear equations and rotational stiffness coefficients contributes to the sufficient evaluation of the elastic critical buckling load of frames consisting of Timoshenko and built-up members.

Next, the 2nd order analysis of imperfect Timoshenko members with arbitrary boundary conditions under the combined effect of axial load and commonly encountered lateral loads is investigated, in order to propose closed-form solutions for the calculation of internal forces and lateral deflections along such members. The incorporation of initial global imperfection according to the 1st global buckling load is achieved by using an approximate magnification factor, which is calculated based on the buckling loads mentioned in the previous paragraph. Lateral loads include uniformly distributed load, concentrated end moments and concentrated end forces and the analysis under their effect is performed with the use of 2nd order slope-deflection equations for Timoshenko members based on Engesser's method. The comparison with numerical models with beam elements leads to very good agreement between them.

The termination of the 2nd order elastic analysis for the calculation of the collapse load is achieved with the use of a proposed simple interaction equation based on the assumption that laced built-up members will fail due to local elastoplastic failure. Thus, the proposed method for laced built-up beam-columns with arbitrary boundary conditions consists of a 2nd order elastic analysis of equivalent Timoshenko members and its termination for the calculation of the collapse load according to the interaction equation. The use of the proposed method for the evaluation of lateral deflections and collapse loads of a large number of laced built-up members proves to be in very satisfactory agreement with the numerical results obtained with geometrically and materially nonlinear imperfection analyses.

Finally, the proposed method is applied to single-story industrial frames with laced built-up columns under symmetrical and anti-symmetrical loadings. In these applications, the frame's girder is replaced by appropriate rotational springs, as they are obtained for the calculation of the elastic critical buckling load of multi-story frames consisting of Timoshenko members, depending on whether the type of loading causes single curvature deformation (non-sway behaviour) or double curvature deformation (sway behaviour). Then, the more compressed column is isolated and the proposed procedure presented in the previous paragraphs for laced members with arbitrary supports is applied. The application of the proposed method to single-story frames with laced members is found to be in satisfactory agreement with numerical results obtained with geometrically and materially nonlinear imperfection analyses.

It is noted that the approach used in modern design practice leads to less accurate results than the proposed method, and in many cases to unsafe predictions. In order to contribute towards improving this shortcoming, the results of this investigation are utilised in order to propose practical design-oriented methods of modelling, analysing and designing laced built-up members.

ΠΕΡΙΕΧΟΜΕΝΑ ΕΚΤΕΝΟΥΣ ΠΕΡΙΛΗΨΗΣ

ΜΗ ΓΡΑΜΜΙΚΗ ΣΥΜΠΕΡΙΦΟΡΑ ΚΑΙ ΣΧΕΔΙΑΣΜΟΣ ΣΥΝΘΕΤΩΝ ΥΠΟΣΤΥΛΩΜΑΤΩΝ ΑΠΟ ΧΑΛΥΒΑ ΥΠΟ ΑΞΟΝΙΚΗ ΚΑΙ ΕΓΚΑΡΣΙΑ ΦΟΡΤΙΣΗ

A.1.	ΕΙΣΑΓΩΓΗ	A-1
A.2.	ΒΙΒΛΙΟΓΡΑΦΙΚΗ ΕΠΙΣΚΟΠΗΣΗ	A-2
A.2.1.	Έρευνα στην απόκριση σύνθετων υποστυλωμάτων.....	A-2
A.2.2.	Έρευνα στην αλληλεπίδραση καθολικής και τοπικής απόκρισης.....	A-3
A.2.3.	Έρευνα στην επιρροή των διατμητικών παραμορφώσεων.....	A-5
A.2.3.1.	Μέθοδος Engesser.....	A-6
A.2.3.2.	Μέθοδος Haringx.....	A-7
A.2.4.	Κανονιστικές διατάξεις EC3	A-8
A.2.4.1.	Σύνθετα υποστυλώματα με ράβδους δικτύωσης	A-8
A.2.4.2.	Σύνθετα υποστυλώματα με λεπίδες σύνδεσης	A-9
A.3.	ΠΕΙΡΑΜΑΤΙΚΗ ΔΙΕΡΕΥΝΗΣΗ	A-9
A.3.1.	Περιγραφή πειραμάτων	A-9
A.3.2.	Περιγραφή αποτελεσμάτων	A-10
A.4.	ΑΡΙΘΜΗΤΙΚΗ ΠΡΟΣΟΜΟΙΩΣΗ ΠΕΙΡΑΜΑΤΩΝ	A-11
A.4.1.	Περιγραφή αριθμητικών προσομοιωμάτων και αναλύσεων.....	A-11
A.4.2.	Περιγραφή αποτελεσμάτων	A-12
A.5.	ΑΡΙΘΜΗΤΙΚΗ ΚΑΙ ΑΝΑΛΥΤΙΚΗ ΔΙΕΡΕΥΝΗΣΗ ΣΥΝΘΕΤΩΝ ΥΠΟΣΤΥΛΩΜΑΤΩΝ	A-13
A.5.1.	Περιγραφή αριθμητικών αναλύσεων και αποτελέσματα	A-13
A.5.2.	Προτεινόμενη μέθοδος	A-14
A.5.3.	Αριθμητική επαλήθευση προτεινόμενης μεθόδου	A-15
A.6.	ΦΟΡΤΙΟ ΛΥΓΙΣΜΟΥ ΠΟΛΥΩΡΟΦΩΝ ΠΛΑΙΣΙΩΝ ΜΕ ΜΕΛΗ TIMOSHENKO.....	A-17
A.6.1.	Περιγραφή προτεινόμενης αναλυτικής μεθόδου	A-17
A.6.2.	Μη γραμμικές σχέσεις για προσδιορισμό φορτίου λυγισμού	A-17
A.6.3.	Εξισώσεις γωνίας-στροφής για μέλη Timoshenko με ημι-άκαμπτες συνδέσεις	A-19
A.6.4.	Στροφικές δυσκαμψίες προς αντικατάσταση μελών	A-20
A.6.5.	Αριθμητική επαλήθευση.....	A-21
A.7.	ΑΝΑΛΥΣΗ 2 ^{ΗΣ} ΤΑΞΗΣ ΜΕΛΩΝ TIMOSHENKO	A-21
A.7.1.	Αρχική ατέλεια	A-21
A.7.2.	Εγκάρσιο ομοιόμορφα κατανεμημένο φορτίο	A-22
A.7.3.	Συγκεντρωμένες ροπές στα άκρα	A-24
A.7.4.	Εγκάρσιες συγκεντρωμένες δυνάμεις στα άκρα	A-24
A.7.5.	Επαλληλία φορτίσεων.....	A-25
A.7.6.	Αριθμητική επαλήθευση.....	A-26
A.8.	ΣΥΜΠΕΡΙΦΟΡΑ ΣΥΝΘΕΤΩΝ ΜΕΛΩΝ ΥΠΟ ΑΞΟΝΙΚΗ ΚΑΙ ΕΓΚΑΡΣΙΑ ΦΟΡΤΙΣΗ	A-27
A.8.1.	Φορτίο αστοχίας σύνθετου μέλους.....	A-27
A.8.2.	Αριθμητικός έλεγχος.....	A-28
A.9.	ΣΥΜΠΕΡΙΦΟΡΑ ΒΙΟΜΗΧΑΝΙΚΩΝ ΠΛΑΙΣΙΩΝ.....	A-30
A.9.1.	Εφαρμογή προτεινόμενης μεθόδου σε βιομηχανικά πλαίσια	A-30

A.9.2. Αριθμητικός έλεγχος.....	A-31
A.10. ΣΥΝΟΨΗ ΚΑΙ ΣΥΜΠΕΡΑΣΜΑΤΑ	A-32
A.11. ΠΡΩΤΟΤΥΠΗ ΣΥΜΒΟΛΗ ΤΗΣ ΔΙΑΤΡΙΒΗΣ.....	A-34
A.11.1. Συμβολή στην επιστήμη του μηχανικού.....	A-34
A.11.2. Συμβολή στη μελετητική πρακτική	A-35

TABLE OF CONTENTS

1	INTRODUCTION.....	1
1.1	PREFACE.....	1
1.2	BUILT-UP COLUMNS.....	1
1.3	LACED BUILT-UP COLUMNS.....	3
1.4	BATTENED BUILT-UP COLUMNS	6
1.5	OBJECTIVE AND CONTENTS OF THE DOCTORAL THESIS.....	7
1.6	REFERENCES	8
2	LITERATURE REVIEW	9
2.1	INTRODUCTION	9
2.2	RESEARCH ON BUILT-UP COLUMNS.....	9
2.3	INTERACTION BETWEEN GLOBAL AND LOCAL BUCKLING.....	17
2.4	THE EFFECT OF SHEAR DEFORMATIONS	19
2.4.1	Shear deformable solid members	19
2.4.2	Engesser's theory.....	21
2.4.3	Haringx's theory.....	25
2.4.4	Application of Engesser's and Haringx's theories in research	28
2.5	MODERN DESIGN CODES	29
2.5.1	Eurocode 3 provisions	29
2.5.1.1	Analysis of built-up columns.....	29
2.5.1.2	Laced built-up columns.....	30
2.5.1.3	Battened built-up columns	36
2.5.1.4	Comparison between laced and battened built-up columns	40
2.5.2	Older German Design Code provisions (DIN 18800 - Part 2).....	42
2.5.3	American Institute of Steel Construction L.R.F.D. provisions.....	42
2.6	CONCLUSIONS	42
2.7	REFERENCES	42
3	EXPERIMENTAL INVESTIGATION	49
3.1	INTRODUCTION.....	49
3.2	DESCRIPTION OF EXPERIMENTS AND EXPERIMENTAL SET-UP	49
3.2.1	Specimen groups	49
3.2.2	Testing frame	52
3.2.3	Testing procedure and measuring devices	53
3.3	MATERIAL PROPERTIES	54
3.4	EXPERIMENTAL RESULTS	56
3.4.1	Group 1	56
3.4.2	Group 2	58
3.4.3	Group 3	61
3.4.4	Group 4.....	64

3.4.5	Group 5.....	67
3.5	COMPARISON OF EXPERIMENTAL RESULTS.....	70
3.5.1	Group 1 - Group 2.....	70
3.5.2	Group 1 - Group 3.....	71
3.5.3	Group 1 - Group 4.....	72
3.5.4	Group 1 - Group 5.....	72
3.6	CONCLUSIONS.....	72
3.7	REFERENCES	73
4	NUMERICAL MODELLING OF EXPERIMENTS.....	75
4.1	INTRODUCTION.....	75
4.2	DESCRIPTION OF NUMERICAL MODELS AND ANALYSES	75
4.3	EXPERIMENTAL AND NUMERICAL RESULTS	78
4.3.1	Group 1.....	78
4.3.2	Group 2.....	81
4.3.3	Group 3.....	85
4.3.4	Group 4.....	89
4.3.5	Group 5.....	93
4.4	EFFECT OF INITIAL IMPERFECTIONS	97
4.4.1	Group 1.....	97
4.4.2	Group 2.....	98
4.4.3	Group 3.....	98
4.4.4	Group 4.....	99
4.4.5	Group 5.....	100
4.5	COMPARISON BETWEEN SHELL AND BEAM ELEMENT MODELS	101
4.5.1	Group 1.....	102
4.5.2	Group 2.....	103
4.5.3	Group 3.....	104
4.5.4	Group 4.....	105
4.5.5	Group 5.....	106
4.6	CONCLUSIONS.....	107
4.7	REFERENCES	108
5	NUMERICAL AND ANALYTICAL INVESTIGATION OF LACED COLUMNS' BEHAVIOUR	111
5.1	INTRODUCTION.....	111
5.2	RESPONSE OF LACED BUILT-UP COLUMNS	111
5.2.1	Perfect laced built-up columns.....	111
5.2.2	Imperfect laced built-up columns.....	113
5.2.2.1	Elastic analyses	114
5.2.2.2	Elastoplastic analyses	117
5.3	EUROCODE 3 PROVISIONS.....	121
5.4	PROPOSED ANALYTICAL APPROACH.....	123

5.5	PARAMETRIC STUDIES	128
5.5.1	First parametric study.....	129
5.5.2	Second parametric study	133
5.5.3	Third parametric study	137
5.6	CONCLUSIONS	141
5.7	REFERENCES	141
6	ELASTIC BUCKLING LOAD OF MULTI-STORY FRAMES CONSISTING OF TIMOSHENKO MEMBERS	143
6.1	INTRODUCTION	143
6.2	ELASTIC BUCKLING LOAD OF TIMOSHENKO COLUMNS	145
6.2.1	General stability matrix.....	145
6.2.2	Buckling equations	147
6.2.2.1	Partially braced frame.....	148
6.2.2.2	Unbraced frame	167
6.2.2.3	Braced frame	168
6.3	SLOPE-DEFLECTION EQUATIONS FOR TIMOSHENKO MEMBERS	172
6.3.1	Semi-rigid connections at the ends	172
6.3.1.1	Second-order analysis	172
6.3.1.2	First-order analysis.....	176
6.3.2	Rigid connections at the ends.....	177
6.3.2.1	Second-order analysis	177
6.3.2.2	First-order analysis.....	178
6.4	ROTATIONAL STIFFNESSES.....	178
6.4.1	Fixed support at the far end and a semi-rigid connection at the near end, without axial force.....	178
6.4.2	Rotationally fixed support at the far end and a rigid connection at the near end, with axial force.....	179
6.4.3	Rotational and translational spring at the far end and a rigid connection at the near end, with axial force.....	180
6.4.4	Members with other boundary conditions at the far end.....	181
6.5	EXAMPLES	186
6.5.1	Example 1.....	186
6.5.2	Example 2.....	189
6.5.3	Example 3.....	190
6.5.4	Example 4.....	191
6.5.5	Example 5.....	191
6.6	CONCLUSIONS	192
6.7	REFERENCES	193
7	SECOND-ORDER ELASTIC ANALYSIS OF IMPERFECT TIMOSHENKO BEAM-COLUMNS WITH ARBITRARY SUPPORTS	195
7.1	INTRODUCTION	195
7.2	IMPERFECT TIMOSHENKO MEMBERS.....	195
7.2.1	Simply-supported case	196
7.2.2	Arbitrary boundary conditions	199
7.2.3	Numerical verification in imperfect Timoshenko members	201

7.2.3.1	Non-sway member	202
7.2.3.2	Partially sway member.....	203
7.2.3.3	Sway member	206
7.3	LATERALLY LOADED TIMOSHENKO MEMBERS	208
7.3.1	Lateral uniformly distributed load.....	208
7.3.2	Concentrated moments at the ends	211
7.3.3	Concentrated forces at the ends	213
7.3.4	Combination of the above load conditions	215
7.4	NUMERICAL VERIFICATION OF THE PROPOSED EQUATIONS	216
7.4.1.1	Non-sway member	216
7.4.1.2	Partially sway member.....	219
7.4.1.3	Sway member	221
7.5	CONCLUSIONS.....	224
7.6	REFERENCES	225
8	BEHAVIOUR OF LACED BEAM-COLUMNS WITH ARBITRARY SUPPORTS	227
8.1	INTRODUCTION.....	227
8.2	INTERACTION EQUATION FOR COLLAPSE LOAD OF LACED MEMBERS.....	227
8.2.1	Interaction equation.....	228
8.2.1.1	Local capacity based on first yield	229
8.2.1.2	Local capacity accounting for plastic reserve	230
8.2.2	Effect of local moments on failure.....	231
8.3	DESIGN OF LACING BARS	232
8.4	VERIFICATION WITH NUMERICAL RESULTS	233
8.4.1	Modelling with beam elements	234
8.4.1.1	Rectangular sections	235
8.4.1.2	I-sections.....	244
8.4.2	Modelling with shell elements	249
8.5	VERIFICATION WITH EXPERIMENTAL RESULTS	253
8.5.1	Klöppel and Ramm experimental results.....	253
8.5.2	Present doctoral thesis's experimental results.....	256
8.6	CONCLUSIONS.....	259
8.7	REFERENCES	260
9	BEHAVIOUR OF INDUSTRIAL FRAMES.....	261
9.1	INTRODUCTION.....	261
9.2	METHODS OF ANALYSIS AND DESIGN FOR LACED MEMBERS.....	261
9.2.1	Modelling procedures	262
9.2.1.1	Euler- Bernoulli beam elements.....	262
9.2.1.2	Timoshenko beam elements.....	262
9.2.1.3	Full laced member with the use of Euler-Bernoulli beam elements.....	262
9.2.1.4	Full laced member with the use of shell elements.....	263

9.2.2	Types of analysis.....	263
9.2.2.1	Linear analysis (LA)	263
9.2.2.2	Linearised Buckling Analysis (LBA).....	263
9.2.2.3	Nonlinear analysis P- Δ	263
9.2.2.4	Nonlinear analysis P- δ	263
9.2.2.5	Geometrically Nonlinear Analysis - Geometrically Nonlinear Imperfection Analysis	264
9.2.2.6	Geometrically and Materially Nonlinear and Geometrically and Materially Nonlinear Imperfection Analyses.....	264
9.2.2.7	Proposed analytical second-order approach including initial imperfections.....	264
9.2.3	Design checks	264
9.2.3.1	Allowable Stress Design	264
9.2.3.2	Interaction equation of Eurocode 3	264
9.2.3.3	Proposed interaction equation.....	265
9.3	EXISTING ANALYSIS AND DESIGN PROCEDURES FOR FRAMES.....	265
9.3.1	Linear elastic analysis and design of the full frame (C.S.1 st)	265
9.3.2	Nonlinear elastic analysis and design of the full frame (C.S.2 nd).....	265
9.3.3	Geometrically and Materially Nonlinear Imperfection Analysis of the full frame (GMNIA).....	265
9.4	APPLICATION OF PROPOSED METHOD TO FRAMES	266
9.4.1	Analytical proposed method applied to frames.....	266
9.4.2	Equivalent Timoshenko frame with GNIA.....	268
9.5	NUMERICAL VERIFICATION IN FRAMES WITH UNIFORM LACED MEMBERS.....	268
9.5.1	Load cases.....	269
9.5.1.1	Load case-A.....	269
9.5.1.2	Load case-B.....	270
9.5.1.3	Load case-C.....	272
9.5.2	Examples.....	273
9.5.2.1	Example 1	273
9.5.2.2	Example 2	281
9.5.2.3	Example 3	288
9.5.2.4	Example 4	296
9.5.2.5	Example 5	304
9.6	FRAMES WITH NON-UNIFORM LACED MEMBERS.....	305
9.7	GUIDELINES FOR PRACTICAL USE.....	308
9.7.1	Linear elastic analysis and design of full frame (C.S.1 st)	308
9.7.2	Nonlinear elastic analysis and design of the full frame (C.S.2 nd).....	308
9.7.3	GNIA of equivalent Timoshenko frame	308
9.7.4	Proposed procedure	309
9.7.5	GMNIA of full frame	309
9.8	CONCLUSIONS.....	310
9.9	REFERENCES	310

10 SUMMARY AND CONCLUSIONS.....	313
10.1 SUMMARY.....	313
10.2 CONCLUDING REMARKS.....	316
10.3 RESEARCH CONTRIBUTION AND INNOVATION.....	318
10.3.1 Contribution to the advancement of engineering science	319
10.3.2 Contribution to the advancement of engineering practice.....	319
10.4 SUGGESTIONS FOR FUTURE RESEARCH	320
10.5 REFERENCES	321

Α ΜΗ ΓΡΑΜΜΙΚΗ ΣΥΜΠΕΡΙΦΟΡΑ ΚΑΙ ΣΧΕΔΙΑΣΜΟΣ ΣΥΝΘΕΤΩΝ ΥΠΟΣΤΥΛΩΜΑΤΩΝ ΑΠΟ ΧΑΛΥΒΑ ΥΠΟ ΑΞΟΝΙΚΗ ΚΑΙ ΕΓΚΑΡΣΙΑ ΦΟΡΤΙΣΗ

A.1. ΕΙΣΑΓΩΓΗ

Τα σύνθετα υποστυλώματα συντίθενται συνήθως από δύο πρότυπες διατομές που βρίσκονται σε απόσταση και συνδέονται μεταξύ τους με τη χρήση είτε ράβδων δικτύωσης είτε λεπίδων σύνδεσης. Οι πρότυπες διατομές αποτελούν τα πέλματα και προσφέρουν αξονική και καμπτική δυσκαμψία. Το συνδετικό μέσο των ράβδων δικτύωσης ή των λεπίδων σύνδεσης εξασφαλίζει τη συνεργασία μεταξύ των πελμάτων και προσφέρει διατμητική δυσκαμψία. Το βασικό χαρακτηριστικό των σύνθετων υποστυλωμάτων που τα χρίζει καταλληλότερα για περιπτώσεις μεγάλων φορτίων και μηκών λυγισμού είναι η διάταξη των μελών που ουσιαστικά βασίζεται στη ροή των εσωτερικών δυνάμεων. Η συγκέντρωση υλικού μακριά από τον ουδέτερο άξονα οδηγεί σε καλύτερη εκμετάλλευση του, ενώ ο προσανατολισμός των πελμάτων με τέτοιο τρόπο ώστε ο ισχυρός τους άξονας να ενεργοποιείται για εκτός επιπέδου συμπεριφορά, οδηγεί στην επίτευξη παρόμοιας αντοχής και δυσκαμψίας και στους δύο άξονες. Τα κατασκευαστικά πλεονεκτήματα των σύνθετων μελών εκτιμήθηκαν στις αρχές του προηγούμενου αιώνα, όταν άρχισαν να χρησιμοποιούνται σε μεγάλης κλίμακας κατασκευές. Παρόλα αυτά η διαφοροποίησή τους από τα συνήθη υποστυλώματα έγινε κατανοητή μετά την κατάρρευση της υπό κατασκευής γέφυρας Quebec στον Καναδά, όπου αποδείχτηκε ότι η αστοχία οφειλόταν σε σύνθετο μέλος που είχε το ρόλο θλιπτήρα.

Τα σύνθετα υποστυλώματα διαφοροποιούνται από τα συνήθως χρησιμοποιούμενα μονομελή ως προς την αλληλεπίδραση καθολικής και τοπικής συμπεριφοράς και ως προς την επιρροή των διατμητικών παραμορφώσεων. Σε αντίθεση με τα μονομελή υποστυλώματα, η τοπική συμπεριφορά των σύνθετων μελών δύναται να επηρεάσει σημαντικά την καθολική απόκριση, τόσο σε ό,τι αφορά τη δυσκαμψία όσο και την αντοχή. Επιπρόσθετα, τα σύνθετα μέλη χαρακτηρίζονται από μικρή διατμητική δυσκαμψία και σημαντική καμπτική, το οποίο σημαίνει πως οι διατμητικές παραμορφώσεις μπορεί να είναι συγκρίσιμου μεγέθους με τις αντίστοιχες καμπτικές. Τα φαινόμενα αυτά θα πρέπει να λαμβάνονται

υπόψη σε συνδυασμό με τη μη γραμμικότητα γεωμετρίας και υλικού για την ορθή αξιολόγηση της συμπεριφοράς.

Τα σύνθετα υποστυλώματα, χαρακτηριζόμενα από μεγάλη αξονική και καμπτική δυσκαμψία, χρησιμοποιούνται σε ένα μεγάλο εύρος κατασκευών. Συνήθως στην πράξη απαντώνται σε μονώροφα βιομηχανικά κτίρια στα οποία κινούνται γερανογέφυρες. Σε τέτοιες περιπτώσεις, γίνεται χρήση διαδοχικών επίπεδων πλαισίων με σύνθετα υποστυλώματα, κατάλληλα προσανατολισμένα ώστε για εντός των πλαισίων συμπεριφορά, να ενεργοποιείται η σύνθετη λειτουργία. Η γερανογέφυρα στηρίζεται στα άκρα της είτε σε κατάλληλα διαμορφωμένο κοντό πρόβολο σε κάποιο ύψος του σύνθετου μέλους είτε στο εσωτερικό πέλμα του σύνθετου υποστυλώματος. Επιπρόσθετα, σύνθετα μέλη χρησιμοποιούνται σε συστήματα δυσκαμψίας και δικτυώματα, κυρίως στη γεφυροποιία.

Η παρούσα διδακτορική διατριβή επικεντρώνεται στη διερεύνηση της στατικής απόκρισης σύνθετων μελών με ράβδους δικτύωσης υπό αξονική θλίψη και συνήθεις εγκάρσιες φορτίσεις. Για λόγους συντομίας στις ενότητες Α.3-Α.11 με τον όρο σύνθετα υποστυλώματα ή μέλη θα αναφέρονται τα σύνθετα υποστυλώματα ή μέλη με ράβδους δικτύωσης.

A.2. ΒΙΒΛΙΟΓΡΑΦΙΚΗ ΕΠΙΣΚΟΠΗΣΗ

Η συμπεριφορά των σύνθετων υποστυλωμάτων έχει ερευνηθεί διεξοδικά σε επίπεδο πειραματικό, αριθμητικό και αναλυτικό με έμφαση σε αξονικά θλιβόμενα αμφιέριστα μέλη. Η αλληλεπίδραση καθολικού και τοπικού λυγισμού καθώς και η επιρροή των διατμητικών παραμορφώσεων έχουν επίσης διερευνηθεί εκτενώς και στην παρούσα ενότητα παρουσιάζονται ενδεικτικές σημαντικές βιβλιογραφικές αναφορές.

A.2.1. Έρευνα στην απόκριση σύνθετων υποστυλωμάτων

Η συμπεριφορά ενός ελαστικού τέλει υποστυλώματος διερευνήθηκε αναλυτικά από τον Euler [2-1], ενώ η ενσωμάτωση των διατμητικών παραμορφώσεων σε ανάλυση λυγισμού πραγματοποιήθηκε από τον Engesser [2-3], [2-4]. Στις αρχές του προηγούμενου αιώνα πραγματοποιήθηκε μεγάλο πλήθος πειραματικών διερευνήσεων [2-7]-[2-15] με έμφαση σε αμφιέριστα μέλη υπό αξονικό θλιπτικό φορτίο και εξήχθησαν κυρίως ποιοτικά συμπεράσματα σε ό,τι αφορά την απόκριση των σύνθετων μελών.

Οι Klöppel και Ramm [2-21] διερεύνησαν αναλυτικά και πειραματικά τη συμπεριφορά 43 έκκεντρα φορτιζόμενων υπό θλιπτική αξονική δύναμη αμφιέριστων σύνθετων υποστυλωμάτων με ράβδους δικτύωσης. Εξήχθησαν συμπεράσματα που αφορούν την επιρροή του μοχλοβραχίονα μεταξύ των πελμάτων, του μήκους του φατνώματος, του μεγέθους της εκκεντρότητας και του είδους της δικτύωσης στην απόκριση και αστοχία των δοκιμών. Επιπρόσθετα, διερευνήθηκε η πιθανή επιρροή των παραμενουσών τάσεων λόγω συγκολλήσεων των ράβδων δικτύωσης στα πέλματα καθώς παρατηρήθηκε πρώιμη πλαστικοποίηση στις περιοχές των συνδέσεων. Οι ίδιοι συγγραφείς [2-22] ανέλυσαν τη συμπεριφορά σύνθετων υποστυλωμάτων με 4 πέλματα που χρησιμοποιούνται ευρέως σε γερανούς. Οι Ramm και Uhlmann [2-23] συνόψισαν τα αποτελέσματα των προαναφερθεισών δημοσιεύσεων και πρότειναν απλές αναλυτικές διαδικασίες για τον έλεγχο σύνθετων μελών στην πράξη που έχουν ενσωματωθεί στις οδηγίες του Ευρωκώδικα 3 (EC3) [2-24].

Οι Lee και Bruneau ασχολήθηκαν πειραματικά [2-37] και αναλυτικά [2-38] με τη σεισμική απόκριση σύνθετων μελών με ράβδους δικτύωσης. Πραγματοποίησαν 12 δοκιμές ψευδο-στατικής φόρτισης και τα αποτελέσματα χρησιμοποιήθηκαν για την εξαγωγή συμπερασμάτων που αφορούσαν την πλαστιμότητα, απορρόφηση ενέργειας, αντοχή και πτώση αντοχής μετά το λυγισμό για διάφορους λόγους καθολικής και τοπικής λυγηρότητας των υποστυλωμάτων. Οι Hashemi και Jafari [2-40] έκαναν μια σύντομη αναφορά για τη συμπεριφορά και τους τρόπους αστοχίας που παρατηρήθηκαν σε υποστυλώματα με λεπίδες σύνδεσης μετά το σεισμό του Bam το 2003, καταλήγοντας πως οι

ανεπαρκείς οδηγίες σχεδιασμού τέτοιων μελών οδήγησαν σε εκτεταμένες αστοχίες. Οι κύριες μορφές αστοχίας που καταγράφηκαν περιλαμβάνουν καθολικό λυγισμό, τοπικό λυγισμό, στρεπτοκαμπτικό λυγισμό, αστοχία των λεπίδων σύνδεσης, αστοχία των συγκολλήσεων των λεπίδων σύνδεσης και πλαστική διατμητική παραμόρφωση των λεπίδων σύνδεσης. Οι ίδιοι συγγραφείς [2-44] πραγματοποίησαν πειράματα ανακυκλιζόμενης φόρτισης σε σύνθετα μέλη με λεπίδες σύνδεσης, καταλήγοντας πως η χρήση τους σε περιοχές υψηλής σεισμικότητας θα πρέπει να αποφεύγεται εξαιτίας της μικρής τους πλαστιμότητας.

Οι Bonab και Hashemi [2-49] πραγματοποίησαν αριθμητικές αναλύσεις σε σύνθετα δικτυωτά μέλη με στατικό σύστημα προβόλων υπό εγκάρσια και αξονική ανακυκλιζόμενη φόρτιση. Στα συμπεράσματα τους αναφέρουν πως όσο μεγαλύτερο είναι το αξονικό φορτίο τόσο μικρότερη η διαθέσιμη πλαστιμότητα και πως οι εσωτερικές ροπές των πελμάτων παίζουν σημαντικό ρόλο. Οι Bonab et al. [2-50] πραγματοποίησαν πειράματα για τον προσδιορισμό του ελαστικού κρίσιμου φορτίου λυγισμού και του φορτίου αστοχίας κεντρικώς θλιβόμενων δικτυωτών μελών και πρότειναν ένα τροποποιημένο διάγραμμα Southwell για την ενσωμάτωση διατμητικών παραμορφώσεων. Κατέληξαν στο συμπέρασμα πως η μέθοδος Engesser για τον υπολογισμό του κρίσιμου φορτίου λυγισμού βρίσκεται σε πολύ καλή συμφωνία με τα πειραματικά αποτελέσματα. Επιπρόσθετα, ανέφεραν πως για τον προσδιορισμό του φορτίου αστοχίας, η μέθοδος Ayrton-Perry οδηγεί σε συντηρητικά αποτελέσματα, ενώ αντίθετα η χρήση καμπυλών πλήρους αντοχής σε υπερεκτίμηση της αντοχής.

A.2.2. Έρευνα στην αλληλεπίδραση καθολικής και τοπικής απόκρισης

Τα σύνθετα υποστυλώματα αποτελούνται από πολλά στοιχεία που συνεργάζονται και συνιστούν μια ενιαία κατασκευή. Συνεπώς η τοπική συμπεριφορά των στοιχείων δύναται να επηρεάσει την καθολική συμπεριφορά της κατασκευής. Δημοσιεύσεις σχετικές με το συγκεκριμένο θέμα παρουσιάζονται σε αυτή την υποενότητα.

Τα σχήματα των ιδιομορφών καθολικού και τοπικού λυγισμού για τυπικό αμφιέριστο δικτυωτό σύνθετο υποστυλόμετρο φαίνονται στο Σχήμα 1. Η ιδιομορφή καθολικού λυγισμού συνδέεται με το φορτίο καθολικού λυγισμού (Σχήμα 1(α)), στο οποίο ολόκληρο το υποστυλόμετρο αποκλίνει από την τέλεια και ευθύγραμμη γεωμετρία του. Στην περίπτωση που η δικτύωση είναι ισχυρή, το φορτίο καθολικού λυγισμού είναι το φορτίο Euler που δίνεται από:

$$P_E = \frac{\pi^2 EI_{eff}}{(KL)^2} \quad (1)$$

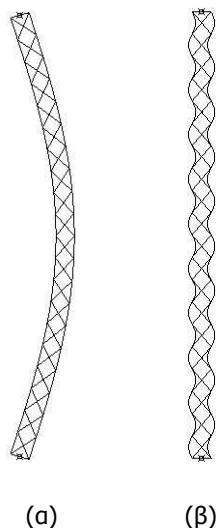
όπου EI_{eff} είναι η καμπτική δυσκαμψία του σύνθετου υποστυλώματος θεωρούμενου ως ενιαίου, K ο συντελεστής ισοδύναμου μήκους λυγισμού ($K=1$ για αμφιέριστα υποστυλώματα) και L είναι το μήκος του υποστυλώματος. Σε περίπτωση σημαντικών διατμητικών παραμορφώσεων θα πρέπει το φορτίο καθολικού λυγισμού να τροποποιηθεί κατάλληλα.

Η ιδιομορφή τοπικού λυγισμού σχετίζεται με τον ανεξάρτητο λυγισμό των φανωμάτων ως αμφιέριστων μελών μεταξύ των συνδέσεων της δικτύωσης με τα πέλματα (Σχήμα 1(β)). Το φορτίο τοπικού λυγισμού προκύπτει από το άθροισμα των φορτίων λυγισμού των φανωμάτων κάθε πέλματος:

$$P_L = \frac{2\pi^2 EI_{ch,z}}{a^2} \quad (2)$$

όπου $EI_{ch,z}$ είναι η εντός επιπέδου καμπτική δυσκαμψία του κάθε πέλματος και a είναι το μήκος του κάθε φανώματος (απόσταση μεταξύ διαδοχικών συνδέσεων).

Το φορτίο τοπικού λυγισμού μπορεί να είναι ελαφρώς μεγαλύτερο σε σύνθετα μέλη με λεπίδες σύνδεσης εξαιτίας της στροφικής δυσκαμψίας που προσφέρουν αυτές στα άκρα των φατνωμάτων. Από την ανωτέρω περιγραφή καθίσταται σαφές πως ο τοπικός λυγισμός σε σύνθετα υποστυλώματα δεν αναφέρεται στον τοπικό λυγισμό πλακοειδών στοιχείων ελατών ή συγκολλητών διατομών.



Σχήμα 1: (α) Ιδιομορφή καθολικού λυγισμού αμφιέριστου δικτυωτού μέλους και (β) ιδιομορφή τοπικού λυγισμού
Το φορτίο πλήρους διαρροής είναι η τρίτη μορφή αστοχίας του τέλειου σύνθετου μέλους:

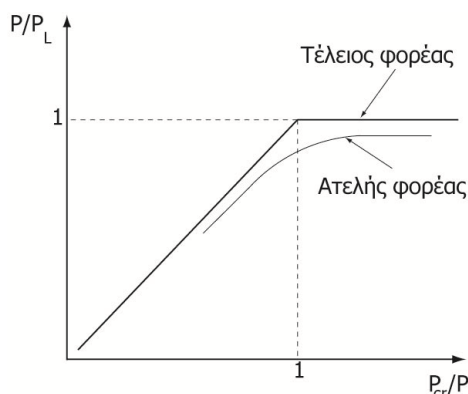
$$P_Y = 2A_{ch} f_y \quad (3)$$

όπου A_{ch} είναι το εμβαδόν της διατομής του κάθε πέλματος και f_y το όριο διαρροής του υλικού. Η κρίσιμη μεταξύ των τριών ανωτέρω μορφών αστοχίας, αγνοώντας την αλληλεπίδραση μεταξύ τους και τα μη γραμμικά φαινόμενα, αντιστοιχεί στην ελάχιστη τιμή φορτίου, όπως υπολογίζεται από τις Εξ. (1)-(3).

Από θεωρητική οπτική γωνία, ο Van der Neut [2-51] ήταν ο πρώτος που ασχολήθηκε με ένα εξιδανικευμένο θλιβόμενο μέλος που αποτελείτο από δύο λεπτότοιχα πέλματα και ένα κορμό που διατηρούσε την ενότητα της κατασκευής. Οι Koiter and Kuiken [2-52] αντιμετώπισαν το ίδιο πρόβλημα και απέδειξαν ότι ο σχεδιασμός με βάση τη βελτιστοποίηση που σχετίζεται με εξίσωση του φορτίων καθολικού και τοπικού λυγισμού οδηγεί σε μεγάλη απώλεια αντοχής λόγω αλληλεπίδρασης ιδιομορφών υπό την παρουσία αρχικών ατελειών. Οι Thompson and Hunt [2-54] πραγματοποιώντας μια ανάλυση με τροποποιημένη καμπτική δυσκαμψία για την ενσωμάτωση αρχικών τοπικών ατελειών στο κρίσιμο φορτίο καθολικού λυγισμού οδηγήθηκαν στα ίδια συμπεράσματα. Οι Svensson and Kragerup [2-58] επιβεβαίωσαν τα προηγούμενα συμπεράσματα και τα επέκτειναν με χρήση ελαστικών αναλύσεων μέχρι την πρώτη διαρροή υλικού. Κατέληξαν στο συμπέρασμα πως η μεγαλύτερη απώλεια αντοχής λαμβάνει χώρα όταν τα φορτία καθολικού λυγισμού, τοπικού λυγισμού και πλήρους διαρροής ταυτίζονται. Αυτή η μείωση γίνεται ιδιαίτερα σημαντική υπό την παρουσία αρχικών ατελειών φτάνοντας μεγέθη της τάξης του 50%.

Μια γραφική απεικόνιση της ευαισθησίας σε αρχικές ατέλειες ελαστικών σύνθετων υποστυλωμάτων φαίνεται στο Σχήμα 2. Στον οριζόντιο άξονα φαίνεται ο λόγος μεταξύ των φορτίων καθολικού και τοπικού λυγισμού, ενώ στον κατακόρυφο άξονα φαίνεται ο λόγος μεταξύ του φορτίου αστοχίας και του φορτίου τοπικού λυγισμού. Απεικονίζεται η απόκριση τόσο του τέλειου όσο και του ατελούς φορέα, καθιστώντας σαφές ότι όταν τα δύο κρίσιμα φορτία λυγισμού ταυτίζονται ($P_{cr}/P_L=1$), η μείωση του φορτίου P εξαιτίας της παρουσίας αρχικών ατελειών είναι πολύ μεγαλύτερη σε σχέση με εκείνη

που αντιστοιχεί σε άλλους λόγους P_{cr}/P_L . Για λόγους P_{cr}/P_L μεγαλύτερους από τη μονάδα η μείωση είναι μεσαίας τάξης, ενώ η μικρότερη μείωση εμφανίζεται για λόγους μικρότερους της μονάδας.



Σχήμα 2: Διάγραμμα ευαισθησίας σε αρχικές ατέλειες για σύνθετο μέλος

A.2.3. Έρευνα στην επιρροή των διατμητικών παραμορφώσεων

Τα μέλη συμπαγούς διατομής υπόκεινται σε καμπτικές, διατμητικές και αξονικές παραμορφώσεις αλλά η επιρροή των δύο τελευταίων στην απόκριση και αντοχή επιτρέπει την αγνόηση τους (μέλη Euler-Bernoulli). Σε υποστυλώματα μικρού μήκους, μεγάλης καμπτικής ή μικρής διατμητικής δυσκαμψίας, ή συνδυασμού των προηγούμενων τριών περιπτώσεων, η επιρροή των διατμητικών παραμορφώσεων μπορεί να είναι σημαντική, και θα πρέπει να ληφθεί υπόψη, καθώς οι καμπτικές παραμορφώσεις γίνονται συγκρίσιμου μεγέθους με τις διατμητικές. Τα μέλη που υπόκεινται σε διατμητικές παραμορφώσεις ονομάζονται μέλη Timoshenko και σε σχέση με τα αντίστοιχα μέλη Euler-Bernoulli έχουν μικρότερα φορτία λυγισμού και υπόκεινται σε σημαντικότερα φαινόμενα 2^{ης} τάξης.

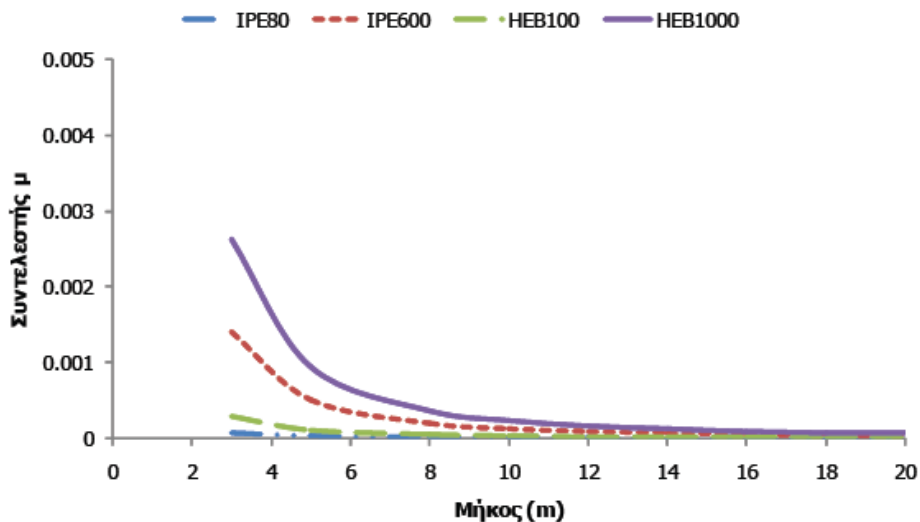
Ο υπολογισμός της καμπτικής δυσκαμψίας βασίζεται στο μέτρο ελαστικότητας E και στη ροπή αδράνειας I της διατομής περί τον εξεταζόμενο άξονα κάμψης. Η διατμητική δυσκαμψία ορίζεται ως το γινόμενο του συντελεστή σχήματος k , του εμβαδού της διατομής και του μέτρου δυστημψίας G . Ο Cowper [2-61], [2-62] παρείχε αναλυτικούς υπολογισμούς για το συντελεστή σχήματος ανάλογα με τα γεωμετρικά χαρακτηριστικά της διατομής και τις ιδιότητες του υλικού. Οι Scheer και Plumeyer [2-63] συμπέραναν πως ο αδιαστατοποιημένος λόγος $1/\mu$ είναι ενδεικτικός της επιρροής των διατμητικών παραμορφώσεων:

$$\frac{1}{\mu} = \frac{kAGL^2}{EI} \quad (4)$$

Με βάση παραμετρική ανάλυση, έδειξαν πως οι διατμητικές παραμορφώσεις θα πρέπει να λαμβάνονται υπόψη για τιμές του λόγου $1/\mu$ μικρότερες του 115 για ισοστατικούς φορείς και 385 για υπερστατικούς φορείς. Γίνεται συνεπώς κατανοητό πως οι υπερστατικοί φορείς αναμένεται να υπόκεινται σε πιο σημαντικές διατμητικές παραμορφώσεις.

Τα σύνθετα υποστυλώματα υπόκεινται συνήθως σε σημαντικές διατμητικές παραμορφώσεις. Πιο συγκεκριμένα, τα σύνθετα υποστυλώματα με ράβδους δικτύωσης χαρακτηρίζονται από μειωμένη διατμητική δυσκαμψία, ενώ ο μεγάλος μοχλοβραχίονας μεταξύ των πελμάτων οδηγεί σε μεγάλη καμπτική δυσκαμψία. Για αυτό το λόγο, παρά το μεγάλο μήκος που συνήθως έχουν, αναπτύσσουν σημαντικές διατμητικές παραμορφώσεις. Παρομοίως, τα σύνθετα υποστυλώματα με λεπίδες σύνδεσης έχουν πολύ μικρή διατμητική δυσκαμψία και παρά το γεγονός πως έχουν μεγάλο μήκος και μικρή καμπτική δυσκαμψία, υπόκεινται επίσης σε σημαντικές διατμητικές παραμορφώσεις. Συνεπώς, και τα δύο είδη σύνθετων μελών χαρακτηρίζονται από μικρούς λόγους $1/\mu$. Η μεταβολή του συντελεστή μ σε

συνάρτηση με το μήκος του μέλους φαίνεται στο Σχήμα 3 για τέσσερις τυπικές διατομές διπλού-ταυ. Ο συντελεστής μ γίνεται μεγάλος (και συνεπώς ο λόγος $1/\mu$ μικρός) για μικρά μήκη υποστυλωμάτων και για διατομές με σχετικά μεγάλη καμπτική δυσκαμψία. Σε σύνθετα μέλη, ο συντελεστής μ συνήθως κυμαίνεται από 0.001 έως 0.1 τονίζοντας τη σημασία των διατμητικών παραμορφώσεων σε τέτοια μέλη.



Σχήμα 3: Επιρροή του μήκους του υποστυλώματος στο συντελεστή μ για τέσσερις τυπικές διατομές I

A.2.3.1. Μέθοδος Engesser

Σύμφωνα με τη μέθοδο Engesser [2-3], [2-4] για την ενσωμάτωση διατμητικών παραμορφώσεων στην ανάλυση αμφιέριστου μέλους με καμπτική δυσκαμψία EI και διατμητική δυσκαμψία S_v που υπόκειται σε θλιπτική αξονική δύναμη P , η συνολική στροφή w' συνίσταται από τη στροφή ψ λόγω κάμψης μόνο και τη διατμητική παραμόρφωση γ :

$$w' = \psi + \gamma \quad (5)$$

Η καμπτική ροπή κατά μήκος του μέλους είναι συνεπώς ίση με:

$$M(x) = -EI\psi'(x) \quad (6)$$

Η τέμνουσα δύναμη που είναι κάθετη στον παραμορφωμένο άξονα είναι ίση με:

$$Q = -EI\psi'' = Pw' \quad (7)$$

Η διατμητική παραμόρφωση γ είναι ίση με:

$$\gamma = \frac{Pw'}{S_v} \quad (8)$$

Η διαφορική εξίσωση που διέπει το πρόβλημα είναι:

$$w'' \left(1 - \frac{P}{S_v} \right) + \frac{Pw}{EI} = 0 \quad (9)$$

και η λύση της ανωτέρω ομογενούς διαφορικής εξίσωσης είναι:

$$w(x) = A_1 \sin(ax) + A_2 \cos(ax) \quad (10)$$

όπου οι συντελεστές A_1 και A_2 αποτελούν σταθερές ολοκλήρωσης, $a^2 = \frac{P}{EI\beta}$ και $\beta = \left(1 - \frac{P}{S_v}\right)$.

Με παρόμοιο τρόπο εξάγεται η ομογενής διαφορική εξίσωση συναρτήσει της στροφής λόγω κάμψης μόνο:

$$EI\psi'''\left(1 - \frac{P}{S_v}\right) + P\psi = 0 \quad (11)$$

Το ελαστικό κρίσιμο φορτίο λυγισμού για αμφιέριστο μέλος Timoshenko σύμφωνα με τη μέθοδο Engesser είναι ίσο με:

$$P_{cr,E} = \frac{P_E}{1 + \frac{P_E}{S_v}} = \frac{1}{\frac{1}{P_E} + \frac{1}{S_v}} \quad (12)$$

όπου P_E είναι το φορτίο λυγισμού Euler του αμφιέριστου μέλους. Επιπρόσθετα, για πολύ κοντά υποστυλώματα που χαρακτηρίζονται από πολύ μεγάλο φορτίο λυγισμού Euler, το κρίσιμο φορτίο λυγισμού είναι ίσο με τη διατμητική δυσκαμψία.

A.2.3.2. Μέθοδος Haringx

Σύμφωνα με τη μέθοδο Haringx [2-65], [2-66] που χρησιμοποιείται για την ενσωμάτωση διατμητικών παραμορφώσεων, στην ανάλυση αμφιέριστου μέλους με καμπτική δυσκαμψία EI και διατμητική δυσκαμψία S_v που υπόκειται σε θλιπτική αξονική δύναμη P , η συνολική στροφή w' συνίσταται από τη στροφή ψ λόγω κάμψης μόνο και τη διατμητική παραμόρφωση γ :

$$w' = \psi + \gamma \quad (13)$$

Η διαφορά από τη μέθοδο Engesser είναι ότι η τέμνουσα δύναμη προκύπτει με βάση τη στροφή λόγω κάμψης μόνο ως:

$$Q(x) = P\psi \quad (14)$$

Κατά αντιστοιχία με τη μέθοδο Engesser, η μέθοδος Haringx οδηγεί στο ακόλουθο φορτίο λυγισμού:

$$P_{cr,H} = \frac{-1 + \sqrt{1 + \frac{4P_E}{S_v}}}{\frac{2}{S_v}} \quad (15)$$

όπου P_E είναι το φορτίο λυγισμού Euler του αμφιέριστου μέλους. Επιπλέον, η χρήση του φορτίου λυγισμού με τη μέθοδο Haringx οδηγεί σε μεγαλύτερη τιμή σε σχέση με εκείνη που προκύπτει με τη μέθοδο Engesser. Σύμφωνα με την έρευνα της παρούσας διδακτορικής διατριβής η μέθοδος Engesser είναι καταλληλότερη για την προσομοίωση σύνθετων υποστυλωμάτων με ισοδύναμα μέλη Timoshenko. Αυτό το συμπέρασμα επιβεβαιώνεται και από τους Bazant και Cedolin [2-73], [2-74] και Gjelsvik [2-67]. Επιπρόσθετα, για πολύ κοντά υποστυλώματα που χαρακτηρίζονται από πολύ μεγάλο

φορτίο λυγισμού Euler, το κρίσιμο φορτίο λυγισμού απειρίζεται, οδηγώντας στο συμπέρασμα πως πρακτικά το μέλος δε λυγίζει.

A.2.4. Κανονιστικές διατάξεις EC3

Στον EC3 [2-24] παρέχονται οδηγίες για την ανάλυση και σχεδιασμό αμφιέριστων σύνθετων υποστυλωμάτων υπό αξονική θλίψη και μικρά εγκάρσια φορτία που προκαλούν παραμόρφωση μονής καμπυλότητας. Τα σύνθετα μέλη προτείνεται να προσομοιώνονται ως μέλη Timoshenko με ισοδύναμη καμπτική και διατμητική δυσκαμψία, ενώ η καθολική ατέλεια συνιστάται να έχει το σχήμα της 1^{ης} ιδιομορφής λυγισμού και να λαμβάνεται ίση με $e_o=L/500$ στο μέσο του ύψους (L =ύψος του σύνθετου μέλους). Για σύνθετο μέλος με δύο όμοια πέλματα, η αξονική δύναμη στο κάθε πέλμα είναι ίση με:

$$N_{ch,Ed} = 0.5N_{Ed} + \frac{M_{Ed}h_oA_{ch}}{2I_{eff}} \quad (16)$$

όπου N_{Ed} είναι η αξονική θλιπτική δύναμη που ασκείται στο σύνθετο μέλος, h_o ο μοχλοβραχίονας μεταξύ των Κ.Β. των πελμάτων, A_{ch} το εμβαδό του κάθε πέλματος, I_{eff} η ισοδύναμη ροπή αδρανείας και M_{Ed} η μέγιστη καμπτική ροπή στο μέσο του ύψους, η οποία είναι ίση με:

$$M_{Ed} = \frac{N_{Ed}e_o + M_{Ed}^I}{1 - \frac{N_{Ed}}{N_{cr}} - \frac{N_{Ed}}{S_v}} \quad (17)$$

όπου M_{Ed}^I είναι η ροπή 1^{ης} τάξης στο μέσο του ύψους λόγω εγκάρσιων φορτίων, S_v η διατμητική δυσκαμψία του μέλους, και N_{cr} το ελαστικό κρίσιμο φορτίο λυγισμού του μέλους αν αγνοηθούν οι διατμητικές παραμορφώσεις, όπως προκύπτει από την ακόλουθη σχέση:

$$N_{cr} = \frac{\pi^2 EI_{eff}}{L^2} \quad (18)$$

Η μέγιστη τέμνουσα δύναμη δίνεται από:

$$V_{Ed} = \pi \frac{M_{Ed}}{L} \quad (19)$$

Στις προδιαγραφές του EC3 αναφέρεται πως απαιτείται κατάλληλη τροποποίηση των προαναφερθεισών οδηγιών για άλλες περιπτώσεις συνοριακών συνθηκών.

A.2.4.1. Σύνθετα υποστυλώματα με ράβδους δικτύωσης

Η ροπή αδρανείας μια σύνθετης διατομής αποτελείται από τις ροπές αδρανείας των πελμάτων και τον όρο Steiner:

$$I_{eff} = \frac{A_{ch}h_o^2}{2} + 2I_{ch} \quad (20)$$

όπου I_{ch} είναι η εντός επιπέδου ροπή αδρανείας του κάθε πέλματος. Η διατμητική δυσκαμψία παρέχεται από τις ράβδους δικτύωσης και εξαρτάται από τη διάταξη τους. Στον EC3 περιέχονται κλειστοί τύποι για τον υπολογισμό της για διάφορους τύπους δικτύωσης. Ο σχεδιασμός του σύνθετου υποστυλώματος βασίζεται στον έλεγχο του πλέον δυσμενέστερου φατνώματος, συγκρίνοντας την αξονική δύναμη σχεδιασμού με την τοπική αντοχή καμπτικού λυγισμού $N_{b,Rd}$ με βάση τις καμπύλες λυγισμού:

$$N_{ch,Ed} \leq N_{b,Rd} \quad (21)$$

Ο συντελεστής ισοδύναμου μήκους λυγισμού μπορεί να ληφθεί ίσος με τη μονάδα. Επιπρόσθετα, θα πρέπει να πραγματοποιηθεί έλεγχος της αξονικής δύναμης που καταπονεί την πλέον δυσμενή ράβδο δικτύωσης στα άκρα του αμφιέριστου μέλους σύμφωνα με τη μέγιστη τέμνουσα δύναμη Q .

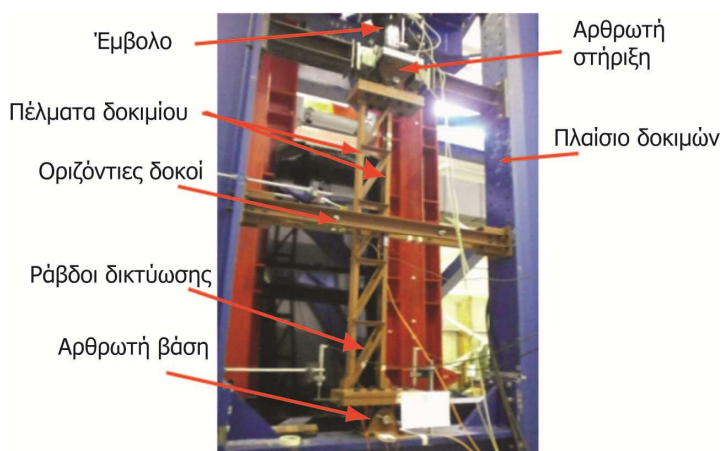
A.2.4.2. Σύνθετα υποστυλώματα με λεπίδες σύνδεσης

Η ανάλυση και ο σχεδιασμός των σύνθετων υποστυλωμάτων με λεπίδες σύνδεσης βρίσκονται σε πλήρη αντιστοιχία με την περίπτωση που το συνδετικό μέσο των πελμάτων είναι οι ράβδοι δικτύωσης. Αναλυτική περιγραφή τους παρουσιάζεται στο πλήρες κείμενο της διδακτορικής διατριβής.

A.3. ΠΕΙΡΑΜΑΤΙΚΗ ΔΙΕΡΕΥΝΗΣΗ

A.3.1. Περιγραφή πειραμάτων

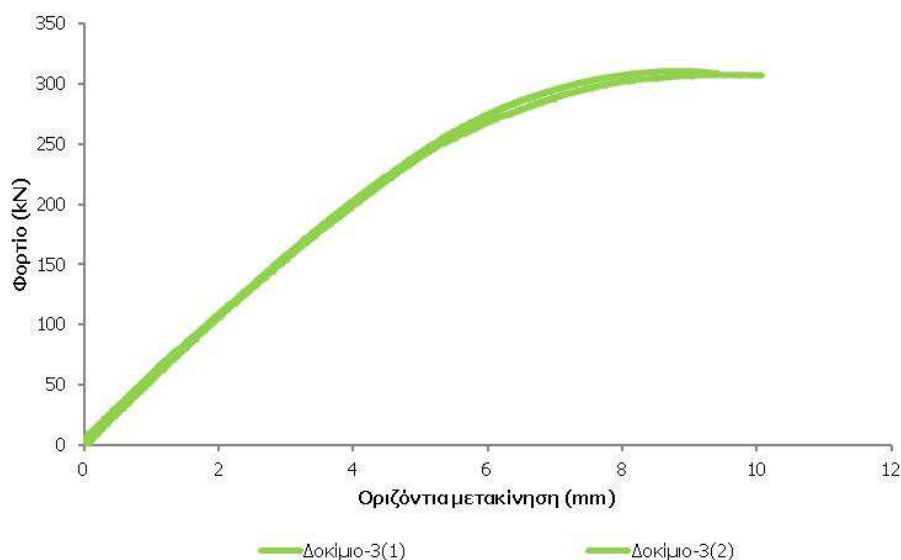
Πραγματοποιήθηκαν πειραματικές δοκιμές σε δέκα αμφιέριστα δοκίμια (πέντε ζεύγη όμοιων δοκιμών για λόγους επαναληψιμότητας) με ρεαλιστικές καθολικές και τοπικές λυγηρότητες, υποκείμενα σε αξονικό θλιπτικό φορτίο και ακραίες συγκεντρωμένες ροπές λόγω εκκεντρότητας του ασκούμενου αξονικού φορτίου. Η Ομάδα 1 αποτέλεσε τη βάση σύγκρισης των πειραματικών δοκιμών, έχοντας διατομές πελμάτων UNP60, μήκος φατνώματος 40cm και ακραίες εκκεντρότητες 10cm προκαλούσες παραμόρφωση μονής καμπυλότητας. Κάθε μια εκ των υπολοίπων ομάδων διέφερε ως προς μια παράμετρο, ώστε η επιρροή αυτής να μπορεί να αξιολογηθεί. Τα δοκίμια της Ομάδας 2 έχουν το μισό μήκος φατνώματος, ενώ η Ομάδα 3 έχει διατομή πελμάτων IPE80. Στα δοκίμια της 4^{ης} Ομάδας ασκούνται ακραίες ροπές προκαλούσες παραμόρφωση διπλής καμπυλότητας, ενώ σε εκείνα της Ομάδας 5 η εκκεντρότητα είναι μισή σε σχέση με εκείνη της Ομάδας 1. Το διάγραμμα τάσεων-παραμορφώσεων του χάλυβα εξήχθη από δοκιμές μονοαξονικού εφελκυσμού σε κατάλληλα διαμορφωμένα δοκίμια. Τα συγκεκριμένα πειράματα διαφέρουν από τα αντίστοιχα βιβλιογραφίας στο ότι χρησιμοποιούνται μεγαλύτερες εκκεντρότητες των φορτίων στα άκρα. Οι μετρήσεις περιελάμβαναν καθολικές μετρήσεις μετακινήσεων και τοπικές μετρήσεις παραμορφώσεων, διευκολύνοντας κατ' αυτόν τον τρόπο την κατανόηση της συμπεριφοράς των δοκιμών. Ένα τυπικό δοκίμιο μετά την τοποθέτηση του στο πλαίσιο δοκιμών φαίνεται στο Σχήμα 4. Διακρίνονται επίσης οι αρθρωτές στηρίξεις στο άνω και κάτω άκρο του δοκιμίου, το έμβολο άσκησης του εξωτερικού φορτίου και οι οριζόντιες δοκοί που απαγορεύουν την εκτός επιπέδου μετακίνηση του δοκιμίου.



Σχήμα 4: Τυπικό δοκίμιο μετά την τοποθέτηση του στο πλαίσιο δοκιμών

A.3.2. Περιγραφή αποτελεσμάτων

Τα αποτελέσματα παρουσιάζονται με χαρακτηριστικές φωτογραφίες για διάφορα επίπεδα φόρτισης, με δρόμους ισορροπίας και με διαγράμματα φορτίου-παραμόρφωσης σε χαρακτηριστικά σημεία. Παρατηρείται πολύ ικανοποιητική συμφωνία ανάμεσα στα αποτελέσματα μεταξύ δοκιμών της ίδιας ομάδας τόσο σε καθολικό όσο και σε τοπικό επίπεδο, κάτι το οποίο αναδεικνύει το γεγονός πως τα πειραματικά αποτελέσματα μπορούν να θεωρηθούν ως αξιόπιστα. Στο Σχήμα 5 φαίνονται ενδεικτικά οι πειραματικοί δρόμοι ισορροπίας των δοκιμών της Ομάδας 3 παρατηρώντας την πολύ καλή συμφωνία μεταξύ τους. Η συμπεριφορά όλων των δοκιμών είναι στην αρχή ελαστική, ενώ για μεγαλύτερα φορτία παρατηρείται σταδιακή μείωση της δυσκαμψίας. Αυτή η μείωση αποδίδεται στην ύπαρξη παραμενουσών τάσεων θερμικής κατεργασίας που οδηγεί σε πρόωρη πλαστικοποίηση των πελμάτων. Το φορτίο που αντιστοιχεί σε μηδενική δυσκαμψία θεωρείται ως το φορτίο αστοχίας, ενώ μετά την επίτευξη του ακολουθεί πτωτικός μεταλυγισμικός κλάδος. Σε όλα τα δοκίμια, τοπική ελαστοπλαστική αστοχία του κρίσιμου φατνώματος οδήγησε σε καθολική αστοχία. Σε αρκετές περιπτώσεις, δοκίμια της ίδιας ομάδας αστόχησαν σε διαφορετικά φατνώματα, τονίζοντας την επιρροή των αρχικών τοπικών ατελειών. Επιπλέον, η ύπαρξη τοπικών εσωτερικών ροπών κατά μήκος των πελμάτων επιβεβαιώνεται από την προς το εσωτερικό των σύνθετων μελών μετακίνηση των κρίσιμων φατνωμάτων σε κάθε ομάδα, ανεξάρτητα από το αν η διατομή των πελμάτων είναι μονής ή διπλής συμμετρίας.



Σχήμα 5: Πειραματικοί δρόμοι ισορροπίας δοκιμών Ομάδας 3

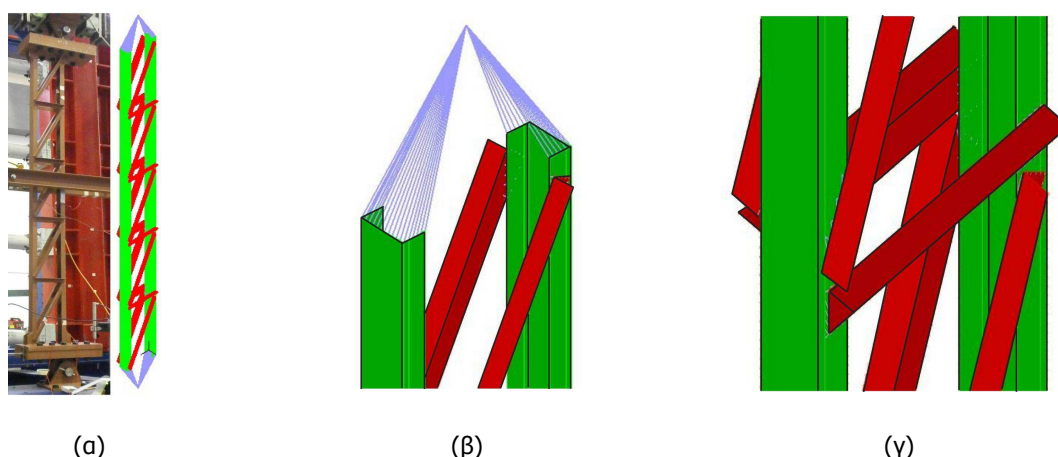
Συγκρίνοντας τις ομάδες μεταξύ τους αξιολογείται η επιρροή των μεταβαλλόμενων παραμέτρων. Από τη σύγκριση των Ομάδων 1 και 2 διαπιστώνεται πως παρά την πύκνωση των ράβδων δικτύωσης δεν υπάρχει σημαντική αύξηση της αντοχής και της δυσκαμψίας. Επιπρόσθετα, δεν εντοπίζεται σημαντική επιρροή των παραμενουσών τάσεων λόγω συγκολλήσεων των ράβδων δικτύωσης στα πέλματα στην περίπτωση της Ομάδας 2. Συγκρίνοντας την Ομάδα 1 με την 3, διαπιστώνεται πως τα πέλματα επηρεάζουν τόσο τη δυσκαμψία όσο και την αντοχή και θα πρέπει να αποτελούν το βασικό κριτήριο σχεδιασμού. Συγκρίνοντας την Ομάδα 1 με την 4, διαπιστώνεται πως η παραμόρφωση διπλής καμπυλότητας οδηγεί σε αύξηση του φορτίου αστοχίας σε σχέση με εκείνο που προκύπτει για παραμόρφωση μονής καμπυλότητας. Τέλος, η μικρότερη εκκεντρότητα στην Ομάδα 5 οδηγεί σε μεγαλύτερη οριακή αντοχή αλλά και σημαντικότερη επιρροή της μη γραμμικότητας γεωμετρίας σε σχέση με τον Ομάδα 1.

A.4. ΑΡΙΘΜΗΤΙΚΗ ΠΡΟΣΟΜΟΙΩΣΗ ΠΕΙΡΑΜΑΤΩΝ

A.4.1. Περιγραφή αριθμητικών προσομοιωμάτων και αναλύσεων

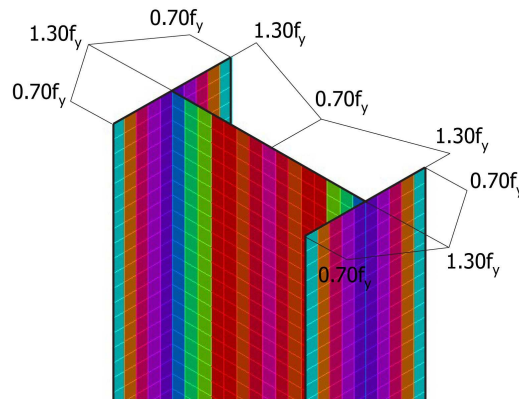
Η πρόοδος που συντελέστηκε τα τελευταία χρόνια στην επιστήμη των υπολογιστών καθιστά πλέον δυνατή την πραγματοποίηση πολύπλοκων αριθμητικών αναλύσεων με βάση προγράμματα πεπερασμένων στοιχείων. Με βάση τα πειράματα, βαθμονομήθηκαν αριθμητικά προσομοιώματα ώστε να είναι δυνατή η χρήση των τελευταίων στη συνέχεια της έρευνας της παρούσας διδακτορικής διατριβής. Για αυτό το σκοπό χρησιμοποιείται το πρόγραμμα πεπερασμένων στοιχείων ADINA [4-3]. Τόσο τα πέλματα όσο και οι ράβδοι δικτύωσης προσομοιώνονται με χρήση επιφανειακών πεπερασμένων στοιχείων, ενώ οι στηρίξεις εισάγονται στα αριθμητικά προσομοιώματα με χρήση άκαμπτων συνδέσμων. Στα άκρα των άκαμπτων συνδέσμων ασκούνται επίσης τα εξωτερικά φορτία ως συγκεντρωμένες δυνάμεις και ροπές. Η αριθμητική προσομοίωση ενός εκ των πειραματικών δοκιμών φαίνεται στο Σχήμα 6. Η δέσμευση της εκτός επιπέδου μετακίνησης επιτυγχάνεται με κατάλληλες στηρίξεις στο μέσο του ύψους των αριθμητικών προσομοιωμάτων.

Η στρατηγική που προτάθηκε από τους Gantes και Fragkopoulos [4-4] για την αριθμητική επαλήθευση των κατασκευών σε οριακή κατάσταση αστοχίας χρησιμοποιήθηκε στην παρούσα διατριβή. Η Γραμμικοποιημένη Ανάλυση Λυγισμού (LBA) αρχικά χρησιμοποιείται για τον υπολογισμό της αντοχής του τέλειου φορέα και των ιδιομορφών λυγισμού. Τα τελικά αποτελέσματα εξάγονται με χρήση Μη Γραμμικής Ανάλυσης Γεωμετρίας και Υλικού Με Αρχικές Ατέλειες (GMNIA) με βάση τη μέθοδο Arc-length [4-6], [4-9] ώστε να προσδιοριστεί και ο μεταλυγισμικός κλάδος.



Σχήμα 6: (α) Τυπικό δοκίμιο και το αντίστοιχο αριθμητικό προσομοίωμα, (β) αριθμητική προσομοίωση της άνω στήριξης και (γ) αριθμητική προσομοίωση των πελμάτων, ράβδων δικτύωσης και συνδέσεων σε ενδιάμεση θέση

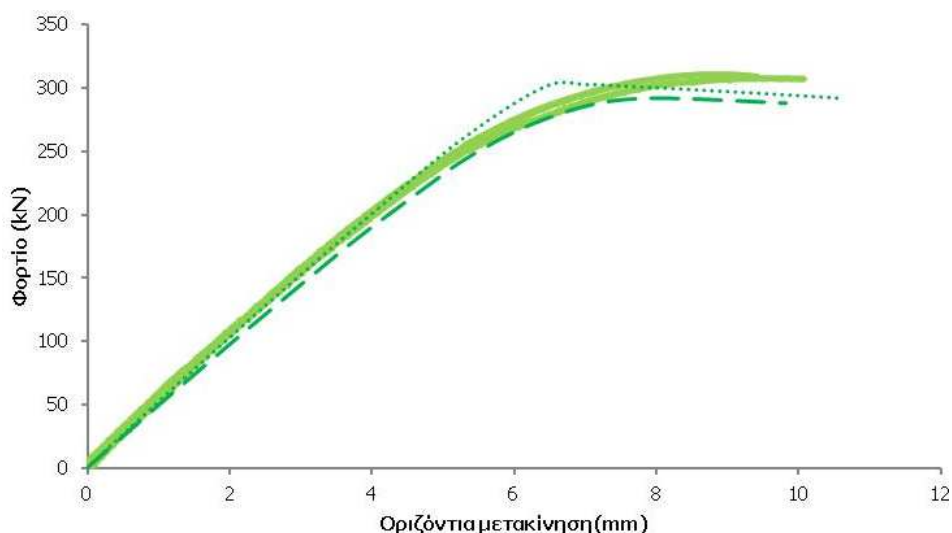
Οι γεωμετρικές καθολικές και τοπικές αρχικές ατέλειες ενσωματώνονται με χρήση των σχημάτων της ιδιομορφής καθολικού και τοπικού λυγισμού, αντίστοιχα. Το μέγεθος των γεωμετρικών ατελειών βασίζεται στις προδιαγραφές του EC3, καθώς δεν πραγματοποιήθηκαν σχετικές μετρήσεις στα πειραματικά δοκίμια. Η επιρροή των παραμενουσών τάσεων λόγω θερμικής κατεργασίας εισάγεται με λεπτομερή διακριτοποίηση της διατομής των πελμάτων σε μικρά τμήματα (Σχήμα 7) και κατάλληλη τροποποίηση του υλικού σε αυτά, ώστε να εφαρμόζονται ορθά η κατανομή και το μέγεθος των παραμενουσών τάσεων, όπως προτείνονται στον ECCS [4-11].



Σχήμα 7: Αριθμητική προσομοίωση παραμενουσών τάσεων σε διατομή IPE80 που υπόκειται σε θλίψη

A.4.2. Περιγραφή αποτελεσμάτων

Με βάση τα αποτελέσματα των αριθμητικών αναλύσεων διαπιστώνεται πως η χρήση GMNIA σε προσομοιώματα με επιφανειακά πεπερασμένα στοιχεία οδηγεί σε πολύ καλή συμφωνία με εκείνα των πειραματικών διερευνήσεων, τόσο σε καθολικό όσο και σε τοπικό επίπεδο. Στην περίπτωση που οι αρχικές γεωμετρικές ατέλειες και παραμένουσες τάσεις αγνοούνται, προβλέπονται μεγαλύτερα φορτία αστοχίας και η πρόωρη πλαστικοποίηση σε υψηλά επίπεδα φόρτισης δεν προσδιορίζεται σε ικανοποιητικό βαθμό. Οι δρόμοι ισορροπίας όπως προκύπτουν από την πειραματική διερεύνηση και τις αριθμητικές αναλύσεις με και χωρίς ενσωμάτωση αρχικών ατελειών (γεωμετρικών ατελειών και παραμενουσών τάσεων θερμικής κατεργασίας) για τα δοκίμια της Ομάδας 3 φαίνονται στο Σχήμα 8. Παρατηρείται η πολύ καλή σύγκριση των πειραματικών και των αριθμητικών αποτελεσμάτων, σε ό,τι αφορά τόσο τη δυσκαμψία όσο και το φορτίο αστοχίας, ιδιαίτερα στην περίπτωση που ενσωματώνονται στα αριθμητικά προσομοιώματα οι αρχικές ατέλειες. Στο Σχήμα 9 διακρίνεται η πειραματική και αριθμητική εικόνα του κρίσιμου φαινομένου δοκιμίου της Ομάδας 5, για φόρτιση που αντιστοιχεί σε σημείο του μεταλυγισμικού κλάδου.



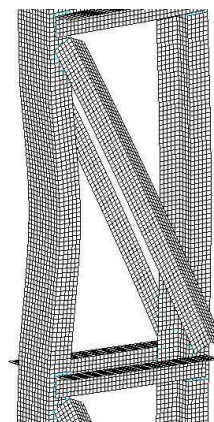
Σχήμα 8: Σύγκριση πειραματικών (συνεχείς γραμμές) και αριθμητικών δρόμων ισορροπίας για τα δοκίμια της Ομάδας 3 για την περίπτωση που λαμβάνονται υπόψη αρχικές ατέλειες (αραιή διακεκομμένη γραμμή) και για την περίπτωση που αγνοούνται οι αρχικές ατέλειες (πυκνή διακεκομμένη γραμμή)

Τέλος, τα αριθμητικά προσομοιώματα με επιφανειακά και με ραβδωτά πεπερασμένα στοιχεία συγκρίνονται μεταξύ τους προκειμένου να αξιολογηθεί η χρήση των τελευταίων. Διαπιστώνεται ότι η

συμπεριφορά των σύνθετων δοκιμών μπορεί να προβλεφθεί πολύ ικανοποιητικά με χρήση ραβδωτών πεπερασμένων στοιχείων, με πολύ μικρότερο υπολογιστικό φόρτο συγκρινόμενο με εκείνον που απαιτείται για χρήση επιφανειακών πεπερασμένων στοιχείων.



(α)



(β)

Σχήμα 9: Σύγκριση πειραματικής και αριθμητικής παραμορφωμένης κατάστασης του κρίσιμου φατνώματος δοκιμίου της Ομάδας 5

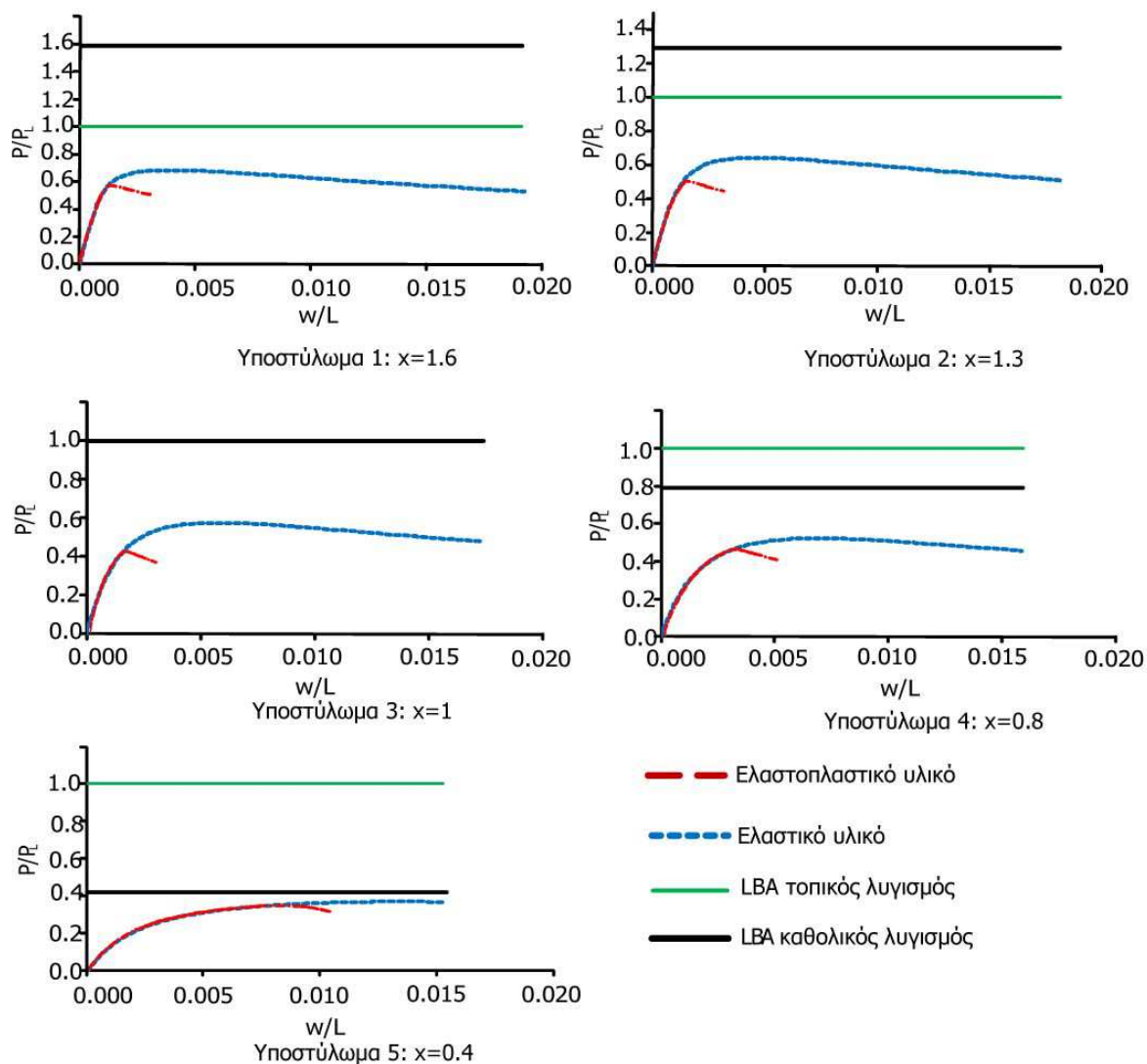
A.5. ΑΡΙΘΜΗΤΙΚΗ ΚΑΙ ΑΝΑΛΥΤΙΚΗ ΔΙΕΡΕΥΝΗΣΗ ΣΥΝΘΕΤΩΝ ΥΠΟΣΤΥΛΩΜΑΤΩΝ

A.5.1. Περιγραφή αριθμητικών αναλύσεων και αποτελέσματα

Μετά την αριθμητική προσομοίωση των πειραμάτων και τη διαπίστωση ότι τα αριθμητικά προσομοιώματα με πεπερασμένα στοιχεία δοκού μπορούν επαρκώς να προβλέψουν τη συμπεριφορά των σύνθετων υποστυλωμάτων με ράβδους δικτύωσης, διερευνάται αριθμητικά η απόκριση ατελών σύνθετων υποστυλωμάτων υπό αξονική θλίψη. Οι πιθανοί τρόποι αστοχίας ενός τέλει σύνθετου υποστυλώματος υπό αξονική θλίψη συνοψίζονται στην υποενότητα A.2.2. Οι αριθμητικές αναλύσεις περιλαμβάνουν τόσο καθολικές όσο και τοπικές ατέλειες, με βάση τα σχήματα των ιδιομορφών καθολικού και τοπικού λυγισμού, αντίστοιχα. Το υλικό θεωρείται είτε ελαστικό είτε διγραμμικό ελαστοπλαστικό χωρίς κράτυνση, ανάλογα με το είδος της ανάλυσης που πραγματοποιείται.

Αρχικά πραγματοποιείται μια εκτεταμένη παραμετρική ανάλυση που περιλαμβάνει 5 σύνθετα υποστυλώματα που διαφέρουν σε ό,τι αφορά το μοχλοβραχίονα μεταξύ των πελμάτων. Κατ' αυτόν τον τρόπο, το καθένα εξ' αυτών αντιστοιχεί σε διαφορετικό λόγο ελαστικού κρίσιμου φορτίου καθολικού λυγισμού προς το αντίστοιχο τοπικού λυγισμού ($x = P_{cr}/P_L$), που αποτελεί βασικό κριτήριο ελέγχου της αλληλεπίδρασης μεταξύ καθολικού και τοπικού λυγισμού. Η πραγματοποίηση Μη Γραμμικών Αναλύσεων Γεωμετρίας με Αρχικές Ατέλειες θεωρώντας ελαστικό υλικό διακρίνεται στην περίπτωση που λαμβάνονται υπόψη αρχικές ατέλειες τόσο καθολικές όσο και τοπικές, και στην περίπτωση που θεωρούνται μόνο καθολικές ατέλειες. Παρατηρείται πως συγκρίνοντας την πρώτη και τη δεύτερη περίπτωση, στην πρώτη υπάρχει μεγαλύτερη μείωση του φορτίου αντοχής και μεγαλύτερες εγκάρσιες καθολικές μετακινήσεις λόγω της επιρροής των τοπικών ατελειών και παραμορφώσεων στην καθολική απόκριση. Επιπλέον, για λόγο x ίσο με τη μονάδα (ταύτιση ελαστικών φορτίων καθολικού και τοπικού λυγισμού), η μείωση της αντοχής είναι μέγιστη. Ακολούθως πραγματοποιούνται Μη Γραμμικές Αναλύσεις Γεωμετρίας και Υλικού με Αρχικές Ατέλειες, τα αποτελέσματα των οποίων συνοψίζονται στο Σχήμα 10. Για λόγο $x=1$, τα φορτία καθολικού λυγισμού, τοπικού λυγισμού και πλήρους διαρροής ταυτίζονται και οδηγούν στη μέγιστη απώλεια αντοχής λόγω

αρχικών ατελειών, όπως διαπιστώθηκε αρχικά από τους Svensson και Kragerup [5-8]. Σε όλες τις περιπτώσεις η αστοχία είναι τοπική ελαστοπλαστική του κρίσιμου φατνώματος.



Σχήμα 10: Δρόμοι ισορροπίας ατελών σύνθετων μελών με ράβδους δικτύωσης με ελαστοπλαστικό υλικό για λόγους $x=1.6$, $x=1.3$, $x=1$, $x=0.8$ και $x=0.4$

A.5.2. Προτεινόμενη μέθοδος

Στον EC3 λαμβάνονται υπόψη οι τρεις μορφές αστοχίας του τέλει φορέα αλλά δεν ενσωματώνεται η επιρροή των τοπικών ατελειών στην καθολική απόκριση του μέλους. Για αυτό το λόγο, στη διατριβή προτείνεται μια τροποποιημένη διαδικασία για την ενσωμάτωση των αρχικών τοπικών ατελειών στην καμπτική δυσκαμψία αμφιέριστου σύνθετου μέλους. Το τελικό βέλος στο μέσο ατελούς σύνθετου μέλους θεωρώντας αρχική καθολική ατέλεια w_0 στο μέσο του είναι:

$$w_T = w_0 \left(\frac{1}{1 - \frac{P}{P_{cr}^*}} \right) \quad (22)$$

όπου P_{cr}^* είναι ένα τροποποιημένο ελαστικό κρίσιμο φορτίο λυγισμού:

$$P_{cr}^* = \frac{1}{\frac{L^2}{\pi^2 EI_{eff}^*} + \frac{1}{S_v}} \quad (23)$$

Στο τροποποιημένο κρίσιμο φορτίο λυγισμού ενσωματώνεται η τροποποιημένη ισοδύναμη καμπτική δυσκαμψία του σύνθετου μέλους EI_{eff}^* :

$$EI_{eff}^* = 0.25h_o^2 (EA_{ch,1}^* + EA_{ch,2}^*) \quad (24)$$

Η αξονική δυστένεια του πλέον θλιβόμενου πέλματος δίνεται από:

$$\frac{1}{EA_{ch,1}^*} = \frac{1}{EA_{ch}} + \frac{\pi^2 \eta^2 (0.5P_L)^2}{2(0.5P_L - P_1)^3} \quad (25)$$

όπου η είναι ο συντελεστής τοπικών ατελειών, θεωρώντας ότι το μέγεθος τους είναι γραμμική συνάρτηση του μήκους του φανώματος a ($z_o = \eta a$) και P_1 είναι η αξονική δύναμη στο πλέον θλιβόμενο πέλμα. Αντίστοιχα υπολογίζεται και η αξονική δυστένεια στο λιγότερο θλιβόμενο πέλμα. Συνεπώς η αξονική δύναμη στο πλέον θλιβόμενο πέλμα δύναται να υπολογιστεί ως:

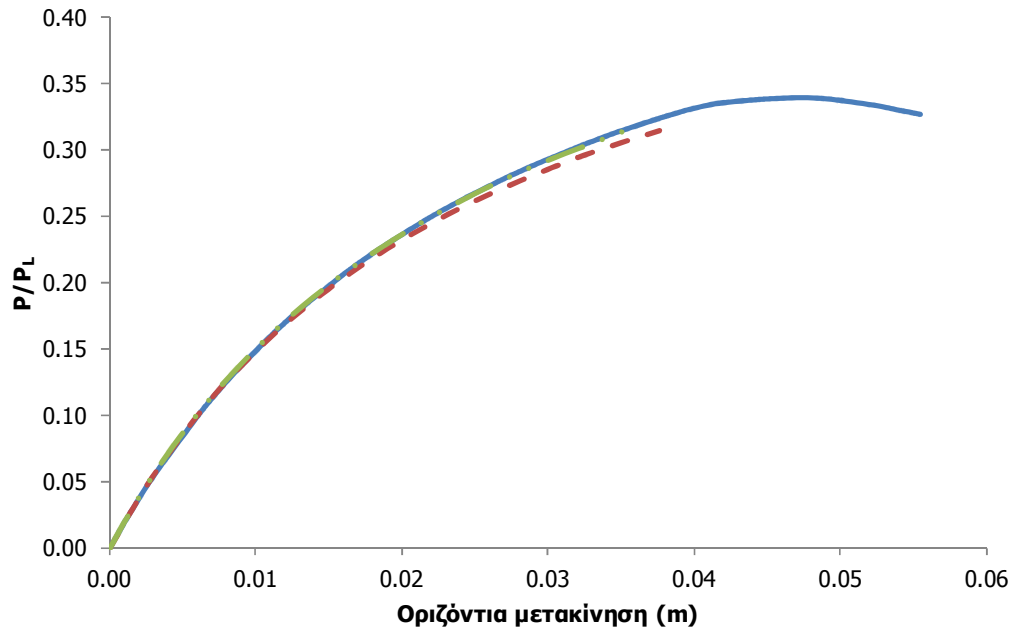
$$0.5P + P \frac{w_o}{1 - \frac{P}{P_{cr}^*}} \frac{1}{h_o} = rN_{ch,Rd} \quad (26)$$

όπου r είναι ένας συντελεστής που κυμαίνεται από 0 έως 1. Για τον υπολογισμό του φορτίου αστοχίας απαιτείται επαναληπτική διαδικασία θεωρώντας διαφορετικές τιμές του r , ως εξής:

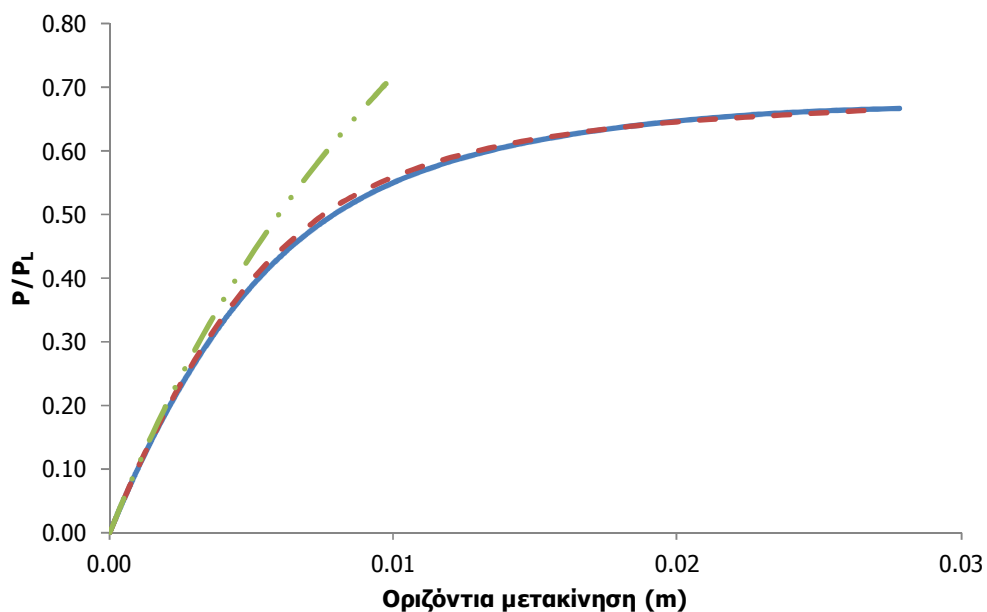
- Υπόθεση $r=1$ και επίλυση της Εξ. (26) ως προς P .
- Επίλυση της Εξ. (26) ως προς P για ελαφρώς μικρότερη τιμή του r .
- Σύγκριση των φορτίων αστοχίας των δύο προηγούμενων βημάτων. Αν το φορτίο του δεύτερου βήματος είναι μικρότερο από εκείνο του πρώτου βήματος, τότε το φορτίο αστοχίας P_u είναι αυτό που υπολογίστηκε στο πρώτο βήμα και η μορφή αστοχίας είναι τοπική ελαστοπλαστική του κρίσιμου φανώματος ($r=1$). Αν όχι, τότε θα πρέπει να πραγματοποιηθεί το επόμενο βήμα.
- Δοκιμή μικρότερων τιμών r μέχρι την εύρεση του μέγιστου φορτίου P . Αυτή η μέγιστη τιμή αντιστοιχεί στο φορτίο αστοχίας P_u . Σε αυτή την περίπτωση, η αστοχία οφείλεται σε καθολική αστάθεια χωρίς τη διαρροή κάποιας διατομής των πελμάτων.

A.5.3. Αριθμητική επαλήθευση προτεινόμενης μεθόδου

Η προτεινόμενη μέθοδος επαληθεύτηκε για ένα μεγάλο πλήθος αριθμητικών προσομοιωμάτων. Τα αποτελέσματα για δύο ενδεικτικές περιπτώσεις παρουσιάζονται στο Σχήμα 11 και στο Σχήμα 12. Η πρώτη περίπτωση αναφέρεται σε σύνθετο υποστυλώμα που αστοχεί λόγω τοπικής ελαστοπλαστικής αστοχίας του κρίσιμου φανώματος. Η διαδικασία του EC3 και η προτεινόμενη μέθοδος δίνουν παραπλήσια αποτελέσματα, τόσο σε ό,τι αφορά τις οριζόντιες μετακινήσεις όσο και σε ό,τι αφορά το φορτίο αστοχίας. Στη δεύτερη περίπτωση, η αστοχία οφείλεται σε ελαστική καθολική αστάθεια και είναι φανερό πως η πρόβλεψη του EC3 είναι κατά της ασφαλείας σε ό,τι αφορά τη δυσκαμψία και την οριακή αντοχή. Αντίθετα, η προτεινόμενη μέθοδος που λαμβάνει υπόψη την επιρροή των τοπικών ατελειών στην καθολική απόκριση του μέλους είναι κοντά στα αριθμητικά αποτελέσματα.



Σχήμα 11: Σύγκριση αριθμητικών (μπλε συνεχής γραμμή), αναλυτικών με βάση τον EC3 (πράσινη αραιή διακεκομμένη γραμμή) και αναλυτικών με βάση την προτεινόμενη μέθοδο (κόκκινη πυκνή διακεκομμένη γραμμή) αποτελεσμάτων για την περίπτωση τοπικής ελαστοπλαστικής αστοχίας



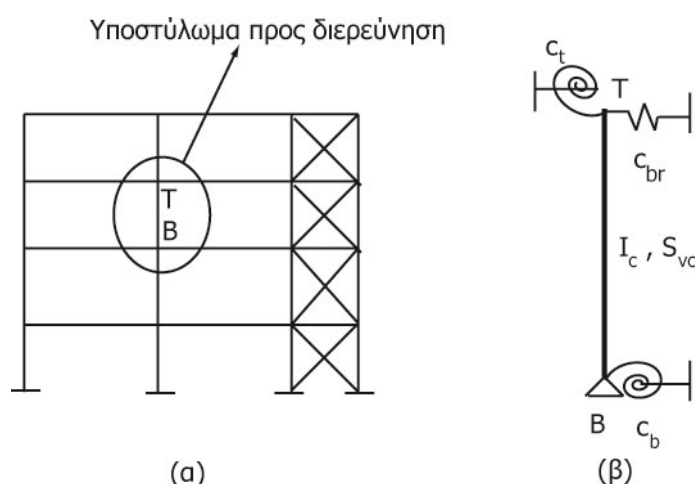
Σχήμα 12: Σύγκριση αριθμητικών (μπλε συνεχής γραμμή), αναλυτικών με βάση τον EC3 (πράσινη αραιή διακεκομμένη γραμμή) και αναλυτικών με βάση την προτεινόμενη μέθοδο (κόκκινη πυκνή διακεκομμένη γραμμή) αποτελεσμάτων για την περίπτωση ελαστικής καθολικής αστοχίας

Ο τύπος αστοχίας που παρατηρείται στην πλειονότητα των περιπτώσεων πρακτικών εφαρμογών οφείλεται σε τοπική ελαστοπλαστική αστοχία του κρίσιμου φατνώματος, κυρίως εξαιτίας των σχετικά μικρών καθολικών και τοπικών ανηγμένων λυγηροτήτων που χρησιμοποιούνται. Συνεπώς, οι προδιαγραφές του EC3 αναμένεται να είναι επαρκείς και η έρευνα στη συνέχεια της διατριβής βασίζεται στη συνηθέστερη αυτή μορφή αστοχίας.

A.6. ΦΟΡΤΙΟ ΛΥΓΙΣΜΟΥ ΠΟΛΥΩΡΟΦΩΝ ΠΛΑΙΣΙΩΝ ΜΕ ΜΕΛΗ TIMOSHENKO

A.6.1. Περιγραφή προτεινόμενης αναλυτικής μεθόδου

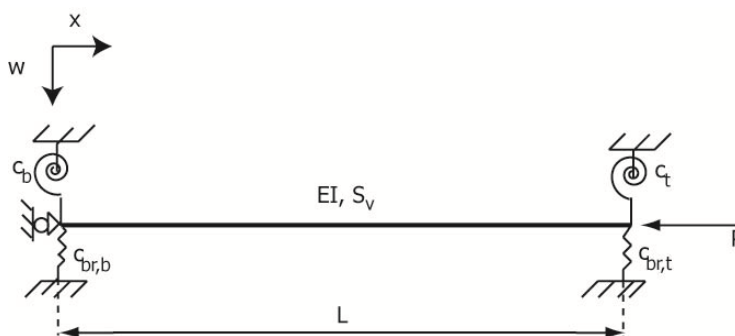
Ο επαρκής υπολογισμός του ελαστικού κρίσιμου φορτίου λυγισμού είναι απαραίτητος για την ορθή αξιολόγηση της αντοχής του τέλειου ελαστικού φορέα που στη συνέχεια χρησιμοποιείται από σύγχρονες κανονιστικές διατάξεις για τον υπολογισμό της ανηγμένης λυγνότητας. Η προτεινόμενη αναλυτική μέθοδος επεκτείνει την αντίστοιχη που προτάθηκε από τους Gantes και Mageirou [6-1], [6-2] για τον υπολογισμό του ελαστικού φορτίου λυγισμού πολυώροφων πλαισίων με άκαμπτες και ημι-άκαμπτες συνδέσεις στην περίπτωση που τα υποστυλώματα και/ή οι δοκοί υπόκεινται σε μη αμελητέες διατμητικές παραμορφώσεις. Η λογική βασίζεται στην απομόνωση του υποστυλώματος προς διερεύνηση με τη χρήση κατάλληλων στροφικών ελατηρίων που προσομοιώνουν τη στροφική δυσκαμψία που προσφέρεται από τα γειτονικά μέλη σε αυτό και κατάλληλου ελατηρίου μετάθεσης που προσομοιώνει τη δυνατότητα σχετικής εγκάρσιας μετακίνησης των δύο άκρων (Σχήμα 13).



Σχήμα 13: (α) Υποστυλώμα TB ως τμήμα πλαισίου και (β) ισοδύναμο προσομοίωμα υποστυλώματος TB

A.6.2. Μη γραμμικές σχέσεις για προσδιορισμό φορτίου λυγισμού

Για αυτό το σκοπό, σε πρώτη φάση θεωρείται το αξονικά θλιβόμενο μέλος Timoshenko με τυχαίες συνοριακές συνθήκες που φαίνεται στο Σχήμα 14 και για το οποίο εξάγεται το μητρώο ευστάθειας. Θέτοντας τη σταθερά του ελατηρίου μετάθεσης $c_{br,b}$ ίση με πολύ μεγάλη τιμή, το μέλος στο Σχήμα 14 μετατρέπεται σε εκείνο που φαίνεται στο Σχήμα 13(β). Τελικά, με χρήση της ορίζουσας ευστάθειας, εξάγονται 3 μη γραμμικές σχέσεις για τον υπολογισμό του φορτίου λυγισμού.



Σχήμα 14: Αξονικά θλιβόμενο μέλος Timoshenko με τυχαίες συνοριακές συνθήκες

Η κάθε μια εξ' αυτών αντιστοιχεί σε μια περίπτωση μεταθετότητας των άκρων του μέλους: μεταθετή, αμετάθετη και μερικώς μεταθετή συμπεριφορά. Για την περίπτωση μερικώς μεταθετής συμπεριφοράς που αποτελεί την πιο γενική περίπτωση προκύπτει:

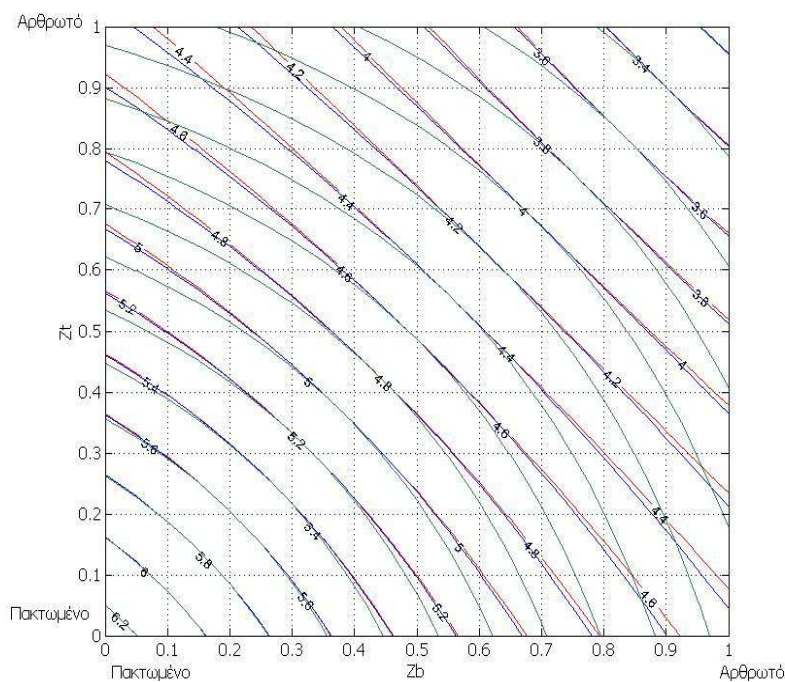
$$\begin{aligned} & -32\overline{c_{br}}(z_t-1)(z_b-1)+4\cos(a_\sigma L)\left[8\overline{c_{br}}(z_t-1)(z_b-1)+(z_t+z_b-2z_tz_b)\left((a_\sigma L)^2\beta_\sigma\overline{c_{br}}-\beta_\sigma^2(a_\sigma L)^4\right)\right]+ \\ & +\sin(a_\sigma L)\left[-16(a_\sigma L)^3\beta_\sigma^2(1-z_t-z_b+z_tz_b)+(a_\sigma L)^5\beta_\sigma^2z_tz_b-(a_\sigma L)^3\beta_\sigma\overline{c_{br}}z_tz_b+ \right. \\ & \left. +4(a_\sigma L)\overline{c_{br}}(4\beta_\sigma-(4\beta_\sigma+1)(z_t+z_b)+(4\beta_\sigma+2)z_tz_b)\right]=0 \end{aligned} \quad (27)$$

$$\text{όπου } c_c = \frac{4EI_c}{L}, \quad z_b = \frac{c_c}{c_c+c_b}, \quad z_t = \frac{c_c}{c_c+c_t}, \quad \overline{c_{br}} = \frac{c_{br}}{EI} L^3 \text{ και } \beta_{cr} = \frac{1}{1+(a_{cr}L)^2 \mu}.$$

Η Εξ. (27) μπορεί να επιλυθεί για τον υπολογισμό του $a_{cr}L = \phi_{cr}$ για διάφορες τιμές του μ που ορίστηκε στην ενότητα Α.2. Το φορτίο λυγισμού μπορεί τότε να υπολογισθεί από την σχέση ($EI = EI_c$):

$$P_{cr} = \frac{\phi_{cr}^2 EI_c}{L^2 + \frac{\phi_{cr}^2 EI_c}{S_v}} \quad (28)$$

Η Εξ. (27) αποτελεί την πιο γενική περίπτωση και συγκλίνει στις αντίστοιχες σχέσεις αμετάθετης και μεταθετής συμπεριφοράς με χρήση κατάλληλης τιμής μετακινησιακού ελατηρίου. Για την περίπτωση της αμετάθετης συμπεριφοράς και για τιμές του μ ίσες με 0.001 (κόκκινες γραμμές), 0.01 (μπλε γραμμές) και 0.1 (πράσινες γραμμές), η γραφική απεικόνιση των λύσεων φαίνεται στο Σχήμα 15. Παρατηρείται πως για ίσες τιμές στρωφικών ελατηρίων στα άκρα και αμετάθετη συμπεριφορά του μέλους, οι λύσεις της Εξ. (27) είναι ανεξάρτητες του μ και ταυτίζονται.



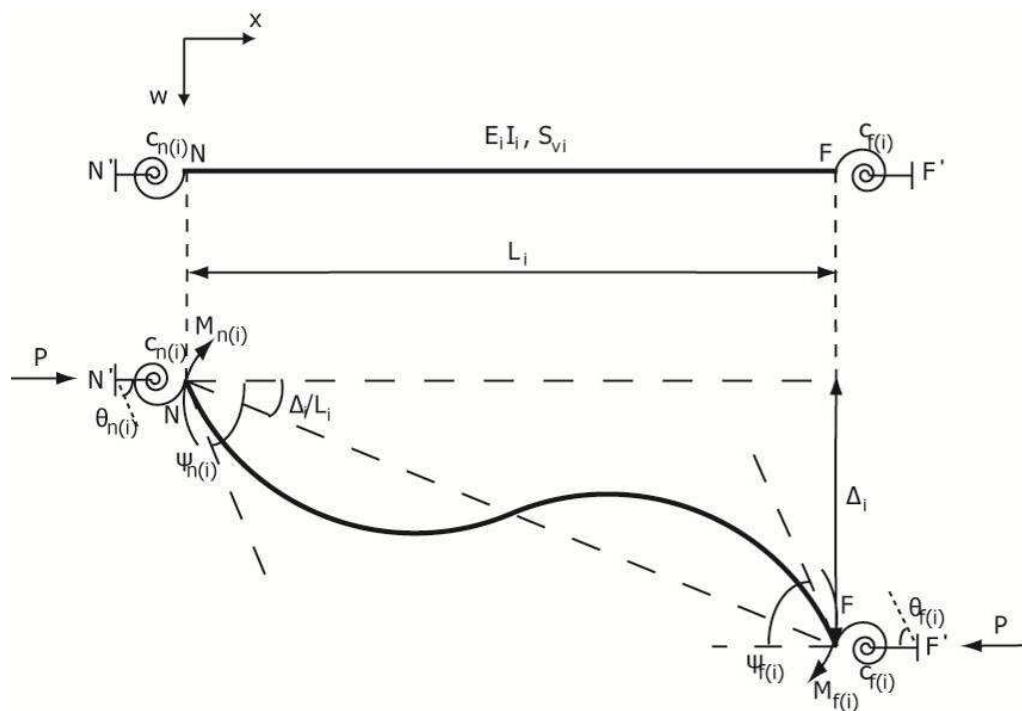
Σχήμα 15: Γραφική απεικόνιση των λύσεων της Εξ. (27) για αμετάθετη συμπεριφορά και τιμές του μ ίσες με 0.001 (κόκκινες γραμμές), 0.01 (μπλε γραμμές) και 0.1 (πράσινες γραμμές)

A.6.3. Εξισώσεις γωνίας-στροφής για μέλη Timoshenko με ημι-άκαμπτες συνδέσεις

Οι προτεινόμενες εξισώσεις γωνίας-στροφής για μέλη Timoshenko με ημι-άκαμπτες συνδέσεις εξάγονται με βάση τη μέθοδο Engesser για την ενσωμάτωση των διατμητικών παραμορφώσεων. Οι υπολογισμοί βασίζονται στην παραμορφωμένη κατάσταση του μέλους όπως φαίνεται στο Σχήμα 16 και θεωρώντας τριγωνομετρικές συναρτήσεις για το συνολικό βέλος w και τη στροφή λόγω κάμψης ψ . Οι ροπές στο κάθε άκρο είναι ίσες με:

$$M_{n(i)} = \frac{E_i I_i}{L_i} A_{11(i)} \left(\theta_{n(i)} - \frac{\Delta_i}{L_i} \right) + \frac{E_i I_i}{L_i} A_{12(i)} \left(\theta_{f(i)} - \frac{\Delta_i}{L_i} \right) \quad (29)$$

$$M_{f(i)} = \frac{E_i I_i}{L_i} A_{21(i)} \left(\theta_{n(i)} - \frac{\Delta_i}{L_i} \right) + \frac{E_i I_i}{L_i} A_{22(i)} \left(\theta_{f(i)} - \frac{\Delta_i}{L_i} \right) \quad (30)$$



Σχήμα 16: Απαραμόρφωτη και παραμορφωμένη κατάσταση μέλους Timoshenko με ημι-άκαμπτες συνδέσεις στα άκρα υπό την επιρροή θλιπτικού αξονικού φορτίου και συγκεντρωμένων ροπών στα άκρα

Ο Πίνακας 1 περιέχει τους συντελεστές δυσκαμψίας περιλαμβάνοντας παραμέτρους που επεξηγήθηκαν προηγουμένως και θα πρέπει να τροποποιηθούν κατάλληλα, ώστε να εφαρμοστούν στο μέλος στο Σχήμα 16. Η επιρροή των ημι-άκαμπτων συνδέσεων υπεισέρχεται στους συντελεστές κατανομής $z_{n(i)}$ και $z_{f(i)}$. Θέτοντας τους συντελεστές κατανομής στα δύο άκρα ίσους με το 0 προκύπτουν οι συντελεστές δυσκαμψίας για μέλος με άκαμπτες συνδέσεις στα άκρα και τα σχετικά αποτελέσματα περιέχονται στον Πίνακα 2. Και στις δύο προαναφερθείσες περιπτώσεις ισχύει ότι $\phi_i = \alpha_i L_i$.

Οι συντελεστές δυσκαμψίας για την περίπτωση χωρίς αξονική δύναμη μπορούν να προσδιορισθούν αν ακολουθηθεί η ίδια αναλυτική διαδικασία αλλά χρησιμοποιηθούν πολυωνυμικές συναρτήσεις για το συνολικό βέλος w και τη στροφή λόγω κάμψης ψ . Προσεγγιστικός υπολογισμός των συντελεστών αυτών μπορεί να επιτευχθεί αν τεθεί σχετικά μικρή τιμή της αξονικής δύναμης P στους συντελεστές δυσκαμψίας που αναφέρονται στην παρούσα υποενότητα.

Πίνακας 1: Συντελεστές δυσκαμψίας για μέλος Timoshenko με ημι-άκαμπτες συνδέσεις υπό αξονική θλίψη

$A_{11(i)} = \frac{(1-z_{n(i)})(1-z_{f(i)}) \left(1 - \frac{\beta_i \varphi_i}{\tan \varphi_i} \right) + \frac{1}{4} (1-z_{n(i)}) z_{f(i)} \beta_i \varphi_i^2}{(1-z_{n(i)})(1-z_{f(i)}) \left(\frac{2 \tan(0.5 \varphi_i)}{\varphi_i} - \beta_i \right) + \frac{1}{4} ((1-z_{n(i)}) z_{f(i)} + (1-z_{f(i)}) z_{n(i)}) \left(1 - \frac{\beta_i \varphi_i}{\tan \varphi_i} \right) + \frac{1}{16} z_{n(i)} z_{f(i)} \beta_i \varphi_i^2}$
$A_{12(i)} = A_{21(i)} = \frac{(1-z_{n(i)})(1-z_{f(i)}) \left(\frac{\beta_i \varphi_i}{\sin \varphi_i} - 1 \right)}{(1-z_{n(i)})(1-z_{f(i)}) \left(\frac{2 \tan(0.5 \varphi_i)}{\varphi_i} - \beta_i \right) + \frac{1}{4} ((1-z_{n(i)}) z_{f(i)} + (1-z_{f(i)}) z_{n(i)}) \left(1 - \frac{\beta_i \varphi_i}{\tan \varphi_i} \right) + \frac{1}{16} z_{n(i)} z_{f(i)} \beta_i \varphi_i^2}$
$A_{22(i)} = \frac{(1-z_{n(i)})(1-z_{f(i)}) \left(1 - \frac{\beta_i \varphi_i}{\tan \varphi_i} \right) + \frac{1}{4} (1-z_{f(i)}) z_{n(i)} \beta_i \varphi_i^2}{(1-z_{n(i)})(1-z_{f(i)}) \left(\frac{2 \tan(0.5 \varphi_i)}{\varphi_i} - \beta_i \right) + \frac{1}{4} ((1-z_{n(i)}) z_{f(i)} + (1-z_{f(i)}) z_{n(i)}) \left(1 - \frac{\beta_i \varphi_i}{\tan \varphi_i} \right) + \frac{1}{16} z_{n(i)} z_{f(i)} \beta_i \varphi_i^2}$

Πίνακας 2: Συντελεστές δυσκαμψίας για μέλος Timoshenko με άκαμπτες συνδέσεις υπό αξονική θλίψη

$S_{11(i)} = S_{22(i)} = \frac{\varphi_i \sin \varphi_i - \beta_i \varphi_i^2 \cos \varphi_i}{-2 \cos \varphi_i - \beta_i \varphi_i \sin \varphi_i + 2}$
$S_{12(i)} = S_{21(i)} = \frac{\beta_i \varphi_i^2 - \varphi_i \sin \varphi_i}{-2 \cos \varphi_i - \beta_i \varphi_i \sin \varphi_i + 2}$

A.6.4. Στροφικές δυσκαμψίες προς αντικατάσταση μελών

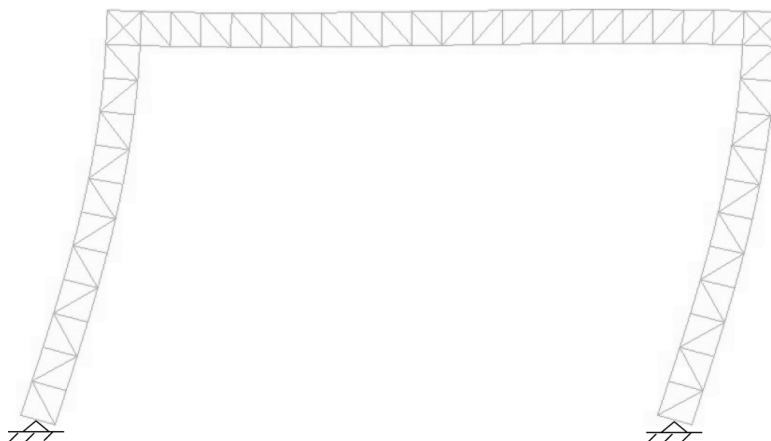
Όπως επεξηγήθηκε προηγουμένως, τα μέλη που συγκλίνουν στο άνω και κάτω άκρο του υπό εξέταση υποστυλώματος, προσφέρουν στροφική δυσκαμψία στα άκρα του και συνεπώς μπορούν να αντικατασταθούν με ισοδύναμο στροφικά ελατήρια. Η τιμή του ισοδύναμου στροφικού ελατηρίου εξαρτάται από το αν το μέλος υπόκειται σε αξονική θλιπτική δύναμη ή όχι και από τη συνοριακή συνθήκη στο απέναντι άκρο του. Για τη γενική περίπτωση που το μέλος υπόκειται σε θλιπτική αξονική δύναμη P_i και έχει άκαμπτο κόμβο στο πλησίον άκρο και τυχαίες συνοριακές συνθήκες στο απέναντι άκρο, το ισοδύναμο στροφικό ελατήριο μπορεί να προσδιοριστεί ως

$$c_i = \frac{E_i I_i}{L_i} \left[S_{11(i)} - \frac{S_{12(i)}^2}{c_{f(i)}^{\#} + S_{11(i)}} - \frac{(S_{11(i)} + S_{12(i)}) \left(\frac{S_{12(i)}}{c_{f(i)}^{\#} + S_{11(i)}} - 1 \right)^2}{2 - \frac{S_{11(i)} + S_{12(i)}}{c_{f(i)}^{\#} + S_{11(i)}} + \frac{c_{br(i)}^{\#} L_i^2 - \frac{P_i L_i^2}{E_i I_i}}{S_{11(i)} + S_{12(i)}}} \right] \quad (31)$$

όπου η τιμή $c^{\#}$ προκύπτει τόσο για το μεταφορικό όσο και για το στροφικό ελατήριο ως $c^{\#} = \frac{c L_i}{E_i I_i}$.

A.6.5. Αριθμητική επαλήθευση

Η χρήση της προτεινόμενης αναλυτικής μεθόδου για τον υπολογισμό του ελαστικού κρίσιμου φορτίου λυγισμού πολυώροφου πλαισίου, που αποτελείται από μέλη Timoshenko, επαληθεύτηκε αριθμητικά σε μεγάλο πλήθος φορέων. Στην παρούσα υποενότητα παρουσιάζονται τα αποτελέσματα για μεταθετό μονώροφο βιομηχανικό πλαίσιο που αποτελείται από σύνθετα υποστυλώματα με ράβδους δικτύωσης και από μια δικτυωτή δοκό. Η ιδιομορφή καθολικού λυγισμού του πλαισίου, όπως προκύπτει αριθμητικά, φαίνεται στο Σχήμα 17 και αντιστοιχεί σε φορτίο λυγισμού 33740kN. Με χρήση της προτεινόμενης μεθόδου προβλέπεται ελαστικό κρίσιμο φορτίο καθολικού λυγισμού ίσο με 33179kN, που βρίσκεται σε ικανοποιητική συμφωνία με το αντίστοιχο αριθμητικό αποτέλεσμα. Η πρόβλεψη του EC3 για το φορτίο λυγισμού είναι ίση με 40270kN, αναδεικνύοντας τη σημασία των διατμητικών παραμορφώσεων στη συγκεκριμένη περίπτωση.



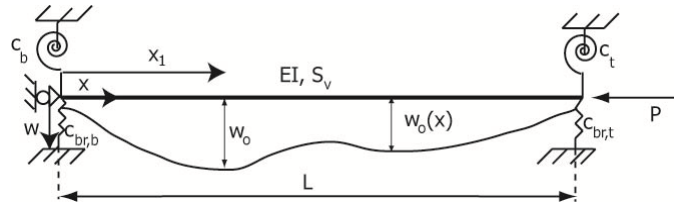
Σχήμα 17: Ιδιομορφή καθολικού λυγισμού μεταθετού μονώροφου βιομηχανικού πλαισίου

A.7. ΑΝΑΛΥΣΗ 2^{ΗΣ} ΤΑΞΗΣ ΜΕΛΩΝ TIMOSHENKO

Στην παρούσα ενότητα παρουσιάζονται κλειστές αναλυτικές σχέσεις για τον προσδιορισμό των μετακινήσεων και των εντατικών μεγεθών κατά μήκος ατελών μελών Timoshenko υπό αξονική θλίψη και συνήθεις εγκάρσιες φορτίσεις. Η ενσωμάτωση των διατμητικών παραμορφώσεων γίνεται σύμφωνα με τη μέθοδο Engesser. Η κάθε μια εκ των περιπτώσεων φόρτισης εξετάζεται αναλυτικά στις ακόλουθες υποενότητες. Στην περίπτωση της αρχικής ατέλειας γίνεται χρήση του μεγεθυντικού συντελεστή που προτάθηκε από τον Young [7-5], ενώ στις εγκάρσιες φορτίσεις γίνεται χρήση των συντελεστών δυσκαμψίας για μέλη Timoshenko με άκαμπτες συνδέσεις στα άκρα που περιέχει ο Πίνακας 2.

A.7.1. Αρχική ατέλεια

Θεωρώντας ένα ατελές μέλος Timoshenko με τυχαίες συννοριακές συνθήκες και λαμβάνοντας υπόψη μόνο την 1^η ιδιομορφή λυγισμού ως σχήμα αρχικής ατέλειας, όπως φαίνεται στο Σχήμα 18, είναι δυνατή η πραγματοποίηση προσεγγιστικής ανάλυσης 2^{ης} τάξης. Τα αποτελέσματα βασίζονται στη χρήση του μεγεθυντικού συντελεστή που χρησιμοποιείται ευρέως από σύγχρονες κανονιστικές διατάξεις. Ο Πίνακας 3 περιέχει τις απαραίτητες αναλυτικές σχέσεις, στις οποίες w_0 είναι η μέγιστη τιμή της αρχικής ατέλειας, P είναι το αξονικό θλιπτικό φορτίο, P_{cr} το ελαστικό κρίσιμο φορτίο λυγισμού του μέλους που συνδέεται άμεσα με το a_{cr} σύμφωνα με την Εξ. (28) και x_1 είναι η θέση κατά μήκος του μέλους όπου η ατέλεια λαμβάνει τη μέγιστη τιμή της (με βάση το σχήμα της 1^{ης} ιδιομορφής λυγισμού).



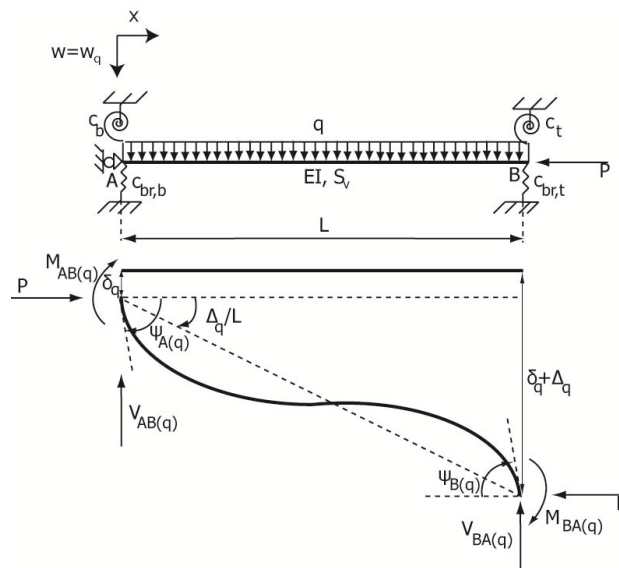
Σχήμα 18: Ατελές μέλος Timoshenko με τυχαίες συνοριακές συνθήκες υπό αξονική θλίψη

Πίνακας 3: Αναλυτικές σχέσεις για την περίπτωση αρχικής ατέλειας σύμφωνα με το σχήμα 1^{ης} ιδιομορφής

Συνολικό βέλος	$w_T(x) = \left(\frac{1}{1 - \frac{P}{P_{cr}}} \right) \frac{w_0 (f_1 \sin(a_{cr}x) + \cos(a_{cr}x) + f_2x + f_3)}{f_1 \sin(a_{cr}x_1) + \cos(a_{cr}x_1) + f_2x_1 + f_3}, \text{ όπου}$ $f_1 = \frac{\frac{a_{cr}^4 \beta_{cr}^2}{c_b^*} \left(\frac{1}{c_{br,b}^*} + \frac{1}{c_{br,t}^*} \right) - \frac{a_{cr}^2 \beta_{cr} L}{c_b^*} + \cos(a_{cr}L) - 1}{a_{cr} \beta_{cr} L \sin(a_{cr}L) - a_{cr}^3 \beta_{cr}^2 \left(\frac{1}{c_{br,b}^*} + \frac{1}{c_{br,t}^*} \right)}, \quad f_2 = -a_{cr} \beta_{cr} \left(\frac{a_{cr}}{c_b^*} + f_1 \right), \quad f_3 = -\frac{a_{cr}^2 \beta_{cr} f_2}{c_{br,b}^*} - 1, \quad c_i^* = \frac{c_i}{EI}$ <p>Το x_1 βρίσκεται μεγιστοποιώντας τη συνάρτηση: $\max(f_1 \sin(a_{cr}x_1) + \cos(a_{cr}x_1) + f_2x_1 + f_3)$</p>
Ροπή κάμψης	$M_{imp}(x) = \frac{Pw_0}{1 - \frac{P}{P_{cr}}} f, \text{ όπου } f = \frac{f_1 \sin(a_{cr}x) + \cos(a_{cr}x)}{f_1 \sin(a_{cr}x_1) + \cos(a_{cr}x_1) + f_2x_1 + f_3}$
Τέμνουσα δύναμη κάθετη στον παραμορφωμένο άξονα	$Q_{imp}(x) = \frac{a_{cr} Pw_0}{1 - \frac{P}{P_{cr}}} f', \text{ όπου } f' = \frac{f_1 \cos(a_{cr}x) - \sin(a_{cr}x)}{f_1 \sin(a_{cr}x_1) + \cos(a_{cr}x_1) + f_2x_1 + f_3}$

A.7.2. Εγκάρσιο ομοιόμορφα κατανεμημένο φορτίο

Το ίδιο μέλος Timoshenko με τυχαίες συνοριακές συνθήκες υπό αξονικό θλιπτικό φορτίο και εγκάρσιο ομοιόμορφα κατανεμημένο φορτίο q φαίνεται στο Σχήμα 19. Θεωρώντας θετικές τις ροπές και στροφές που είναι σύμφωνες με την ωρολογιακή φορά είναι δυνατή η πραγματοποίηση ανάλυσης 2^{ης} τάξης και ο Πίνακας 4 περιέχει τις κλειστές αναλυτικές λύσεις του προβλήματος.



Σχήμα 19: Μέλος Timoshenko υπό αξονική θλίψη και εγκάρσιο ομοιόμορφα κατανεμημένο φορτίο

Πίνακας 4: Αναλυτικές σχέσεις για την περίπτωση εγκάρσιου ομοιόμορφου κατανεμημένου φορτίου

Ροπή κάμψης στο άκρο A	$M_{AB(q)} = \frac{EI}{L} S_{11} \left(\psi_{A(q)} - \frac{\Delta_q}{L} \right) + \frac{EI}{L} S_{12} \left(\psi_{B(q)} - \frac{\Delta_q}{L} \right) - M_F$ $, \text{όπου } M_F = \frac{q}{a^2} \left[1 - \frac{La}{2\beta} \cot \left(\frac{aL}{2} \right) \right] + \frac{EI}{S_v} q$
Ροπή κάμψης στο άκρο B	$M_{BA(q)} = \frac{EI}{L} S_{12} \left(\psi_{A(q)} - \frac{\Delta_q}{L} \right) + \frac{EI}{L} S_{11} \left(\psi_{B(q)} - \frac{\Delta_q}{L} \right) + M_F$
Τέμνουσα δύναμη στο άκρο A	$V_{AB(q)} = 0.5qL - \frac{M_{AB(q)} + M_{BA(q)} + P\Delta_q}{L}$
Τέμνουσα δύναμη στο άκρο B	$V_{BA(q)} = 0.5qL + \frac{M_{AB(q)} + M_{BA(q)} + P\Delta_q}{L}$
Βέλος στο άκρο A	$\delta_q = \frac{qL - c_{br,t} \Delta_q}{c_{br,b} + c_{br,t}}$
Διαφορικό βέλος μεταξύ άκρων A και B	$\frac{\Delta_q}{L} = \frac{\rho_1 (-c_b \psi_{A(q)} - c_t \psi_{B(q)}) + \chi_q}{\omega}, \text{ όπου } \rho_1 = 1 + c_{br,t}/c_{br,b}, \rho_2 = 1 - c_{br,t}/c_{br,b}, \chi_q = 0.5q\rho_2 L^2 \text{ και}$ $\omega = L^2 \left(c_{br,t} - \rho_1 \frac{P}{L} \right)$
Στροφή λόγω κάμψης στο άκρο A	$\psi_{A(q)} = \frac{(\omega S_{12} + S\rho_1 c_t) \left(\frac{-\omega M_F L}{EI} + S\chi_q \right) - (\omega S_{11} + \omega c_t^\# + S\rho_1 c_t) \left(\frac{\omega M_F L}{EI} + S\chi_q \right)}{(\omega S_{12} + S\rho_1 c_b)(\omega S_{12} + S\rho_1 c_t) - (\omega S_{11} + \omega c_t^\# + S\rho_1 c_t)(\omega S_{11} + \omega c_b^\# + S\rho_1 c_b)}, \text{ όπου}$ $S = S_{11} + S_{12} \text{ και } c_i^\# = \frac{c_i L}{EI}$
Στροφή λόγω κάμψης στο άκρο B	$\psi_{B(q)} = \frac{\chi_q S + \frac{\omega M_F L}{EI} - (\omega(S_{11} + c_b^\#) + S\rho_1 c_b) \psi_{A(q)}}{\omega S_{12} + S\rho_1 c_t}$
Ροπή κάμψης	$M_q(x) = -EI\psi_q'(x) = M_{AB(q)} + V_{AB(q)}x + P(w_q(x) - \delta_q) - 0.5qx^2$
Τέμνουσα δύναμη κάθετη στον παραμορφωμένο άξονα	$Q_q(x) = -EI\psi_q''(x) = V_{AB(q)} + Pw_q'(x) - qx$
Συνολικό βέλος	$w_q(x) = \frac{\frac{1}{P} \left(- \left(M_{AB(q)} + q \left(\frac{1}{a^2} + \frac{EI}{S_v} \right) \right) \cos aL + M_{AB(q)} + V_{AB(q)}L + q \left(\frac{1}{a^2} + \frac{EI}{S_v} - 0.5L^2 \right) \right) + \Delta_q}{\sin aL} \sin ax +$ $+ \frac{1}{P} \left(M_{AB(q)} + q \left(\frac{1}{a^2} + \frac{EI}{S_v} \right) \right) \cos ax + \frac{1}{P} \left(-M_{AB(q)} - V_{AB(q)}x + P\delta_q + q \left(-\frac{1}{a^2} - \frac{EI}{S_v} + 0.5x^2 \right) \right)$
Συνολική στροφή	$w_q'(x) = a \frac{\frac{1}{P} \left(- \left(M_{AB(q)} + q \left(\frac{1}{a^2} + \frac{EI}{S_v} \right) \right) \cos aL + M_{AB(q)} + V_{AB(q)}L + q \left(\frac{1}{a^2} + \frac{EI}{S_v} - 0.5L^2 \right) \right) + \Delta_q}{\sin aL} \cos ax -$ $- \frac{a}{P} \left(M_{AB(q)} + q \left(\frac{1}{a^2} + \frac{EI}{S_v} \right) \right) \sin ax + \frac{1}{P} (-V_{AB(q)} + qx)$

A.7.3. Συγκεντρωμένες ροπές στα άκρα

Χρησιμοποιείται το ίδιο μέλος Timoshenko με τυχαίες συνοριακές συνθήκες (Σχήμα 19) υπό αξονικό θλιπτικό φορτίο και συγκεντρωμένες ροπές στα άκρα M_1 και M_2 , αντίστοιχα, θεωρώντας θετικές τις ροπές και στροφές που είναι σύμφωνες με την ωρολογιακή φορά (οι δείκτες q γίνονται M). Ο Πίνακας 5 περιέχει τις κλειστές αναλυτικές λύσεις του προβλήματος.

Πίνακας 5: Αναλυτικές σχέσεις για την περίπτωση συγκεντρωμένων ροπών στα άκρα

Ροπή κάμψης στο άκρο A	$M_{AB(M)} = \frac{EI}{L} S_{11} \left(\psi_{A(M)} - \frac{\Delta_M}{L} \right) + \frac{EI}{L} S_{12} \left(\psi_{B(M)} - \frac{\Delta_M}{L} \right)$
Ροπή κάμψης στο άκρο B	$M_{BA(M)} = \frac{EI}{L} S_{12} \left(\psi_{A(M)} - \frac{\Delta_M}{L} \right) + \frac{EI}{L} S_{11} \left(\psi_{B(M)} - \frac{\Delta_M}{L} \right)$
Τέμνουσα δύναμη στο άκρο A	$V_{AB(M)} = -\frac{M_{AB(M)} + M_{BA(M)} + P\Delta_M}{L}$
Τέμνουσα δύναμη στο άκρο B	$V_{BA(M)} = \frac{M_{AB(M)} + M_{BA(M)} + P\Delta_M}{L}$
Βέλος στο άκρο A	$\delta_M = -\frac{c_{br,t} \Delta_M}{c_{br,b} + c_{br,t}}$
Διαφορικό βέλος μεταξύ άκρων A και B	$\frac{\Delta_M}{L} = \frac{\rho_1 \left(-c_b \psi_{A(M)} - c_t \psi_{B(M)} \right) + \chi_M}{\omega}, \text{ όπου } \chi_M = (M_1 + M_2) \rho_1$
Στροφή λόγω κάμψης στο άκρο A	$\psi_{A(M)} = \frac{(\omega S_{12} + S \rho_1 c_t) \left(\frac{\omega M_2 L}{EI} + S \chi_M \right) + (\omega S_{11} + \omega c_t^\# + S \rho_1 c_t) \left(\frac{-\omega M_1 L}{EI} - S \chi_M \right)}{(\omega S_{12} + S \rho_1 c_b)(\omega S_{12} + S \rho_1 c_t) - (\omega S_{11} + \omega c_t^\# + S \rho_1 c_t)(\omega S_{11} + \omega c_b^\# + S \rho_1 c_b)}$
Στροφή λόγω κάμψης στο άκρο B	$\psi_{B(M)} = \frac{\chi_M S + \frac{\omega M_1 L}{EI} - (\omega(S_{11} + c_b^\#) + S \rho_1 c_b) \psi_{A(M)}}{\omega S_{12} + S \rho_1 c_t}$
Ροπή κάμψης	$M_M(x) = M_{AB(M)} + V_{AB(M)} x + P(w_M(x) - \delta_M)$
Τέμνουσα δύναμη κάθετη στον παραμορφωμένο άξονα	$Q_M(x) = V_{AB(M)} + P w_M'(x)$
Συνολικό βέλος	$w_M(x) = \frac{M_{AB(M)}}{P} \frac{(1 - \cos \alpha L)}{\sin \alpha L} + \frac{V_{AB(M)} L}{P} \sin \alpha x + \frac{M_{AB(M)}}{P} \cos \alpha x + \frac{1}{P} \left(-M_{AB(M)} - V_{AB(M)} x + P \delta_M \right)$
Συνολική στροφή	$w_M'(x) = \alpha \frac{M_{AB(M)}}{P} \frac{(1 - \cos \alpha L)}{\sin \alpha L} + \frac{V_{AB(M)} L}{P} \cos \alpha x - \alpha \frac{M_{AB(M)}}{P} \sin \alpha x - \frac{V_{AB(M)}}{P}$

A.7.4. Εγκάρσιες συγκεντρωμένες δυνάμεις στα άκρα

Χρησιμοποιείται το ίδιο μέλος Timoshenko με τυχαίες συνοριακές συνθήκες (Σχήμα 19) υπό αξονικό θλιπτικό φορτίο και συγκεντρωμένα εγκάρσια φορτία στα άκρα H_1 και H_2 , αντίστοιχα, θεωρούμενα ως θετικά αν έχουν τη φορά του θετικού άξονα των εγκάρσιων βελών. Επίσης θεωρούνται θετικές οι ροπές και στροφές που είναι σύμφωνες με την ωρολογιακή φορά (οι δείκτες q γίνονται H). Ο Πίνακας 6 περιέχει τις κλειστές αναλυτικές λύσεις του προβλήματος.

Πίνακας 6: Αναλυτικές σχέσεις για την περίπτωση συγκεντρωμένων εγκάρσιων δυνάμεων στα άκρα

Ροπή κάμψης στο άκρο A	$M_{AB(H)} = \frac{EI}{L} S_{11} \left(\psi_{A(H)} - \frac{\Delta_H}{L} \right) + \frac{EI}{L} S_{12} \left(\psi_{B(H)} - \frac{\Delta_H}{L} \right)$
Ροπή κάμψης στο άκρο B	$M_{BA(H)} = \frac{EI}{L} S_{12} \left(\psi_{A(H)} - \frac{\Delta_H}{L} \right) + \frac{EI}{L} S_{11} \left(\psi_{B(H)} - \frac{\Delta_H}{L} \right)$
Τέμνουσα δύναμη στο άκρο A	$V_{AB(H)} = - \frac{M_{AB(H)} + M_{BA(H)} + P\Delta_H}{L}$
Τέμνουσα δύναμη στο άκρο B	$V_{BA(H)} = \frac{M_{AB(H)} + M_{BA(H)} + P\Delta_H}{L}$
Βέλος στο άκρο A	$\delta_H = \frac{H_1 + H_2 - c_{br,t} \Delta_H}{c_{br,b} + c_{br,t}}$
Διαφορικό βέλος μεταξύ άκρων A και B	$\frac{\Delta_H}{L} = \frac{\rho_1 \left(-c_b \psi_{A(H)} - c_t \psi_{B(H)} \right) + \chi_H}{\omega}, \text{ όπου } \chi_H = L(H_2 - H_1 c_{br,t} / c_{br,b})$
Στροφή λόγω κάμψης στο άκρο A	$\psi_{A(H)} = \frac{(\omega S_{12} - \omega S_{11} - \omega c_t^{\#})(S\chi_H)}{(\omega S_{12} + S\rho_1 c_b)(\omega S_{12} + S\rho_1 c_t) - (\omega S_{11} + \omega c_t^{\#} + S\rho_1 c_t)(\omega S_{11} + \omega c_b^{\#} + S\rho_1 c_b)}$
Στροφή λόγω κάμψης στο άκρο B	$\psi_{B(H)} = \frac{\chi_H S - (\omega(S_{11} + c_b^{\#}) + S\rho_1 c_b) \psi_{A(H)}}{\omega S_{12} + S\rho_1 c_t}$
Ροπή κάμψης	$M_H(x) = M_{AB(H)} + V_{AB(H)}x + P(w_H(x) - \delta_H)$
Τέμνουσα δύναμη κάθετη στον παραμορφωμένο άξονα	$Q_H(x) = V_{AB(H)} + Pw_H'(x)$
Συνολικό βέλος	$w_H(x) = \frac{M_{AB(H)}}{P} \frac{(1 - \cos \alpha L)}{\sin \alpha L} + \frac{V_{AB(H)}L}{P} \sin \alpha x + \frac{M_{AB(H)}}{P} \cos \alpha x + \frac{1}{P} \left(-M_{AB(H)} - V_{AB(H)}x + P\delta_H \right)$
Συνολική στροφή	$w_H'(x) = a \frac{M_{AB(H)}}{P} \frac{(1 - \cos \alpha L)}{\sin \alpha L} + \frac{V_{AB(H)}L}{P} \cos \alpha x + \frac{M_{AB(H)}}{P} \sin \alpha x - \frac{V_{AB(H)}}{P}$

A.7.5. Επαλληλία φορτίσεων

Οι ξεχωριστά εξεταζόμενες περιπτώσεις αρχικής ατέλειας, εγκάρσιου ομοιόμορφα κατανεμημένου φορτίου, συγκεντρωμένων ροπών στα άκρα και συγκεντρωμένων εγκάρσιων φορτίων στα άκρα δύνανται να επαλληλιστούν στην περίπτωση ανάλυσης 2^{ης} τάξης για σταθερό αξονικό φορτίο P. Συνεπώς προκύπτει ότι η συνδυασμένη επιρροή τους στην καμπτική ροπή, τέμνουσα δύναμη κάθετη στον παραμορφωμένο άξονα και εγκάρσιο βέλος υπολογίζεται αντίστοιχα ως:

$$M(x) = M_{imp}(x) + M_q(x) + M_M(x) + M_H(x) \quad (32)$$

$$Q(x) = Q_{imp}(x) + Q_q(x) + Q_M(x) + Q_H(x) \quad (33)$$

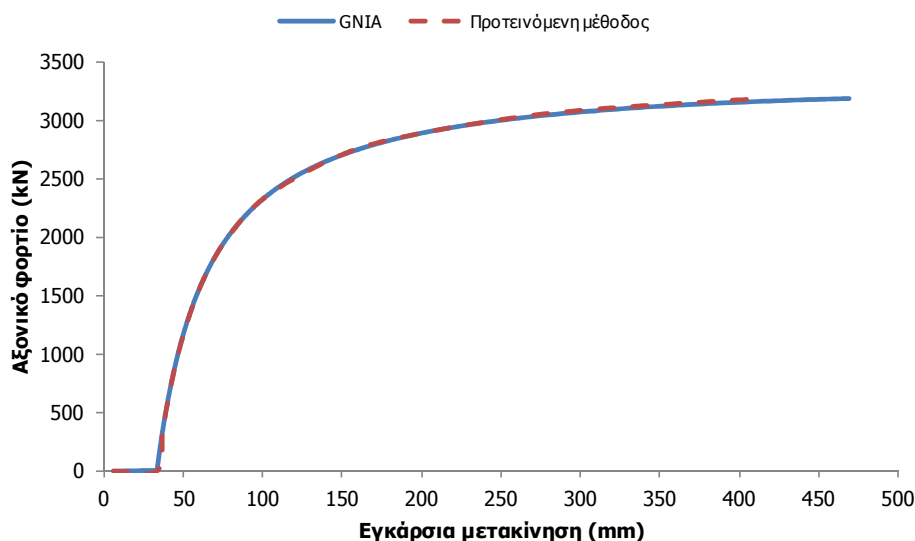
$$w(x) = w_T(x) + w_q(x) + w_M(x) + w_H(x) \quad (34)$$

A.7.6. Αριθμητική επαλήθευση

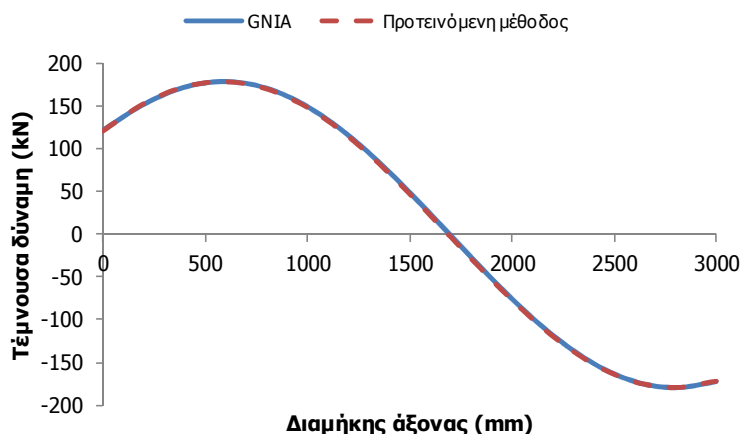
Οι προαναφερθείσες κλειστές αναλυτικές σχέσεις ελέγχθηκαν έναντι Μη Γραμμικών Αναλύσεων Γεωμετρίας με Αρχική Ατέλεια GNIA σε πλήθος μελών Timoshenko με αμετάθετα, μερικώς μεταθετά και μεταθετά άκρα υπό την επιρροή τυχαίων φορτίσεων.

Στην παρούσα υποενότητα παρουσιάζονται τα αποτελέσματα που εξήχθησαν για την περίπτωση μερικώς μεταθετού μέλους Timoshenko με μήκος $L=3\text{m}$, και διατομή από χάλυβα (μέτρο ελαστικότητας $E=210\text{GPa}$ και λόγο Poisson $\nu=0.3$) με διατμητική δυσκαμψία $S_v=16154\text{kN}$ και ροπή αδρανείας περί τον άξονα κάμψης ίση με $I=8.33\text{e-}6\text{m}^4$. Στα άκρα οι συνοριακές συνθήκες ορίζονται με βάση ελατήρια σταθερών $c_b=2000\text{kNm}$, $c_{br,b}\rightarrow\infty$, $c_t\rightarrow\infty$ και $c_{br,t}=1000\text{kN/m}$. Το μέλος Timoshenko έχει συντελεστή $\mu=0.012$ και θα μπορούσε να αντιστοιχεί σε ένα σύνθετο υποστύλωμα με ράβδους δικτύωσης. Το ελαστικό κρίσιμο φορτίο λυγισμού υπολογίζεται αριθμητικά ίσο με $P_{cr}=3438\text{kN}$, ενώ αναλυτικά με βάση την Εξ. (27) ίσο με $P_{cr}=3454\text{kN}$. Η αρχική ατέλεια θεωρείται ίση με $w_0=L/500=0.006\text{m}$ και βασίζεται στην 1^η ιδιομορφή λυγισμού του μέλους. Οι εγκάρσιες φορτίσεις περιλαμβάνουν εγκάρσιο ομοιόμορφο κατανεμημένο φορτίο q , συγκεντρωμένες ροπές στα άκρα M_1 και M_2 και συγκεντρωμένα φορτία στα άκρα H_1 και H_2 που είναι ίσα με 10kN/m , 50kNm , -100kNm , 50kN και 10kN , αντίστοιχα.

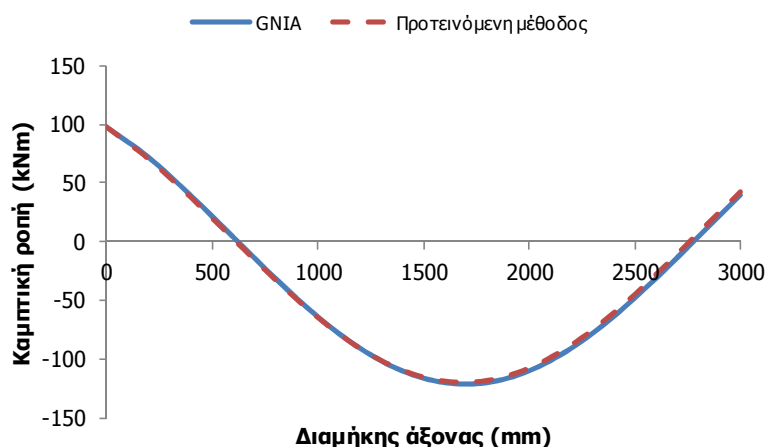
Ο δρόμος ισορροπίας με βάση την εγκάρσια μετακίνηση σε τυχαίο σημείο παρουσιάζεται στο Σχήμα 20 και παρατηρείται πολύ καλή σύγκριση μεταξύ του αριθμητικού αποτελέσματος και της προτεινόμενης αναλυτικής μεθόδου. Η προσεγγιστική αναλυτική μέθοδος χάνει την ακρίβεια της για μεγάλο αξονικό φορτίο πλησίον του ελαστικού κρίσιμου φορτίου λυγισμού. Για αξονικό φορτίο ίσο με $0.8P_{cr}$ τα διαγράμματα τεμνουσών δυνάμεων καθέτων στον παραμορφωμένο άξονα και καμπτικών ροπών φαίνονται στο Σχήμα 21 και στο Σχήμα 22, αντίστοιχα.



Σχήμα 20: Δρόμος ισορροπίας για το εξεταζόμενο μέλος Timoshenko με τυχαίες συνοριακές συνθήκες



Σχήμα 21: Διάγραμμα τεμνουσών δυνάμεων καθέτων στον παραμορφωμένο άξονα κατά μήκος του εξεταζόμενου μέλους για αξονική δύναμη ίση με $0.8P_{cr}$



Σχήμα 22: Διάγραμμα καμπτικών ροπών κατά μήκος του εξεταζόμενου μέλους για αξονική δύναμη ίση με $0.8P_{cr}$

A.8. ΣΥΜΠΕΡΙΦΟΡΑ ΣΥΝΘΕΤΩΝ ΜΕΛΩΝ ΥΠΟ ΑΞΟΝΙΚΗ ΚΑΙ ΕΓΚΑΡΣΙΑ ΦΟΡΤΙΣΗ

A.8.1. Φορτίο αστοχίας σύνθετου μέλους

Η διαδικασία υπολογισμού της συμπεριφοράς σύνθετων μελών με ράβδους δικτύωσης βασίζεται στην παραδοχή ότι μπορούν να προσομοιωθούν ως μέλη Timoshenko με ισοδύναμη καμπτική και διατμητική δυσκαμψία. Η προτεινόμενη αναλυτική διαδικασία που παρουσιάστηκε στην ενότητα A.7 και βασίζεται σε υπολογιστικά εργαλεία και ποιοτικά συμπεράσματα που παρουσιάστηκαν στις ενότητες A.3-A.6, δύναται να χρησιμοποιηθεί στον υπολογισμό των εντατικών μεγεθών και μετακινήσεων κατά μήκος ενός ατελούς μέλους Timoshenko που υπόκειται σε διάφορες εγκάρσιες φορτίσεις και σε αξονική θλίψη. Προκειμένου να προσδιοριστεί το φορτίο αστοχίας σύνθετου μέλους με ράβδους δικτύωσης θα πρέπει αυτά τα εντατικά μεγέθη να χρησιμοποιηθούν για τον υπολογισμό των εντατικών μεγεθών των συστατικών μερών (πέλματα και ράβδοι δικτύωσης) του σύνθετου μέλους. Εφόσον τα συστατικά μέρη των σύνθετων μελών με ράβδους δικτύωσης καταπονούνται κυρίως από αξονικές δυνάμεις, ο τερματισμός της ελαστικής ανάλυσης 2^{ης} τάξης επιτυγχάνεται με χρήση μιας κατάλληλης σχέσης αλληλεπίδρασης που συνδέεται αποκλειστικά με αυτές. Η σχέση αλληλεπίδρασης βασίζεται στο συμπέρασμα ότι η συνηθέστερη μορφή αστοχίας στην πράξη είναι τοπική ελαστοπλαστική αστοχία του κρίσιμου φατνώματος (συνήθως υπό θλίψη) που οδηγεί σε καθολική κατάρρευση του μέλους.

Θέτοντας την αξονική δύναμη στο πλέον θλιβόμενο πέλμα ίση με την τοπική αντοχή σε λυγισμό του φαινώματος προκύπτει:

$$\frac{P}{2} + \frac{|M_{\max}|}{h_0} = N_L \quad (35)$$

όπου P είναι το αξονικό φορτίο επί του σύνθετου μέλους και M_{\max} είναι η μέγιστη καμπτική ροπή κατά μήκος του ισοδύναμου μέλους Timoshenko (προκύπτει μεγιστοποιώντας την Εξ. (32)). Η Εξ. (35) τροποποιείται στην περίπτωση που η μέγιστη καμπτική ροπή εμφανίζεται στα άκρα του μέλους (στο $x=0$ ή L) και συγκλίνει διαγώνια ράβδος στο άκρο του κρίσιμου φαινώματος, λαμβάνοντας κατ' αυτόν τον τρόπο υπόψη το γεγονός ότι ένα τμήμα της αξονικής δύναμης παραλαμβάνεται από τη διαγώνια ράβδο (είτε σε θλίψη είτε σε εφελκυσμό ανάλογα με τη φορά της τέμνουσας δύναμης). Η τέμνουσα δύναμη Q υπολογίζεται με χρήση της Εξ. (33). Για την περίπτωση δικτύωσης X και X με ορθοστάτες η Εξ. (35) γίνεται:

$$\frac{P}{2} + \frac{|M_{\max}(0;L)|}{h_0} \pm \frac{|Q(0;L)| \tan \phi_l}{2} = N_L \quad (36)$$

Στις περιπτώσεις δικτύωσης N , V και Z , η Εξ. (35) γίνεται:

$$\frac{P}{2} + \frac{|M_{\max}(0;L)|}{h_0} \pm |Q(0;L)| \tan \phi_l = N_L \quad (37)$$

Οι άγνωστες παράμετροι στις σχέσεις αλληλεπίδρασης είναι τόσο το φορτίο αστοχίας P όσο και η θέση μεγιστοποίησης της καμπτικής ροπής κατά μήκος του εξεταζόμενου μέλους και συνεπώς απαιτείται μια επαναληπτική διαδικασία για την εύρεση του φορτίου αστοχίας. Στην τοπική αντοχή N_L λαμβάνεται υπόψη η επιρροή των τοπικών ατελειών και της διαρροής. Το κρίσιμο φαινόμενο μπορεί να θεωρηθεί απλοποιητικά ως αμφιέριστο, κάτι το οποίο δεν είναι πάντα ακριβές αλλά οδηγεί σε συντηρητικές προβλέψεις αντοχής. Η τοπική αντοχή μπορεί να βασίζεται είτε στην 1^η διαρροή της διατομής είτε να λαμβάνει υπόψη και την επέκταση της διαρροής για την επίτευξη ακριβέστερων αποτελεσμάτων.

A.8.2. Αριθμητικός έλεγχος

Η προτεινόμενη μέθοδος για ατελή σύνθετα μέλη υπό αξονική και εγκάρσια φόρτιση ελέγχεται στην παρούσα υποενότητα με χρήση αποτελεσμάτων πεπερασμένων στοιχείων που εξήχθησαν με το πρόγραμμα ADINA. Οι αριθμητικές αναλύσεις χρησιμοποιούνται για τον υπολογισμό του φορτίου αστοχίας και ενσωματώνουν μη γραμμικότητα τόσο γεωμετρίας όσο και υλικού. Οι καθολικές και τοπικές ατέλειες βασίζονται στα αντίστοιχα σχήματα ιδιομορφών λυγισμού. Το μέγεθος της καθολικής ατέλειας λαμβάνεται ίσο με $L/500$, ενώ το μέγεθος της τοπικής ατέλειας βασίζεται είτε στην προδιαγραφή του EC3 είτε λαμβάνεται ίσο με $a/500$. Σε κάθε περίπτωση η τοπική ατέλεια έχει τέτοια φορά ώστε να οδηγεί στο ελάχιστο φορτίο αντοχής. Η ποιότητα του χάλυβα θεωρείται ίση με S355 και το διάγραμμα τάσεων-παραμορφώσεων διγραμμικό χωρίς κράτυνση. Η αστοχία των ράβδων δικτύωσης αποκλείεται από τις εξεταζόμενες περιπτώσεις, καθώς θεωρείται πως έχουν σχεδιαστεί με ικανοποιητική υπεραντοχή (ως είθισται στην πράξη). Οι μέθοδοι που χρησιμοποιούνται και ελέγχονται είναι:

- GMNIA: Μη Γραμμική Ανάλυση Γεωμετρίας και Υλικού με Αρχικές Ατέλειες. Το φορτίο αστοχίας που προκύπτει θεωρείται το μέτρο σύγκρισης, καθώς βασίζεται στη βέλτιστη μέθοδο από άποψη ακρίβειας αποτελεσμάτων.
- Προτεινόμενη Μέθοδος-A (Πρ. Μέθοδος-A): Το φορτίο αστοχίας προκύπτει με χρήση των αναλυτικών σχέσεων που προτάθηκαν στις υποενότητες A.6 και A.7 και της κατάλληλης σχέσης

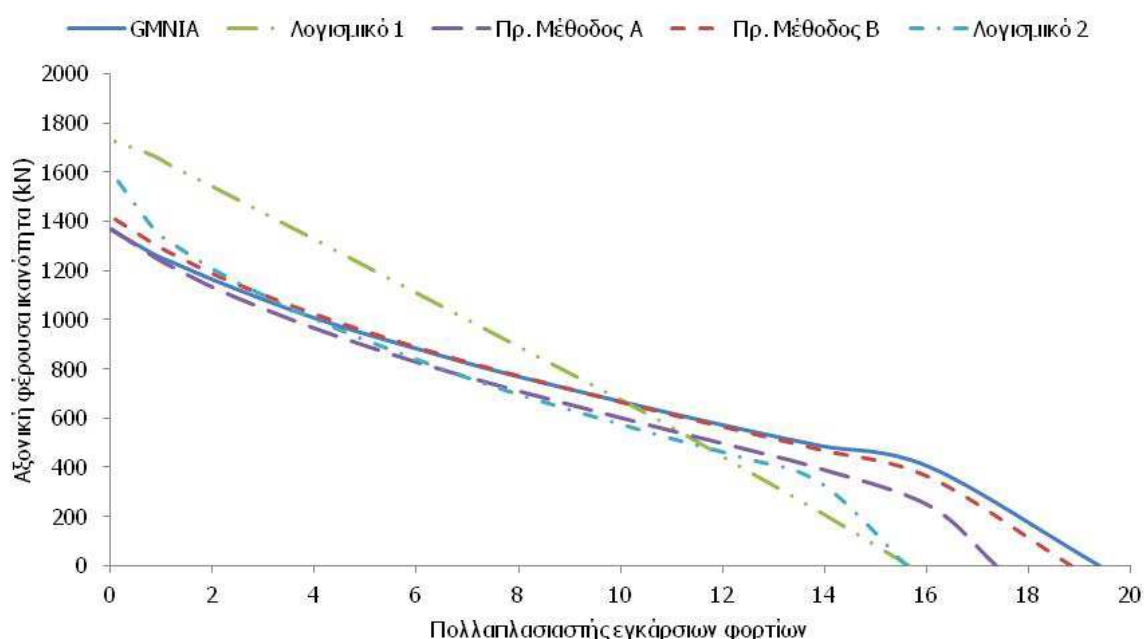
αλληλεπίδρασης εκ των Εξ. (35)-(37). Η τοπική αντοχή βασίζεται στην 1^η διαρροή του κρίσιμου φαινώματος.

- Προτεινόμενη Μέθοδος-B (Πρ. Μέθοδος-B): Το φορτίο αστοχίας προκύπτει με χρήση των αναλυτικών σχέσεων που προτάθηκαν στις υποενότητες A.6 και A.7 και της κατάλληλης σχέσης αλληλεπίδρασης εκ των Εξ. (35)-(37). Στην τοπική αντοχή λαμβάνεται υπόψη η επέκταση της διαρροής στη διατομή του κρίσιμου φαινώματος.
- Λογισμικό 1 και Λογισμικό 2: Χρήση εμπορικού λογισμικού για την εκτέλεση ανάλυσης 1^{ης} τάξης (Λογισμικό 1) και μη γραμμικής ανάλυσης γεωμετρίας με φαινόμενα P-Δ (Λογισμικό 2) όπου δε λαμβάνονται υπόψη αρχικές καθολικές ατέλειες. Φορτίο αστοχίας θεωρείται εκείνο που οδηγεί σε οριακή ικανοποίηση της κατωτέρω ανίσωσης:

$$\frac{N}{\chi_z A_{ch} f_y} + k_{zz} \frac{M_z}{M_{z,pl,Rd}} \leq 1 \quad (38)$$

όπου N και M_z είναι η αξονική δύναμη και η καμπτική ροπή στην εξεταζόμενη διατομή του πέλματος, χ_z ο μειωτικός συντελεστής για καμπτικό λυγισμό περί τον ασθενή άξονα (λαμβάνοντας έμμεσα την επιρροή αρχικών τοπικών ατελειών), k_{zz} ο συντελεστής αλληλεπίδρασης όπως ορίζεται από τη Μέθοδο 2 του EC3 και $M_{z,pl,Rd}$ η πλαστική ροπή αντοχής της διατομής για κάμψη περί τον ασθενή άξονα.

Ενδεικτικά για την περίπτωση σύνθετου υποστυλώματος με ράβδους δικτύωσης και τυχαίες συνοριακές συνθήκες που υπόκειται σε αξονική και σε διάφορες εγκάρσιες φορτίσεις, το διάγραμμα αλληλεπίδρασης φαίνεται στο Σχήμα 23. Παρατηρείται πολύ καλή σύγκριση μεταξύ GMNIA και των προτεινόμενων μεθόδων, ειδικά της Προτεινόμενης Μεθόδου-B που λαμβάνει υπόψη την επέκταση της διαρροής στη διατομή. Η χρήση εμπορικού λογισμικού και ανάλυσης με φαινόμενα P-Δ (Λογισμικό 2) οδηγεί σε ικανοποιητικά αποτελέσματα, εκτός της περίπτωσης συμπεριφοράς υποστυλώματος που είναι κατά της ασφαλείας. Η χρήση γραμμικής ελαστικής ανάλυσης με εμπορικό λογισμικό (Λογισμικό 1) οδηγεί σε αποτελέσματα τόσο κατά όσο και υπέρ της ασφαλείας και θα πρέπει να αποφεύγεται.



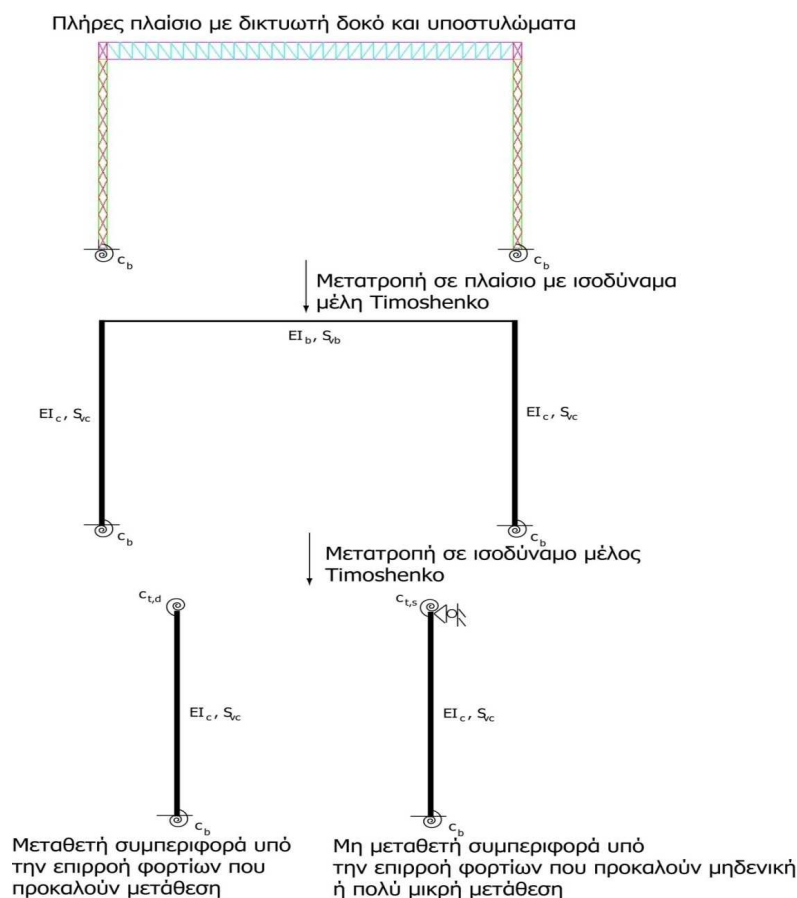
Σχήμα 23: Διάγραμμα αλληλεπίδρασης για σύνθετο μέλος με τυχαίες συνοριακές συνθήκες και συνύπαρξη αξονικής δύναμης και εγκάρσιων φορτίσεων

Η χρήση της προτεινόμενης διαδικασίας για τον υπολογισμό των μετακινήσεων και των φορτίων αστοχίας ελέγχθηκε σε μεγάλο πλήθος αριθμητικών προσομοιωμάτων σύνθετων υποστυλωμάτων με ράβδους δικτύωσης με χρήση διάφορων εγκάρσιων φορτίσεων. Εξήχθη το συμπέρασμα ότι ευρίσκεται σε πολύ καλή συμφωνία με αριθμητικά αποτελέσματα που προκύπτουν από πλήρως μη γραμμικές αναλύσεις, σε ό,τι αφορά τόσο τη δυσκαμψία όσο και το φορτίο αντοχής. Επιπρόσθετα, αποδείχτηκε ότι η προτεινόμενη μέθοδος είναι επαρκέστερη συγκρινόμενη με τη συνήθη μελετητική πρακτική που βασίζεται σε γραμμική ελαστική ανάλυση και η οποία μπορεί να είναι κατά της ασφαλείας σε περιπτώσεις λυγρών φορέων που υπόκεινται σε σημαντική μη γραμμικότητα γεωμετρίας.

A.9. ΣΥΜΠΕΡΙΦΟΡΑ ΒΙΟΜΗΧΑΝΙΚΩΝ ΠΛΑΙΣΙΩΝ

A.9.1. Εφαρμογή προτεινόμενης μεθόδου σε βιομηχανικά πλαίσια

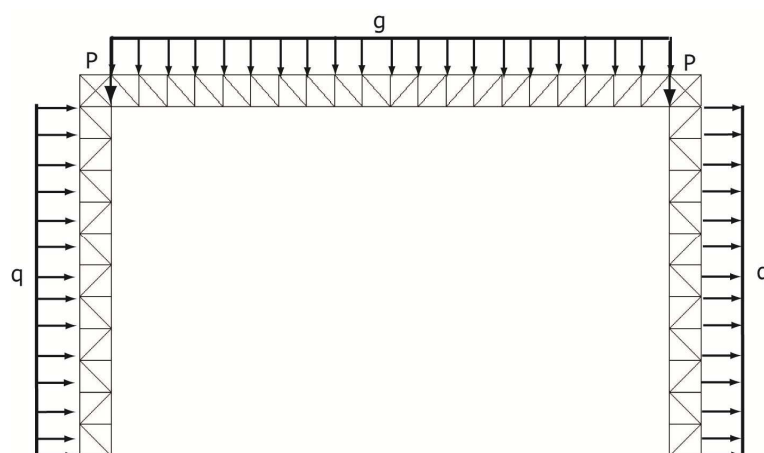
Η προτεινόμενη μέθοδος εφαρμόζεται σε μονώροφα βιομηχανικά πλαίσια με σύνθετα υποστυλώματα υπό συμμετρικές και αντισυμμετρικές φορτίσεις. Στις εφαρμογές αυτές, η δοκός του πλαισίου αντικαθίσταται από κατάλληλα στρωφικά ελατήρια, όπως αυτά εξήχθησαν για τον υπολογισμό του ελαστικού φορτίου λυγισμού πολυώρων κατασκευών από μέλη Timoshenko, ανάλογα με το αν η φόρτιση προκαλεί παραμόρφωση μονής (αμετάθετη συμπεριφορά) ή διπλής (μεταθετή συμπεριφορά) καμπυλότητας. Ακολούθως απομονώνεται το δυσμενέστερο υποστυλόμενο και εφαρμόζεται η διαδικασία που περιγράφηκε στην προηγούμενη παράγραφο για μεμονωμένα σύνθετα μέλη με τυχαίες συνοριακές συνθήκες. Η διαγραμματική απεικόνιση της μετατροπής του πλαισίου σε ισοδύναμο στατικό προσομοίωμα μέλους Timoshenko φαίνεται στο Σχήμα 24.



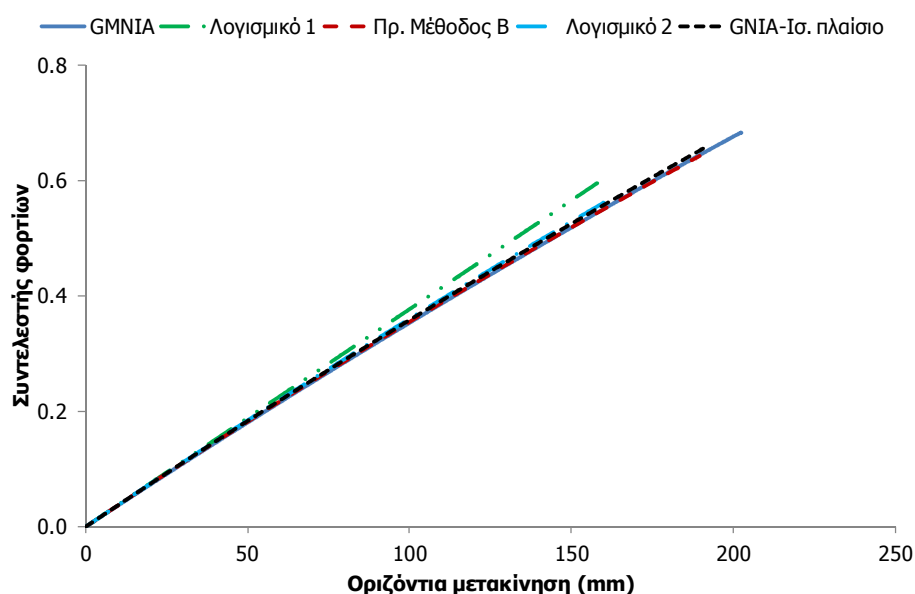
Σχήμα 24: Μετατροπή πλήρους πλαισίου σε στατικό ισοδύναμο προσομοίωμα μέλους Timoshenko

A.9.2. Αριθμητικός έλεγχος

Στην παρούσα υποενότητα παρουσιάζεται ένα ενδεικτικό αριθμητικό παράδειγμα του αμφίπακτου μονώροφου βιομηχανικού πλαισίου που φαίνεται στο Σχήμα 25. Εξετάζεται η περίπτωση συνδυασμού κατακόρυφων και οριζόντιων φορτίσεων. Οι μέθοδοι που χρησιμοποιούνται και ελέγχονται είναι ίδιες με εκείνες που παρουσιάστηκαν στην ενότητα A.8. Επιπλέον εξετάζεται και η περίπτωση Μη Γραμμικής Ανάλυσης Γεωμετρίας (GNIA) του ισοδύναμου πλαισίου Timoshenko για τον προσδιορισμό των οριζόντιων μετακινήσεων και έπειτα εφαρμογή της κατάλληλης σχέσης αλληλεπίδρασης εκ των Εξ. (35)-(37) για τον προσδιορισμό του φορτίου αστοχίας. Οι δρόμοι ισορροπίας παρουσιάζονται στο Σχήμα 26 για όλες τις μεθόδους. Διακρίνεται η σημαντική απόκλιση της γραμμικής ελαστικής ανάλυσης (Λογισμικό 1) που οδηγεί σε υποεκτίμηση των οριζόντιων μετακινήσεων αλλά σε ασφαλή πρόβλεψη του φορτίου αστοχίας. Η χρήση μη γραμμικής ελαστικής ανάλυσης (Λογισμικό 2) οδηγεί σε βελτίωση της πρόβλεψης των οριζόντιων μετακινήσεων και σε συντηρητική πρόβλεψη του φορτίου αστοχίας. Η χρήση της Προτεινόμενης Μεθόδου-B οδηγεί σε πολύ ικανοποιητική πρόβλεψη τόσο των οριζόντιων μετακινήσεων όσο και του φορτίου αστοχίας. Η καλύτερη σύγκριση με τις πλήρως μη γραμμικές αναλύσεις GMNIA επιτυγχάνεται με χρήση GNIA σε ισοδύναμο πλαίσιο με μέλη Timoshenko.



Σχήμα 25: Εξεταζόμενο μονώροφο βιομηχανικό πλαίσιο υπό συνδυασμό κατακόρυφων και οριζόντιων φορτίσεων



Σχήμα 26: Δρόμοι ισορροπίας για το εξεταζόμενο μονώροφο βιομηχανικό πλαίσιο υπό συνδυασμό κατακόρυφων και οριζόντιων φορτίσεων

Μη γραμμική συμπεριφορά και σχεδιασμός σύνθετων υποστυλωμάτων από χάλυβα υπό αξονική και εγκάρσια φόρτιση

Πραγματοποιήθηκε πλήθος εφαρμογών και εξήχθησαν παρόμοια συμπεράσματα. Εν κατακλείδι, η εφαρμογή της προτεινόμενης μεθόδου σε μονώροφα πλαίσια με σύνθετα μέλη με ράβδους δικτύωσης βρίσκεται σε ικανοποιητική συμφωνία με αριθμητικά αποτελέσματα που εξάγονται με τη χρήση πλήρως μη γραμμικών αναλύσεων GMNIA. Η χρήση της σύγχρονης μελετητικής πρακτικής σχεδιασμού οδηγεί σε λιγότερο ακριβή αποτελέσματα από εκείνα της προτεινόμενης μεθόδου που σε αρκετές περιπτώσεις είναι κατά της ασφαλείας.

Τέλος, διερευνήθηκε η απόκριση μονώροφων βιομηχανικών πλαισίων με μη ομοιόμορφα καθ' ύψος σύνθετα υποστυλώματα με ράβδους δικτύωσης που απαντώνται συχνά σε περιπτώσεις που απαιτείται στήριξη γερανογέφυρας στο εσωτερικό πέλμα των υποστυλωμάτων. Αριθμητικές αναλύσεις έδειξαν πως αυτή η πρακτική οδηγεί σε σημαντική μείωση του φορτίου αντοχής και σε σημαντική αύξηση των εγκάρσιων μετακινήσεων, κάτι το οποίο αποδίδεται στη μη πλήρη συνεργασία μεταξύ δοκού και υποστυλωμάτων. Η χρήση ενός κοντού προβόλου σε ενδιάμεσο ύψος για τη στήριξη της γερανογέφυρας ίσως είναι καταλληλότερη.

A.10. ΣΥΝΟΨΗ ΚΑΙ ΣΥΜΠΕΡΑΣΜΑΤΑ

Στόχος της παρούσας διδακτορικής διατριβής είναι η μελέτη της συμπεριφοράς σύνθετων υποστυλωμάτων με ράβδους δικτύωσης και τυχαίες συννοριακές συνθήκες υπό αξονική και εγκάρσια φόρτιση και η διατύπωση οδηγιών για το σχεδιασμό τους. Για την επίτευξη αυτού του στόχου ακολουθείται συνδυασμένη πειραματική, αριθμητική και αναλυτική προσέγγιση.

Αρχικά, παρουσιάζεται ο σχεδιασμός και η εκτέλεση μιας σειράς πειραματικών δοκιμών σε δέκα αμφιέριστα σύνθετα υποστυλώματα με ράβδους δικτύωσης (πέντε ομάδες με δύο ίδια υποστυλώματα στην κάθε μία για λόγους επαναληψιμότητας) με ρεαλιστικές καθολικές και τοπικές ανηγμένες λυγνότητες. Τα δοκίμια υποβάλλονται σε αξονικά θλιπτικά φορτία και συγκεντρωμένες ακραίες ροπές προκαλούμενες λόγω εκκεντρότητας των αξονικών φορτίων. Τα αποτελέσματα για κάθε δοκίμιο παρουσιάζονται με φωτογραφίες τους για διάφορα επίπεδα φόρτισης, και δρόμους ισορροπίας με τη μορφή διαγραμμάτων φορτίου-εγκάρσιας μετακίνησης καθώς και φορτίου-παραμόρφωσης σε χαρακτηριστικές θέσεις. Η συμπεριφορά όλων των δοκιμών είναι αρχικά ελαστική, ενώ διαπιστώνεται πως σε όλες τις ομάδες η τοπική ελαστοπλαστική αστοχία ενός φατνώματος οδηγεί σε καθολική αστοχία χωρίς περιθώρια ανακατανομής της έντασης. Με βάση την τοπική συμπεριφορά των κρίσιμων φατνωμάτων καταδεικνύεται η επιρροή των αρχικών τοπικών ατελειών και των τοπικών εσωτερικών ροπών.

Στη συνέχεια, πραγματοποιείται αριθμητική προσομοίωση των πειραμάτων με τη μέθοδο πεπερασμένων στοιχείων, με στόχο τη βαθμονόμηση των αριθμητικών προσομοιωμάτων έχοντας ως βάση τα πειραματικά αποτελέσματα, ώστε να μπορούν να χρησιμοποιηθούν στη μετέπειτα πορεία της έρευνας. Για την προσομοίωση τόσο των πελμάτων όσο και των ράβδων δικτύωσης χρησιμοποιούνται αρχικά επιφανειακά πεπερασμένα στοιχεία. Προκειμένου να ληφθεί υπόψη η παρουσία παραμενουσών τάσεων λόγω θερμικής κατεργασίας η διατομή των πελμάτων χωρίζεται κατάλληλα σε τμήματα, σε κάθε ένα εκ των οποίων αποδίδεται διαφορετική ποιότητα χάλυβα. Οι καθολικές και τοπικές γεωμετρικές ατέλειες ενσωματώνονται στις αριθμητικές αναλύσεις σύμφωνα με τις πρώτες ιδιομορφές καθολικού και τοπικού λυγισμού, αντίστοιχα. Από τις αριθμητικές αναλύσεις προκύπτει πως εφόσον ληφθούν υπόψη στην ανάλυση η μη γραμμικότητα γεωμετρίας και υλικού, οι αρχικές γεωμετρικές καθολικές και τοπικές ατέλειες και οι παραμένουσες τάσεις θερμικής κατεργασίας, υπάρχει μια πολύ καλή συμφωνία μεταξύ αριθμητικών και πειραματικών αποτελεσμάτων, σε όρους μετακινήσεων, παραμορφώσεων και αντοχής. Επιπλέον, η σύγκριση των αριθμητικών προσομοιωμάτων με επιφανειακά πεπερασμένα στοιχεία με αντίστοιχα ραβδωτών πεπερασμένων στοιχείων οδηγεί στο

συμπέρασμα πως η χρήση των δεύτερων μπορεί να προβλέψει ικανοποιητικά τη συμπεριφορά των σύνθετων μελών με αισθητά μικρότερο υπολογιστικό κόστος.

Στη συνέχεια, με χρήση αριθμητικών προσομοιωμάτων κυρίως ραβδωτών πεπερασμένων στοιχείων, διερευνάται η απόκριση σύνθετων υποστυλωμάτων με ράβδους δικτύωσης με καθολικές και τοπικές ατέλειες. Διαπιστώνεται ότι η αστοχία εκδηλώνεται συνήθως ως τοπική ελαστοπλαστική αστοχία του κρίσιμου φατνώματος, ή σπανιότερα ως καθολική ελαστική αστοχία. Στη δεύτερη περίπτωση η αλληλεπίδραση μεταξύ καθολικού και τοπικού λυγισμού είναι σημαντική και θα πρέπει να λαμβάνεται υπόψη, ενώ στην πρώτη μπορεί να ενσωματωθεί έμμεσα στην τοπική αντοχή του κρίσιμου φατνώματος. Η μεγαλύτερη μείωση του φορτίου αστοχίας του ατελούς φορέα σε σχέση με τον τέλειο πραγματοποιείται και στις δύο περιπτώσεις όταν τα φορτία καθολικού λυγισμού, τοπικού λυγισμού και πλήρους διαρροής ταυτίζονται, ενώ η μικρότερη όταν το κρίσιμο φορτίο καθολικού λυγισμού είναι μικρότερο από του τοπικού. Η αδυναμία της ικανοποιητικής πρόβλεψης του φορτίου αστοχίας από τις διατάξεις του Ευρωκώδικα 3 στην περίπτωση της δεύτερης μορφής αστοχίας, καθώς δε λαμβάνεται εκεί υπόψη η αλληλεπίδραση καθολικού και τοπικού λυγισμού, αποτελεί κίνητρο για τη δημιουργία μιας προσεγγιστικής αναλυτικής διαδικασίας που προβλέπει επαρκώς την απόκριση των σύνθετων μελών και στις δύο περιπτώσεις αστοχίας. Παρόλα αυτά, η πλέον συχνή μορφή αστοχίας στην πράξη είναι η πρώτη, λόγω χρήσης μελών με μικρές ως μέτριες καθολικές και τοπικές ανηγμένες λυγηρότητες και λόγω συνύπαρξης σημαντικών εγκάρσιων φορτίων, και με βάση αυτή συνεχίζεται η παρούσα έρευνα.

Εν συνεχεία, εφόσον η προσομοίωση των σύνθετων μελών με ράβδους δικτύωσης ως μελών Timoshenko κρίνεται επαρκής και αξιόπιστη, η έρευνα επικεντρώνεται στην πρόβλεψη του ελαστικού κρίσιμου φορτίου λυγισμού μελών Timoshenko με τυχαίες συνοριακές συνθήκες με τη μέθοδο του Engesser. Προτείνεται για αυτό το σκοπό ένα μητρώο ευστάθειας 3×3 που οδηγεί σε τρεις μη γραμμικές σχέσεις για αμετάθετα, μερικώς μεταθετά και μεταθετά μέλη. Εξάγονται επίσης εξισώσεις γωνίας στροφής με τη μέθοδο Engesser για μέλη Timoshenko με ημι-άκαμπτες συνδέσεις στα άκρα τους. Με βάση αυτές, υπολογίζονται στρεφικές δυσκαμψίες για τα προς αντικατάσταση μέλη Timoshenko σε πλαίσια, ανάλογα με τη συνοριακή συνθήκη στο απέναντι άκρο τους και την παρουσία ή όχι αξονικής δύναμης. Η χρήση των μη γραμμικών σχέσεων και των στρεφικών δυσκαμψιών συμβάλλει στον επαρκή υπολογισμό του ελαστικού κρίσιμου φορτίου λυγισμού πλαισίων που αποτελούνται από μέλη Timoshenko και από σύνθετα μέλη.

Ακολούθως, διερευνάται η ανάλυση 2^{ης} τάξης ατελών μελών Timoshenko με τυχαίες συνοριακές συνθήκες υπό συνδυασμό αξονικού φορτίου και συνήθων εγκάρσιων φορτίων, με στόχο να προταθούν κλειστές σχέσεις για τον υπολογισμό εντατικών μεγεθών και μετακινήσεων κατά μήκος των μελών. Η ενσωμάτωση αρχικής καθολικής ατέλειας σύμφωνα με το σχήμα της 1^{ης} ιδιομορφής καθολικού λυγισμού γίνεται με χρήση προσεγγιστικού μεγεθυντικού συντελεστή που υπολογίζεται με βάση τα φορτία λυγισμού της προηγούμενης παραγράφου. Οι εγκάρσιες φορτίσεις περιλαμβάνουν ομοιόμορφα κατανομημένο φορτίο, ακραίες συγκεντρωμένες ροπές και ακραίες συγκεντρωμένες δυνάμεις και η ανάλυση υπό την επίδρασή τους πραγματοποιείται με χρήση των εξισώσεων γωνίας στροφής 2^{ης} τάξης με τη μέθοδο Engesser για μέλη Timoshenko. Η σύγκριση με αριθμητικά προσομοιώματα ραβδωτών πεπερασμένων στοιχείων οδηγεί σε πολύ ικανοποιητική συμφωνία μεταξύ τους.

Ο τερματισμός της ελαστικής ανάλυσης 2^{ης} τάξης για τον υπολογισμό του φορτίου αστοχίας τους πραγματοποιείται με χρήση μιας προτεινόμενης απλής σχέσης αλληλεπίδρασης που βασίζεται στο συμπέρασμα ότι τα σύνθετα μέλη με ράβδους δικτύωσης αστοχούν συνήθως λόγω τοπικής ελαστοπλαστικής αστοχίας. Συνεπώς, συνολικά η προτεινόμενη μέθοδος για μεμονωμένα σύνθετα μέλη με τυχαίες συνοριακές συνθήκες περιλαμβάνει την ελαστική ανάλυση 2^{ης} τάξης των ισοδύναμων μελών Timoshenko και τον τερματισμό αυτής για τον προσδιορισμό του φορτίου αστοχίας με βάση τη σχέση αλληλεπίδρασης. Η χρήση της προτεινόμενης διαδικασίας για τον υπολογισμό των μετακινήσεων

Μη γραμμική συμπεριφορά και σχεδιασμός σύνθετων υποστυλωμάτων από χάλυβα υπό αξονική και εγκάρσια φόρτιση

και των φορτίων αστοχίας μεγάλου πλήθους σύνθετων υποστυλωμάτων με ράβδους δικτύωσης αποδεικνύεται ότι ευρίσκεται σε πολύ καλή συμφωνία με αριθμητικά αποτελέσματα που προκύπτουν από πλήρως μη γραμμικές αναλύσεις.

Τέλος, η προτεινόμενη μέθοδος εφαρμόζεται σε μονώροφα βιομηχανικά πλαίσια με σύνθετα υποστυλώματα υπό συμμετρικές και αντισυμμετρικές φορτίσεις. Στις εφαρμογές αυτές, η δοκός του πλαισίου αντικαθίσταται από κατάλληλα στροφικά ελατήρια, όπως αυτά εξήχθησαν για τον υπολογισμό του ελαστικού φορτίου λυγισμού πολυώροφων κατασκευών από μέλη Timoshenko, ανάλογα με το αν η φόρτιση προκαλεί παραμόρφωση μονής (αμετάθετη συμπεριφορά) ή διπλής (μεταθετή συμπεριφορά) καμπυλότητας. Ακολουθώντας απομονώνεται το δυσμενέστερο υποστυλώμα και εφαρμόζεται η διαδικασία που περιγράφηκε στην προηγούμενη παράγραφο για μεμονωμένα σύνθετα μέλη με τυχαίες συννοριακές συνθήκες. Η εφαρμογή της προτεινόμενης μεθόδου σε μονώροφα πλαίσια με σύνθετα μέλη βρίσκεται σε ικανοποιητική συμφωνία με αριθμητικά αποτελέσματα που εξάγονται με τη χρήση πλήρως μη γραμμικών αναλύσεων. Η χρήση της σύγχρονης μελετητικής πρακτικής σχεδιασμού οδηγεί σε λιγότερο ακριβή αποτελέσματα από εκείνα της προτεινόμενης μεθόδου και σε αρκετές περιπτώσεις είναι κατά της ασφαλείας. Τέλος, με βάση αυτή τη διερεύνηση προτείνονται πρακτικοί τρόποι προσομοίωσης, ανάλυσης και ελέγχου επάρκειας των σύνθετων μελών, με στόχο τη βελτίωση της αξιοπιστίας κατά το σχεδιασμό τους σε επίπεδο μελετητικής πρακτικής.

A.11. ΠΡΩΤΟΤΥΠΗ ΣΥΜΒΟΛΗ ΤΗΣ ΔΙΑΤΡΙΒΗΣ

Η παρούσα διδακτορική διατριβή ασχολείται με τη μη γραμμική συμπεριφορά και το σχεδιασμό σύνθετων μελών με ράβδους δικτύωσης υπό αξονική και εγκάρσια φόρτιση λαμβάνοντας υπόψη την επιρροή αρχικών καθολικών και τοπικών ατελειών. Για την επίτευξη αυτού του στόχου, πραγματοποιείται πειραματική, αριθμητική και αναλυτική διερεύνηση που περιλαμβάνει επιστημονική πρωτοτυπία. Βάσει αυτής, διατυπώνονται επίσης βασικές οδηγίες ανάλυσης και σχεδιασμού σύνθετων μελών με ράβδους δικτύωσης, συμβάλλοντας έτσι στην πρόοδο της μελετητικής πρακτικής στο συγκεκριμένο θέμα.

A.11.1. Συμβολή στην επιστήμη του μηχανικού

Η συμβολή στην επιστήμη του μηχανικού περιλαμβάνει:

- Εκτέλεση πρωτότυπων πειραμάτων σε δοκίμια σύνθετων μελών με ράβδους δικτύωσης με ρεαλιστικές καθολικές και τοπικές ανηγμένες λυγηρότητες που περιλαμβάνουν τόσο καθολικές όσο και τοπικές μετρήσεις διευκολύνοντας την ποιοτική και ποσοτική ερμηνεία της απόκρισης των δοκιμίων ([10-1], [10-2]).
- Χρήση Μη Γραμμικών Αναλύσεων Γεωμετρίας και Υλικού με Αρχικές Ατέλειες (GMNIA), συμπεριλαμβάνοντας την επιρροή παραμενοουσών τάσεων θερμής έλασης βασιζόμενοι σε ένα υπολογιστικό τέχνασμα τροποποίησης της αντοχής του υλικού σε συγκεκριμένες περιοχές της διατομής, με στόχο τη βαθμονόμηση των αριθμητικών προσομοιωμάτων με βάση τα πειραματικά αποτελέσματα. Η αριθμητική προσομοίωση τέτοιου τύπου είναι πρωτότυπη και συμπεράσματα που εξάγονται κατά τη διάρκεια της αριθμητικής προσομοίωσης μπορεί να αποδειχτούν χρήσιμα για άλλους ερευνητές ([10-1], [10-2]).
- Πραγματοποίηση εκτεταμένων παραμετρικών αναλύσεων και εξαγωγή του συμπεράσματος ότι ατελή σύνθετα υποστυλώματα με ράβδους δικτύωσης αστοχούν είτε λόγω καθολικής ελαστικής αστοχίας είτε λόγω τοπικής ελαστοπλαστικής αστοχίας του κρίσιμου φατνώματος, με τη δεύτερη περίπτωση να απαντάται συχνότερα στην πράξη. Προτείνεται αναλυτική μέθοδος που μπορεί να προβλέψει ικανοποιητικά τη συμπεριφορά των σύνθετων μελών και στις δύο περιπτώσεις. Ελλείψει υπάρχουσών αναλυτικών μεθόδων που να μπορούν να χρησιμοποιηθούν για την ικανοποιητική

πρόβλεψη και των δύο μηχανισμών αστοχίας, η μόνη εναλλακτική μέθοδος είναι η χρήση μη γραμμικής αριθμητικής ανάλυσης που απαιτεί πολύ μεγαλύτερο υπολογιστικό φόρτο από την προτεινόμενη αναλυτική διαδικασία ([10-3]).

- Πρόταση αναλυτικής μεθόδου για τον υπολογισμό του ελαστικού κρίσιμου φορτίου λυγισμού πολυώροφων πλαισίων με μέλη Timoshenko με βάση τη μέθοδο Engesser. Για αυτό το σκοπό, μορφώνονται μητρώο ευστάθειας για μέλος Timoshenko με τυχαίες συνοριακές συνθήκες και εξισώσεις γωνίας στροφής για μέλη Timoshenko με ημι-άκαμπτες συνδέσεις με βάση τη μέθοδο Engesser. Προτείνονται επίσης στρωφικές δυσκαμψίες για τα προς αντικατάσταση μέλη που συντρέχουν στον άνω και κάτω κόμβο του εξεταζόμενου υποστυλώματος ([10-4]).
- Εξαγωγή κλειστών σχέσεων για τον άμεσο υπολογισμό των εντατικών μεγεθών και μετακινήσεων κατά μήκος ατελούς μέλους Timoshenko με τυχαίες συνοριακές συνθήκες που υπόκειται σε αξονική θλίψη και εγκάρσιες φορτίσεις. Η ενσωμάτωση των διατμητικών παραμορφώσεων πραγματοποιείται με τη μέθοδο Engesser. Οι εγκάρσιες φορτίσεις περιλαμβάνουν εγκάρσιο ομοιόμορφα κατανομημένο φορτίο, συγκεντρωμένες ροπές στα άκρα και συγκεντρωμένες εγκάρσιες δυνάμεις στα άκρα ([10-5], [10-6], [10-7]).
- Χρήση των αναλυτικών αποτελεσμάτων των δύο προηγούμενων παραγράφων, για τον τερματισμό της ελαστικής ανάλυσης 2^{ης} τάξης με βάση μια απλή σχέση αλληλεπίδρασης προς υπολογισμό του φορτίου αστοχίας καθολικά και τοπικά ατελούς σύνθετου υποστυλώματος με τυχαίες συνοριακές συνθήκες υπό αξονική θλίψη και τυπικές εγκάρσιες φορτίσεις, είτε το σύνθετο μέλος είναι μεμονωμένο είτε θεωρείται μέλος μονώροφου βιομηχανικού πλαισίου ([10-5], [10-6], [10-7]).

A.11.2. Συμβολή στη μελετητική πρακτική

Στην τρέχουσα μελετητική πρακτική προβλέπεται τρόπος σχεδιασμού αμφιέρειστων υποστυλωμάτων, ενώ στην πράξη τα σύνθετα μέλη είναι τμήματα μεγαλύτερων πλαισίων. Για αυτό το λόγο, οι υπάρχουσες αναλυτικές προβλέψεις δεν είναι δυνατό να χρησιμοποιηθούν σε πιο περίπλοκες περιπτώσεις και απαιτούνται κατάλληλες τροποποιήσεις. Η κύρια συνεισφορά της παρούσας διδακτορικής διατριβής στη μελετητική πρακτική συνοψίζεται ως:

- Η προτεινόμενη μέθοδος, βασιζόμενη σε αναλυτικούς υπολογισμούς και σε απλή σχέση αλληλεπίδρασης, μπορεί να χρησιμοποιηθεί για τον προσδιορισμό της συμπεριφοράς σύνθετων μελών, ανεξάρτητα από το αν αποτελούν μέρος πλαισίων ή όχι. Αυτό διευκολύνει την άμεση χρήση από τους μηχανικούς της πράξης. Η προτεινόμενη μέθοδος οδηγεί σε υπολογισμό των εντατικών μεγεθών και εγκάρσιων βελών σε κάθε στάθμη φόρτισης και σε επαρκή προσδιορισμό της αντοχής του σύνθετου μέλους.
- Η προτεινόμενη μέθοδος βασίζεται σε αναλυτικές σχέσεις που είναι σχετικά εύκολες στη χρήση, ιδιαίτερα αν ενσωματωθούν με τη μορφή κώδικα σε κατάλληλο λογισμικό. Προσφέρουν κατ' αυτόν τον τρόπο ακριβή αποτελέσματα με σχετικά μικρό υπολογιστικό κόστος. Συνεπώς μπορούν να χρησιμοποιηθούν σε εκτεταμένες παραμετρικές αναλύσεις κατά τη διάρκεια προμελέτης και για τον έλεγχο των αποτελεσμάτων που εξάγονται από αριθμητικές αναλύσεις με εμπορικά λογισμικά.
- Χρήσιμα συμπεράσματα εξάγονται για την ανάλυση και σχεδιασμό σύνθετων μελών στην πράξη συγκρίνοντας τις συνήθεις μελετητικές πρακτικές ανάλυσης και σχεδιασμού με αποτελέσματα που προκύπτουν από πλήρως μη γραμμικές αναλύσεις. Η χρήση ελαστικής γραμμικής ανάλυσης αποδεικνύεται αξιόπιστη μόνο στην περίπτωση που το πλαίσιο συμπεριφέρεται πολύ δύσκαμπτα, ενώ η ενσωμάτωση της μη γραμμικότητας γεωμετρίας στην ανάλυση είναι εν γένει σκόπιμη. Η πρόβλεψη της αντοχής μπορεί να βελτιωθεί αν στην Εξ. (38) συμπεριληφθεί μόνο ο όρος που συνδέεται με την αξονική δύναμη.

- Η προσομοίωση του πλήρους πλαισίου με μέλη Timoshenko, η πραγματοποίηση μη γραμμικής ανάλυσης γεωμετρίας και η χρήση της προτεινόμενης σχέσης αλληλεπίδρασης οδηγεί σε πολύ ικανοποιητικά αποτελέσματα, σε ό,τι αφορά τόσο εγκάρσιες μετακινήσεις όσο και το φορτίο αστοχίας. Η συγκεκριμένη διαδικασία δεν απαιτεί λεπτομερή προσομοίωση των σύνθετων μελών και συνεπώς είναι πιο γρήγορη και κατάλληλη σε φάση προμελέτης.
- Η χρήση μη ομοιόμορφων καθ' ύψος σύνθετων υποστυλωμάτων, για παράδειγμα σε περιπτώσεις χρήσης γερανογέφυρας και στήριξης αυτής στο εσωτερικό πέλμα, θα πρέπει να αποφεύγεται. Αριθμητικές αναλύσεις έδειξαν πως οδηγεί σε σημαντική μείωση του φορτίου αντοχής και σε σημαντική αύξηση των εγκάρσιων μετακινήσεων, κάτι το οποίο αποδίδεται στη μη πλήρη συνεργασία μεταξύ δοκού και υποστυλωμάτων. Η χρήση ενός κοντού προβόλου σε ενδιάμεσο ύψος για τη στήριξη της γερανογέφυρας ίσως είναι καταλληλότερη.

1 INTRODUCTION

1.1 PREFACE

Columns may be defined as compressed longitudinal structural members. Metal columns appeared in the late 18th century as wrought-iron members and their use was based on empirical evaluations. With the introduction of steel to constructional engineering and with the larger demand for safe and economical structures, the necessity for a thorough investigation of steel columns' behaviour became prominent.

After the observation by Leonhard Euler [1-1] that the column's strength was not only a problem of crushing but also of stability, many theories [1-2], [1-3] were developed accounting for these failure modes. The combination of theoretical and experimental investigation that took place during the first half of the 21st century was strengthened by the advances in computer engineering during the second half of the same century, allowing for complicated calculations and advanced types of analyses. These decades of analytical, experimental and numerical research included plasticity, large deflections, residual stresses and initial imperfections and resulted in the single and multiple column curves that are incorporated in modern code provisions for the efficient design of columns [1-4]. In practice structural members are usually subjected to both axial and lateral loads and in such cases they are called beam-columns. Axial forces and bending moments of comparable magnitude coexist along the beam-columns and both should be considered in their design. To that purpose modern design guides contain appropriate interaction formulae that account for both geometrical and material nonlinearity.

Columns with single and solid cross-section along their length have been thoroughly investigated over the last century and modern codes provide sufficient guidance to engineers for the design of such members. Despite that fact, in many structures, the existing cross-sections may not satisfy in an economical way strength and/or serviceability criteria. A powerful alternative in steel buildings and bridges providing economical solutions in cases of large spans, large buckling lengths and/or heavy loads is the use of built-up columns.

1.2 BUILT-UP COLUMNS

Built-up columns consist of the longitudinal chords (or flanges) and the shear system that provides shear rigidity and structural integrity by connecting the chords between each other. They have a

double-symmetrical cross-section and are characterized by large static indeterminacy. Both the flanges and the shear system are constructed by either rolled or welded cross-sections. Usually built-up columns have two chords and depending on the type of the shear system they are distinguished in two main categories: laced and battened built-up members. The shear system consists of lacing bars and batten plates in the first and second category, respectively, which are usually constructed in two parallel planes. The built-up behaviour corresponds to the plane of the shear system. In the response perpendicular to the plane of the shear system, the two chords work as two closely spaced cross-sections. Typical views of an I-profile column, a laced built-up column and a battened built-up member are shown in Figure 1-1(a)-(c), respectively. In the first case, the flanges are continuously connected with the web along the height of the column. In the laced and battened columns of this example, U-profiles are used as flanges while the lacing bars and the batten plates play the role of the web.

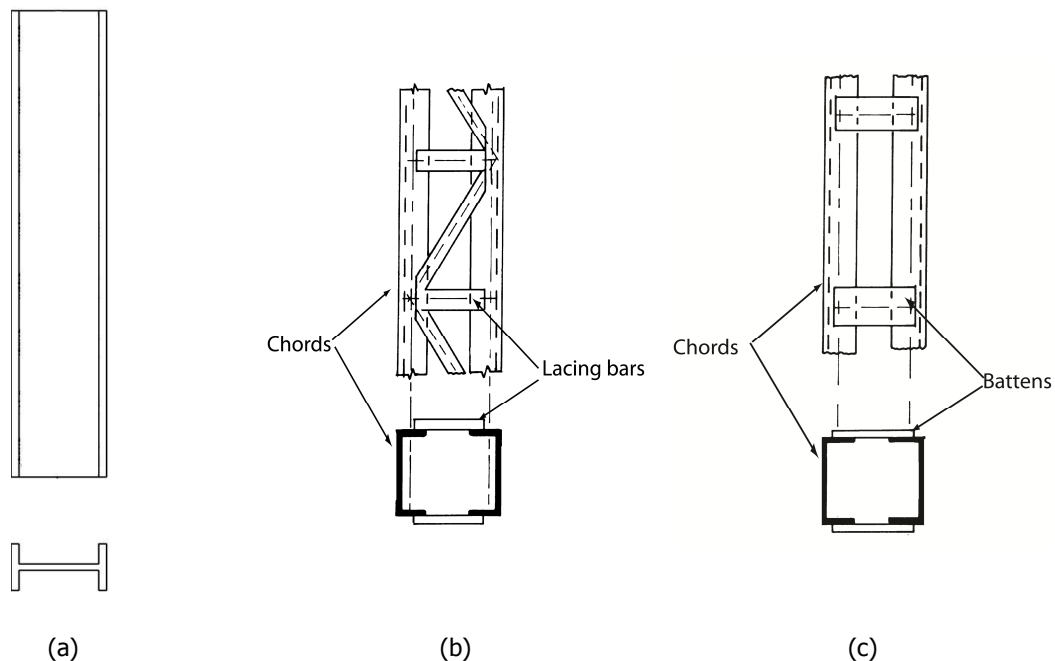


Figure 1-1: (a) I-profile column (b) laced built-up column and (c) battened built-up column

The key characteristic that makes built-up columns structurally more efficient than solid web members is the arrangement of the single counterparts, which follows the flux of the internal forces. The concentration of material far from the cross-section's elastic neutral axis results in its better exploitation. By orienting the cross-section of the built-up columns' flanges in a way that its strong axis is activated for out-of plane (perpendicular to the plane of the shear system) bending as shown in Figure 1-1, strength and stiffness of similar magnitude can be achieved for both axes.

The structural advantages of built-up struts were appreciated from the beginning of the 21st century, when they were used in large scale constructions. At the same time, their differentiation from other structural members became clear in the most tragic way in Canada. The Quebec Bridge [1-5] covering the width of St. Lawrence River collapsed in 15 seconds during its construction in 1907, leading to death 75 workers from a total of 86 working that day. The failure was attributed to the buckling of a built-up diagonal. New efforts took place and the bridge was totally reconstructed in 1919 (Photo 1-1). Built-up columns are differentiated from commonly used columns in two aspects. The first one is the important and detrimental effect of shear deformations, which is attributed to their significantly deformable shear systems. The second is the interaction between global and local behavior of such columns. The interaction should be taken into account because the arrangement of the diagonal bars

or of the batten plates leads to the appearance of several panels in elevation which make the consideration of the local behavior necessary.



(a)



(b)

Photo 1-1 (a) The collapse of the Quebec Bridge in 1907 and (b) the Quebec Bridge today

1.3 LACED BUILT-UP COLUMNS

As already mentioned, laced built-up columns usually consist of two flanges that are connected between each other with the use of diagonal bars constructed in two parallel planes. The lever arm between the two flanges is relatively large and the diagonals can be either bolted or welded on the flanges, forming triangles and resulting in a truss like static system. The lacing system can vary depending on the arrangement of diagonals. Some of the ones encountered often in practice are presented in Figure 1-2. The bending and axial rigidities are provided by the longitudinal chords, while the shear rigidity is mainly offered by the lacing bars. As will be pointed out in the following chapters, laced members are usually characterized by large bending and shear rigidities making them suitable for resisting both axial and lateral loading.

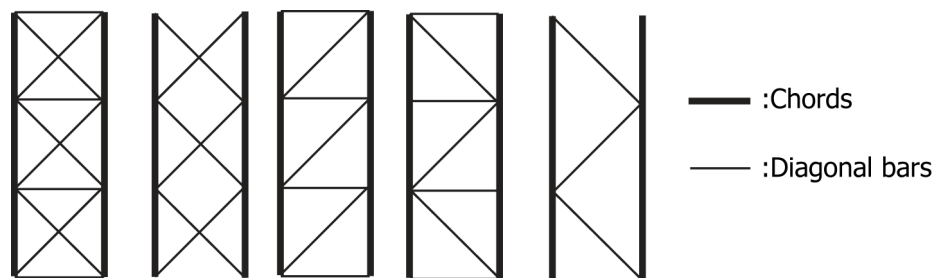


Figure 1-2: Different arrangements of lacing bars

Laced built-up columns are often used in industrial buildings carrying crane bridges such as the one depicted in Figure 1-3. The demand for large columns' height, heavy loads and small displacements in such structures makes laced columns a tempting solution. In general, industrial buildings consist of consecutive planar frames in which laced columns are positioned appropriately so that for in-plane loads the built-up behaviour is activated. The crane bridge is usually directly supported by the inner chord of the laced columns, while the outer chord is used for the connection of the columns with the frame girder as shown in Figure 1-3 [1-6].

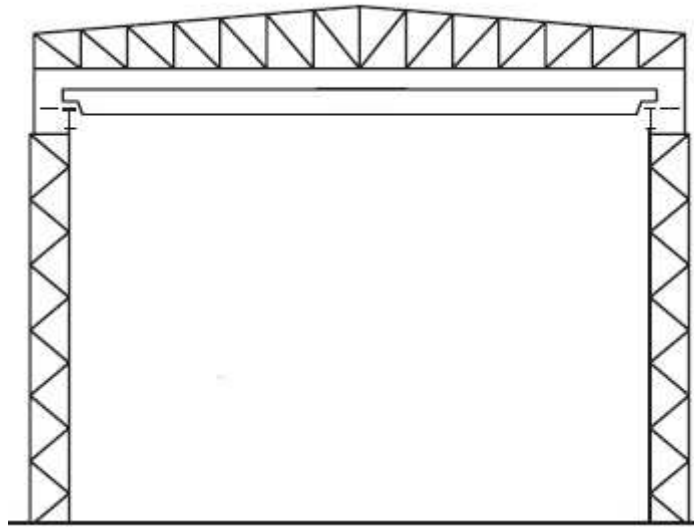


Figure 1-3: Typical industrial frame with laced built-up columns carrying crane bridge

Extensive use of laced columns in industrial frames (naval stations and hangars) serving military purposes took place over the last century, satisfying the need for protecting massive military equipment under large covered areas as depicted in Photo 1-2. A typical example of laced columns used in a modern industrial structure in Greece is shown in Photo 1-3 (a)-(b). In Photo 1-3 (c)-(d), the first transformer plant of Hyundai in the United States [1-7] that was completed at the end of 2011 is shown. The use of massive laced columns was necessary for supporting the 6000-ton transformer plant covered by large jack trusses.



Photo 1-2: Laced built-up columns in a naval station

Laced columns have also been extensively used in bridge engineering, especially throughout the United States, either as frames' columns or as bracing members. Four cases are shown in Photo 1-4, in which the lacing bars are riveted on the flanges. Photo 1-4 (a) comes from the recent retrofit of San-Francisco-Oakland Bay Bridge [1-8], at which the strengthening took place while the bridge was still open to traffic. The use of laced ties aimed at protecting the bridge from severe seismic actions. Photo 1-4 (b) was taken from the historical Gale Road Bridge in Michigan [1-9] which was built in 1897 with the use of riveted laced columns and trusses.



(a)



(b)



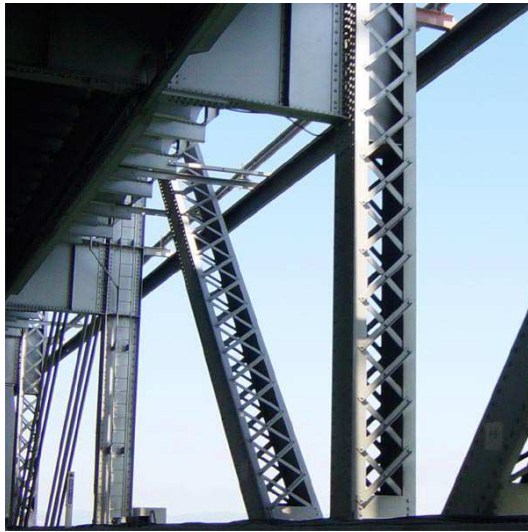
(c)



(d)

Photo 1-3 (a)-(d) Laced built-up column in modern industrial buildings with welded connection of the lacing bars on the chords

Another use of laced columns is related to tower cranes used often in large construction sites. The need for sufficiently large stiffness and strength in both axes of bending without the use of laterally supportive systems makes laced columns a unique solution. Usually laced columns used as tower cranes consist of four chords connected between each other with four planes of lacing serving the previously mentioned needs. Significant bending moments due to load eccentricities and lateral loads can be safely delivered to the ground with the use of a limited amount of steel. A view of a tower crane at the Mont Blanc mountain top is shown in Photo 1-5 [1-10].



(a)



(b)

Photo 1-4: Steel laced built-up struts used as (a) bracing members and (b) part of frames in bridge engineering in the United States



Photo 1-5: Laced tower crane at Mont Blanc

1.4 BATTENED BUILT-UP COLUMNS

Battened built-up columns usually consist of two flanges that are connected between each other with the use of batten plates (battens) constructed in two parallel planes. The lever arm between the two flanges is relatively small in comparison to laced built-up columns and the battens are welded on the flanges, resulting in a static system similar to the Vierendeel truss. The rigid connection between the battens and the chords is necessary for the transmission of shear between the longitudinal flanges. In the case that the battens are attached to the flanges by hinged connections, the column is called spaced and the flanges work individually. In battened members the bending rigidity is offered by the longitudinal chords while the shear rigidity is offered by both the chords and the battens. As will be pointed out in the following chapters, battened members are usually characterized by small shear

rigidity making them suitable for resisting mainly axial loading. Due to this disadvantage battened built-up columns are not permitted by U.S. design provisions.

Battened members are usually used as compression struts, like in the bridge cases depicted in Photo 1-6 [1-11]. The use of bracing systems in the plane of the battens in these photos verifies that battened columns are not usually designed for resisting significant lateral forces. A similar use of battened struts can be seen in Photo 1-7 [1-12], in an arch-shaped structure belonging to a hydro-electrical plant in Pueblo Nuevo Vinas in Guatemala. The static system of the arch clarifies that the battened members act as transverse and diagonal truss bars, mainly stressed by axial forces.



(a)



(b)

Photo 1-6: (a)-(b) Steel battened built-up struts used in bridge engineering



Photo 1-7: Steel battened built-up struts in a hydro-electrical structure in Pueblo Nuevo Vinas in Guatemala

1.5 OBJECTIVE AND CONTENTS OF THE DOCTORAL THESIS

This thesis focuses on built-up beam-columns, especially on laced ones that are more frequently used in practice. The main purpose of this research is to thoroughly investigate and to provide useful guidelines for their analysis and design. The present research is based on the three main aspects used in modern civil engineering research which include analytical procedures, numerical calculations and experimental tests.

The introduction to columns in general and built-up columns in particular, presented in this first chapter, is followed by Chapter 2 that contains a literature review regarding the behaviour of laced and battened built-up members, the second-order analysis of Timoshenko beam-columns and provisions incorporated in modern design codes related to the analysis and design of built-up

columns. Chapter 3 describes in detail the set-up and the results of an experimental work that took place at the Institute of Metal Structures at the School of Civil Engineering of the National Technical University of Athens, in the context of the present doctoral thesis. In Chapter 4, the experimental outcomes are compared with numerical results for the calibration of the numerical models and useful conclusions are drawn about the numerical modelling of laced columns. Chapter 5 presents the types of failure that laced built-up members can exhibit and a proposed interaction equation for the calculation of the collapse load of imperfect simply-supported laced built-up columns is presented. In Chapter 6, the problem of the calculation of the elastic critical buckling load of frames consisting of Timoshenko members is thoroughly examined and an analytical procedure is proposed. In Chapter 7, imperfect Timoshenko beam-columns with arbitrary supports under axial compressive and lateral loading are examined and closed-form solutions are proposed for calculating their second-order elastic response. In Chapter 8, the structural behaviour of imperfect steel built-up beam-columns with any type of boundary conditions subjected to combined axial and lateral actions is investigated by making also use of the results obtained in Chapters 5, 6 and 7. Chapter 9 provides examples for the practical use of the proposed procedures in the calculation of the response and failure load of laced built-up columns belonging to planar and symmetrical industrial frames. Additionally, guidelines for their design and numerical modelling in practice are provided. Finally, Chapter 10 includes a summary of the present doctoral thesis, the main contribution to the research field related to it and recommendations for future research.

1.6 REFERENCES

- [1-1] Van den Broeck, J. A. "English translation of Euler's on the strength of columns", American Journal of Physics, 15, July 1947
- [1-2] Bleich, F. "Buckling strength of metal structures", McGraw-Hill, New York, 1952
- [1-3] Salmon, E. H. "Columns, A treatise on the strength and design of compression members", Oxford Technical Publications, London, 1921
- [1-4] Tall L. "Centrally compressed members", In Axially Compressed Structures, Stability and Strength, ed. R. Narayanan, Applied Science Publishers, London, 1982, pp. 1-40
- [1-5] http://en.wikipedia.org/wiki/Quebec_Bridge
- [1-6] Richard J. Tremblay R., Koboevic S., MacCrimmon R.A. "Seismic analysis and design approaches for crane-supporting steel structures, Proceedings of STESSA, 2009
- [1-7] http://www.ids-inc.net/project_details.php?id=4549
- [1-8] http://en.wikipedia.org/wiki/San_Francisco%E2%80%93Oakland_Bay_Bridge
- [1-9] <http://www.historicbridges.org/bridges/browser/?bridgebrowser=truss/gale/>
- [1-10] [http://en.wikipedia.org/wiki/Crane_\(machine\)](http://en.wikipedia.org/wiki/Crane_(machine))
- [1-11] Kirozis A., Lempesis J. "Analytical, numerical and code-based investigation of built-up columns", Diploma thesis, School of Civil Engineering, National Technical University of Athens, 2008 (in Greek)
- [1-12] http://www.greenstands.eu/en/410_green-projects.php?proid=7

2 LITERATURE REVIEW

2.1 INTRODUCTION

The structural response of built-up columns has been studied extensively and many relevant publications can be encountered in the literature. They include analytical methods, numerical simulations and experimental tests covering all possible research approaches in the field of structural engineering. These works are mainly related to simply-supported built-up columns under axial loading. Two main aspects that differentiate built-up columns from commonly used struts have been thoroughly investigated: (i) the modelling of built-up members as equivalent Timoshenko struts including the effect of shear deformations and (ii) the effect of interaction between global and local behaviour. In this chapter, a review of the existing literature for the response and failure types of laced and battened built-up columns will be initially presented. Then, publications related to interaction between global and local buckling will be mentioned, focusing on the effect of global and local imperfections on the overall behaviour. Additionally, as will be illustrated in the following chapters, modelling built-up struts as equivalent Timoshenko members is very convenient in analytical procedures. Therefore research with emphasis on the second-order response of Timoshenko beam-columns will be summarized. Finally, the provisions of modern design codes for built-up columns will be presented and conclusions on the literature review will be drawn. All research topics into which this chapter is separated are directly connected between each other. Their separate presentation is used for the reader's facilitation and is based on the field to which each research work made the largest contribution.

2.2 RESEARCH ON BUILT-UP COLUMNS

Built-up columns consist of many counterparts and as a result their behaviour differs from the one of solid struts. In the present section, publications related to experimental tests and analytical procedures, either empirical or not, will be presented. It will be shown that during the last century researchers tried to approach the behaviour of built-up members using various approximations, sometimes very far from reality. A typical laced column and its cross-section are depicted in Figure 2-1. The two flanges offer both axial and bending rigidity and the lever arm between them is h_0 . In this specific example the chords consist of I-shaped cross-sections positioned in such a way that their strong axis y - y is parallel to the plane of the lacing. Therefore, for behaviour in the lacing's plane the

weak axis $z-z$ is activated. The total length L of the built-up column is divided in a finite number of smaller parts usually called panels. Each panel's length is denoted as " a " and is equal to the distance between adjacent joints. The diagonal and transverse bars (the angle between them is denoted as ϕ_1) offer the necessary shear rigidity to the built-up member. They are usually welded on the flanges ensuring integrity between them. The end transverse bars may have the same cross-section as intermediate transverse members or much larger ones, leading to the so called "end rigid plates". The technical terminology of laced struts applies also for the case of battened columns, with the difference that diagonal bars are absent and transverse members (battens) are rigidly connected to the flanges.

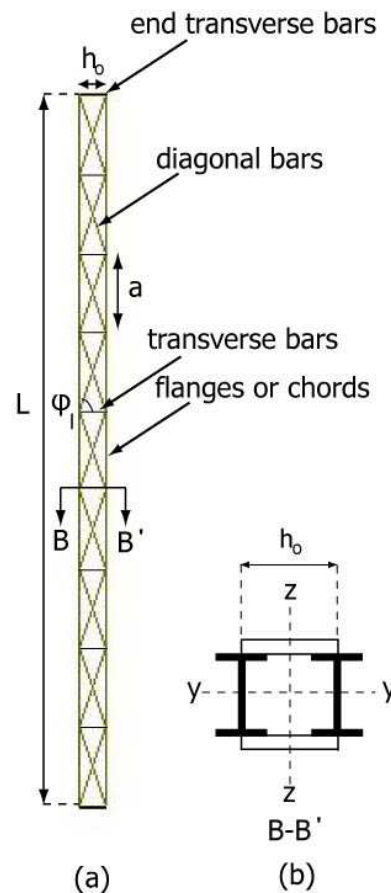


Figure 2-1: (a) Typical laced built-up column and (b) its cross-section B-B'

The buckling of an elastic perfect column under axial compressive load was initially mathematically investigated by Euler [2-1]. The distinction of the behaviour between stocky and slender columns was made by Tetmajer [2-2] who proposed that Euler's formula could be applied in the elastic region of slender members. Engesser [2-3], [2-4] was the first one to incorporate into the elastic critical buckling load of built-up columns the effect of both bending and shear deformations. His theoretical analyses on battened columns resulted in analytical formulas, which take into consideration the deformations of battened column's counterparts. Until today, one of the existing methods for incorporating shear deformations in buckling analyses bears his name.

Emperger [2-5] published the results of tests on flat ended riveted battened built-up columns, concluding that the action of the column as a whole can be achieved with double riveted batten plates, while single riveted battens were unable to transfer shear from one chord to another. The author also concluded that the capacity of a built-up member could not be larger than the equivalent solid column's as a whole whatever the strength of the lacing bars. Krohn [2-6] analyzed battened built-up columns considering that the totally applied load was unevenly distributed between the two

chords as the column deflected. Additionally, he proposed that the shear force transferred to the battens at the ends of a simply-supported column could be calculated by considering a sinusoidal deflection.

Müller-Breslau [2-7] worked on eccentrically loaded battened built-up columns, considering them as homogeneous members in cases of more than four panels and sufficiently stiff battens. Surprisingly, one of his conclusions was that the effect of shear on the capacity of battened members was negligible. This is incorrect, as today it is well-known that built-up members may be susceptible to significant shear deformations capable of reducing their bearing capacity. In 1910, Talbot and Moore [2-8] presented an experimental effort related to the investigation of steel and wrought-iron built-up columns' behaviour under load. The research aimed at determining experimentally the variation of compressive stresses and strains along the length of the chords and other components. It is interesting that the concepts of local non-straightness and non homogeneity of the material were clearly mentioned by the authors.

With the aid of the American Railway Engineering Association in 1918, tests were performed [2-9] on battened steel columns with flat ends, investigating the effect of the panels' length on the capacity. They concluded that the larger the unrestricted panels' length, the smaller the overall strength of the column, highlighting that the local behaviour affected the overall one. Furthermore, the American Society of Civil Engineers in 1927 supported the performance of a few more tests [2-10] on eccentrically loaded battened members examining the case of opposite eccentricities, too. They verified that battened columns were suitable for use in cases of small eccentricities and therefore of small shear forces. On the contrary, large shear forces caused significant shear deformation resulting in excessive local bending of the chords and of the battens.

Petermann [2-11] published the results of tests conducted by Müller-Breslau, observing large variations when comparing them with empirical calculation procedures. In 1931 the same author [2-12] reported experimental results of ten more battened columns based on which he recommended local slenderness ratios for the panels. In 1936, Timoshenko [2-13] provided a theoretically based formula for the calculation of the elastic critical buckling load of built-up columns accounting for the effect of the flexibility of battens and chords on the shear rigidity of the built-up members.

In 1940, Holt [2-14] published tests on fifteen built-up columns of structural aluminium alloys and two of structural steel. He investigated the effect of the shape of section on the strength of built-up columns. It is worth mentioning that he noticed failure by local buckling at stresses less than the material's yield strength for relatively large width-to-thickness ratios. Ng [2-15] in his doctoral thesis tested battened columns with various panel lengths and with welded joints instead of riveted ones as in previously mentioned tests. He drew qualitative conclusions on the capacity's decrease in cases of larger panels and suggested that the slenderness ratio of the unrestricted panels should not exceed 50. Furthermore, he concluded that the numerous welds did not significantly affect the strength of the columns.

Pippard [2-16] worked on a battened built-up column and considered the effect of the battens as similar to that of a continuous web that offered only flexural restraint to the chords in elevation and did not contribute to the second moment of inertia of the built-up cross-section. It is interesting to note that Pippard came to the conclusion that the larger the number of battens (and the smaller the panels' length), the smaller the column's capacity. This is surprising, as a large number of battens leads to reduction of shear deformations and strengthening of the local behaviour (as the panels' lengths decrease and they become stocky), resulting in solid column behaviour with larger capacity.

Bleich [2-17] presented a closed-form solution for the critical load of battened members, making the assumption that points of inflection appear at the middle of the panels' and battens' length

(Vierendeel truss). In order to ensure that the local behaviour would not be more critical than the global one, Bleich recommended that the local slenderness should be smaller than the global one. Additionally, he assumed a sinusoidal deformed shape and proposed that the battens should be designed for a shear force corresponding to the deflection for which the column's concave side yielded. As will be later shown, modern design codes adopted formulas based on the philosophy behind Bleich's formula.

Koenigsberger et al. [2-18] performed tests on battened members and concluded that the optimum ratio of local to global slenderness was 0.4 for riveted members and 0.47 for welded ones. They also mentioned that the local slenderness should be calculated with an effective buckling factor of 1 for riveted joints (Figure 2-2(a)) and 0.85 for welded joints (Figure 2-2(b)), accounting in this way for the flexural restraint that the rigid connections would offer in local buckling. Their method for calculating the collapse load was in good agreement with their tests and with the tests performed by Müller-Breslau [2-7].

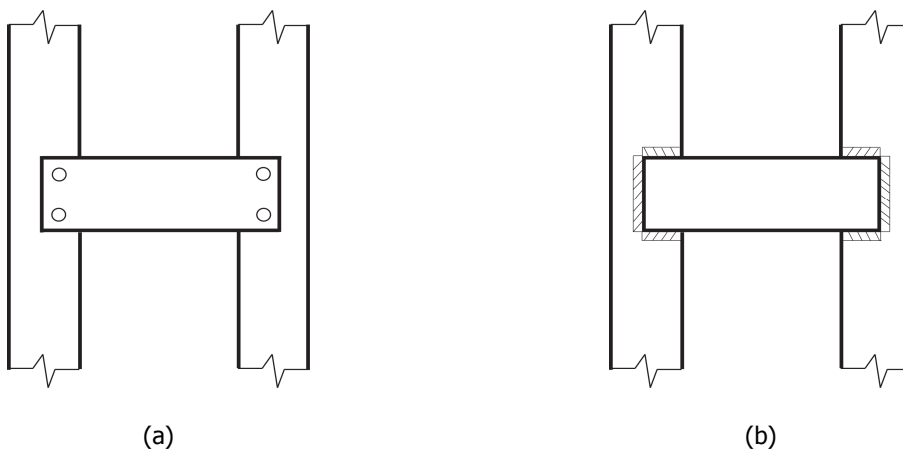


Figure 2-2: Connection of batten to chords (a) with rivets and (b) with perimetrical welding

Mohsin [2-19] worked analytically on the behaviour of battened members under eccentric loading and concluded that the elastic critical buckling load of such members depended on the load's eccentricity unlike to solid columns. This conclusion seemed to be valid, as loading one chord more than the other resulted in different response between them. Nevertheless, it should be mentioned that the modern design concept states that elastic critical buckling loads should be related to elastic perfect columns under concentric loading, and that any existing load eccentricities should be taken into account by using second-order analysis.

Klöppel and Uhlmann [2-20] performed an extensive experimental and analytical study of eccentrically loaded simply-supported battened columns and investigated the effect of various parameters on the response and capacity, such as the panels' length, the residual stresses, the magnitude of eccentricity and the lever arm between the chords. They concluded that battened members exhibit elastoplastic behaviour, which could be taken into account in an elastic procedure by either incorporating or omitting the moment of inertia of the chords in calculating the moment of inertia of the whole built-up column. They also mentioned that in columns with flanges that are continuously interconnected with the web, larger slendernesses led to larger effect of plasticity. This comes in contrast with the case of solid members, for which plasticity plays a more significant role for small values of slenderness. Additionally, they concluded that residual stresses due to welding between battens and chords do not have a significant effect on load carrying capacity. They summarised that the possible types of failure are:

- Failure of the panels due to bending and axial force.

- Failure of the battens due to bending and shear force.
- Panel mechanism, when the shear force is significant at the ends of a simply-supported column and four plastic hinges appear at the four ends of the critical panels.

Klöppel and Ramm [2-21] examined analytically and experimentally the behaviour of 43 eccentrically loaded simply-supported laced columns with various types of lacing. Apart from investigating factors like the ones mentioned in the previous publication, they searched for the effect of residual stresses due to welding between lacing bars and chords, as they observed that in the joints between lacing members and chords, premature plastification took place. For that purpose, they tested 3 columns with annealing in order to eliminate the magnitude of welding residual stresses, concluding that they do play a role and that in practice denser lacings may result in loss of stiffness and strength. The same authors [2-22] worked also on the behaviour of laced columns with four chords, which are commonly used for constructing crane booms. Ramm and Uhlmann [2-23] summarized the previously mentioned publications' results and proposed simple analytical procedures for checking the capacity of built-up members in practice. Their procedures became the basis for the analysis and design of built-up columns in Eurocode 3 [2-24] and will be thoroughly explained in the following sections.

Vroonland [2-25] and Brolin et al. [2-26] worked on latticed crane booms under axial and lateral load and noted that failure took place in the tests when the compressive force in a chord reached the failure load of the unrestricted length between the joints. This conclusion will be the basis of the present doctoral thesis for the design of laced columns, as will be presented in the following chapters. Lin et al. [2-27] used a non-dimensional factor for the constant shear flexibility of battened and laced members with end rigid stay plates and derived a system of second-order slope-deflection equations under distributed line load. Hinges were assumed at the joints in laced struts and in the middle of the panels' and battens' length in battened members.

Toossi [2-28] investigated the out-of plane buckling of battened built-up columns by converting the discrete problem to a continuous one. He proposed a general relationship between the external loads and the cross-section's properties for this type of instability. Porter and Williams [2-29] treated battened columns as an assembly of cells and with the use of stability functions formed the stiffness matrix of the structure, finally used for the calculation of the exact elastic critical buckling load. A major advantage of this procedure was the fact that cells could have different characteristics in elevation, facilitating the analysis of non-uniform built-up members. A significant disadvantage was related to the cumbersome calculation process.

Halabia [2-30] in his doctoral thesis continued the work of the previous authors [2-29] and examined the behaviour of uniform and non-uniform battened columns under concentric or eccentric loading from a theoretical and an experimental point of view. He came up with conclusions related to possible types of failure of such columns (excluding any type of failure in battens), which were summarised as:

- Single central hinge in a bending mode corresponds to the type in which failure initiates from the middle cross-section of a simply-supported battened column due to the appearance of a plastic hinge. This type of collapse mechanism is equivalent to the solid columns type of failure. It is expected in types of battened columns with relatively small panels' length (small intervals between battens).
- Panel mechanism appears due to significant shear forces that result in significant bending moments at the panels' ends and consequently to the formation of plastic hinges. In battened columns with varying panels' length, the panel mechanism is expected in the largest panel. The author pointed out that this mechanism is not usually a primary one and it appears at the post-buckling branch of the equilibrium path.

- Four hinge short cell mechanism appears in cases with short cells due to the formation of three plastic hinges at the ends and middle of the critical panels.
- Four hinge long cell mechanism appears in some cases, when a panel's length is much larger than the length of the other panels.
- Three hinge short cell mechanism appears either in the elastic or in the elastoplastic range due to the formation of three plastic hinges that in the deformed configuration all lie on the same straight line. This type of failure is exhibited either prior to any other collapse mechanism (and therefore is the critical one) or in the post-buckling range (more often).

A computer program used for the calculation of elastic critical buckling load and failure load of battened members was developed for the prediction of the failure modes. Halabia additionally proposed ways for incorporating his findings into the pertinent British codes of practice, which make use of Ayrton-Perry's formula.

Gjelsvik [2-31] used the main concept of Engesser's theory for investigating the elastic buckling of built-up columns with end stay plates. End stay plates prohibit the appearance of shear deformations at the ends of the column and, using a layered sandwich cross-section, he obtained a sixth-order differential equation, which was convenient for applying the two additional boundary conditions. The model's chords sustained axial forces, shear forces and bending moments, while the web was loaded by shear forces. The results were given in the form of graphs, facilitating their use from engineers of practice. A main conclusion was that the existence of end stay plates provides significant increase in the elastic critical buckling load of built-up columns. This increase is much larger for more shear-weak members and for columns with small ratio between overall second-moment of inertia and second-moment of inertia of the single chord. Therefore, it can be concluded that end stay plates are more useful in battened members rather than in laced ones.

Paul expanded Gjelsvik's procedure for other possible boundary conditions and considered that the column's web could also transmit axial forces and bending moments, making the model applicable to built-up columns with continuous web. His experimental findings [2-32] showed good agreement with analytical results [2-33] and the Engesser's method without the effect of end stay plates was always on the safe side. Ermopoulos et al. [2-34] investigated built-up columns with linear variation of depth with various practical support conditions and analysed them as rigid-jointed frameworks. By performing rigorous analyses they obtained critical buckling loads and assessed the effect of many parameters, such as the degree of non-uniformity, number of panels, stiffness and length of components on them. Chang and Sher [2-35] presented a numerical procedure for the elastoplastic post-buckling behaviour of perfect and imperfect built-up columns. As a model they considered two slightly separated identical members connected at their ends and middle with rigid links.

Sahoo and Rai [2-36] tested battened cantilevers under constant axial load and gradually increasing lateral force. The formation of the plastic hinge was expected at the base of the specimens. The configuration of the battens varied by considering constant batten intervals in elevation, denser arrangement of battens in the region in which plastic hinge formation was expected, and box-type cross-section in the plastic hinge region. The authors concluded that reducing the panels' length in critical regions (i.e. at the beam-columns' ends) or creating a box-type cross-section proved beneficial in terms of energy dissipation, lateral stiffness, lateral strength and moment rotation characteristics. They pointed out that the significant weaknesses of battened members (relatively small lateral stiffness and capacity) that make them inappropriate for use in seismic areas can be overcome with these modifications. Views of Sahoo and Rai's specimens after failure are depicted in Figure 2-3. It can be seen that the local lateral deflections of the chords in the first case were much larger than the ones in the two latter cases.

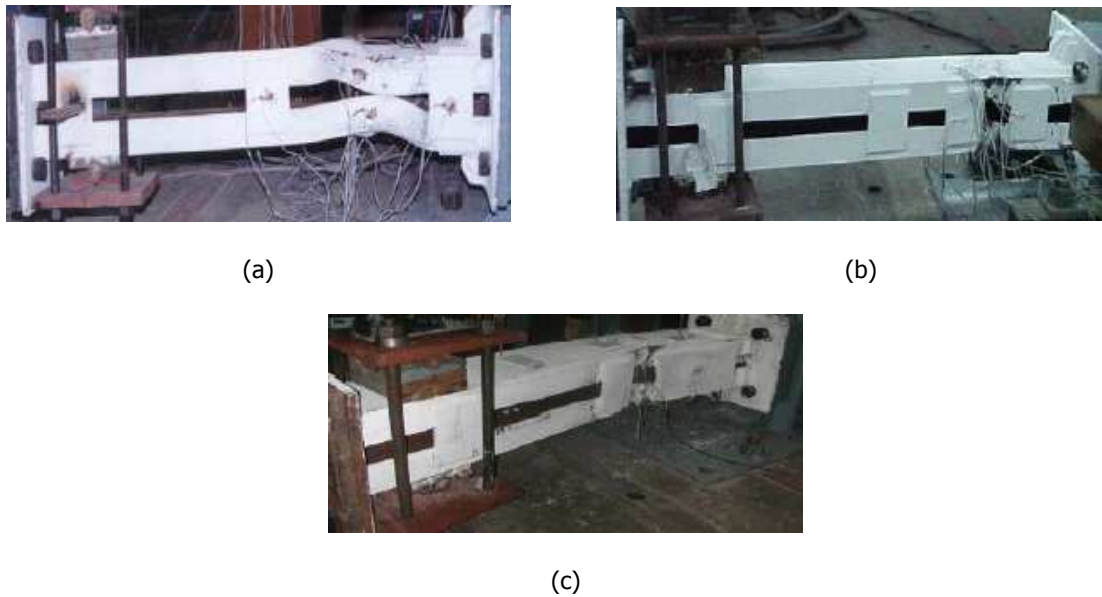


Figure 2-3: Specimens with (a) constant distance between battens, (b) denser arrangement of battens in the expected plastic hinge region and (c) box-type cross-section in the expected plastic hinge regions after failure [2-36]

Lee and Bruneau investigated both experimentally [2-37] and analytically [2-38] the seismic performance of built-up laced steel brace members. Quasi-static testing of 12 columns was conducted and the data were used for drawing conclusions regarding ductility, energy dissipation, capacity and strength degradation after buckling for different global and local slenderness ratios. The global in-plane buckling of one of their laced built-up specimens is depicted in Figure 2-4. Richard et al. [2-39] performed elastic time history analyses on planar single-story moment-resisting frames with fixed base supports of their laced built-up columns. They concluded that the median horizontal displacements and accelerations were well predicted by the code equivalent static force procedure and response spectrum method. They additionally observed that inelastic buckling at the base of such structures may take place, leading to structural response characterised by low ductility.



Figure 2-4: Global in-plane buckling of laced built-up specimen [2-37]

Hashemi and Jafari [2-40] presented a brief review of the behaviour and failure modes observed in battened columns after the Bam earthquake in 2003, concluding that insufficient design provisions for such members resulted in an excessive amount of failures. The main failure types were summarized as overall buckling, local buckling, lateral-torsional buckling, rupture of battens, rupture of battens' welds, plastic shear deformation of battens and splice failures. Hashemi and Jafari [2-41] evaluated

experimentally the elastic critical buckling load of battened columns with end stay plates and proposed a modified Southwell plot [2-42] accounting for interaction between global and local buckling, as will be discussed in the following section. They concluded that Paul's method [2-32], [2-33] gave the most satisfactory results when compared with tests. The same authors [2-43] used Ayrton-Perry formula and ultimate capacity curves for predicting the collapse load of battened struts and concluded that the first one was conservative and the second one against safety, suggesting that a mean value of the two should be better considered. The same authors [2-44] performed cyclic tests on battened cantilevers subjected to axial and lateral point loads. Their main conclusion was that their use should be avoided in high seismicity areas due to their relatively low ductility.

Guo and Wang [2-45] worked on the instability behaviour of axially loaded simply-supported prismatic multi-tube latticed steel columns depicted in Figure 2-5. They proposed simple formulas for the calculation of their slenderness ratio in practical design. Razdolsky [2-46], [2-47], [2-48] investigated the elastic critical buckling load of laced columns with two different lacing types by considering the column as a statically indeterminate structure. To that effect, he proposed an analytical procedure which was capable of capturing both global and local buckling modes.

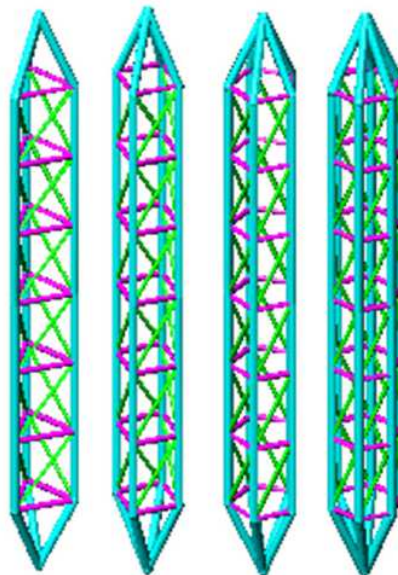


Figure 2-5: View of the different prismatic multi-tube latticed columns that Guo and Wang [2-45] worked on

Bonab and Hashemi [2-49] performed a numerical investigation of the cyclic behaviour of laced columns by using cantilevers laterally and axially loaded. In their conclusions they mentioned that the higher the applied axial load the lower the available ductility, and that the behaviour of laced columns was significantly affected by internal bending moments in the chords. Bonab et al. [2-50] investigated experimentally the elastic buckling load and collapse load of centrally compressed laced built-up columns and proposed a slightly modified Southwell plot for accounting for shear deformations. They concluded that Engesser's method for accounting for shear deformations and calculating the critical load was in the best agreement with experimental results. Additionally, they found that applying Ayrton-Perry formula to the built-up column considered as a whole for the evaluation of the collapse load gave conservative results, while the use of ultimate capacity curves resulted in unsafe ones.

2.3 INTERACTION BETWEEN GLOBAL AND LOCAL BUCKLING

Solid columns consist of plates continuously interconnected between each other. This interconnection guarantees cooperation between the plates but local buckling of cross-sections' plate components may appear and affect the global response. Cross-sections prone to local buckling are unable to develop their full plastic capacity and cross-section classification aims at accounting for local buckling in Eurocode 3 and other codes. In a similar manner, built-up columns consist of many local counterparts that cooperate and form a unity and therefore, global behaviour where built-up members act as a whole may be affected by the local behaviour of their counterparts. Publications related to this type of problem will be presented in the present section.

Global and local buckling mode shapes of a typical simply-supported laced column are shown in Figure 2-6. The global buckling mode is related to the global buckling load (Figure 2-6(a)), at which the whole column deflects from its perfect and straight configuration. If the lacing is very stiff, this load would be the Euler buckling load of the system:

$$P_E = \frac{\pi^2 EI_{eff}}{(KL)^2} \quad (2-1)$$

where EI_{eff} is the bending rigidity of the built-up column as a whole, K is the effective buckling length factor ($K=1$ for simply-supported columns) and L is the length of the column. In case of significant shear deformation, Eq. (2-1) should be modified accordingly.

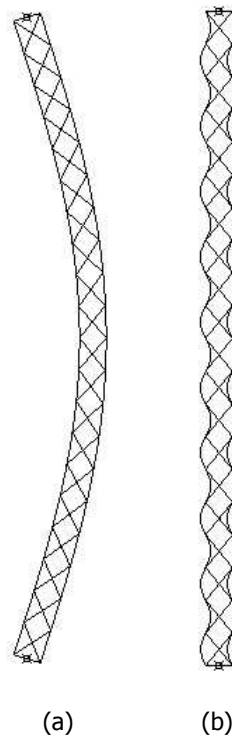


Figure 2-6: (a) Global buckling mode of simply-supported laced column and (b) local buckling mode

The local buckling mode is related to the individual buckling of the panels as simply-supported columns between lacing joints (Figure 2-6(b)). The local buckling load is given by the summation of the buckling loads of each chord's panels individually:

$$P_L = \frac{2n^2 EI_{ch,z}}{a^2} \quad (2-2)$$

where $EI_{ch,z}$ is the in-plane bending rigidity of each chord and a is the length of each panel (distance between connectors). The local buckling load may be somewhat larger than the one calculated with Eq. (2-2) in battened built-up columns due to the rotational stiffness that relatively stiff battens will offer at the ends of the panels. From the above description, it can be concluded that local buckling in built-up members does not refer to the local buckling in cross-sections' plate components.

The squash load is the third possible type of failure of perfect built-up columns and is given by:

$$P_Y = 2A_{ch} f_y \quad (2-3)$$

where A_{ch} is the cross-sectional area of each chord and f_y is the yield stress of the material. The prevailing failure mode of perfect built-up columns neglecting mode interaction and nonlinear effects would thus be the one corresponding to the smallest of the loads calculated by Eqs. (2-1), (2-2) and (2-3).

From a theoretical point of view Van der Neut [2-51] was the first one to work on an idealized compression member consisting of two thin-walled flanges and a web that maintained the integrity of the structure. Koiter and Kuiken [2-52] addressed the same problem using the same cross-section and by making use of potential energy expressions and orthogonalised buckling modes, showed that "naive" optimization associated with equal global and local buckling loads leads to a large loss of capacity due to buckling mode interaction in the presence of initial imperfections. This result is in accordance with Koiter's 1/2 power law [2-53].

Thompson and Hunt [2-54] obtained, following a linearised "smearing" analysis, the same set of indices as the ones found by Koiter. Miller and Hedgepeth [2-55] worked on the detrimental effect of global and local imperfections on built-up struts. Their results were presented in charts illustrating the reduction of the elastic critical load as a fraction of the Euler critical load of perfect members. Crawford and Hedgepeth [2-56] and Crawford and Benton [2-57] obtained similar results to the ones obtained by the previous authors.

Svensson and Kragerup [2-58] confirmed the previous results and extended them concluding, by means of elastic analyses up to yielding, that the largest loss of capacity happens when local and global Euler critical stresses and the yield stress coincide. This reduction in capacity becomes prominent in the presence of initial imperfections, reaching magnitudes of 50%. A graphical representation of the imperfection sensitivity in elastic built-up columns is shown in Figure 2-7. On the horizontal axis the ratio between the global and local buckling loads is depicted, while on the vertical one the ratio between the governing critical load P and the local buckling load is shown. Both the perfect and imperfect structures' responses are plotted. It is clear that when the two buckling loads coincide ($P_{cr}/P_L=1$), the decrease of load P due to the existence of initial imperfections is much larger than for other ratios of P_{cr}/P_L . For ratios P_{cr}/P_L larger than unity the decrease is moderate, while for ratios less than one the smallest decrease is observed.

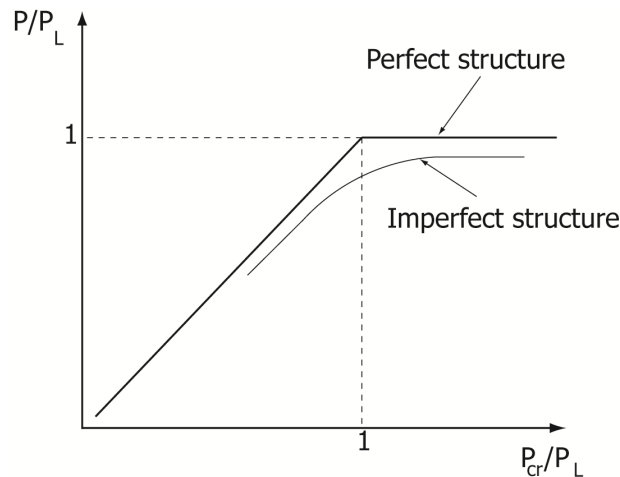


Figure 2-7: Graphical representation of the imperfection sensitivity in built-up columns

Tong and Chen [2-59] confirmed the unfavourable mode interaction in centrally compressed built-up columns using the assumptions by Svensson and Kragerup but still assuming elastic material. They additionally proposed an iterative procedure for calculating the collapse load of such members. Duan et al. [2-60] investigated the effect of compound buckling on the compression strength of elastic built-up members and performed extensive parametric studies for identifying cases in which this effect is important. They showed that code provisions that do not account for mode interaction result in unsafe results.

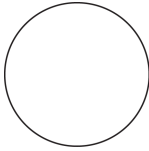
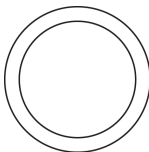
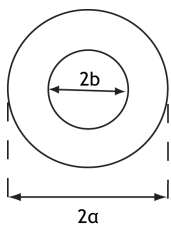
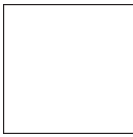
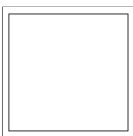
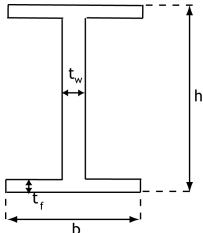
2.4 THE EFFECT OF SHEAR DEFORMATIONS

2.4.1 Shear deformable solid members

In solid columns bending, shear and axial deformations coexist but the effect of the last two on the response and capacity allows for their omission (Euler-Bernoulli members). In columns with either short length or large bending rigidity or small shear rigidity or a combination of the previous cases, the effect of shear deformations cannot be neglected, as they may be of comparable magnitude with bending deformations. Shear deformable columns are also called Timoshenko columns and compared with Euler-Bernoulli members have smaller critical loads and exhibit larger second-order effects.

The calculation of bending rigidity is related to the elastic modulus E and the second moment of inertia of the cross-section I . Shear rigidity for solid cross-sections is defined as the product of shape factor k (also called shear correction factor), the area of the cross-section A and the shear modulus G . The shape factor is inserted in the shear rigidity in order to account for the non-uniformity of the shear stresses over the cross-section. Cowper [2-61], [2-62] provided accurate predictions of shape factors depending on the geometrical characteristics of the cross-section and the material properties. He suggested for example that the shape factor for solid rectangular steel sections is equal to 0.83 while for rectangular hollow steel sections it is taken as 0.153, coming up with the conclusion that the second ones are more susceptible to shear deformations. Typical values of shape factors for various cross-sections in terms of the Poisson ratio ν of the material according to Cowper are given in Table 2-1.

Table 2-1: Shape factor for various cross-sections according to Cowper [2-61]

Description of cross-section	Cross-section	Shape factor
Circular		$k = \frac{6(1+\nu)}{7+6\nu}$
Thin-walled CHS		$k = \frac{2(1+\nu)}{4+3\nu}$
CHS		$k = \frac{6(1+\nu)(1+m^2)^2}{(7+6\nu)(1+m^2)^2 + (20+12\nu)m^2}$, $m = b/a$
Square		$k = \frac{10(1+\nu)}{12+11\nu}$
Thin-walled SHS		$k = \frac{20(1+\nu)}{48+39\nu}$
I section		<p>Shear force parallel to the weak axis: $k = \frac{A_w}{A}$</p> <p>Shear force parallel to the strong axis: $k = \frac{2A_f}{1.2A}$</p> <p>A=total cross-sectional area, A_w=web's area, A_f=flange's area</p>

Scheer and Plumeyer [2-63] concluded that the non-dimensionless ratio $1/\mu$ could be indicative of the importance of shear deformations in structural analyses:

$$\frac{1}{\mu} = \frac{kAGL^2}{EI} \quad (2-4)$$

Based on a parametric study, they showed that the work done by the shear forces should be taken into account for values of $1/\mu$ smaller than 115 for determinate and 385 for indeterminate structures.

Based on this criterion, it can be concluded that indeterminate structures are much more susceptible to shear deformations than determinate ones.

Built-up columns are usually susceptible to significant shear deformations. To be more specific, laced columns have reduced shear rigidity due to the lacing, while the large lever arms between the flanges lead to large bending rigidities. Therefore, despite the fact that their length is relatively large, they are subjected to significant shear deformations. Similarly, battened columns are generally characterized by even smaller shear rigidity than laced struts and despite the fact that their length is usually large and their bending rigidity relatively small, they are also prone to shear deformations. Both are characterized by small values of $1/\mu$. For four typical I cross-sections subjected to shear parallel to their strong axis, the values of factor μ are plotted against the length of the column in Figure 2-8. It can be seen that factor μ becomes large (and therefore $1/\mu$ small) for small columns' lengths and for cross-sections with relatively large bending rigidity. In such cases shear deformations play an important role and should be taken into account. For built-up members, factor μ usually varies between 0.001 and 0.1 highlighting that the importance of shear deformations in such members is large.

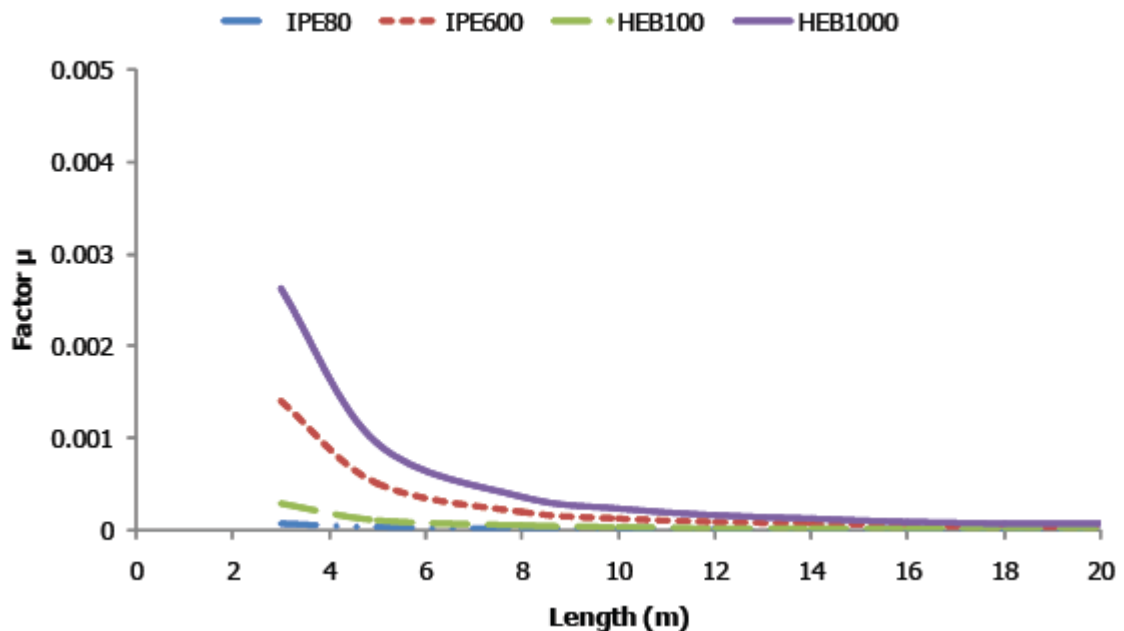


Figure 2-8: Effect of column's length on factor μ for four typical I cross-sections

For a typical column with length equal to 23.8m and a steel cross-section HEB450 subjected to shear forces parallel to its weak axis (bending about its strong axis), the value of $1/\mu$ is approximately equal to 1700 ($\mu=0.00059$) showing that shear deformations are not significant, whether it belongs to a determinate or an indeterminate structure. For the same column the use of two steel cross-sections HEB450 at a distance equal to 40cm between each other in order to form a laced built-up column modifies its susceptibility to shear deformations. The use of typical lacing systems can lead to values of $1/\mu$ that vary from 50 to 100 showing that the incorporation of shear deformations in its structural analysis is necessary.

2.4.2 Engesser's theory

Engesser [2-3], [2-4] was the first to include in the calculation of the elastic critical buckling load of columns the effect of both bending and shear deformations, by incorporating in the differential equation provided by Euler an additional term of curvature due to shear deformations. The stability

problem of a Timoshenko simply-supported column is briefly described afterwards. A perfect and elastic simply-supported column under an axial load P is shown in its undeformed and buckled configuration in Figure 2-9. The column is characterised by bending rigidity EI and shear rigidity S_v . The longitudinal axis is denoted as x and the transverse one as w . It can be seen that the transverse deformation depends on the location along the longitudinal axis.

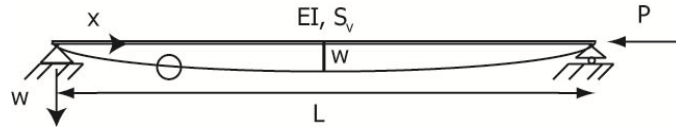


Figure 2-9: Undeformed and buckled configuration of Timoshenko column under compressive force P

A close view of the circled region is shown in Figure 2-10 in which the deformed axis KK' is rotated by w' in relation to the horizontal axis if the differentiation with respect to the longitudinal axis x is denoted as prime. Cross-section BB' is perpendicular to the deformed axis KK' , while cross-section AA' corresponds to rotation due to bending only, ψ . In Timoshenko beam theory, the total rotation of the cross-section w' consists of two parts:

$$w' = \psi + \gamma \quad (2-5)$$

where ψ is the rotation due to bending only and γ is the shear deformation. In Euler-Bernoulli theory the two cross-sections AA' and BB' coincide, as the total rotation is only due to bending and shear deformation is considered equal to zero.

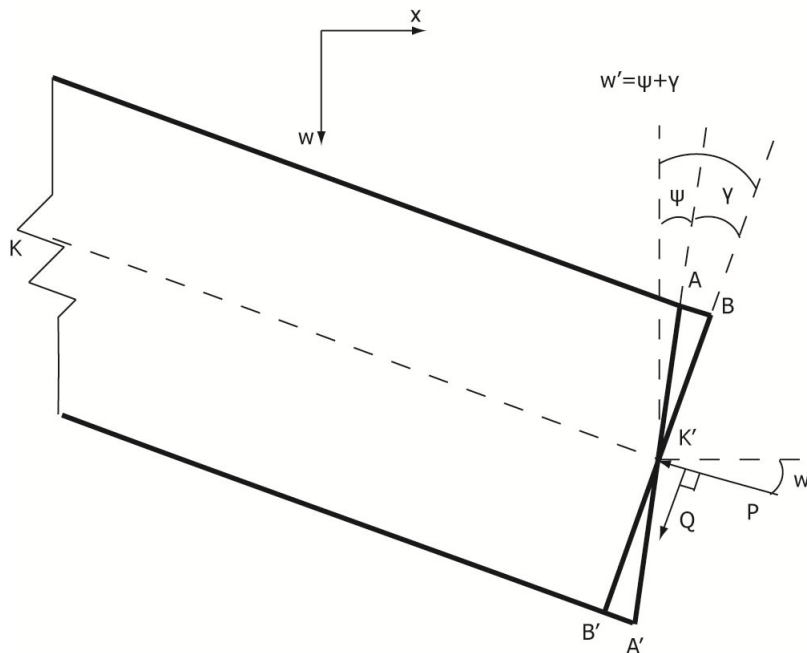


Figure 2-10: Deformed cross-sections and applied forces according to Engesser's theory

The axial force applied P is approximately equal to the one which is perpendicular to cross-section BB' , as the cosine of the total rotation w' is close to unity, while the shear force perpendicular to the deformed axis is denoted as Q . It can be seen that the deformed axis KK' is no longer perpendicular to the rotated due to bending cross-section AA' , while the assumption that plane sections remain plane is still valid. The equilibrium of infinitesimally small parts of the Timoshenko member with their cross-sections perpendicular to the deformed and undeformed axes are shown in Figure 2-11(a) and

(b), respectively, in which M is used for internal bending moment and V for the shear force perpendicular to the undeformed axis.

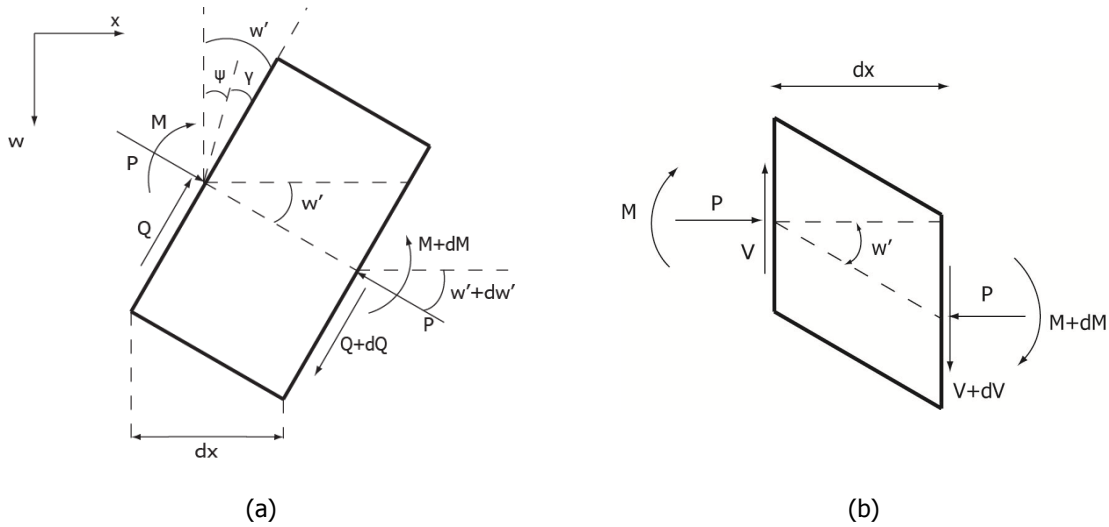


Figure 2-11: Infinitesimally small parts of a Timoshenko member with their cross-sections perpendicular to the (a) deformed axis and (b) the undeformed axis

The external bending moment along the longitudinal axis x due to the applied axial force considering the column's deformed configuration is:

$$M(x) = Pw(x) \quad (2-6)$$

The internal bending moment as a function of curvature due to bending only is given by:

$$M(x) = -EI\psi'(x) \quad (2-7)$$

For simplicity reasons, parameters depending on the examined location along the longitudinal axis will be next denoted only with their symbol (i.e. $M(x) = M$). By equating the external and internal bending moments based on Eqs. (2-6) - (2-7) the expression of curvature due to bending can be obtained as a function of the transverse deflection:

$$\psi' = -\frac{Pw}{EI} \quad (2-8)$$

The shear force perpendicular to the deformed axis Q can be found by considering equilibrium in the column's part shown in Figure 2-11(a) as:

$$Q = \frac{dM}{dx} \quad (2-9)$$

From Eqs. (2-6), (2-7) and (2-9):

$$Q = -EI\psi'' = Pw' \quad (2-10)$$

Considering that shear deformation γ is equal to the shear force Q divided by the shear rigidity of the column S_v the following expression arises:

$$\gamma = \frac{Pw'}{S_v} \quad (2-11)$$

The shear force perpendicular to the undeformed axis V can be found from equilibrium in the column's part depicted in Figure 2-11(b) as:

$$V = \frac{dM}{dx} - Pw' \quad (2-12)$$

The expression of Eq. (2-12) can be modified with the use of Eq. (2-10) as:

$$V = -EI\psi'' - Pw' = Q - Pw' \quad (2-13)$$

Eq. (2-5) by differentiation with respect to x and based on Eqs. (2-8) - (2-11) gives the differential equation with respect to the total deflection w that controls the problem:

$$\frac{\partial^2 w}{\partial x^2} = \frac{P}{S_v} w'' - \frac{P}{EI} w \quad (2-14)$$

which can be written:

$$w'' \left(1 - \frac{P}{S_v} \right) + \frac{Pw}{EI} = 0 \quad (2-15)$$

Eq. (2-15) is valid for a simply-supported column as the number of constants in the solution can satisfy its boundary conditions and its general solution in sinusoidal form is:

$$w(x) = A_1 \sin(\alpha x) + A_2 \cos(\alpha x) \quad (2-16)$$

where A_1 and A_2 are integration constants,

$$\alpha^2 = \frac{P}{EI\beta} \quad (2-17)$$

and

$$\beta = \left(1 - \frac{P}{S_v} \right) \quad (2-18)$$

Eq. (2-16) is sufficient for Euler-Bernoulli members for which only bending deformations are significant if the shear rigidity is set equal to infinity, but this is not the case in Timoshenko columns for which an additional differential equation should be used, with respect either to the rotation due to bending only ψ or to the shear deformation γ .

Using Eq. (2-5) and solving Eqs. (2-8) and (2-11) for w' the following equation is obtained:

$$-\frac{EI\psi''}{P} = \psi + \frac{P}{S_v} \left(-\frac{EI\psi''}{P} \right) \quad (2-19)$$

Rearrangement of Eq. (2-19) gives:

$$EI\psi''\left(1 - \frac{P}{S_v}\right) + P\psi = 0 \quad (2-20)$$

Observing Eqs. (2-15) and (2-20) one can realise that the only difference from the classical Euler-Bernoulli differential equation is the factor $1 - P/S_v$. The elastic critical buckling load of a simply-supported column according to Engesser's theory is equal to:

$$P_{cr,E} = \frac{P_E}{1 + \frac{P_E}{S_v}} = \frac{1}{\frac{1}{P_E} + \frac{1}{S_v}} \quad (2-21)$$

where P_E is the Euler critical buckling load of the same column. This solution can be found in many structural textbooks and based on it, it can be concluded that if shear rigidity becomes very large and shear deformations are negligible, one obtains the Euler buckling load. Additionally, it can be seen that for very short columns characterised by a very large Euler critical load, the critical load according to Engesser's theory approaches their shear rigidity.

2.4.3 Haringx's theory

In 1925, Biezeno and Koch [2-64] used Engesser's approach for the stability of helical springs under compression and they found divergence of the theoretical results from the experimental ones, which questioned its validity. To be more specific, experiments showed that very short helical springs could never buckle in practice, while Engesser's approach stated that their critical buckling load would be equal to their shear rigidity. In order to overcome this problem, a few years later in 1948 Haringx [2-65], [2-66], proposed a different method known in the literature as "Modified Approach". The theoretical results obtained with this procedure were in good agreement with the experimental ones for helical springs and the Modified Approach was commonly accepted in the field of mechanical engineering. A brief description of the applicability of Modified Approach to a Timoshenko simply-supported column is presented next.

The main difference of the concept behind the Modified Approach is that the shear force Q is no longer perpendicular to the deformed beam axis but instead is applied to the rotated due to bending only cross-section AA' , as shown in Figure 2-12. The applied axial force P is no longer perpendicular to the deformed cross-section BB' and its angle with the horizontal axis is ψ . The divergence of the applied axial force P from the axis of the member's centre of gravity is depicted in Figure 2-12 and was characterised by Gjelsvik [2-67] as "wrong assumption".

The shear force Q becomes:

$$Q(x) = P\psi \quad (2-22)$$

It should be noted that the shear force Q is no longer the first derivative of the external bending moment.

The shear deformation γ becomes:

$$\gamma = \frac{P\psi}{S_v} \quad (2-23)$$

The shear force perpendicular to the undeformed axis is similar to the one in Engesser's theory:

$$V = Q - P\psi \quad (2-24)$$

Based on Eqs. (2-5), (2-23) and (2-24) the following expression can be obtained:

$$V = S_v (w' - \psi) - P\psi \quad (2-25)$$

By differentiating Eq. (2-5) once and using Eq. (2-23) the following differential equation with respect to the total deflection w is obtained:

$$\frac{\partial^2 w}{\partial x^2} = \psi' \left(1 + \frac{P}{S_v} \right) \quad (2-26)$$

Rearranging the terms in Eq. (2-26) the following equation is found:

$$w'' \left(\frac{1}{1 + \frac{P}{S_v}} \right) + \frac{Pw}{EI} = 0 \quad (2-27)$$

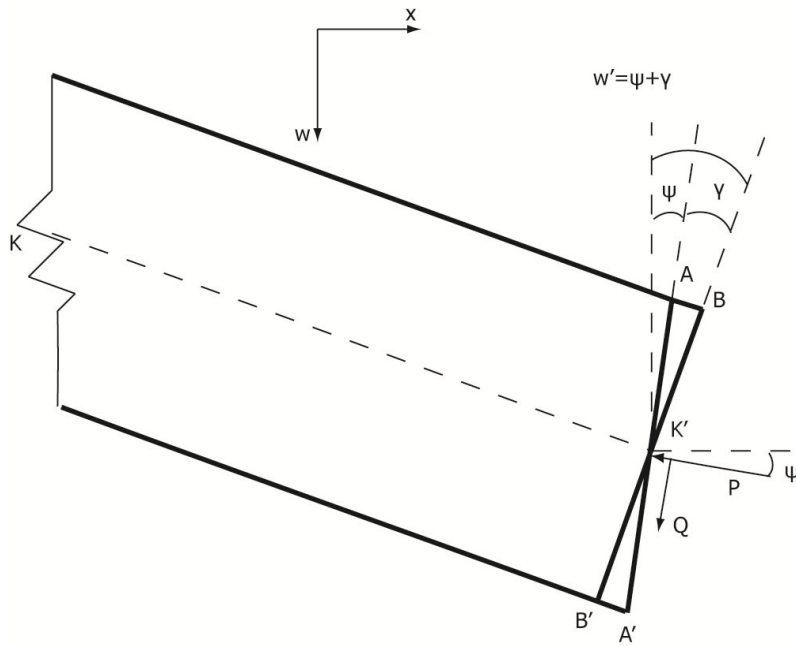


Figure 2-12: Deformed cross-sections and applied forces according to Haringx's theory

The solution of Eq. (2-27) is given in a sinusoidal form as:

$$w(x) = A_1 \sin(\alpha' x) + A_2 \cos(\alpha' x) \quad (2-28)$$

where A_1 and A_2 are integration constants,

$$\alpha'^2 = \frac{P\beta'}{EI} \quad (2-29)$$

and

$$\beta' = \left(1 + \frac{P}{S_v} \right) \quad (2-30)$$

By comparing Eq. (2-16) with Eq. (2-30) it can be seen that the difference is between the β and β' terms.

The differential equation with respect to ψ can be obtained with the use of Eq. (2-5), (2-8) and (2-23):

$$-\frac{EI\psi''}{P} = \psi \left(1 + \frac{P}{S_v} \right) \quad (2-31)$$

Rearranging Eq. (2-31) gives:

$$\psi'' \left(\frac{1}{1 + \frac{P}{S_v}} \right) + \left(\frac{P}{EI} \right) \psi = 0 \quad (2-32)$$

The elastic critical buckling load of a Timoshenko column according to Haringx's theory is equal to:

$$P_{cr,H} = \frac{-1 + \sqrt{1 + \frac{4P_E}{S_v}}}{\frac{2}{S_v}} \quad (2-33)$$

Eqs. (2-21) and (2-33) contain the same terms and have both been used for the calculation of built-up columns' critical loads. Timoshenko and Gere [2-68] stated that Eq. (2-33) is more appropriate for use in built-up columns despite the fact that it predicts a larger critical load. Nanni [2-69], Ziegler [2-70], Gjelsvik [2-67] and Blaauwendraad [2-71], [2-72] worked analytically on the applicability of the previously described methods to the analysis of Timoshenko members and concluded that Engesser's method is expected to approach reality in a better way. Bazant and Cedolin [2-73], [2-74] stated that both methods are equivalent if the definition of shear rigidity is different for each procedure. Bazant and Beghini [2-75], [2-76] investigated the applicability of the analytical procedures to the buckling of soft-core sandwich columns. They concluded that whenever a sandwich structure is in small strain and a constant shear modulus is used in the calculations, the Engesser theory should be preferred.

In general, formulas commonly used for shear rigidity correspond to Engesser's approach, while helical springs should be analyzed according to Haringx's theory. Commercial finite element software incorporates shear deformations in an approximate way, leading to results close to Engesser's method. It should be noted that the two methods of incorporating shear deformation differ only in the case of second-order analysis, while when no geometrical nonlinearity is considered they both lead to the same results.

A comparison between the critical loads obtained with Haringx's and Engesser's methods (Eqs. (2-33) and (2-21), respectively) is shown in Figure 2-13 for simply-supported Timoshenko columns with Euler critical buckling loads varying from 10000kN to 100kN. It can be seen that Eq. (2-33) yields always higher critical loads and that the difference between the two methods becomes larger as the shear

rigidity is reduced. Additionally, this divergence is much more important in cases that the Euler critical load is much larger than the shear rigidity.

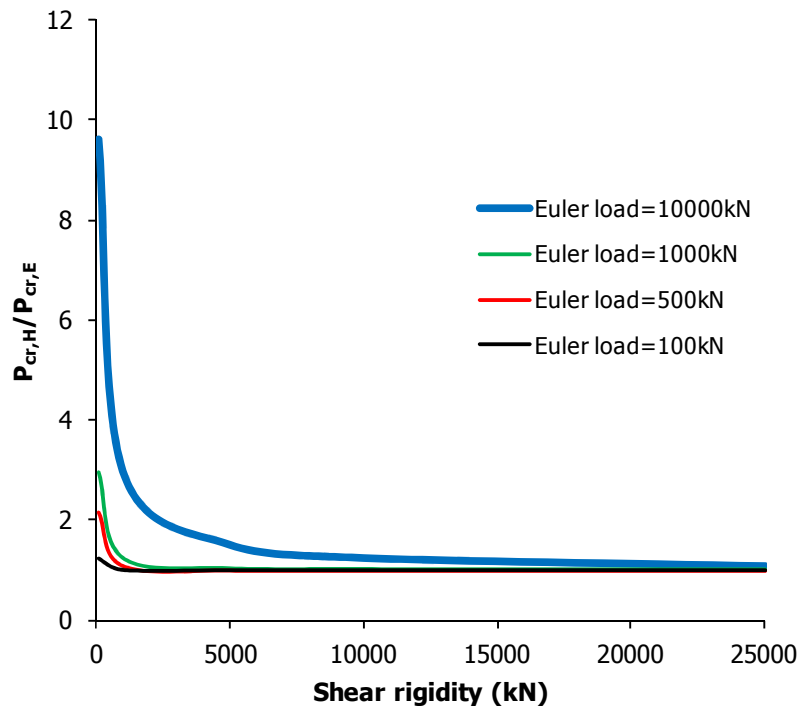


Figure 2-13: Comparison between Haringx's and Engesser's method

2.4.4 Application of Engesser's and Haringx's theories in research

Haringx's method was used by Kelly [2-77] in the buckling analysis under tension of elastomeric bearings. Aristizabal-Ochoa [2-78] proposed a stability matrix for evaluating the elastic buckling load of Timoshenko members with arbitrary supports based on Haringx's procedure. The same author [2-79] proposed first and second order slope-deflection equations suitable for the analysis of either determinate or indeterminate structures.

Aristizabal-Ochoa [2-80] also compared different analytical procedures for the buckling analysis of Euler-Bernoulli and Timoshenko members confirming the previously mentioned merits of each method, stating that Modified Approach is capable of capturing buckling under tension, too. He then [2-81] proposed a method for the large deflection and post-buckling behaviour of Timoshenko beam-columns with semi-rigid connections including axial effects. Finally, Aristizabal-Ochoa [2-82] expanded the matrix method for the stability and second-order analysis of Timoshenko beam-columns with semi-rigid connections.

Bryant and Baile [2-83] performed slope-deflection analysis on Timoshenko members under transverse loading. Absi [2-84] proposed a set of slope-deflection equations for Timoshenko members with rigid connections at their ends based on Engesser's method. Banerjee and Williams [2-85], based on Engesser's method, investigated the validity of Eq. (2-21) in columns with other boundary conditions, among them many standard cases. It was shown to be valid in standard cases such as hinged-hinged, clamped-free and clamped-clamped columns and in members with end rotational springs of equal stiffnesses. However, it is not valid for the common clamped-hinged case and for hinged-hinged cases with end rotational springs of unequal stiffnesses, with the discrepancy reaching in some cases a magnitude of 20%.

Marinetti and Olivetto [2-86] proposed a second-order numerical method for the analysis of frameworks consisting of Timoshenko members. Their nonlinear equations can be solved either with the method of successive approximations or with procedures of the Newton-Raphson type. The authors presented examples highlighting the significant effect of shear deformations in cases that built-up members are used.

Wang et al. [2-87] proposed an 8x8 matrix, providing exact stability criteria for Timoshenko columns with intermediate and end concentrated axial loads. Gengshu et al. [2-88] investigated the buckling and second-order effects in dual shear-flexural structural systems. They proved that the total buckling load was a simple summation of the buckling loads of the two component structures when they acted independently, and that the distribution of vertical loads among the two components played no role. Additionally, they proposed a simple formula for the amplification factor for the displacements and bending moments in such structural types.

2.5 MODERN DESIGN CODES

In this section, the design provisions of modern design codes for the analysis and design of laced and battened built-up columns will be presented. Emphasis will be given to Eurocode 3, which is the code used in European countries, containing much information based on the research mentioned in the previous sections. In all cases, the provisions concern built-up members with a constant cross-section along their length.

2.5.1 Eurocode 3 provisions

2.5.1.1 Analysis of built-up columns

Eurocode 3 [2-24] provides guidance for simply-supported laced built-up columns under compression and small lateral loads causing single curvature deformation. It suggests that simply-supported laced columns with at least three panels are treated as Timoshenko columns with equivalent bending and shear rigidities, like the one shown in Figure 2-14. The initial imperfection is based on the first buckling mode of simply-supported columns having the half wavelength and a maximum magnitude at the mid-height. Eurocode 3 suggests that the imperfection's value at mid-height should be equal to $e_o = L/500$, a value experimentally characterised as sufficiently safe for all types of built-up columns by Uhlmann [2-89].

For a built-up column with two similar flanges the axial force applied to the more compressed chord can be calculated as:

$$N_{ch,Ed} = 0.5N_{Ed} + \frac{M_{Ed}h_oA_{ch}}{2I_{eff}} \quad (2-34)$$

where N_{Ed} is the applied axial compressive force, h_o is the lever arm between the centres of gravity of the chords (Figure 2-15), A_{ch} is the cross-sectional area of the chords, I_{eff} is the equivalent second moment of inertia of the built-up member (that will be defined next) and M_{Ed} is the maximum bending moment at mid-height.

The maximum bending moment is given by:

$$M_{Ed} = \frac{N_{Ed}e_0 + M_{Ed}^I}{1 - \frac{N_{Ed}}{N_{cr}} - \frac{N_{Ed}}{S_v}} \quad (2-35)$$

where M_{Ed}^I is the first-order bending moment at the mid-height due to transverse loads, S_v is the shear rigidity of the column (depends on the type of the shear system as it will be illustrated in the following sections) and N_{cr} is the elastic critical buckling load of the built-up member if shear deformations are neglected, given by:

$$N_{cr} = \frac{\pi^2 EI_{eff}}{L^2} \quad (2-36)$$

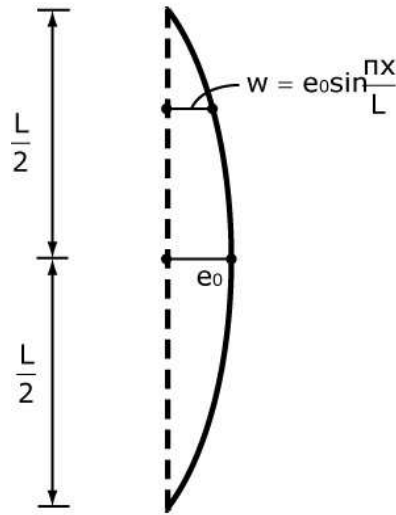


Figure 2-14: Imperfect simply-supported column in its undeformed imperfect configuration [2-24]

The maximum shear force at the ends of the built-up member is given by:

$$V_{Ed} = \pi \frac{M_{Ed}}{L} \quad (2-37)$$

Eurocode 3 states that these provisions should be accordingly modified for other types of boundary conditions without providing any further instructions.

2.5.1.2 Laced built-up columns

The equivalent second moment of inertia of a built-up cross-section consists of the inertia of the chords as individuals and of the Steiner term:

$$I_{eff} = \frac{A_{ch} h_0^2}{2} + 2I_{ch} \quad (2-38)$$

where I_{ch} is the in-plane moment of inertia of the chords (usually the moment of inertia about z-z axis) as depicted in Figure 2-15. It can be seen that built-up columns have significantly increased stiffness when compared to solid members due to the distance of the material from the elastic neutral

axis of the cross-section. The chords' moment of inertia is usually much smaller than the Steiner term in laced columns and can even be neglected.

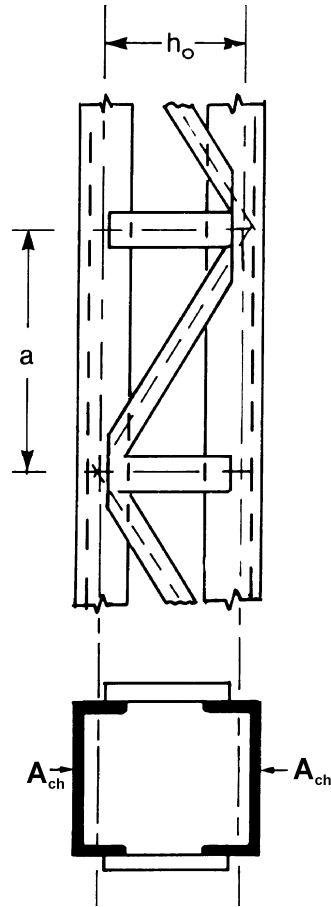


Figure 2-15: Part of a typical laced column and its built-up cross-section [2-24]

The shear rigidity in laced columns is offered by the lacing bars, and depends on the arrangement. Commonly encountered cases are shown in Figure 2-16. Eurocode 3 contains formulas for calculating the shear rigidity only for the first three cases, but expressions for all five cases were provided by Ramm and Uhlmann [2-23] and will be presented here for completeness.

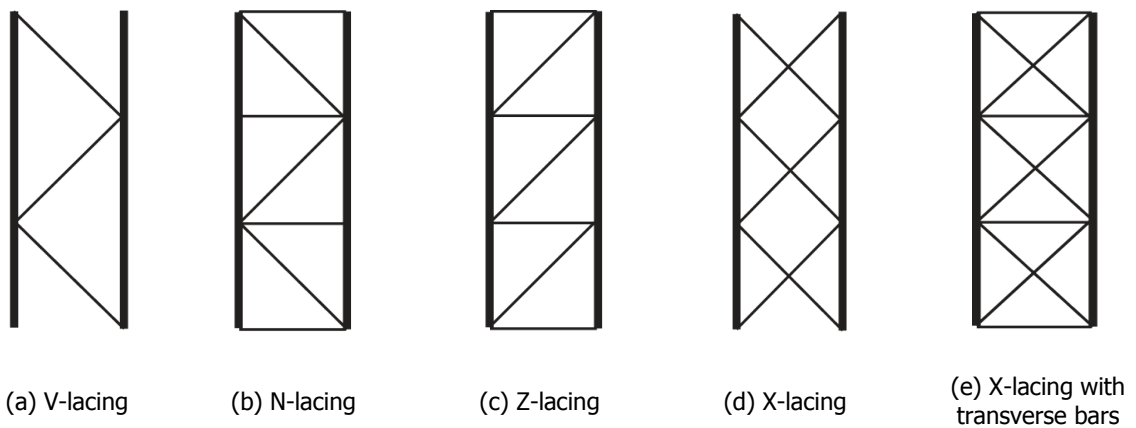


Figure 2-16: Different types of lacing systems

For obtaining the shear rigidity, the model of a single cell can be considered, assuming that all component members are subjected only to axial forces (each component is pin-ended). The lacing in Figure 2-16(c) is analysed here for better explanation of the procedure. The application of shear forces Q at the top and bottom nodes of a single cell (Figure 2-17) leads to the shear deformation of the whole cell. The total shear deformation can be described as the summation of two components:

$$Y = Y_1 + Y_2 \quad (2-39)$$

where y_1 is the shear deformation due to the axial extension of the diagonal and y_2 is the shear deformation due to the axial extension of the transverse bar.

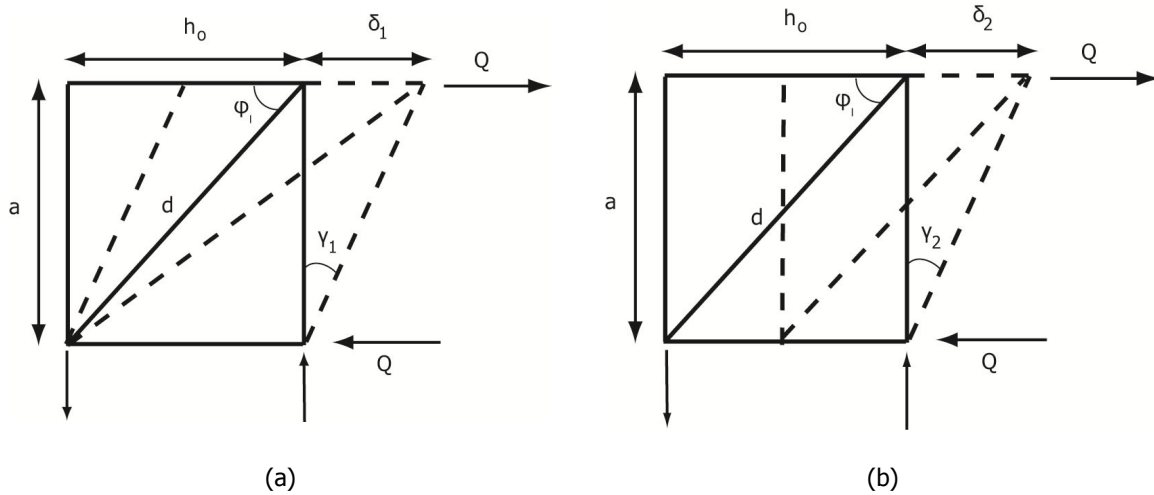


Figure 2-17: Deformation of cell due to axial extension of (a) diagonal and (b) transverse bar

The force applied to the diagonal is equal to $Q/\cos\phi_1$ and the displacement δ_1 becomes:

$$\delta_1 \cos\phi_1 = \frac{Q}{\cos\phi_1} \frac{d}{A_d E} = \frac{Qa}{A_d E \cos\phi_1 \sin\phi_1} \quad (2-40)$$

where ϕ_1 is the angle between the diagonal and the transverse bar, E is the Young's modulus, A_d the cross-sectional area of the diagonal, d the length of the diagonal and a the length of the panel.

The shear deformation y_1 is therefore equal to:

$$y_1 = \frac{\delta_1}{a} = \frac{Q}{A_d E} \frac{1}{\cos^2\phi_1 \sin\phi_1} \quad (2-41)$$

The displacement δ_2 is equal to (A_v =transverse bar's cross-sectional area):

$$\delta_2 = \frac{Qh_0}{A_v E} \quad (2-42)$$

Similarly, the shear deformation y_2 based on Eq. (2-42) is equal to:

$$y_2 = \frac{\delta_2}{a} = \frac{Q}{A_v E} \frac{1}{\tan\phi_1} \quad (2-43)$$

By considering that shear deformation is the ratio between the shear force and the shear rigidity and by combining Eqs. (2-39), (2-41) and (2-43), the shear rigidity for Z-lacing can be calculated as:

$$S_v = \frac{EA_d ah_o^2}{d^3 \left[1 + \frac{A_d h_o^3}{A_v d^3} \right]} \quad (2-44)$$

The corresponding expression in Eurocode 3 contains the influence of the number of planes n and Eq. (2-44) becomes:

$$S_v = \frac{nEA_d ah_o^2}{d^3 \left[1 + \frac{A_d h_o^3}{A_v d^3} \right]} \quad (2-45)$$

Formulas for the calculation of shear rigidities for different lacing arrangements are given in Table 2-2. It can be concluded that in all cases the shear rigidity depends on the axial stiffness and geometrical parameters that include the panels' length a , the lever arm between the chords h_o and the length of the diagonal bars d . It can be concluded that the larger the axial stiffness nEA_d of the diagonal bars, the larger the shear rigidity of the lacing system. If the value nEA_d is considered to be constant, the effect of angle ϕ_l (which deals with the geometrical parameters) on the shear rigidity can be investigated and expressed in an "effectiveness factor" that its expressions are provided in Table 2-3. The relation between the effectiveness factor and angle ϕ_l is graphically presented in Figure 2-18. It can be concluded that the lacing systems become more efficient leading to increased shear rigidities for angles ϕ_l between 30 and 50 degrees. For other values of angle ϕ_l the lacing bars are not fully exploited and this becomes prominent for large angle values.

Table 2-2: Formulas for shear rigidities of different lacing arrangements

V-lacing	N-lacing	Z-lacing	X-lacing and X-lacing with transverse members
$S_v = \frac{nEA_d ah_o^2}{2d^3}$	$S_v = \frac{nEA_d ah_o^2}{d^3}$	$S_v = \frac{nEA_d ah_o^2}{d^3 \left[1 + \frac{A_d h_o^3}{A_v d^3} \right]}$	$S_v = \frac{2nEA_d ah_o^2}{d^3}$

Table 2-3: Formulas for effectiveness factor of different lacing arrangements

V-lacing	N-lacing	Z-lacing	X-lacing and X-lacing with transverse members
$\frac{\sin\phi_l (\cos\phi_l)^2}{2}$	$\sin\phi_l (\cos\phi_l)^2$	$\frac{\tan\phi_l (\cos\phi_l)^3}{1 + (\cos\phi_l)^3}$	$2\sin\phi_l (\cos\phi_l)^2$

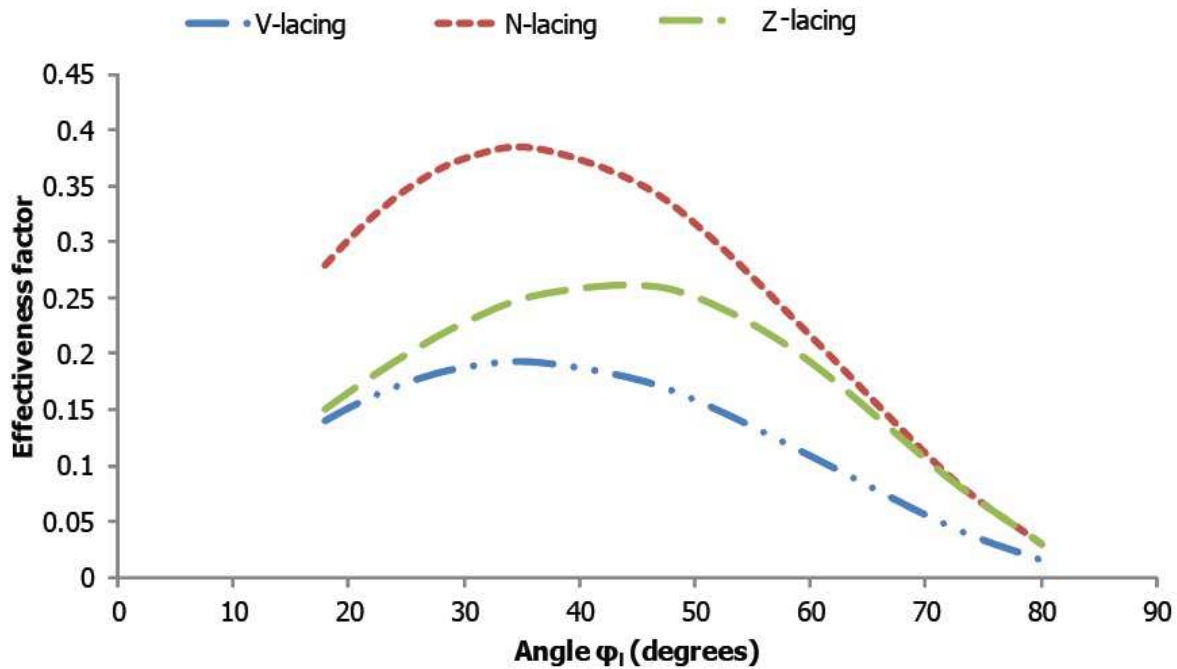


Figure 2-18: Relation between the effectiveness factor and angle ϕ_l in lacing systems

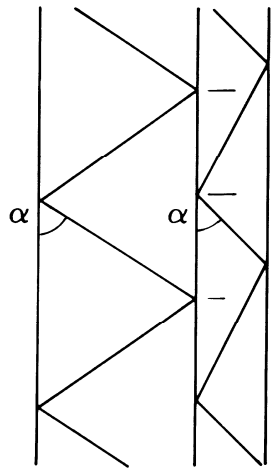
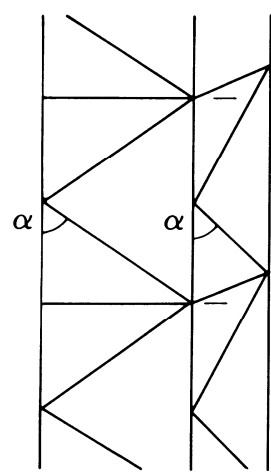
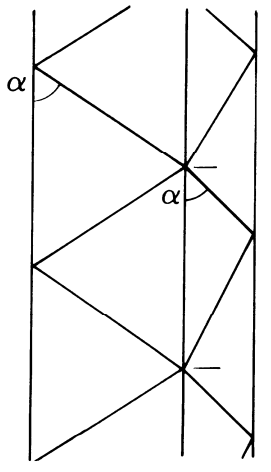
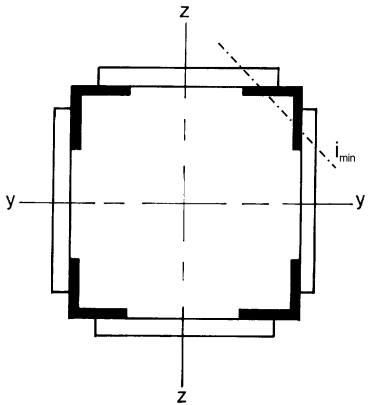
Laced columns' chords between connectors should be checked against axial forces considering their buckling capacities according to the provided buckling curves. Each chord should satisfy the following inequality:

$$\frac{N_{ch,Ed}}{N_{b,Rd}} \leq 1,0 \quad (2-46)$$

where $N_{ch,Ed}$ is the maximum axial force applied along the chord as obtained by Eq. (2-34) and $N_{b,Rd}$ is the buckling strength of the chord between successive lacing connections at mid-height. The effective buckling length factor is taken equal to unity considering that the mid-height panel behaves as a simply-supported member. In this way the rotational stiffness that adjacent panels and lacing bars offer to the critical panel is ignored. Similarly, the diagonal bars at the ends should be checked against axial forces that are calculated based on the shear force perpendicular to the deformed axis of the column as obtained by Eq. (2-37).

The buckling length of each panel L_{ch} can be considered according to Table 2-4 for four-pieced laced columns. In two-pieced laced columns it can be taken equal to a .

Table 2-4: Lacing bars in four planes and corresponding effective buckling lengths L_{ch} [2-24]

 <p style="text-align: center;">$L_{ch} = 1.52a$</p>	 <p style="text-align: center;">$L_{ch} = 1.28a$</p>
 <p style="text-align: center;">$L_{ch} = a$</p>	

Some recommended constructional details include:

- Parallel planes should be in accordance as in Figure 2-19(a) for avoiding torsional effects that will be significant in the case of Figure 2-19(b).
- At the ends of each laced column and at connections with other members, linking elements should be provided.

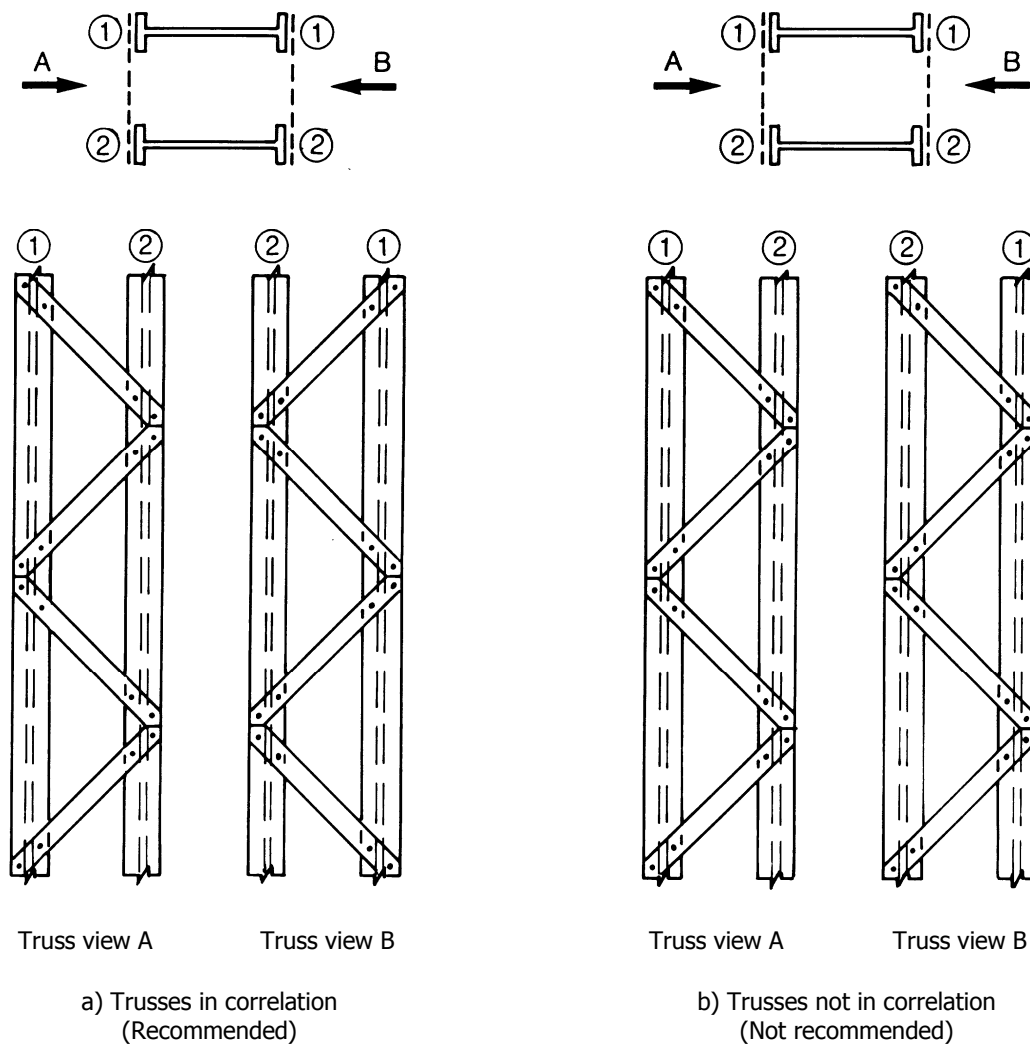


Figure 2-19: (a) Recommended and (b) unacceptable arrangement of lacing bars in parallel planes [2-24]

2.5.1.3 Battened built-up columns

The equivalent second moment of inertia of a battened column's (Figure 2-20) built-up cross-section consists of the inertia of the chords as individuals and of the Steiner term:

$$I_{\text{eff}} = \frac{A_{\text{ch}} h_o^2}{2} + 2\mu' I_{\text{ch}} \quad (2-47)$$

The factor μ' was introduced according to the work of Klöppel and Uhlmann [2-20] in order to account for the effect of plasticity. To be more specific, the authors concluded that battened built-up struts enter the elastoplastic range, in which the bending stiffness is reduced, due to the plastification of outer fibres. This can happen before the chords reach their ultimate strength leading to increased displacements and compressive forces applied to the chords. The authors performed analytical and numerical calculations taking into account plastification and elastic calculations considering both $\mu'=0$ (lower bound) and $\mu'=1$ (upper bound). They concluded that in very slender battened built-up struts (characterised by very large values of global slenderness λ) the effect of plastified regions on the global response is much more important than in less slender ones. This conclusion is clearly expressed in Table 2-5, where the proposed value of μ' is equal to zero for large slenderness leading to small bending stiffness and equal to unity for small slenderness leading to full exploitation of the chords'

bending stiffness. Intermediate slendernesses lie between the two boundaries. It can be seen that obtaining a solution requires an iterative procedure.

Table 2-5: Efficiency factor μ' [2-24]

criterion	Efficiency factor μ'
$\lambda \geq 150$	0
$75 < \lambda < 150$	$2 - \lambda/75$
$\lambda \leq 75$	1.0
where λ is the slenderness of the whole column considering the full second moment of inertia	

It is worth mentioning that this finding is quite surprising as exactly the opposite happens in solid members. In solid columns the influence of plasticity is much more important in the range of small slendernesses while very slender columns behave almost elastically. The authors attributed this deviation from normal behaviour to the many counterparts that exist in a battened built-up column and to the continuous connection between the flanges and the battens that lead to a complex interaction between the whole column and the individual panels.

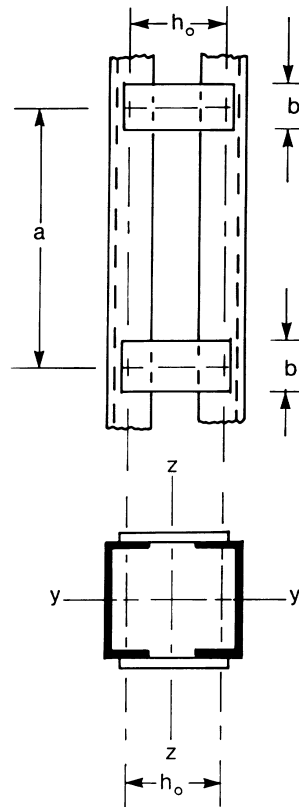


Figure 2-20: Part of a typical battened column and its built-up cross-section [2-24]

The shear rigidity in battened columns with constant interval between battens is offered by both the flanges and the battens. The general derivation based on the concept of the Vierendeel truss, presented by Timoshenko and Gere [2-68] and incorporated in Eurocode 3, will be presented here for completeness. In a Vierendeel truss points of inflection are considered to be located at the middle of each panel and at the middle of each batten. Therefore, a statically determinate structure can be separated and considered for structural analysis. Consider a part of a typical battened column between successive points of inflection along the chords, as shown in Figure 2-21, subjected to shear

forces Q at its ends. The total shear deformation results from the deformation of the battens and flanges:

$$\gamma = \frac{\delta_1 + \delta_2}{\frac{a}{2}} \quad (2-48)$$

where δ_1 is the displacement at the tip due to the batten's deformation and δ_2 is the displacement at the tip due to the flange's deformation. The rotation θ at the ends of the batten is equal to:

$$\theta = \frac{h_0}{6EI_b} M \quad (2-49)$$

where I_b is the second moment of inertia of the batten about its axis of bending and M is the applied moment at the ends of the batten. The bending moment at the ends of the batten M is equal to $Qa/2$ and substituting in Eq. (2-49) gives:

$$\theta = \frac{Qah_0}{12EI_b} \quad (2-50)$$

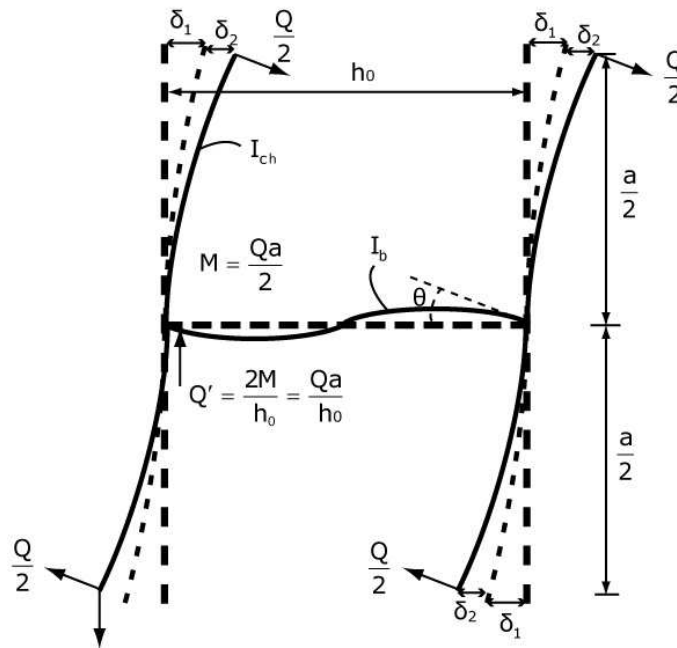


Figure 2-21: Deformed shape of battened column's part subjected to shear forces at its ends

The displacement δ_1 based on Eq.(2-50) is equal to:

$$\delta_1 = \frac{\theta a}{2} = \frac{Qa^2h_0}{24EI_b} \quad (2-51)$$

The displacement δ_2 considering the deflection formula for a cantilever under an end point load is:

$$\delta_2 = \frac{Q}{2} \left(\frac{a}{2} \right)^3 \frac{1}{3EI_{ch}} = \frac{Qa^3}{48EI_{ch}} \quad (2-52)$$

The inverse of the shear rigidity arises by using Eqs. (2-48), (2-51) and (2-52):

$$\frac{1}{S_v} = \frac{\gamma}{Q} = \frac{ah_0}{12EI_b} + \frac{a^2}{24EI_{ch}} \quad (2-53)$$

After some manipulation Eq. (2-53) becomes:

$$S_v = \frac{24EI_{ch}}{a^2 \left(1 + \frac{2I_{ch}}{I_b} \frac{h_0}{a} \right)} \quad (2-54)$$

If the number of battens' planes is denoted as n , the shear rigidity incorporated in Eurocode 3 is obtained:

$$S_v = \frac{24EI_{ch}}{a^2 \left(1 + \frac{2I_{ch}}{nI_b} \frac{h_0}{a} \right)} \quad (2-55)$$

It can be seen that in Eq. (2-54) only the bending deformations of the components are considered. In the case of very short battens and/or panels the effect of shear deformations may have to be considered, too.

Additionally, it can be observed that the length $a/2$ of each cantilever is measured from the centres of gravity of the battens and the length of each batten h_0 is measured from the centres of gravity of the chords. These lengths can be refined in cases of welded joints, as within the finite dimensions of the rigid welded connections deformations are rather limited. Using Eq. (2-54) is always on the safe side in that respect.

Eurocode 3 requires that the shear rigidity obtained with Eq. (2-54) should satisfy the following inequality:

$$S_v \leq \frac{2n^2EI_{ch}}{a^2} \quad (2-56)$$

Eq. (2-56) was obtained by Klöppel and Uhlmann [2-20] considering rigid batten-plates and comparing the critical load of a single panel with that of the whole member. It corresponds to the case that a single panel would buckle elastically and its contribution to the shear rigidity would be cancelled due to the second-order effects in the flanges. The concept behind the upper limit set in Eurocode 3 was previously considered by other researchers [2-13], [2-18] too, with the introduction of a second-order magnification factor to the term related to the chords in the shear rigidity formula.

The chords in battened columns should be checked against the combination of axial forces $N_{ch,Ed}$ applied to the chords and the bending moment $V_{Ed}a/4$ which are shown in Figure 2-22. Apart from the cross-sectional checks, the chords should be checked against buckling with use of the interaction formulae included in Appendices A and B of Eurocode 3 for methods 1 [2-90] and 2 [2-91], respectively.

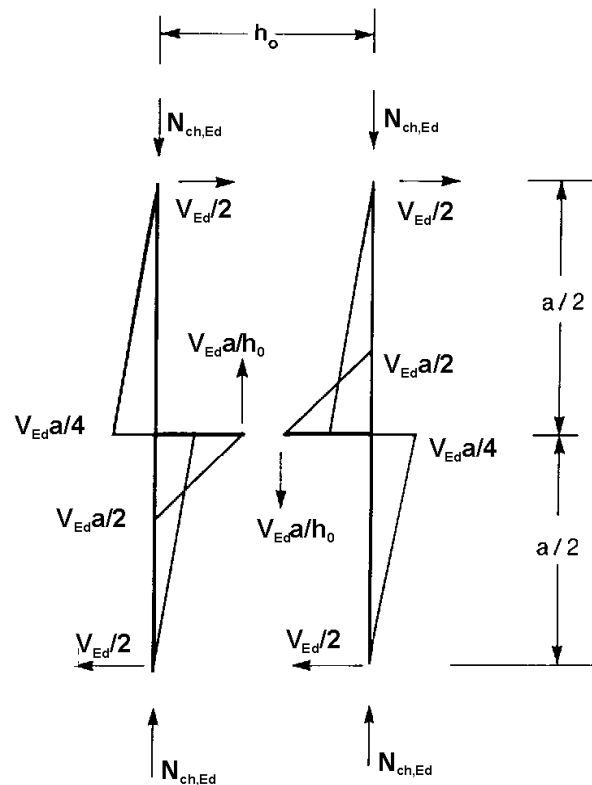


Figure 2-22: Axial forces and bending moments in a part of a battened column [2-24]

The following recommended constructional details are included in Eurocode 3:

- Batten plates at each column's end should be provided.
- Two parallel battens should be placed at every joint.
- Battens should be provided at intermediate points at which either loads are applied or lateral supports converge.

2.5.1.4 Comparison between laced and battened built-up columns

Laced and battened built-up columns have different shear systems, something that differentiates their structural response and behaviour. As it was shown in the previous subsection, in laced built-up columns only the lacing bars participate in the shear system while in battened ones both battens and chords do. In this subsection a qualitative and quantitative comparison between the efficiency of the shear systems of the two built-up columns types is made by varying the lever arm h_o and the panels' length a .

A simply-supported column with a length of 12m and a chords' cross-section HEB300 will be examined in laced (Z-lacing) and battened configuration. Lacing bars and battens have a rectangular cross-section 31x10 and 100x10, respectively. In the first parametric study, the panels' length is kept constant and equal to 60cm while the lever arm h_o varies from 20cm to 90cm affecting the elastic critical buckling load, too. The results are summarized in Figure 2-23 in which the lever arm is plotted on the horizontal axis and the ratio between the Euler buckling load and the shear rigidity (indicative of the effect of shear deformations on the elastic critical buckling load of simply-supported Timoshenko members as shown in Eq. (2-21)) is plotted on the vertical axis. The larger the value of this ratio becomes, the more significant the effect of the shear deformations on the elastic critical buckling load is. It can be observed that for small values of the lever arm the battened member has

larger shear rigidity than the laced one as the battens have a small length and small bending deformations. Meanwhile, for small values of the lever arm in the laced column, the angle φ_1 is very large and the lacing system less effective as shown in Figure 2-18. For values of the lever arm larger than approximately 30cm, the shear rigidity of the battened column reduces significantly while this is not the case for the laced member in which a mild reduction takes place. For this reason, the use of battened members in cases of large lever arms is expected to lead to large effects of shear deformations.

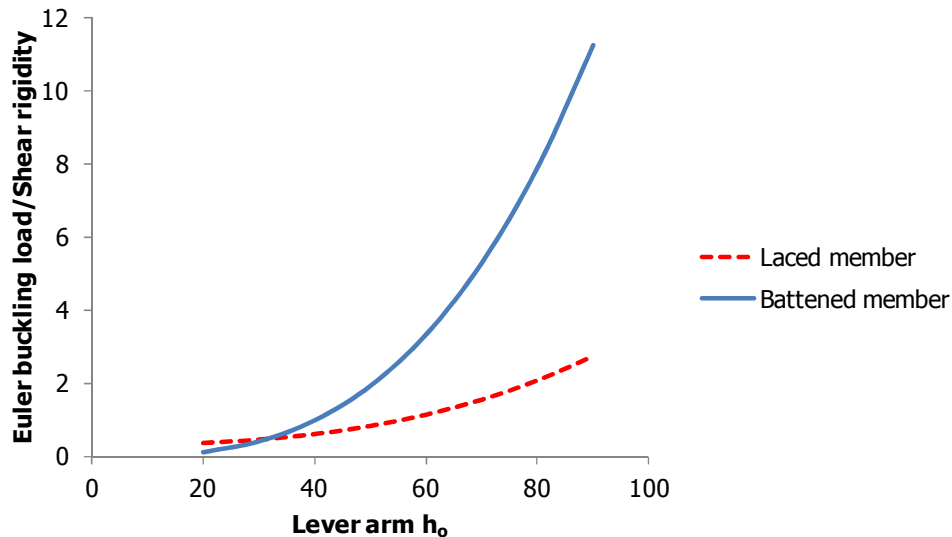


Figure 2-23: Effect of lever arm h_o on the ratio between the Euler buckling load and the shear rigidity

In the second parametric study, the lever arm is kept constant and equal to 60cm while the length of the panels varies from 43cm to 240cm. The results are summarised in Figure 2-24 in which the panels' length is plotted on the horizontal axis and the ratio between the Euler buckling load and the shear rigidity is plotted on the vertical axis. In all cases, the shear rigidity of the battened member is less than the one of the laced column, resulting in similar conclusions to the first parametric study.

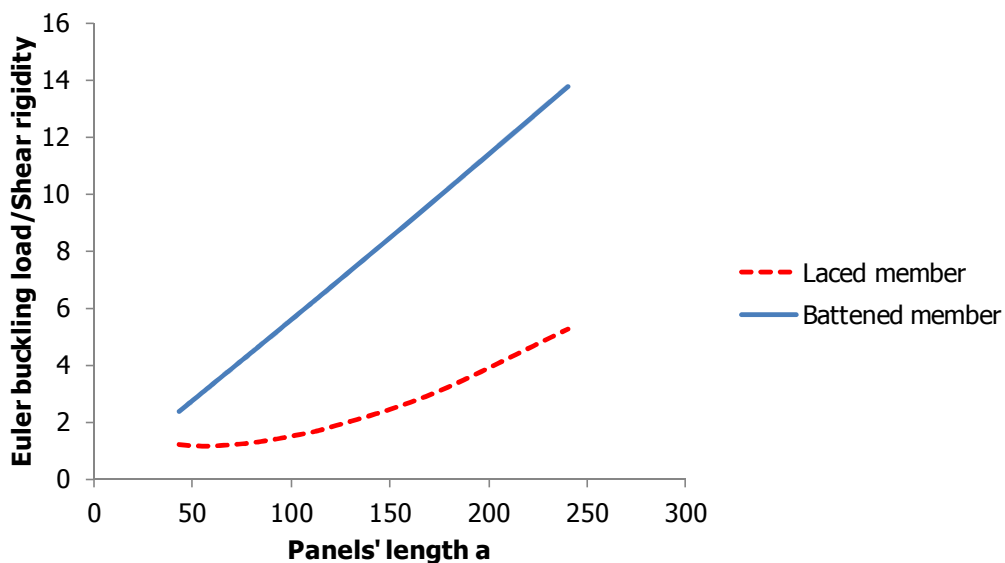


Figure 2-24: Effect of panels' length a on the ratio between the Euler buckling load and the shear rigidity

Therefore, it is made clear that laced columns are much more efficient in terms of shear rigidity in most cases. For this reason, they are preferred in cases of important lateral loads that require both large bending and shear rigidity. The battened columns are commonly used either in cases in which no significant shear forces are expected in the structure or in cases that a bracing system is used for transferring the transverse loads in their plane.

2.5.2 Older German Design Code provisions (DIN 18800 - Part 2)

The design concepts presented for Eurocode 3 [2-24] can also be found in DIN 18800-Part 2 [2-92] and will not be repeated.

2.5.3 American Institute of Steel Construction L.R.F.D. provisions

L.R.F.D. [2-93] focuses on the design of closely spaced built-up columns, in which the two flanges are connected with the use of interconnectors. Therefore, it considers the effect of shearing due to the deformation of the interconnectors and of the flanges, battens and laces. Closely spaced built-up columns are out of the research area of the present doctoral thesis and will not be further discussed.

2.6 CONCLUSIONS

In this chapter, the existing literature regarding laced and battened built-up columns is described. Initially, the existing research work on built-up members is presented focusing on experimental, numerical and analytical procedures from the very beginning of the 21st century until the main issues that differentiate them from solid members became clearer. The effect of compound buckling and shear deformations in built-up columns is then summarised. Finally, the guidance of Eurocode 3 regarding simply-supported columns is thoroughly described and light is shed on issues that are not clearly explained in the code.

Based on the literature review and code specifications described in this chapter, it can be concluded that they are mainly related to simply-supported laced members subjected to axial loads. Additionally, the effect of compound buckling is not fully investigated and the existing numerical methods for incorporating its effect on structural analysis of laced members are computationally demanding. On the other hand, in practice, laced members are subjected to both axial and lateral loads and belong to industrial frames. As a result, they rarely belong to the limited categories that literature and codes cover and there is not a sufficient procedure that an engineer of practice can use for their accurate design.

The present doctoral thesis aims at bridging this gap by investigating the structural behaviour of laced built-up columns including the effects of shear deformations and compound buckling. In this way, it intends to provide guidance for the analysis and design of laced members with arbitrary supports under both axial and lateral loading. In order to achieve this goal, it includes experimental tests, numerical procedures and analytical methods contributing to both engineering practice and scientific knowledge.

2.7 REFERENCES

- [2-1] Van den Broeck, J. A. "English translation of Euler's on the strength of columns", American Journal of Physics, Vol. 15, July 1947
- [2-2] Tetmajer, L. "Die Gesetze der Knickungs – und der Zusammengesetzten Druckfestigkeit der technisch wichtigsten Baustoffe", Bulletin No. 8 of the Materials Testing Institute, Zurich, ETH, 1896

- [2-3] Engesser, F. "Die Knickfestigkeit gerader Stäbe", Zentralblatt der Bauverwaltung, Vol. 11, pp. 483-486, Berlin, 1891
- [2-4] Engesser, F. "Über die Knickfestigkeit von Rahmenstäben", Zentralblatt der Bauverwaltung, p. 136, Berlin, 1909
- [2-5] Emperger, F.V. "Welchen Querverband bedarf eine Eisensaule", Beton und Eisen, p. 71, 1908
- [2-6] Krohn, R. "Beitrag der Untersuchung der Knickfestigkeit gegliederter Stäbe", Zentralblatt der Bauverwaltung, p. 559, Berlin, 1908
- [2-7] Müller-Breslau, H. "Über exzentrisch gedruckte gegliederte Stäbe", Sitzungsberichte D.K. Press Akad. den Wissenschaften, p.166, Berlin, 1910
- [2-8] Talbot, A.N., Moore, H.F. "An investigation of built-up columns under load", Engineering Bulletin, No. 44, University of Illinois, 1910
- [2-9] Final report on built-up columns, Proceedings of the American Railway Engineering Associations, Vol. 19, pp. 789-811, 1918
- [2-10] Progress report of the special committee on steel column research, Transactions of the American Society of Civil Engineers, Vol. 89, pp. 1485-1549, 1926
- [2-11] Petermann, "Müller-Breslau's Knickversuche mit Rahmenstäben", Der Bauingenieur, Vol. 7, pp. 979-981 and pp. 1009-1016, 1926
- [2-12] Petermann, "Knickversuche mit Rahmenstäben aus st 48", Der Bauingenieur, Vol. 12, pp. 509-515, 1931
- [2-13] Timoshenko, S. "Buckling of battened struts", Theory of Elastic Stability, pp. 144-147 and pp. 155-156, 1936
- [2-14] Holt, M. "Tests on built-up columns of structural aluminium alloys", Transactions of the American Society of Civil Engineers, Vol. 105, pp. 196-217, 1940
- [2-15] Ng, W.H. "The behaviour and design of battened structural members", Doctoral thesis, University of Cambridge, U.K., 1947
- [2-16] Pippard, A.J.S. "The critical load of a battened column", Studies in Elastic Structures, pp. 193-201, London, 1952
- [2-17] Bleich, F. "Buckling strength of metal structures", Engineering Societies Monographs, McGraw-Hill, New York, 1952
- [2-18] Koenigsberger, F., Mohsin, M.E. "Design and load carrying capacity of welded battened struts", The Structural Engineer, Vol. 34, No. 6, pp. 183-203, 1956
- [2-19] Mohsin, M.E. "The critical load of unsymmetrical welded battened struts", The Structural Engineer, Vol. 43, No. 11, 1965
- [2-20] Klöppel, K., Uhlmann, W. "Versuchsmässige und rechnerische Bestimmung der Traglasten mehrteiliger Rahmenstäbe unter Verwendung elektronischer Rechenautomaten", Der Stahlbau, Vol. 34, p. 161, 199 and 231, 1965
- [2-21] Klöppel, K., Ramm, W., "Versuche und Berechnung zur Bestimmung der Traglast mehrteiliger Gitterstäbe unter aussermittiger Belastung", Der Stahlbau, Vol. 37 p. 164 and 236, 1968
- [2-22] Klöppel, K., Ramm, W., "Zur Stabilitätsuntersuchung von mehrteiligen Gitterstäben", Der Stahlbau, Vol. 41 pp. 14-21, 1972

- [2-23] Ramm, W., Uhlmann W. "Zur Anpassung des Stabilitätsnachweises für mehrteilige Druckstäbe an das europäische Nachweiskonzept", *Der Stahlbau*, Vol. 50, pp. 161-172, 1981
- [2-24] Eurocode 3: Design of Steel Structures. Part 1.1: General structural rules. CEN-European Committee for Standardisation, Brussels, EN1993-1-1, 2005
- [2-25] Vroonland, E.J., "Analysis of pendant-supported latticed crane booms", *SAE Trans*, Vol. 80, Pap. 710697, 1971
- [2-26] Brolin, C.A., Durscher, H.E., Serentha, G. "Destructive testing of crane booms", *SAE Transactions*, Vol. 81, Pap. 720784, 1972
- [2-27] Lin, F.J., Glauser, E.C., Johnston, B.G., "Behaviour of laced and battened structural members", *Journal of the Structural Division, American Society of Civil Engineers (A.S.C.E.)*, Vol. 96, No. ST7, pp. 1377-1401, 1970
- [2-28] Toossi, M. "On the out-of-plane buckling of battened columns", *International Journal of Mechanical Sciences*, Vol. 14, pp. 511-521, 1972
- [2-29] Porter, D.M., Williams, F.W. "Critical load of built-up columns and a pocket calculator program", *Proceedings of Institute of Civil Engineers*, Vol. 64, Part 2, pp. 761-771, 1978
- [2-30] Halabia, S.L. "Stability and behaviour of battened steel struts", *Doctoral thesis, University of Wales, U.K.*, 1981
- [2-31] Gjelsvik, A. "Buckling of built-up columns with or without stay plates", *Journal of Engineering Mechanics*, Vol. 116, No. 5, pp. 1142-1159, 1990
- [2-32] Paul, M. "Theoretical and experimental study on buckling of built-up columns", *Journal of Engineering Mechanics*, Vol. 121, No. 10, pp. 1098-1105, 1995
- [2-33] Paul, M. "Buckling loads for built-up columns with stay plates", *Journal of Engineering Mechanics*, Vol. 121, No. 10, pp. 1200-1208, 1995
- [2-34] Ermopoulos J.C., Ioannidis S.S., Kounadis A.N. "Stability of battened columns with and without taper", *Engineering Structures*, Vol. 13, No. 3, pp. 237-241, 1991
- [2-35] Chang, J.S., Sher, H.F. "Elastoplastic postbuckling behaviour of perfect and imperfect built-up columns", *Computers and Structures*, Vol. 44, No. 5, pp. 1037-1046, 1992
- [2-36] Sahoo, D.R., Rai, D.C. "Built-up battened columns under lateral cyclic load", *Thin-walled structures*, Vol. 45, pp. 552-562, 2007
- [2-37] Lee, K., Bruneau, M. "Seismic vulnerability evaluation of axially loaded steel built-up laced members I: experimental results", *Earthquake Engineering and Engineering Vibration*, Vol. 7, No. 2, pp. 113-124, 2008
- [2-38] Lee, K., Bruneau, M. "Seismic vulnerability evaluation of axially loaded steel built-up laced members II: evaluations", *Earthquake Engineering and Engineering Vibration*, Vol. 7, No. 2, pp. 125-136, 2008
- [2-39] Richard, J., Tremblay, R., Koboevic, S., MacCrimmon, R.A. "Seismic analysis and design approaches for crane-supporting steel structures", *Proceedings of the Behaviour of Steel Structures in Seismic Areas*, pp. 511-517, Philadelphia, United States, 2009
- [2-40] Hashemi, B.H., Jafari, M.A. "Performance of batten columns in steel buildings during the Bam earthquake of 26 December 2003", *Journal of Seismology and Earthquake Engineering: Special Issue on Bam Earthquake*, pp. 101-109, 2004

- [2-41] Hashemi, B.H., Jafari, M.A. "Experimental evaluation of elastic critical load in batten columns", *Journal of Constructional Steel Research*, Vol. 65, pp. 125-131, 2009
- [2-42] Southwell R.V. "On the analysis of observations in problems of elastic stability", *Proceedings of the Royal Society of London*, Vol. 135, Part A, pp. 601-616, 1932
- [2-43] Hashemi, B.H., Jafari, M.A. "Evaluation of Ayrton-Perry formula to predict the compressive strength of batten columns", *Journal of Constructional Steel Research*, Vol. 68, pp. 89-96, 2012
- [2-44] Hashemi, B.H., Jafari, M.A. "Experimental evaluation of cyclic behaviour of batten columns", *Journal of Constructional Steel Research*, Vol. 78, pp. 88-96, 2012
- [2-45] Guo, Y., Wang, J. "Instability behaviour and application of prismatic multi-tube latticed steel column", *Journal of Constructional Steel Research*, Vol. 65, pp. 12-22, 2009
- [2-46] Razdolsky, A.G. "Euler critical force calculation for laced columns", *Journal of Engineering Mechanics (A.S.C.E.)*, Vol. 131, No.5, pp. 997-1003, 2005
- [2-47] Razdolsky, A.G. "Flexural buckling of laced column with serpentine lattice", *The IES Journal Part A: Civil and Structural Engineering*, Vol. 3, No. 1, pp. 38-49, 2010
- [2-48] Razdolsky, A.G. "Calculation of slenderness ratio for laced columns with serpentine and crosswise lattices", *Journal of Constructional Steel Research*, Vol. 67, pp. 25-29, 2011
- [2-49] Bonab, A.P., Hashemi, B.H. "Analytical investigation of cyclic behaviour of laced built-up columns", *Journal of Constructional Steel Research*, Vol. 73, pp. 128-138, 2012
- [2-50] Bonab, A.P., Hashemi, B.H., Hosseini, M. "Experimental evaluation of the elastic buckling and compressive capacity of laced columns", *Journal of Constructional Steel Research*, Vol. 86, pp. 66-73, 2013
- [2-51] Van der Neut, A. "The interaction of local buckling and column failure of thin-walled compression members", *Proceedings of the 12th international congress of applied mechanics*, Stanford University, United States, August 26-31, 1968
- [2-52] Koiter, W.T., Kuiken, G.D.C. "The interaction between local buckling and overall buckling on the behaviour of built-up columns", *Laboratory of Engineering Mechanics*, Report No. 447, Delft, 1971
- [2-53] Koiter W.T. "Over de stabiliteit van het elastische evenwicht", *Doctoral thesis*, T.U. Delft, The Netherlands, 1945
- [2-54] Thompson, J.M.T., Hunt, G.W. "A General Theory of Elastic Stability", John Wiley, London, 1973
- [2-55] Miller, R.K., Hedhepeth, J.M. "The buckling of latticed columns with stochastic imperfections", *International Journal of Solid Structures*, Vol. 15, pp. 71-84, 1979
- [2-56] Crawford, R.F., Hedgepeth, J.M. "Effects of initial waviness on the strength and design of built-up structures", *AIAA Journal*, Vol. 13, No. 5, p. 672, 1975
- [2-57] Crawford, R.F., Benton, M.D. "Strength of initially wavy lattice columns", *AIAA Journal*, Vol. 18, No. 5, p. 581, 1980
- [2-58] Svensson, S.E., Kragerup, J. "Collapse loads of laced column", *Journal of Structural Division, American Society of Civil Engineers*, Vol. 108(ST6), pp. 1367-84, 1982

- [2-59] Tong Geng-Shu., Chen Shao-Fan "An interactive buckling theory for built-up beam-columns and its application to centrally compressed built-up members", *Journal of Constructional Steel Research*, Vol. 14, pp. 221-241, 1989
- [2-60] Duan L., Reno M., Uang CM. "Effect of compound buckling on compression strength of built-up members", *Journal of Engineering (American Institute of Steel Construction)*, 1st Quarter, pp. 30-37, 2002
- [2-61] Cowper, Gr. "The shear coefficient in Timoshenko's beam theory", *Journal of Applied Mechanics, Transactions of the American Society of Mechanical Engineers*, Vol. 33, pp. 335-340, 1966
- [2-62] Cowper, Gr. "On the accuracy of Timoshenko's beam theory", *Proceedings of the American Society of Civil Engineers*, EM6, pp. 1447-1453, 1968
- [2-63] Scheer, J., Plumeyer, K. "Zu Verformungen stählerner Biegeträger aus Querkraften", *Bauingenieur*, Vol. 63, pp. 475-478, 1988
- [2-64] Biezeno, C.B., Koch, J.J. "Knickung von Schraubenfedern", *Zeitschrift für Angewandte Mathematik und Mechanik*, Vol. 5, pp. 279-280, 1925
- [2-65] Haringx, J.A. "On the buckling and lateral rigidity of helical springs", *Proceedings of the Koninklijke Nederlandse Akademie van Wetenschappen*, pp. 45-533, 1942
- [2-66] Haringx, J.A. "On highly compressible helical springs and rubber rods, and their application for vibration-free mountings", I-III, Reprints R 94, 101, 109, Philips research reports, pp. 1-97, Eindhoven, 1948.
- [2-67] Gjelsvik, A. "Stability of built-up columns", *Journal of Engineering Mechanics*, Vol. 117, No. 6, pp. 1331-1345, 1991
- [2-68] Timoshenko, S., Gere, J.M. "Theory of elastic stability", 2nd edition New York: McGraw-Hill Book Company, 1961
- [2-69] Nanni, J. "Das Eulersche Knickproblem unter Berücksichtigung der Querkraft", *Zeitschrift für Angewandte Mathematik und Mechanik*, Vol. 22, pp. 156-185, 1971
- [2-70] Ziegler, H. "Arguments for and against Engesser's Buckling Formulas", *Ingenieur-Archiv*, Vol. 52, pp. 105-113, 1981
- [2-71] Blaauwendraad, J. "Timoshenko beam-column buckling. Does Dario stand the test?", *Engineering Structures*, Vol. 30, pp. 3389-3393, 2008
- [2-72] Blaauwendraad, J. "Shear in structural stability: On the Engesser-Haringx discord", *Journal of Applied Mechanics*, Vol. 77, No. 3, 2010
- [2-73] Bazant, Z.P., Cedolin, L. "Stability of Structures", New York: Oxford University Press, 1991
- [2-74] Bazant, Z.P. "Discussion of "stability of built-up columns"" by A. Gjelsvik (author), *Journal of Engineering Mechanics*, Vol. 118, No. 6, pp. 1279-1281, 1992
- [2-75] Bazant, Z.P., Beghini, A. "Sandwich buckling formulas and applicability of standard computational algorithm for finite strain", *Composites: Part B*, Vol. 35, pp. 573-581, 2004
- [2-76] Bazant, Z.P., Beghini, A. "Stability and finite strain of homogenized structures soft in shear: sandwich or fibre composites and layered bodies", *International Journal of Solids and Structures*, Vol. 43, pp. 1571-1593, 2006

- [2-77] Kelly, J.M. "Tension buckling in multilayer elastomeric bearings", *Journal of Engineering Mechanics*, Vol. 129, No. 12, pp. 1363-1368, 2003
- [2-78] Aristizabal-Ochoa, J.D. "Column stability and minimum lateral bracing: effects of shear deformations", *Journal of Engineering Mechanics*, Vol. 130, No. 10, pp. 1223-1232, 2004
- [2-79] Aristizabal-Ochoa, J.D. "Slope-deflection equations for stability and second-order analysis of Timoshenko beam-column structures with semi-rigid connections", *Journal of Engineering Structures*, Vol. 30, No. 9, pp. 2517-2527, 2008
- [2-80] Aristizabal-Ochoa, J.D. "Stability of columns with semi-rigid connections including shear effects using Engesser, Haringx and Euler approaches", *Journal of Engineering Structures*, Vol. 33, No. 3, pp. 868-880, 2011
- [2-81] Aristizabal-Ochoa, J.D. "Large deflection and postbuckling behaviour of Timoshenko beam-columns with semi-rigid connections including shear and axial effects", *Journal of Engineering Structures*, Vol. 29, pp. 991-1003, 2007
- [2-82] Aristizabal-Ochoa, J.D. "Matrix method for stability and second-order analysis of Timoshenko beam-column structures with semi-rigid connections", *Journal of Engineering Structures*, Vol. 34, pp. 289-302, 2012
- [2-83] Bryant, R.H., Baile, O.C. "Slope deflection analysis including transverse shear", *Journal of the Structural Division (A.S.C.E.)*, Vol. 103, No. 2, pp. 443-446, 1977
- [2-84] Absi, E. "Equations intrinseques d'une poutre droite a section constant", *Annales de l'Institut Technique du Batiment et des Travaux Publics*, Vol. 21(229), pp. 151-167, 1967
- [2-85] Banerjee, J.R., Williams, F.W. "The effect of shear deformation on the critical buckling of columns", *Journal of Sound and Vibration*, Vol. 174, No. 5, pp. 607-616, 1994
- [2-86] Marinetti, A., Oliveto, G. "Second order analysis of elastic frames with Timoshenko members", *Engineering Analysis*, Vol. 1, No. 2, pp. 92-98, 1984
- [2-87] Wang, C.M., Ng, K.H., Kitipornchai, S. "Stability criteria for Timoshenko columns with intermediate and end concentrated axial loads", *Journal of Constructional Steel Research*, Vol. 58, pp. 1177-1193, 2002
- [2-88] Gengshu, T., Pi, Y.-L., Bradford, M., Tin-Loi, F. "Buckling and second-order effects in dual shear-flexural systems", *Journal of Structural Engineering*, Vol. 134, No. 11, pp. 1726-1732, 2008
- [2-89] Uhlmann, W. "Some problems concerning design recommendations for centrally compressed built-up members", *Proceedings of the 2nd Conference on Stability of Steel Structures*, Preliminary Report, pp. 121-130, Liege, 1977
- [2-90] Boissonnade, N., Jaspart, J.-P., Muzeau, J.-P., Villette, M. "New interaction formulae for beam-columns in Eurocode 3: The French-Belgian approach", *Journal of Constructional Research*, Vol. 60, pp. 421-431, 2004
- [2-91] Greiner, R., Lindner, J. "Interaction formulae for members subjected to bending and axial compression in EUROCODE 3 - The Method 2 approach", *Journal of Constructional Research*, Vol. 62, pp. 757-770, 2006
- [2-92] DIN 18800, Teil 2: Stahlbauten, 1990
- [2-93] Load and resistance factor design specification for structural steel buildings, American Institute of Steel Construction Inc., Chicago, 1999

3 EXPERIMENTAL INVESTIGATION

3.1 INTRODUCTION

In this chapter the experiments of laced built-up columns that took place in the context of the present doctoral thesis will be presented. Main purpose of this experimental work was the in-plane testing of scaled Z-lacing type built-up columns under significant eccentricities of the applied axial loading at the ends. Parameters like the magnitude and direction of eccentricity, the profile of the chords and the density of the lacing varied, in order to address their effect on the columns' capacity. The measurements performed during the tests can be classified in two categories: (i) global measurements that characterise the overall structural response of the specimens in terms of load-displacement curves with the use of LVDTs, and (ii) local measurements that characterise the local structural response of the specimens in terms of load-strain curves with the use of strain gauges. In general, previous experimental tests focused only on the first category of measurements and identification of local failures was mainly based on visual observations. Apart from the assessment of the structural behaviour and failure of laced columns, the present experimental investigation was also used as the basis for the calibration of numerical models.

3.2 DESCRIPTION OF EXPERIMENTS AND EXPERIMENTAL SET-UP

3.2.1 Specimen groups

A total number of 10 simply-supported eccentrically loaded columns have been tested (5 pairs of similar columns for repeatability purposes) at the Institute of Steel Structures in the School of Civil Engineering of the National Technical University of Athens. The specimens were constructed by the Greek company NOE Constructions S.A. [3-1] that is active in the field of the design, fabrication and erection of many kinds of steel structures. Balance between the desirable research aspects and the limitations imposed by the existing equipment in the laboratory on the specimens and the maximum load that the actuator could apply led to the selection of geometry and cross-section of specimens. The total available height is approximately equal to 3.9m within which the actuator, the top and bottom supports and the specimen should be placed, thus leading to an available height of 234.5cm for the specimens. Additionally, the maximum load that the actuator could safely apply is equal to 500kN.

Each specimen was named according to the group it belonged to, followed by the number 1 or 2 (i.e. the two specimens of group 1 were named 1(1) and 1(2)). Indicative sketches of the column specimens in the five groups together with their top and bottom hinged supports and eccentricities (e_{top} and e_{bot}) are shown in Figure 3-1. The numbering of the panels is also shown, as measured starting from the bottom support. The nominal length L of all specimens was equal to 202cm, while their effective length L_e , as measured from the top pinned support to the bottom one, was equal to 234.5cm (satisfying the maximum height limitation). In all cases the lacing bars had an angle cross-section L25x25x3 and were welded on the chords. Additional characteristics for each specimen group including panels' lengths, flanges' cross-sections, magnitude and direction of eccentricities of the loads at the ends (considered as positive when resulting in clockwise end moment), are listed in Table 3-1.

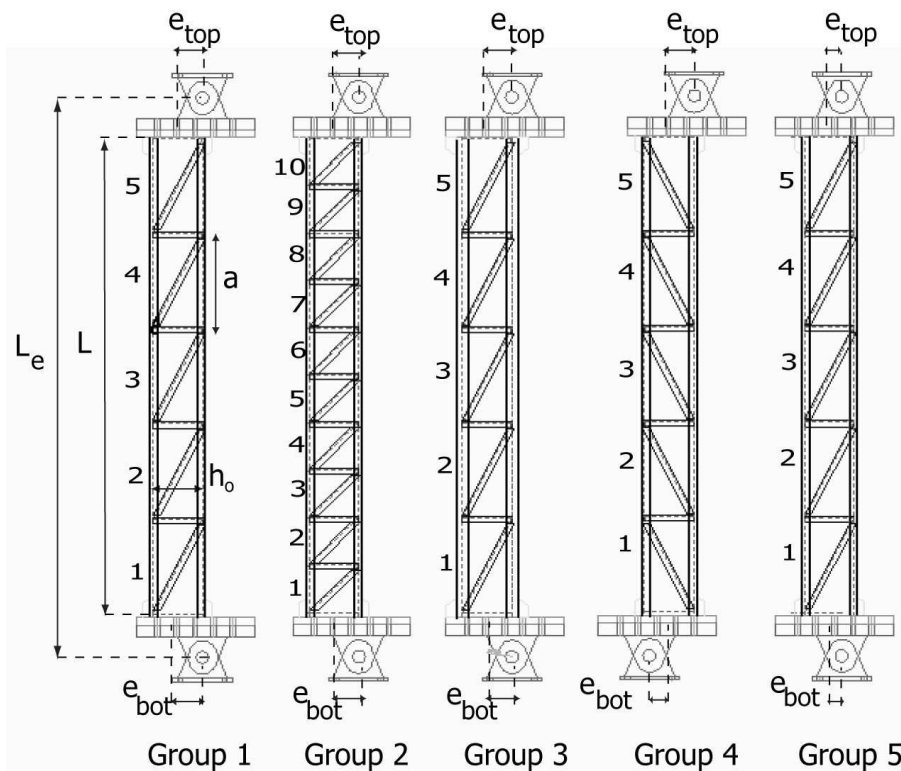


Figure 3-1: Specimen groups

Table 3-1: Characteristics of the five specimen groups

Group	Panel's length a (cm)	Flanges' cross-section	e_{top} (cm)	e_{bot} (cm)
1	40	UNP60	10	-10
2	20	UNP60	10	-10
3	40	IPE80	10	-10
4	40	UNP60	10	8
5	40	UNP60	5	-5

The design of the specimens was based on allowing failure to take place only along the chords. The specimens' diagonal bars were selected to have sufficient over-strength, in accordance with common practice. This was one of the main reasons for selecting angle cross-sections for the diagonal bars, as they are characterised by larger buckling strengths when compared to rectangular cross-sections of the same area. Observing the eccentricities of the loads at the top and bottom of the specimens, it can be concluded that in Groups 1, 2, 3 and 5, the specimens were subjected to end moments of opposite direction (single curvature) and in Group 4 to end moments of the same direction (double curvature). The first two groups differed only as far as the density of the lacing is concerned, in order

to investigate the effect of a stiffer lacing, of the total number of welds and of the smaller length of panels on the structural response and bearing capacity of the columns. Group 1 had a mono-symmetric UNP60 cross-section, while Group 3 had a doubly symmetric IPE80 cross-section. Based on their comparison it could be observed whether the eccentrically loaded UNP chords exhibit significantly different behaviour from the centrally loaded IPE chords. Comparison between Group 1 (single curvature deformation) and Group 4 (double curvature deformation) would highlight the differences between initiation of failure from an intermediate and from an end panel. Finally, Group 5 had half magnitude of eccentricity at its ends in comparison with Group 1, so that axial load would play a more important role than the end bending moments, leading in this way to more pronounced geometrical nonlinearity. Three-dimensional views of the specimen groups are shown in Figure 3-2. The bolts that were used for connecting the main body of the specimens with the supports, and the supports with the testing frame at the bottom and actuator at the top, are also depicted. These bolts were prestressed in order to achieve full cooperation between the connecting elements, thus allowing the consideration that they acted as one.

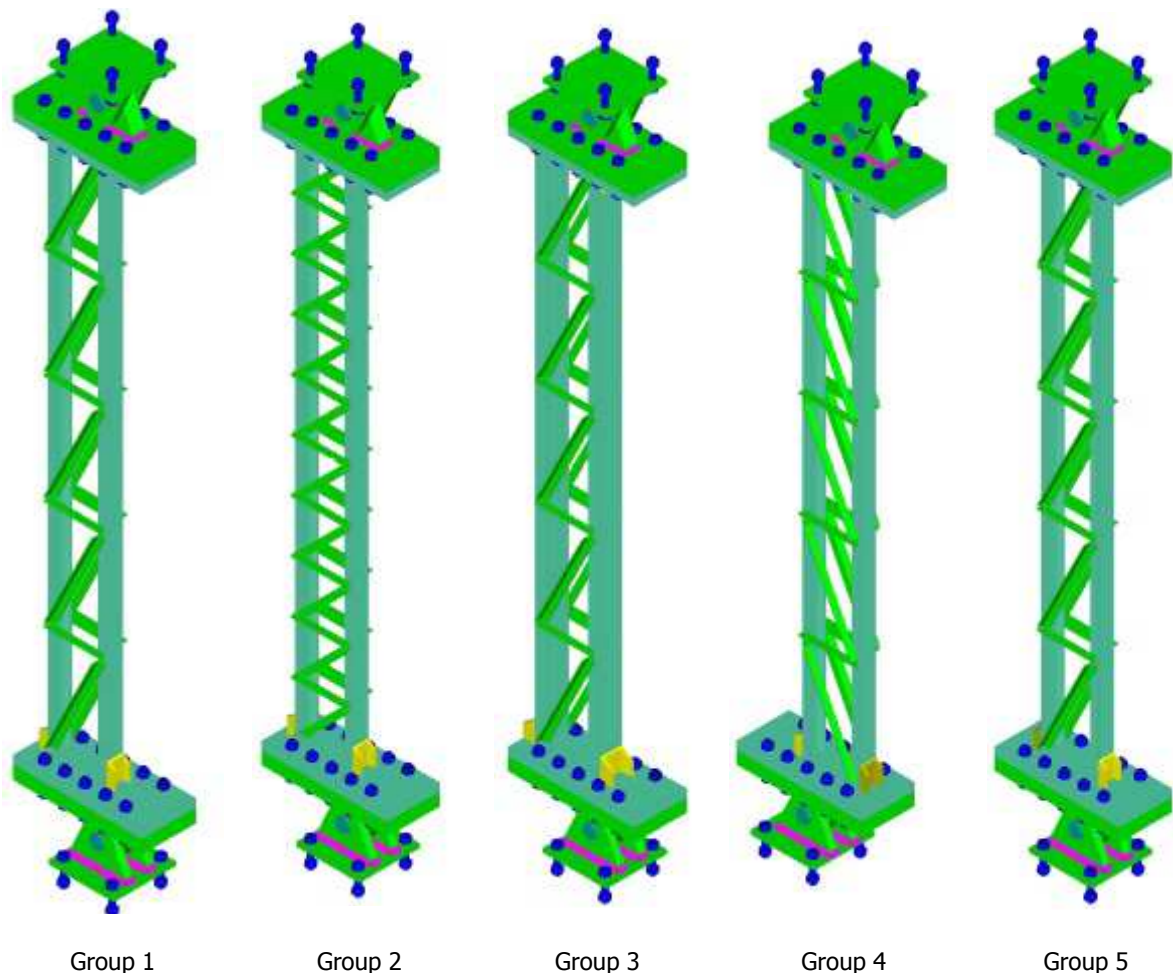


Figure 3-2: Three-dimensional views of the five specimen groups

The maximum load expected for the geometry and cross-sections selected, was calculated for Group 3. According to the conservative calculations of Eurocode 3, it was approximately equal to 159kN and 227kN for S235 and S355 steel, respectively. The possibility of obtaining a larger collapse load due to higher steel's strength and/or due to smaller initial global and local imperfections would not be worrying as a sufficiently safe margin was left from the 500kN that the actuator could apply.

3.2.2 Testing frame

A typical specimen after its vertical placement in the testing frame is depicted in Figure 3-3. At the top and bottom of the specimens hinged supports were used for the connection with the actuator and frame, respectively. The supports' design was based on the concept that for the expected magnitude and direction of load they should behave elastically and be sufficiently rigid. Horizontal beams were placed at specimens' mid-height in order to restrict out-of plane movement. The horizontal beams were at a very small distance from the specimens so that any undesirable contact between them would be avoided.

Due to the type of loading imposed on the specimens both vertical and horizontal reactions were expected to appear at the supports. The vertical reactions could be safely transferred to the testing frame through the top and bottom supports. The horizontal reaction at the bottom could also be directly transferred to the testing frame, but this was not the case at the top. In order to avoid stressing the actuator horizontally, due to horizontal reactions at the top end of the column, a special device was constructed and placed at the top of each column as shown in Figure 3-4. This device consisted of two cantilevers that were rigidly connected to the frame and had rollers at their free end, facilitating in this way the vertical movement of the actuator. It was crucial that the rollers move freely and transfer no vertical load from the actuator to the cantilevers.

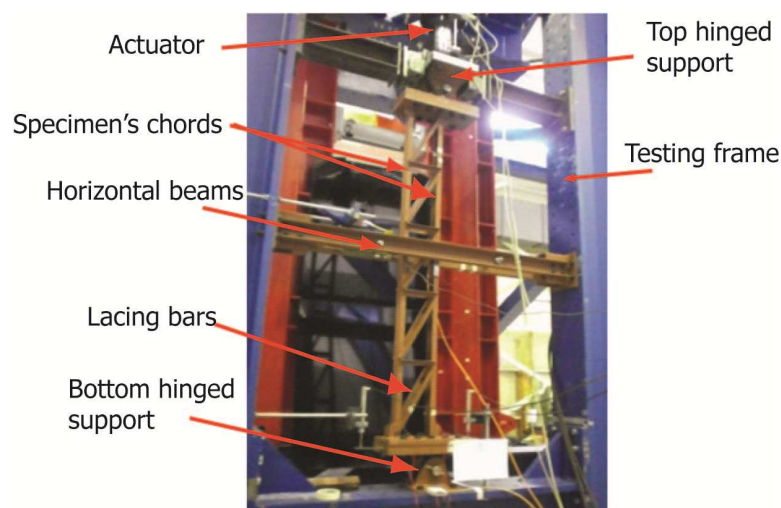


Figure 3-3: View of typical specimen at the testing frame

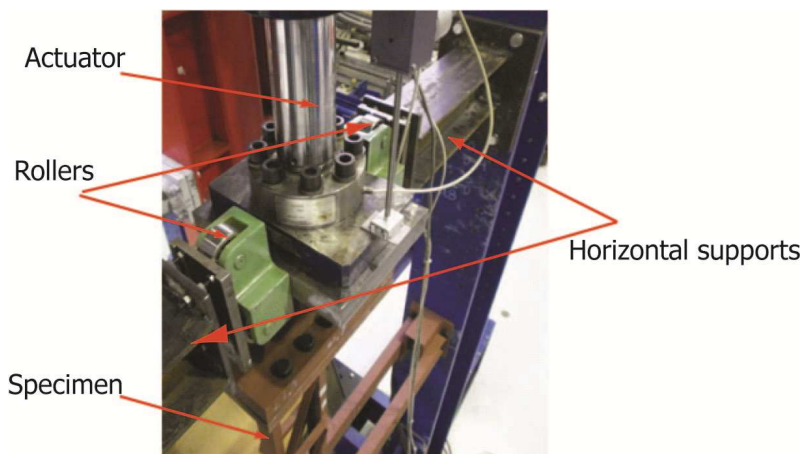


Figure 3-4: Close view of top support

3.2.3 Testing procedure and measuring devices

The tests were performed with the use of a 500kN actuator of maximum pressure equal to 250bar constructed by company MALVASIA [3-2] operating in displacement control. The rate control of the applied displacement was in all cases equal 0.0025mm/s. The machine controlling the actuator measured the applied vertical displacement and automatically transformed it into load.

In Figure 3-5 the locations of measuring devices are depicted. LVDTs (Linear Variable Differential Transformers) by company KYOWA [3-3] (Figure 3-6) were used for measuring the deflections at the mid-height (Groups 1, 2, 3, 5) and at a distance equal to 1/5 of the actual length from the bottom and top support of the column (Group 4). Their measurements were used for obtaining load-horizontal displacement graphs and identifying the global response of the columns. The measurement of the strains took place with the use of sensing elements that electrically detect micro mechanical changes through a change of their resistance. The strain gauges were provided by KYOWA [3-3] and had a nominal resistance of 120 Ω . Additionally, strain gauges were placed at various locations on the web of the compressed chords (named A, B and C in Figure 3-5) along the columns (Figure 3-7) and on the side of the end diagonal bar (denoted as D in Figure 3-5) welded on the chords. Their measurements were related to the axial strain which was used for observing the local response of the panels. The locations of the strain gauges were selected to be such that the local behaviour of many panels could be identified, including regions that remained elastic and those that entered the plastic region. Special care was given for the correct placement of the strain gauges by polishing the desirable location in order to ensure a satisfactory contact between the strain gauge and the surface.

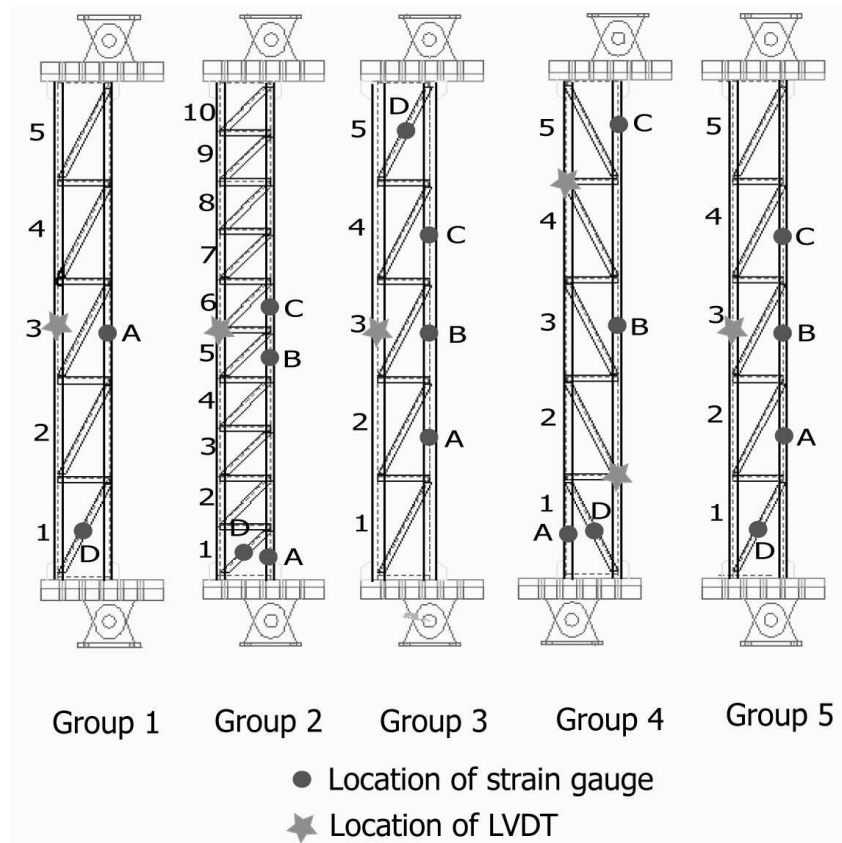


Figure 3-5: Specimen groups with locations of measuring devices



Figure 3-6: LVDT placed at mid-height of specimen



Figure 3-7: Strain gauge placed at the web of the chord

3.3 MATERIAL PROPERTIES

The material properties of the steel used for manufacturing the specimens were extracted through tensile tests with the use of displacement control in appropriately designed coupons obtained from the columns' flanges. The geometry of the coupons and the testing procedure was based on the guidance provided by DIN 50125 [3-4]. The tensile tests took place at a servo-hydraulic testing frame by INSTRON [3-5] that is capable of applying 300kN. The results were given in terms of applied load and corresponding displacement of the coupons' edges from which the engineering stress (σ_e) and engineering strain (ϵ_e) could be calculated. The true stress (σ_t) and true strain (ϵ_t) that account for the change of the coupons' width during the loading process were calculated according to the following formulas:

$$\sigma_t = \sigma_e (1 + \epsilon_e) \quad (3-1)$$

$$\epsilon_t = \ln(1 + \epsilon_e) \quad (3-2)$$

A view of a typical coupon at its final shape before testing is shown in Figure 3-8 and during testing in Figure 3-9. The width's reduction at the mid-height of the coupon due to Poisson's effect is clearly seen.



Figure 3-8: Typical tensile coupon



Figure 3-9: Coupon during the tensile test

The average Young's modulus for all specimens was 210GPa. The yield stress for each coupon was taken as the 0.2% proof stress found in the plateau following the elastic branch. The mean yield stresses for each group are given in Table 3-2. A typical true stress-true strain graph is given in Figure 3-10.

Table 3-2: Mean yield stresses of specimen groups

	Group 1	Group 2	Group 3	Group 4	Group 5
Yield stress (MPa)	338	338	395	335	302

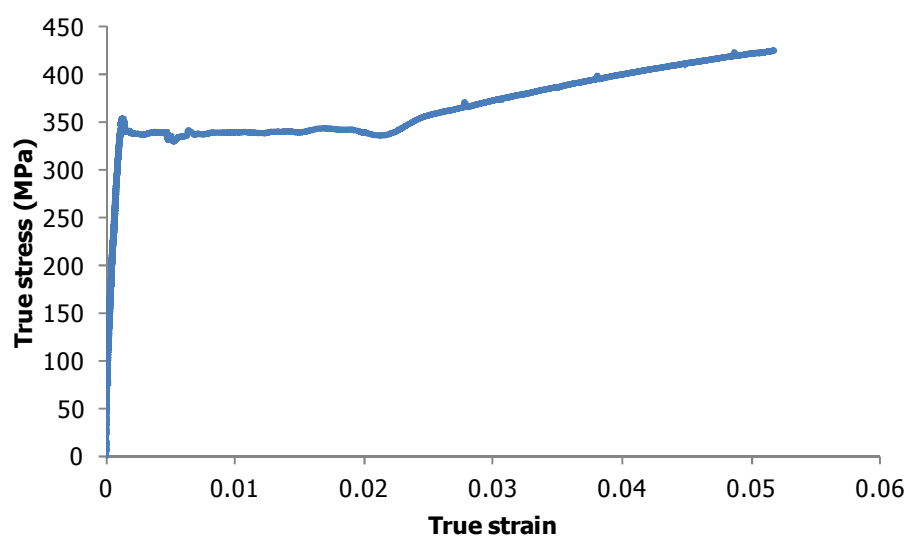


Figure 3-10: True stress-true strain relationship for the steel of Group 1

3.4 EXPERIMENTAL RESULTS

The experimental results are summarized in the following sections for every group separately. Equilibrium paths, indicative load-strain diagrams and indicative deformed shapes are presented. The maximum load along the equilibrium paths was considered to be the collapse load. The panel from which failure initiated and had the largest local lateral deflections will be characterised as critical panel in the following sections. Global buckling will refer to buckling of the column as a whole and local buckling to buckling of one of the chords between adjacent connections.

3.4.1 Group 1

The equilibrium paths of the specimens 1(1) and 1(2) are depicted in Figure 3-11. The collapse load of the specimens was 200kN. In the post-buckling range, the second panel buckled inwards for both specimens 1(1) and 1(2), as shown in Figure 3-12(a) - (b). It was thus concluded that the critical panels were the second ones in both specimens, although all three intermediate panels were expected to have similar high level of stress. This was verified by the strain measurements at location A (panel 3), shown in Figure 3-13, where buckling was not observed but a strain magnitude larger than the one that corresponded to the yield strain was reached.

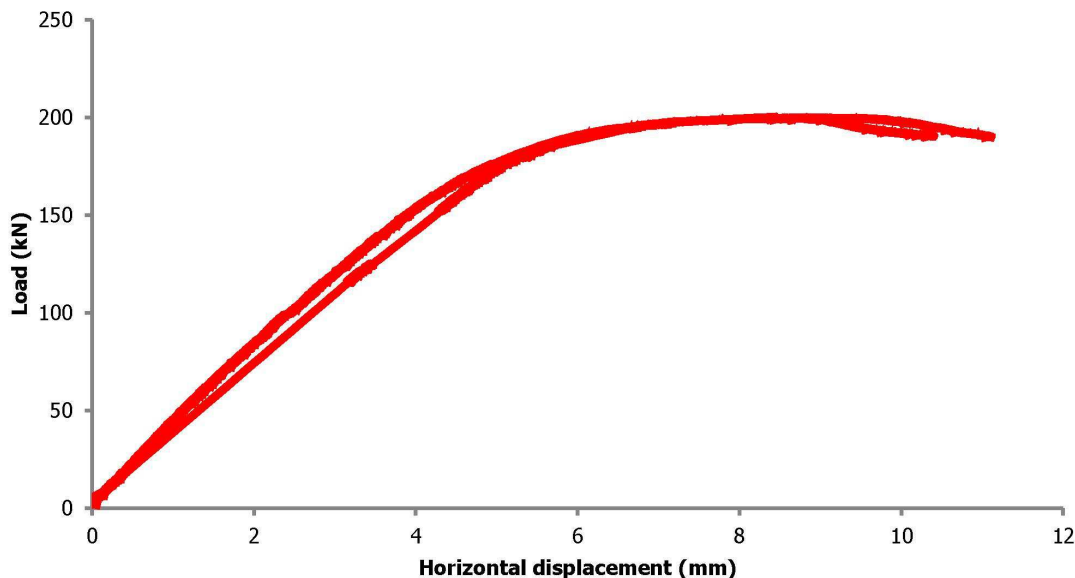


Figure 3-11: Equilibrium paths of specimens 1(1) and 1(2)

The strain measurements of the end diagonal at location D are depicted in Figure 3-14. It can be seen that a satisfactory agreement between them exists and that the strains appearing along the end diagonals were relatively small, as single curvature deformations did not lead to significant shear forces at the ends of simply-supported columns. Their existence therefore was attributed to the relatively small shear forces and to arbitrary unmeasurable parameters that differed in the two tests. The diagonals remained in the elastic region.

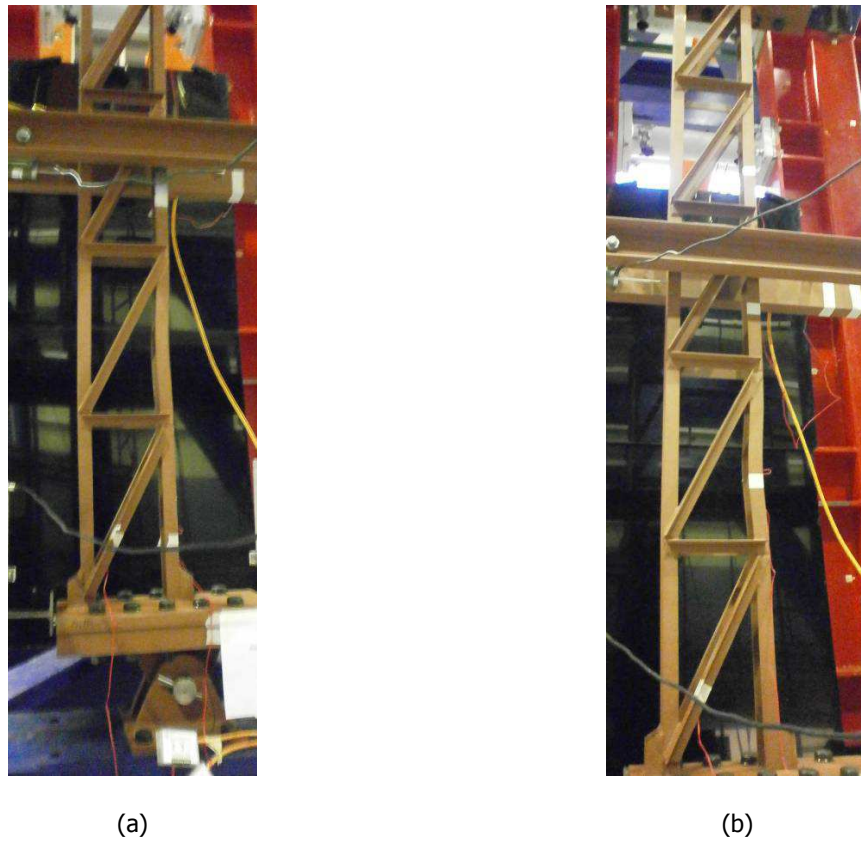


Figure 3-12: Deformed shape of specimens (a) 1(1) and (b) 1(2)

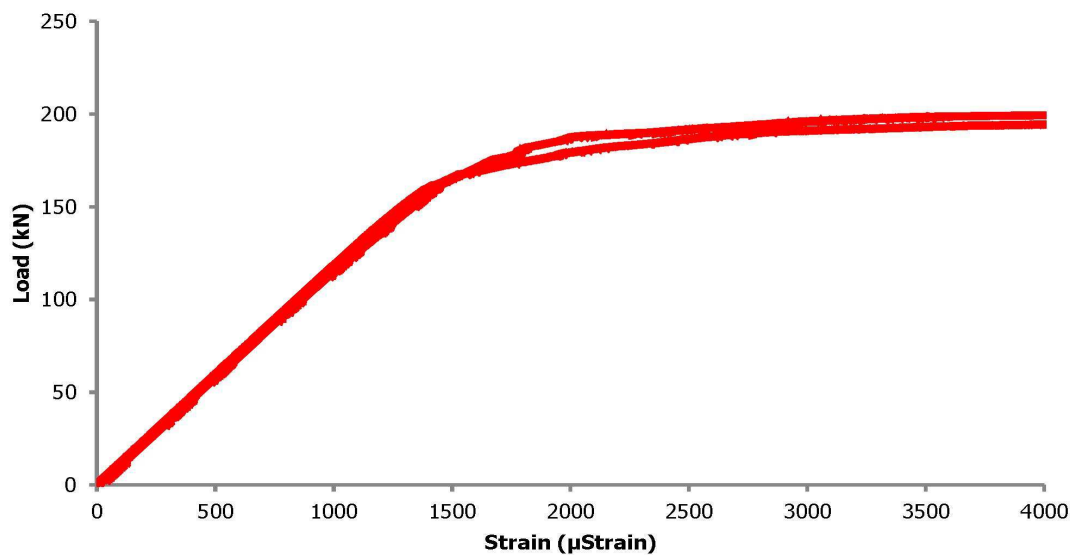


Figure 3-13: Load-strain relationship at location A of Group 1 specimens

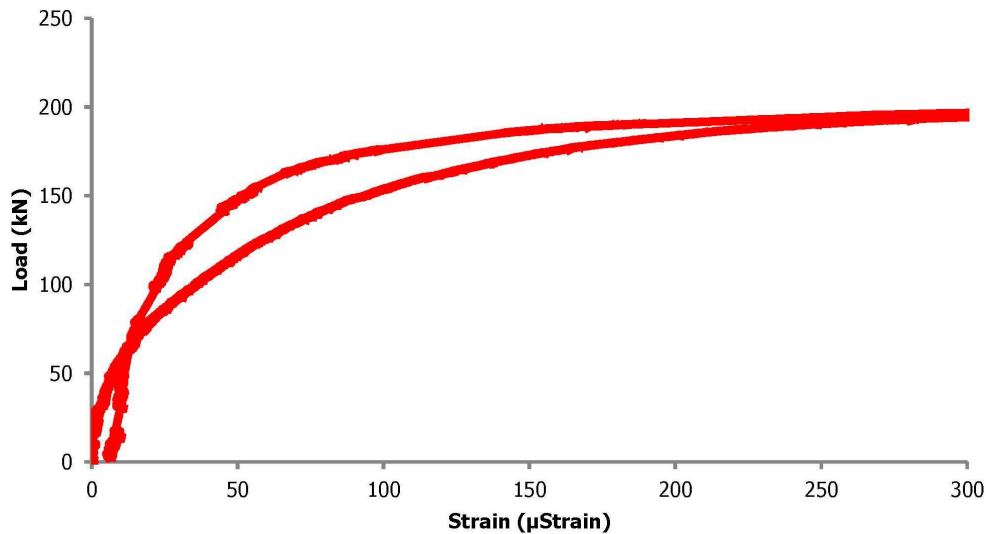


Figure 3-14: Load-strain relationship at location D of Group 1 specimens

3.4.2 Group 2

The equilibrium paths of specimens 2(1) and 2(2) based on the horizontal mid-height displacement are depicted in Figure 3-15. The collapse load of the specimens was 206kN and the more dense lacing arrangement offered only a small increase in the capacity in these specific cases. The stocky behaviour of the specimens at local level resulted in no local buckling of the panels. The single curvature deformed configurations of specimens 2(1) and 2(2) in the post-failure range are shown in Figure 3-16(a) - (b). The strain measurements along the compressed chord at locations A, B and C are shown in Figure 3-17 to Figure 3-19, respectively. The regions B and C reached high levels of strain, revealing that plastification initiated earlier at these locations. From this remark, it was concluded that the critical panels were the fifth and sixth ones in both specimens. This was verified by the strain measurements at location B (panel 5) which reached a magnitude larger than the one corresponding to yield strain.

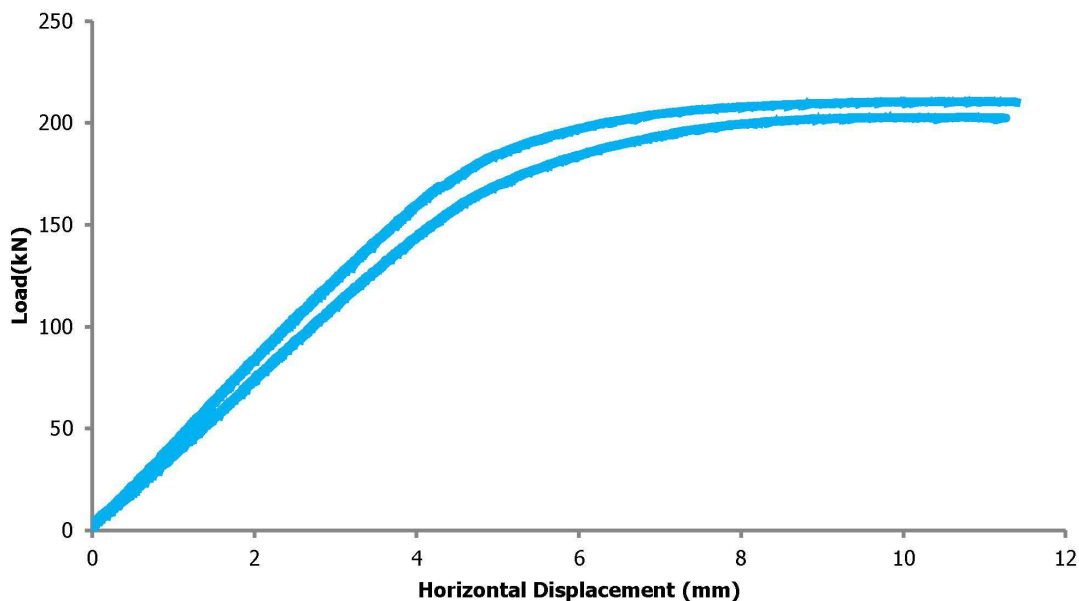


Figure 3-15: Equilibrium paths of specimens 2(1) and 2(2)

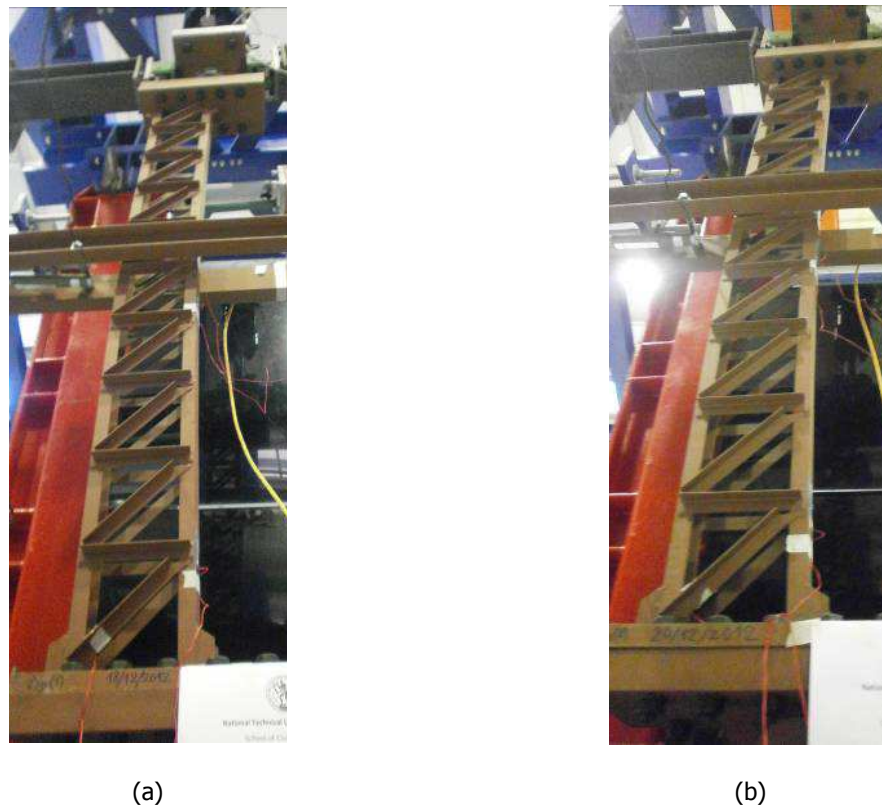


Figure 3-16: Deformed shape of specimens (a) 2(1) and (b) 2(2)

The strain measurements of the end diagonal at location D are shown in Figure 3-20. It can be seen that the strains appearing along the end diagonals were relatively small, as single curvature deformations did not lead to significant shear forces at the ends of simply-supported columns. Their existence was attributed, as for Group 1, to the small shear forces and to random factors that were not measured and resulted in differences between them. The diagonals remained elastic during the tests.

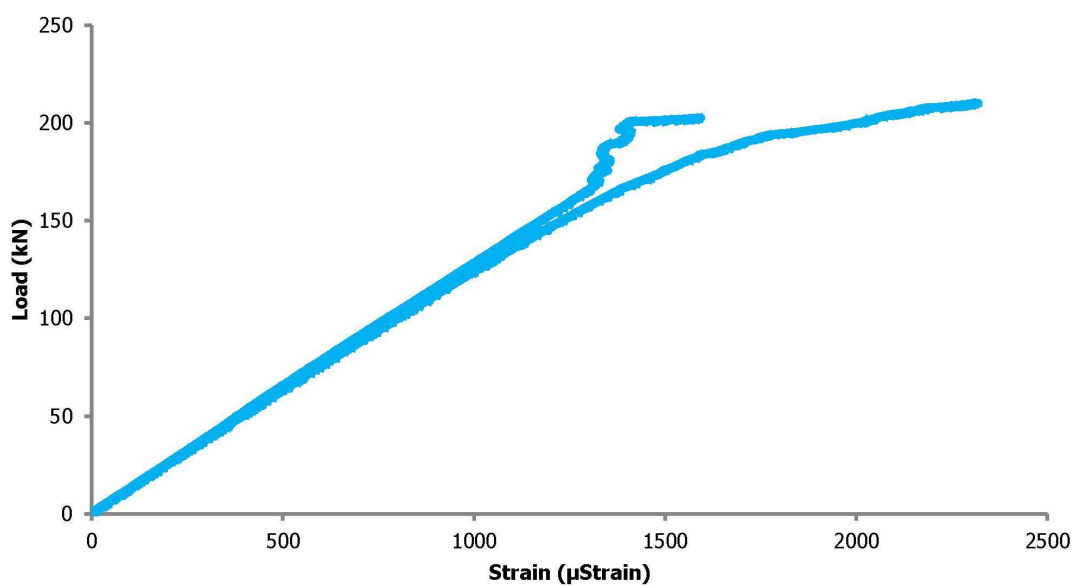


Figure 3-17: Load-strain relationship at location A of Group 2 specimens

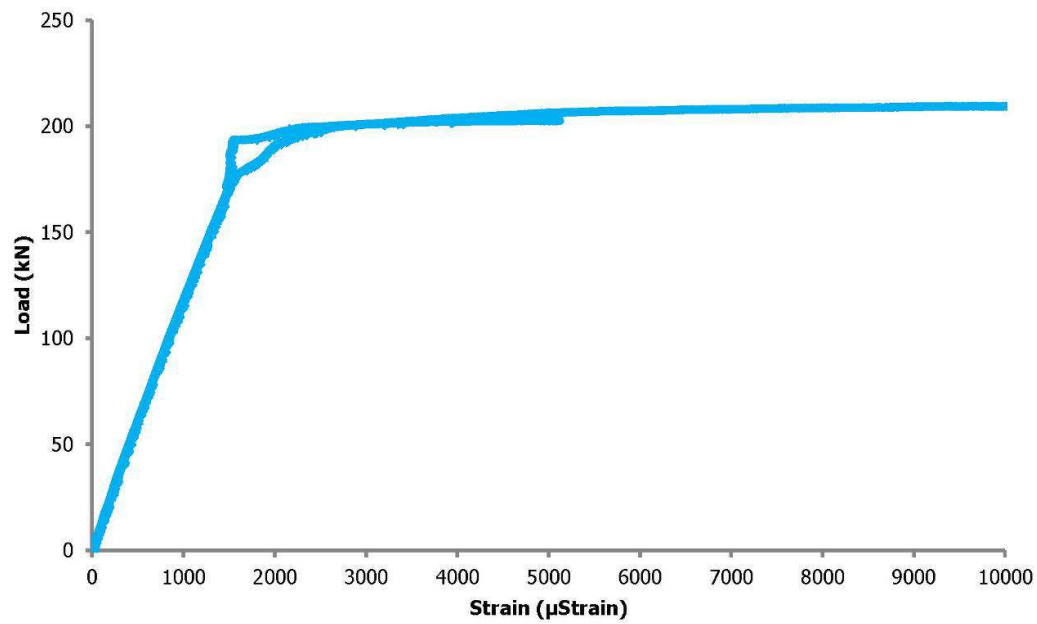


Figure 3-18: Load-strain relationship at location B of Group 2 specimens

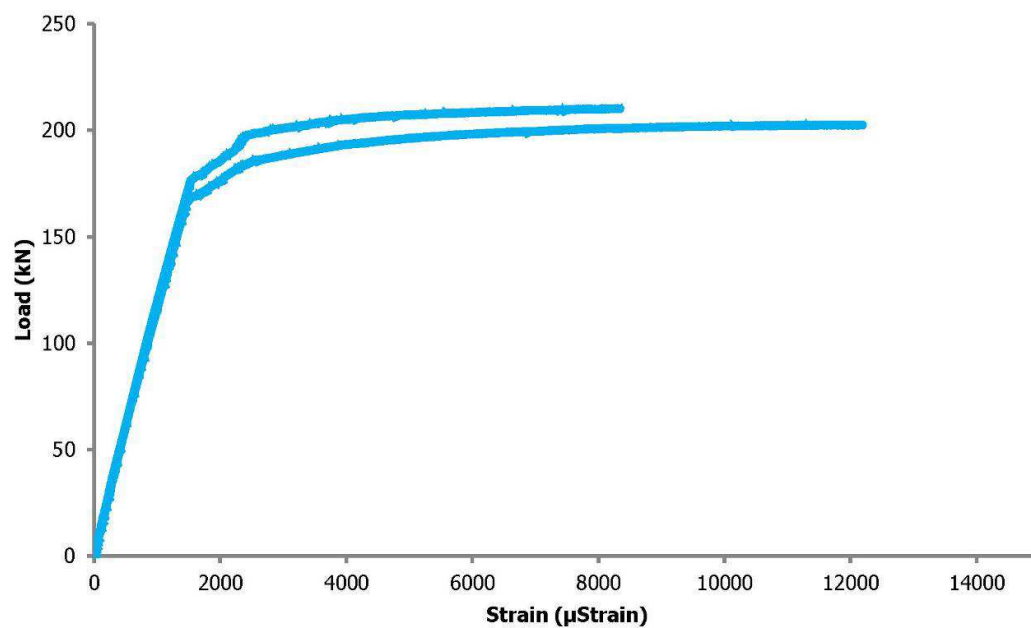


Figure 3-19: Load-strain relationship at location C of Group 2 specimens

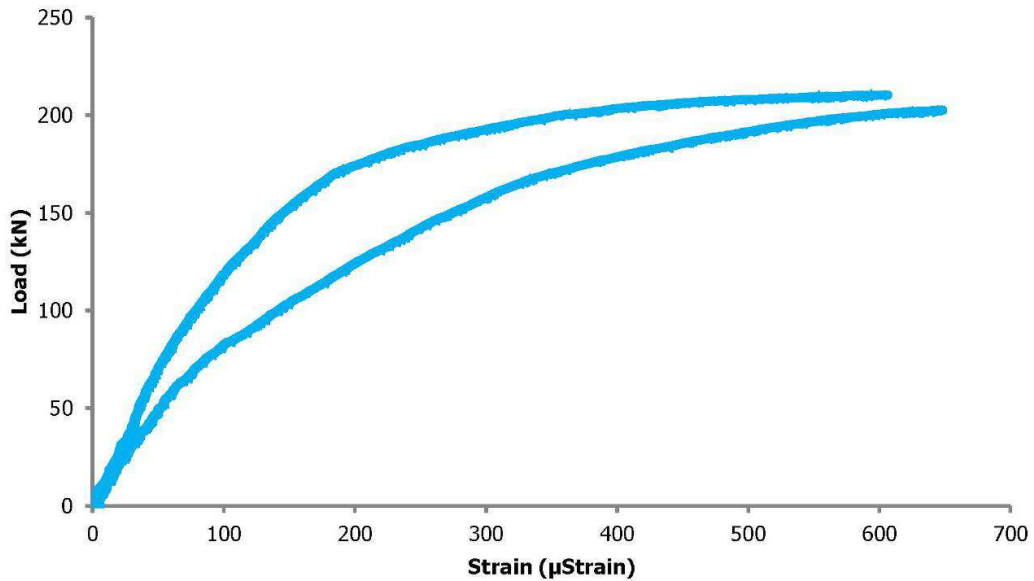


Figure 3-20: Load-strain relationship at location D of Group 2 specimens

3.4.3 Group 3

The equilibrium paths of specimens 3(1) and 3(2) based on the horizontal mid-height displacement are shown in Figure 3-21. The collapse load of the specimens was 309kN, larger than in Groups 1 and 2. This was attributed to the stronger chords used (IPE80 instead of UNP60) in terms of both axial and bending rigidity. The single curvature deformed configurations of specimens 3(1) and 3(2) in the post-failure range are shown in Figure 3-22(a) - (b). It can be seen that the fourth and third panels buckled inwards in specimens 3(1) and 3(2), respectively. As in the previous cases, the intermediate panels were expected to have similar stress levels and therefore the different locations of local buckling in Group 3 indicated the presence of initial imperfections. These initial imperfections could be attributed either to material non-homogeneity or geometrical out-of-straightness or combination of these. The strain measurements along the compressed chord at locations A, B and C are shown in Figure 3-23 - Figure 3-25, respectively, revealing that the material yielded in all three regions.

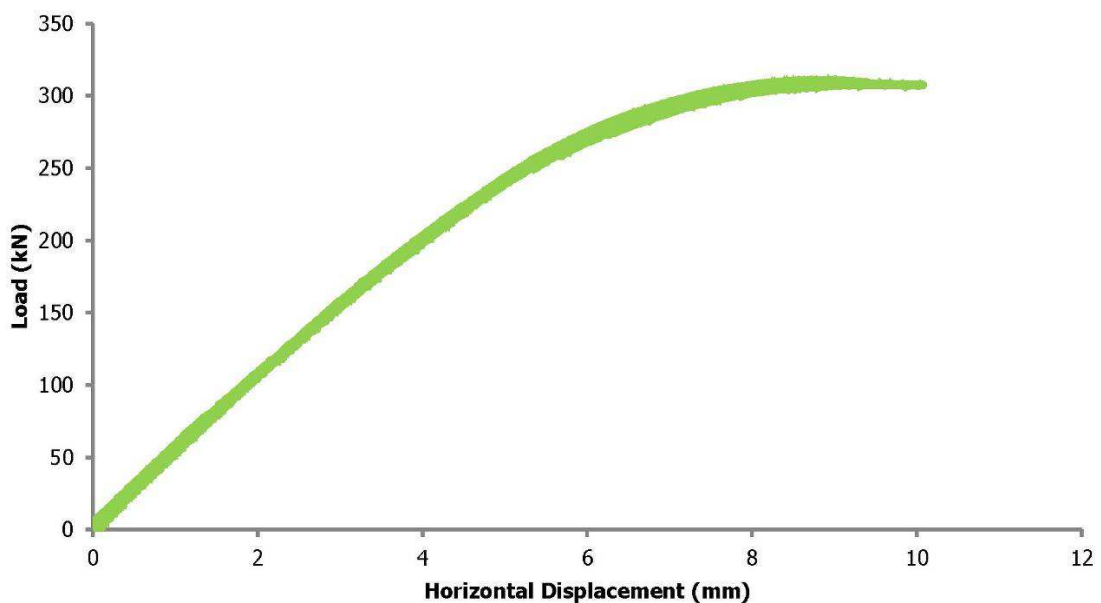


Figure 3-21: Equilibrium paths of specimens 3(1) and 3(2)

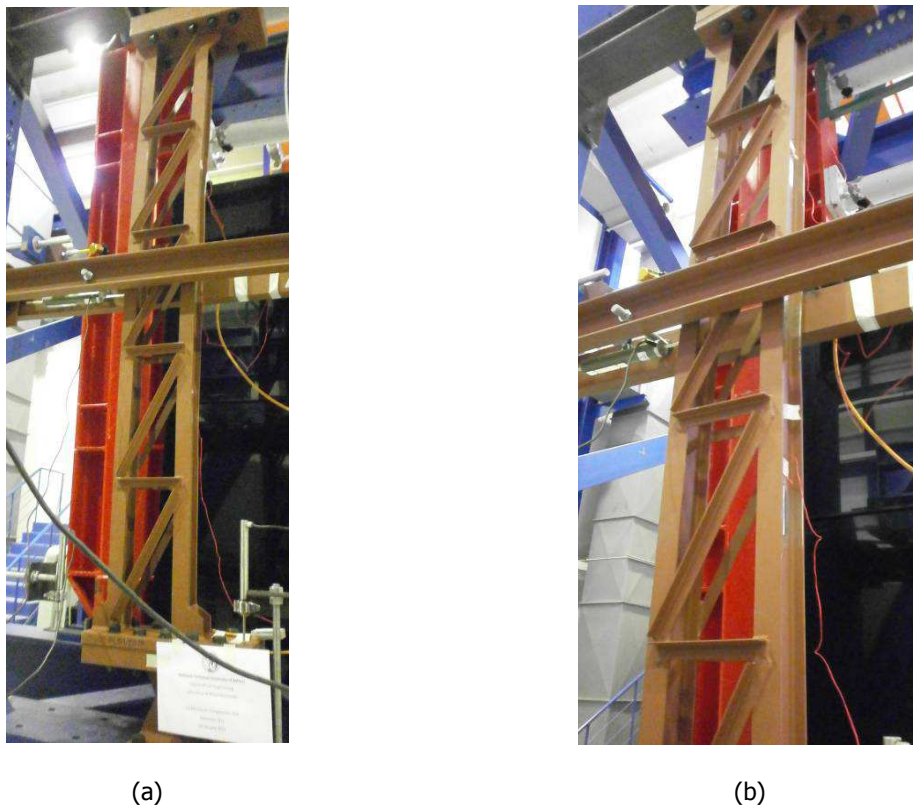


Figure 3-22: Deformed shape of specimens (a) 3(1) and (b) 3(2)

The strain measurements of the end diagonal at location D are presented in Figure 3-26. It can be seen that the strains appearing along the end diagonals were relatively small as in the previous groups. Additionally, they differed significantly between each other highlighting that for such small magnitudes many unknown factors may have played a role in them. The diagonal bars remained elastic throughout the tests.

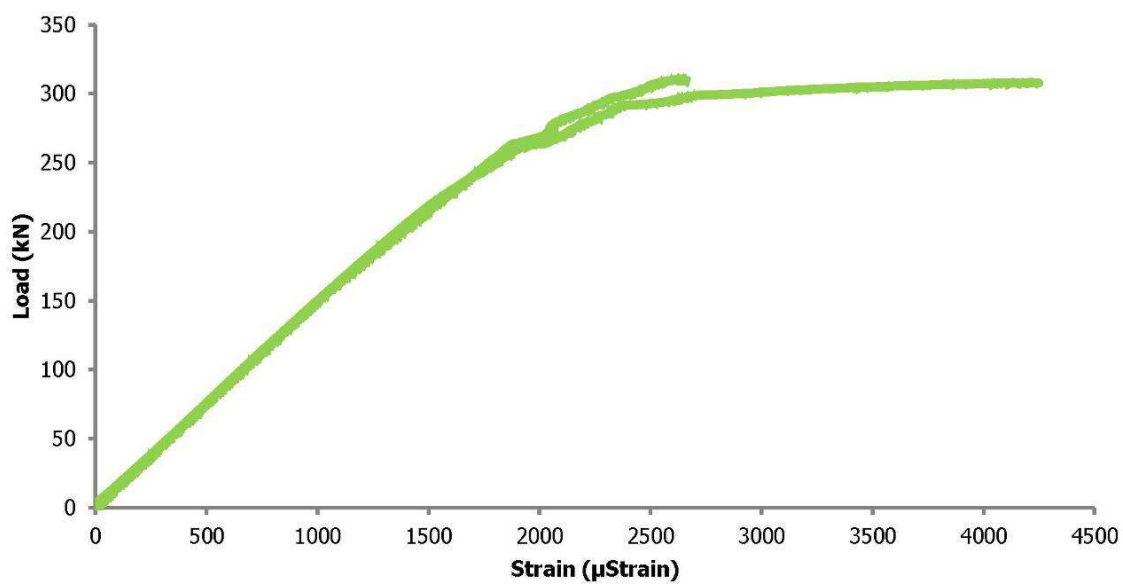


Figure 3-23: Load-strain relationship at location A of Group 3 specimens

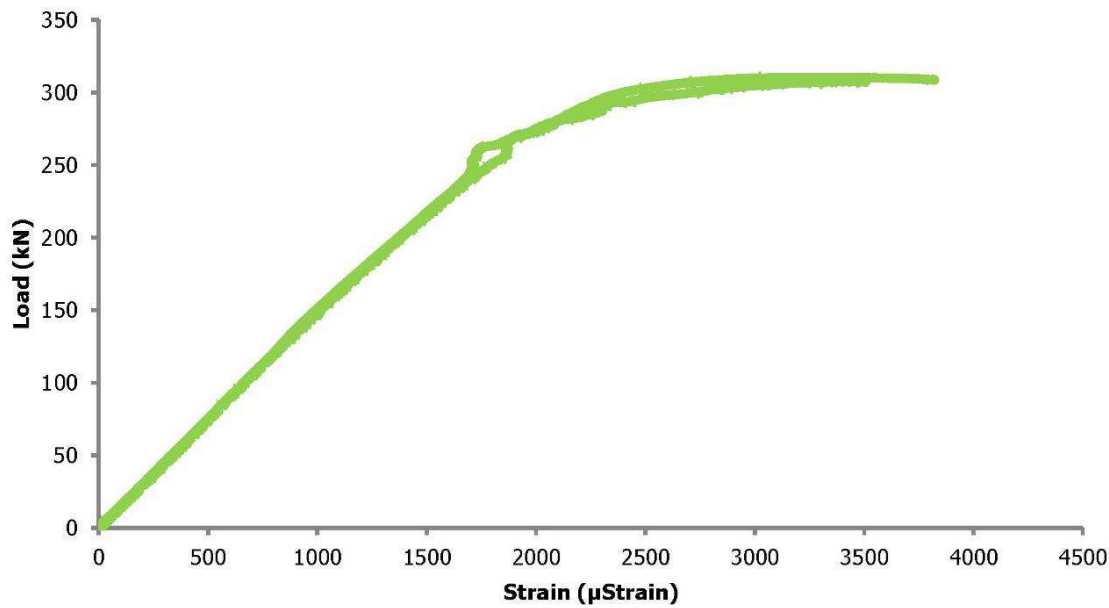


Figure 3-24: Load-strain relationship at location B of Group 3 specimens

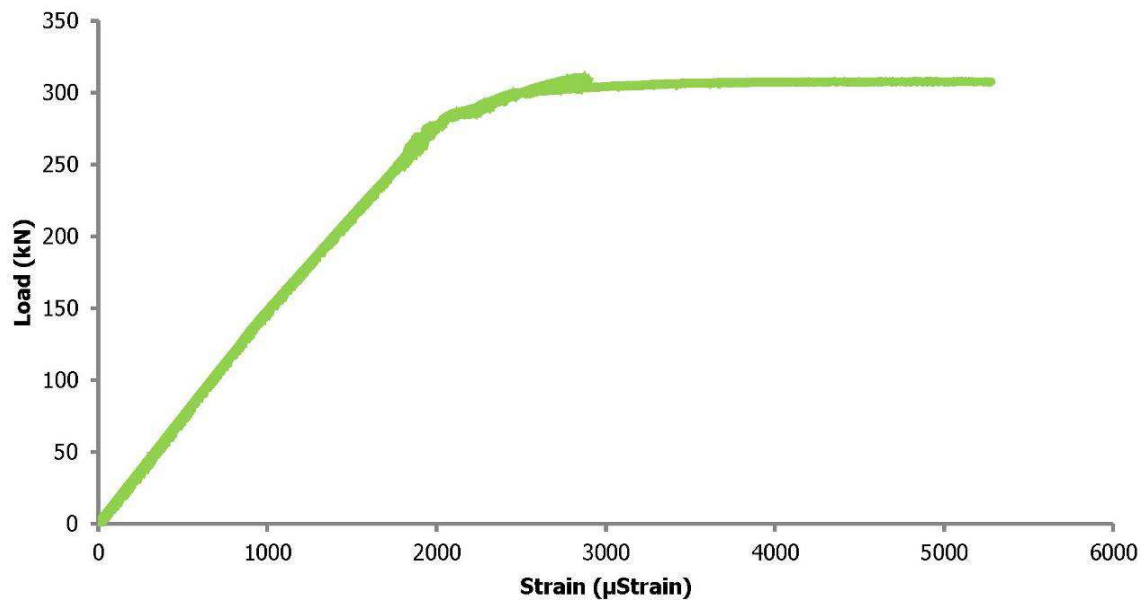


Figure 3-25: Load-strain relationship at location C of Group 3 specimens

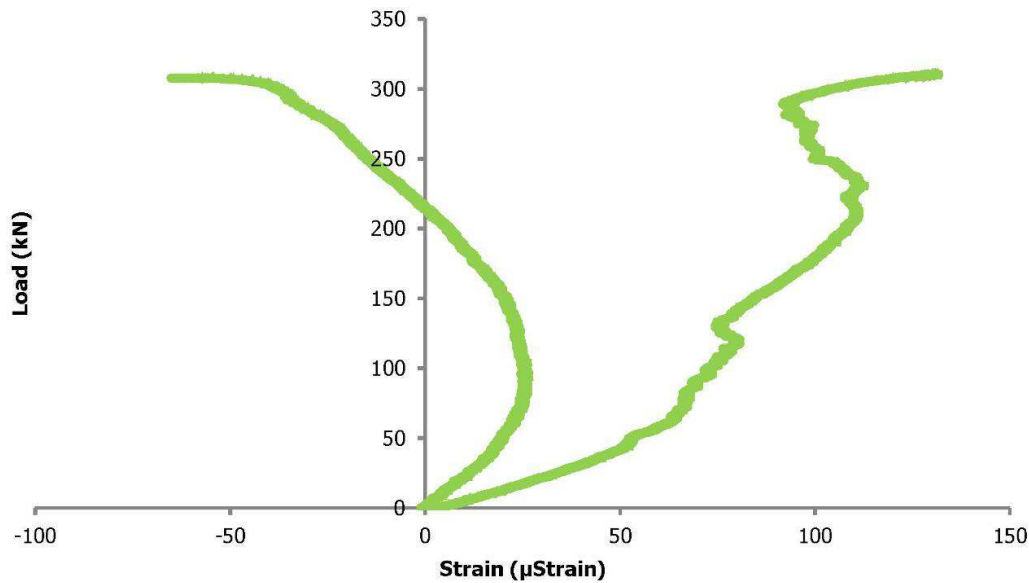


Figure 3-26: Load-strain relationship at location D of Group 3 specimens

3.4.4 Group 4

The equilibrium paths of specimens 4(1) and 4(2) are presented in Figure 3-27 for the displacement at the top and in Figure 3-28 for the displacement at the bottom. The collapse loads were equal to 230kN and 209kN for specimens 4(1) and 4(2), respectively. Double curvature deformation led to very small horizontal displacements which differed significantly at the bottom between the two tests. The deformed configurations of specimens 4(1) and 4(2) in the post-failure range are shown in Figure 3-29(a) - (b). It should be noted that the eccentricity at the top was slightly larger than at the bottom (see Table 3-1) and for this reason the fifth panel buckled inwards in both specimens. The strain measurements along the compressed chords at locations A, B and C are shown in Figure 3-30 - Figure 3-32, respectively. It can be concluded that the material at locations A and B remained elastic, while at location C it was plastified.

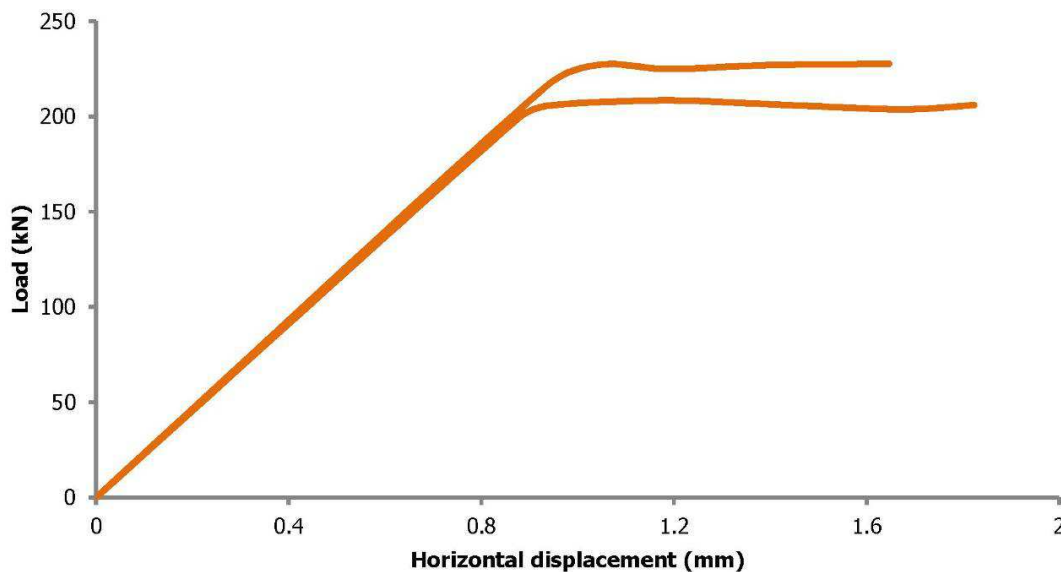


Figure 3-27: Equilibrium paths of specimens 4(1) and 4(2) based on horizontal displacement at the top

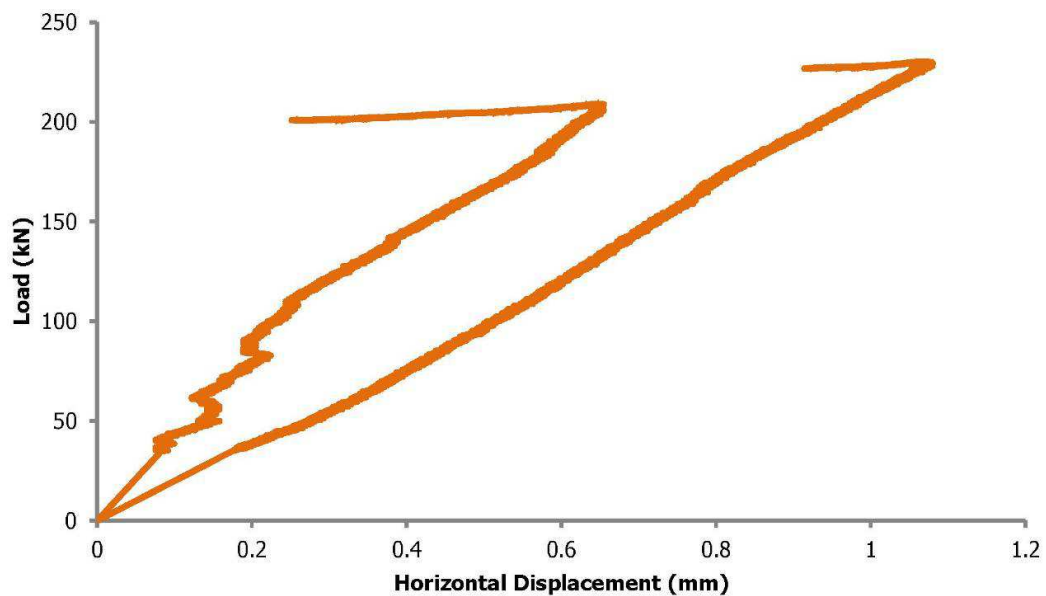
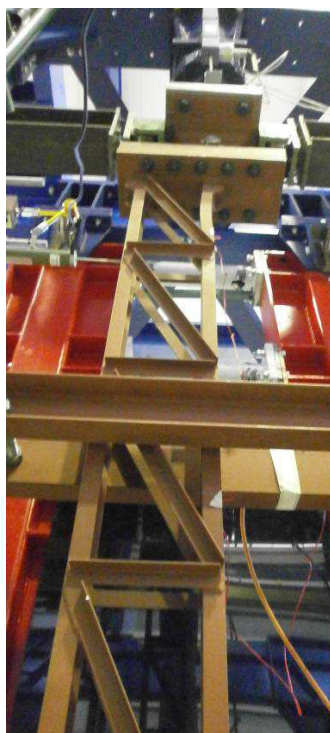
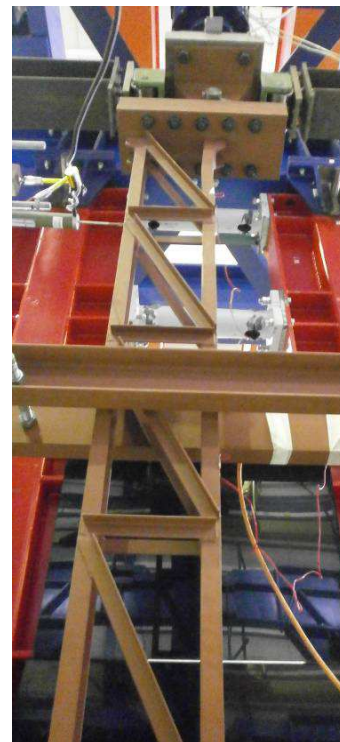


Figure 3-28: Equilibrium paths of specimens 4(1) and 4(2) based on the horizontal displacement at the bottom



(a)



(b)

Figure 3-29: Deformed shape of specimens (a) 4(1) and (b) 4(2)

The strain measurements of the end diagonal at location D are shown in Figure 3-33. It can be seen that the strains appearing along the end diagonals were relatively large due to the fact that double curvature caused large shear force at the ends of the columns. The two tests were in good agreement and the diagonals did not yield despite the larger magnitude of strains.

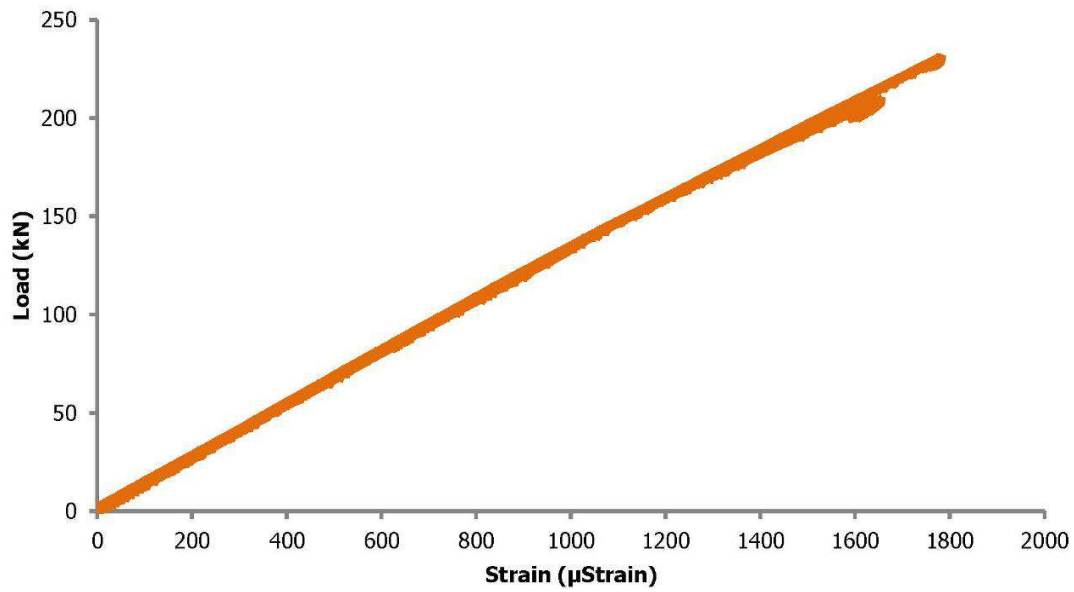


Figure 3-30: Load-strain relationship at location A of Group 4 specimens

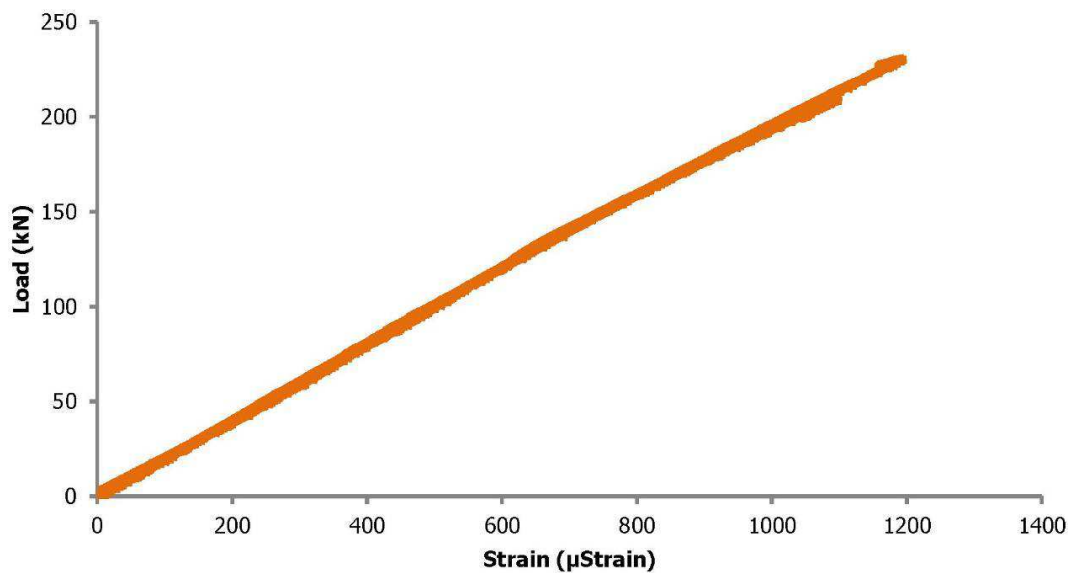


Figure 3-31: Load-strain relationship at location B of Group 4 specimens

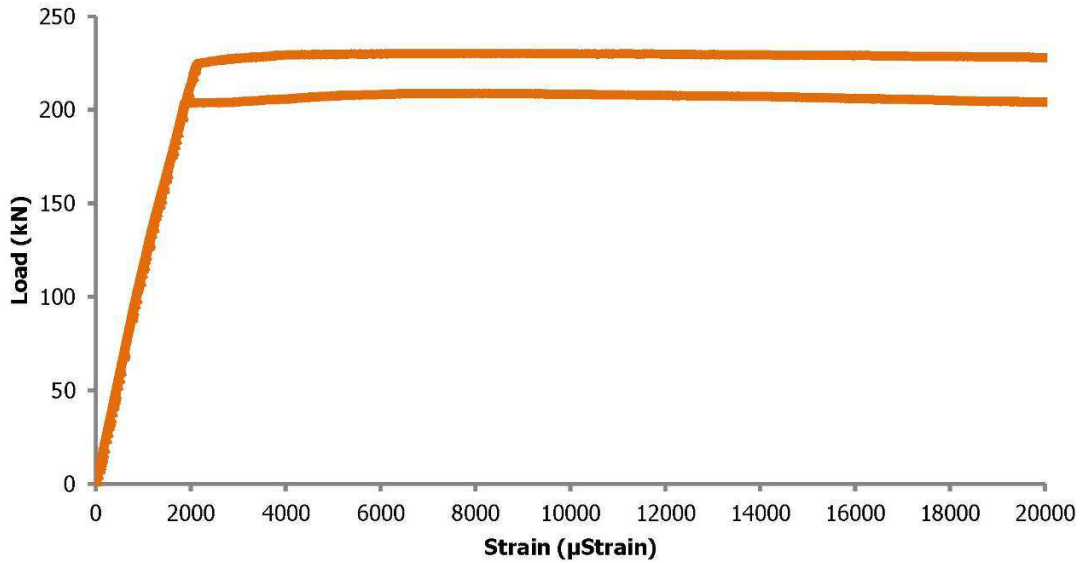


Figure 3-32: Load-strain relationship at location C of Group 4 specimens

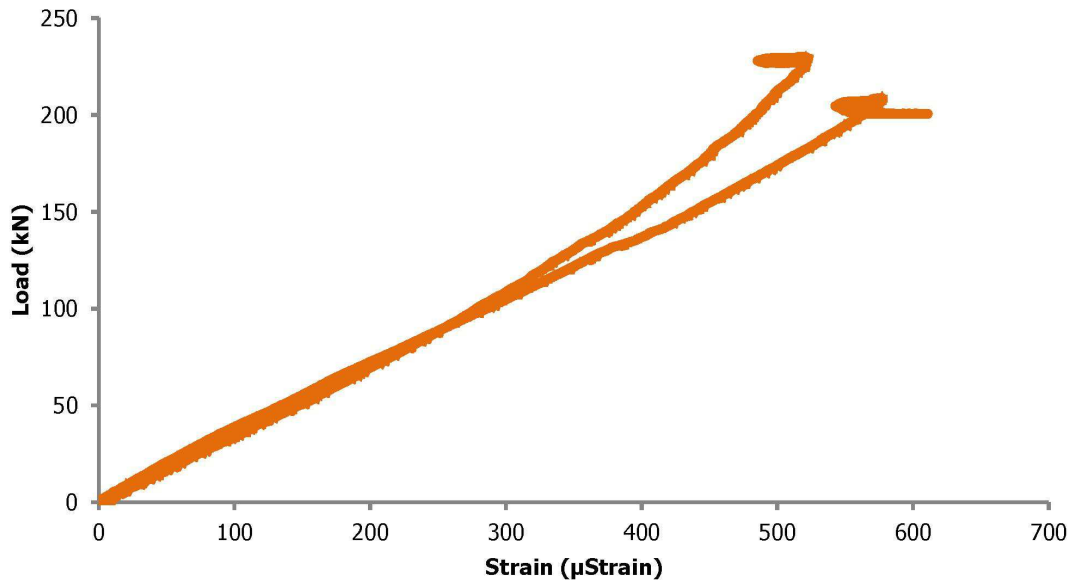


Figure 3-33: Load-strain relationship at location D of Group 4 specimens

3.4.5 Group 5

The equilibrium paths of the specimens 5(1) and 5(2) related to the horizontal mid-height displacement are presented in Figure 3-34. The collapse load of the specimens was 247kN, larger than in Group 1 due to the smaller eccentricity at the ends. The single curvature deformed configurations of specimens 5(1) and 5(2) in the post-failure range are shown in Figure 3-35(a) - (b). It can be seen that the second and fourth panels buckled inwards in specimens 5(1) and 5(2), respectively. As in Group 3, the intermediate panels were expected to have similar stress levels and therefore the different locations of local buckling in Group 5 indicated the presence of initial imperfections. The strain measurements along the compressed chord at locations A, B and C are shown in Figure 3-36 - Figure 3-38, respectively.

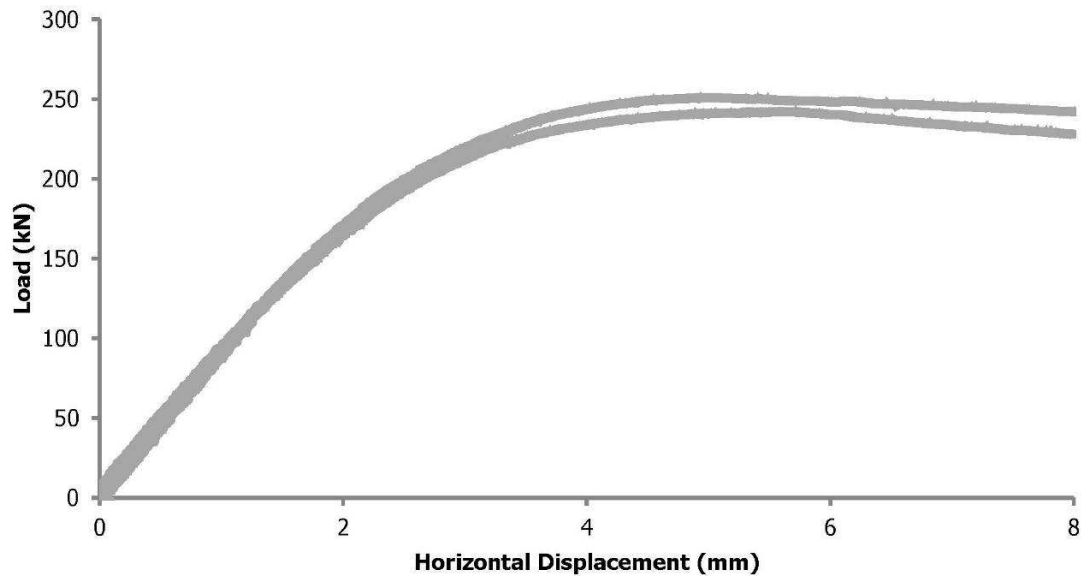
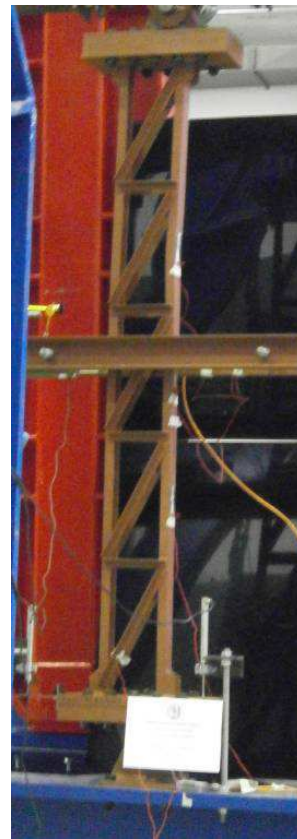


Figure 3-34: Equilibrium paths of specimens 5(1) and 5(2)



(a)



(b)

Figure 3-35: Deformed shape of specimens (a) 5(1) and (b) 5(2)

The strain measurements of the end diagonal at location D are depicted in Figure 3-39. The conclusions were the same as the ones drawn for Groups 1, 2 and 3 (single curvature deformation).

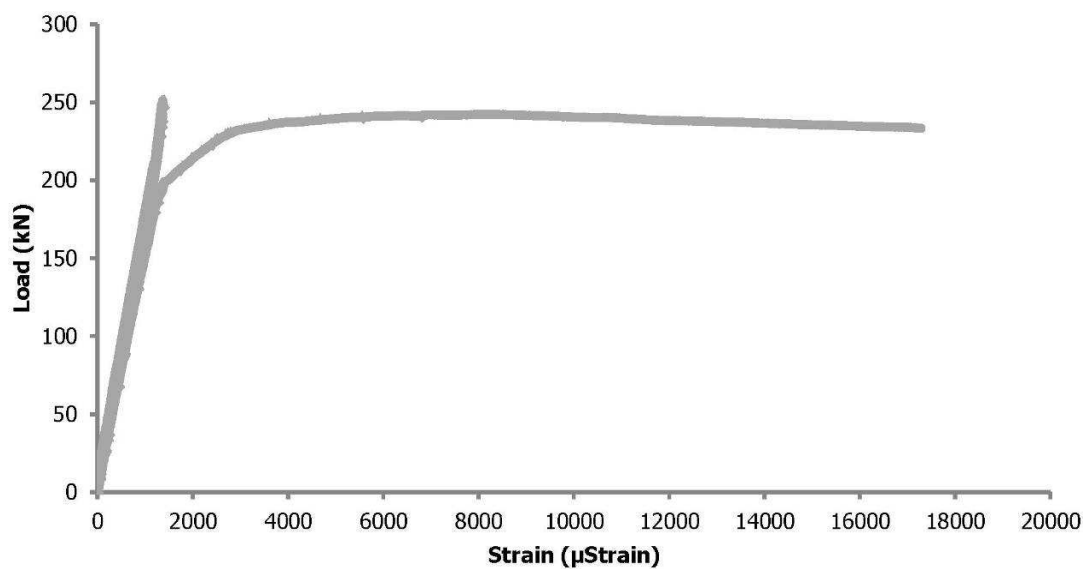


Figure 3-36: Load-strain relationship at location A of Group 5 specimens

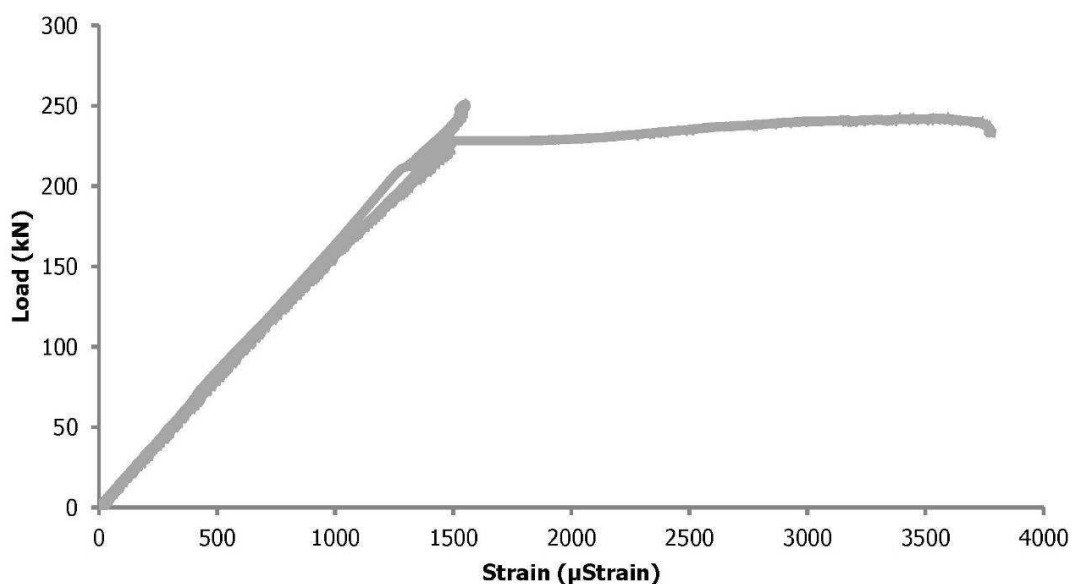


Figure 3-37: Load-strain relationship at location B of Group 5 specimens

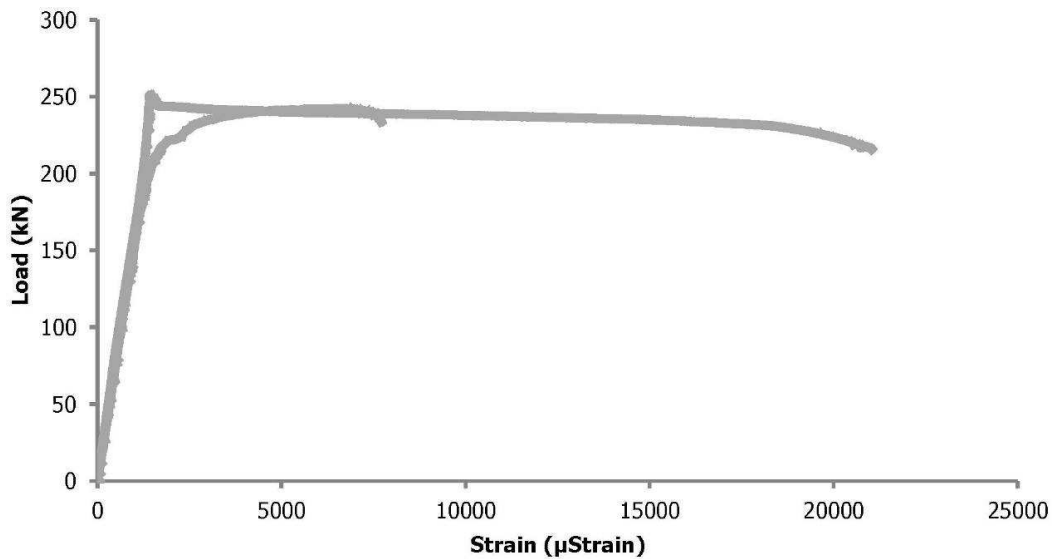


Figure 3-38: Load-strain relationship at location C of Group 5 specimens

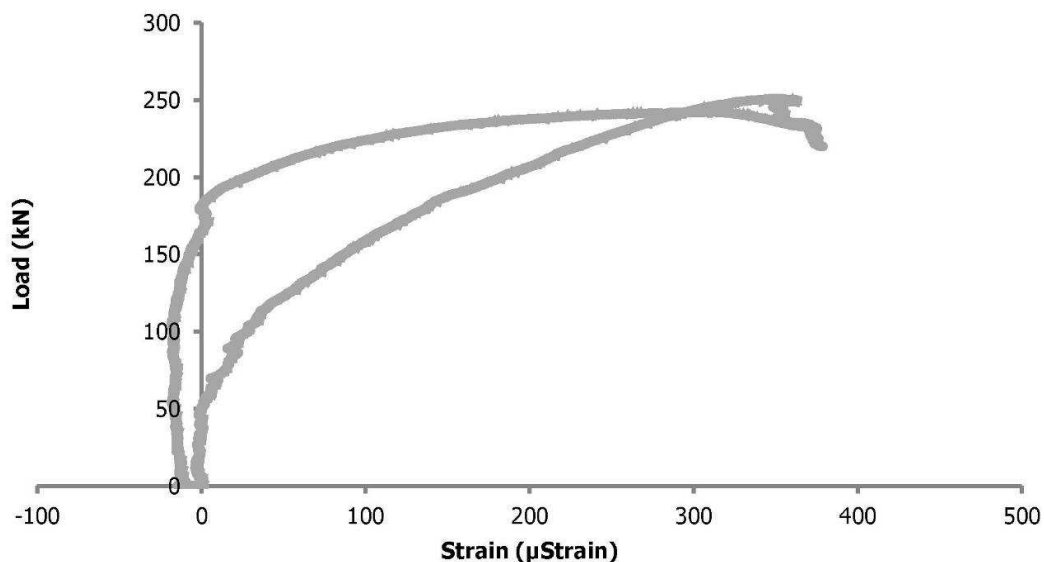


Figure 3-39: Load-strain relationship at location D of Group 5 specimens

3.5 COMPARISON OF EXPERIMENTAL RESULTS

The comparison between tests can shed light on the effect of various parameters, thus in this section the testing results of the different groups will be appropriately compared with each other. The comparison will be based on the experimentally obtained equilibrium paths.

3.5.1 Group 1 - Group 2

Based on Figure 3-40 where the equilibrium paths of specimens of Group 1 and 2 are compared, it can be concluded that the denser lacing arrangement resulted only in a small increase in stiffness and collapse load. Meanwhile, the larger number of welds required for the connection between the chords and the lacing bars in Group 2 did not lead to an obvious premature decrease of the stiffness due to the welding residual stresses. Of course this conclusion cannot be generalized, as welding procedures

differ significantly and may result in miscellaneous welding residual stress distributions and magnitudes.

In their experimental work on laced built-up columns Klöppel and Ramm [3-6] compared the experimental results with an analytical procedure and concluded that the analytical results were on the unsafe side for cases with very stiff lacing (and therefore numerous welds). The observation of premature plastification of the chords at the joints and the fact that internal bending moments could not be the only reason for this, made them test three more columns with annealed welded connections. The results showed that the columns behaved elastically until the ultimate load. As annealing is not a common practice in civil engineering constructions due to its cost, the authors proposed a conservative global imperfection of $L/500$ to be used in any type of lacing system.

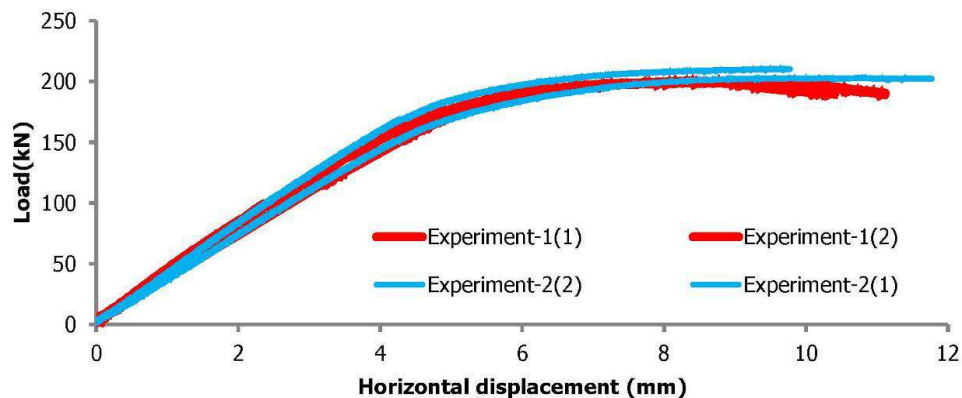


Figure 3-40: Comparison of equilibrium paths of Groups 1 and 2

3.5.2 Group 1 - Group 3

The material of the two groups was not the same and for this reason a quantitative comparison cannot be directly done. Observing Figure 3-41, in which the equilibrium paths of specimens of Groups 1 and 3 are compared, it can be concluded that the larger area of the chords' cross-section affected directly both the stiffness and capacity of the columns. Additionally, in Group 1 the critical panels deflected inwards after buckling and this could not be attributed only to the small eccentricity (distance between the cross-section's centre of gravity and the point of loading) in the loading of the mono-symmetric UNP60 chords, as the same observation was made for Group 3 (double-symmetric IPE80 cross-section). This behaviour was attributed to the existence of small internal bending moments about the chords' weak axis that triggered this direction of deflection.

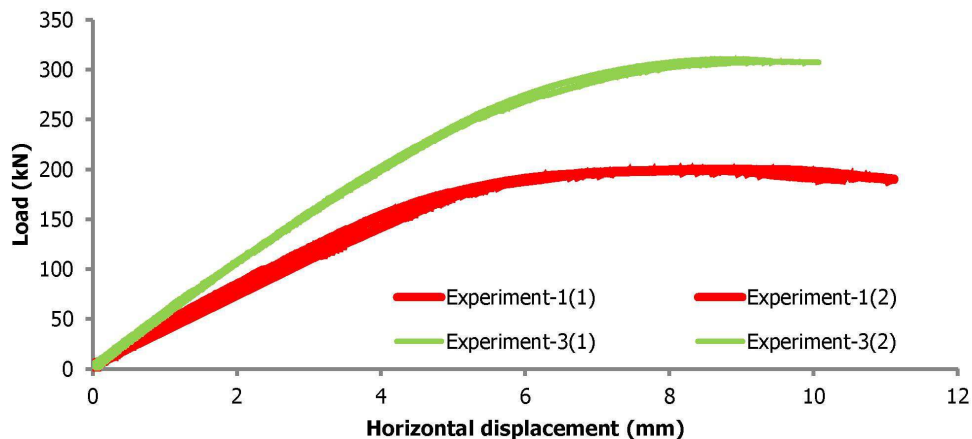


Figure 3-41: Comparison of equilibrium paths of Groups 1 and 3

3.5.3 Group 1 - Group 4

The material of the two groups was almost the same and the comparison between specimens of Groups 1 and 4 can be based on quantitative conclusions. In this subsection the comparison between specimens of Groups 1 and 4 is discussed. Group 1 and Group 4 had the same geometrical and loading characteristics but exhibited an opposite type of deformation. In Group 1 intermediate panels were more stressed, while in Group 4 the top end panels were expected to fail. Equilibrium paths could not be directly compared, as they referred to displacement at different locations of the column in elevation. Quantitative conclusions were drawn, as Group 1 and Group 4 had similar material yield strength. Double curvature deformation led to much smaller deflections and to 10% increase of collapse load (220kN mean value in Group 4 compared to 200kN in Group 1). Despite the different boundary conditions that the intermediate panels had when compared with end panels, no significant differences were observed in the type of local failure in specimens of Group 1 compared with the ones of Group 4.

3.5.4 Group 1 - Group 5

The material of Group 5 had a lower yield stress when compared with the one of Group 1. Nevertheless, when comparing Groups 1 and 5, by observing the equilibrium paths of their specimens presented in Figure 3-42, it can be concluded that the smaller eccentricity in Group 5 resulted in a larger collapse load and in smaller lateral deflections. The elastic part of the equilibrium paths of Group 5 was slightly more nonlinear due to the larger effect of the applied axial load. In the three out of four tests belonging to these groups failure initiated from the second panel, while in the fourth one from the fourth panel. As all other parameters were the same for the four specimens, this differentiation was attributed to the existence of initial imperfections that differed even among specimens of the same group.

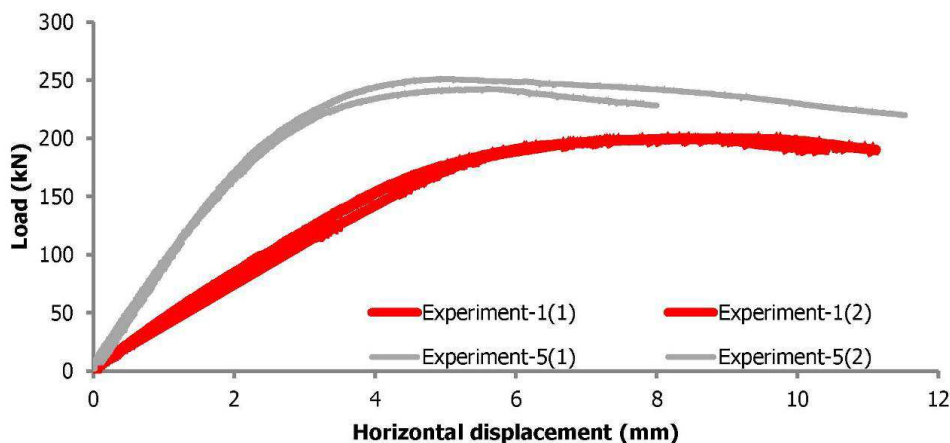


Figure 3-42: Comparison of equilibrium paths of Groups 1 and 5

3.6 CONCLUSIONS

In the present chapter the work and results related to the experimental effort made in the context of the present doctoral thesis were presented. Ten specimens (five pairs of similar specimens) were tested under combined axial load and end concentrated moments. The results related to both global and local responses were presented with the use of equilibrium paths and load-strain curves, respectively. Each group's specimens were compared in a satisfactory way with each other verifying the existence of repeatability between the tests. The main technical conclusions can be summarised in the following:

- The global response and collapse load were affected mainly by the cross-sectional area of the chords and the magnitude and direction of eccentricity at the columns' ends.
- Overall collapse took place due to plastification of the more compressed chords and no plastic reserve was observed in the specimens.
- In cases of relatively slender panels, local buckling of the critical panels was observed in the post-buckling range. In cases of stocky panels only global deformation was seen.
- The large number of welds in Group 2 did not lead to detrimental effect of welding residual stresses on the collapse load in the specific cases examined.
- The critical panels buckled inwards in all cases highlighting that local behaviour was affected by internal bending moments about the weak axis of the chords that triggered this direction of deformation.
- The local buckling of different intermediate panels even in specimens (Group 3 and Group 5) of the same group revealed that local initial imperfections existed. This was not the case in Group 4, where the end panels were much more stressed than the other panels and initial imperfections could not modify the location of failure.

The obtained experimental results led to qualitative and quantitative conclusions as presented in this chapter. Nevertheless, the performance of a very large number of tests is practically difficult as they require financial funding and are very time consuming. For this reason, the calibration of numerical models according to experimental results, and the use of them for performing a large number of analyses (in order to draw additional qualitative and quantitative conclusions) can prove beneficial in the field of structural engineering. Based on this concept, in Chapter 4 numerical models will be calibrated relying on the experimental results of Chapter 3.

3.7 REFERENCES

- [3-1] www.noe.gr
- [3-2] <http://www.malvasiaelectronics.gr/>
- [3-3] <http://www.kyowa-ei.co.jp/eng>
- [3-4] DIN 50125, Test pieces for the tensile testing of metallic materials, April 1991
- [3-5] www.instron.com
- [3-6] Klöppel, K. Ramm, W. "Versuche und Berechnung zur Bestimmung der Traglast mehrteiliger Gitterstäbe unter aussermittiger Belastung", Der Stahlbau, Vol. 37, p. 164 and 236, 1968

4 NUMERICAL MODELLING OF EXPERIMENTS

4.1 INTRODUCTION

The advances made in the fields of both numerical methods and computer engineering in recent years facilitated the development and use of finite element software that can approach natural phenomena in an efficient way. In the civil engineering field, the finite element method is commonly used in the analysis and design of structures and in many other areas. The calibration of numerical models according to experimental results gives researchers the opportunity to perform a large number of numerical analyses in many different cases, being confident that they can reliably predict real behaviour. Method 2 included in Appendix B of Eurocode 3 [4-1], [4-2] for the buckling of beam-columns under combined axial force and biaxial bending is a classical example of this procedure, as it was based on experimental results and on approximately 25000 calibrated numerical analyses. In the present chapter, the numerical modelling of the experimental work presented in Chapter 3 is thoroughly described. The corresponding numerical models, types of finite elements and methods of analyses are presented. The numerical results are then compared with the experimental ones and useful conclusions are drawn as far as the efficiency of the numerical approach is concerned. The comparison takes place at two different levels. The first one contains the comparison of the tests with nonlinear analysis of numerical models based on detailed geometrical modelling and shell elements. The second one concerns the comparison of the numerical models with shell elements with the ones with beam elements. Based on these comparisons a validation of the performance of shell and beam elements is presented for the modelling of built-up members.

4.2 DESCRIPTION OF NUMERICAL MODELS AND ANALYSES

Finite element software ADINA [4-3] was used for the numerical analyses. Both flanges and diagonal bars were modelled with 4-noded shell elements. The welded connections between the flanges and the diagonals were inserted with rigid links and this type of modelling was considered to be realistic as it accounted for the finite dimensions and rigidity of the connections. A uniform and sufficiently dense meshing was used. The supports were modelled using rigid links, at the ends of which the boundary conditions and the external loads were applied, accounting in this way for the difference between the column's nominal and effective length (from bottom to top pinned connection). The use of simple elastic static analyses proved that the behaviour of the testing frame was sufficiently stiff for the type

and amount of loading applied during the tests, therefore there was no need for incorporating its effect on the specimen's response. Views of a typical specimen after its placement in the testing frame and the corresponding numerical model are shown in Figure 4-1(a). Details of the numerical modelling of the top support and connections are shown in Figure 4-1(b)-(c).

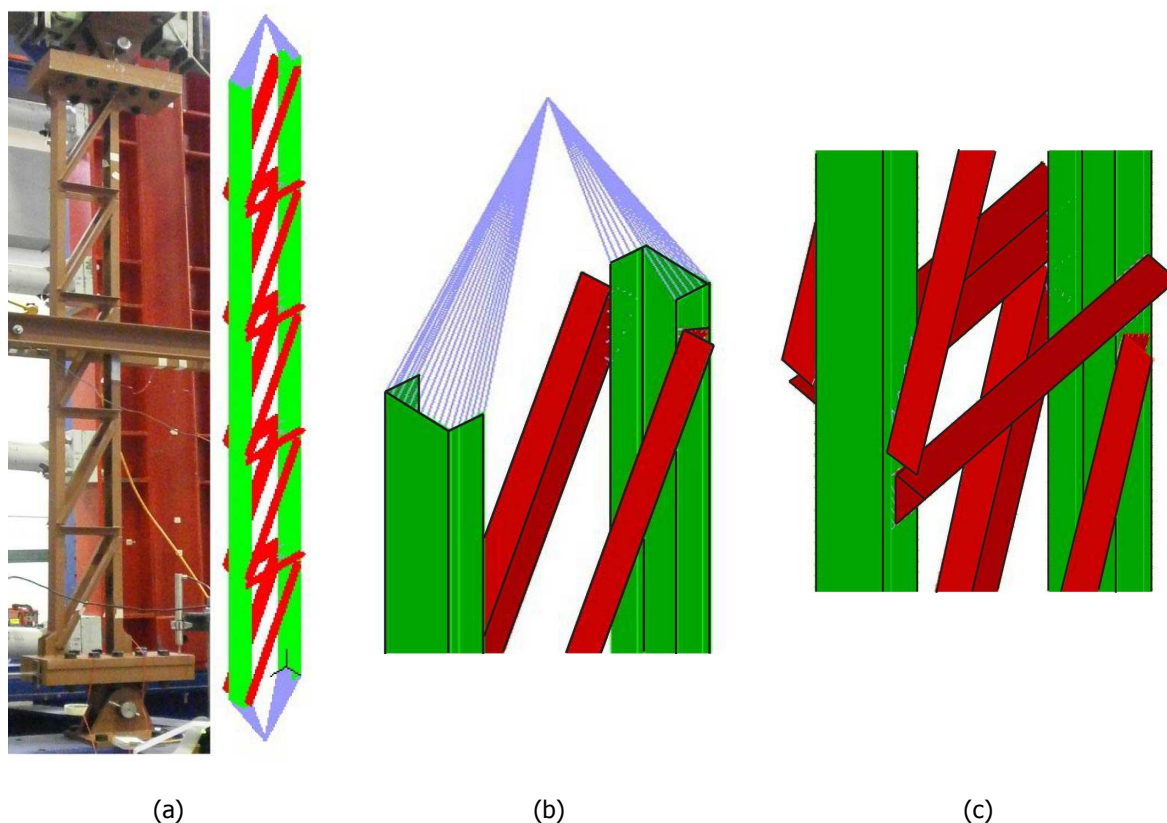


Figure 4-1: (a) Typical specimen at the testing frame and corresponding numerical model, (b) numerical modelling of top support and (c) close view of connections between flanges and diagonal bars

The strategy proposed by Gantes and Fragkopoulos [4-4] for the numerical verification of steel structures at the ultimate limit state was used in the present study. Linearised Buckling Analyses (LBA) using appropriate algorithms taking into account the work of Dimopoulos and Gantes [4-5] were used for obtaining the buckling loads for a prediction of the capacity of the perfect elastic structure and for obtaining the buckling mode shapes. The final numerical results were based on Geometrically and Materially Nonlinear Imperfection Analyses (GMNIA), in order to account for both large displacements and material plastification. The initial imperfections were inserted according to the buckling mode shapes obtained with LBA. The arc-length method originally developed by Riks [4-6], [4-7] and Wempner [4-8] and later modified by many researchers (i.e. [4-9], [4-10]) was used for obtaining the post-buckling branch of the structural response, too. The results include load - displacement curves (equilibrium paths), load - strain diagrams, snapshots of deformed shapes at characteristic locations and indicative stress distributions for the better understanding of the structural behaviour of the members.

Columns are affected by the appearance of geometrical imperfections and residual stresses, either thermally induced or due to welding procedures and fabrication. Neither of them was measured in the present study, instead code provisions were used for their incorporation into numerical models. Eurocode 3 [4-1] considers that equivalent global geometrical imperfections should be used to account for both out-of-straightness and residual stresses due to welding procedures. The

disadvantage of this concept is that the effect of residual stresses appears only after the stresses in the cross-section exceed a certain magnitude, while equivalent imperfections affect the response from its onset. Nevertheless, it is convenient for analytical calculations as it overcomes the difficulty of modelling residual stresses in cross-sections, especially the ones related to welding procedures that are also in general tough to measure. Based on Eurocode 3 [4-1], the maximum equivalent global imperfection was considered to be equal to $L_e/500$ and was inserted in the nonlinear analyses using the shape of the 1st global buckling mode obtained with Linearised Buckling Analyses (LBA).

Locally, Eurocode 3 [4-1] suggests that each panel should be considered as a separate simply-supported column and that its local capacity should be calculated according to the buckling curves. The imperfection used for the buckling curves consists of a geometrical part with amplitude equal to $a/1000$ and an additional part related to the thermally induced residual stresses. The distribution and magnitude of thermally induced residual stresses due to fabrication have been investigated for many years and pertinent guidelines are included in ECCS provisions [4-11]. In the numerical analyses, the local geometrical imperfection was set to $a/1000$ and inserted based on the local buckling mode shape. The thermally induced residual stresses were incorporated in the chords' cross-sections in order to capture in a satisfactory way the gradual plastification of the column. Their modelling relied on discretising the cross-section of the chords (UNP60 and IPE80) in sufficiently small shell elements and on using appropriate material yield strengths in each element group, so that the residual stress distribution would be correctly applied. The material yield strength of each element group depended on whether it belonged to a location with tensile or compressive residual stresses and on the yield strength measured through tensile tests as described in Chapter 3. The different shell element groups (each element group has its own colour) of an IPE80 cross-section expected to be subjected to compressive normal stresses are depicted in Figure 4-2. It can be seen that the doubly-symmetrical IPE80 cross-section had symmetrical residual stress pattern in order to satisfy self-equilibrium.

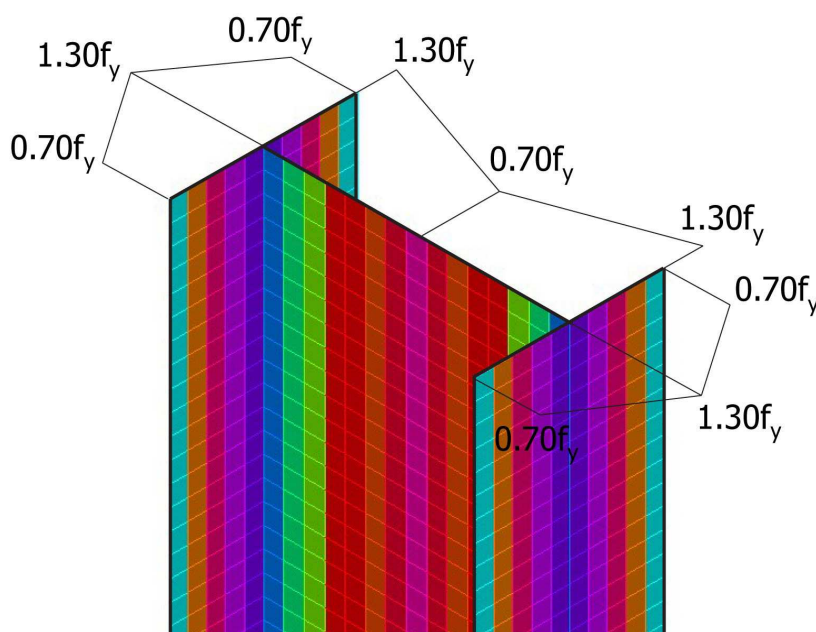


Figure 4-2: Modelling of residual stresses in an IPE80 cross-section subjected to compressive normal stresses

The concept behind this type of modelling can be explained with a simple example, in which at a specific location of the cross-section the residual stress is compressive and equal to the 30% of the yield stress. This means that the compressive strength of this location is equal to 70% of the yield stress and the tensile strength equal to 130% of the yield stress if this specific location is subjected to

compression. This type of modelling residual stresses is convenient but its main drawback is that it is useful in cases that the type of stresses that will appear in the cross-section is known in prior.

4.3 EXPERIMENTAL AND NUMERICAL RESULTS

In this section the Linearised Buckling Analysis (LBA) results will be initially shown and afterwards experimental results (solid lines) will be presented in comparison with the numerical ones (dotted lines) obtained with Geometrically and Materially Nonlinear Imperfection Analyses (GMNIA) for every group separately. Equilibrium paths, indicative load-strain diagrams, characteristic deformed shapes and stress distributions will be presented. The maximum load along the equilibrium paths will be considered to be the collapse load. The panel from which failure initiated and had the largest lateral deflections at the post-buckling state will be characterised as critical panel in the following sections. Global buckling will be used for characterising global behaviour, local buckling for deformation of the chords between successive connections and local plate buckling for the description of the out-of-plane deformation of the web and/or flanges of the cross-sections.

4.3.1 Group 1

The local and global buckling mode shapes for Group 1 are shown in Figure 4-3. The local and global buckling loads (of the modes used for incorporating the initial imperfections) are equal to 2227kN and 3134kN, respectively. It is observed that at these high levels of loading the buckling modes capture the out-of-plane buckling of the lacing bars which affects the global and local buckling loads. When the out-of-plane degrees of freedom of the model are deactivated in order to reduce these effects, the local and global buckling loads increase and become equal to 2515kN and 3481kN, respectively.



Figure 4-3: (a) Local and (b) global buckling modes obtained numerically for Group 1

In Figure 4-4 the experimental and numerical equilibrium paths obtained for the horizontal displacement at mid-height of specimens of Group 1 are shown. It can be seen that the numerical model predicts in a satisfactory way the elastic stiffness, collapse load and post-buckling branch. The critical panel is the second one in the two tests and the third one in the numerical analysis (Figure 4-5). Despite that fact the intermediate panels have similar stress levels and no obvious difference between the experimental and numerical results is observed. No local plate buckling or torsional effects are observed in the numerical results as the material plastification imposes relatively small levels of loading.

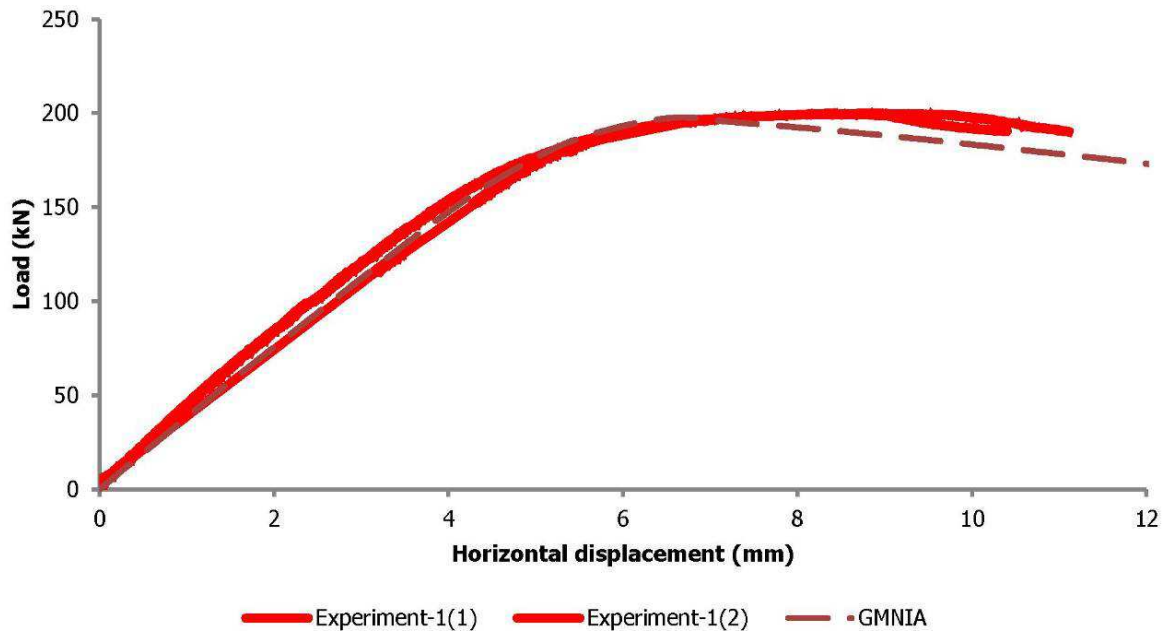


Figure 4-4: Equilibrium paths obtained experimentally and numerically for Group 1

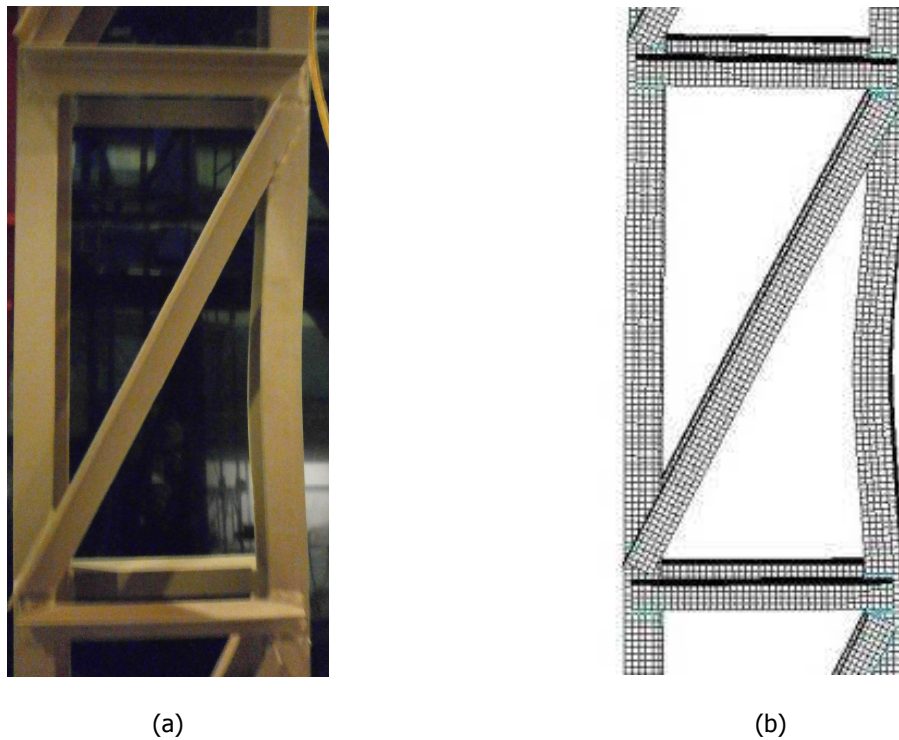


Figure 4-5: Critical panels at a post-buckling state obtained (a) experimentally and (b) numerically for Group 1

The load-strain curves for location A as obtained experimentally and numerically are shown in Figure 4-6 showing good agreement at a local level. The load-strain curves for location D are depicted in Figure 4-7 and it can be seen that the numerical prediction cannot accurately approach the test results. The magnitude of strains is relatively small and, as was explained in Chapter 3, these strains are attributed to the small shear forces and to random parameters that are not possible to measure and differed even between the two specimens. In Figure 4-8 the deformed shape (magnified for better observation), the von Mises stress distribution and the plastification of the critical panel at

collapse load level are shown. It can be seen that apart from the critical panel, adjacent panels enter the plastic region, too.

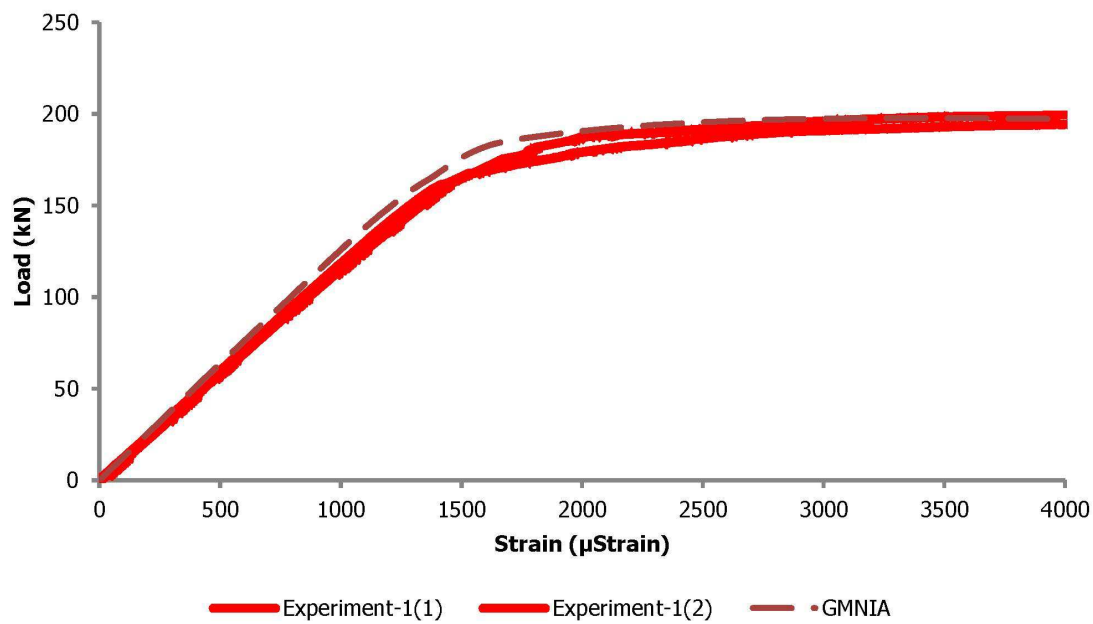


Figure 4-6: Load-strain curves obtained experimentally and numerically for Group 1 at location A

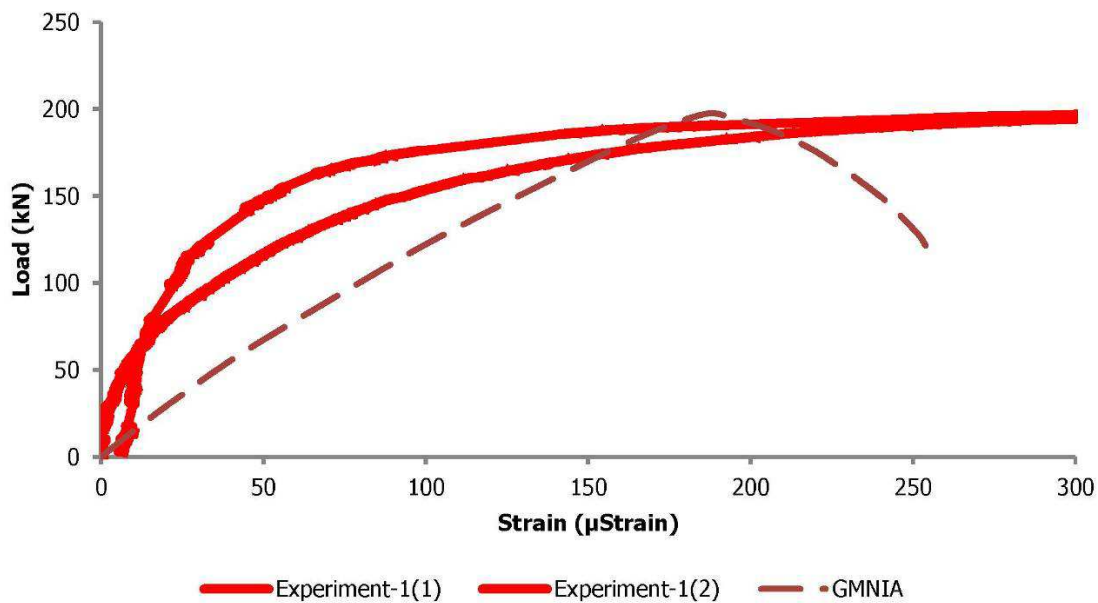


Figure 4-7: Load-strain curves obtained experimentally and numerically for Group 1 at location D

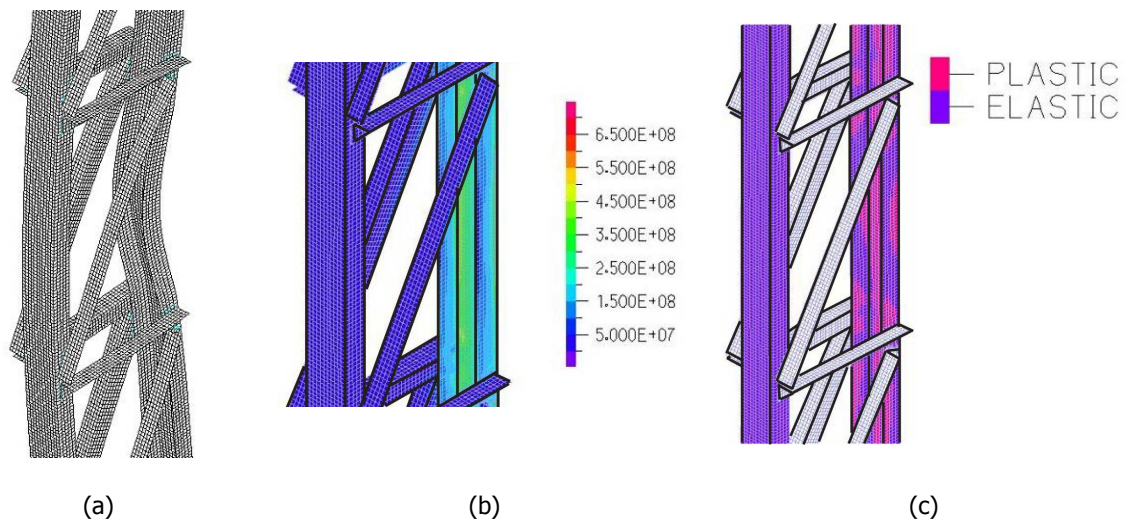


Figure 4-8: Critical panel's for Group 1 (a) deformed view, (b) von Mises stress distribution and (c) plastification at collapse load level

4.3.2 Group 2

The global buckling mode shape for Group 2, corresponding to a critical load of 3945kN, is shown in Figure 4-9. The local buckling mode shape is related to a much greater buckling load due to the small panels' length and is not captured with the use of LBA. Out-of-plane buckling of lacing bars is observed at these high levels of loading and when out-of-plane degrees of freedom are restricted in order to diminish them the global buckling load becomes equal to 4709kN.

In Figure 4-10 the experimental and numerical equilibrium paths obtained for the horizontal displacement at mid-height of specimens of Group 2 are shown. The numerical results are very close to the experimental ones in this case, too. The critical panels are the fifth and sixth ones in both tests and numerical analyses. No geometrical indication of local buckling is observed in both experimental and numerical results, as the panels are characterised by small non-dimensional slenderness. No local plate buckling and torsional effects are observed in the numerical results. The global response of specimen 2(1) (the same as specimen 2(2)) and numerical model at a post-buckling state is depicted in Figure 4-11.



Figure 4-9: Global buckling mode obtained numerically for Group 2

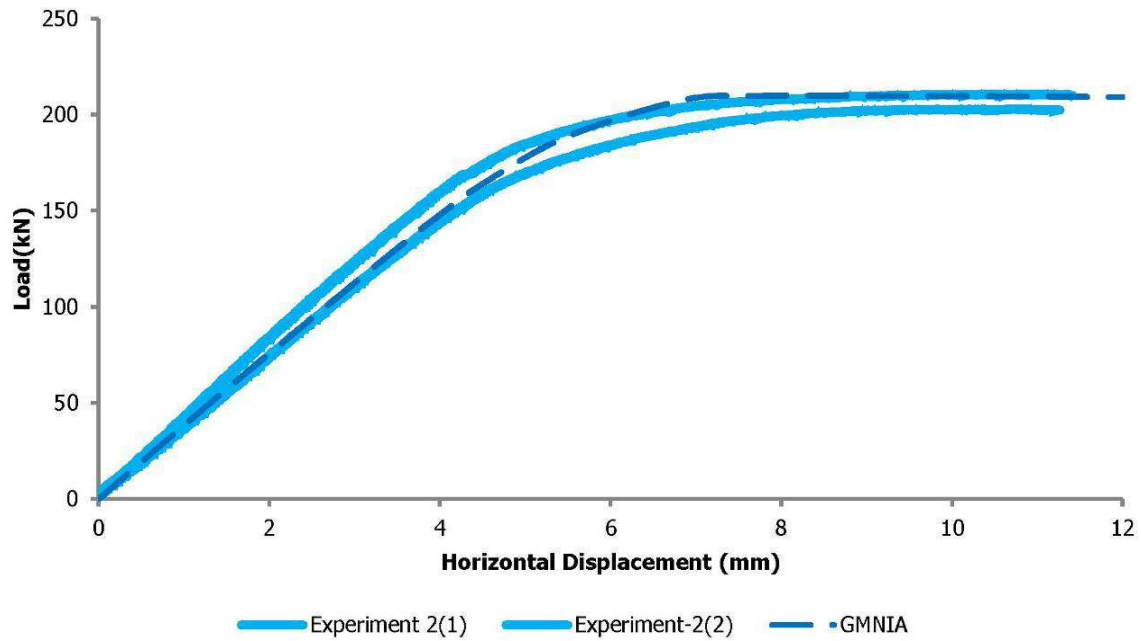


Figure 4-10: Equilibrium paths obtained experimentally and numerically for Group 2



Figure 4-11: Laced columns at a post-buckling state obtained (a) experimentally and (b) numerically for Group 2

The load-strain curves for locations A, B, C and D as obtained experimentally and numerically are shown in Figure 4-12 to Figure 4-15, showing good agreement at a local level. In Figure 4-15, related

to the end diagonal's strain, the numerical prediction is not satisfactory for the reasons explained in Group 1. The deformed shape (magnified for better observation), the von Mises stress distribution and the plastification of the critical panel at collapse load level, are shown in Figure 4-16. It can be seen that the intermediate panels are fully plastified, which is a verification that they fail as stocky columns.

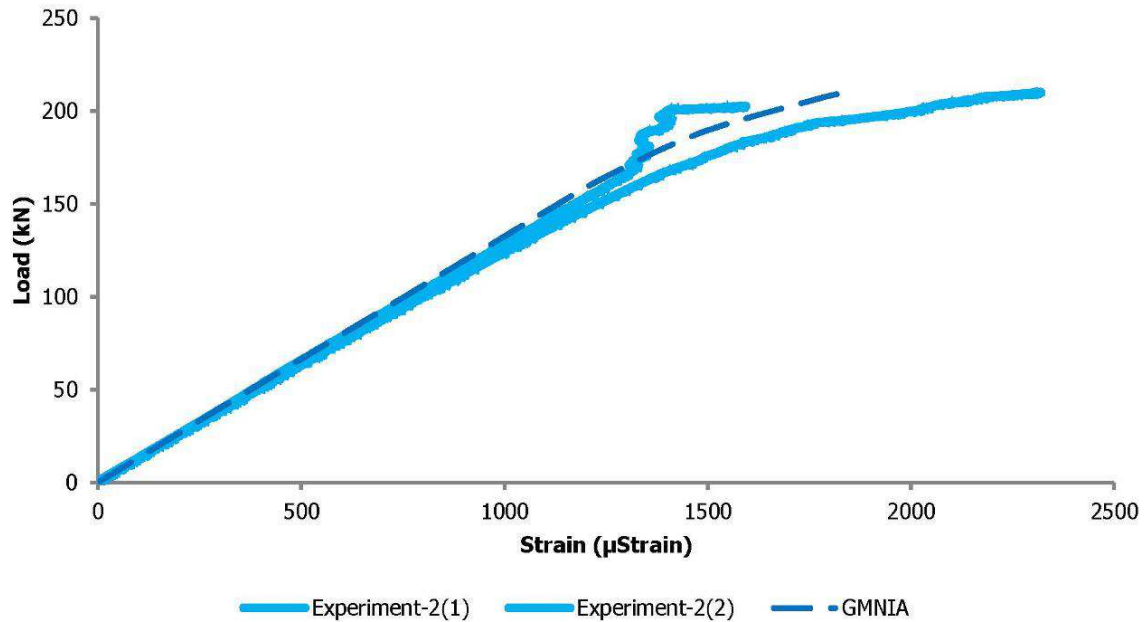


Figure 4-12: Load-strain curves obtained experimentally and numerically for Group 2 at location A

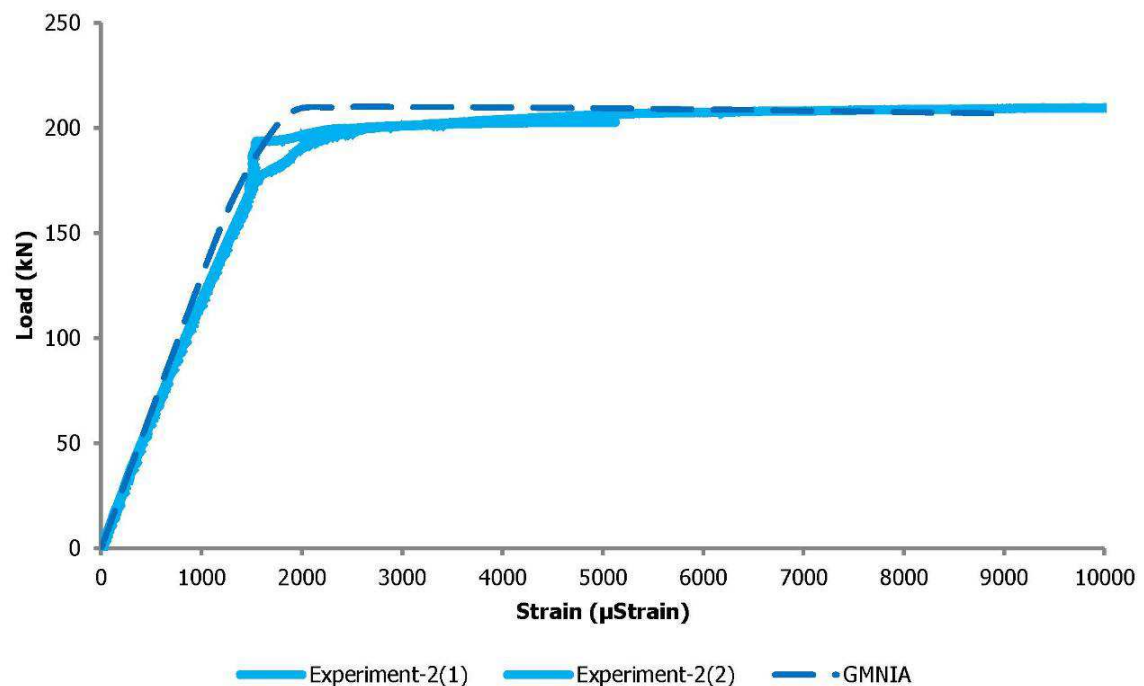


Figure 4-13: Load-strain curves obtained experimentally and numerically for Group 2 at location B

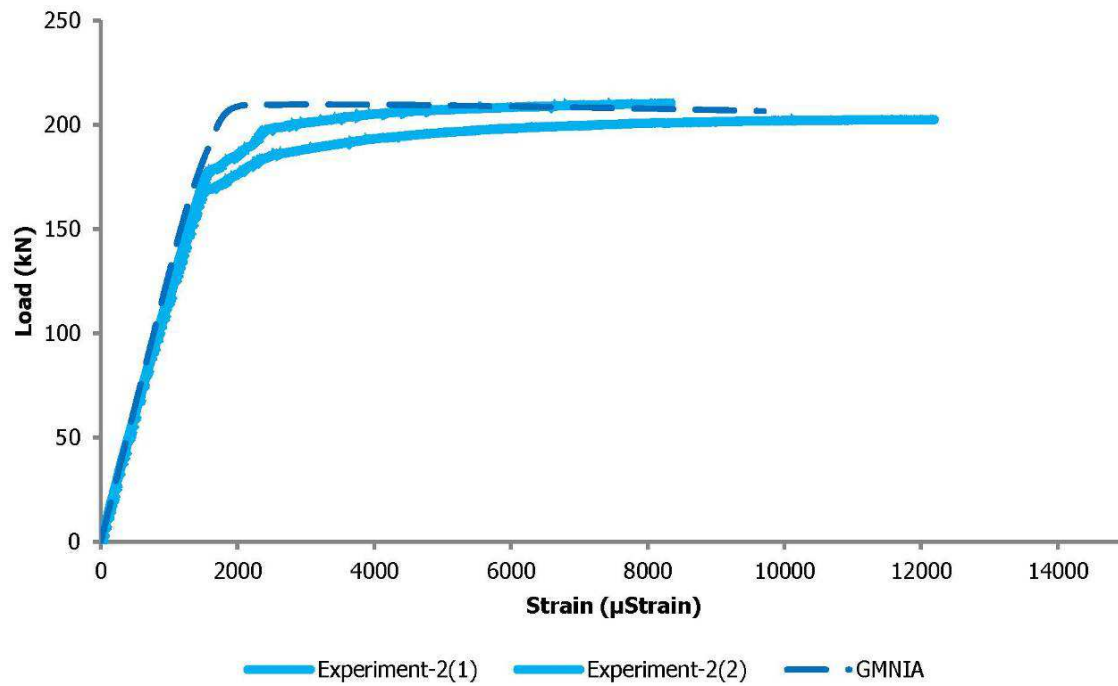


Figure 4-14: Load-strain curves obtained experimentally and numerically for Group 2 at location C

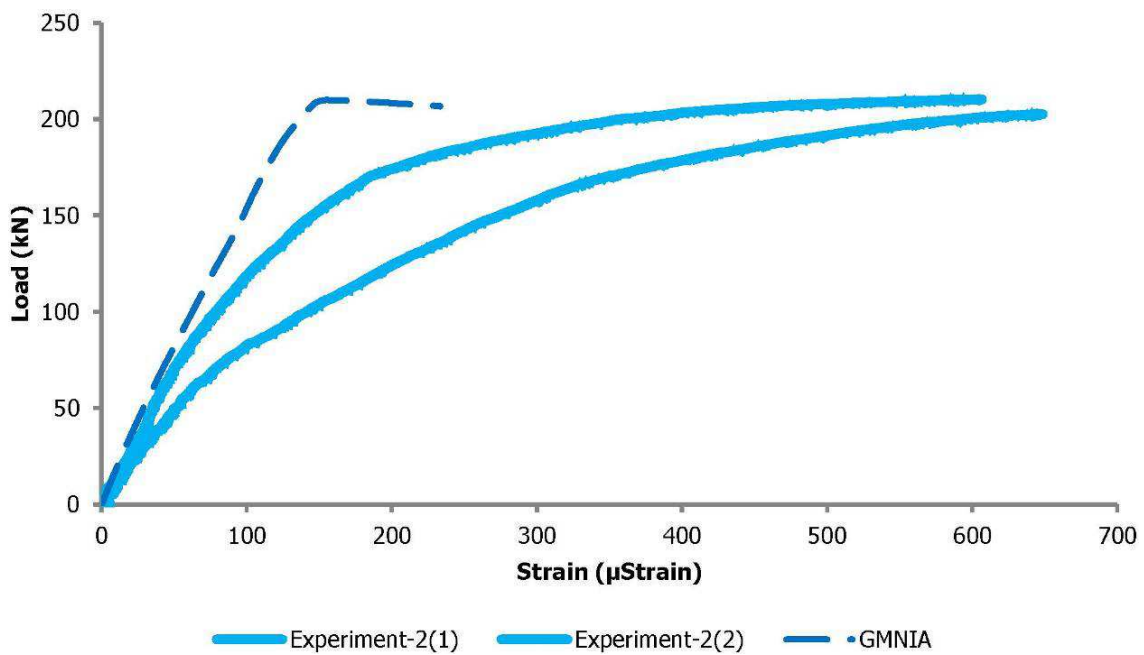


Figure 4-15: Load-strain curves obtained experimentally and numerically for Group 2 at location D

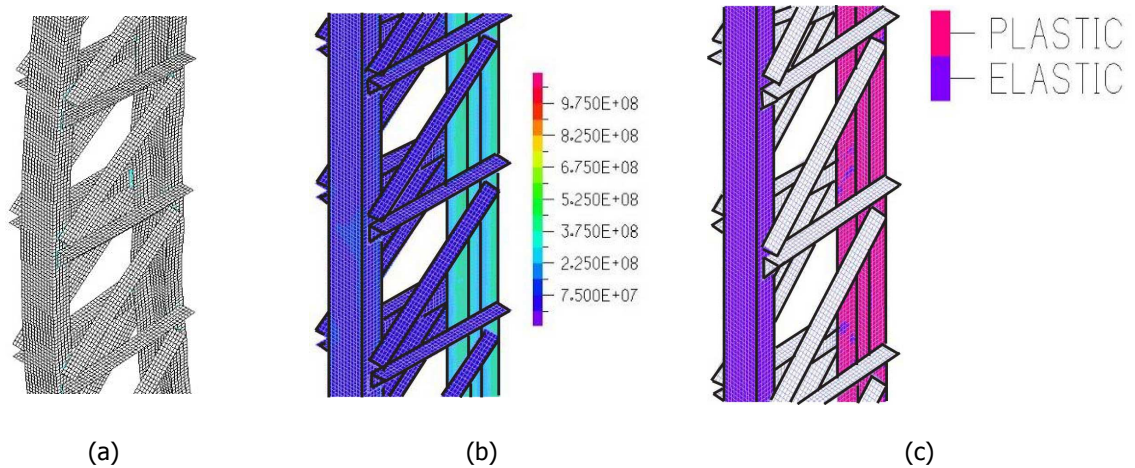


Figure 4-16: Critical panel's for Group 2 (a) deformed view, (b) von Mises stress distribution and (c) plastification at collapse load level

4.3.3 Group 3

The local and global buckling mode shapes for Group 3 are depicted in Figure 4-17. The local and global buckling loads (of the modes used for incorporating the initial imperfections) are equal to 3544kN and 3874kN, respectively. It is observed that at these high levels of loading the buckling modes capture out-of-plane buckling of lacing bars. When the out-of-plane degrees of freedom of the model are deactivated in order to reduce these effects, the local and global buckling loads are equal to 4068kN and 4470kN, respectively.

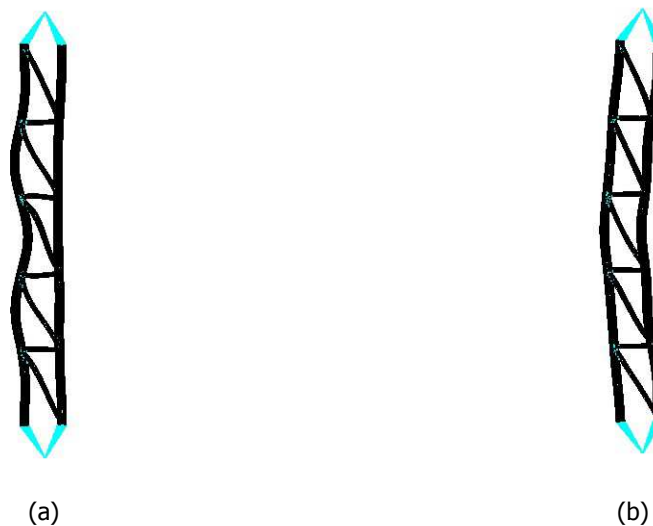


Figure 4-17: (a) Local and (b) global buckling modes obtained numerically for Group 3

In Figure 4-18 the experimental and numerical equilibrium paths obtained for the horizontal displacement at mid-height of specimens of Group 3 are shown. The agreement between the numerical and experimental results is satisfactory. The critical panels are the fourth and third ones in specimens 3(1) and 3(2), respectively, while in the numerical analyses the fourth panel initially fails. In all cases the critical panel deflects inwards. The local response of the critical panel experimentally (specimen 3(1)) and as predicted by the numerical model at a post-buckling state is depicted in Figure 4-19.

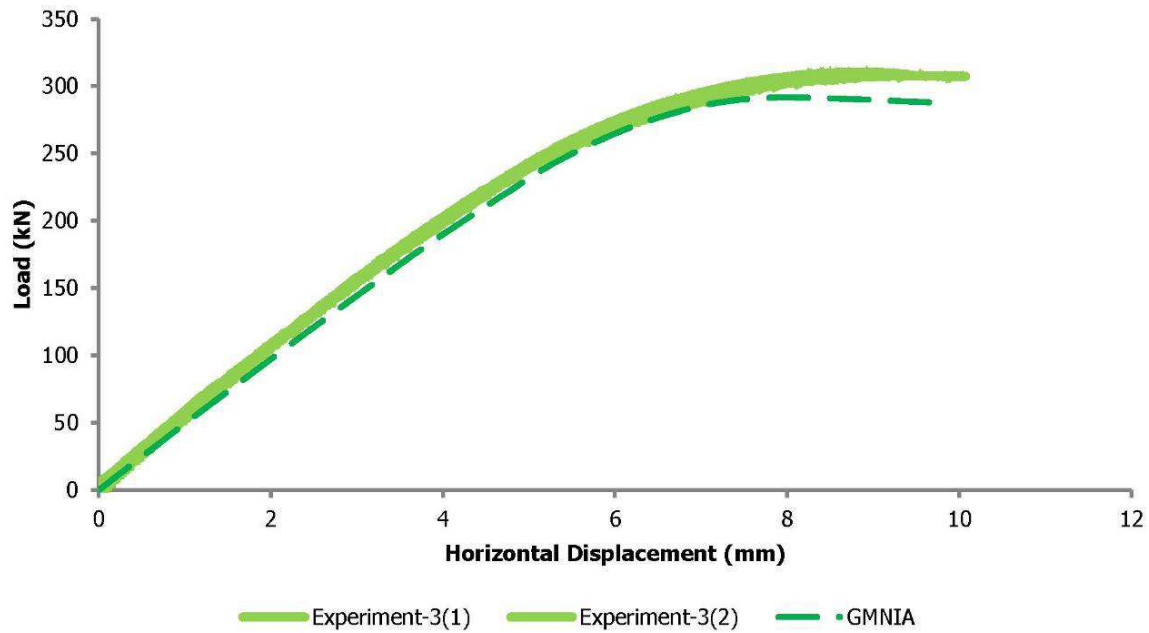


Figure 4-18: Equilibrium paths obtained experimentally and numerically for Group 3

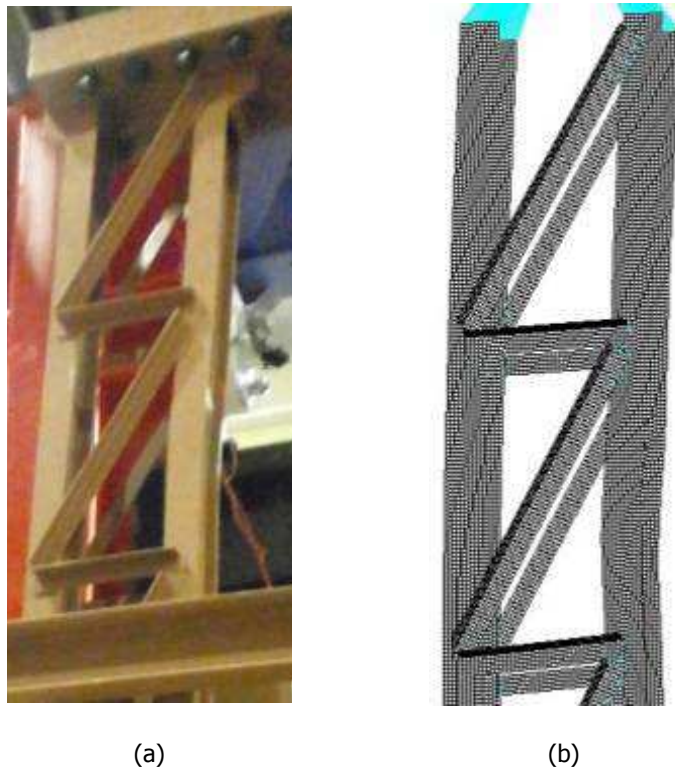


Figure 4-19: Critical panel at a post-buckling state obtained (a) experimentally and (b) numerically for Group 3

The load-strain curves for locations A, B, C and D as obtained experimentally and numerically are shown in Figure 4-20 to Figure 4-23, revealing sufficient agreement between the two. In Figure 4-23, related to the end diagonal's strain, the numerical prediction is not satisfactory for the reasons explained for Group 1. The deformed shape (magnified for better observation), the von Mises stress distribution and the plastification of the critical panel at collapse load level are shown in Figure 4-24. It can be seen that in addition to the critical panel the adjacent ones enter the plastic region, as well.

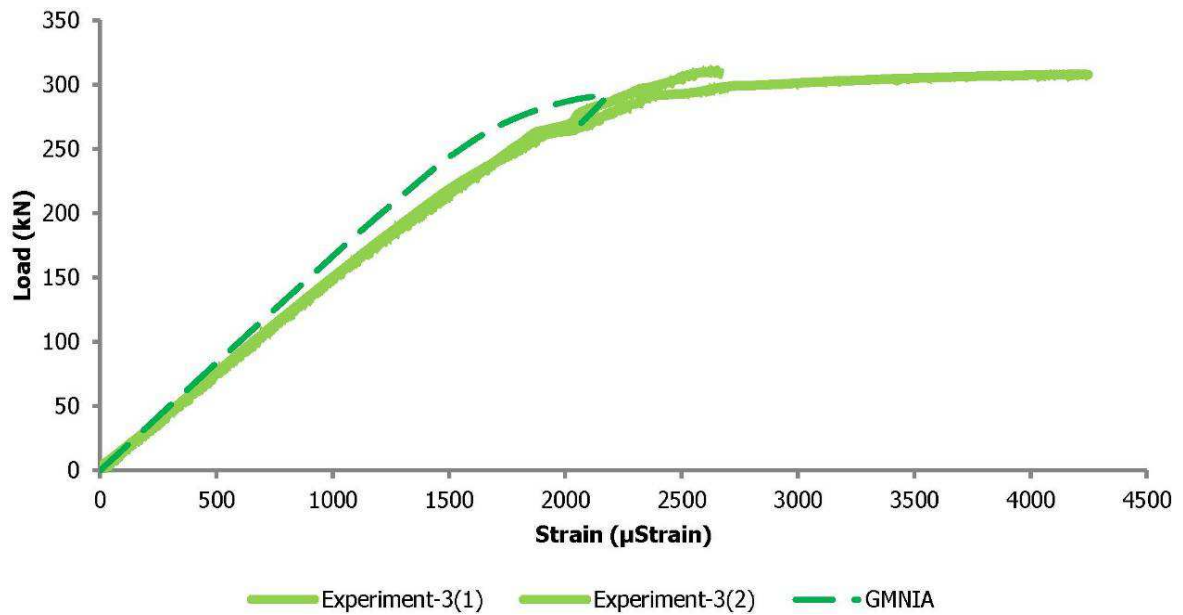


Figure 4-20: Load-strain curves obtained experimentally and numerically for Group 3 at location A

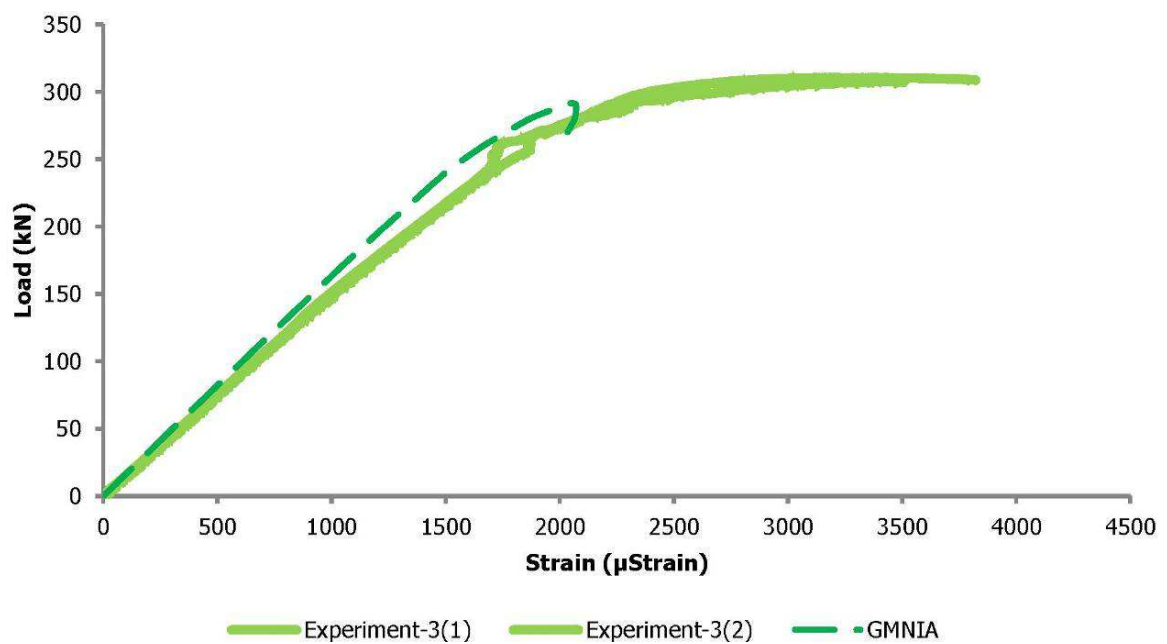


Figure 4-21: Load-strain curves obtained experimentally and numerically for Group 3 at location B

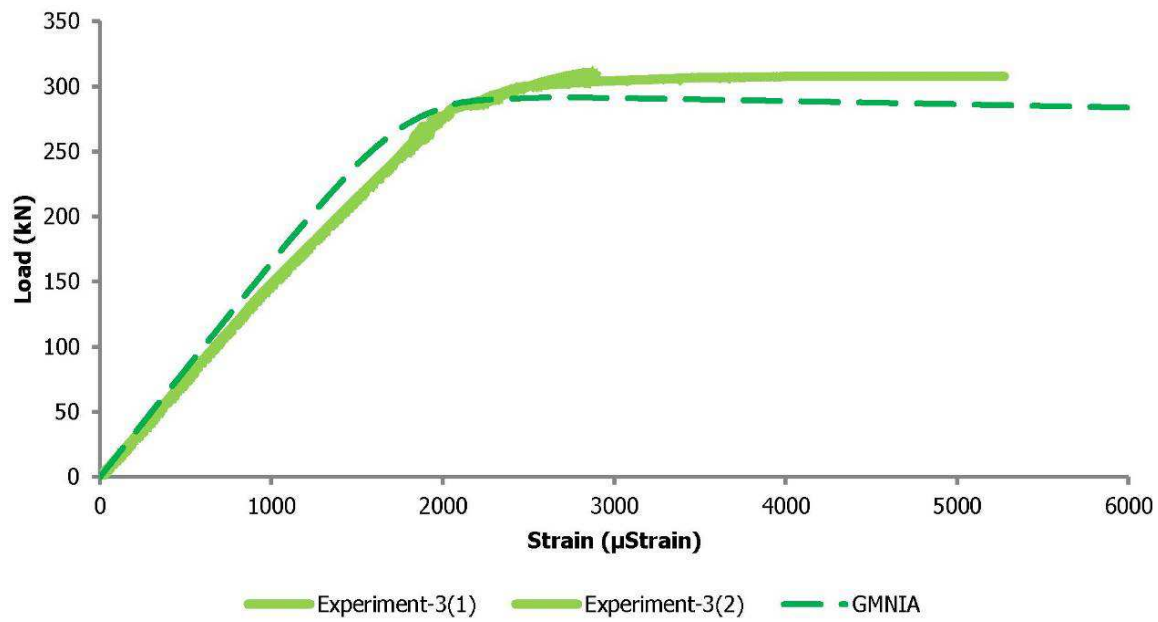


Figure 4-22: Load-strain curves obtained experimentally and numerically for Group 3 at location C

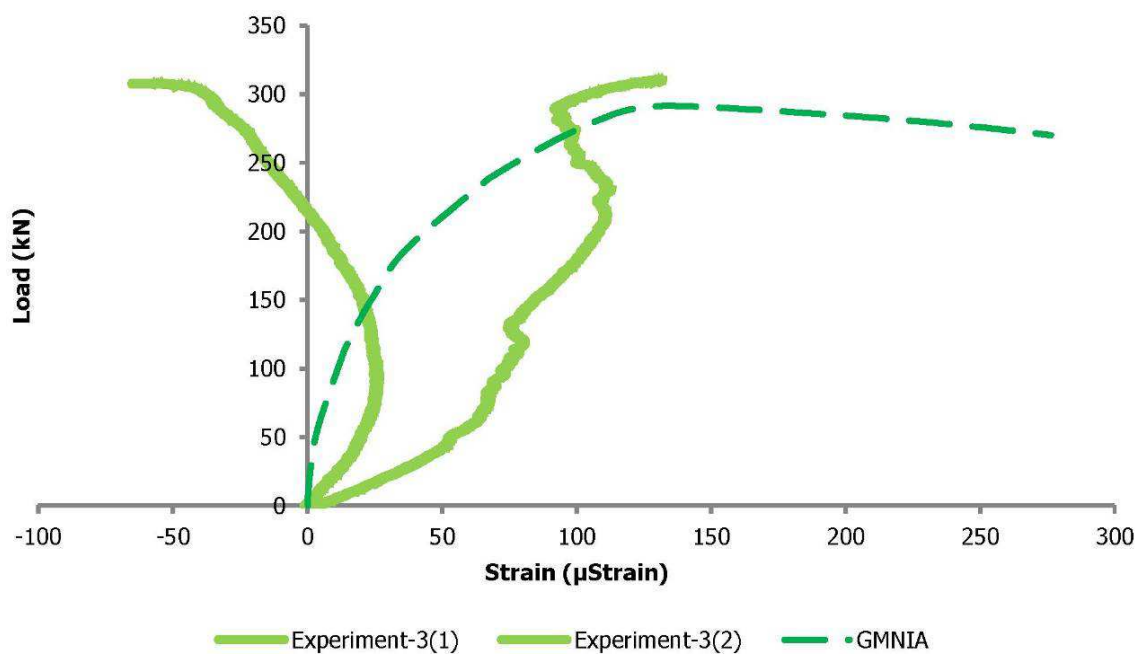


Figure 4-23: Load-strain curves obtained experimentally and numerically for Group 3 at location D

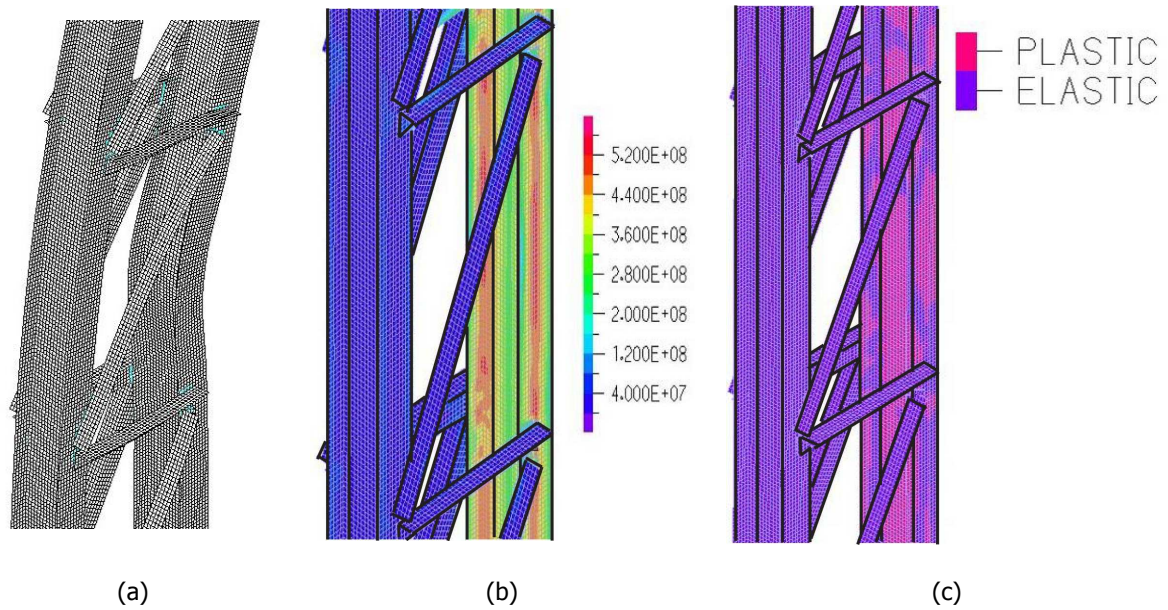


Figure 4-24: Critical panel's for Group 3 (a) deformed view, (b) von Mises stress distribution and (c) plastification at collapse load level

4.3.4 Group 4

The local and global buckling modes of Group 4 are similar to the ones obtained for Group 1, as shown in Figure 4-3. In Figure 4-25 and Figure 4-26 the experimental and numerical equilibrium paths obtained for the horizontal displacement at top and bottom of specimens of Group 4, respectively, are shown. The numerical and experimental results are satisfactory for the collapse load but differ as far as the magnitude of the displacements is concerned. The critical panel is the fifth panel in all cases, as its stress level is much larger than in the rest of the column. It also deflects inwards in all cases. The local response of the critical panel experimentally (specimen 4(1)) and as predicted by the numerical model at a post-buckling state is depicted in Figure 4-27. No local plate buckling and torsional effects are observed in the numerical results.

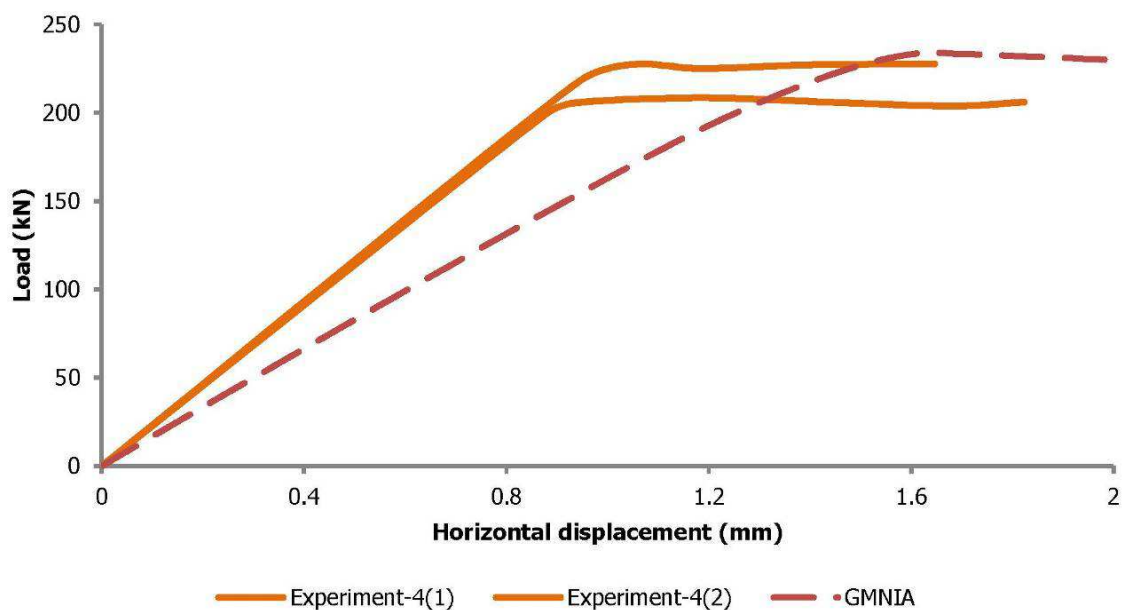


Figure 4-25: Equilibrium paths obtained experimentally and numerically at the top of the specimens for Group 4

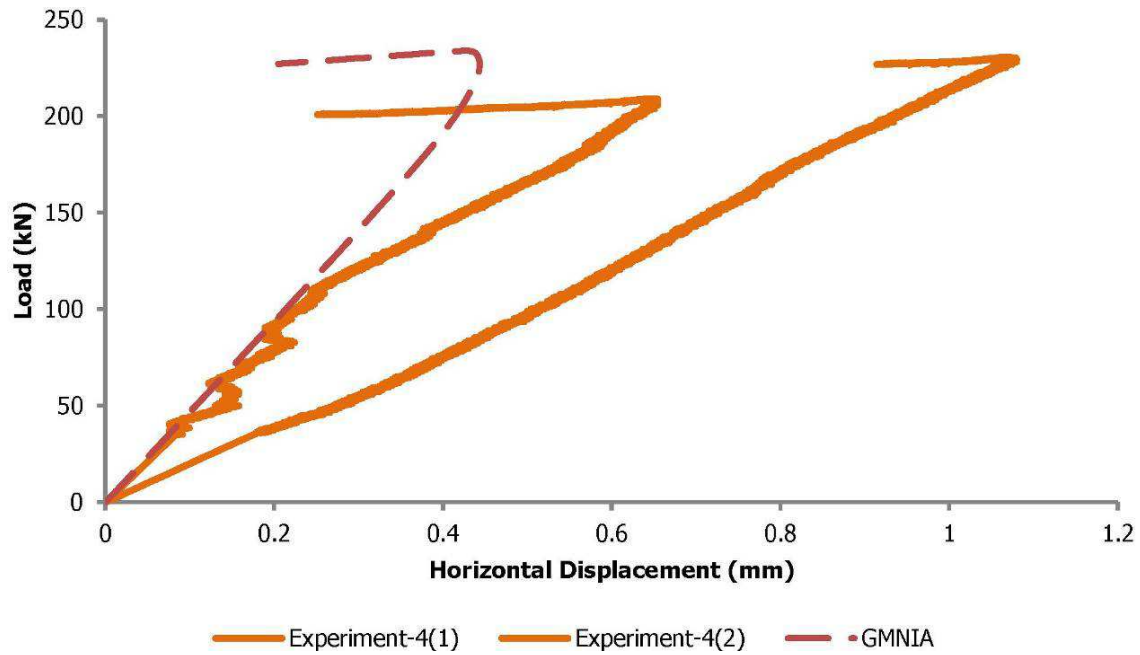
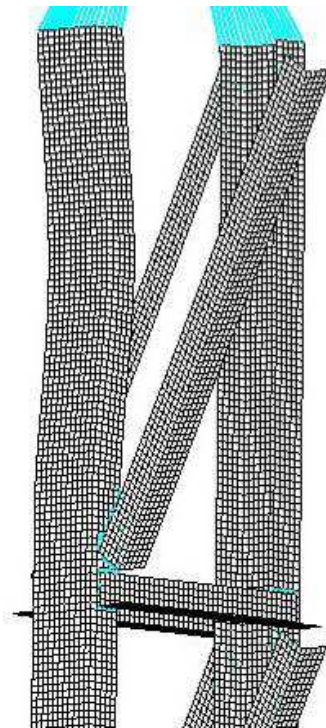


Figure 4-26: Equilibrium paths obtained experimentally and numerically at the bottom of the specimens for Group 4



(a)



(b)

Figure 4-27: Critical panel at a post-buckling state obtained (a) experimentally and (b) numerically for Group 4

The load-strain curves for locations A, B, C and D as obtained experimentally and numerically, are shown in Figure 4-28 to Figure 4-31 showing good agreement at a local level. In Figure 4-31 related to the end diagonal's strain, the numerical prediction is satisfactory because double curvature deformation is related to large shear forces at the ends of the column. For this reason, the effect of

random parameters that are difficult to measure and differ even between specimens of the same group is not visible in the results. The deformed shape (magnified for better observation), the von Mises stress distribution and the plastification of the critical panel at collapse load level, are shown in Figure 4-32. It can be seen that the critical panel is plastified, while only a small part of the adjacent one enters the plastic region.

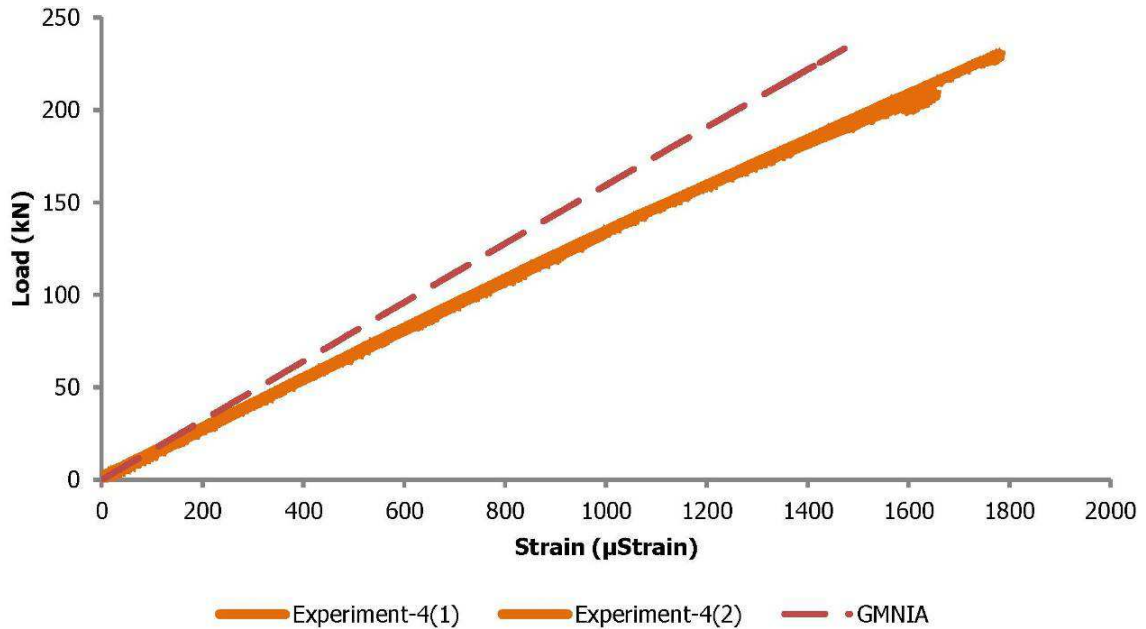


Figure 4-28: Load-strain curves obtained experimentally and numerically for Group 4 at location A

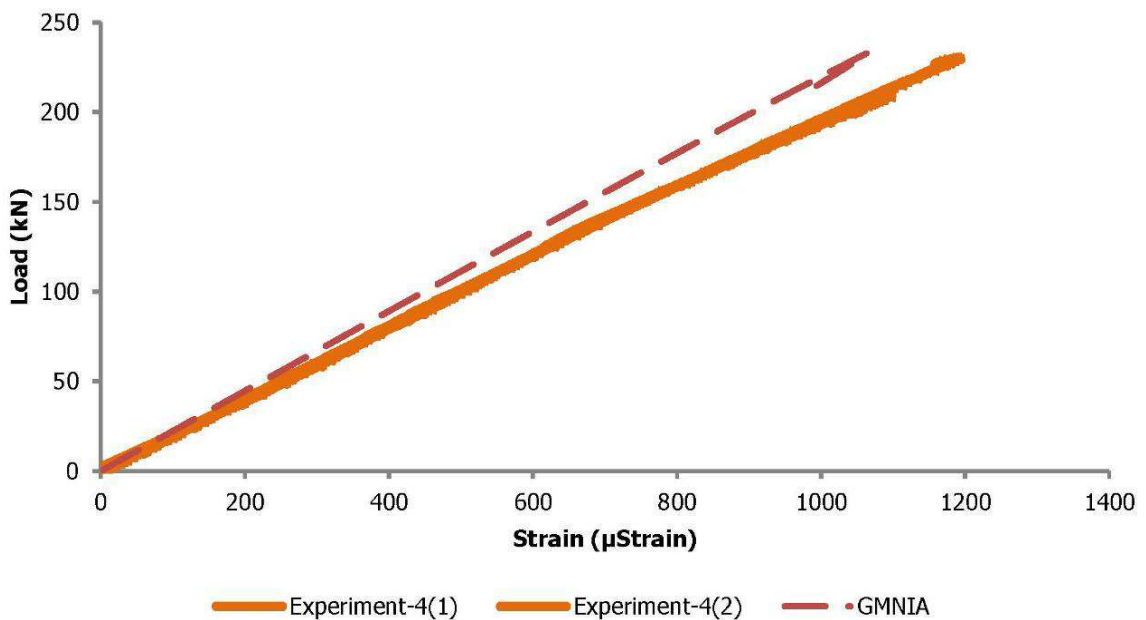


Figure 4-29: Load-strain curves obtained experimentally and numerically for Group 4 at location B

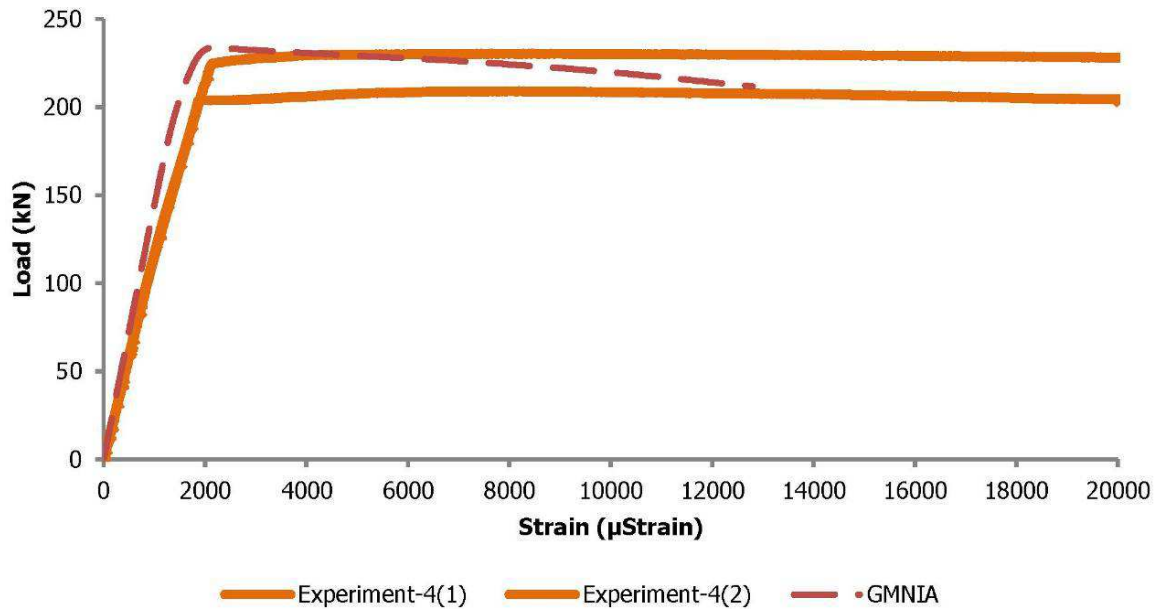


Figure 4-30: Load-strain curves obtained experimentally and numerically for Group 4 at location C

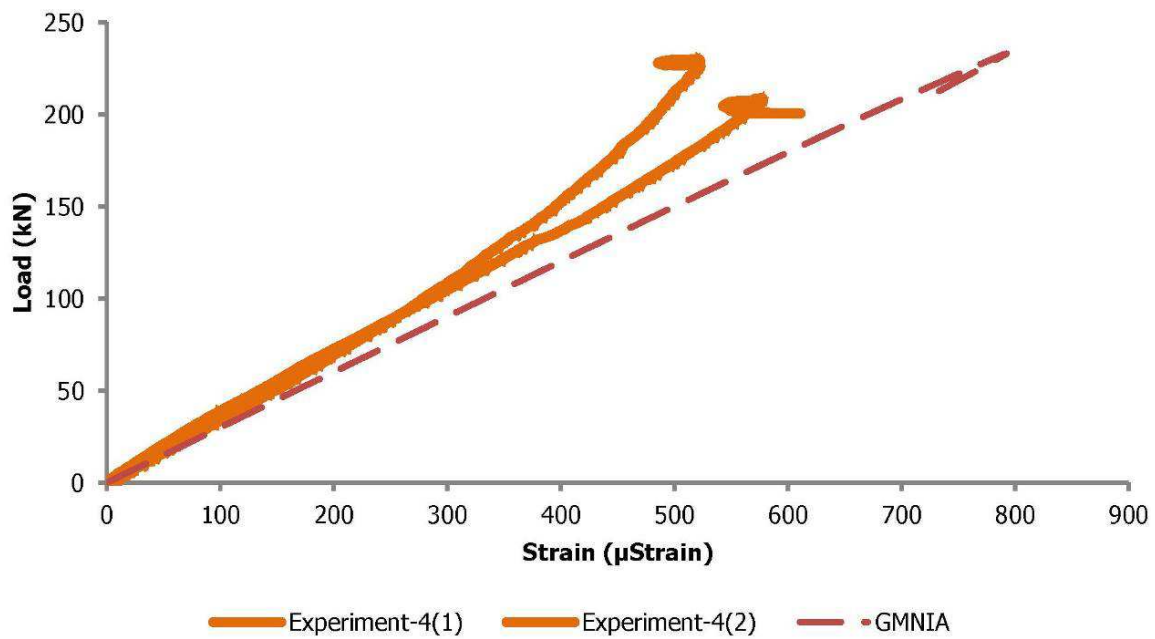


Figure 4-31: Load-strain curves obtained experimentally and numerically for Group 4 at location D

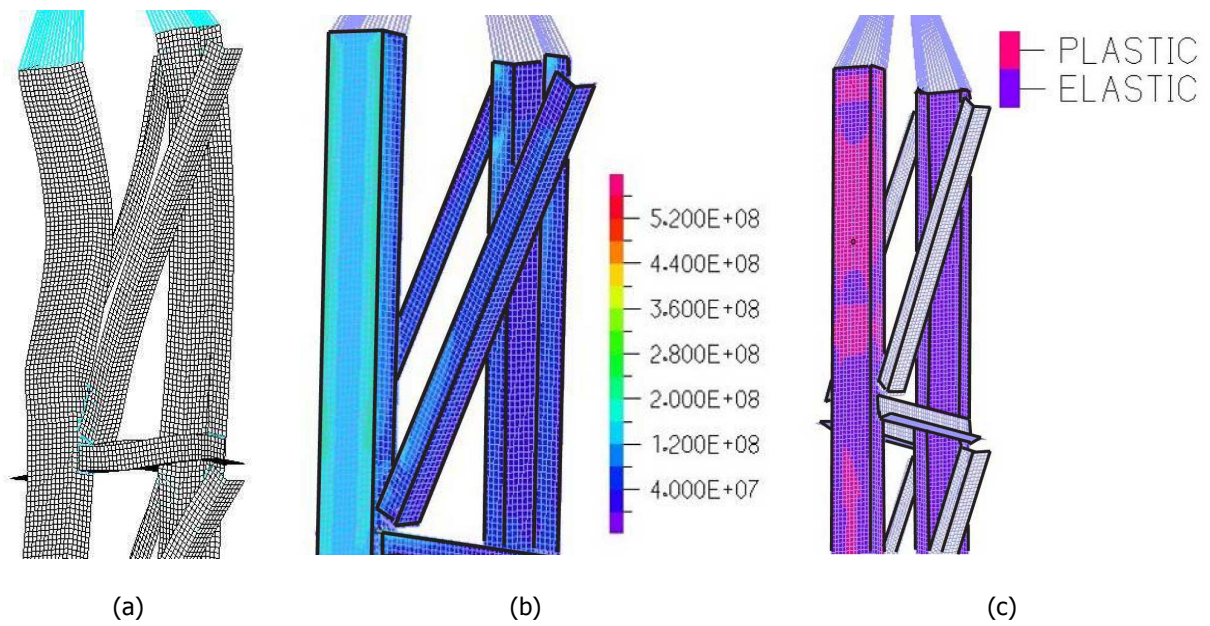


Figure 4-32: Critical panel's for Group 4 (a) deformed view, (b) von Mises stress distribution and (c) plastification at collapse load level

4.3.5 Group 5

The local and global buckling modes of Group 5 are similar to the ones obtained for Group 1, as shown in Figure 4-3. In Figure 4-33 the experimental and numerical equilibrium paths obtained for the horizontal displacement at mid-height of specimens of Group 5 are shown. The agreement between the numerical and experimental results is satisfactory. A small difference is observed in the elastic part of the equilibrium paths that is clearly attributed to the fact that global imperfection plays an important role in these cases (small eccentricity of the applied load and as a result larger effect of global imperfection on global deflections) and leads to more conservative results (as this global imperfection is based on the conservative provisions of Eurocode 3).

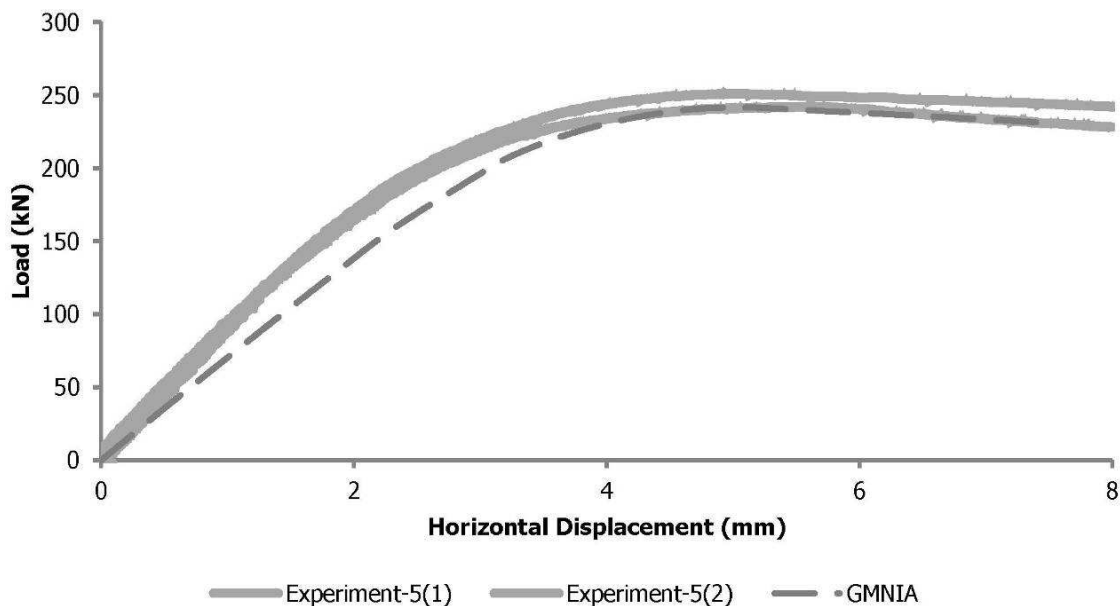


Figure 4-33: Equilibrium paths obtained experimentally and numerically for Group 5

The critical panels are the second and fourth ones in specimens 5(1) and 5(2), respectively, while in the numerical analyses the third panel initially fails. Despite that fact, as intermediate panels have the same stress level, no significant deviation of the numerical results from the experimental ones is observed in terms of collapse load. In all cases the critical panel deflects inwards. The local response of the critical panel experimentally (specimen 5(1)) and as predicted by the numerical model at a post-buckling state is depicted in Figure 4-34. No local plate buckling and torsional effects are observed in the numerical results.

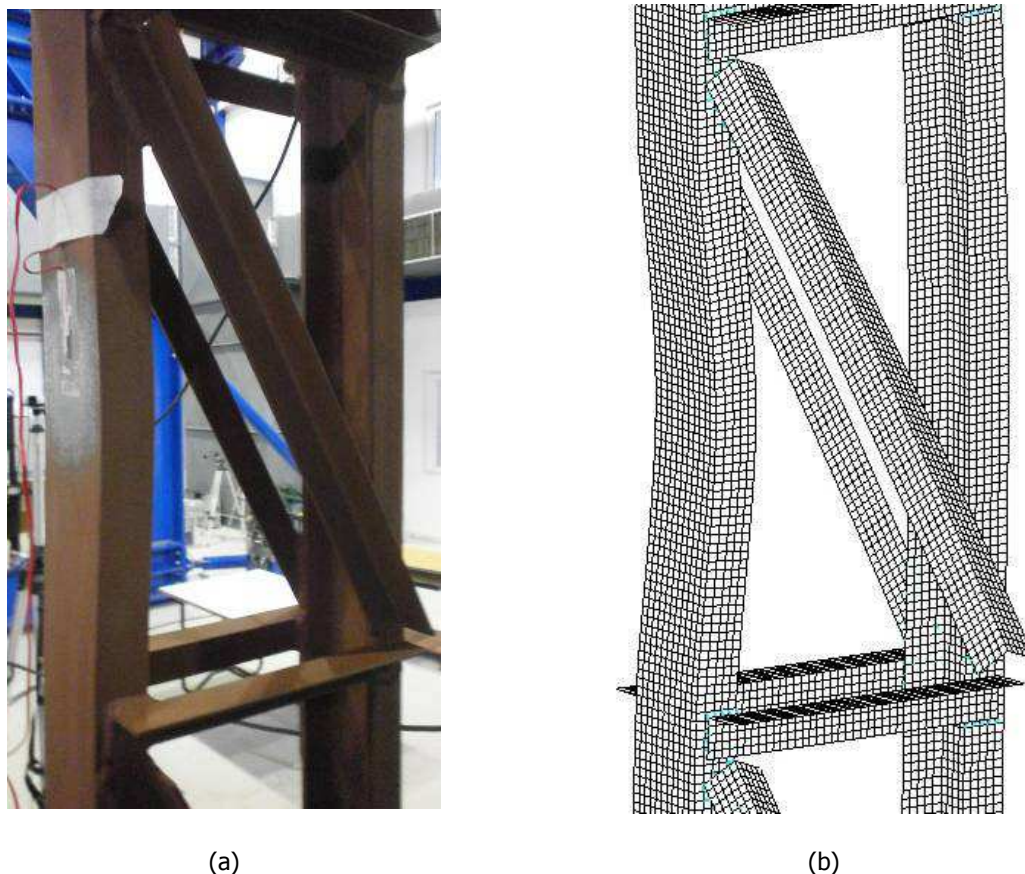


Figure 4-34: Critical panel at a post-buckling state obtained (a) experimentally and (b) numerically for Group 5

The load-strain curves for the locations A, B, C and D as obtained experimentally and numerically are shown in Figure 4-35 - Figure 4-38 and verified that at a local level a good agreement between tests and analyses is achieved. In Figure 4-38 related to the end diagonal's strain the numerical prediction is not satisfactory for the reasons explained in Group 1. The deformed shape (magnified for better observation), the von Mises stress distribution and the plastification of the critical panel at collapse load level, are shown in Figure 4-39. Similarly to Groups 1, 2 and 3, the critical panel and the adjacent ones are plastified. The non-critical chord remains elastic with a very low stress level.

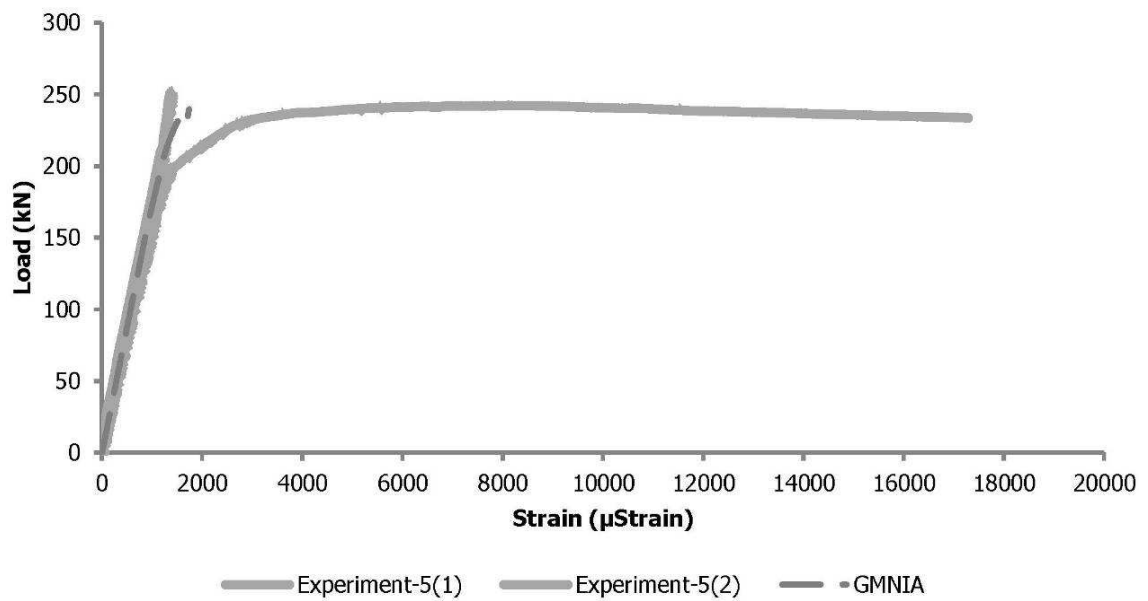


Figure 4-35: Load-strain curves obtained experimentally and numerically for Group 5 at location A

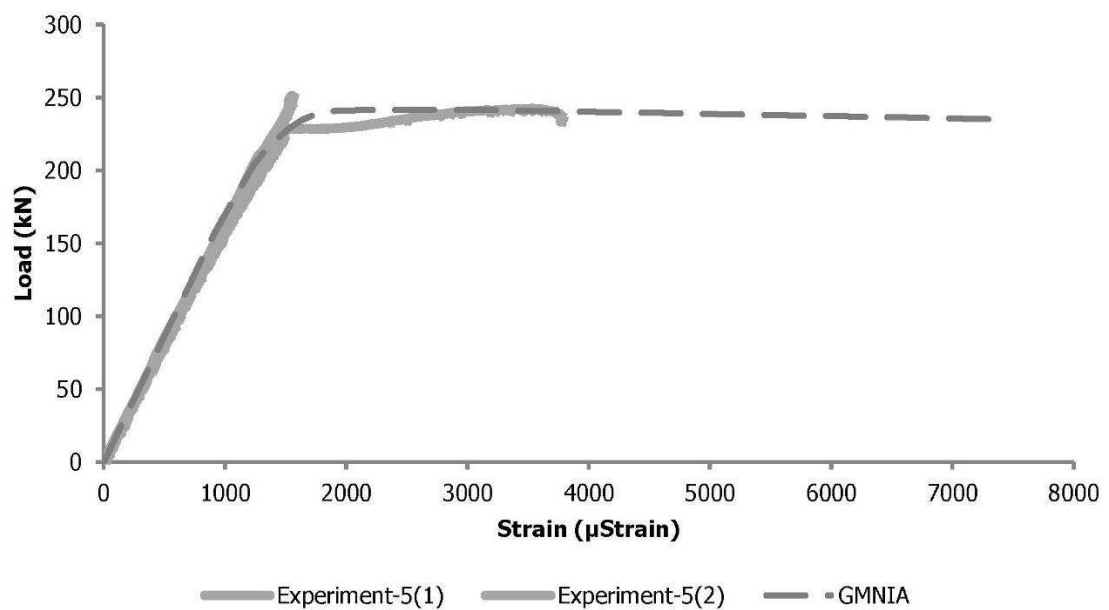


Figure 4-36: Load-strain curves obtained experimentally and numerically for Group 5 at location B

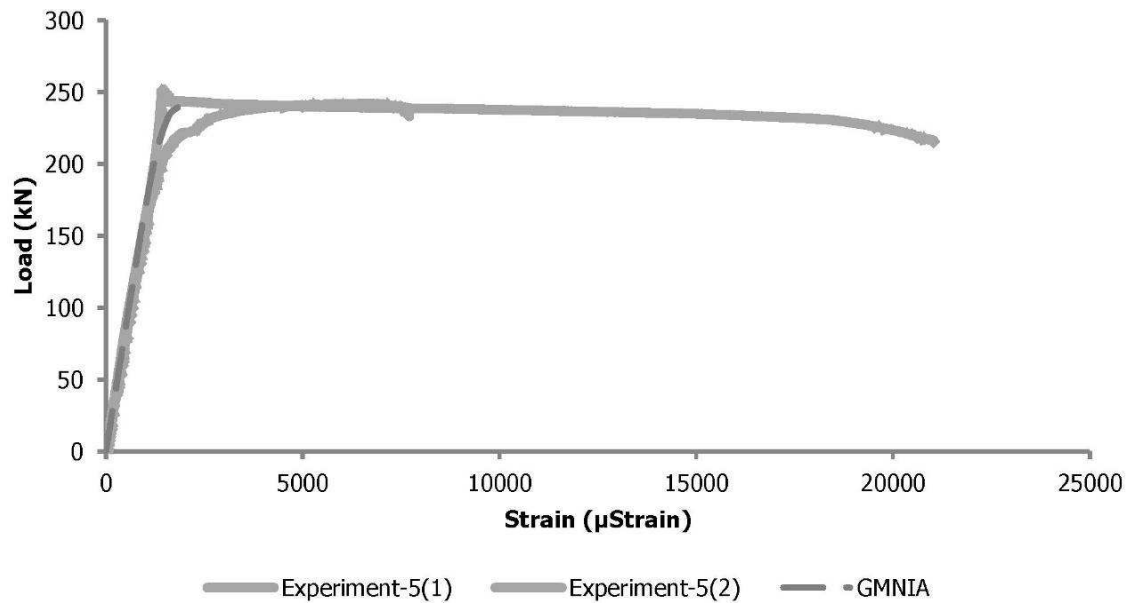


Figure 4-37: Load-strain curves obtained experimentally and numerically for Group 5 at location C

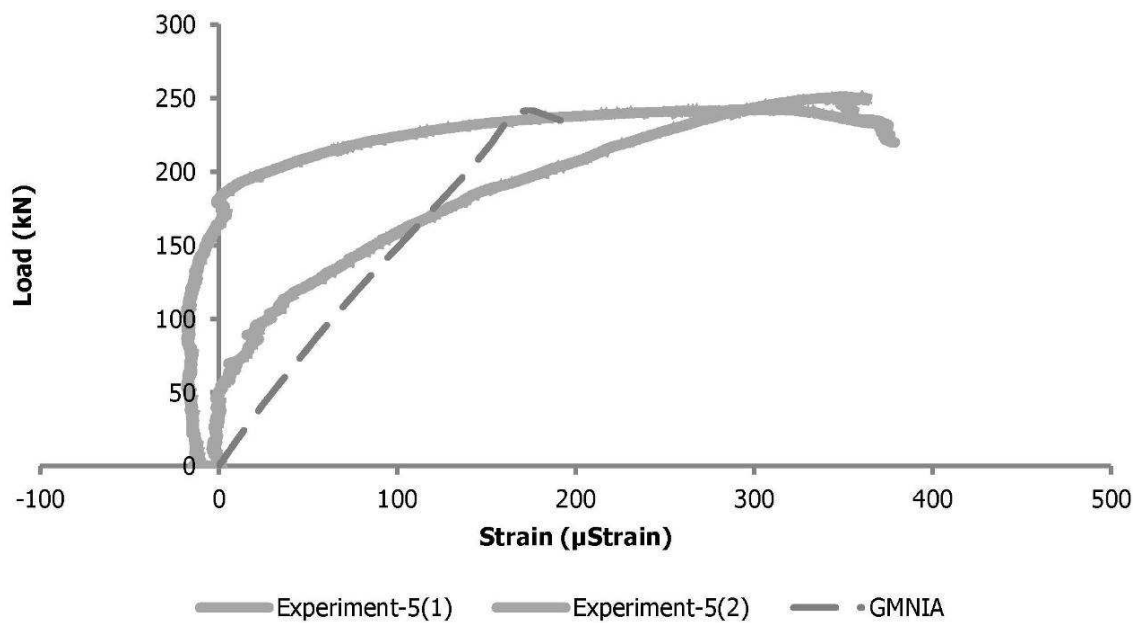


Figure 4-38: Load-strain curves obtained experimentally and numerically for Group 5 at location D

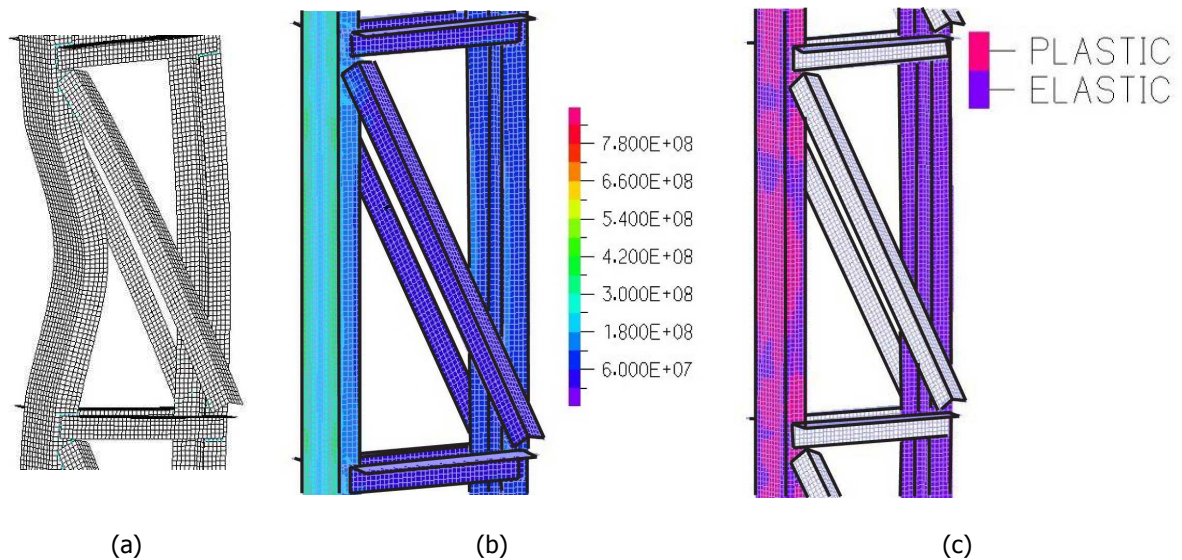


Figure 4-39: Critical panel's for Group 5 (a) deformed view, (b) von Mises stress distribution and (c) plastification at collapse load level

4.4 EFFECT OF INITIAL IMPERFECTIONS

Initial imperfections always exist in structures and should be taken into account. Their effect on the structural response is usually detrimental leading to reduction of the structure's capacity, especially in members characterised by a large non-dimensional slenderness. Their magnitude and distribution may also differ significantly from one structure to another as they depend on various parameters. The effect of initial imperfections can be observed by performing numerical analyses without the incorporation of initial geometrical imperfections and thermally induced residual stresses (GMNA) and comparing them with the tests and with numerical analyses accounting for initial imperfections (GMNIA). In this section this comparison will be presented with the use of the equilibrium paths for each group separately.

4.4.1 Group 1

The equilibrium paths obtained experimentally, numerically with the use of GMNIA and numerically with the use of GMNA are shown in Figure 4-40 for Group 1. It can be seen that the initial imperfection results in a slightly reduced elastic stiffness that gradually decreases due to the existence of thermally induced residual stresses resulting in a smaller collapse load. On the other hand, if GMNA is performed, the equilibrium path obtained has an elastic part until the collapse load while the post-buckling descending branch is very similar to the one obtained with GMNIA. The collapse load obtained with the use of GMNIA is close to the experimental one and on the safe side while the use of GMNA results in a collapse load on the unsafe side. Capturing the gradual plastification of the member is not important for structural design but accurately predicting the collapse load is and reveals that initial imperfections should be taken into account.

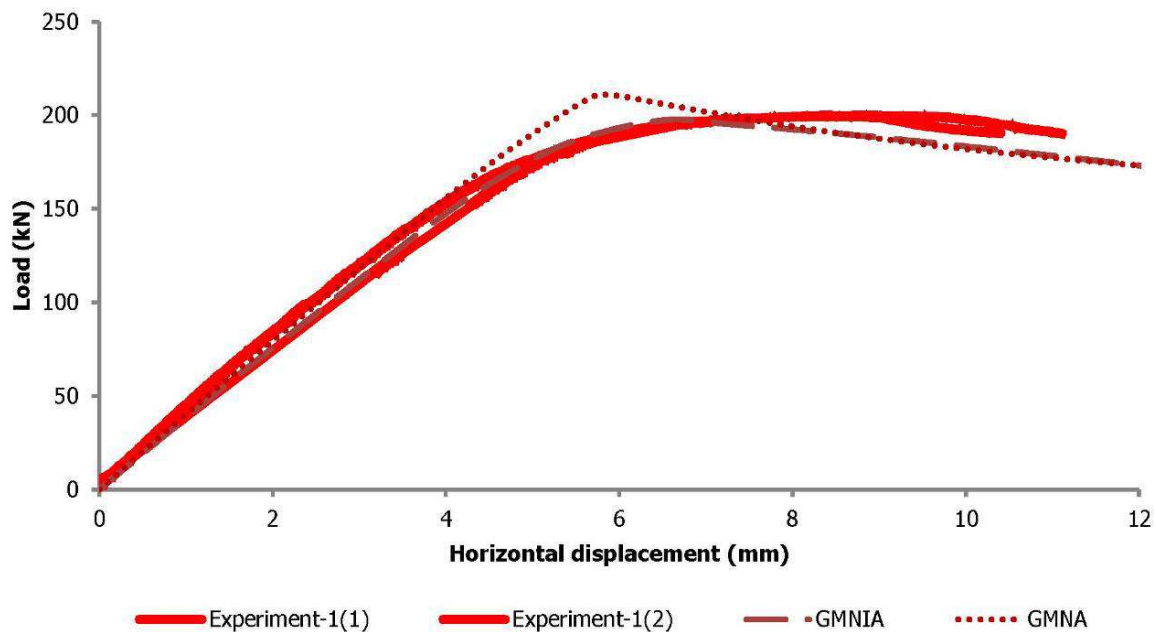


Figure 4-40: Equilibrium paths obtained experimentally and numerically (GMNIA and GMNA) for Group 1

4.4.2 Group 2

The equilibrium paths obtained experimentally, numerically with the use of GMNIA and numerically with the use of GMNA are shown in Figure 4-41 for Group 2. Similar conclusions to Group 1 are drawn in this case, too.

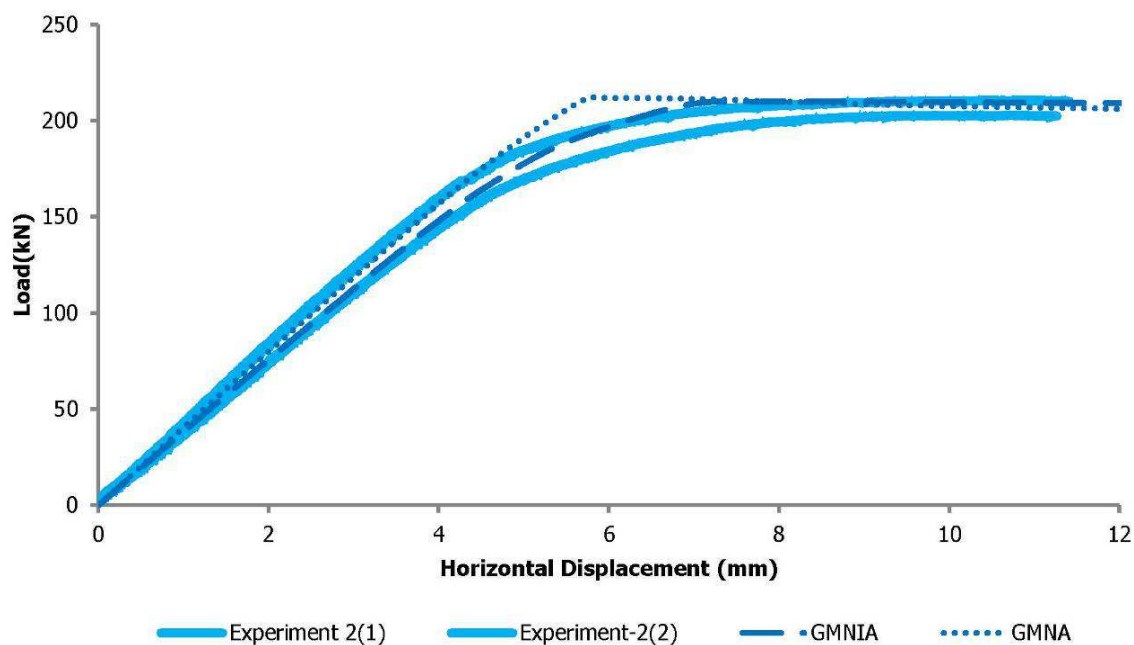


Figure 4-41: Equilibrium paths obtained experimentally and numerically (GMNIA and GMNA) for Group 2

4.4.3 Group 3

The equilibrium paths obtained experimentally, numerically with the use of GMNIA and numerically with the use of GMNA are shown in Figure 4-42 for Group 3. The elastic stiffness and collapse load without initial imperfections are closer to the experimental ones due to the conservatism of the

magnitude of global imperfection incorporated in GMNIA. In GMNA the decrease of stiffness due to thermally induced residual stresses is not captured and the member behaves elastically up to the ultimate load.

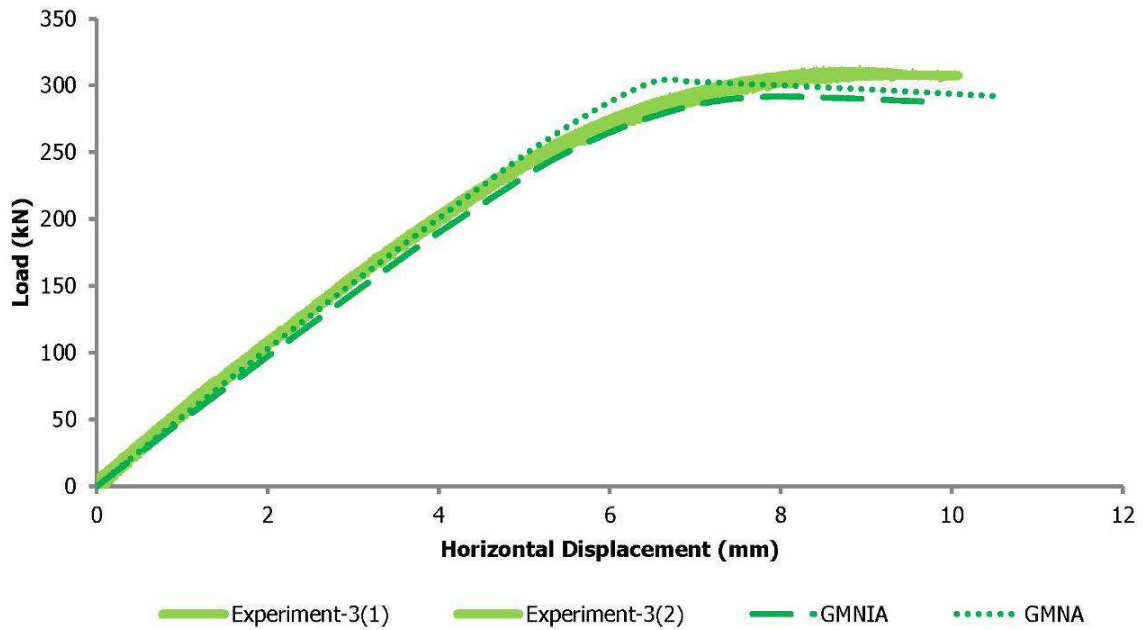


Figure 4-42: Equilibrium paths obtained experimentally and numerically (GMNIA and GMNA) for Group 3

4.4.4 Group 4

The equilibrium paths obtained experimentally, numerically with the use of GMNIA and numerically with the use of GMNA are shown in Figure 4-43 and Figure 4-44 for Group 4 and for top and bottom measurements, respectively. The effect of residual stresses and initial imperfections is the smallest when compared with the other four groups due to the type of loading and deformation that result in elastic behaviour of a relatively large part of the column.

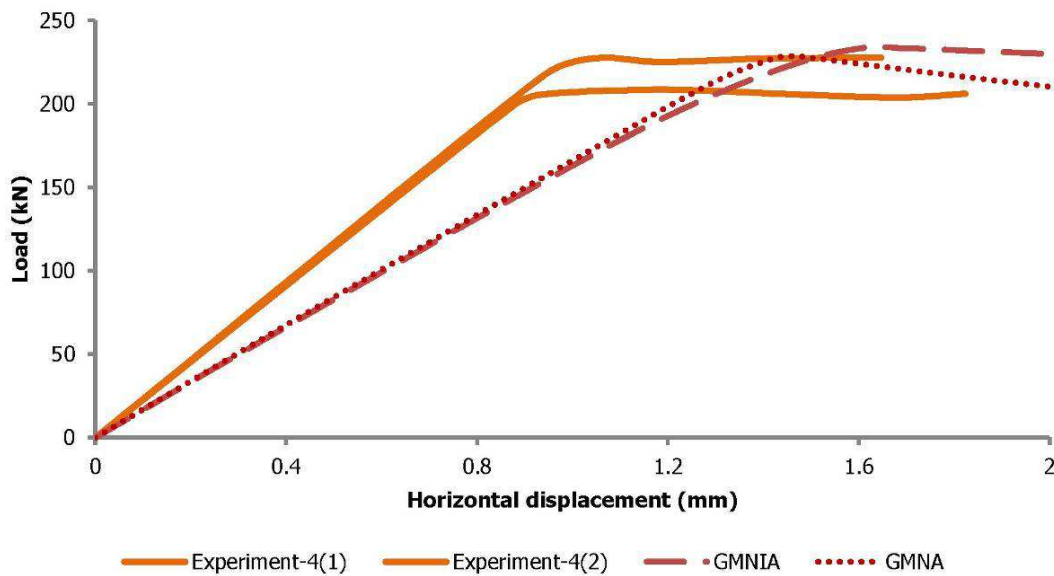


Figure 4-43: Equilibrium paths obtained experimentally and numerically (GMNIA and GMNA) for the top displacement for Group 4

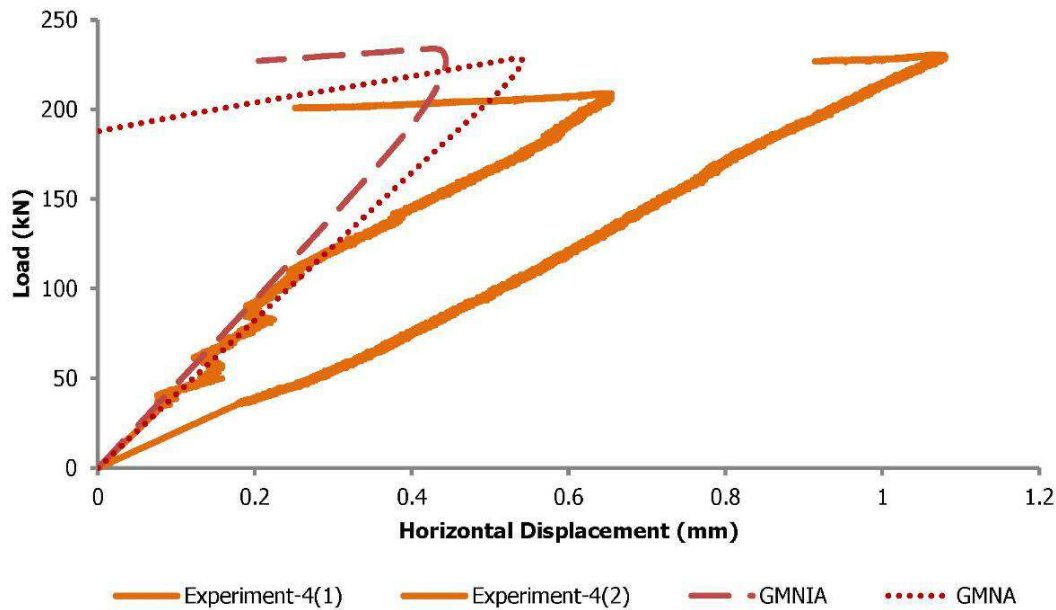


Figure 4-44: Equilibrium paths obtained experimentally and numerically (GMNIA and GMNA) for the bottom displacement for Group 4

4.4.5 Group 5

The equilibrium paths obtained experimentally, numerically with the use of GMNIA and numerically with the use of GMNA are shown in Figure 4-45 for Group 5. The elastic stiffness without initial imperfections is closer to the experimental one due to the conservatism of the magnitude of global imperfection incorporated in GMNIA. In GMNA the decrease of stiffness due to thermally induced residual stresses is not captured and the member behaves elastically up to the ultimate load.

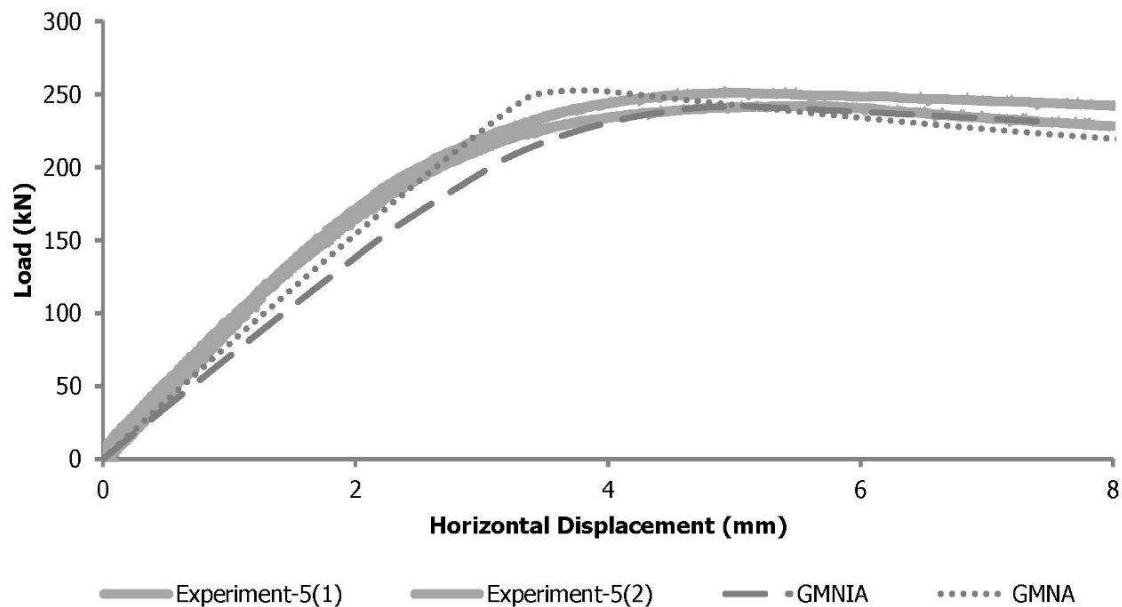


Figure 4-45: Equilibrium paths obtained experimentally and numerically (GMNIA and GMNA) for Group 5

4.5 COMPARISON BETWEEN SHELL AND BEAM ELEMENT MODELS

In the previous sections the calibration of the shell element numerical models was presented and the conclusion that they approached experimental results efficiently was drawn. It should be noted, though that the use of shell elements is in general time-consuming and computationally demanding. One of their main advantages is that they can efficiently capture local plate buckling of cross-sections and torsional effects, which however were not observed in the tests. The cross-sections used in the tests belong to class 1 according to Eurocode 3 [4-1] cross-section classification, which means that the use of a simpler type of element for their modelling could also be sufficient.

In this section, planar beam element numerical models are compared with the calibrated shell element numerical models in order to examine their usefulness in such cases. A comparative view of a typical shell element model and beam element model for a laced column belonging to Group 1 is depicted in Figure 4-46. Both the chords and diagonals of the built-up members are modelled with the use of Hermitian beam elements with six degrees of freedom at each end. Bending moment releases are incorporated at the ends of the diagonals and at the ends of the chords. The chords are considered to be continuous in elevation. It should be also noted that the planar nature of the beam element model requires the use of a cross-section of double area for the diagonals in order to sufficiently model the two lacing planes. The stiff supports are modelled with rigid links as in the shell element cases. Additionally, initial imperfections are incorporated in the chords of the beam element models by inserting equivalent geometrical imperfections according to Eurocode 3 [4-1], as the modelling of residual stresses in the beam elements' cross-sections is not possible. Failure of the lacing bars is not considered in the present analyses and no initial imperfections are used for diagonals and transverse bars. Finally, no eccentricities are taken into account for the connection between the lacing bars and the chords, as usually done when modelling such structures.

Comparison between the two types of modelling follows in the next sections for each group separately based on equilibrium paths obtained with Geometrically and Materially Nonlinear Imperfection Analyses (GMNIA). The elastic stiffness, the collapse load and the post-buckling behaviour are compared and discussed.

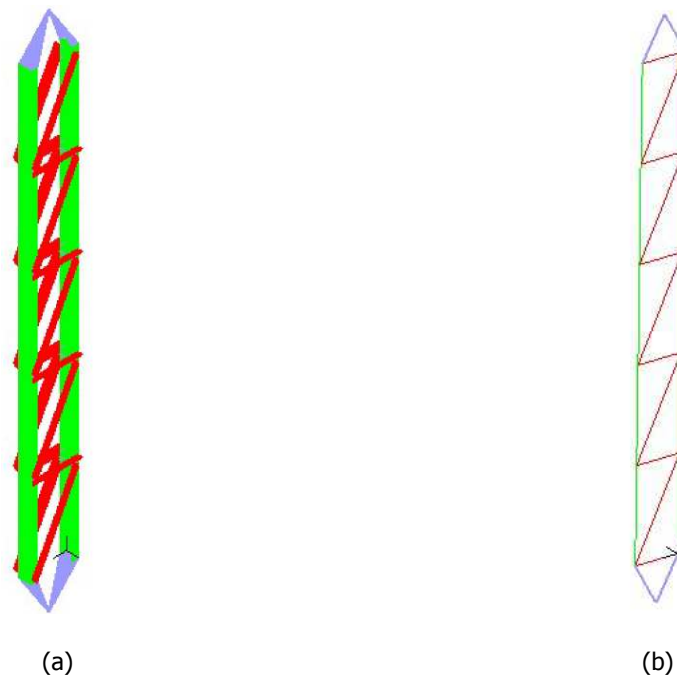


Figure 4-46: (a) Shell element and (b) beam element numerical models for typical laced member of Group 1

4.5.1 Group 1

The beam element model's local and global buckling loads are equal to 1164kN and 3377kN, respectively and the corresponding buckling modes are depicted in Figure 4-47. The shell element model's local and global buckling loads are equal to 2227kN and 3134kN, respectively. The incorporation of bending moment releases at the diagonal ends and the fact that the panels' unrestricted length is larger in the beam element models (due to the omission of the finite dimensions of the chord to lacing connections) resulted in these differences at a local level. An explanation of the unrestricted length (a') and the restricted length (a) is shown in Figure 4-48. In the tests the unrestricted length is approximately equal to 75% of the restricted one due to scaling reasons imposed by limitations in the specimens' dimensions. This value is expected to be larger in practical built-up members as the connections' dimensions will be much smaller compared to the total length of the panels. The global buckling load obtained for planar behaviour of the shell element models (3481kN) is in very good comparison with the result obtained with the beam element model, while these values are larger than the ones found from shell element models that include out-of-plane buckling of the lacing bars (3134kN).

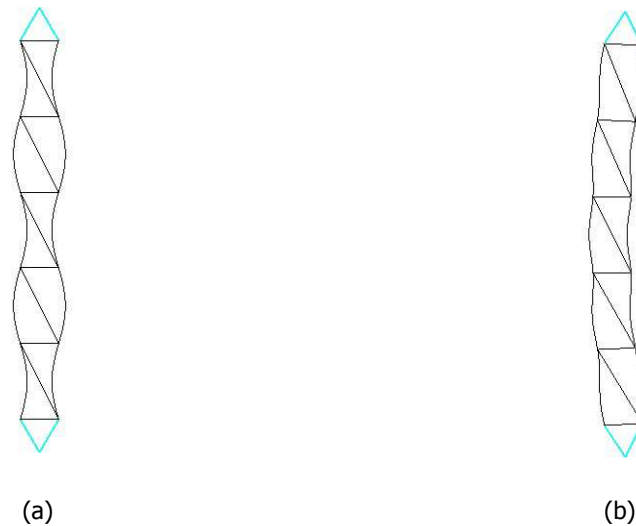


Figure 4-47: (a) Local and (b) global buckling mode shapes of the beam element model of Group 1

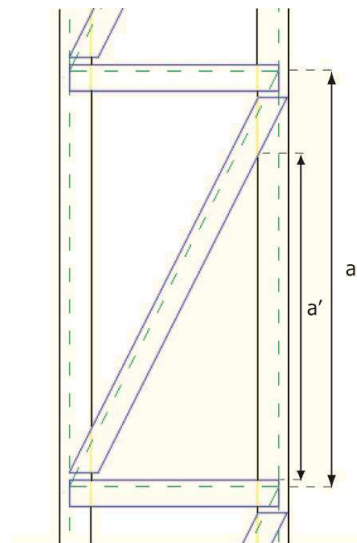


Figure 4-48: Unrestricted (a') and restricted (a) lengths of panel

The equilibrium paths obtained with numerical analyses with the use of shell and beam elements for Group 1 are shown in Figure 4-49. It can be seen that the beam element model predicts the same elastic stiffness and a slightly smaller collapse load. To be more specific the collapse loads of the numerical analyses with beam elements and shell elements are equal to 180kN and 197kN, respectively. As the global response is the same for the two cases and the global buckling load is larger for the beam element model, it is concluded that the difference in the local behaviour results in the deviation of the collapse loads. The post-buckling response is slightly more abrupt in the beam element case.

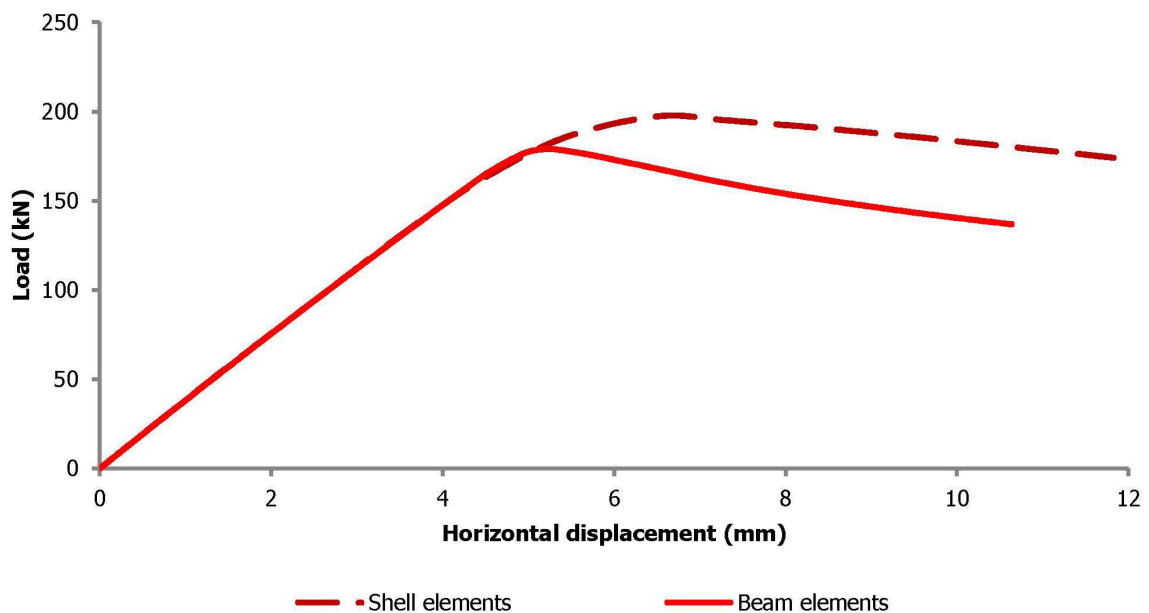


Figure 4-49: Equilibrium paths obtained numerically with shell and beam elements for Group 1

4.5.2 Group 2

The global buckling mode shape is shown in Figure 4-50 and corresponds to a load equal to 4682kN, larger than 3945kN which is the one obtained with shell elements. As in Group 1, the global buckling load obtained with the use of beam elements is larger because it does not account for out-of-plane buckling of the diagonals. In the case that out-of-plane degrees of freedom are deactivated the shell element model's global buckling load becomes 4709kN, a value close to the one found with the beam element model. The equilibrium paths obtained with numerical analyses with the use of shell and beam elements for Group 2 are shown in Figure 4-51. A good correlation of both the elastic stiffness and collapse load is achieved. The local behaviour is not significantly affected by the finite dimensions of the connections between chords and lacings because the panels are relatively stocky and full plastification of the cross-section is the prevailing local type of failure (thus the length of the panel does not play any important role). To be more specific the collapse loads are equal to 207kN and 210kN in the beam and shell element models, respectively. The post-buckling responses differ significantly probably because the full plastification of the cross-section in the beam element model leads to problems in the numerical convergence.



Figure 4-50: Global buckling mode obtained numerically with the use of beam elements for Group 2

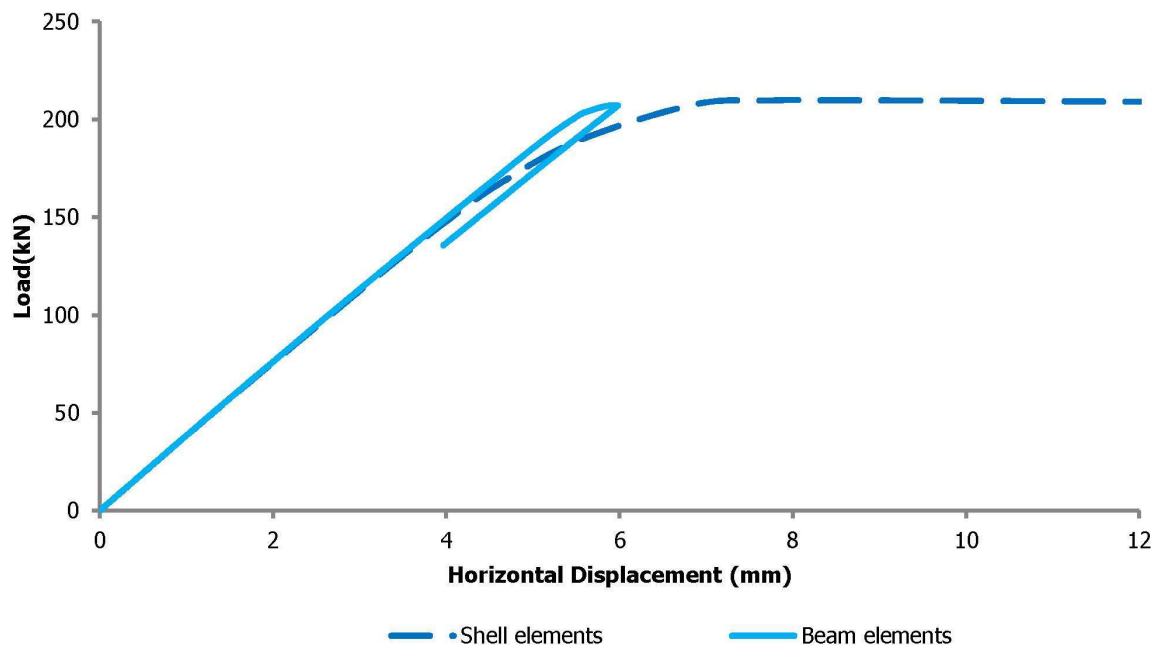


Figure 4-51: Equilibrium paths obtained numerically with shell and beam elements for Group 2

4.5.3 Group 3

The beam element model's local and global buckling loads are equal to 2358kN and 4231kN, respectively. The shell element model's local and global buckling loads for the case that out-of-plane buckling of the diagonal bars is included are equal to 3544kN and 3874kN, respectively. In the case that out-of-plane degrees of freedom are deactivated they become 4068kN and 4470kN, respectively. The corresponding buckling mode shapes are shown in Figure 4-52. The equilibrium paths obtained with numerical analyses with the use of shell and beam elements for Group 3 are shown in Figure 4-53. It can be seen that the beam element model is very close to the shell element one in terms of elastic stiffness and collapse load. The collapse loads are equal to 268.5 and 291.5 in the beam and shell element models, respectively. The post-buckling branch is slightly more descending for the beam element model.

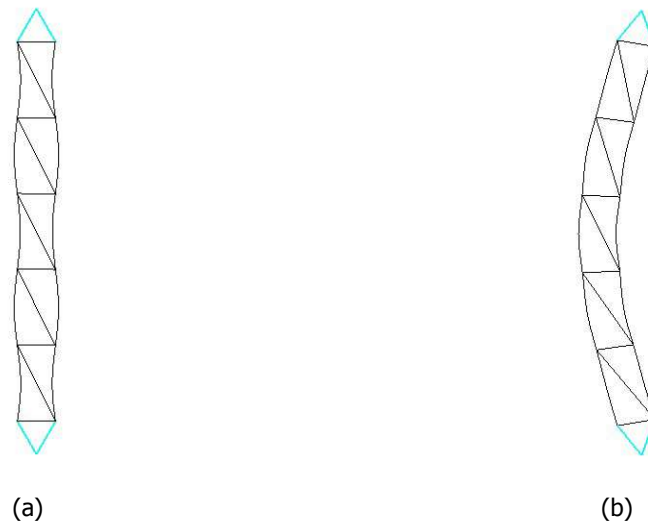


Figure 4-52: (a) Local and (b) global buckling mode shapes of the beam element model of Group 3

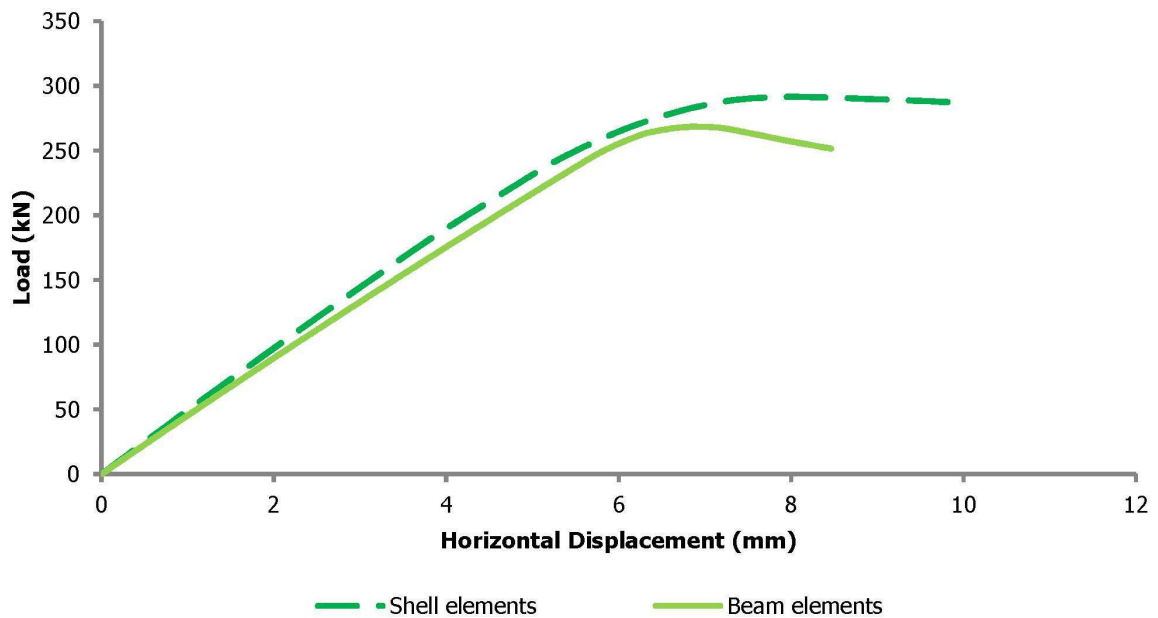


Figure 4-53: Equilibrium paths obtained numerically with shell and beam elements for Group 3

4.5.4 Group 4

The beam and shell element models' global and local buckling loads are the same as the ones of Group 1. The corresponding buckling mode shapes are shown in Figure 4-47. The equilibrium paths obtained with numerical analyses with the use of shell and beam elements for Group 4 are shown in Figure 4-54 and Figure 4-55 for the top and bottom measurement, respectively. A good agreement is found for the elastic stiffness, collapse load and post-buckling branch. The collapse loads are equal to 222kN and 233kN for the beam and shell element model, respectively.

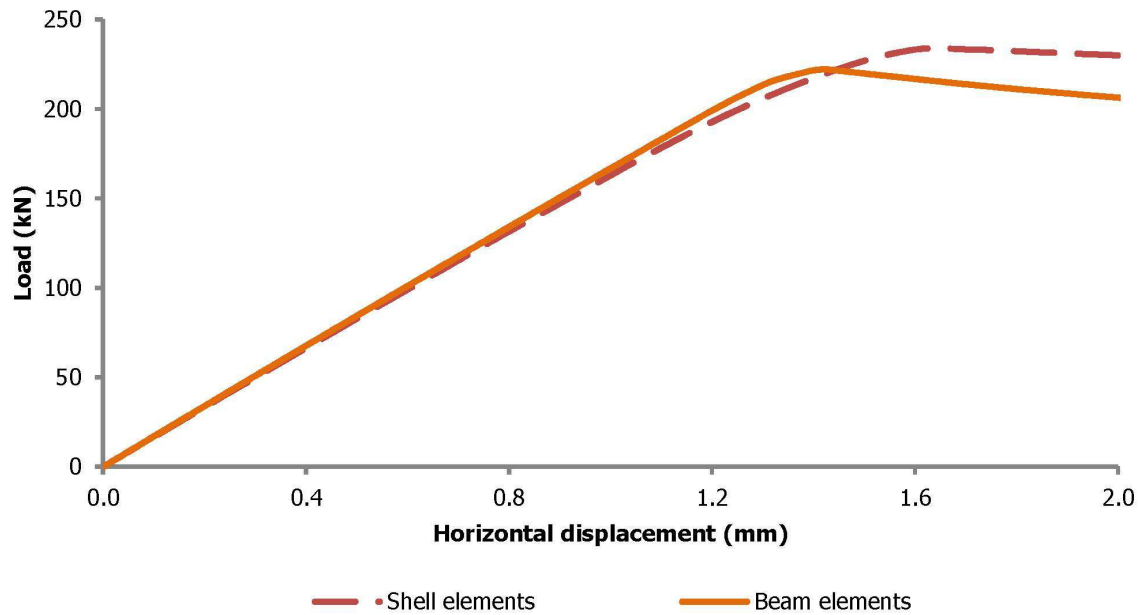


Figure 4-54: Equilibrium paths obtained numerically with shell and beam elements for the top measurement of Group 4

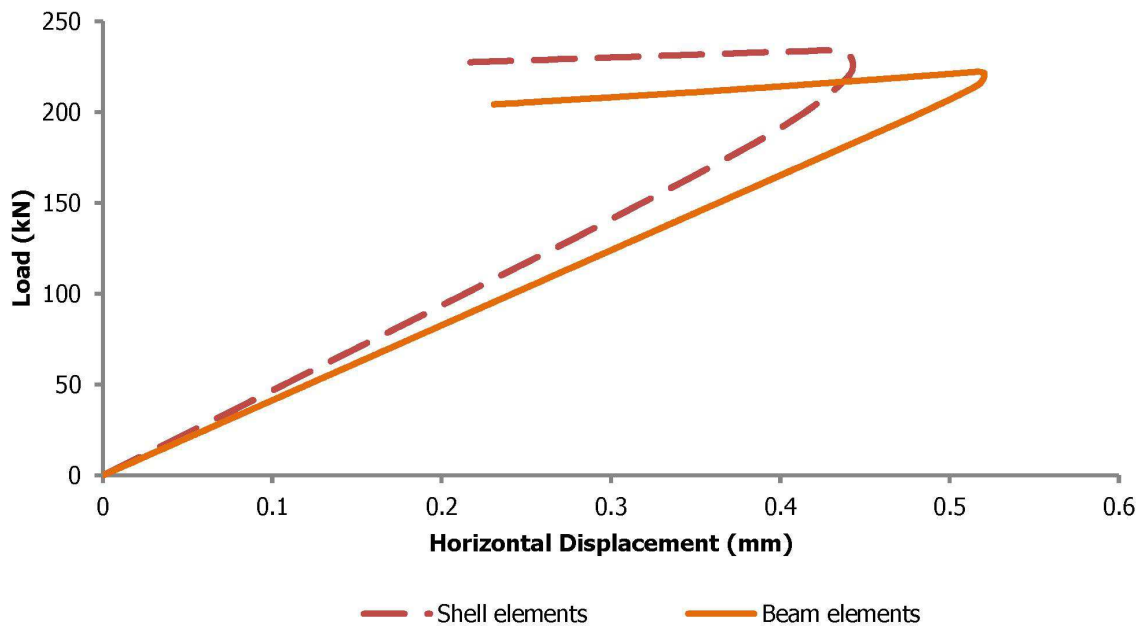


Figure 4-55: Equilibrium paths obtained numerically with shell and beam elements for the bottom measurement of Group 4

4.5.5 Group 5

The beam and shell element models' global and local buckling loads are the same as the ones of Group 1. The corresponding buckling mode shapes are shown in Figure 4-47. The equilibrium paths obtained with numerical analyses with the use of shell and beam elements for Group 5 are shown in Figure 4-56. It can be seen that the beam element model results in the same elastic stiffness and a slightly smaller collapse load. The collapse loads are equal to 226.5kN and 241.5kN in the beam and shell element models, respectively. The post-buckling response is more descending in the beam element case.

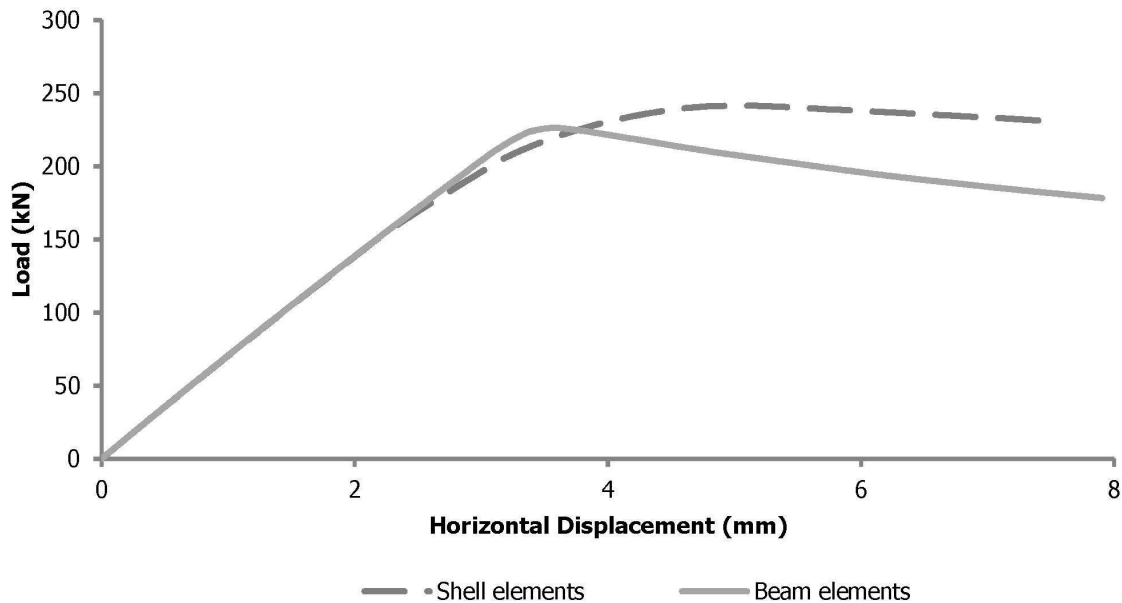


Figure 4-56: Equilibrium paths obtained numerically with shell and beam elements for Group 5

4.6 CONCLUSIONS

In the present chapter the numerical analyses of the tests performed in the context of the present doctoral thesis were presented. Finite element software ADINA [4-3] was used for this purpose with which Linearised Buckling Analyses (LBA), Geometrically and Materially Nonlinear Imperfection Analyses (GMNIA) and Geometrically and Materially Nonlinear Analyses (GMNA) were performed. The results were presented with the use of load-displacement curves (equilibrium paths), load-strain diagrams, von Mises stress distributions and deformed shapes at characteristic locations. The numerical analyses were separated into two different levels.

Initially, shell element models were used to perform LBA and GMNIA resulting in very satisfactory results when compared with the experimental ones at both global and local level. The incorporation of code provisions for initial imperfections affected the structural response and collapse load. Modelling thermally induced residual stresses with a simple concept of modifying appropriately the material yield strength captured the gradual degradation of the elastic stiffness of the equilibrium paths. It is recommended that initial imperfections are incorporated in the structural analyses of laced built-up columns. The collapse loads obtained experimentally and numerically with the use of shell element models are summarised in Table 4-1. The mean error of the shell element models' prediction of the collapse load is approximately equal to 3%.

Afterwards, shell element models were compared with beam element ones. The beam element models were based on the type of modelling commonly used in practice and in analytical methods. Beam elements predicted satisfactorily laced built-up members' elastic stiffness and gave collapse loads close to the shell element models' but always smaller as they did not account for the finite dimensions and rigidity of the connections between the lacing bars and the chords. A summary of the collapse loads obtained with the use of beam elements is given in Table 4-1. The mean error of the beam element models' prediction of the collapse load is approximately equal to 6.6%.

Table 4-1: Summary of collapse loads obtained experimentally and with different numerical models

Group	Experimental tests (kN)	GMNIA-shell elements (kN)	GMNIA-beam elements (kN)	Error (%) shell elements	Error (%) beam elements
1	200	197	180	1.50	10.00
2	206	210	207	-1.94	-0.49
3	309	291.5	268.5	5.67	13.11
4	220	233	222	-5.91	-0.91
5	247	241.5	226.5	2.23	8.30

Based on the numerical investigation of the experimental tests, it can be concluded that both beam and shell elements are expected to be a useful tool for the research and design of laced built-up columns. The conservatism of the beam elements is attributed to the fact that the finite dimensions of the connections of the lacing bars to the chords are neglected leading to difference between the restricted and unrestricted lengths as described in Figure 4-48. In the tests, this difference was important due to geometrical restrictions, but in practice these lengths are expected to be close to each other. For this reason, it is recommended that in cases that local buckling of the plate elements is not expected, beam element models are preferred as they are computationally less demanding without any significant loss of accuracy.

4.7 REFERENCES

- [4-1] Eurocode 3: Design of Steel Structures. Part 1.1: General structural rules. CEN-European Committee for Standardisation, Brussels, EN1993-1-1, 2005
- [4-2] Greiner, R., Lindner, J. "Interaction formulae for members subjected to bending and axial compression in EUROCODE 3 - The Method 2 approach", Journal of Constructional Research, Vol. 62, pp. 757-770, 2006
- [4-3] ADINA System 8.5, Release Notes. ADINA R & D Inc., 71 Elton Avenue, Watertown, MA 02472; USA. 2008
- [4-4] Gantes, C.J., Fragkopoulos, E. "Strategy for numerical verification of steel structures at the ultimate limit state", Structure and Infrastructure Engineering, Vol. 6, pp. 225-255, 2010
- [4-5] Dimopoulos C.A., Gantes, C.J. "Comparison of alternative algorithms for buckling analysis of slender steel structures", Structural Engineering and Mechanics, Vol. 44, No. 2, pp. 219-238, 2012
- [4-6] Riks, E. "The application of Newton's method to the problem of elastic stability", Journal of Applied Mechanics, Vol. 39, pp. 1060-1065, 1972
- [4-7] Riks, E. "An incremental approach to the solution of snapping and buckling problems", International Journal of Solids and Structures, Vol. 15, pp. 529-551, 1979
- [4-8] Wempner, G.A. "Discrete approximation related to nonlinear theories of solids", International Journal of Solids and Structures, Vol. 7, pp. 1581-1599, 1971.
- [4-9] Crisfield, M.A. "A fast incremental/iterative solution procedure that handles snap-through", Computers and Structures, Vol. 13, pp. 55-62, 1981
- [4-10] Bathe, K.J., Dvorkin E.N. "On the automatic solution of nonlinear finite element equations", Computers and Structures, Vol. 17, pp. 871-879, 1983

- [4-11] European Convention for Constructional Steelwork (ECCS), Ultimate Limit State Calculation of Sway Frames with Rigid Joints, ECCS, Technical Working Group 8.2., Systems, Publication No. 33, 1983

5 NUMERICAL AND ANALYTICAL INVESTIGATION OF LACED COLUMNS' BEHAVIOUR

5.1 INTRODUCTION

Following the numerical calibration of the experimental tests, the use of numerical models for the prediction of the behaviour of laced built-up columns will be presented in this chapter. The structural response and collapse load of axially compressed laced columns will be investigated from a numerical point of view. The interaction between global buckling, local buckling and yield strength will be presented and a parametric study will be utilised for observing their effect on the stiffness, collapse load and post-buckling response. Afterwards, an approximate analytical procedure will be proposed for accounting for this type of interaction in the calculation of the structural response of laced members. The capacity obtained with the proposed method, Eurocode 3 (EC3) [5-1] and Geometrically and Materially Nonlinear Imperfection Analyses (GMNIA) [5-2]-[5-3] with the use of finite element software ADINA [5-4] will be finally presented and compared and useful conclusions will be drawn.

5.2 RESPONSE OF LACED BUILT-UP COLUMNS

5.2.1 Perfect laced built-up columns

A perfect column, that consists of two flange components widely spaced between each other and connected with a lacing system, under an axially compressive load can exhibit three possible types of failure. The first two are global and local buckling, while the third one is due to plastification of the two flanges, at a load known as squash load. Consider a laced member with equivalent bending rigidity EI_{eff} and shear rigidity S_v , as described in Chapter 2. The equivalent second moment of inertia consists of the inertia of the chords and of the Steiner term:

$$I_{\text{eff}} = \frac{A_{\text{ch}} h^2}{2} + 2I_{\text{ch}} \quad (5-1)$$

where A_{ch} is the cross-sectional area of the chords, h_o is the lever arm between the centres of gravity of each chord and I_{ch} is the in-plane moment of inertia of the chords (usually the moment of inertia about z-z axis). In laced columns the chords' moment of inertia is usually much smaller than the Steiner term and can be neglected while the shear rigidity depends on the arrangement of the lacing bars. In Chapter 2, formulas for the calculation of the shear rigidity were provided, depending on the axial rigidities and lengths of the lacing bars.

The global buckling mode (Figure 5-1(a)) occurs at the global buckling load at which the whole column deflects from its perfect and straight configuration. If the lacing is very stiff, this load is equal to the Euler buckling load of the system as:

$$P_E = \frac{\pi^2 EI_{eff}}{(KL)^2} \quad (5-2)$$

where K is the effective buckling length factor ($K=1$ for simply-supported columns) and L is the total length of the column. In case of non-negligible shear deformation and with the use of Engesser's theory the global buckling load becomes:

$$P_{cr} = \frac{1}{\frac{1}{P_E} + \frac{1}{S_v}} \quad (5-3)$$

The local buckling load is associated with the individual buckling of the panels as simply-supported columns (Figure 5-1(b)). The total local buckling load is given by the summation of the buckling loads of each chord's panels individually:

$$P_L = \frac{2\pi^2 EI_{ch,z}}{a^2} \quad (5-4)$$

where $EI_{ch,z}$ is the in-plane bending rigidity of each chord and a is the length of each panel (distance between connectors).

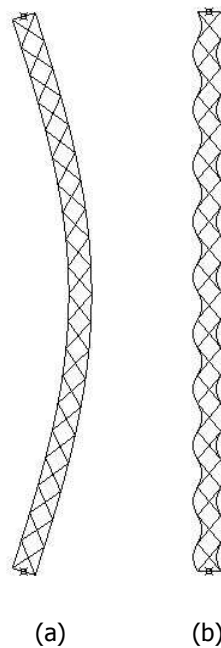


Figure 5-1: (a) Global and (b) local buckling mode of simply-supported laced column

The squash load is the third possible type of failure of perfect built-up columns and is given by the summation of the squash loads of the chords:

$$P_Y = 2A_{ch}f_y \quad (5-5)$$

where A_{ch} is the cross-sectional area of each chord and f_y is the yield stress of the material, idealised as elastic-perfectly plastic. The prevailing failure mode of perfect built-up columns neglecting mode interaction and nonlinear effects would thus be the one corresponding to the smallest of the loads obtained with Eqs. (5-3), (5-4) and (5-5).

5.2.2 Imperfect laced built-up columns

In reality, however, there are always imperfections in structural members that modify their behaviour and their ultimate strength. In this section the behaviour of imperfect built-up columns is investigated numerically by means of geometrically and materially nonlinear analyses. Useful conclusions for both pre- and post-buckling structural behaviour can thus be reached, which will then be utilised for the formulation of the proposed analytical approach.

Numerical models of simply supported laced built-up columns subjected to a concentrated compressive load at one end are created in ADINA using Hermitian beam elements. The lacing bars are modelled with moment releases at their ends and the two flanges as continuous members. All members are discretised in an appropriate way so that the results can be considered as sufficiently accurate. The shape of initial global and local imperfections is chosen to be consistent with the global and local mode shapes, respectively, as obtained by LBA. The maximum global and local imperfections are equal to $w_0 = \xi \cdot L = L/500$ and $z_0 = \eta \cdot a = a/500$, respectively. The maximum value of global imperfection appears in the middle of the simply-supported columns investigated, while the local one appears in the middle of each span between connectors.

Five different laced built-up columns are analysed, corresponding to varying values of the ratio x between global and local elastic critical buckling loads:

$$x = \frac{P_{cr}}{P_L} \quad (5-6)$$

Namely the five examples correspond to values of x equal to 1.6, 1.3, 1.0, 0.8 and 0.4, thus exhibiting qualitatively different structural behaviour. For that purpose, typical geometrical and cross-section characteristics are used, summarised in Table 5-1, while the desired variation of ratio x is achieved by varying the lever arm between the flange components, h_0 .

Table 5-1: Geometrical and cross-section characteristics of parametric study

Length L (cm)	Panel's length a (cm)	Flanges' cross-sectional area A_{ch} (cm ²)	$I_{ch,z}$ (cm ⁴)	h_0 (cm)
1350	150	30	142	varied

Analysis results are shown in the following two sections for elastic and inelastic material behaviour, respectively, by means of equilibrium paths plotting on the horizontal axis the horizontal displacement at mid-height, w , divided by the column height, L , and on the vertical axis the applied load P , divided by the elastic critical local buckling load, P_L . The collapse analysis option of ADINA is employed (Arc-length method), thus obtaining also results beyond the collapse loads, associated with limit points of the equilibrium paths.

5.2.2.1 Elastic analyses

The results for the case of elastic material are illustrated in Figure 5-2 for the five example columns described above. The values of elastic critical buckling loads, both global and local, are shown with black and green horizontal lines, respectively. The prevailing type of failure corresponds to the smaller buckling load. Equilibrium paths from geometrically nonlinear analysis with global imperfections only (sparse dotted red line), as well as both global and local imperfections (dense dotted blue line), are also shown.

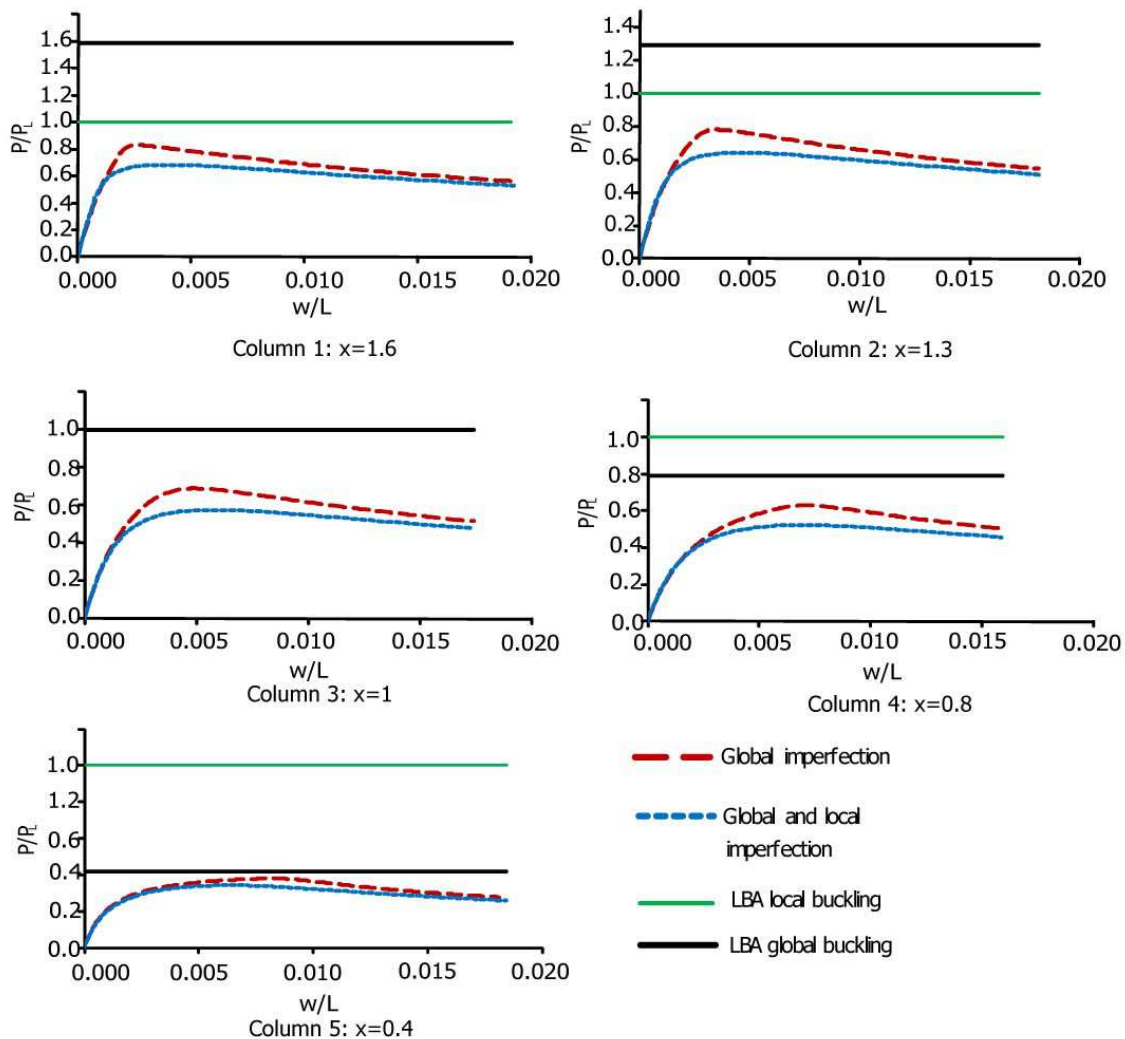


Figure 5-2: Equilibrium paths for elastic geometrically imperfect systems at (a) $x=1.6$, (b) $x=1.3$, (c) $x=1$, (d) $x=0.8$ and (e) $x=0.4$

Initially the deflections are the same regardless of whether global imperfections only or both global and local imperfections are introduced. At a larger load level the horizontal displacement becomes larger for the case that both types of imperfections are used. It is also observed that, even when only global imperfections are used, all equilibrium paths exhibit limit points, thus no post-buckling resistance. Moreover, collapse loads, associated with limit points, are always smaller than the smallest among the global and local critical buckling loads. Collapse loads decrease even more in case both global and local imperfections are introduced.

In order to better understand this, it is interesting to observe the deformed shapes at characteristic points ((a) pre-buckling state, (b) collapse load level and (c) post-buckling state) along the equilibrium

paths of the columns corresponding to $x=1.6$ (column 1) and $x=0.4$ (column 5). For the first case, the deformed shapes are shown in Figure 5-3 if elastic material and no local imperfections are used. It can be seen that both global and local deformations appear. In Figure 5-4, the deformed shapes obtained for $x=1.6$ with the use of elastic material and both global and local imperfections are depicted.

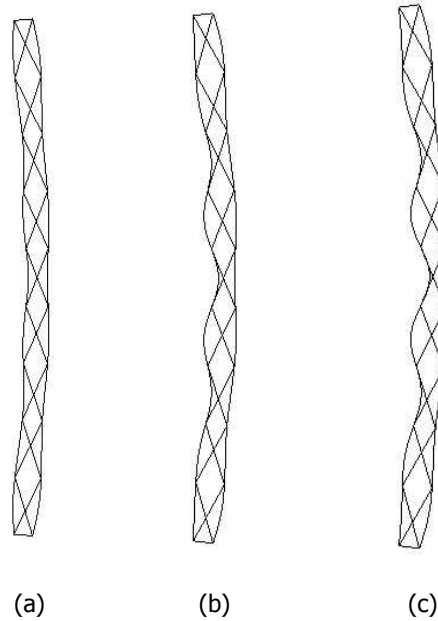


Figure 5-3: Deformed shapes of column 1 with elastic material and no local imperfections at (a) pre-buckling state, (b) collapse load level and (c) post-buckling state

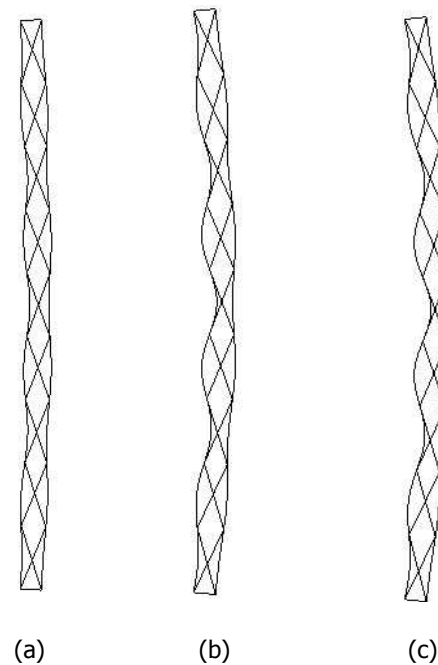


Figure 5-4: Deformed shapes of column 1 with elastic material and both local and global imperfections at (a) pre-buckling state, (b) collapse load level and (c) post-buckling state

For the second case (column 5), the deformed shapes are shown in Figure 5-5 if elastic material and no local imperfections are used. It can be seen that both global and local deformations appear despite

the fact that no local imperfections are inserted in the analysis. In Figure 5-6, the deformed shapes obtained for $x=0.4$ with the use of elastic material and both global and local imperfections are depicted. It is observed that the local deformations are more prominent than in Figure 5-5.

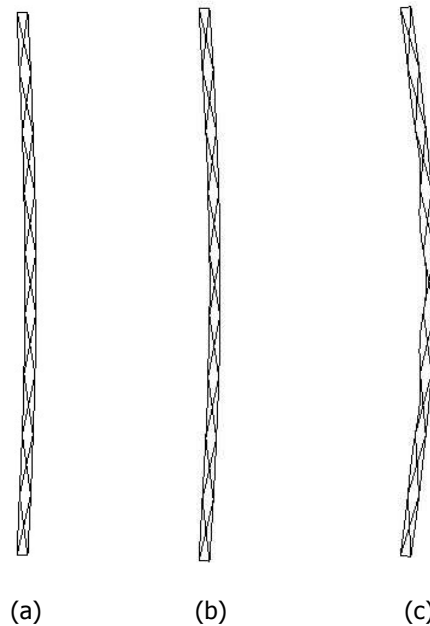


Figure 5-5: Deformed shapes of column 5 with elastic material and no local imperfections at (a) pre-buckling state, (b) collapse load level and (c) post-buckling state

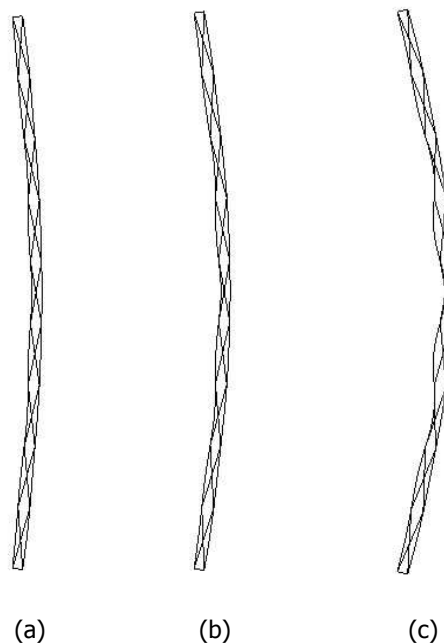


Figure 5-6: Deformed shapes of column 5 with elastic material and both local and global imperfections at (a) pre-buckling state, (b) collapse load level and (c) post-buckling state

It can be observed that not only global but also local deformations develop, even if only global imperfections are used. This is more pronounced for column 1, where the local mode occurs for a much smaller load than the corresponding global mode, and less so for column 5, where the opposite is the case. Nevertheless, an interaction between the two modes is observed in all cases, independently of whether also a local imperfection is used or not, and this is believed to be the reason

for the systematic decrease of collapse load with respect to both linearised buckling loads, as well as for the descending post-buckling branch. Of course, when both global and local imperfections are introduced, the resulting local deformations are relatively larger, particularly for larger values of ratio x , therefore, the resulting collapse load is smaller and the overall equilibrium path is lower. Additionally lateral deflections in this case are larger than in the case that only global imperfections exist, highlighting this interaction. It is also observed that the largest reduction of collapse load with respect to the linearised buckling loads is when x is equal to unity, in other words when global and local buckling loads coincide. These observations are in accordance with the findings of Van der Neut [5-5] and Koiter and Kuiken [5-6], [5-7].

5.2.2.2 Elastoplastic analyses

The results for the case of inelastic material are illustrated in Figure 5-7 for the five example columns described above. The material used is considered to be elastic-perfectly plastic with yield stress equal to 44kN/cm^2 . This value is chosen so that the squash load given by Eq. (5-5) would be equal to the local buckling load given by Eq. (5-4). The values of elastic critical buckling loads, both global and local, are shown again with black and green horizontal lines, respectively. Equilibrium paths from geometrically nonlinear analysis with both global and local imperfections and both elastic (blue dotted line) and elastoplastic (red dotted line) material are also shown.

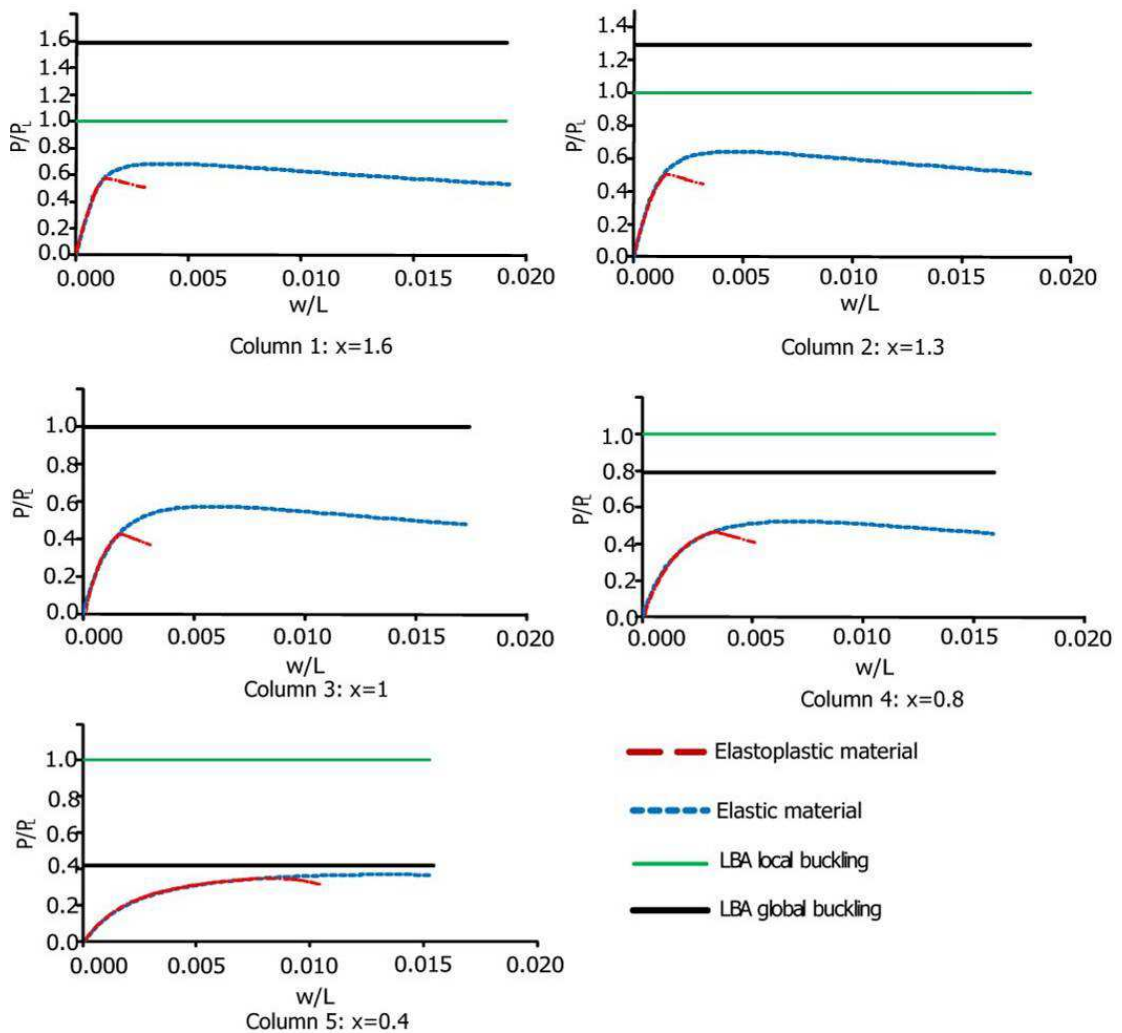


Figure 5-7: Equilibrium paths of imperfect laced built-up columns with elastoplastic material at (a) $x=1.6$, (b) $x=1.3$, (c) $x=1$, (d) $x=0.8$ and (e) $x=0.4$

In all cases examined the failure is related to local yielding. This type of failure leads to a smaller collapse load than the elastic one and is associated with more sharply descending post-buckling branches. The largest loss of capacity compared to the linearised buckling loads takes place in the case they coincide with each other and with the squash load (Figure 5-7(c)), as initially found by Svensson and Kragerup [5-8]. The influence of material yielding is practically negligible for column 5, characterised by a small value of x , thus having a large ratio of global to local slenderness.

The deformed shapes of column 1, when elastoplastic material and both initial global and local imperfections are used, are shown at a pre-buckling state, collapse load level and post-buckling state in Figure 5-8. In all cases local deformations appear and are magnified due to the increase of the axial load. Additionally, the axial force diagram and bending moment diagram along the chords are presented in Figure 5-9 and Figure 5-10, respectively. The largest axial forces appear at the mid-height of the column due to the existence of global imperfections of sinusoidal shape (largest deflection at mid-height). Additionally, the bending moment distribution follows the local buckling mode shape (sinusoidal shape).

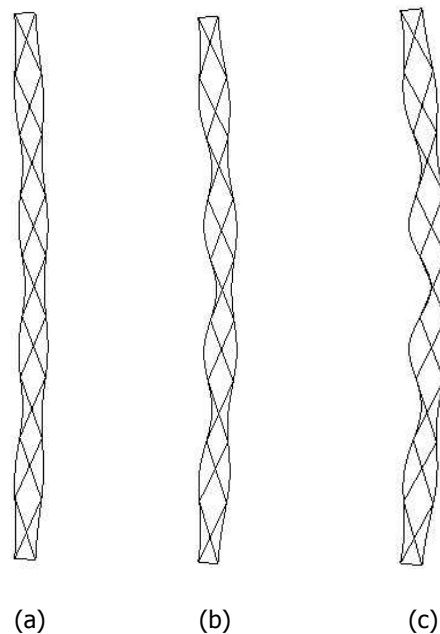


Figure 5-8: Deformed shapes of column 1 with elastoplastic material and both local and global imperfections at (a) pre-buckling state, (b) collapse load level and (c) post-buckling state

For the specific case presented, the normal stresses related to the maximum axial force and to the corresponding local bending moment are in general close to each other. Therefore it can be concluded that in cases that local buckling is the critical one (as for column 1 with $x=1.6$), local imperfections and deformations are expected to have a significant effect on the collapse load. An analysis without the use of local imperfections is not of practical importance in such cases but can prove useful for differentiating their effect on the collapse load. If local imperfections are neglected, the normal stresses related to the maximum axial force are in general larger than the ones related to the corresponding bending moment. Thus, it can be seen that even without the existence of initial local imperfections, the appearance of local deformations may lead to local bending moments that result in normal stresses. Despite that fact, initial local imperfections are the ones that lead to significant local bending moments.

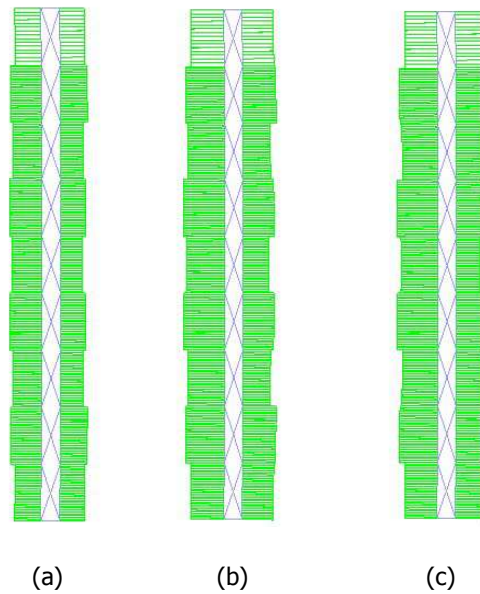


Figure 5-9: Axial force diagrams of column 1 with elastoplastic material and both local and global imperfections at (a) pre-buckling state, (b) collapse load level and (c) post-buckling state

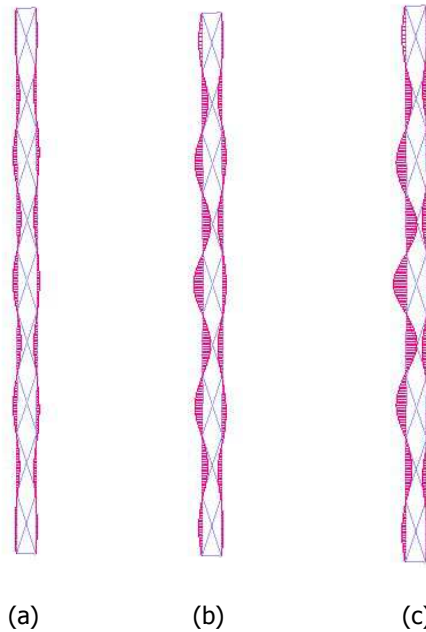


Figure 5-10: Bending moment diagrams of column 1 with elastoplastic material and both local and global imperfections at (a) pre-buckling state, (b) collapse load level and (c) post-buckling state

The deformed shapes of column 5, when elastoplastic material and both initial global and local imperfections are used, are shown at a pre-buckling state, collapse load level and post-buckling state in Figure 5-11. In all cases local deformations appear and are magnified due to the increase of the axial load. Additionally, the axial force diagram and bending moment diagram along the chords are presented in Figure 5-12 and Figure 5-13, respectively. The largest axial forces appear at the mid-height of the column due to the existence of global imperfections of sinusoidal shape (largest deflection at mid-height). Additionally, the bending moment distribution follows the local buckling mode shape (sinusoidal shape).

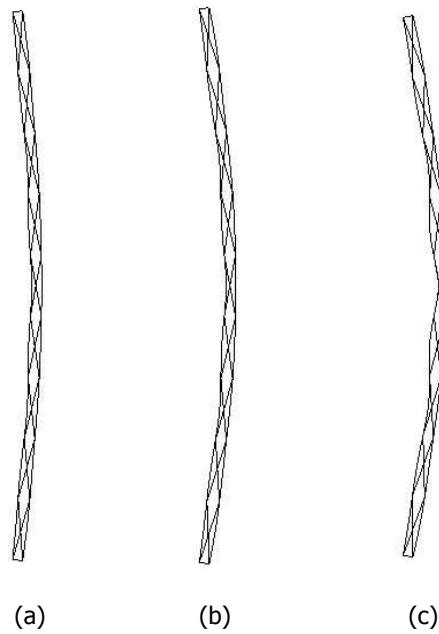


Figure 5-11: Deformed shapes of column 5 with elastoplastic material at characteristic points along the equilibrium path at (a) pre-buckling state, (b) collapse load level and (c) post-buckling state

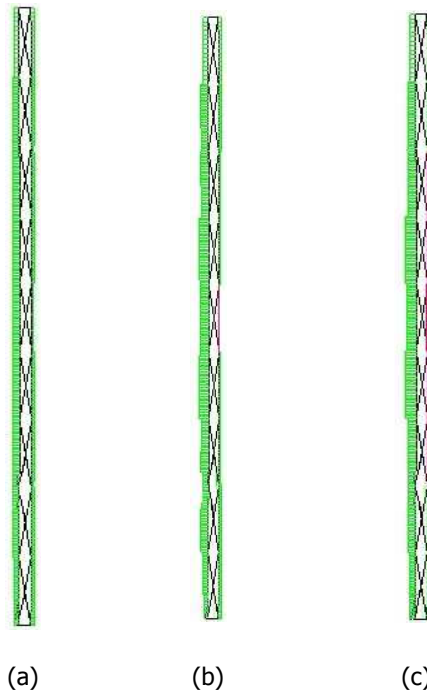


Figure 5-12: Axial force diagrams of column 5 with elastoplastic material at characteristic points along the equilibrium path at (a) pre-buckling state, (b) collapse load level and (c) post-buckling state

For the specific case presented, the normal stresses related to the maximum axial force and to the corresponding local bending moment are in general close to each other. Therefore, as for column 1, it can be concluded that in cases that local buckling is not the critical one (as for column 5 with $x=0.4$), local imperfections and deformations are expected to have an effect on the collapse load. If local imperfections are neglected, the normal stresses related to the maximum axial force are in general larger than the ones related to the corresponding bending moment. Thus, it can be seen that even

without the existence of initial local imperfections, local bending moments appear due to continuity of the chords and result in normal stresses. As for column 1, local imperfections are the ones that lead to significant local bending moments.

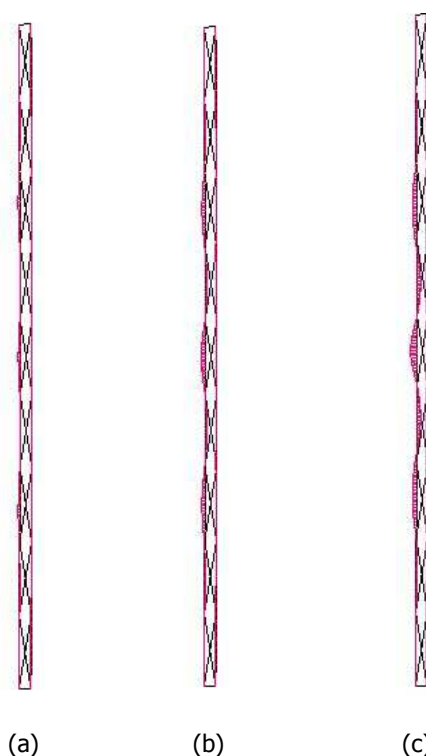


Figure 5-13: Bending moment diagrams of column 5 with elastoplastic material at characteristic points along the equilibrium path at (a) pre-buckling state, (b) collapse load level and (c) post-buckling state

When comparing lateral deflections, it can be concluded that they are larger in the cases that both global and local imperfections are used than in the ones that only global imperfections are used. This result highlights that there is interaction between global and local buckling that leads to an increase of $P-\Delta$ effects. In solid columns, the types of failure can be attributed either to elastoplastic buckling or to elastic buckling. In the first case, material's yielding and column's buckling lead to overall failure. In the latter case material remains elastic and failure takes place due to instability.

The types of failure of laced built-up columns can be summarised as:

- Local failure due to inelastic buckling of the chord between lacing joints. In this case the compressive force developing in the middle of the most compressed chord reaches the capacity of the chord between connectors and local failure leads to collapse.
- Overall failure of the column due to elastic (or almost elastic) global buckling. In this case the compressive force developing in the middle of the most compressed chord is smaller than the capacity of the chord between connectors. Nevertheless, overall instability leads to collapse.

5.3 EUROCODE 3 PROVISIONS

In Chapter 2 a general introduction to the Eurocode 3 (EC3) provisions for laced built-up members was made. In EC3 guidance for simply-supported columns is given assuming that the maximum bending moment appears at the mid-height of the member, even in the case that small lateral loads exist. Laced built-up members are truss-like structural systems and therefore their primary type of stress is due to axial forces while the secondary one is due to bending moments, usually about the

weak axis of the chords. In EC3 bending moments are neglected and only the axial forces are considered. In the case of a simply-supported laced column considering only global imperfections the equilibrium of vertical forces and moments at mid-height gives

$$P = P_1 + P_2 \quad (5-7)$$

$$(P_1 - P_2) \frac{h_o}{2} = (P_1 + P_2) w_T \quad (5-8)$$

where P is the total compressive force applied on the built-up column, P_1 is the total force of the more compressed flange at the cross-section at mid-height, P_2 is the corresponding total force of the less compressed flange and w_T is the total deflection of the column at the cross-section at mid-height due to the existence of initial global imperfections (Figure 5-14). The total deflection is the sum of the initial global imperfection w_o and of the additional deflection w due to second-order effects.

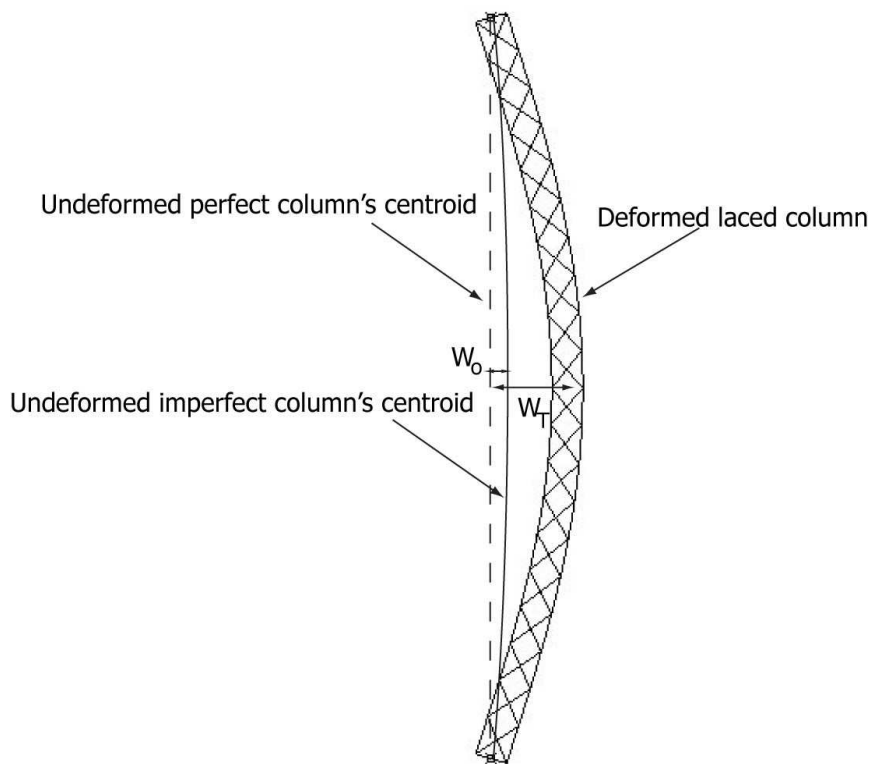


Figure 5-14: Global undeformed and deformed configurations of typical laced column

In order to avoid heavy computational work, without significant loss of accuracy, the magnification factor proposed by Thomas Young [5-9] and incorporated into many structural engineering code specifications is used for expressing the total deflection of the column w_T in terms of the initial imperfection w_o as

$$w_T = \frac{w_o}{1 - \frac{P}{P_{cr}}} \quad (5-9)$$

P_{cr} corresponds to the elastic critical buckling load of the Timoshenko member having equivalent bending and shear rigidities. In Eurocode 3 checking the maximum axial force of the chords (at mid-height) against the buckling resistance of the chord between connectors and the maximum axial force

of the diagonal bars (at the ends) against the buckling resistance of a diagonal bar is required. The design procedure is thoroughly described in Chapter 2. As diagonal bars are not usually designed marginally, the load at which according to Eurocode 3 failure will take place is the first one. Making use of Eq. (5-7), Eq. (5-8) and Eq. (5-9) and based on the fact that collapse will take place when the force in the more compressed flange (i.e. P_1) reaches the local capacity $N_{ch,Rd}$ of the geometrically imperfect chord, EC3 provisions result in the collapse load as

$$P = P_{cr} \left[\left(\frac{N_{ch,Rd}}{P_{cr}} + \frac{w_o}{h_o} + 0.5 \right) - \sqrt{\left(\frac{N_{ch,Rd}}{P_{cr}} + \frac{w_o}{h_o} + 0.5 \right)^2 - \frac{2N_{ch,Rd}}{P_{cr}}} \right] \quad (5-10)$$

Eq. (5-10) contains all three different types of failure of a perfect laced member. Global response is inserted with the use of global imperfection and the global elastic critical buckling load. Local behaviour is described by $N_{ch,Rd}$ which is the capacity of the part of the chord between successive lacing joints assuming simply-supported behaviour. The local capacity $N_{ch,Rd}$ can be obtained with the use of the buckling curves provided by Eurocode 3 and incorporates local buckling and yielding.

Local imperfections are taken into account in Eq. (5-10) only in the calculation of $N_{ch,Rd}$ and their influence on the value of the overall deflection at mid-height, due to their interaction with global imperfections, is ignored. This effect may be significant, as was demonstrated previously by the parametric study, where the resulting total deflections at mid-height when both global and local imperfections were introduced were found to be larger than the corresponding ones when only global imperfections were used, by approximately 15% at collapse load levels. Therefore, a modification of the EC3 procedure will be proposed in the next session, addressing this issue in an approximate but efficient manner.

5.4 PROPOSED ANALYTICAL APPROACH

Consider a simply-supported built-up column with both global and local initial imperfections which is axially loaded by a force P . It is modelled for computational convenience as a Timoshenko column with equivalent bending and shear rigidity. The internal bending moment is equal to:

$$M(x) = -EI_{eff} w_b''(x) \quad (5-11)$$

where $w_b(x)$ is the deflection due to bending only.

The external bending moment is equal to:

$$M(x) = P(w(x) + w_o(x)) \quad (5-12)$$

By equating Eq. (5-11) and Eq. (5-12), Eq. (5-13) is obtained

$$EI_{eff} \left(1 - \frac{P}{S_v} \right) w_b''(x) + Pw_b(x) = -Pw_o(x) \quad (5-13)$$

The effect of global imperfections $w_o(x)$ is directly included in the right-hand side of the differential moment equilibrium (5-13) with respect to the additional deflections due to bending $w_b(x)$, while the effect of local imperfections can be taken into account by properly modifying the effective bending rigidity EI_{eff} of the member, replacing it by a reduced value EI_{eff}^* . Then Eq. (5-13) becomes:

$$EI_{\text{eff}}^* \left(1 - \frac{P}{S_v} \right) w_b''(x) + Pw_b(x) = -Pw_o(x) \quad (5-14)$$

By considering that EI_{eff}^* is constant and based on Eq. (5-14), the additional deflection due to bending only w_b becomes equal to:

$$w_b(x) = \frac{w_o(x)}{\frac{a_{\text{cr}}^2}{a^{*2}} - 1} \quad (5-15)$$

where

$$a^{*2} = \frac{P}{EI_{\text{eff}}^* \beta} \quad (5-16)$$

Additionally, $\beta = 1 - P/S_v$ and for the simply-supported case the value of a_{cr} is:

$$a_{\text{cr}}^2 = \frac{n^2}{L^2} \quad (5-17)$$

As the shear deformation is directly related to the shear force perpendicular to the deformed axis Q , it is expressed in terms of the rotation due to bending only. By integrating once, the additional deflection due to shear deformation can be obtained as:

$$w_s(x) = -\frac{EI_{\text{eff}}^*}{S_v} \left(\frac{-a_{\text{cr}}^2 w_o(x)}{\frac{a_{\text{cr}}^2}{a^{*2}} - 1} \right) \quad (5-18)$$

The additional deflection w is equal to the sum of the additional deflection due to bending (Eq. (5-15)) and the additional deflection due to shear deformation (Eq.(5-18)) resulting in the following expression after some manipulation:

$$w(x) = w_o(x) \frac{1}{\beta_{\text{cr}}^* \left(\frac{a_{\text{cr}}^2}{a^{*2}} - 1 \right)} \quad (5-19)$$

where

$$\beta_{\text{cr}}^* = 1 - \frac{P_{\text{cr}}^*}{S_v} \quad (5-20)$$

The total deflection $w_T(x)$ of the column is given by adding the initial imperfection and the additional deflection due to both bending and shear deformation $w(x)$:

$$w_T(x) = w_o(x) + w(x) = w_o \left(1 + \frac{1}{\beta_{cr}^* \left(\frac{\pi^2 EI_{eff}^* \left(1 - \frac{P}{S_v} \right)}{PL^2} - 1 \right)} \right) \sin\left(\frac{\pi x}{L}\right) \quad (5-21)$$

Thus, the maximum total deflection at the middle is obtained as:

$$w_T = w_o \left(\frac{1}{1 - \frac{P}{P_{cr}^*}} \right) \quad (5-22)$$

where P_{cr}^* is a modified "elastic critical global buckling load", obtained by replacing in Eq. (5-2) the effective bending stiffness EI_{eff} by the modified one, EI_{eff}^* :

$$P_{cr}^* = \frac{1}{\frac{L^2}{\pi^2 EI_{eff}^*} + \frac{1}{S_v}} \quad (5-23)$$

The reduced bending rigidity can be obtained by considering a "smeared" analysis similar to the one introduced by Thompson & Hunt [5-10], including the effect of local imperfections on global response.

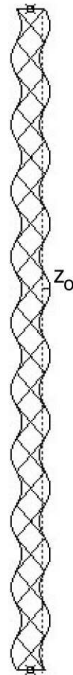


Figure 5-15: Local imperfections of typical laced column

This analysis is slightly modified here to account for the different axial forces in the two flanges of the built-up column. Consider that in the more compressed chord, the existence of initial local imperfections $z_0(x)$ with $z_0(L/2)=\eta \cdot a$ (Figure 5-15) has a sinusoidal form:

$$z_0(x) = \eta a \sin\left(\frac{\pi x}{a}\right) \quad (5-24)$$

The additional local deflection due to the application of the compressive axial force P_1 is equal to:

$$z(x) = z \sin\left(\frac{\pi x}{a}\right) \quad (5-25)$$

The relation between the initial local imperfection and the additional local deflection at the mid-height is obtained with the use of the magnification factor for Euler-Bernoulli members:

$$z = \eta a \frac{P_1}{0.5P_L - P_1} \quad (5-26)$$

The 2nd order axial shortening between two adjacent lacing joints is equal to:

$$u_{ch,1} = \frac{1}{2} \int_0^a \left[\left(z'_0(x) + z'(x) \right)^2 - \left(z'_0(x) \right)^2 \right] dx \quad (5-27)$$

where prime denotes differentiation with respect to x . By incorporating Eq. (5-26) in Eq. (5-25) and by making use of it in combination with Eq. (5-24) the above integral leads to:

$$u_{ch,1} = \frac{n^2 \eta^2 a P_1 (P_L - P_1)}{4 (0.5P_L - P_1)^2} \quad (5-28)$$

By adding to the 2nd order shortening the 1st order one, the total shortening is obtained, which is a non-linear function of the applied compressive load. By differentiating it once with respect to P_1 , the tangential compliance of the more compressed chord is calculated:

$$\frac{1}{EA_{ch,1}^*} = \frac{1}{EA_{ch}} + \frac{n^2 \eta^2 (0.5P_L)^2}{2 (0.5P_L - P_1)^3} \quad (5-29)$$

A similar procedure can be followed for obtaining the axial compliance of the less compressed chord by substituting $P - P_1$ instead of P_1 . The effective bending stiffness of a laced built-up column containing the reduced axial stiffness of both chords (neglecting the individual second-moment of inertia of each chord) is then given by:

$$EI_{eff}^* = 0.25 h_o^2 (EA_{ch,1}^* + EA_{ch,2}^*) \quad (5-30)$$

The force in the more compressed flange will be equal to:

$$P_1 = 0.5P + P \frac{w_o}{1 - \frac{P}{P_{cr}^*}} \frac{1}{h_o} \quad (5-31)$$

It is convenient to express this force as a ratio r of the local capacity of the flange $N_{ch,Rd}$:

$$P_1 = rN_{ch,Rd} \quad (5-32)$$

Factor r varies from 0 to 1, with 0 corresponding to no loading and 1 to local flange failure. Combining Eqs. (5-31) and (5-32), the following nonlinear equation relating the applied load P to factor r can be obtained:

$$0.5P + P \frac{w_o}{1 - \frac{P}{P_{cr}^*}} \frac{1}{h_o} = rN_{ch,Rd} \quad (5-33)$$

in which P_{cr}^* is substituted by using Eqs. (5-23) and (5-30).

The proposed method is expected to be conservative as it is based on the force in the more compressed panel P_1 for the calculation of a uniform reduction of the bending stiffness due to initial local imperfections along the laced column's length. In reality smaller forces than P_1 are applied to the rest of the column but this assumption is convenient for computational reasons. As seen from Figure 5-2 the elastic nonlinear equilibrium paths of the column have the shape shown with blue dotted line which is also depicted in Figure 5-16. Considering also the inelastic curves of Figure 5-7, collapse occurs on the ascending part of the equilibrium path in case of local flange failure, corresponding to $r=1$ (Figure 5-16(a)), or on the limit point of the equilibrium path in case of global elastic failure, corresponding to $r<1$ (Figure 5-16(b)). Based on this remark, Eq. (5-33) can be solved iteratively for P , aiming at obtaining its value P_u corresponding to failure.

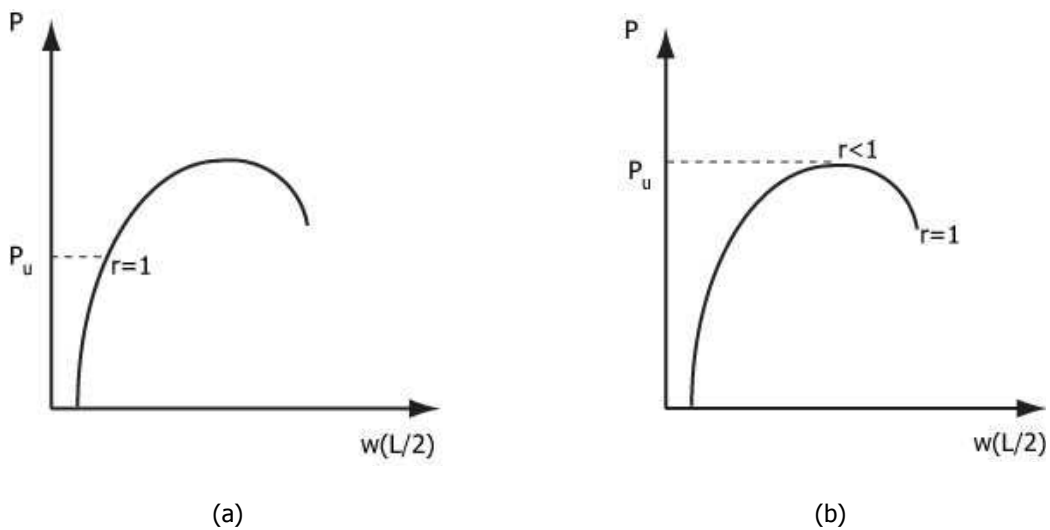


Figure 5-16: Graphical explanation of the proposed analytical approach with (a) local failure and (b) global failure

The proposed iterative procedure can be summarised as follows:

- Assume $r=1$ and solve Eq. (5-33) for P .
- Try a slightly smaller value of r (i.e. 0.95) and solve Eq. (5-33) for P .
- Compare the loads calculated in the previous two steps. If the load of the second step is smaller than the one of the first step, then the collapse load P_u has been reached at the first step and corresponds to local flange failure due to yielding and $r=1$ (Figure 5-16(a)). If not then go to the next step.

- Try smaller values of r (a procedure which can be optimized for faster convergence) until a maximum of P is reached. This maximum value is the collapse load P_u (Figure 5-16(b)). In such a case, the column failed globally without exceeding the yield stress at any cross-section in elevation.

The iterative procedure is shown graphically for the cases of global elastic and local elastoplastic failure in Figure 5-17. It can be seen that the computational effort required for the case of local elastoplastic failure is similar to EC3's, while for global elastic failure it is larger. The proposed method can be used for the prediction of the equilibrium paths (starting from zero applied axial load) until the collapse load. The equilibrium path can be evaluated by calculating the total deflection for different values of the axial load P with the use of Eq. (5-22).

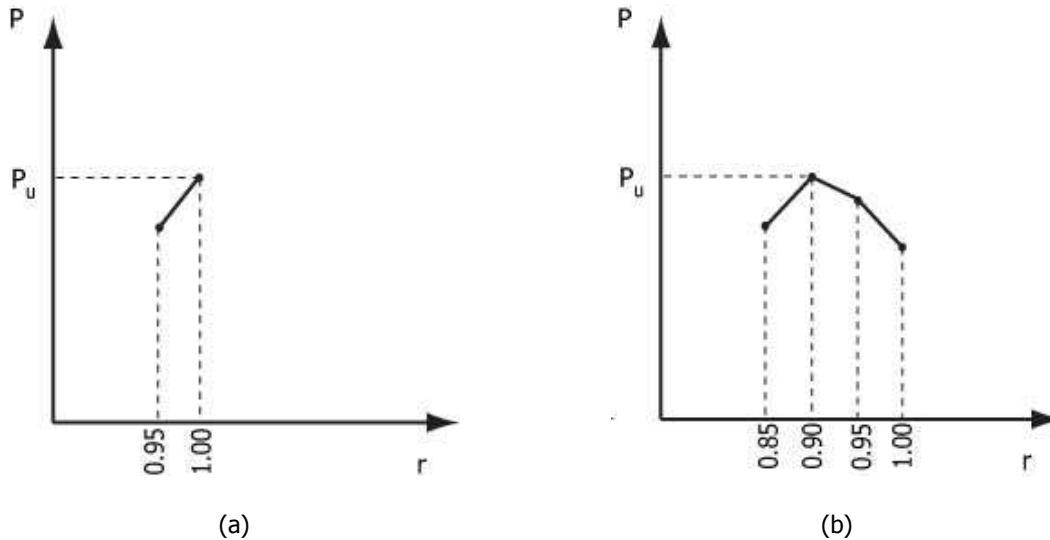


Figure 5-17: Graphical explanation of the proposed analytical approach with (a) local failure and (b) global failure

The proposed method is consistent with the concept of Eurocode 3 that the laced column will behave elastically until failure takes place, whether it is related to global elastic collapse or to local elastoplastic one.

5.5 PARAMETRIC STUDIES

The parametric studies that are presented in this section aim at investigating both the imperfection sensitivity of built-up columns and the effectiveness of EC3 and of the proposed method. The results are presented with the use of two types of diagrams. In the first one, the equilibrium paths used have the horizontal displacement (also called transverse displacement) plotted on the horizontal axis and the non-dimensional ratio P/P_L on the vertical one. In the second one, the graphs used have on the horizontal axis ratio x between global and local elastic critical buckling loads P_{cr}/P_L and on the vertical axis the ratio y of the collapse load P_u to the local buckling load P_L .

$$y = \frac{P_u}{P_L} \quad (5-34)$$

The solutions corresponding to a perfect structure and obtained with LBA [5-4] are shown in the graphs with a bilinear solid line. The results of the imperfect structures obtained with GMNIA performed with finite element software ADINA [5-4], EC3 [5-1] and the proposed method are also illustrated. Three separate parametric studies are presented, each achieving the variation of ratio x in a different way. The global and local imperfections are assumed to be equal to $L/500$ and $150\text{cm}/500=0.3\text{cm}$, respectively, in all cases. The results are presented in terms of equilibrium paths

and collapse loads. The equilibrium paths are obtained with the use of Eq. (5-9) and Eq. (5-22) for Eurocode 3 and the proposed method, respectively. The collapse loads are calculated with the use of Eq. (5-10) for Eurocode 3 and with the iterative procedure described for the proposed method previously.

5.5.1 First parametric study

In the first parametric study, simply-supported laced columns are examined for which the global buckling load and the squash load are chosen to be equal and remain constant. Built-up columns are generally characterised by large global buckling loads and in order to achieve equality between the two previously mentioned loads, unrealistic yield strength equal to 70kN/cm^2 is chosen. This unrealistic value is not expected to influence the parameters examined as they are based on non-dimensional factors. The local buckling load varies by changing the spacing of lacing joints (panel's length) from 71.05cm to 150cm . In this way the ratio x also varies. The geometrical and inertial characteristics of the columns used are summarised in Table 5-2.

Table 5-2: Geometrical and cross-section characteristics of the first parametric study

Length L (cm)	Panel's length a (cm)	Flanges' cross-sectional area A_{ch} (cm^2)	$I_{ch,z}$ (cm^4)	h_o (cm)
1350	varied	30	150	50

Failure in all cases is local elastoplastic and the proposed method converges to collapse loads for value of r equal to 1, despite the fact that high yield strength is used for the material. The equilibrium paths for each one of the cases examined are shown in Figure 5-18 to Figure 5-23. The equilibrium paths of the proposed procedure and EC3 stop at the collapse load they predict. In all cases a good comparison between the analytical procedures and the numerical results is observed.

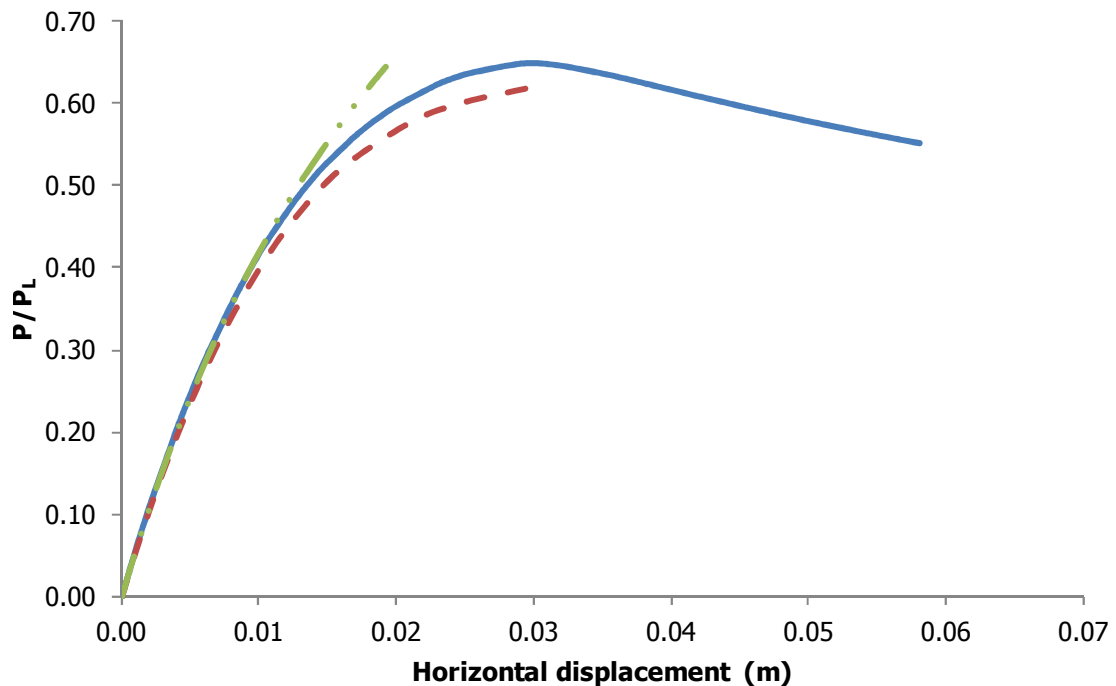


Figure 5-18: Equilibrium paths of the first parametric study's cases based on GMNIA (blue solid line), the proposed method (red densely dotted line) and EC3 (green sparsely dotted line) for $a=150\text{cm}$ ($x=1.55$)

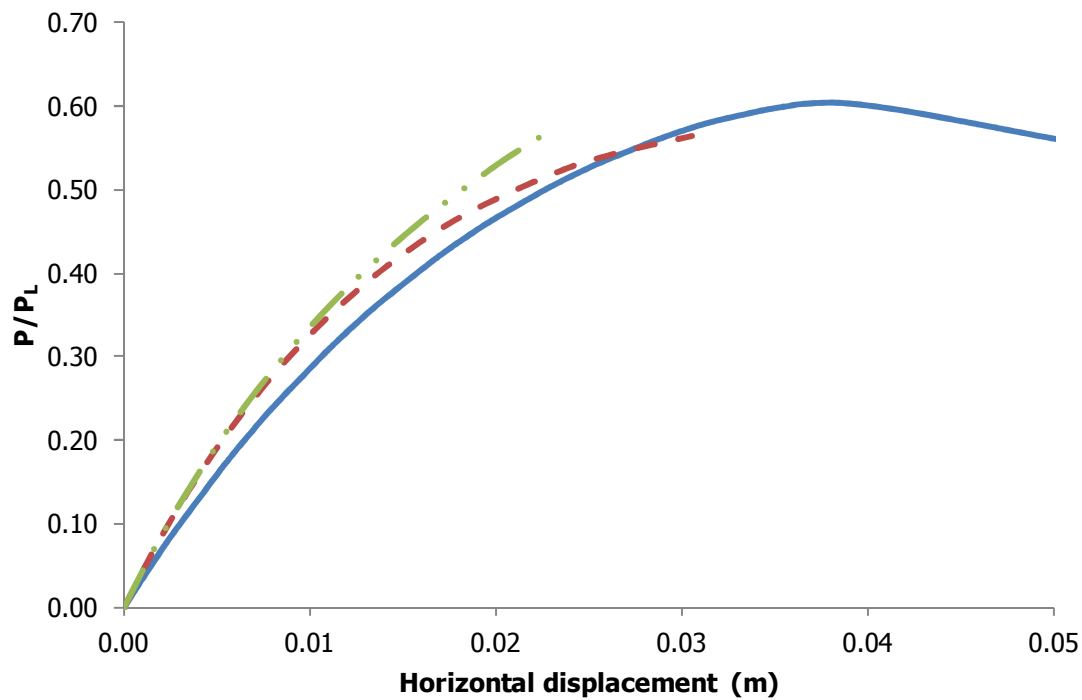


Figure 5-19: Equilibrium paths of the first parametric study's cases based on GMNIA (blue solid line), the proposed method (red densely dotted line) and EC3 (green sparsely dotted line) for $a=135\text{cm}$ ($x=1.26$)

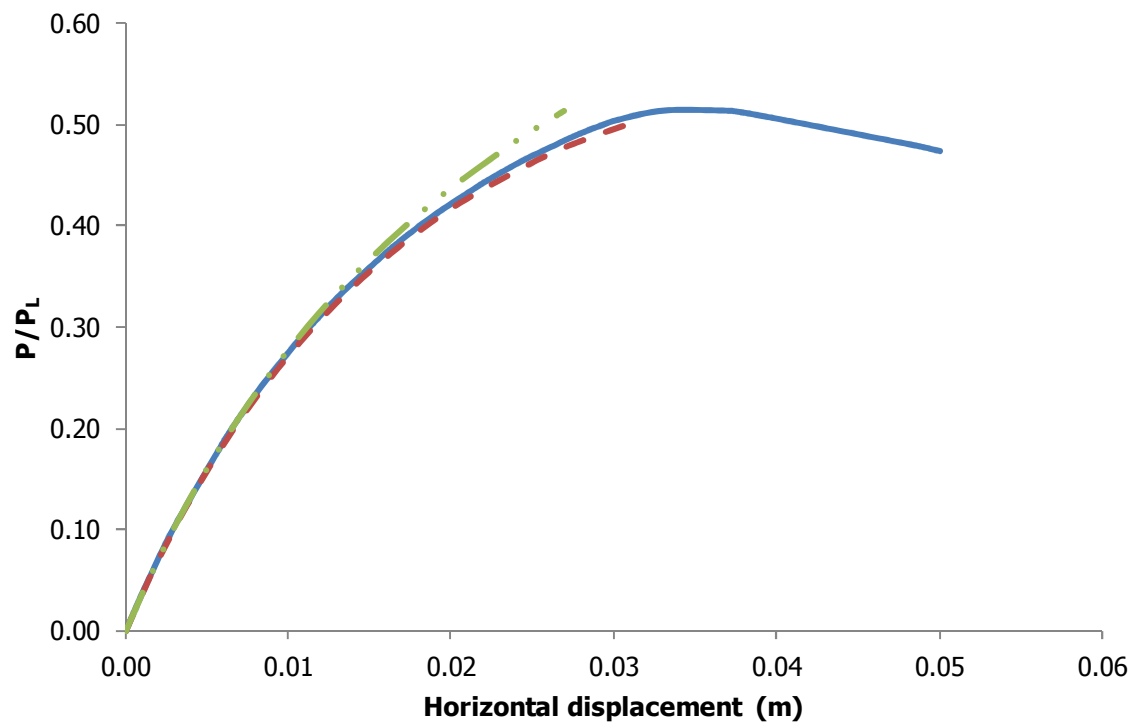


Figure 5-20: Equilibrium paths of the first parametric study's cases based on GMNIA (blue solid line), the proposed method (red densely dotted line) and EC3 (green sparsely dotted line) for $a=122.73\text{cm}$ ($x=1.04$)

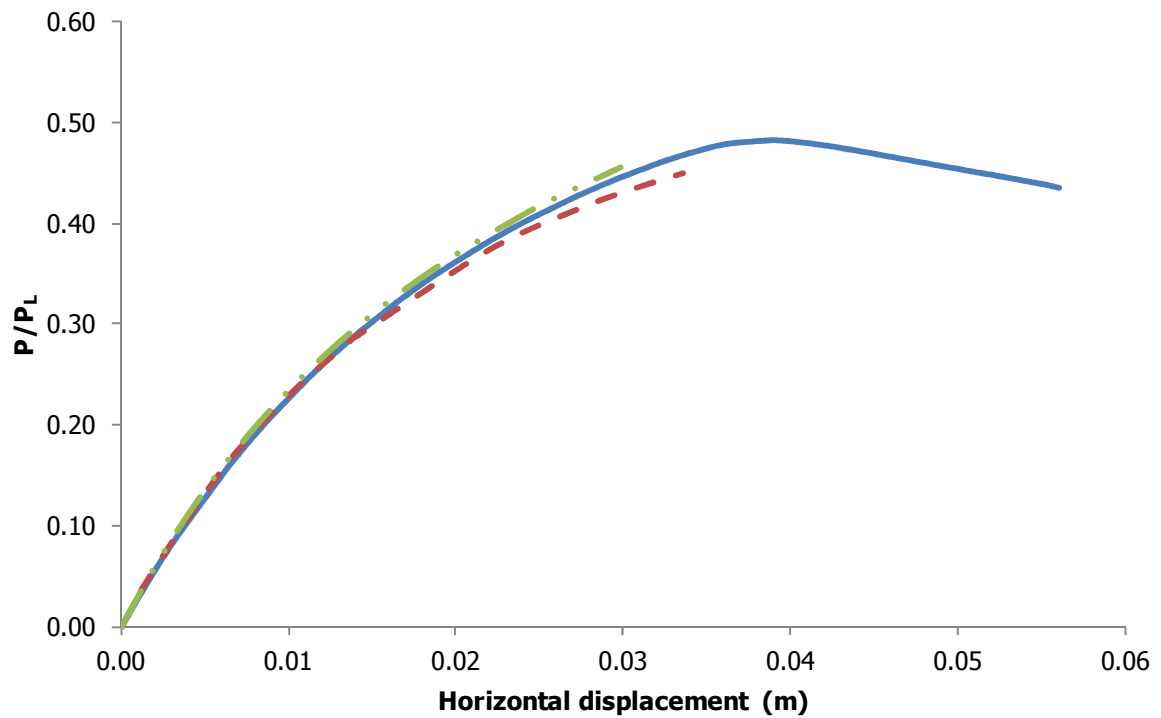


Figure 5-21: Equilibrium paths of the first parametric study's cases based on GMNIA (blue solid line), the proposed method (red densely dotted line) and EC3 (green sparsely dotted line) for $a=112.5\text{cm}$ ($x=0.88$)

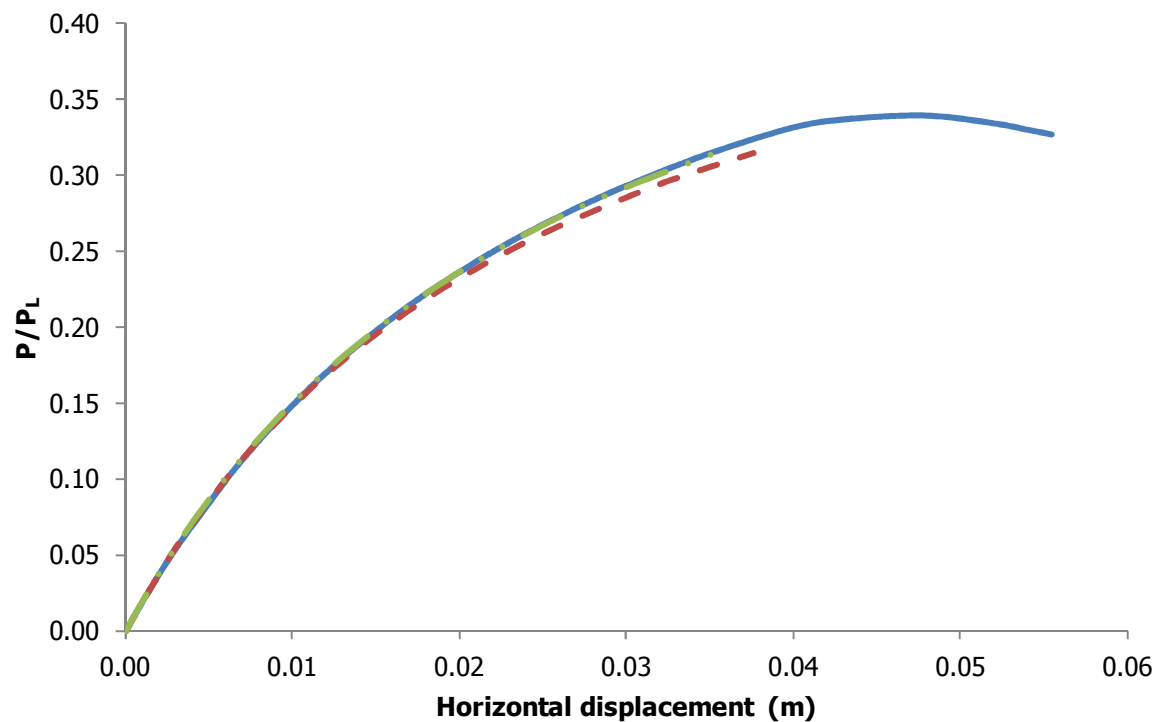


Figure 5-22: Equilibrium paths of the first parametric study's cases based on GMNIA (blue solid line), the proposed method (red densely dotted line) and EC3 (green sparsely dotted line) for $a=90\text{cm}$ ($x=0.56$)

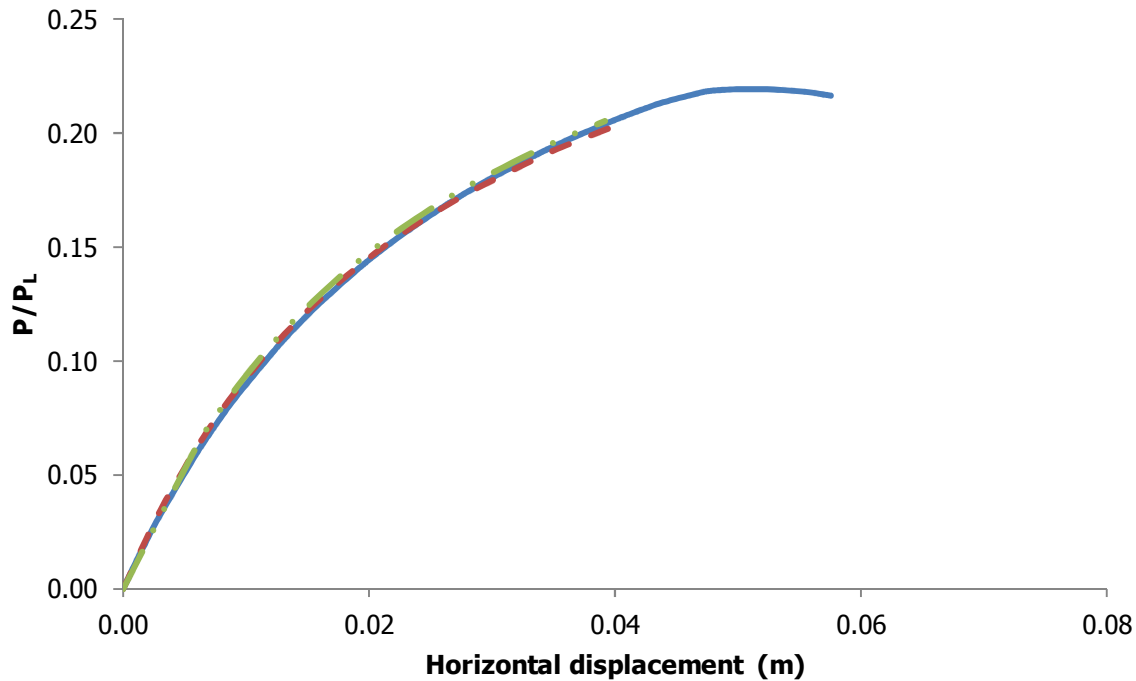


Figure 5-23: Equilibrium paths of the first parametric study's cases based on GMNIA (blue solid line), the proposed method (red densely dotted line) and EC3 (green sparsely dotted line) for $a=71.05\text{cm}$ ($x=0.35$)

The collapse loads obtained by the different analyses are shown in Figure 5-24 and in Table 5-3. The collapse loads obtained with both analytical methods, the one proposed in this work and the one included in EC3 specifications are in very good agreement with each other and with numerical results, with the largest difference being approximately 5.5%. The collapse loads predicted by the proposed method are slightly more conservative than EC3 results when compared with numerical results. The largest loss of capacity due to the existence of initial imperfections takes place when the stresses of local buckling, global buckling and yielding of the material all coincide, as initially observed by Svensson and Kragerup [5-8]. In this example the loss of capacity with respect to the perfect system due to the existence of imperfections for coinciding buckling and squash loads is equal to 46.1%.

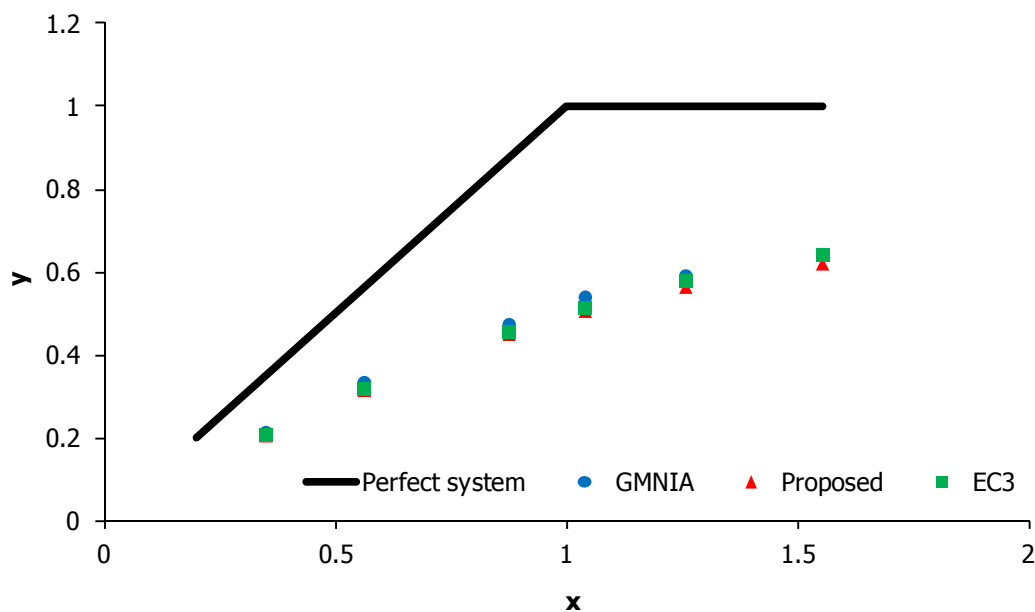


Figure 5-24: Imperfection sensitivity diagram for the first parametric study

Table 5-3: Values of y varying x for the first parametric study

x	GMNIA	Proposed method	EC3
0.35	0.21	0.20	0.21
0.56	0.33	0.31	0.32
0.88	0.47	0.45	0.45
1.04	0.54	0.51	0.51
1.26	0.59	0.56	0.58
1.55	0.64	0.62	0.64

5.5.2 Second parametric study

In the second parametric study, simply-supported laced columns are examined for which the local buckling load and the squash load are chosen to be equal and remain constant, while the overall buckling load varies by changing the lever arm between the flanges from 25cm to 50cm. In this way the ratio x varies, too. The yield strength of the steel used is taken equal to 44kN/cm². The geometrical and inertial characteristics of the laced columns of the second parametric study are summarised in Table 5-4.

Table 5-4: Geometrical and cross-section characteristics of the second parametric study

Length L (cm)	Panel's length a (cm)	Flanges' cross-sectional area A_{ch} (cm ²)	$I_{ch,z}$ (cm ⁴)	h_o (cm)
1350	150	30	142	varied

The equilibrium paths for each case separately are depicted in Figure 5-25 to Figure 5-30 as obtained numerically (blue solid line) and analytically with the proposed procedure (red densely dotted line) and EC3's provisions (green sparsely dotted line). The proposed method gives similar results for small values of applied axial load as the effect of local imperfections does not affect much the overall response. For large axial forces, the proposed method is more conservative and in some cases overestimates the effect of local imperfections as it considers a constant reduction of the bending stiffness along the column's length. EC3 provisions give very satisfactory results for both the elastic response and the collapse load of the columns. Both analytical procedures predict sufficiently the collapse load obtained with the numerical tools.

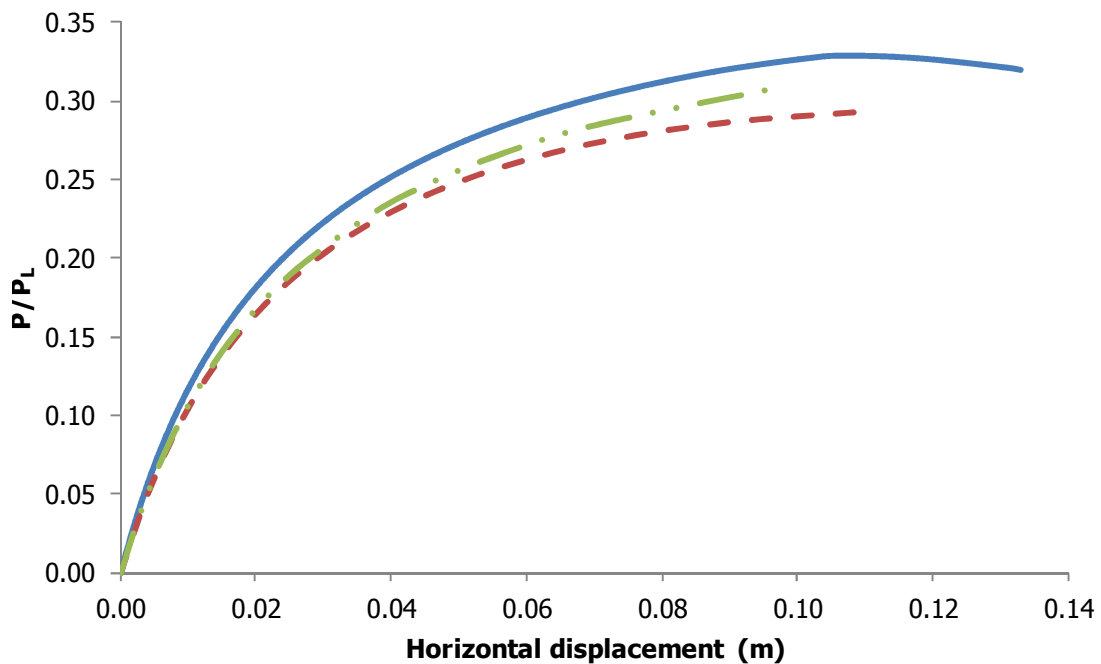


Figure 5-25: Equilibrium paths of the second parametric study's cases based on GMNIA (blue solid line), the proposed method (red densely dotted line) and EC3 (green sparsely dotted line) for $h_o=25$ cm ($x=0.42$)

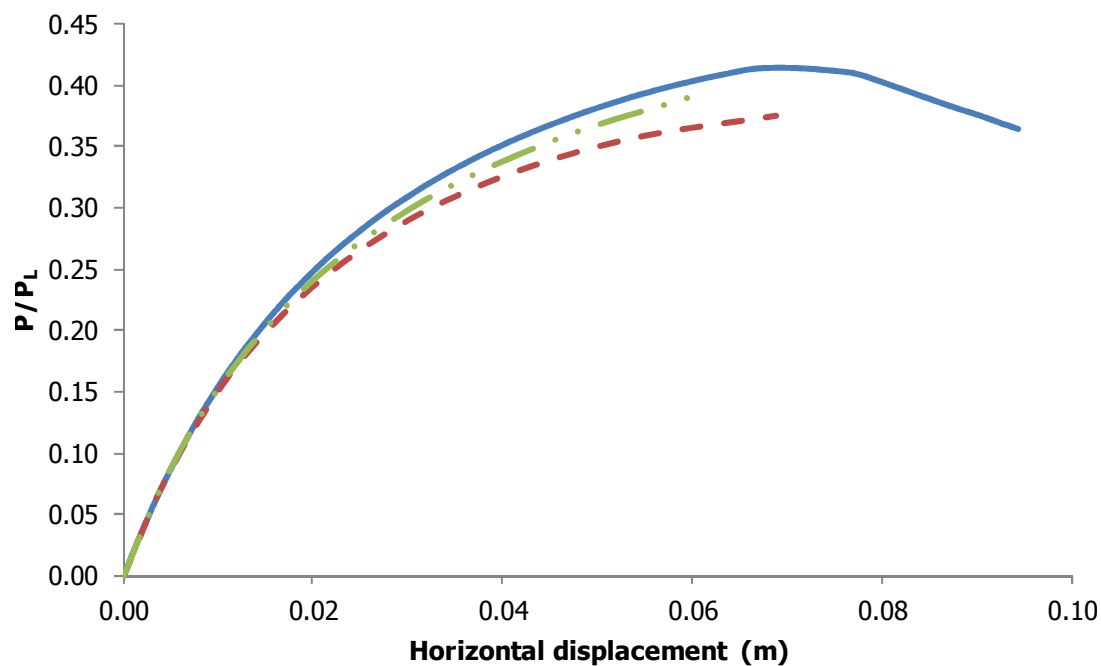


Figure 5-26: Equilibrium paths of the second parametric study's cases based on GMNIA (blue solid line), the proposed method (red densely dotted line) and EC3 (green sparsely dotted line) for $h_0=30\text{cm}$ ($x=0.58$)

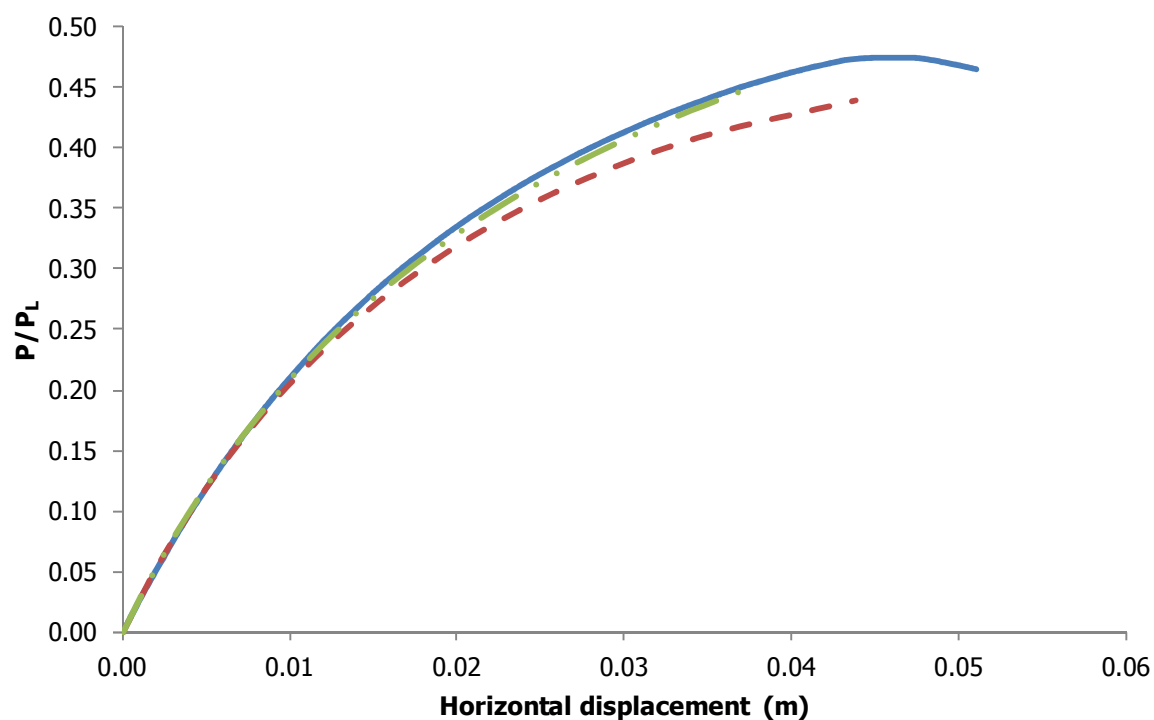


Figure 5-27: Equilibrium paths of the second parametric study's cases based on GMNIA (blue solid line), the proposed method (red densely dotted line) and EC3 (green sparsely dotted line) for $h_0=35\text{cm}$ ($x=0.79$)

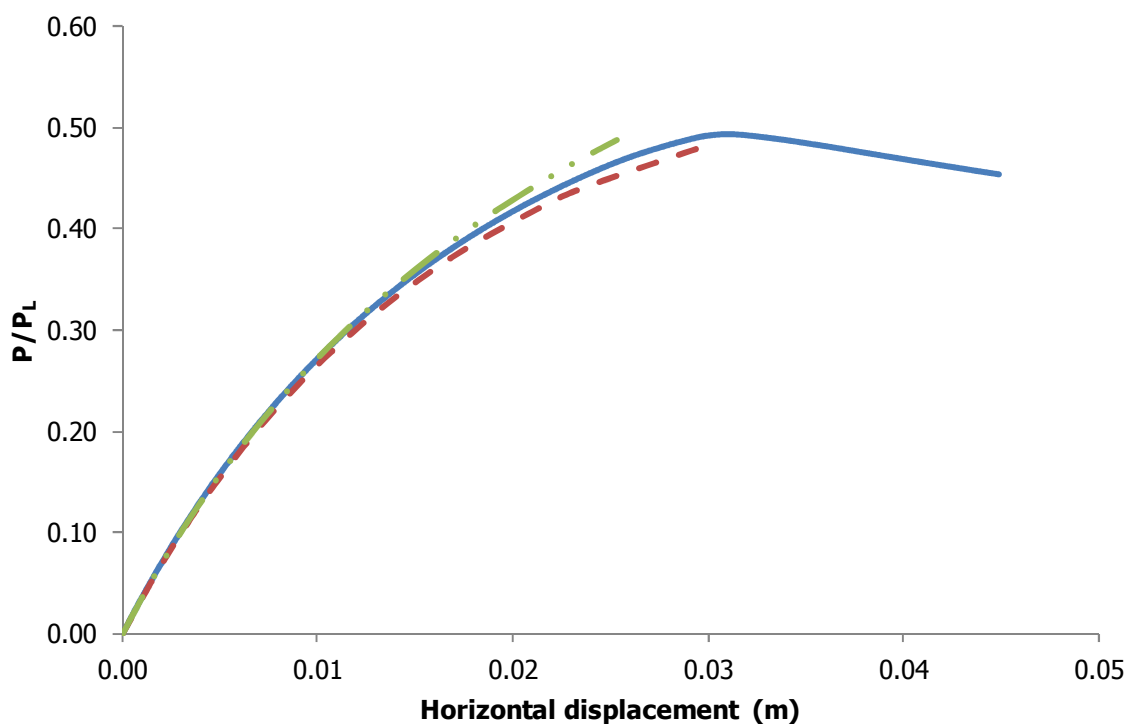


Figure 5-28: Equilibrium paths of the second parametric study's cases based on GMNIA (blue solid line), the proposed method (red densely dotted line) and EC3 (green sparsely dotted line) for $h_o=40\text{cm}$ ($x=1.02$)

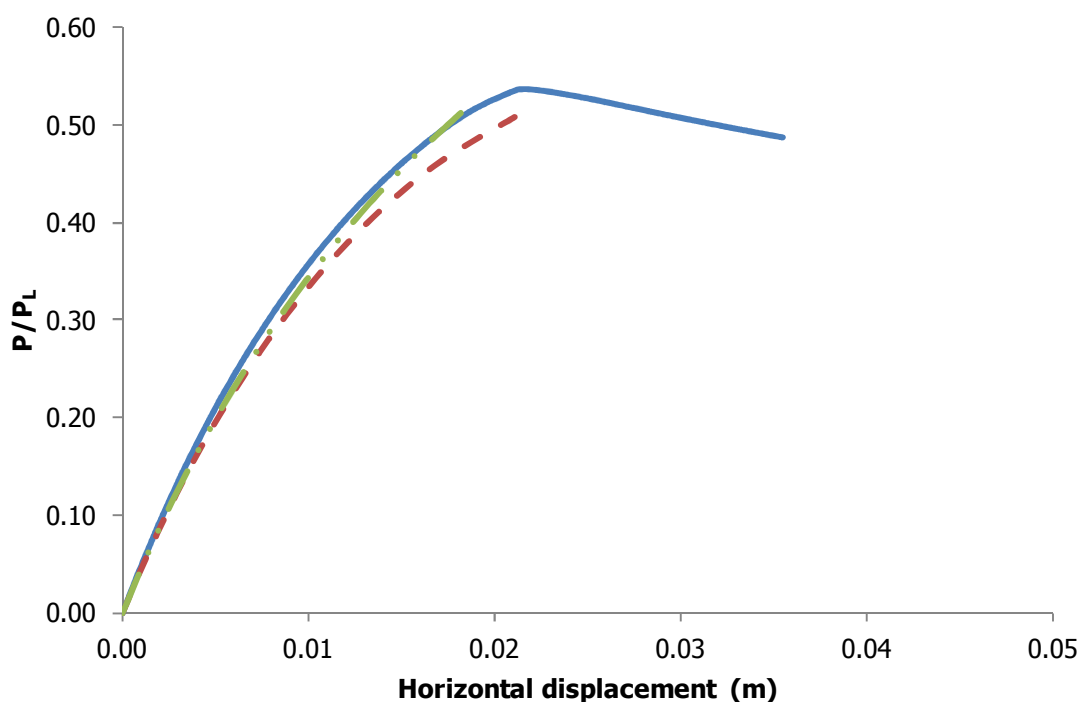


Figure 5-29: Equilibrium paths of the second parametric study's cases based on GMNIA (blue solid line), the proposed method (red densely dotted line) and EC3 (green sparsely dotted line) for $h_o=45\text{cm}$ ($x=1.29$)

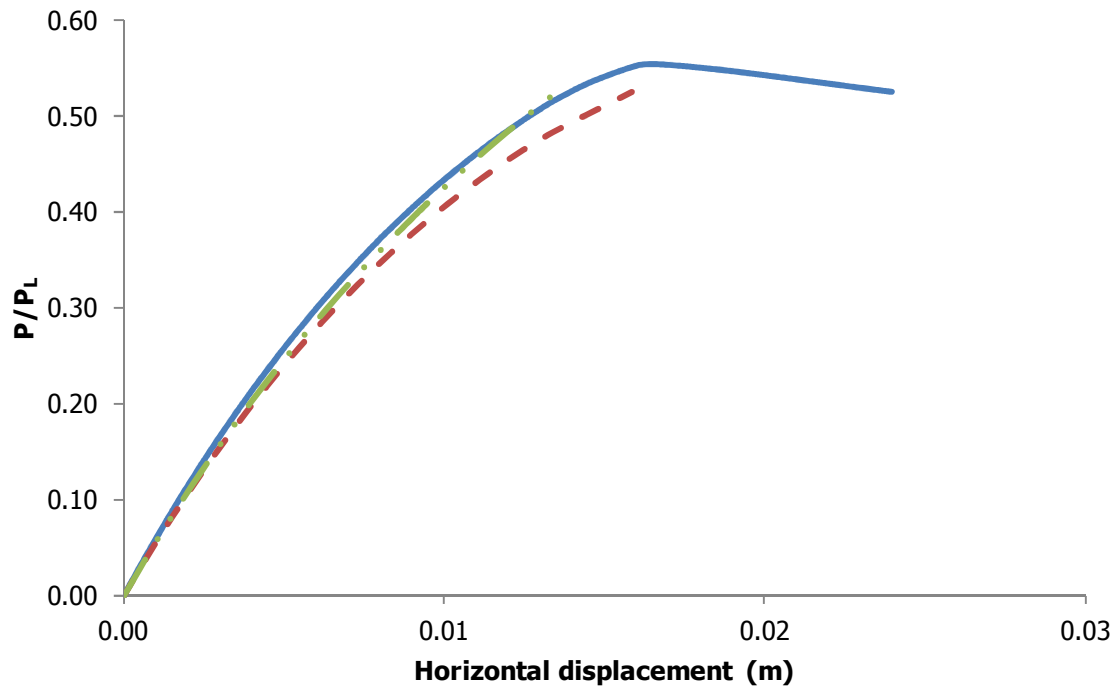


Figure 5-30: Equilibrium paths of the second parametric study's cases based on GMNIA (blue solid line), the proposed method (red densely dotted line) and EC3 (green sparsely dotted line) for $h_0=50\text{cm}$ ($\chi=1.59$)

The results obtained by the different analyses are shown in the sensitivity diagram of Figure 5-31. Failure in all cases is again elastoplastic. Similar conclusions as for the first parametric study are drawn, with the largest difference between alternative approaches being less than 5% and the largest imperfection sensitivity at $x=1$ being equal to 51.7%. A summary of the ratio γ for different ratios x as obtained with the different methods is presented in Table 5-5.

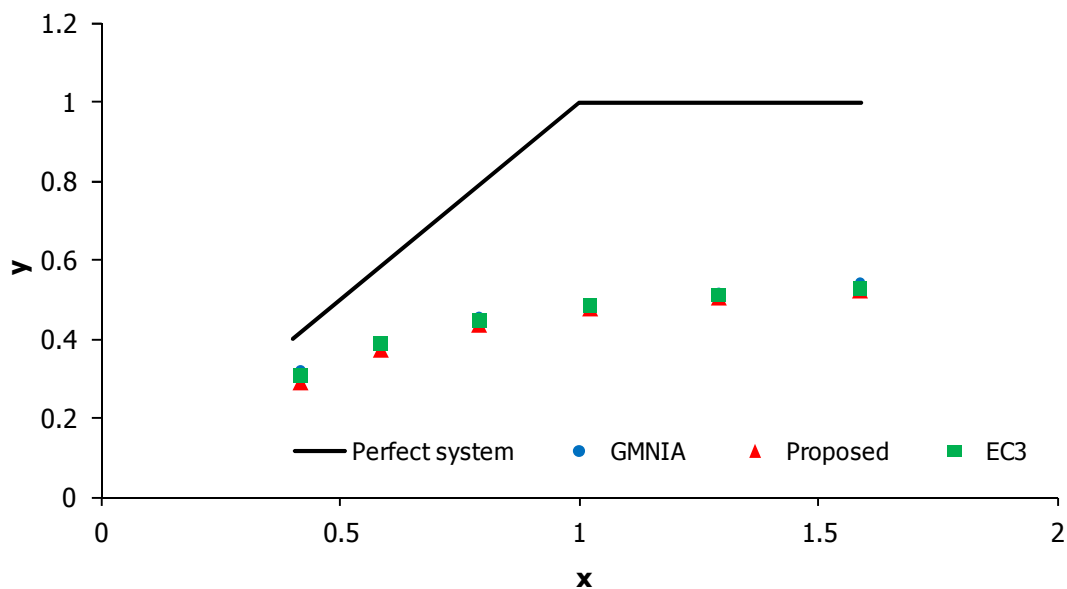


Figure 5-31: Imperfection sensitivity diagram for the second parametric study

Table 5-5: Values of y varying x for the second parametric study

x	GMNIA	Proposed method	EC3
0.42	0.32	0.29	0.31
0.58	0.39	0.37	0.39
0.79	0.46	0.44	0.45
1.02	0.48	0.48	0.49
1.29	0.52	0.51	0.51
1.59	0.55	0.52	0.53

5.5.3 Third parametric study

In the third parametric study, laced cantilevers are examined for which the local buckling load and squash load remain constant while the global buckling load varies by modifying the lever arm between the chords from 25cm to 50cm. In this way the ratio x varies, too. The yield strength of the steel used is taken equal to 42kN/cm^2 . The laced cantilevers' geometrical and inertial characteristics are summarised in Table 5-6.

Table 5-6: Geometrical and cross-section characteristics of the third parametric study

Length L (cm)	Panel's length a (cm)	Flanges' cross-sectional area A_{ch} (cm ²)	$I_{ch,z}$ (cm ⁴)	h_o (cm)
1350	150	13.2	27.7	varies

The equilibrium paths of the six cases of the third parametric study follow in Figure 5-32 to Figure 5-37. They are obtained with the use of GMNIA (blue solid line), the proposed procedure (red densely dotted line) and with the use of the concept of EC3 (green sparsely dotted line). It can be seen that the geometrical nonlinearity is important for all six cases according to GMNIA. All cases deal with global elastic failure except for $x \approx 2$, which is related to local elastoplastic failure, but at a load level close to the one corresponding to global failure. More pronounced differences between the three approaches are observed. The proposed procedure is capable of accurately capturing the nonlinear response and collapse load in contrast with EC3 that gives unsafe results and predicts much stiffer response for large values of the ratio x when compared with GMNIA.

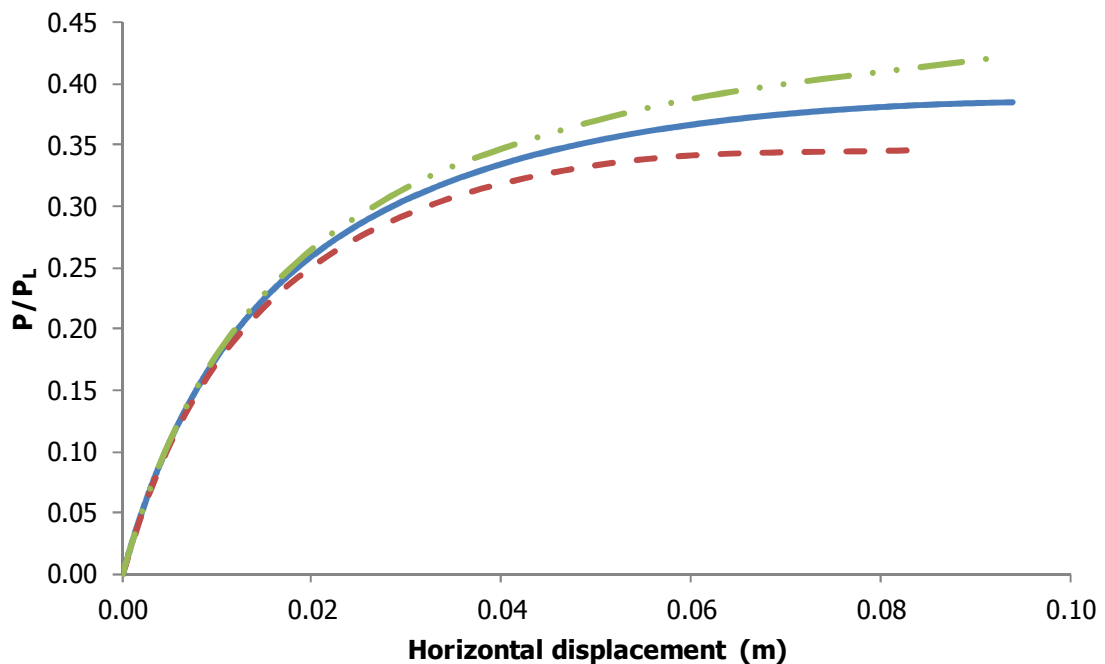


Figure 5-32: Equilibrium paths of the third parametric study's cases based on GMNIA (blue solid line), the proposed method (red densely dotted line) and EC3 (green sparsely dotted line) for $h_o=25\text{cm}$ ($x=0.51$)

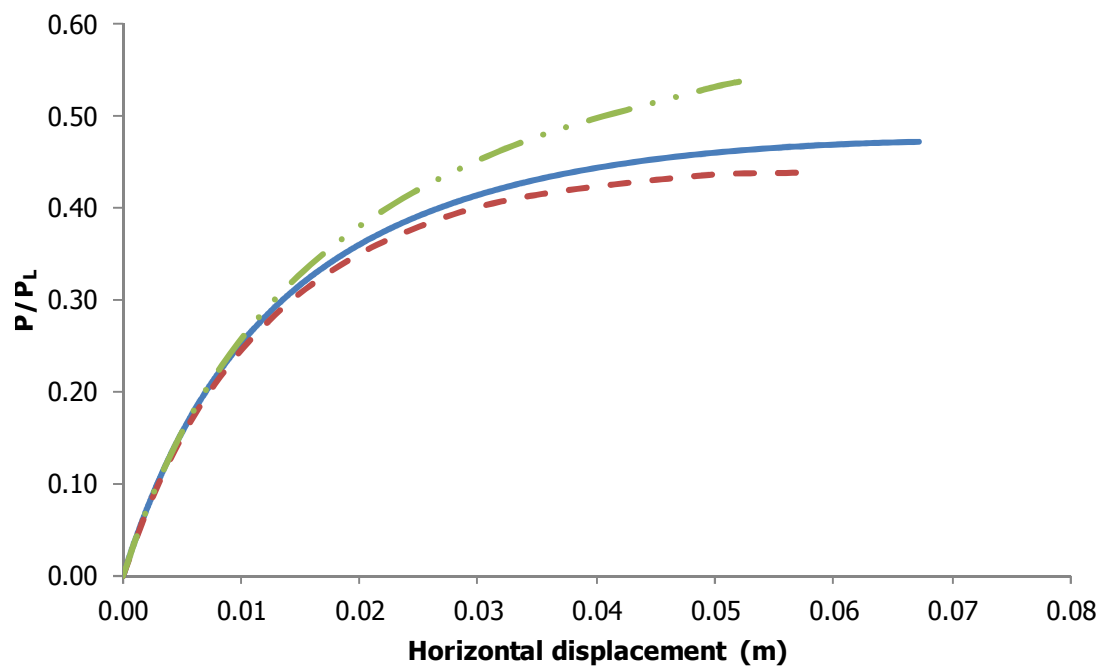


Figure 5-33: Equilibrium paths of the third parametric study's cases based on GMNIA (blue solid line), the proposed method (red densely dotted line) and EC3 (green sparsely dotted line) for $h_o=30\text{cm}$ ($x=0.74$)

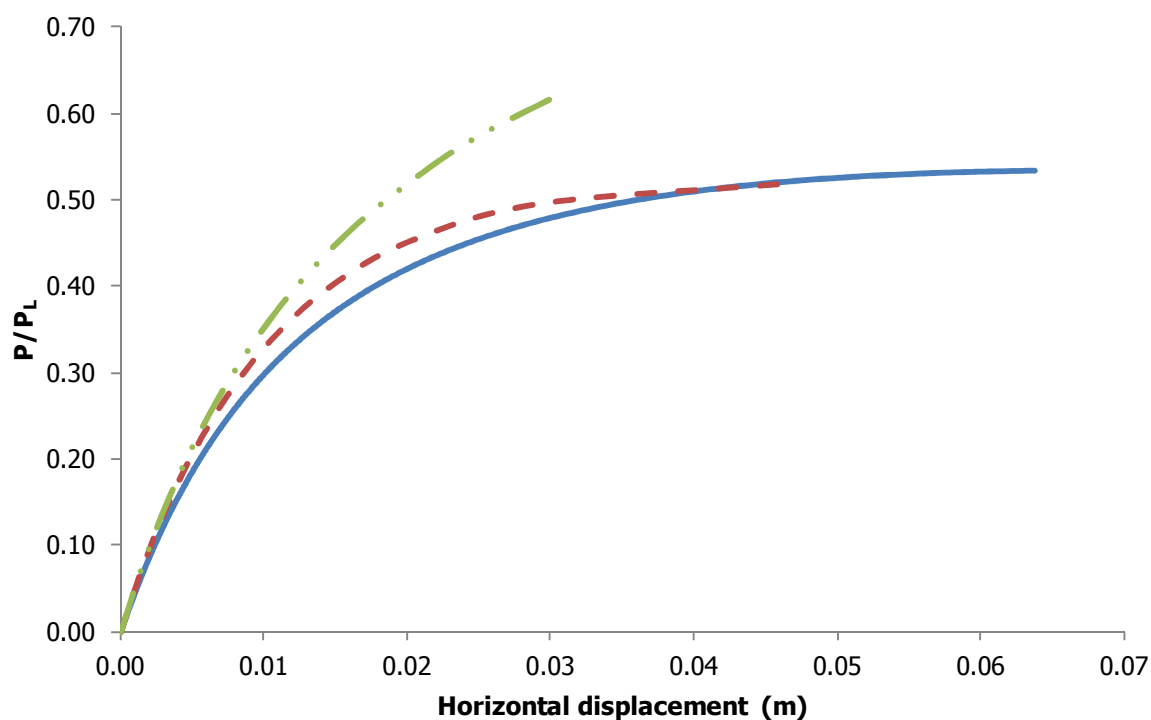


Figure 5-34: Equilibrium paths of the third parametric study's cases based on GMNIA (blue solid line), the proposed method (red densely dotted line) and EC3 (green sparsely dotted line) for $h_o=35\text{cm}$ ($x=1.00$)

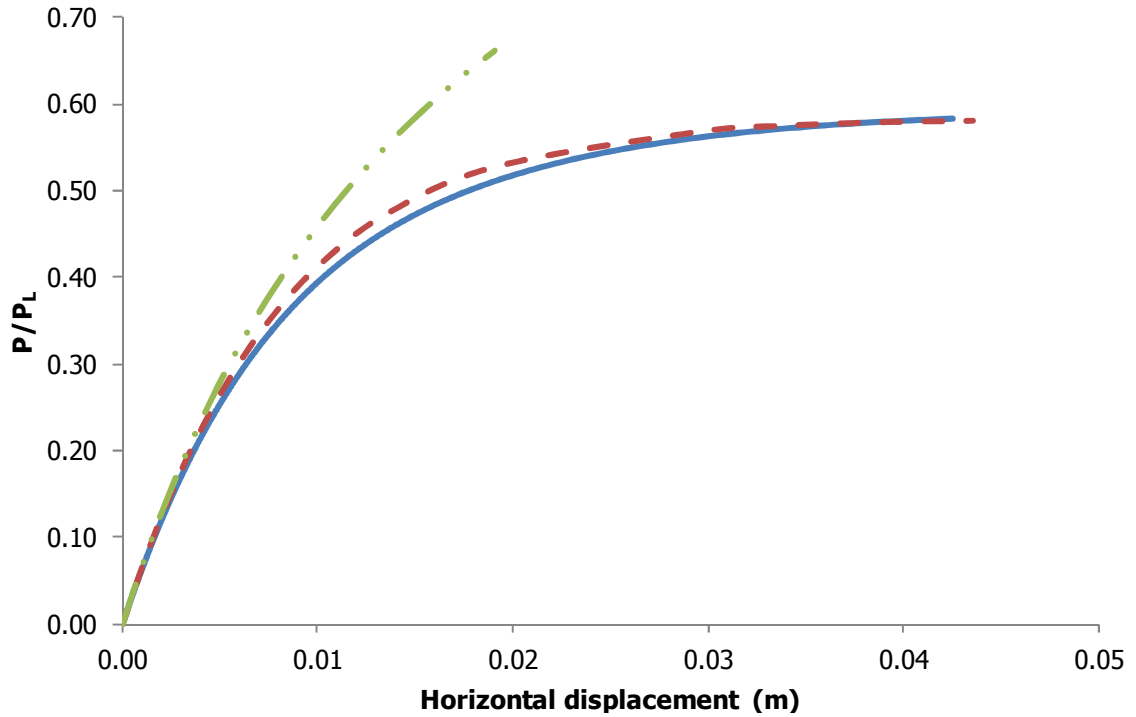


Figure 5-35: Equilibrium paths of the third parametric study's cases based on GMNIA (blue solid line), the proposed method (red densely dotted line) and EC3 (green sparsely dotted line) for $h_0=40\text{cm}$ ($x=1.30$)

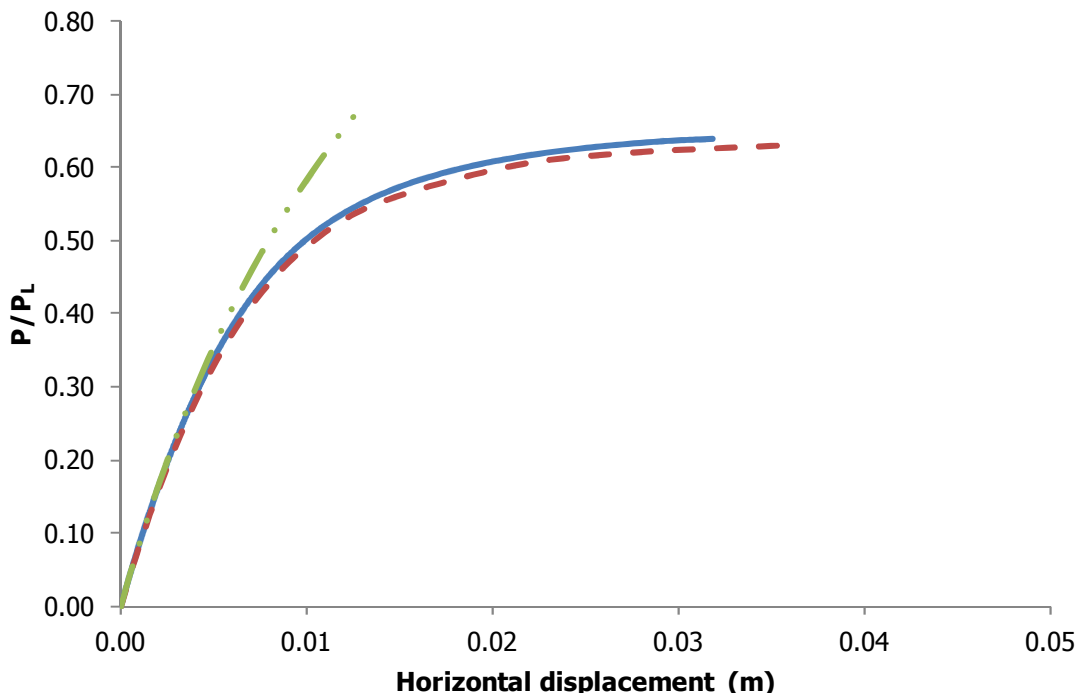


Figure 5-36: Equilibrium paths of the third parametric study's cases based on GMNIA (blue solid line), the proposed method (red densely dotted line) and EC3 (green sparsely dotted line) for $h_0=45\text{cm}$ ($x=1.64$)

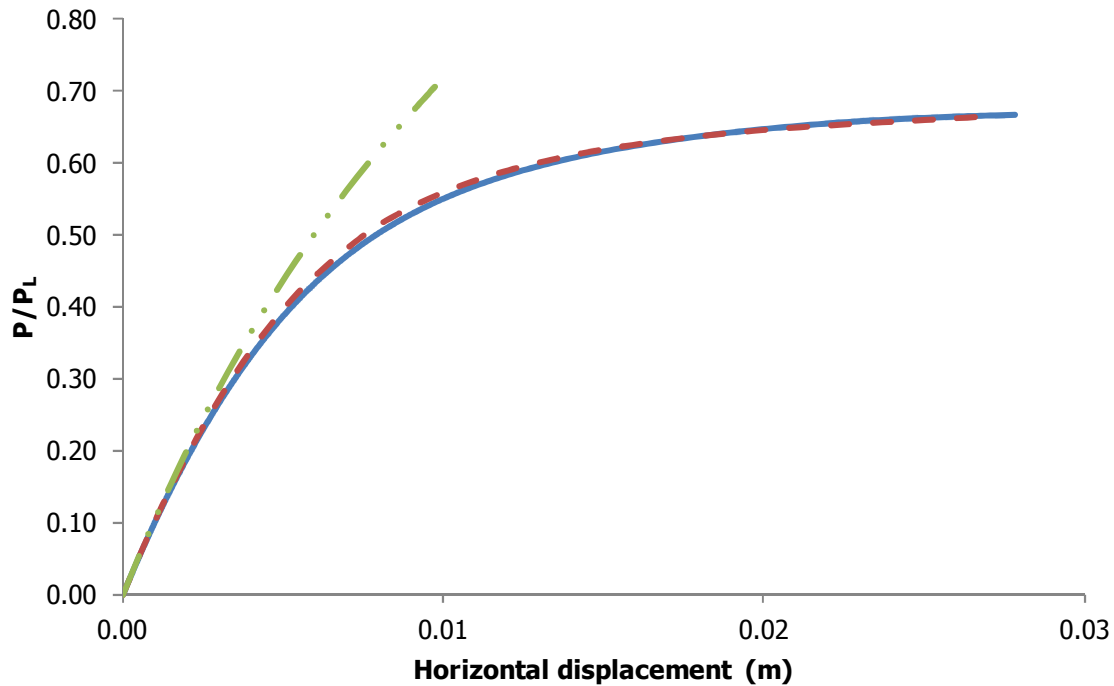


Figure 5-37: Equilibrium paths of the third parametric study's cases based on GMNIA (blue solid line), the proposed method (red densely dotted line) and EC3 (green sparsely dotted line) for $h_o=50\text{cm}$ ($x=2.01$)

The results are also summarised in Figure 5-38, in which the corresponding imperfection sensitivity diagram is depicted, and in Table 5-7. The proposed method approximates better the numerical results, being always on the safe side, while EC3 is on the unsafe side with the largest error being equal to 15%. The smallest difference between the three methods corresponds to the case of $x \approx 2$ and is in the order of 5%.

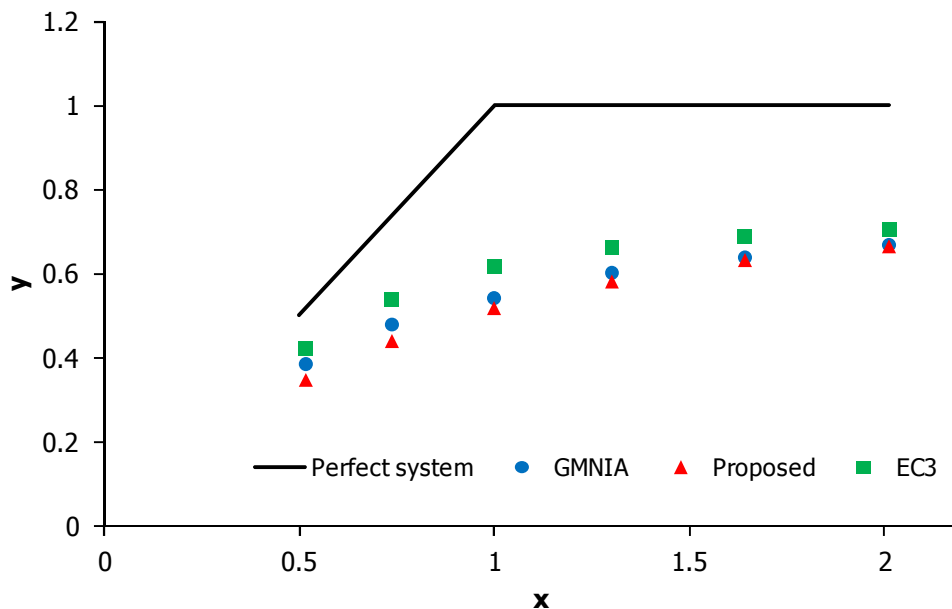


Figure 5-38: Imperfection sensitivity diagram for the third parametric study

Table 5-7: Values of y varying x for the third parametric study

x	GMNIA	Proposed method	EC3
0.51	0.39	0.35	0.42
0.74	0.48	0.44	0.54
1.00	0.54	0.52	0.62
1.30	0.60	0.58	0.66
1.64	0.64	0.63	0.69
2.01	0.67	0.67	0.71

5.6 CONCLUSIONS

In this chapter the behaviour of perfect and imperfect laced built-up columns was investigated from a numerical and analytical point of view. GNI and GMNI analyses were used for observing that the relation of the three types of failure of perfect laced members associated with the global buckling load, local buckling load and squash load between each other affects the overall response and collapse load. EC3 accounts for all three types of failure but does not consider the effect of local imperfections on the global response. For this reason a modified procedure was proposed that incorporates the initial imperfections in the bending stiffness of the laced column. The proposed method requires an iterative procedure for its solution.

Based on the three parametric studies presented, it was concluded that the proposed method and EC3 give similar results when local elastoplastic failure governs. This is not the case when elastic global failure is the critical one, in which case the proposed method provides a better approximation of the "exact" numerical results, while EC3 is consistently on the unsafe side. This is explained by considering that in the case of elastoplastic failure overall deformations are rather small, thus the increase of global deformations due to the interaction between global and local imperfections is not important and therefore in such cases the proposed method is not significantly different from EC3.

It was also pointed out that when the type of failure is local, both the proposed method and EC3 require comparable computational effort and provide results that are close to the numerical ones. In the case of elastic overall failure the proposed method requires some iterations, thus more computational effort than EC3, but is expected to yield more accurate and safe results in comparison to EC3 approach. The error of EC3 on the unsafe side reaches in some cases a magnitude of 15%. The appearance of elastic overall failure in general requires axially loaded slender columns at both a global and local level constructed with the use of a material of relatively high yield strength. In most practical built-up members that are also transversely loaded (reducing in this way the importance of the geometrical nonlinearity), local elastoplastic failure is expected to govern and the philosophy used by EC3 is sufficient.

Finally, more general conclusions of the numerical and analytical procedures described in this chapter are that a laced built-up column can be sufficiently modelled as Timoshenko member with equivalent bending and shear rigidities and be assumed that behaves elastically until failure either it is related to global elastic collapse or local elastoplastic one. Therefore, it is important that a straight-forward method for their elastic analysis is proposed and this is the main objective of the next two chapters.

5.7 REFERENCES

- [5-1] Eurocode 3: Design of Steel Structures. Part 1.1: General structural rules. CEN-European Committee for Standardisation, Brussels, EN1993-1-1, 2005
- [5-2] Riks, E. "The application of Newton's method to the problem of elastic stability", Journal of Applied Mechanics, Vol. 39, pp. 1060-1065, 1972

- [5-3] Riks, E. "An incremental approach to the solution of snapping and buckling problems", *International Journal of Solids and Structures*, Vol. 15, pp. 529-551, 1979
- [5-4] ADINA System 8.5, Release Notes. ADINA R & D Inc., 71 Elton Avenue, Watertown, MA 02472; USA. 2008
- [5-5] Van der Neut, A. "The interaction of local buckling and column failure of thin-walled compression members", *Proceedings of the 12th International Congress of Applied Mechanics*, Stanford University, United States, August 26-31, 1968
- [5-6] Koiter, W.T., Kuiken, G.D.C. "The interaction between local buckling and overall buckling on the behaviour of built-up columns", *Laboratory of Engineering Mechanics*, Report No. 447, Delft, 1971
- [5-7] Koiter W.T. "Over de stabiliteit van het elastische evenwicht", *Doctoral thesis*, T.U. Delft, The Netherlands, 1945
- [5-8] Svensson, S.E., Kragerup, J. "Collapse loads of laced column", *Journal of Structural Division*, American Society of Civil Engineers, Vol. 108(ST6), pp. 1367-84, 1982
- [5-9] Young, T. "A course of lectures on Natural Philosophy and the Mechanical arts" Reprint of 1807 edition, Thoemmes Press, Bristol, 2002
- [5-10] Thompson, J.M.T., Hunt, G.W. "A General Theory of Elastic Stability", John Wiley, London, 1973

6 ELASTIC BUCKLING LOAD OF MULTI-STORY FRAMES CONSISTING OF TIMOSHENKO MEMBERS

6.1 INTRODUCTION

In Chapter 5, it was shown that a laced built-up column can be modelled as an equivalent Timoshenko member, and therefore, reliable calculation of its elastic critical buckling load is crucial. In this chapter the elastic buckling loads of Timoshenko members with arbitrary supports at their ends, and those of multi-story frames consisting of Timoshenko members, will be presented. The main objective of this effort is to expand the method proposed by Gantes and Mageirou [6-1], [6-2] for the calculation of the elastic buckling load of multi-story frames with rigid or semi-rigid connections for the case that columns and/or beams are susceptible to shear deformations. It is worth mentioning here that elastic critical buckling loads are used by all modern steel design codes, including Eurocode 3 [6-3], in order to calculate slenderness ratios, which are then inserted into buckling curves for obtaining the member's ultimate strength, thus also taking indirectly into account the influence of imperfections, residual stresses and material nonlinearity. Therefore, reliable calculation of elastic buckling loads is not merely of academic interest, but also has significant practical value. It is noted that in many of the examples presented by Gantes and Mageirou codes' specifications gave over conservative results (see for instance example 3 of reference [6-1]). As elastic buckling loads depend heavily on boundary conditions, namely the relative transverse displacements of the two ends and the rotational restrictions at the two ends, the task of their correct calculation consists of two different parts, which are both addressed: (i) how to obtain the critical buckling load of a shear-weak member in compression for any set of given boundary conditions, and (ii) how to obtain rotational stiffnesses for taking into account the effect of other shear-weak members, converging at the end nodes of the member in question, using equivalent elastic springs.

It can be concluded from Figure 6-1 that the overall stability of the frame can be examined by focusing on the behaviour of a critical column or a number of critical columns. For this reason the effect of members converging at the top and bottom node of the column in question is taken into account by replacing them with equivalent rotational springs. The ability of the column to translate horizontally depends on the eventual presence of lateral bracing and this is incorporated in the model

by using a translational spring at the top node of the column. This is shown schematically in Figure 6-1, where the buckling strength of column TB of the frame in Figure 6-1(a) is investigated by means of the simplified model of the individual column in Figure 6-1(b). The restriction provided by the other members of the frame to the rotations of nodes T and B is modelled via rotational springs with constants c_t and c_b respectively, while the resistance provided by the bracing system to relative transverse translation of nodes T and B is modelled via the translational spring with constant c_{br} . The stiffness of the bottom and top rotational springs is obtained by summing up the contributions of members converging at the bottom and top ends, respectively:

$$c_b = \sum_i c_{b,i}, \quad c_t = \sum_j c_{t,j} \quad (6-1)$$

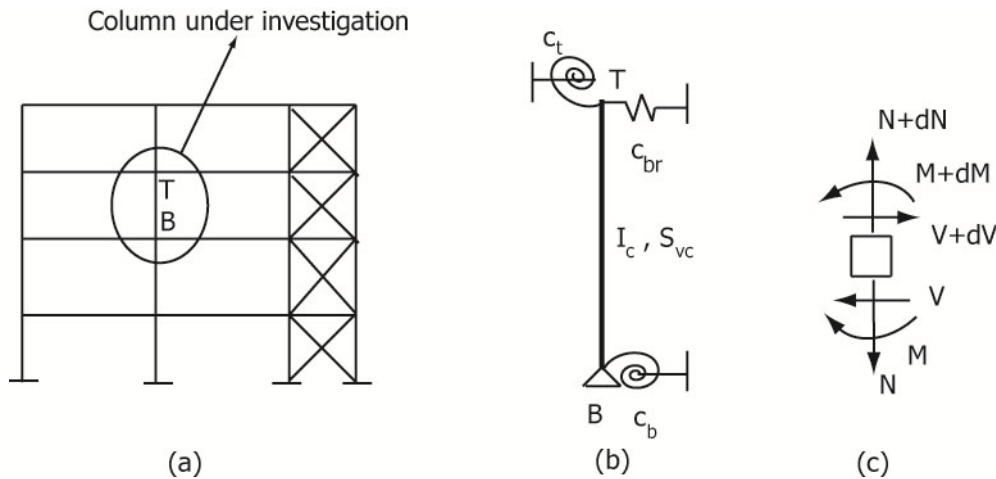


Figure 6-1: (a) Column TB as a part of a frame, (b) structural model of column TB and (c) sign convention (Gantes and Mageirou [6-1])

Individual member stiffnesses are obtained by making use of slope-deflection equations. Such equations were initially introduced by Maney [6-4] for Euler-Bernoulli members without axial force, and express the member's end moments in terms of rotation angles. These equations are given, including the presence of axial force, in a familiar form by Salmon and Johnson [6-5] and many other structural textbooks. They were expanded for the case of Timoshenko beam-columns by Absi [6-6]. Lin et al. [6-7] derived slope-deflections equations for built-up members with end-rigid plates at their ends. Aristizabal-Ochoa [6-8], making use of Haringx's approach, proposed slope-deflection equations for Timoshenko members with semi-rigid connections in a similar way to the one presented next.

In order to achieve the objective of the present chapter, a 3x3 stability matrix is derived for a shear-weak member with arbitrary boundary conditions, from which three stability equations for members belonging to unbraced, partially braced and braced frames are obtained. Indicative graphs containing the solutions of the stability equations for braced, partially braced and unbraced frames are provided. Afterwards, slope-deflection equations for shear-weak members with semi-rigid connections are derived based on Engesser's method and used for the calculation of a complete set of rotational stiffness coefficients, which are then used for the replacement of members converging at the bottom and top ends of the column in question by equivalent springs. All possible rotational and translational boundary conditions at the far end of these members, as well as the eventual presence of axial force, are considered. Finally, five examples are presented for verification of the proposed approach, two of three-story frames with rigid and semi-rigid beam to column connections, one of a three-story frame with asymmetrically applied load, one of a partially braced frame and one of a sway frame consisting of built-up members.

6.2 ELASTIC BUCKLING LOAD OF TIMOSHENKO COLUMNS

6.2.1 General stability matrix

The differential equations that control the buckling problem of a simply-supported shear-weak column with bending and shear rigidity EI and S_v , respectively, that is loaded axially by a compressive force P were presented in Chapter 2 and are repeated here briefly for easy reference. If the column buckles, due to its deformed shape, second order moments develop along its length. If the differentiation with respect to the longitudinal axis is denoted as prime, the total rotation of a cross-section, which is attributed to both bending and shear deformation (ψ and γ , respectively), is stated below:

$$w' = \psi + \gamma \quad (6-2)$$

According to Timoshenko beam-theory, the differential equations for a simply-supported beam refer to both total and bending rotations as follows:

$$w'' \left(1 - \frac{P}{S_v} \right) + \frac{Pw}{EI} = 0 \quad (6-3)$$

$$\psi'' \left(1 - \frac{P}{S_v} \right) + \frac{P\psi}{EI} = 0 \quad (6-4)$$

Now, consider the simplified model of the structural member shown in Figure 6-2. At each end a translational and a rotational spring resist lateral deflection and bending rotation, respectively. The member has length L and is characterised by bending and shear rigidities EI and S_v , respectively. The sensitivity of the member to shear deformations can be identified by calculating its dimensionless shear parameter μ :

$$\mu = \frac{EI}{S_v L^2} \quad (6-5)$$

The effect of shear deformations is smaller for smaller values of μ . It can be seen that apart from reduced shear rigidity and/or small length, a column can be significantly affected by shear deformations if the bending rigidity is relatively large making bending deformations small and of comparable magnitude with those due to shear.

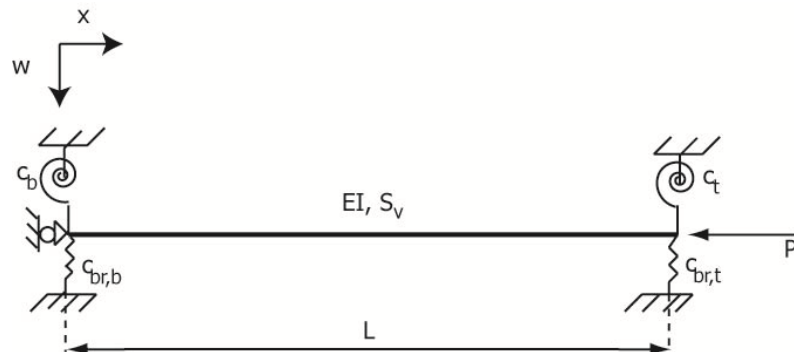


Figure 6-2: Shear-weak member with rotational and translational springs at each end, subjected to axial compressive load

By differentiating Eqs. (6-3) and (6-4) twice, the equations for members with arbitrary boundary conditions are obtained, such as the one shown in Figure 6-2. Thus, Eqs. (6-6) and (6-7), that were initially derived by Banerjee and Williams [6-9], are obtained:

$$w'''' \left(1 - \frac{P}{S_v} \right) + \frac{Pw''}{EI} = 0 \quad (6-6)$$

$$\psi'''' \left(1 - \frac{P}{S_v} \right) + \frac{P\psi''}{EI} = 0 \quad (6-7)$$

The solutions of fourth order differential Eqs. (6-6) and (6-7) are:

$$w(x) = A_1 \sin(\alpha x) + A_2 \cos(\alpha x) + A_3 x + A_4 \quad (6-8)$$

$$\psi(x) = (-\alpha\beta) A_2 \sin(\alpha x) + (\alpha\beta) A_1 \cos(\alpha x) + A_3 \quad (6-9)$$

where

$$\alpha^2 = \frac{P}{EI\beta} \quad (6-10)$$

$$\beta = \left(1 - \frac{P}{S_v} \right) \quad (6-11)$$

or

$$\beta = \frac{1}{1 + (\alpha L)^2 \mu} \quad (6-12)$$

The integration constants of the solution of the differential Eq. (6-7) are expressed in terms of those of Eq. (6-8) by making use of Eq. (6-2).

The boundary conditions can be introduced by considering the shear force perpendicular to the undeformed axis V and moment M at each end and by making use of Eqs. (6-8) and (6-9). The equations for the shear force V and bending moment M were presented for the simply-supported case in Chapter 2 and are also applicable for the case of arbitrary boundary supports:

$$V = -EI\psi'' - Pw' = Q - Pw' \quad (6-13)$$

and

$$M(x) = -EI\psi'(x) \quad (6-14)$$

Thus, four equations related to internal shear force V and bending moment M in terms of the unknowns A_i appear, two for each end:

$$V(0) = Q(0) - Pw'(0) = -EI\psi''(0) - Pw'(0) \quad (6-15)$$

$$V(L) = Q(L) - Pw'(L) = -EI\psi''(L) - Pw'(L) \quad (6-16)$$

$$M(0) = -EI\psi'(0) \quad (6-17)$$

$$M(L) = -EI\psi'(L) \quad (6-18)$$

The corresponding external expressions for shear force V and bending moment M are:

$$V(0) = c_{br,b} w(0) \quad (6-19)$$

$$V(L) = -c_{br,t} w(L) \quad (6-20)$$

$$M(0) = -c_b \psi(0) \quad (6-21)$$

$$M(L) = c_t \psi(L) \quad (6-22)$$

By equating the expressions of internal and external moments and shear forces four equations arise that are expressed in terms of the four integration constants. These equations can be written in a 4x4 matrix form. By adding the ones that are obtained from equating the shear forces, constant A_4 is eliminated, and the matrix's dimensions are reduced by one. A non-trivial solution is obtained only if the determinant of the stability matrix is equal to zero as shown in Eq. (6-23):

$$\det \begin{bmatrix} a_{cr} \beta_{cr} & \frac{a_{cr}^2 \beta_{cr}}{c_b^*} & 1 \\ -\frac{a_{cr}^2 \beta_{cr} \sin(a_{cr} L)}{c_t^*} + a_{cr} \beta_{cr} \cos(a_{cr} L) & -\frac{a_{cr}^2 \beta_{cr} \cos(a_{cr} L)}{c_t^*} - a_{cr} \beta_{cr} \sin(a_{cr} L) & 1 \\ -\sin(a_{cr} L) & 1 - \cos(a_{cr} L) & \frac{a_{cr}^2 \beta_{cr}}{c_{br,t}^*} + \frac{a_{cr}^2 \beta_{cr}}{c_{br,b}^*} - L \end{bmatrix} = 0 \quad (6-23)$$

where $c_i^* = c_i/EI$.

In that case the critical values of α and β are obtained as α_{cr} and β_{cr} , respectively. This yields a so-called stability equation, from which the elastic critical load of the beam-column P_{cr} can be calculated.

6.2.2 Buckling equations

The structural model of Figure 6-2 can be easily transformed to the one of Figure 6-1(b) if the translational spring at the bottom node is assigned infinite stiffness. In order to obtain non-dimensional stability equations in which the rotational springs' stiffnesses vary from zero (fixed support) to unity (pinned support), the distribution factors z_t and z_b that were introduced by Gantes and Mageirou [6-1], [6-2] are used. These are obtained by non-dimensionalisation of end rotational stiffnesses c_b and c_t with respect to the column's flexural stiffness c_c :

$$z_b = \frac{c_c}{c_c + c_b}, \quad z_t = \frac{c_c}{c_c + c_t} \quad (6-24)$$

where

$$c_c = \frac{4EI_c}{L} \quad (6-25)$$

The elastic buckling load is given in terms of parameter $\phi_{cr} = a_{cr}L$ by the following formula:

$$P_{cr} = \frac{\phi_{cr}^2 EI_c}{L^2 + \frac{\phi_{cr}^2 EI_c}{S_v}} \quad (6-26)$$

This approach is next used to obtain the buckling equations for the special cases of partially braced, unbraced and braced frames.

6.2.2.1 Partially braced frame

The buckling equation can be derived by substituting $1/c_{br,b}$ equal to zero and $c_{br,t} = c_{br}$ in the stability matrix and setting its determinant equal to zero:

$$\begin{aligned} & -32\overline{c_{br}}(z_t-1)(z_b-1) + 4\cos(a_{cr}L) \left[8\overline{c_{br}}(z_t-1)(z_b-1) + (z_t+z_b-2z_tz_b) \left((a_{cr}L)^2 \beta_{cr} \overline{c_{br}} - \beta_{cr}^2 (a_{cr}L)^4 \right) \right] + \\ & + \sin(a_{cr}L) \left[-16(a_{cr}L)^3 \beta_{cr}^2 (1-z_t-z_b+z_tz_b) + (a_{cr}L)^5 \beta_{cr}^2 z_tz_b - (a_{cr}L)^3 \beta_{cr} \overline{c_{br}} z_tz_b + \right. \\ & \left. + 4(a_{cr}L) \overline{c_{br}} (4\beta_{cr} - (4\beta_{cr}+1)(z_t+z_b) + (4\beta_{cr}+2)z_tz_b) \right] = 0 \end{aligned} \quad (6-27)$$

where

$$\overline{c_{br}} = c_{br}^* L^3 \quad (6-28)$$

Eq. (6-27) can be solved numerically for $\phi_{cr} = a_{cr}L$. The solution is obtained for specific values of the dimensionless parameter μ (β_{cr} is directly connected with ϕ_{cr} as illustrated in Eq. (6-12)) and the stiffness of the translational spring. The value of ϕ_{cr} can then be substituted into Eq. (6-26) for the calculation of the elastic critical load of the member. If shear deformations are neglected, Eq. (6-27) is transformed to the one obtained by Gantes and Mageirou [6-1], [6-2] for partially braced frames consisting of Euler-Bernoulli columns.

The results obtained from Eq. (6-27) for different values of the distribution factors varying from zero (fixed support) to unity (hinged support), the translational spring's stiffness and the value of the parameter μ are summarised from Table 6-1 to Table 6-18 covering a large variety of possible cases. Each table is square and symmetric and for this reason only the diagonal and the top half is shown. The results are shown graphically in Figure 6-3 to Figure 6-20 obtained with the use of Matlab [6-10]. For values of μ equal to 0.001, 0.01 and 0.1 the graphs have red, blue and green colour, respectively. It should be noted that in Chapter 2, it was seen that solid cross-sections have a value of μ usually less than 0.003 highlighting that the effect of shear deformations on them is negligible.

Table 6-1: Value of ϕ_{cr} for $\bar{c}_{br}=0.2$ and $\mu=0.001$

zt/zb	0	0.05	0.1	0.15	0.2	0.25	0.3	0.35	0.4	0.45	0.5	0.55	0.6	0.65	0.7	0.75	0.8	0.85	0.9	0.95	1
0	3.168	3.128	3.084	3.038	2.988	2.934	2.876	2.815	2.749	2.679	2.605	2.526	2.443	2.357	2.265	2.170	2.070	1.966	1.857	1.742	1.622
0.05		3.089	3.046	3.001	2.952	2.900	2.843	2.783	2.718	2.650	2.577	2.500	2.418	2.333	2.243	2.148	2.049	1.946	1.837	1.723	1.603
0.1			3.006	2.961	2.914	2.863	2.808	2.749	2.686	2.619	2.547	2.471	2.391	2.307	2.218	2.124	2.026	1.924	1.816	1.702	1.582
0.15				2.919	2.872	2.823	2.769	2.712	2.650	2.585	2.515	2.440	2.362	2.279	2.191	2.099	2.002	1.900	1.793	1.680	1.560
0.2					2.828	2.779	2.728	2.672	2.612	2.548	2.480	2.407	2.330	2.248	2.162	2.071	1.975	1.874	1.768	1.655	1.536
0.25						2.733	2.683	2.628	2.570	2.508	2.442	2.371	2.295	2.215	2.130	2.041	1.946	1.846	1.740	1.628	1.509
0.3							2.634	2.582	2.526	2.465	2.400	2.331	2.258	2.179	2.096	2.008	1.914	1.815	1.711	1.599	1.481
0.35								2.531	2.477	2.419	2.356	2.289	2.217	2.140	2.058	1.972	1.880	1.782	1.678	1.568	1.449
0.4									2.425	2.368	2.307	2.242	2.172	2.097	2.018	1.933	1.842	1.746	1.643	1.533	1.415
0.45										2.314	2.255	2.192	2.124	2.051	1.973	1.890	1.801	1.706	1.604	1.495	1.377
0.5											2.198	2.137	2.072	2.001	1.925	1.844	1.756	1.663	1.562	1.454	1.336
0.55												2.079	2.015	1.946	1.872	1.793	1.707	1.615	1.515	1.408	1.290
0.6													1.953	1.887	1.815	1.737	1.653	1.563	1.464	1.357	1.240
0.65														1.823	1.753	1.677	1.595	1.505	1.408	1.301	1.183
0.7															1.685	1.611	1.530	1.442	1.345	1.239	1.120
0.75																1.538	1.459	1.372	1.276	1.169	1.049
0.8																	1.381	1.295	1.199	1.091	0.968
0.85																		1.208	1.112	1.002	0.875
0.9																			1.013	0.900	0.765
0.95																				0.779	0.630
1																					0.447

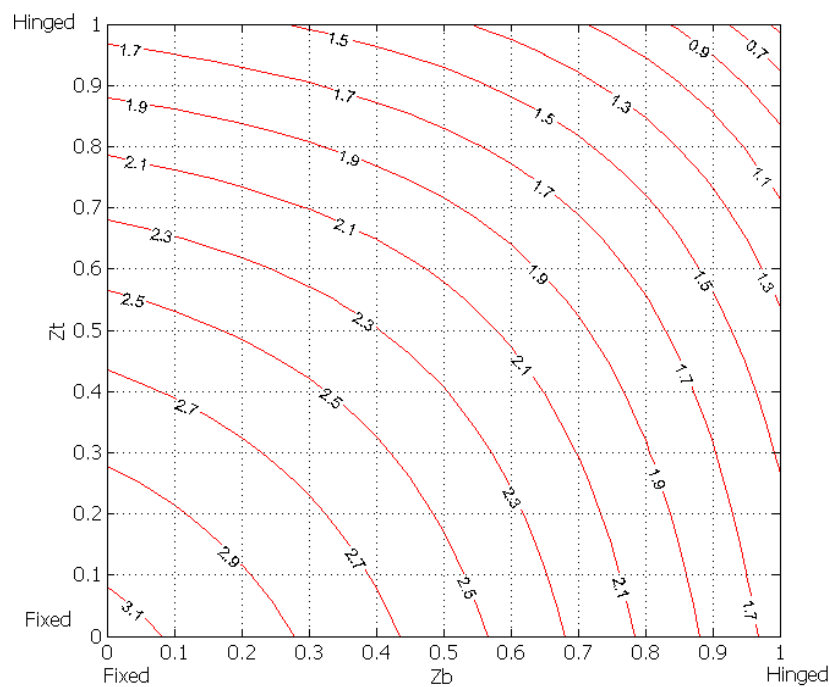
Figure 6-3: Graphical representation of the solution of buckling equation for partially-braced frames $\bar{c}_{br}=0.2$ and $\mu=0.001$

Table 6-2: Value of ϕ_{cr} for $\bar{c}_{br}=0.2$ and $\mu=0.01$

zt/zb	0	0.05	0.1	0.15	0.2	0.25	0.3	0.35	0.4	0.45	0.5	0.55	0.6	0.65	0.7	0.75	0.8	0.85	0.9	0.95	1
0	3.173	3.132	3.089	3.043	2.992	2.939	2.881	2.819	2.753	2.683	2.609	2.530	2.447	2.360	2.269	2.173	2.073	1.969	1.860	1.745	1.624
0.05		3.093	3.051	3.006	2.957	2.904	2.848	2.787	2.723	2.654	2.581	2.504	2.422	2.336	2.246	2.152	2.052	1.949	1.840	1.726	1.605
0.1			3.010	2.966	2.919	2.867	2.812	2.753	2.690	2.623	2.551	2.475	2.395	2.310	2.221	2.128	2.030	1.927	1.818	1.705	1.584
0.15				2.923	2.877	2.827	2.774	2.716	2.655	2.589	2.519	2.444	2.366	2.282	2.195	2.102	2.005	1.903	1.795	1.682	1.562
0.2					2.832	2.784	2.732	2.676	2.616	2.552	2.484	2.411	2.334	2.252	2.165	2.074	1.978	1.877	1.770	1.658	1.538
0.25						2.737	2.687	2.633	2.575	2.512	2.446	2.375	2.299	2.219	2.134	2.044	1.949	1.849	1.743	1.631	1.511
0.3							2.638	2.586	2.530	2.469	2.405	2.335	2.261	2.183	2.099	2.011	1.917	1.818	1.713	1.602	1.483
0.35								2.536	2.481	2.423	2.360	2.292	2.220	2.144	2.062	1.975	1.883	1.785	1.681	1.570	1.451
0.4									2.429	2.372	2.311	2.246	2.176	2.101	2.021	1.936	1.845	1.749	1.646	1.536	1.417
0.45										2.318	2.259	2.196	2.128	2.055	1.977	1.893	1.804	1.709	1.607	1.498	1.380
0.5											2.202	2.141	2.075	2.004	1.928	1.847	1.759	1.665	1.565	1.456	1.338
0.55												2.082	2.018	1.950	1.876	1.796	1.710	1.618	1.518	1.410	1.292
0.6													1.957	1.890	1.818	1.740	1.656	1.565	1.467	1.359	1.242
0.65														1.826	1.756	1.680	1.597	1.508	1.410	1.303	1.185
0.7															1.688	1.613	1.533	1.444	1.348	1.241	1.122
0.75																1.541	1.462	1.374	1.278	1.171	1.051
0.8																	1.383	1.297	1.201	1.093	0.970
0.85																		1.210	1.114	1.004	0.876
0.9																			1.015	0.901	0.766
0.95																				0.780	0.631
1																					0.448

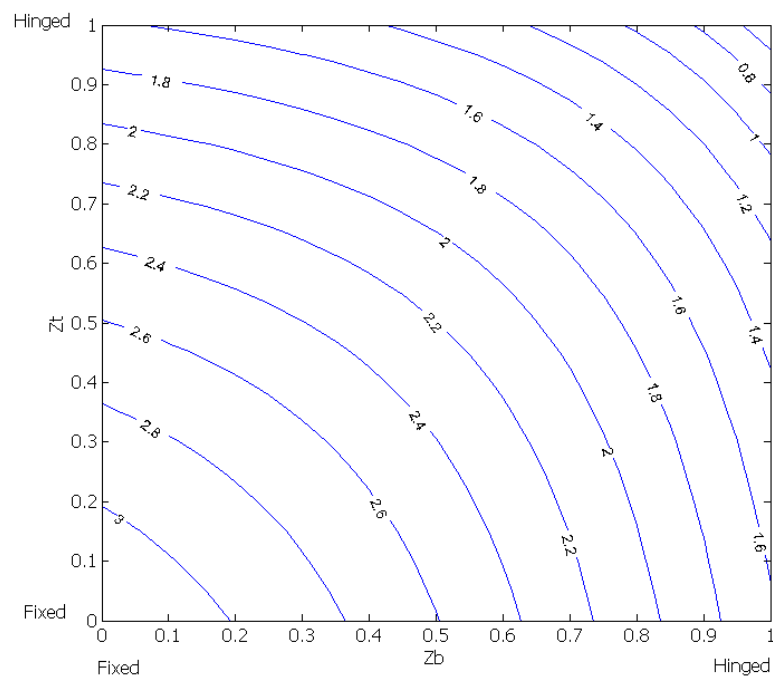
Figure 6-4: Graphical representation of the solution of buckling equation for partially-braced frames $\bar{c}_{br}=0.2$ and $\mu=0.01$

Table 6-3: Value of ϕ_{cr} for $\bar{c}_{br}=0.2$ and $\mu=0.1$

zt/zb	0	0.05	0.1	0.15	0.2	0.25	0.3	0.35	0.4	0.45	0.5	0.55	0.6	0.65	0.7	0.75	0.8	0.85	0.9	0.95	1
0	3.244	3.203	3.159	3.112	3.060	3.005	2.946	2.882	2.814	2.741	2.665	2.583	2.498	2.408	2.313	2.215	2.112	2.004	1.892	1.774	1.650
0.05		3.164	3.121	3.074	3.024	2.970	2.912	2.850	2.783	2.712	2.637	2.557	2.472	2.384	2.290	2.193	2.091	1.984	1.872	1.754	1.631
0.1			3.079	3.034	2.985	2.933	2.876	2.815	2.750	2.681	2.607	2.528	2.445	2.357	2.265	2.169	2.068	1.962	1.850	1.734	1.610
0.15				2.990	2.943	2.892	2.837	2.778	2.714	2.646	2.574	2.497	2.415	2.329	2.238	2.143	2.043	1.938	1.827	1.711	1.588
0.2					2.897	2.848	2.794	2.737	2.675	2.609	2.538	2.463	2.383	2.298	2.209	2.115	2.016	1.912	1.802	1.686	1.563
0.25						2.800	2.748	2.693	2.633	2.568	2.499	2.426	2.348	2.265	2.177	2.084	1.986	1.883	1.774	1.659	1.537
0.3							2.698	2.645	2.587	2.524	2.457	2.386	2.310	2.228	2.142	2.051	1.954	1.852	1.744	1.630	1.508
0.35								2.593	2.537	2.477	2.412	2.342	2.268	2.189	2.104	2.015	1.920	1.819	1.712	1.598	1.476
0.4									2.483	2.425	2.362	2.295	2.222	2.145	2.063	1.975	1.881	1.782	1.676	1.563	1.441
0.45										2.369	2.308	2.243	2.173	2.098	2.017	1.931	1.840	1.742	1.637	1.524	1.403
0.5											2.250	2.187	2.119	2.046	1.968	1.884	1.794	1.697	1.594	1.482	1.361
0.55												2.127	2.061	1.990	1.914	1.832	1.744	1.649	1.546	1.435	1.315
0.6													1.998	1.929	1.855	1.775	1.689	1.595	1.494	1.384	1.263
0.65														1.863	1.791	1.713	1.629	1.537	1.436	1.327	1.206
0.7															1.721	1.645	1.562	1.472	1.372	1.263	1.141
0.75																1.571	1.490	1.400	1.302	1.192	1.069
0.8																	1.409	1.321	1.222	1.112	0.986
0.85																		1.233	1.133	1.021	0.891
0.9																			1.033	0.916	0.778
0.95																				0.792	0.639
1																					0.452

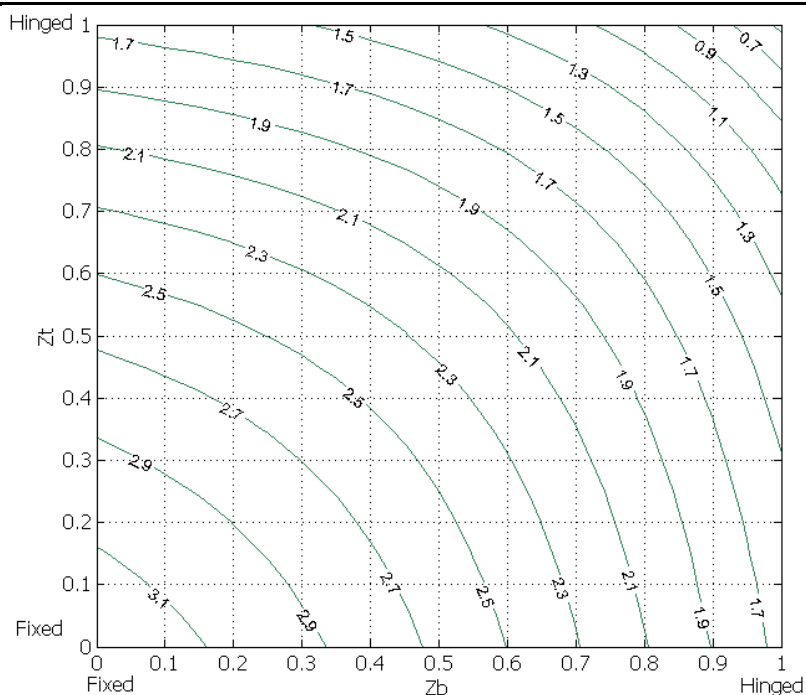
Figure 6-5: Graphical representation of the solution of buckling equation for partially-braced frames $\bar{c}_{br}=0.2$ and $\mu=0.1$

Table 6-4: Value of ϕ_{cr} for $\bar{c}_{br}=0.6$ and $\mu=0.001$

zt/zb	0	0.05	0.1	0.15	0.2	0.25	0.3	0.35	0.4	0.45	0.5	0.55	0.6	0.65	0.7	0.75	0.8	0.85	0.9	0.95	1
0	3.220	3.181	3.139	3.094	3.045	2.993	2.936	2.876	2.812	2.744	2.672	2.595	2.514	2.430	2.341	2.248	2.151	2.050	1.944	1.834	1.719
0.05		3.143	3.102	3.058	3.011	2.960	2.905	2.846	2.783	2.716	2.645	2.570	2.491	2.407	2.320	2.228	2.132	2.031	1.927	1.817	1.702
0.1			3.063	3.020	2.974	2.924	2.871	2.813	2.752	2.687	2.617	2.543	2.465	2.383	2.297	2.206	2.111	2.011	1.907	1.798	1.684
0.15				2.978	2.934	2.886	2.834	2.778	2.718	2.655	2.587	2.514	2.438	2.357	2.272	2.182	2.088	1.990	1.887	1.778	1.664
0.2					2.891	2.844	2.794	2.740	2.682	2.620	2.553	2.483	2.408	2.328	2.245	2.156	2.064	1.966	1.864	1.756	1.643
0.25						2.799	2.750	2.698	2.642	2.582	2.517	2.448	2.375	2.297	2.215	2.128	2.037	1.941	1.840	1.733	1.620
0.3							2.704	2.653	2.599	2.541	2.478	2.411	2.340	2.264	2.183	2.098	2.008	1.913	1.813	1.707	1.595
0.35								2.605	2.552	2.496	2.435	2.370	2.301	2.227	2.148	2.065	1.976	1.883	1.784	1.679	1.567
0.4									2.502	2.448	2.389	2.326	2.259	2.187	2.110	2.029	1.942	1.850	1.752	1.648	1.537
0.45										2.396	2.339	2.279	2.213	2.144	2.069	1.989	1.904	1.814	1.717	1.614	1.504
0.5											2.285	2.227	2.164	2.096	2.024	1.946	1.863	1.774	1.679	1.577	1.468
0.55												2.171	2.110	2.045	1.974	1.899	1.818	1.731	1.637	1.537	1.428
0.6													2.052	1.989	1.921	1.847	1.768	1.683	1.591	1.492	1.384
0.65														1.928	1.862	1.791	1.714	1.631	1.540	1.443	1.336
0.7															1.799	1.730	1.655	1.573	1.485	1.388	1.282
0.75																1.663	1.590	1.510	1.423	1.327	1.222
0.8																	1.519	1.441	1.355	1.260	1.154
0.85																		1.364	1.279	1.185	1.078
0.9																			1.195	1.100	0.992
0.95																				1.004	0.893
1																					0.775

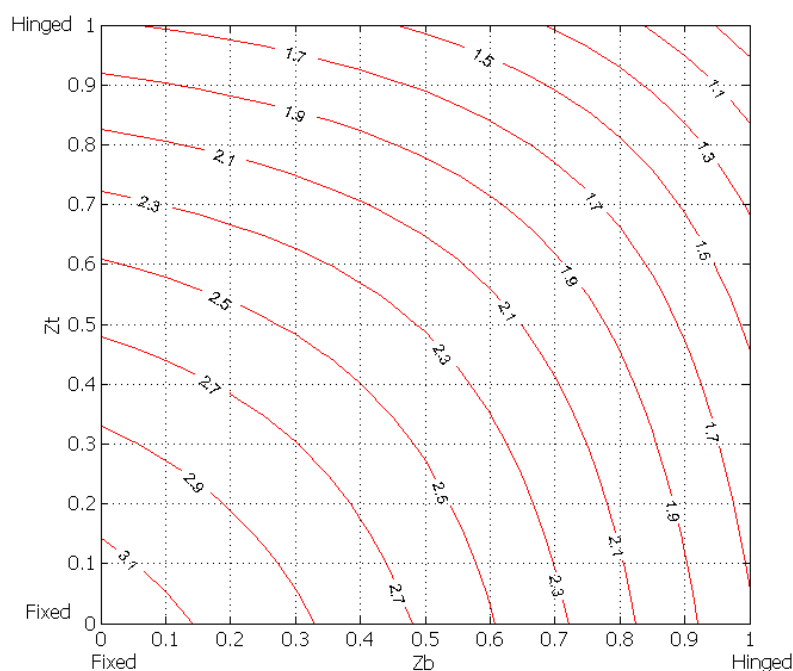


Table 6-5: Value of ϕ_{cr} for $\bar{c}_{br}=0.6$ and $\mu=0.01$

zt/zb	0	0.05	0.1	0.15	0.2	0.25	0.3	0.35	0.4	0.45	0.5	0.55	0.6	0.65	0.7	0.75	0.8	0.85	0.9	0.95	1
0	3.234	3.195	3.153	3.108	3.059	3.007	2.950	2.890	2.825	2.757	2.684	2.607	2.526	2.441	2.351	2.258	2.160	2.059	1.952	1.842	1.726
0.05		3.157	3.116	3.072	3.025	2.974	2.919	2.860	2.797	2.729	2.658	2.582	2.502	2.418	2.330	2.238	2.141	2.040	1.935	1.825	1.709
0.1			3.077	3.034	2.988	2.938	2.884	2.827	2.765	2.700	2.630	2.555	2.477	2.394	2.307	2.216	2.120	2.020	1.916	1.806	1.691
0.15				2.993	2.948	2.899	2.847	2.791	2.732	2.667	2.599	2.526	2.449	2.368	2.282	2.192	2.098	1.999	1.895	1.786	1.671
0.2					2.904	2.858	2.807	2.753	2.695	2.632	2.566	2.495	2.419	2.339	2.255	2.166	2.073	1.975	1.872	1.764	1.650
0.25						2.813	2.764	2.711	2.655	2.594	2.530	2.460	2.387	2.308	2.226	2.138	2.046	1.950	1.848	1.740	1.627
0.3							2.717	2.666	2.612	2.553	2.490	2.423	2.351	2.275	2.194	2.108	2.017	1.922	1.821	1.714	1.601
0.35								2.618	2.565	2.508	2.448	2.382	2.312	2.238	2.159	2.075	1.986	1.891	1.792	1.686	1.574
0.4									2.515	2.460	2.401	2.338	2.270	2.198	2.121	2.038	1.951	1.858	1.760	1.655	1.544
0.45										2.408	2.351	2.290	2.225	2.154	2.079	1.999	1.913	1.822	1.725	1.622	1.511
0.5											2.297	2.238	2.175	2.107	2.034	1.955	1.872	1.782	1.687	1.584	1.475
0.55												2.182	2.121	2.055	1.984	1.908	1.826	1.739	1.645	1.544	1.435
0.6													2.062	1.999	1.930	1.856	1.777	1.691	1.599	1.499	1.391
0.65														1.938	1.872	1.800	1.722	1.638	1.548	1.449	1.342
0.7															1.808	1.738	1.663	1.581	1.492	1.394	1.287
0.75																1.671	1.598	1.517	1.430	1.333	1.227
0.8																	1.526	1.447	1.361	1.266	1.159
0.85																		1.370	1.285	1.190	1.083
0.9																			1.200	1.104	0.996
0.95																				1.008	0.896
1																					0.777

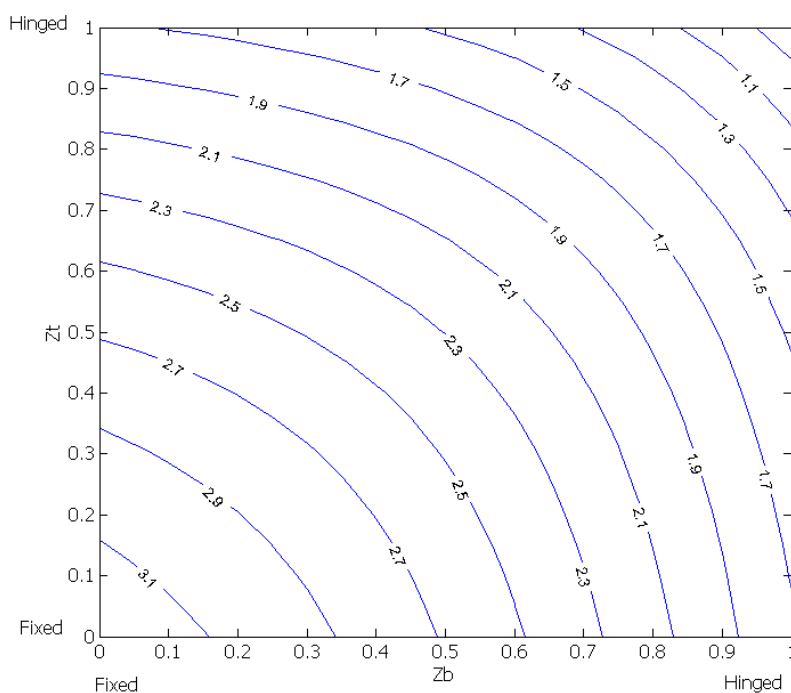
Figure 6-7: Graphical representation of the solution of buckling equation for partially-braced frames $\bar{c}_{br}=0.6$ and $\mu=0.01$

Table 6-6: Value of ϕ_{cr} for $\bar{c}_{br}=0.6$ and $\mu=0.1$

zt/zb	0	0.05	0.1	0.15	0.2	0.25	0.3	0.35	0.4	0.45	0.5	0.55	0.6	0.65	0.7	0.75	0.8	0.85	0.9	0.95	1
0	3.454	3.413	3.369	3.321	3.268	3.212	3.150	3.084	3.013	2.937	2.856	2.771	2.680	2.586	2.487	2.384	2.277	2.165	2.050	1.929	1.804
0.05		3.374	3.331	3.284	3.233	3.178	3.118	3.053	2.984	2.909	2.830	2.746	2.657	2.564	2.466	2.364	2.257	2.147	2.032	1.912	1.787
0.1			3.289	3.244	3.194	3.140	3.082	3.019	2.951	2.879	2.801	2.718	2.631	2.539	2.443	2.342	2.236	2.127	2.012	1.893	1.769
0.15				3.200	3.152	3.100	3.043	2.982	2.916	2.845	2.769	2.689	2.603	2.512	2.417	2.318	2.214	2.105	1.992	1.873	1.749
0.2					3.106	3.055	3.001	2.941	2.877	2.809	2.735	2.656	2.572	2.483	2.390	2.292	2.189	2.081	1.969	1.851	1.727
0.25						3.007	2.954	2.897	2.835	2.768	2.697	2.620	2.538	2.451	2.360	2.263	2.162	2.055	1.944	1.827	1.704
0.3							2.904	2.849	2.789	2.725	2.655	2.581	2.501	2.416	2.326	2.232	2.132	2.027	1.916	1.800	1.678
0.35								2.796	2.739	2.677	2.610	2.537	2.460	2.378	2.290	2.197	2.099	1.995	1.886	1.771	1.649
0.4									2.684	2.624	2.560	2.490	2.415	2.335	2.250	2.159	2.063	1.961	1.853	1.739	1.618
0.45										2.567	2.506	2.439	2.366	2.289	2.206	2.117	2.023	1.923	1.817	1.704	1.584
0.5											2.446	2.382	2.313	2.238	2.158	2.072	1.980	1.881	1.777	1.665	1.546
0.55												2.321	2.254	2.182	2.105	2.021	1.931	1.835	1.733	1.623	1.504
0.6													2.191	2.122	2.047	1.966	1.878	1.785	1.684	1.575	1.458
0.65														2.055	1.983	1.905	1.820	1.729	1.630	1.522	1.406
0.7															1.914	1.838	1.756	1.667	1.570	1.464	1.348
0.75																1.765	1.686	1.599	1.503	1.399	1.284
0.8																	1.608	1.523	1.430	1.326	1.211
0.85																		1.440	1.348	1.245	1.129
0.9																			1.256	1.153	1.036
0.95																				1.049	0.928
1																					0.799

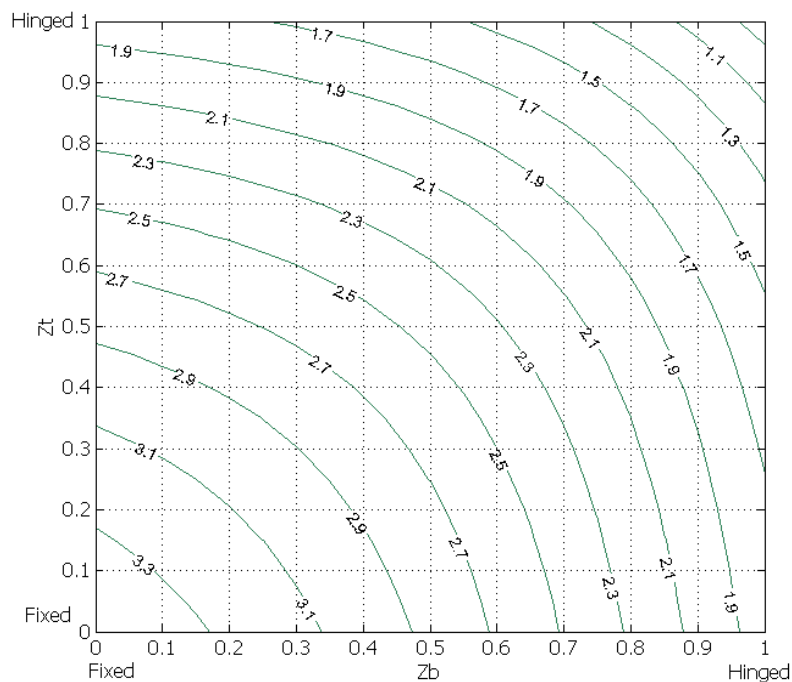
Figure 6-8: Graphical representation of the solution of buckling equation for partially-braced frames $\bar{c}_{br}=0.6$ and $\mu=0.1$

Table 6-7: Value of φ_{cr} for $\bar{c}_{br}=1$ and $\mu=0.001$

zt/zb	0	0.05	0.1	0.15	0.2	0.25	0.3	0.35	0.4	0.45	0.5	0.55	0.6	0.65	0.7	0.75	0.8	0.85	0.9	0.95	1
0	3.270	3.233	3.192	3.148	3.101	3.050	2.995	2.937	2.874	2.808	2.737	2.662	2.583	2.500	2.413	2.323	2.228	2.130	2.028	1.921	1.811
0.05		3.196	3.157	3.114	3.068	3.018	2.965	2.908	2.847	2.781	2.712	2.639	2.561	2.479	2.394	2.304	2.211	2.113	2.012	1.906	1.796
0.1			3.118	3.077	3.032	2.984	2.932	2.877	2.817	2.753	2.685	2.613	2.537	2.457	2.373	2.284	2.192	2.095	1.995	1.889	1.780
0.15				3.037	2.994	2.947	2.897	2.843	2.785	2.723	2.656	2.586	2.511	2.432	2.349	2.262	2.171	2.076	1.976	1.871	1.762
0.2					2.952	2.907	2.858	2.806	2.750	2.689	2.625	2.556	2.483	2.406	2.324	2.239	2.149	2.054	1.955	1.852	1.743
0.25						2.864	2.817	2.766	2.712	2.653	2.590	2.524	2.452	2.377	2.297	2.213	2.124	2.031	1.933	1.831	1.723
0.3							2.772	2.723	2.670	2.614	2.553	2.488	2.419	2.345	2.267	2.185	2.097	2.006	1.909	1.808	1.701
0.35								2.676	2.626	2.571	2.512	2.450	2.382	2.311	2.235	2.154	2.068	1.978	1.883	1.783	1.677
0.4									2.577	2.525	2.468	2.408	2.343	2.273	2.199	2.120	2.036	1.948	1.854	1.755	1.650
0.45										2.475	2.421	2.362	2.299	2.232	2.160	2.083	2.002	1.915	1.823	1.725	1.621
0.5											2.369	2.313	2.252	2.188	2.118	2.043	1.964	1.879	1.788	1.692	1.589
0.55												2.259	2.201	2.139	2.072	1.999	1.922	1.839	1.750	1.655	1.554
0.6													2.146	2.086	2.021	1.951	1.876	1.795	1.708	1.615	1.515
0.65														2.028	1.966	1.899	1.826	1.747	1.663	1.571	1.472
0.7															1.906	1.841	1.771	1.695	1.612	1.522	1.425
0.75																1.779	1.711	1.637	1.556	1.469	1.373
0.8																	1.645	1.573	1.495	1.409	1.314
0.85																		1.504	1.427	1.343	1.249
0.9																			1.352	1.269	1.176
0.95																				1.187	1.094
1																					1.001

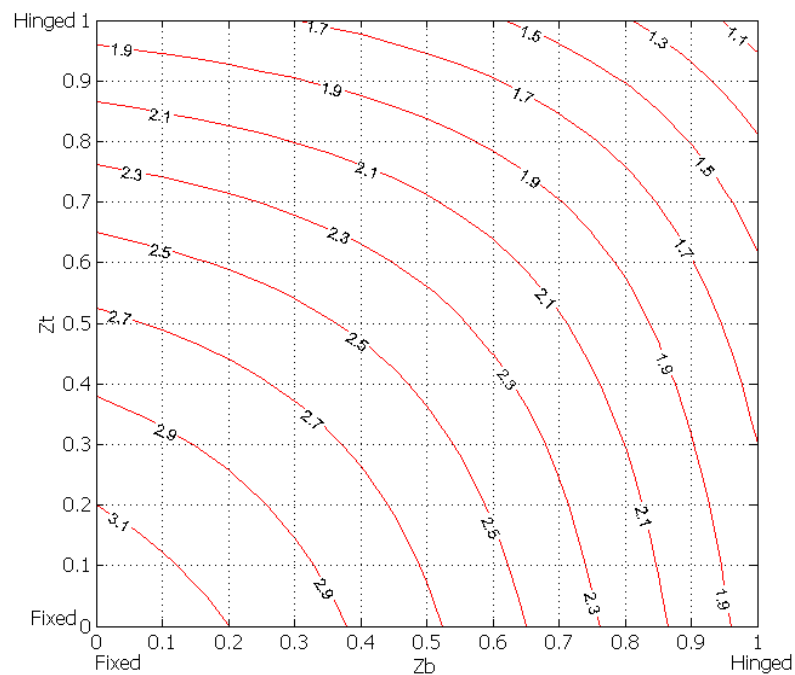
Figure 6-9: Graphical representation of the solution of buckling equation for partially-braced frames $\bar{c}_{br}=1$ and $\mu=0.001$

Table 6-8: Value of ϕ_{cr} for $\bar{c}_{br}=1$ and $\mu=0.01$

zt/zb	0	0.05	0.1	0.15	0.2	0.25	0.3	0.35	0.4	0.45	0.5	0.55	0.6	0.65	0.7	0.75	0.8	0.85	0.9	0.95	1
0	3.294	3.257	3.216	3.172	3.124	3.073	3.018	2.959	2.896	2.829	2.758	2.682	2.602	2.519	2.431	2.339	2.244	2.145	2.041	1.934	1.822
0.05		3.220	3.181	3.138	3.092	3.042	2.988	2.930	2.869	2.803	2.733	2.659	2.580	2.498	2.411	2.321	2.226	2.128	2.025	1.918	1.807
0.1			3.142	3.101	3.056	3.007	2.955	2.899	2.839	2.775	2.706	2.633	2.557	2.475	2.390	2.301	2.207	2.110	2.008	1.902	1.791
0.15				3.061	3.017	2.970	2.920	2.865	2.807	2.744	2.677	2.606	2.531	2.451	2.367	2.279	2.187	2.090	1.989	1.884	1.774
0.2					2.975	2.930	2.881	2.828	2.771	2.711	2.645	2.576	2.502	2.424	2.342	2.255	2.164	2.069	1.969	1.864	1.755
0.25						2.886	2.839	2.788	2.733	2.674	2.611	2.544	2.472	2.395	2.315	2.229	2.140	2.046	1.947	1.843	1.734
0.3							2.794	2.745	2.692	2.635	2.574	2.508	2.438	2.364	2.285	2.201	2.113	2.020	1.923	1.820	1.712
0.35								2.698	2.647	2.592	2.533	2.469	2.401	2.329	2.252	2.170	2.084	1.993	1.896	1.795	1.688
0.4									2.598	2.545	2.488	2.427	2.362	2.291	2.216	2.136	2.052	1.962	1.867	1.767	1.661
0.45										2.495	2.440	2.381	2.318	2.250	2.177	2.100	2.017	1.929	1.836	1.737	1.632
0.5											2.388	2.332	2.271	2.205	2.135	2.059	1.979	1.893	1.801	1.704	1.600
0.55												2.278	2.219	2.156	2.088	2.015	1.936	1.853	1.763	1.667	1.564
0.6													2.163	2.103	2.037	1.966	1.890	1.809	1.721	1.627	1.525
0.65														2.045	1.982	1.914	1.840	1.760	1.675	1.582	1.482
0.7															1.921	1.856	1.784	1.707	1.624	1.533	1.435
0.75																1.793	1.724	1.649	1.567	1.479	1.382
0.8																	1.658	1.585	1.505	1.418	1.323
0.85																		1.514	1.437	1.351	1.257
0.9																			1.361	1.277	1.183
0.95																				1.194	1.100
1																					1.005

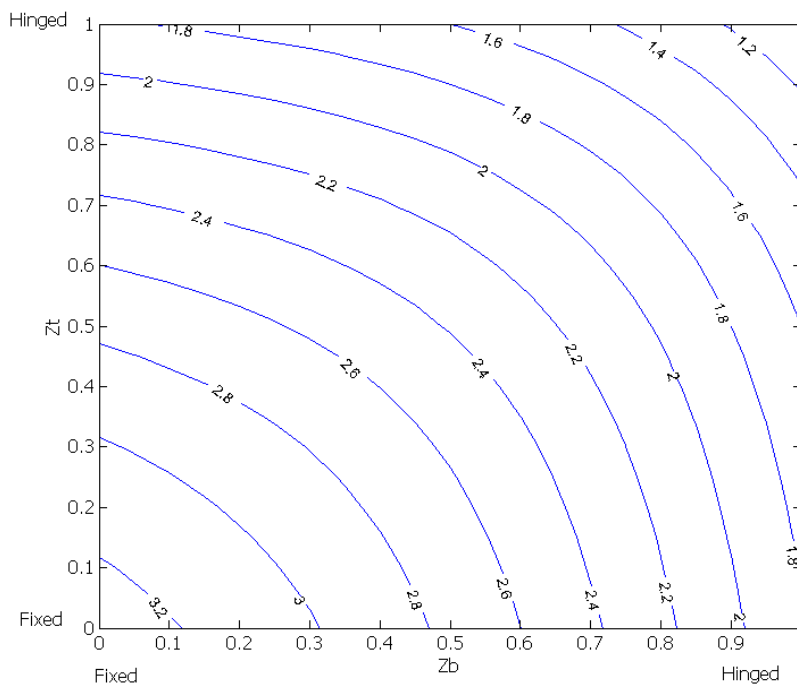
Figure 6-10: Graphical representation of the solution of buckling equation for partially-braced frames $\bar{c}_{br}=1$ and $\mu=0.01$

Table 6-9: Value of ϕ_{cr} for $\bar{c}_{br}=1$ and $\mu=0.1$

zt/zb	0	0.05	0.1	0.15	0.2	0.25	0.3	0.35	0.4	0.45	0.5	0.55	0.6	0.65	0.7	0.75	0.8	0.85	0.9	0.95	1
0	3.669	3.629	3.585	3.537	3.483	3.425	3.362	3.293	3.218	3.138	3.053	2.962	2.867	2.766	2.662	2.553	2.441	2.325	2.205	2.081	1.953
0.05		3.590	3.547	3.500	3.449	3.392	3.330	3.263	3.190	3.112	3.028	2.939	2.845	2.746	2.643	2.535	2.424	2.308	2.189	2.066	1.938
0.1			3.506	3.461	3.411	3.356	3.296	3.230	3.160	3.083	3.001	2.914	2.821	2.724	2.622	2.515	2.405	2.290	2.172	2.049	1.922
0.15				3.417	3.369	3.316	3.258	3.194	3.125	3.051	2.971	2.885	2.795	2.699	2.599	2.494	2.384	2.271	2.153	2.031	1.904
0.2					3.322	3.271	3.215	3.154	3.088	3.015	2.938	2.854	2.766	2.672	2.573	2.470	2.362	2.249	2.133	2.011	1.885
0.25						3.222	3.169	3.110	3.046	2.976	2.901	2.820	2.733	2.642	2.545	2.443	2.337	2.226	2.110	1.990	1.864
0.3							3.118	3.061	3.000	2.933	2.860	2.781	2.697	2.608	2.513	2.414	2.309	2.200	2.085	1.966	1.841
0.35								3.008	2.949	2.885	2.815	2.739	2.658	2.571	2.479	2.381	2.279	2.171	2.058	1.940	1.816
0.4									2.893	2.832	2.765	2.692	2.614	2.530	2.440	2.345	2.245	2.139	2.028	1.911	1.788
0.45										2.773	2.710	2.640	2.565	2.484	2.398	2.305	2.207	2.103	1.994	1.879	1.757
0.5											2.649	2.583	2.512	2.434	2.350	2.261	2.165	2.064	1.957	1.843	1.723
0.55												2.521	2.453	2.378	2.298	2.212	2.119	2.020	1.915	1.804	1.685
0.6													2.388	2.317	2.240	2.157	2.068	1.972	1.869	1.760	1.642
0.65														2.250	2.177	2.097	2.011	1.918	1.818	1.711	1.595
0.7															2.107	2.031	1.948	1.858	1.761	1.656	1.542
0.75																1.959	1.879	1.792	1.698	1.595	1.483
0.8																	1.803	1.719	1.628	1.527	1.417
0.85																		1.639	1.549	1.451	1.342
0.9																			1.463	1.366	1.258
0.95																				1.271	1.163
1																					1.054

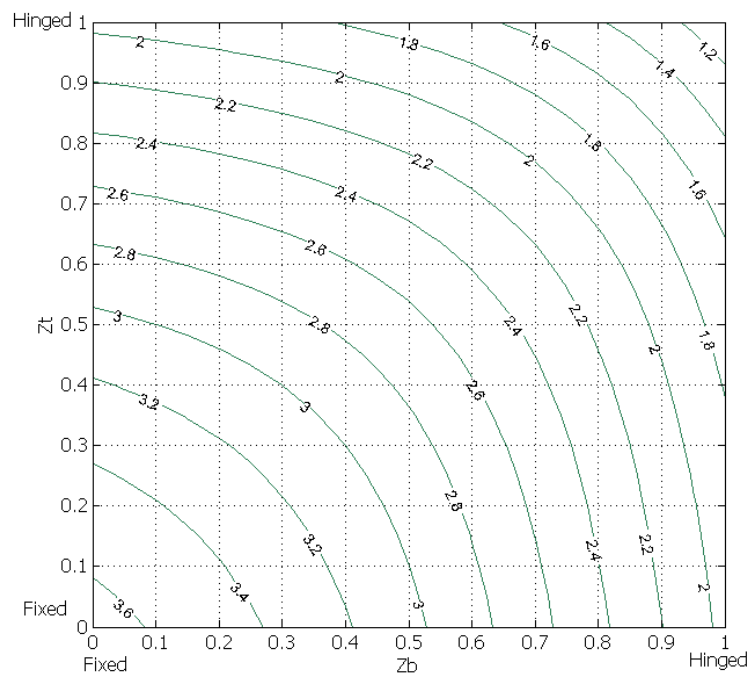
Figure 6-11: Graphical representation of the solution of buckling equation for partially-braced frames $\bar{c}_{br}=1$ and $\mu=0.1$

Table 6-10: Value of ϕ_{cr} for $\bar{c}_{br}=2.5$ and $\mu=0.001$

zt/zb	0	0.05	0.1	0.15	0.2	0.25	0.3	0.35	0.4	0.45	0.5	0.55	0.6	0.65	0.7	0.75	0.8	0.85	0.9	0.95	1
0	3.454	3.421	3.384	3.345	3.302	3.256	3.207	3.153	3.095	3.034	2.968	2.899	2.825	2.748	2.668	2.583	2.496	2.405	2.312	2.215	2.116
0.05		3.388	3.353	3.315	3.274	3.229	3.181	3.129	3.072	3.012	2.948	2.880	2.808	2.732	2.653	2.570	2.484	2.394	2.301	2.205	2.107
0.1			3.319	3.283	3.243	3.199	3.153	3.102	3.047	2.989	2.927	2.860	2.790	2.715	2.637	2.555	2.470	2.381	2.290	2.195	2.097
0.15				3.247	3.209	3.167	3.122	3.073	3.020	2.963	2.903	2.838	2.769	2.696	2.619	2.539	2.455	2.368	2.277	2.183	2.086
0.2					3.172	3.132	3.088	3.041	2.990	2.936	2.877	2.814	2.747	2.675	2.600	2.521	2.439	2.353	2.263	2.170	2.074
0.25						3.094	3.052	3.007	2.958	2.905	2.848	2.787	2.722	2.653	2.579	2.502	2.421	2.336	2.248	2.156	2.061
0.3							3.012	2.969	2.922	2.872	2.817	2.758	2.695	2.628	2.556	2.481	2.402	2.318	2.231	2.141	2.046
0.35								2.928	2.883	2.835	2.783	2.726	2.665	2.600	2.531	2.458	2.380	2.299	2.213	2.124	2.031
0.4									2.841	2.795	2.745	2.691	2.633	2.570	2.503	2.432	2.356	2.277	2.193	2.105	2.014
0.45										2.751	2.704	2.652	2.597	2.537	2.472	2.403	2.330	2.253	2.171	2.085	1.995
0.5											2.659	2.610	2.557	2.500	2.438	2.372	2.301	2.226	2.147	2.062	1.974
0.55												2.564	2.514	2.460	2.401	2.337	2.269	2.197	2.119	2.037	1.951
0.6													2.467	2.416	2.360	2.299	2.234	2.164	2.089	2.010	1.925
0.65														2.367	2.314	2.257	2.195	2.128	2.056	1.979	1.897
0.7															2.265	2.211	2.152	2.088	2.019	1.945	1.865
0.75																2.160	2.104	2.044	1.978	1.907	1.830
0.8																	2.052	1.995	1.932	1.864	1.790
0.85																		1.941	1.882	1.817	1.747
0.9																			1.826	1.765	1.698
0.95																				1.707	1.643
1																					1.583

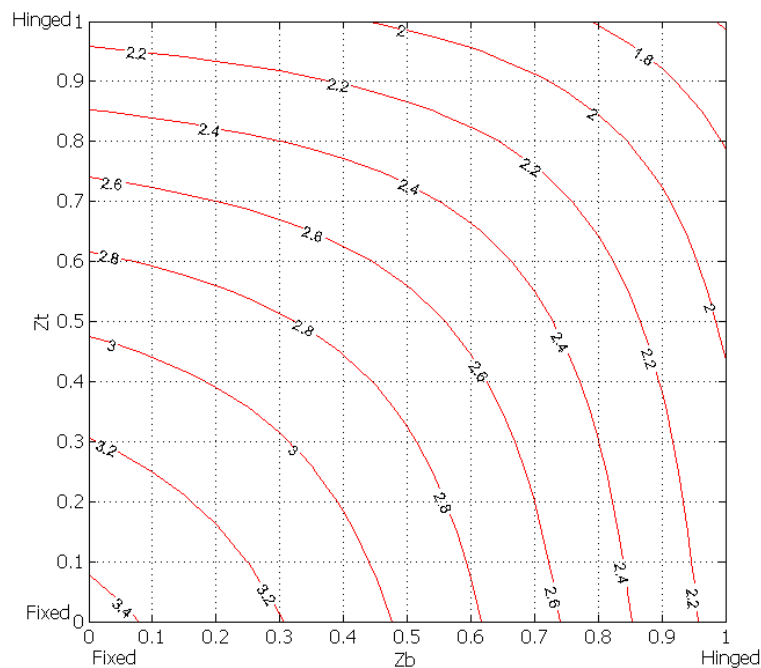
Figure 6-12: Graphical representation of the solution of buckling equation for partially-braced frames $\bar{c}_{br}=2.5$ and $\mu=0.001$

Table 6-11: Value of ϕ_{cr} for $\bar{c}_{br}=2.5$ and $\mu=0.01$

zt/zb	0	0.05	0.1	0.15	0.2	0.25	0.3	0.35	0.4	0.45	0.5	0.55	0.6	0.65	0.7	0.75	0.8	0.85	0.9	0.95	1
0	3.514	3.480	3.444	3.404	3.361	3.314	3.264	3.209	3.150	3.087	3.020	2.949	2.873	2.794	2.711	2.624	2.534	2.441	2.345	2.246	2.143
0.05		3.448	3.413	3.374	3.332	3.287	3.238	3.185	3.128	3.066	3.000	2.931	2.856	2.778	2.697	2.611	2.522	2.430	2.334	2.236	2.134
0.1			3.379	3.342	3.301	3.257	3.210	3.158	3.103	3.043	2.979	2.910	2.838	2.761	2.681	2.597	2.509	2.417	2.323	2.225	2.124
0.15				3.306	3.267	3.225	3.179	3.129	3.075	3.017	2.955	2.888	2.818	2.743	2.663	2.581	2.494	2.404	2.310	2.214	2.113
0.2					3.230	3.189	3.145	3.097	3.045	2.989	2.929	2.864	2.795	2.722	2.644	2.563	2.478	2.389	2.297	2.201	2.102
0.25						3.151	3.109	3.063	3.013	2.959	2.900	2.838	2.771	2.699	2.624	2.544	2.460	2.373	2.282	2.187	2.089
0.3							3.068	3.024	2.977	2.925	2.869	2.808	2.743	2.674	2.601	2.523	2.441	2.355	2.265	2.172	2.074
0.35								2.983	2.937	2.888	2.834	2.776	2.713	2.647	2.575	2.499	2.419	2.335	2.247	2.155	2.059
0.4									2.894	2.847	2.796	2.741	2.681	2.616	2.547	2.473	2.396	2.313	2.227	2.136	2.042
0.45										2.803	2.754	2.701	2.644	2.582	2.516	2.445	2.369	2.289	2.205	2.116	2.023
0.5											2.708	2.659	2.604	2.545	2.481	2.413	2.340	2.262	2.180	2.093	2.002
0.55												2.611	2.560	2.504	2.443	2.378	2.308	2.233	2.153	2.068	1.978
0.6													2.512	2.459	2.401	2.339	2.272	2.199	2.122	2.040	1.953
0.65														2.409	2.355	2.296	2.232	2.163	2.088	2.009	1.924
0.7															2.304	2.248	2.188	2.122	2.050	1.974	1.891
0.75																2.196	2.139	2.076	2.008	1.935	1.855
0.8																	2.085	2.026	1.962	1.891	1.815
0.85																		1.971	1.910	1.843	1.770
0.9																			1.852	1.789	1.720
0.95																				1.730	1.664
1																					1.601

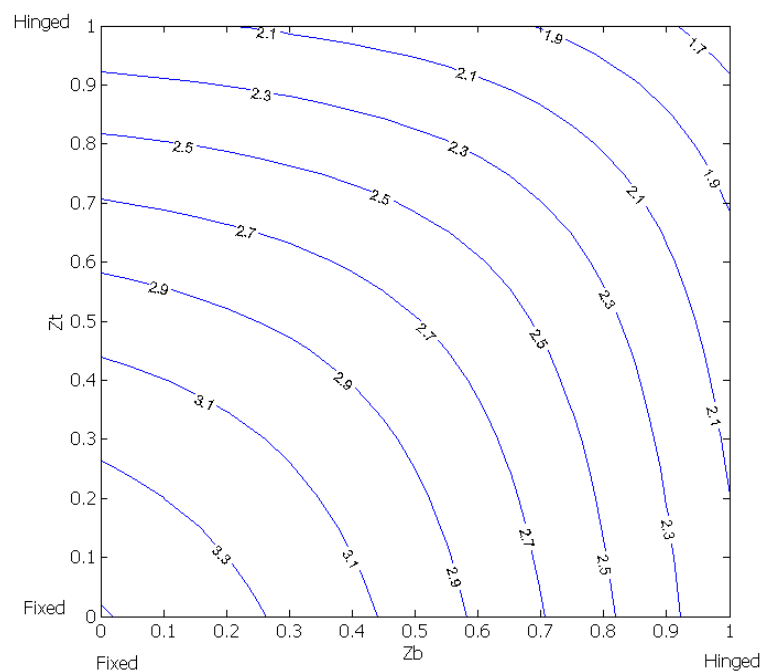


Table 6-12: Value of ϕ_{cr} for $\bar{c}_{br}=2.5$ and $\mu=0.1$

zt/zb	0	0.05	0.1	0.15	0.2	0.25	0.3	0.35	0.4	0.45	0.5	0.55	0.6	0.65	0.7	0.75	0.8	0.85	0.9	0.95	1
0	4.494	4.462	4.425	4.381	4.331	4.272	4.204	4.125	4.036	3.937	3.828	3.711	3.587	3.457	3.322	3.185	3.045	2.903	2.760	2.616	2.471
0.05		4.431	4.396	4.354	4.306	4.249	4.183	4.107	4.020	3.922	3.815	3.699	3.576	3.447	3.313	3.176	3.037	2.896	2.753	2.609	2.464
0.1			4.362	4.323	4.276	4.222	4.158	4.084	4.000	3.905	3.800	3.686	3.564	3.436	3.303	3.167	3.028	2.887	2.745	2.601	2.456
0.15				4.285	4.241	4.190	4.129	4.058	3.977	3.884	3.782	3.670	3.550	3.423	3.292	3.156	3.018	2.878	2.736	2.593	2.448
0.2					4.200	4.152	4.094	4.027	3.949	3.860	3.760	3.651	3.533	3.408	3.278	3.144	3.007	2.867	2.726	2.583	2.438
0.25						4.106	4.053	3.990	3.916	3.831	3.735	3.628	3.513	3.391	3.263	3.130	2.994	2.855	2.714	2.572	2.427
0.3							4.003	3.945	3.876	3.795	3.704	3.602	3.490	3.370	3.244	3.113	2.978	2.841	2.701	2.559	2.415
0.35								3.891	3.827	3.753	3.666	3.569	3.462	3.345	3.222	3.094	2.961	2.824	2.686	2.545	2.401
0.4									3.770	3.701	3.621	3.530	3.427	3.316	3.196	3.071	2.940	2.805	2.668	2.528	2.386
0.45										3.639	3.566	3.482	3.386	3.280	3.165	3.043	2.915	2.783	2.648	2.509	2.368
0.5											3.501	3.424	3.336	3.236	3.127	3.010	2.886	2.757	2.624	2.487	2.347
0.55												3.356	3.275	3.184	3.082	2.970	2.851	2.726	2.596	2.462	2.324
0.6													3.204	3.121	3.027	2.922	2.809	2.689	2.563	2.432	2.296
0.65														3.047	2.962	2.865	2.759	2.645	2.524	2.396	2.264
0.7															2.885	2.798	2.700	2.593	2.477	2.355	2.226
0.75																2.720	2.631	2.531	2.423	2.306	2.181
0.8																	2.550	2.459	2.358	2.248	2.129
0.85																		2.377	2.284	2.181	2.069
0.9																			2.199	2.104	1.998
0.95																				2.016	1.917
1																					1.826

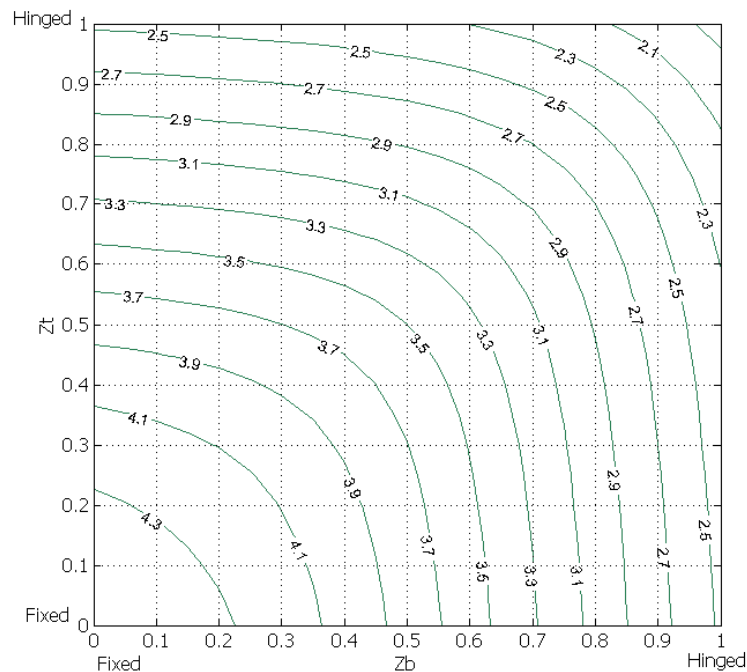
Figure 6-14: Graphical representation of the solution of buckling equation for partially-braced frames $\bar{c}_{br}=2.5$ and $\mu=0.1$

Table 6-13: Value of ϕ_{cr} for $\bar{c}_{br}=7.5$ and $\mu=0.001$

zt/zb	0	0.05	0.1	0.15	0.2	0.25	0.3	0.35	0.4	0.45	0.5	0.55	0.6	0.65	0.7	0.75	0.8	0.85	0.9	0.95	1
0	4.004	3.981	3.955	3.927	3.896	3.862	3.824	3.782	3.736	3.685	3.630	3.570	3.506	3.438	3.366	3.291	3.212	3.131	3.048	2.964	2.877
0.05		3.959	3.935	3.908	3.878	3.845	3.809	3.768	3.724	3.674	3.621	3.563	3.500	3.433	3.362	3.287	3.210	3.129	3.047	2.962	2.877
0.1			3.912	3.887	3.858	3.827	3.792	3.753	3.710	3.663	3.611	3.554	3.493	3.427	3.357	3.284	3.207	3.127	3.045	2.961	2.876
0.15				3.863	3.836	3.806	3.773	3.736	3.695	3.649	3.599	3.544	3.484	3.420	3.352	3.279	3.203	3.125	3.043	2.960	2.875
0.2					3.811	3.783	3.752	3.717	3.678	3.634	3.586	3.533	3.475	3.413	3.346	3.275	3.200	3.122	3.041	2.958	2.873
0.25						3.757	3.728	3.695	3.658	3.617	3.571	3.520	3.465	3.404	3.339	3.269	3.195	3.118	3.039	2.956	2.872
0.3							3.701	3.670	3.636	3.597	3.554	3.506	3.452	3.394	3.331	3.263	3.191	3.115	3.036	2.954	2.871
0.35								3.642	3.611	3.575	3.534	3.489	3.438	3.382	3.321	3.255	3.185	3.111	3.033	2.952	2.869
0.4									3.582	3.549	3.512	3.469	3.422	3.369	3.311	3.247	3.178	3.106	3.029	2.949	2.867
0.45										3.520	3.486	3.447	3.403	3.353	3.298	3.237	3.171	3.100	3.025	2.946	2.865
0.5											3.455	3.420	3.380	3.334	3.283	3.225	3.161	3.093	3.020	2.943	2.863
0.55												3.389	3.354	3.312	3.264	3.210	3.150	3.085	3.014	2.939	2.860
0.6													3.322	3.285	3.242	3.193	3.137	3.075	3.006	2.933	2.856
0.65														3.253	3.216	3.171	3.120	3.062	2.997	2.927	2.852
0.7															3.184	3.145	3.099	3.046	2.986	2.919	2.846
0.75																3.113	3.074	3.027	2.972	2.909	2.840
0.8																	3.041	3.001	2.953	2.896	2.831
0.85																		2.969	2.928	2.878	2.819
0.9																			2.896	2.855	2.803
0.95																				2.823	2.780
1																					2.749

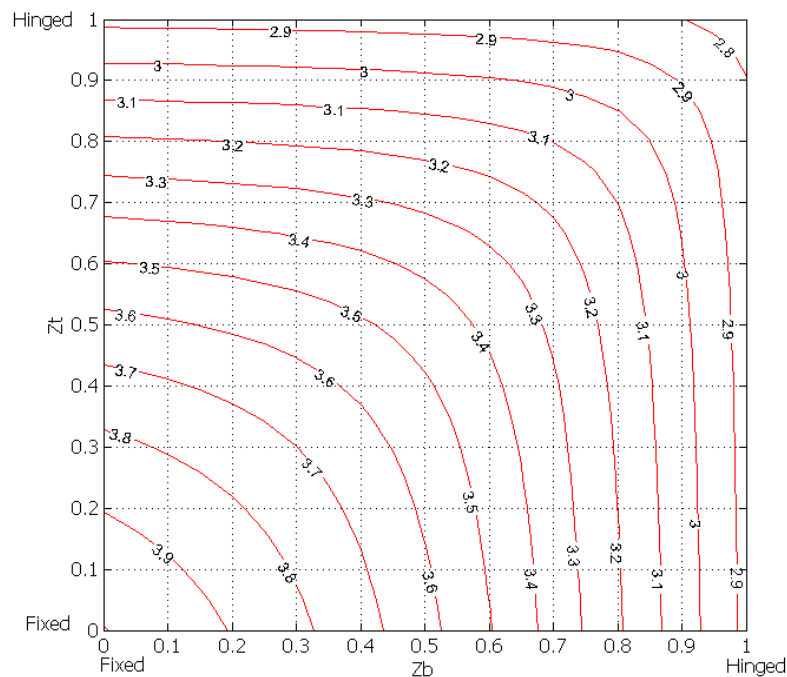
Figure 6-15: Graphical representation of the solution of buckling equation for partially-braced frames $\bar{c}_{br}=7.5$ and $\mu=0.001$

Table 6-14: Value of ϕ_{cr} for $\bar{c}_{br}=7.5$ and $\mu=0.01$

zt/zb	0	0.05	0.1	0.15	0.2	0.25	0.3	0.35	0.4	0.45	0.5	0.55	0.6	0.65	0.7	0.75	0.8	0.85	0.9	0.95	1
0	4.180	4.158	4.133	4.104	4.073	4.037	3.997	3.953	3.903	3.848	3.788	3.722	3.651	3.575	3.495	3.410	3.323	3.234	3.142	3.048	2.954
0.05		4.136	4.112	4.086	4.055	4.021	3.983	3.940	3.892	3.839	3.780	3.715	3.645	3.571	3.491	3.408	3.321	3.232	3.141	3.048	2.953
0.1			4.090	4.064	4.036	4.003	3.967	3.926	3.880	3.828	3.771	3.708	3.640	3.566	3.488	3.405	3.319	3.231	3.140	3.047	2.953
0.15				4.041	4.014	3.983	3.949	3.910	3.865	3.816	3.761	3.700	3.633	3.561	3.484	3.402	3.317	3.229	3.138	3.046	2.952
0.2					3.989	3.960	3.928	3.891	3.849	3.802	3.749	3.690	3.625	3.555	3.479	3.399	3.314	3.227	3.137	3.045	2.952
0.25						3.934	3.904	3.869	3.830	3.786	3.735	3.679	3.616	3.547	3.473	3.395	3.311	3.225	3.136	3.044	2.951
0.3							3.876	3.845	3.808	3.767	3.719	3.665	3.605	3.539	3.467	3.390	3.308	3.222	3.134	3.043	2.950
0.35								3.816	3.783	3.744	3.700	3.650	3.593	3.529	3.459	3.384	3.304	3.219	3.132	3.041	2.949
0.4									3.753	3.718	3.678	3.631	3.578	3.517	3.450	3.377	3.299	3.216	3.129	3.040	2.948
0.45										3.687	3.651	3.609	3.559	3.503	3.439	3.369	3.293	3.212	3.126	3.038	2.947
0.5											3.619	3.582	3.537	3.485	3.426	3.359	3.286	3.207	3.123	3.035	2.945
0.55												3.549	3.510	3.463	3.409	3.347	3.277	3.200	3.119	3.032	2.943
0.6													3.477	3.436	3.388	3.331	3.265	3.192	3.113	3.029	2.941
0.65														3.402	3.361	3.310	3.250	3.182	3.106	3.025	2.938
0.7															3.327	3.284	3.231	3.169	3.097	3.019	2.935
0.75																3.249	3.205	3.150	3.085	3.011	2.930
0.8																	3.171	3.125	3.069	3.001	2.924
0.85																		3.091	3.045	2.986	2.915
0.9																			3.011	2.963	2.901
0.95																				2.929	2.881
1																					2.847

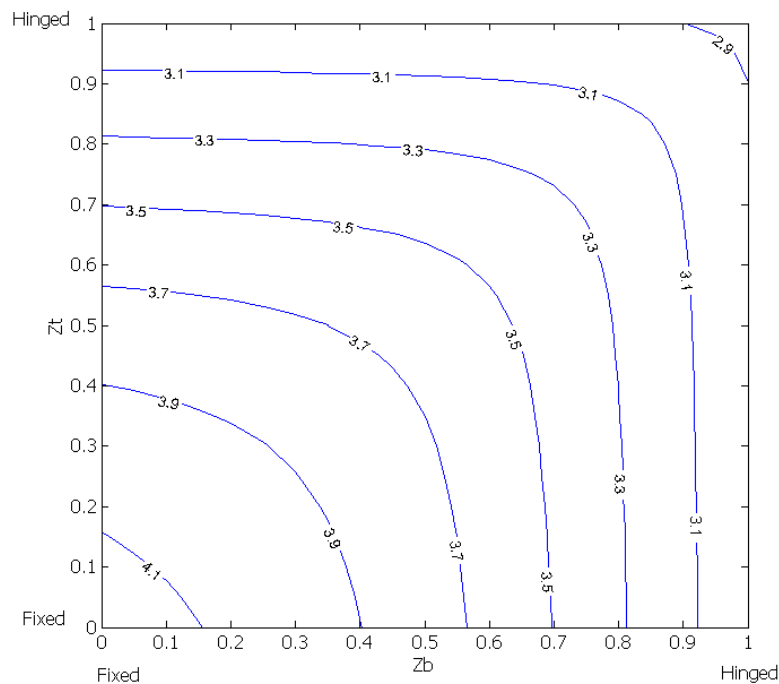
Figure 6-16: Graphical representation of the solution of buckling equation for partially-braced frames $\bar{c}_{br}=7.5$ and $\mu=0.01$

Table 6-15: Value of ϕ_{cr} for $\bar{c}_{br}=7.5$ and $\mu=0.1$

zt/zb	0	0.05	0.1	0.15	0.2	0.25	0.3	0.35	0.4	0.45	0.5	0.55	0.6	0.65	0.7	0.75	0.8	0.85	0.9	0.95	1
0	6.208	6.200	6.113	6.018	5.916	5.806	5.689	5.565	5.434	5.296	5.151	5.002	4.847	4.689	4.527	4.363	4.197	4.031	3.864	3.697	3.530
0.05		6.122	6.037	5.945	5.847	5.742	5.629	5.510	5.383	5.250	5.111	4.966	4.817	4.663	4.505	4.345	4.183	4.019	3.855	3.690	3.525
0.1			5.955	5.867	5.773	5.672	5.565	5.450	5.329	5.202	5.068	4.929	4.784	4.635	4.482	4.326	4.167	4.007	3.845	3.682	3.519
0.15				5.784	5.694	5.598	5.495	5.386	5.271	5.149	5.022	4.888	4.749	4.605	4.457	4.305	4.150	3.993	3.834	3.674	3.513
0.2					5.609	5.518	5.421	5.318	5.209	5.093	4.972	4.844	4.711	4.572	4.429	4.282	4.131	3.978	3.822	3.665	3.506
0.25						5.433	5.342	5.245	5.142	5.033	4.918	4.796	4.669	4.537	4.399	4.257	4.111	3.962	3.810	3.655	3.499
0.3							5.257	5.167	5.070	4.968	4.860	4.745	4.624	4.498	4.367	4.230	4.089	3.944	3.795	3.644	3.491
0.35								5.083	4.994	4.898	4.797	4.689	4.576	4.456	4.331	4.200	4.064	3.924	3.780	3.632	3.482
0.4									4.911	4.823	4.729	4.629	4.523	4.410	4.292	4.167	4.037	3.902	3.763	3.619	3.472
0.45										4.743	4.656	4.564	4.465	4.360	4.249	4.131	4.007	3.878	3.743	3.604	3.460
0.5											4.578	4.493	4.403	4.305	4.202	4.091	3.974	3.851	3.722	3.587	3.448
0.55												4.417	4.334	4.245	4.150	4.047	3.937	3.821	3.698	3.568	3.434
0.6													4.260	4.180	4.092	3.998	3.896	3.787	3.670	3.547	3.417
0.65														4.107	4.029	3.943	3.849	3.748	3.639	3.523	3.399
0.7															3.959	3.882	3.797	3.705	3.604	3.495	3.378
0.75																3.814	3.739	3.656	3.564	3.463	3.353
0.8																	3.673	3.599	3.517	3.425	3.324
0.85																		3.536	3.463	3.381	3.289
0.9																			3.401	3.330	3.249
0.95																				3.270	3.200
1																					3.142

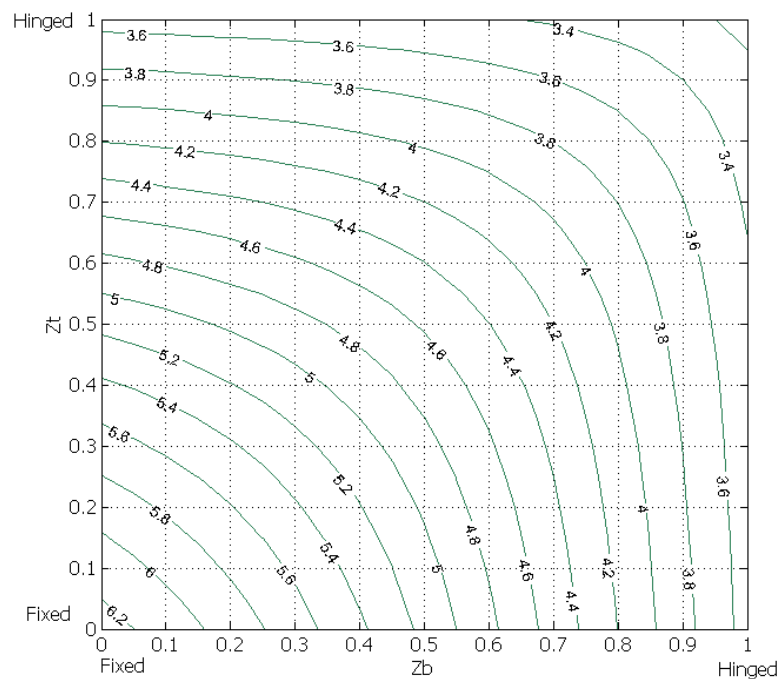
Figure 6-17: Graphical representation of the solution of buckling equation for partially-braced frames $\bar{c}_{br}=7.5$ and $\mu=0.1$

Table 6-16: Value of ϕ_{cr} for $\bar{c}_{br}=100$ and $\mu=0.001$

zt/zb	0	0.05	0.1	0.15	0.2	0.25	0.3	0.35	0.4	0.45	0.5	0.55	0.6	0.65	0.7	0.75	0.8	0.85	0.9	0.95	1
0	6.283	6.202	6.115	6.023	5.927	5.829	5.728	5.625	5.523	5.421	5.320	5.220	5.123	5.028	4.935	4.845	4.757	4.673	4.591	4.512	4.435
0.05		6.122	6.038	5.948	5.855	5.758	5.659	5.559	5.458	5.358	5.258	5.160	5.064	4.969	4.878	4.788	4.702	4.618	4.536	4.457	4.381
0.1			5.955	5.868	5.777	5.683	5.586	5.488	5.389	5.291	5.193	5.096	5.001	4.908	4.817	4.729	4.643	4.560	4.479	4.400	4.324
0.15				5.784	5.695	5.603	5.509	5.413	5.316	5.220	5.124	5.029	4.935	4.844	4.754	4.667	4.582	4.499	4.419	4.341	4.266
0.2					5.609	5.520	5.428	5.334	5.240	5.146	5.052	4.958	4.867	4.776	4.688	4.602	4.518	4.436	4.357	4.280	4.205
0.25						5.433	5.344	5.253	5.161	5.069	4.977	4.886	4.795	4.707	4.620	4.535	4.452	4.372	4.293	4.217	4.143
0.3							5.257	5.169	5.079	4.989	4.900	4.810	4.722	4.635	4.550	4.466	4.385	4.305	4.227	4.152	4.079
0.35								5.083	4.996	4.908	4.821	4.733	4.647	4.562	4.478	4.396	4.315	4.237	4.160	4.086	4.013
0.4									4.911	4.826	4.740	4.655	4.571	4.487	4.405	4.324	4.245	4.168	4.092	4.018	3.947
0.45										4.743	4.659	4.576	4.493	4.412	4.331	4.251	4.174	4.097	4.023	3.950	3.879
0.5											4.578	4.497	4.416	4.335	4.256	4.178	4.102	4.027	3.953	3.881	3.811
0.55												4.417	4.338	4.259	4.182	4.105	4.030	3.956	3.883	3.812	3.743
0.6													4.260	4.183	4.107	4.032	3.957	3.885	3.813	3.743	3.674
0.65														4.107	4.033	3.959	3.886	3.814	3.743	3.674	3.606
0.7															3.959	3.886	3.814	3.743	3.673	3.605	3.538
0.75																3.814	3.743	3.673	3.604	3.537	3.470
0.8																	3.673	3.604	3.536	3.469	3.403
0.85																		3.536	3.468	3.402	3.336
0.9																			3.401	3.336	3.271
0.95																				3.270	3.206
1																					3.142

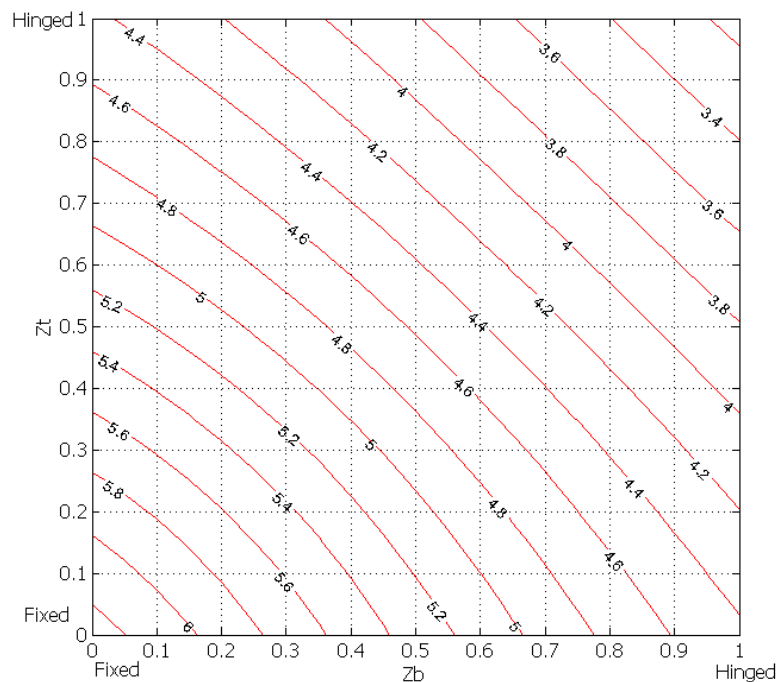
Figure 6-18: Graphical representation of the solution of buckling equation for partially-braced frames $\bar{c}_{br}=100$ and $\mu=0.001$

Table 6-17: Value of φ_{cr} for $\overline{c_{br}}=100$ and $\mu=0.01$

zt/zb	0	0.05	0.1	0.15	0.2	0.25	0.3	0.35	0.4	0.45	0.5	0.55	0.6	0.65	0.7	0.75	0.8	0.85	0.9	0.95	1
0	6.283	6.202	6.115	6.023	5.927	5.828	5.727	5.624	5.521	5.418	5.315	5.214	5.114	5.017	4.921	4.828	4.737	4.649	4.563	4.480	4.399
0.05		6.122	6.038	5.948	5.855	5.758	5.658	5.558	5.456	5.355	5.254	5.154	5.056	4.959	4.865	4.773	4.683	4.595	4.510	4.427	4.347
0.1			5.955	5.868	5.777	5.683	5.586	5.487	5.388	5.288	5.189	5.091	4.994	4.899	4.806	4.714	4.626	4.539	4.455	4.373	4.293
0.15				5.784	5.695	5.603	5.508	5.412	5.315	5.218	5.120	5.024	4.929	4.835	4.744	4.654	4.566	4.480	4.397	4.316	4.237
0.2					5.609	5.520	5.428	5.334	5.239	5.144	5.049	4.955	4.861	4.769	4.679	4.590	4.504	4.419	4.337	4.257	4.178
0.25						5.433	5.344	5.253	5.160	5.068	4.975	4.882	4.791	4.701	4.612	4.525	4.440	4.356	4.275	4.196	4.118
0.3							5.257	5.169	5.079	4.989	4.898	4.808	4.719	4.630	4.543	4.458	4.374	4.292	4.212	4.133	4.057
0.35								5.083	4.996	4.908	4.820	4.732	4.644	4.558	4.473	4.389	4.306	4.226	4.147	4.069	3.994
0.4									4.911	4.826	4.740	4.654	4.569	4.484	4.401	4.319	4.238	4.158	4.081	4.004	3.930
0.45										4.743	4.659	4.576	4.492	4.410	4.328	4.247	4.168	4.090	4.013	3.938	3.865
0.5											4.578	4.496	4.415	4.334	4.254	4.175	4.098	4.021	3.946	3.872	3.799
0.55												4.417	4.338	4.259	4.180	4.103	4.027	3.951	3.877	3.805	3.733
0.6													4.260	4.183	4.106	4.030	3.955	3.882	3.809	3.737	3.667
0.65														4.107	4.032	3.958	3.884	3.812	3.740	3.670	3.600
0.7															3.959	3.886	3.814	3.742	3.672	3.602	3.534
0.75																3.814	3.743	3.673	3.603	3.535	3.467
0.8																	3.673	3.604	3.535	3.468	3.401
0.85																		3.536	3.468	3.401	3.335
0.9																			3.401	3.335	3.270
0.95																				3.270	3.206
1																					3.142

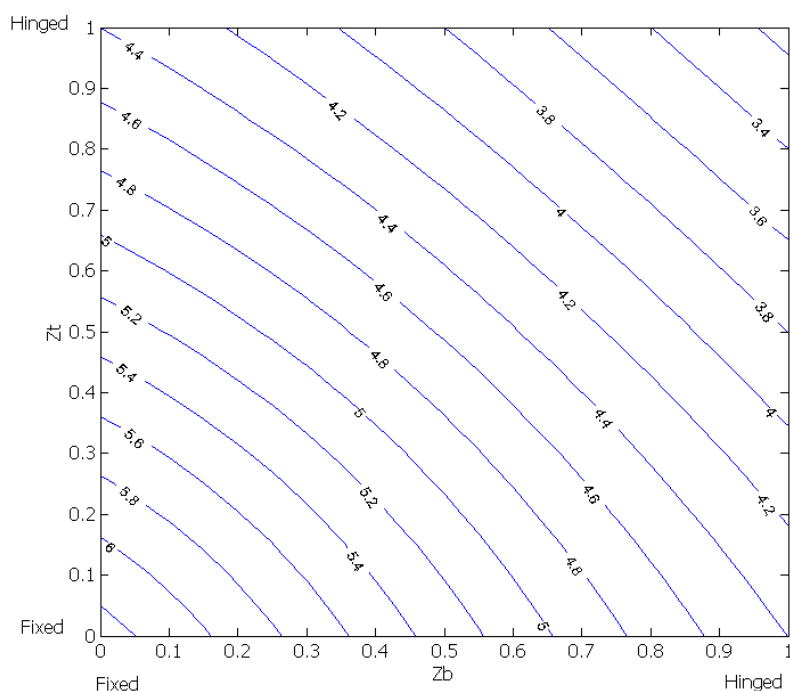
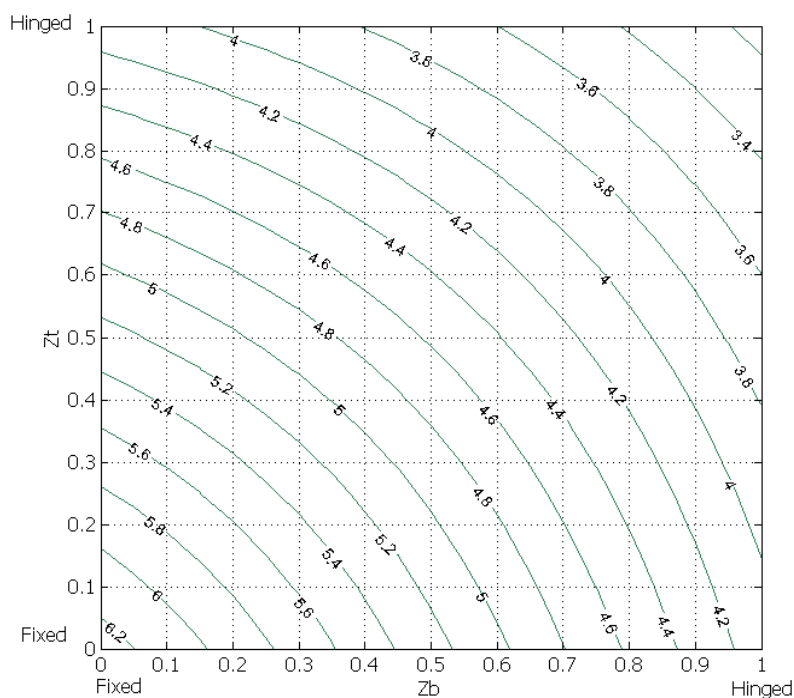
Figure 6-19: Graphical representation of the solution of buckling equation for partially-braced frames $\overline{c_{br}}=100$ and $\mu=0.01$

Table 6-18: Value of ϕ_{cr} for $\bar{c}_{br}=100$ and $\mu=0.1$

zt/zb	0	0.05	0.1	0.15	0.2	0.25	0.3	0.35	0.4	0.45	0.5	0.55	0.6	0.65	0.7	0.75	0.8	0.85	0.9	0.95	1
0	6.283	6.202	6.115	6.023	5.926	5.825	5.720	5.613	5.502	5.390	5.276	5.160	5.043	4.926	4.808	4.690	4.572	4.454	4.337	4.220	4.103
0.05		6.122	6.038	5.948	5.854	5.755	5.653	5.548	5.440	5.330	5.218	5.105	4.991	4.876	4.761	4.645	4.530	4.414	4.299	4.184	4.069
0.1			5.955	5.868	5.776	5.681	5.581	5.479	5.374	5.267	5.158	5.048	4.936	4.824	4.711	4.598	4.485	4.372	4.259	4.146	4.034
0.15				5.784	5.695	5.602	5.506	5.406	5.304	5.200	5.095	4.987	4.879	4.769	4.660	4.549	4.439	4.328	4.218	4.107	3.997
0.2					5.609	5.519	5.426	5.330	5.232	5.131	5.028	4.924	4.819	4.713	4.606	4.498	4.391	4.283	4.175	4.067	3.959
0.25						5.433	5.343	5.251	5.156	5.058	4.959	4.859	4.757	4.654	4.550	4.446	4.341	4.236	4.130	4.025	3.919
0.3							5.257	5.168	5.077	4.983	4.888	4.790	4.692	4.592	4.492	4.391	4.289	4.187	4.084	3.981	3.878
0.35								5.083	4.995	4.905	4.813	4.720	4.625	4.529	4.432	4.334	4.235	4.136	4.036	3.936	3.836
0.4									4.911	4.825	4.737	4.647	4.556	4.463	4.370	4.275	4.179	4.083	3.987	3.889	3.792
0.45										4.743	4.658	4.572	4.485	4.396	4.306	4.214	4.122	4.029	3.935	3.841	3.746
0.5											4.578	4.496	4.412	4.326	4.240	4.152	4.063	3.973	3.883	3.791	3.699
0.55												4.417	4.337	4.255	4.172	4.088	4.002	3.915	3.828	3.740	3.650
0.6													4.260	4.182	4.102	4.022	3.939	3.856	3.772	3.686	3.600
0.65														4.107	4.031	3.954	3.875	3.795	3.714	3.632	3.548
0.7															3.959	3.885	3.809	3.733	3.655	3.575	3.495
0.75																3.814	3.742	3.669	3.594	3.517	3.440
0.8																	3.673	3.603	3.531	3.458	3.383
0.85																		3.536	3.467	3.397	3.325
0.9																			3.401	3.334	3.266
0.95																				3.270	3.204
1																					3.142

Figure 6-20: Graphical representation of the solution of buckling equation for partially-braced frames $\bar{c}_{br}=100$ and $\mu=0.1$

6.2.2.2 Unbraced frame

The buckling equation for a frame free to sway can be derived by substituting c_{br} equal to zero in the buckling equation of the partially braced frame:

$$4(z_t(2z_b-1)-z_b)a_{cr}L\cos(a_{cr}L)+\left[z_tz_b(a_{cr}L)^2-16(z_t-1)(z_b-1)\right]\sin(a_{cr}L)=0 \quad (6-29)$$

It can be seen that Eq. (6-29) does not contain parameter β_{cr} (and in consequence parameter μ) and therefore its solution depends only on the distribution factors. It can be iteratively solved for $\varphi_{cr}=a_{cr}L$. The results for the unbraced frame are summarised in Table 6-19 and are the same as the ones found for unbraced Euler-Bernoulli members. The graphical presentation of the results in Table 6-19 is shown in Figure 6-21 as obtained with the use of Matlab [6-10].

Table 6-19: Value of φ_{cr} for unbraced frames

zt/zb	0	0.05	0.1	0.15	0.2	0.25	0.3	0.35	0.4	0.45	0.5	0.55	0.6	0.65	0.7	0.75	0.8	0.85	0.9	0.95	1
0	3.142	3.101	3.057	3.01	2.959	2.904	2.846	2.783	2.716	2.646	2.57	2.491	2.407	2.319	2.227	2.130	2.029	1.923	1.811	1.694	1.571
0.05		3.061	3.018	2.972	2.922	2.869	2.812	2.751	2.685	2.616	2.542	2.464	2.381	2.294	2.203	2.107	2.007	1.901	1.791	1.674	1.55
0.1			2.977	2.932	2.883	2.831	2.776	2.716	2.652	2.584	2.511	2.435	2.353	2.268	2.177	2.083	1.983	1.878	1.768	1.652	1.528
0.15				2.888	2.841	2.791	2.736	2.678	2.616	2.549	2.478	2.403	2.323	2.238	2.149	2.056	1.957	1.853	1.744	1.628	1.505
0.2					2.796	2.747	2.694	2.637	2.576	2.511	2.442	2.368	2.29	2.207	2.119	2.027	1.929	1.826	1.717	1.602	1.479
0.25						2.699	2.648	2.593	2.534	2.471	2.403	2.331	2.254	2.173	2.086	1.995	1.899	1.797	1.688	1.573	1.451
0.3							2.599	2.545	2.488	2.427	2.361	2.29	2.215	2.136	2.051	1.961	1.866	1.764	1.657	1.543	1.420
0.35								2.494	2.438	2.379	2.315	2.246	2.173	2.095	2.012	1.924	1.830	1.730	1.623	1.509	1.386
0.4									2.385	2.327	2.265	2.199	2.127	2.051	1.970	1.883	1.790	1.691	1.586	1.472	1.35
0.45										2.272	2.212	2.147	2.078	2.003	1.924	1.839	1.747	1.650	1.545	1.432	1.309
0.5											2.154	2.091	2.024	1.952	1.874	1.790	1.700	1.604	1.500	1.387	1.265
0.55												2.031	1.966	1.895	1.819	1.737	1.649	1.554	1.451	1.339	1.215
0.6													1.902	1.834	1.760	1.68	1.593	1.499	1.396	1.284	1.160
0.65														1.767	1.695	1.617	1.531	1.438	1.336	1.224	1.099
0.7															1.625	1.548	1.464	1.371	1.270	1.157	1.030
0.75																1.472	1.389	1.297	1.196	1.082	0.951
0.8																	1.307	1.215	1.112	0.996	0.860
0.85																		1.123	1.018	0.897	0.753
0.9																			0.909	0.781	0.621
0.95																				0.638	0.443
1																					0.314

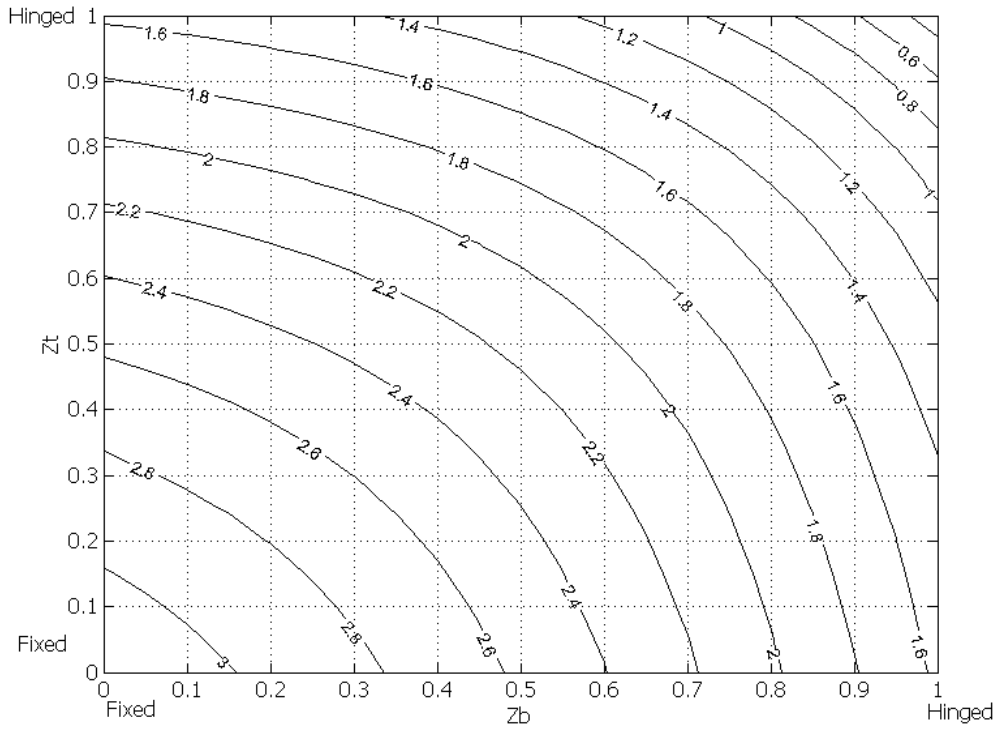


Figure 6-21: Graphical representation of the solution of buckling equation for unbraced frames

6.2.2.3 Braced frame

The buckling equation for a non-sway frame can be derived by substituting $1/c_{br}$ equal to zero in the buckling equation of the partially braced frame:

$$\begin{aligned}
 & 32(z_t - 1)(z_b - 1) - 4\cos(a_{cr}L) \left[8(z_t - 1)(z_b - 1) + (z_t + z_b - 2z_t z_b)(a_{cr}L)^2 \beta_{cr} \right] + \\
 & + \sin(a_{cr}L) \left[-16\beta_{cr}(a_{cr}L) + (z_t + z_b) \left(4(a_{cr}L) + 16\beta_{cr}(a_{cr}L) \right) + \right. \\
 & \left. + z_t z_b \left(\beta_{cr}(a_{cr}L)^3 - 8(a_{cr}L) - 16\beta_{cr}(a_{cr}L) \right) \right] = 0
 \end{aligned} \tag{6-30}$$

It can be seen that Eq. (6-30) can be iteratively solved for $\phi_{cr} = a_{cr}L$ for different values of the distribution factor and the parameter μ (that exists in parameter β_{cr}). The only case that it vanishes from the nonlinear equation is for springs with equal values of rotational stiffness as initially observed by Banerjee and Williams [6-9]. The results for values of the parameter μ equal to 0.001, 0.01 and 0.1 are shown in Table 6-20, Table 6-21 and Table 6-22 and graphically (as obtained with Matlab [6-10]) in Figure 6-22, Figure 6-23 and Figure 6-24, respectively. Red, blue and green colours are used for the graphs for μ equal to 0.001, 0.01 and 0.1, respectively.

Table 6-20: Value of ϕ_{cr} for braced frames and $\mu=0.001$

zt/zb	0	0.05	0.1	0.15	0.2	0.25	0.3	0.35	0.4	0.45	0.5	0.55	0.6	0.65	0.7	0.75	0.8	0.85	0.9	0.95	1
0	6.283	6.2	6.115	6.02	5.93	5.83	5.729	5.628	5.527	5.427	5.328	5.232	5.138	5.046	4.958	4.872	4.79	4.71	4.634	4.56	4.489
0.05		6.12	6.038	5.95	5.85	5.76	5.66	5.561	5.462	5.363	5.266	5.17	5.077	4.987	4.899	4.814	4.731	4.653	4.576	4.503	4.432
0.1			5.955	5.87	5.78	5.68	5.587	5.49	5.392	5.295	5.199	5.105	5.013	4.924	4.837	4.752	4.670	4.592	4.516	4.442	4.372
0.15				5.78	5.69	5.6	5.509	5.414	5.319	5.224	5.129	5.037	4.946	4.857	4.771	4.688	4.606	4.529	4.453	4.38	4.309
0.2					5.61	5.52	5.428	5.335	5.242	5.149	5.056	4.965	4.876	4.788	4.703	4.621	4.540	4.463	4.388	4.315	4.245
0.25						5.43	5.344	5.253	5.162	5.071	4.98	4.891	4.803	4.717	4.633	4.551	4.471	4.395	4.32	4.248	4.178
0.3							5.257	5.169	5.08	4.991	4.902	4.814	4.728	4.643	4.56	4.48	4.401	4.325	4.251	4.179	4.11
0.35								5.083	4.996	4.909	4.822	4.736	4.651	4.568	4.486	4.407	4.329	4.254	4.18	4.109	4.04
0.4									4.911	4.826	4.741	4.657	4.573	4.491	4.411	4.332	4.255	4.181	4.109	4.038	3.97
0.45										4.743	4.659	4.577	4.495	4.414	4.335	4.258	4.182	4.108	4.037	3.967	3.899
0.5											4.578	4.497	4.416	4.337	4.259	4.183	4.108	4.035	3.964	3.895	3.827
0.55												4.417	4.338	4.26	4.183	4.108	4.033	3.962	3.891	3.823	3.756
0.6													4.26	4.183	4.108	4.033	3.960	3.889	3.819	3.751	3.685
0.65														4.107	4.033	3.959	3.887	3.816	3.747	3.68	3.614
0.7															3.959	3.886	3.814	3.745	3.676	3.609	3.543
0.75																3.814	3.743	3.674	3.606	3.539	3.474
0.8																	3.673	3.604	3.537	3.47	3.405
0.85																		3.536	3.468	3.402	3.338
0.9																			3.401	3.336	3.271
0.95																				3.27	3.206
1																					3.142

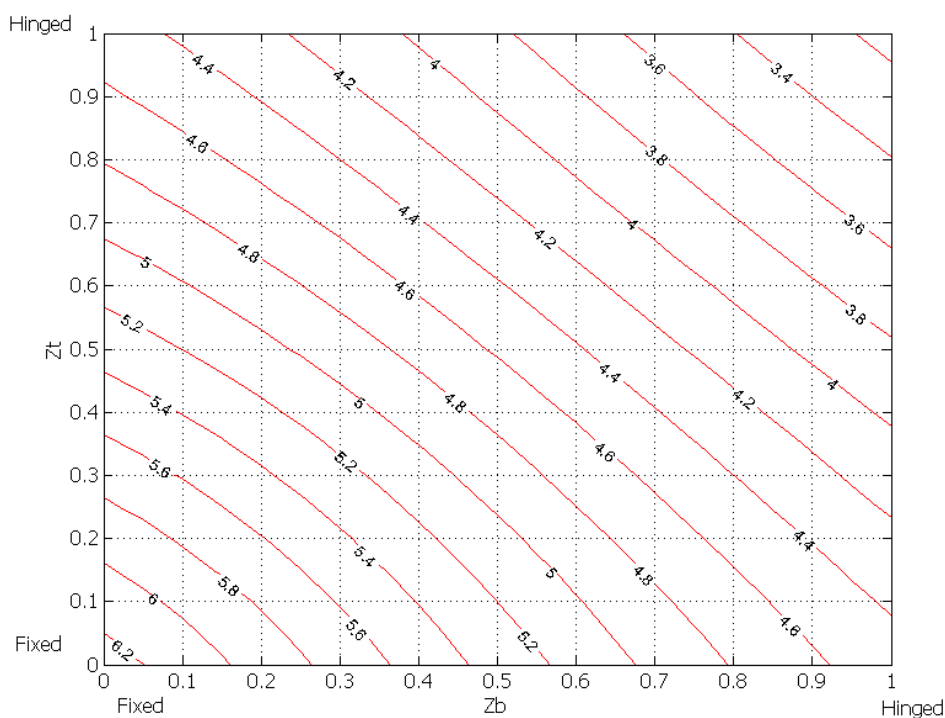
Figure 6-22: Graphical representation of the solution of buckling equation for braced frames and $\mu=0.001$

Table 6-21: Value of ϕ_{cr} for braced frames and $\mu=0.01$

zt/zb	0	0.05	0.1	0.15	0.2	0.25	0.3	0.35	0.4	0.45	0.5	0.55	0.6	0.65	0.7	0.75	0.8	0.85	0.9	0.95	1
0	6.283	6.2	6.115	6.02	5.93	5.83	5.728	5.626	5.524	5.423	5.323	5.224	5.128	5.033	4.942	4.853	4.767	4.684	4.603	4.525	4.449
0.05		6.12	6.038	5.95	5.85	5.76	5.66	5.56	5.459	5.359	5.261	5.163	5.068	4.975	4.884	4.796	4.71	4.627	4.547	4.469	4.394
0.1			5.955	5.87	5.78	5.68	5.586	5.489	5.39	5.292	5.195	5.099	5.005	4.913	4.823	4.736	4.651	4.569	4.489	4.412	4.337
0.15				5.78	5.69	5.6	5.509	5.413	5.317	5.221	5.126	5.031	4.939	4.848	4.759	4.673	4.589	4.507	4.428	4.351	4.277
0.2					5.61	5.52	5.428	5.335	5.241	5.147	5.053	4.96	4.869	4.78	4.692	4.607	4.524	4.443	4.365	4.289	4.215
0.25						5.43	5.344	5.253	5.161	5.069	4.978	4.887	4.798	4.71	4.624	4.539	4.457	4.378	4.3	4.225	4.151
0.3							5.257	5.169	5.08	4.99	4.9	4.811	4.724	4.637	4.553	4.47	4.389	4.31	4.233	4.159	4.086
0.35								5.083	4.996	4.909	4.821	4.734	4.648	4.563	4.48	4.399	4.319	4.241	4.165	4.091	4.02
0.4									4.911	4.826	4.741	4.656	4.571	4.488	4.406	4.326	4.248	4.171	4.096	4.023	3.952
0.45										4.743	4.659	4.576	4.494	4.412	4.332	4.253	4.176	4.1	4.026	3.954	3.884
0.5											4.578	4.497	4.416	4.336	4.257	4.179	4.103	4.029	3.956	3.884	3.815
0.55												4.417	4.338	4.259	4.182	4.106	4.031	3.957	3.885	3.815	3.746
0.6													4.26	4.183	4.107	4.032	3.958	3.886	3.814	3.745	3.677
0.65														4.107	4.033	3.959	3.886	3.814	3.744	3.675	3.608
0.7															3.959	3.886	3.814	3.744	3.674	3.606	3.539
0.75																3.814	3.743	3.673	3.605	3.537	3.471
0.8																	3.673	3.604	3.536	3.469	3.403
0.85																		3.536	3.468	3.402	3.337
0.9																			3.401	3.336	3.271
0.95																				3.27	3.206
1																					3.142

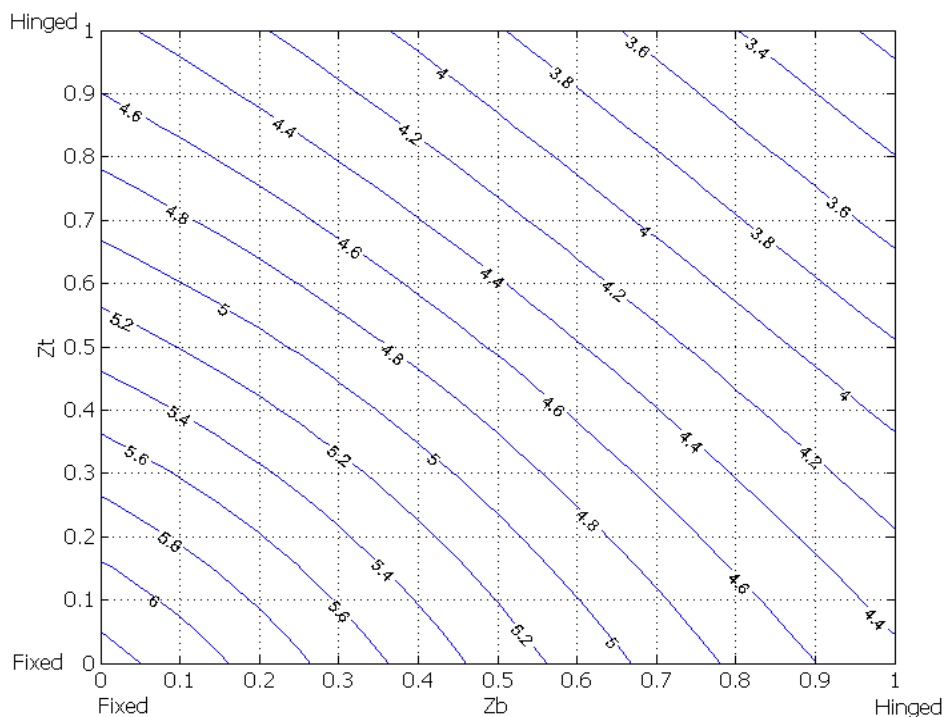
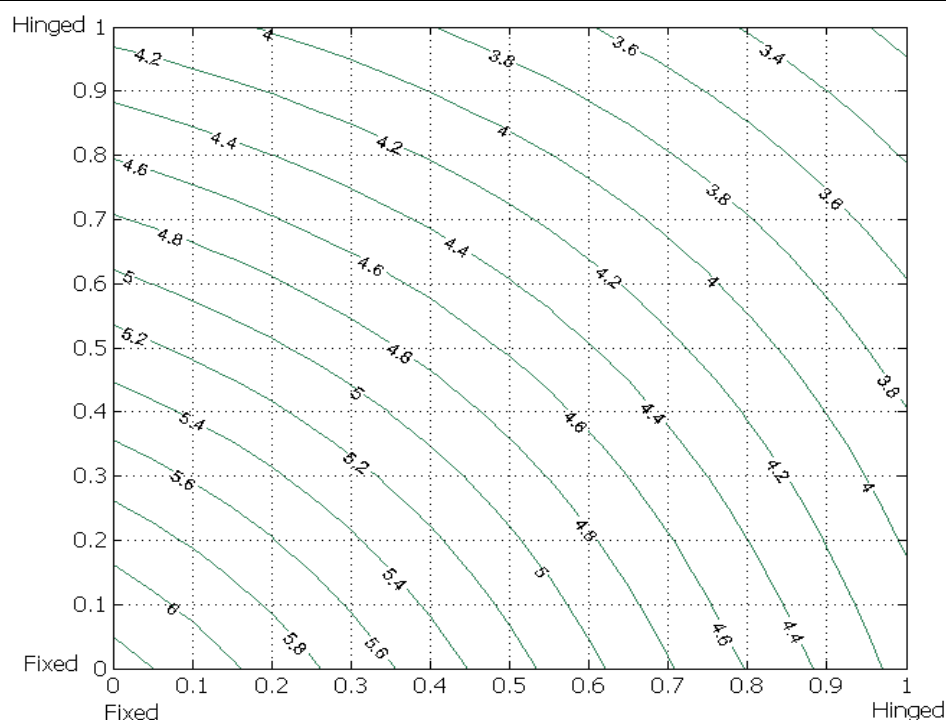
Figure 6-23: Graphical representation of the solution of buckling equation for braced frames and $\mu=0.01$

Table 6-22: Value of ϕ_{cr} for braced frames and $\mu=0.1$

zt/zb	0	0.05	0.1	0.15	0.2	0.25	0.3	0.35	0.4	0.45	0.5	0.55	0.6	0.65	0.7	0.75	0.8	0.85	0.9	0.95	1
0	6.283	6.2	6.115	6.02	5.93	5.83	5.721	5.614	5.504	5.393	5.279	5.165	5.05	4.935	4.819	4.704	4.588	4.473	4.359	4.245	4.132
0.05		6.12	6.038	5.95	5.85	5.76	5.654	5.549	5.442	5.332	5.222	5.11	4.997	4.884	4.771	4.658	4.544	4.432	4.319	4.208	4.097
0.1			5.955	5.87	5.78	5.68	5.582	5.48	5.375	5.269	5.161	5.052	4.942	4.831	4.72	4.61	4.499	4.388	4.278	4.169	4.059
0.15				5.78	5.69	5.6	5.506	5.407	5.306	5.202	5.097	4.991	4.884	4.776	4.668	4.559	4.451	4.343	4.235	4.128	4.021
0.2					5.61	5.52	5.426	5.331	5.232	5.132	5.03	4.927	4.823	4.718	4.613	4.507	4.402	4.296	4.191	4.086	3.981
0.25						5.43	5.343	5.251	5.156	5.059	4.961	4.861	4.76	4.658	4.556	4.453	4.35	4.247	4.145	4.042	3.939
0.3							5.257	5.168	5.077	4.984	4.889	4.792	4.694	4.596	4.497	4.397	4.297	4.197	4.097	3.996	3.896
0.35								5.083	4.995	4.906	4.814	4.721	4.627	4.532	4.436	4.339	4.242	4.145	4.047	3.949	3.852
0.4									4.911	4.825	4.737	4.648	4.557	4.465	4.373	4.279	4.185	4.091	3.996	3.901	3.806
0.45										4.743	4.658	4.573	4.485	4.397	4.308	4.218	4.127	4.035	3.943	3.851	3.758
0.5											4.578	4.496	4.412	4.327	4.241	4.154	4.066	3.978	3.889	3.799	3.709
0.55												4.417	4.337	4.255	4.173	4.089	4.004	3.919	3.833	3.746	3.659
0.6													4.26	4.182	4.103	4.022	3.941	3.859	3.776	3.692	3.607
0.65														4.107	4.032	3.954	3.876	3.797	3.717	3.636	3.554
0.7															3.959	3.885	3.81	3.734	3.656	3.578	3.499
0.75																3.814	3.742	3.669	3.595	3.519	3.443
0.8																	3.673	3.603	3.532	3.459	3.385
0.85																		3.536	3.467	3.397	3.327
0.9																			3.401	3.334	3.266
0.95																				3.27	3.205
1																					3.142



It is also interesting to compare the effect of factor μ on the value of $\phi_{cr}=a_{cr}L$ by plotting the results for the different values of μ in the same graph (Figure 6-25). As it was previously mentioned, the only case in which parameter μ vanishes from the nonlinear equation is for springs with equal values of rotational stiffness ($z_b=z_t$). For this reason, the value of ϕ_{cr} is exactly the same along the diagonal (from 0 to 1) of the plot.

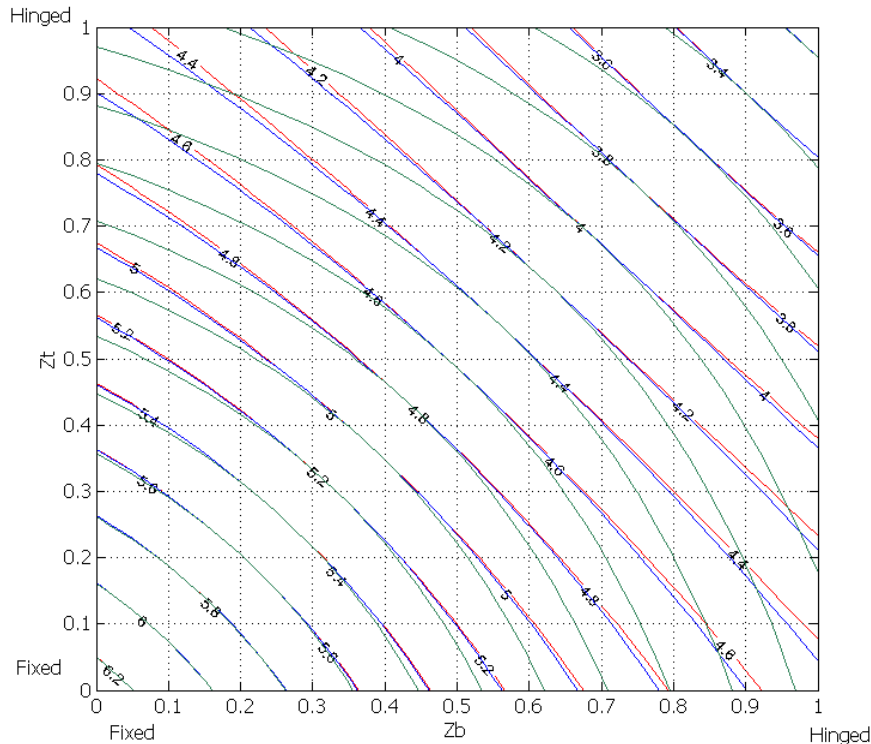


Figure 6-25: Effect of μ on value of $\phi_{cr}=a_{cr}L$

6.3 SLOPE-DEFLECTION EQUATIONS FOR TIMOSHENKO MEMBERS

Slope-deflection equations are used for the static analysis of determinate and indeterminate structures. Using equilibrium and compatibility conditions, the deflections and rotations can be calculated. Afterwards, the reactions can be evaluated leading to the calculation of bending moments, shear forces and axial forces in the structure's members. In this section, slope-deflection equations for Timoshenko members (based on Engesser's theory) either with rigid or semi-rigid connections are presented for both second-order and first-order analyses.

6.3.1 Semi-rigid connections at the ends

Connections have specific rotational stiffness that varies between the hinged and the rigid case. In the first case the connections have zero rotational stiffness, while in the second case the rotational stiffness approaches infinity. In this section, slope-deflection equations for Timoshenko members with semi-rigid connections are presented.

6.3.1.1 Second-order analysis

Consider the Timoshenko member i of Figure 6-26 that has semi-rigid connections at its ends and is subjected to axial compressive force and clockwise moments at the ends. At its ends the effect of semi-rigid connections is taken into account with the use of rotational springs. The deformed configuration with the corresponding displacements and rotations at the ends are also depicted. The

parameters to be used were described in Chapter 2. The bending moment along the member is equal to:

$$M = -EI_i \psi' = M_{n(i)} - \frac{M_{n(i)} + M_{f(i)} + P\Delta_i}{L_i} x + Pw \quad (6-31)$$

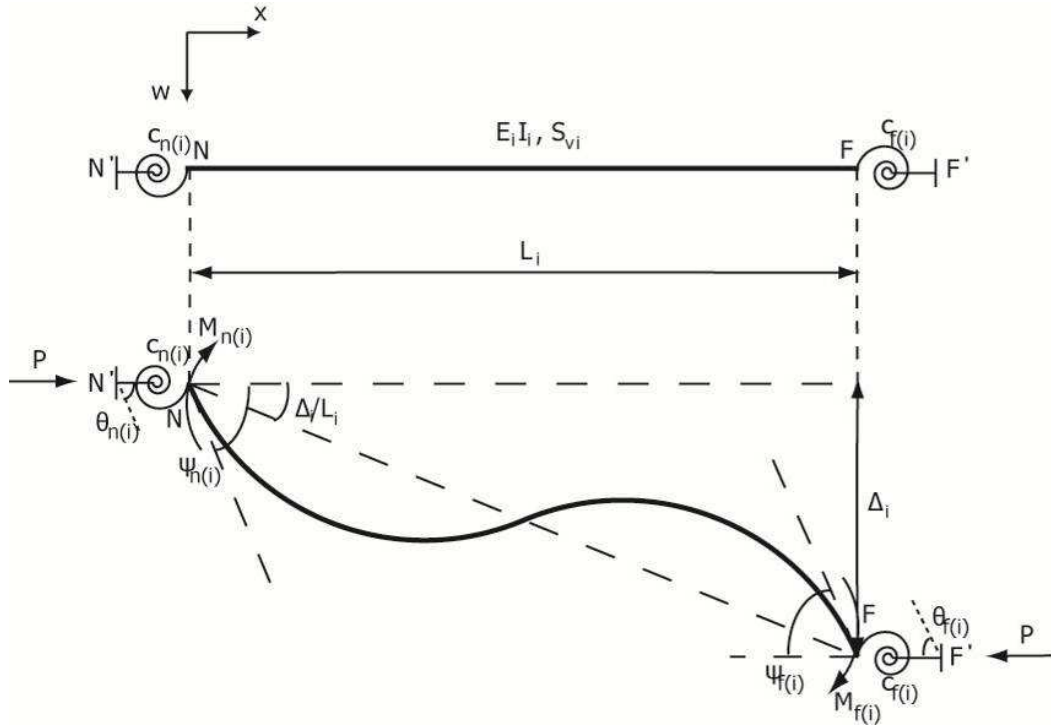


Figure 6-26: Undeformed and deformed shapes of a shear-weak member with semi-rigid connections at its ends under the application of axial compressive force and clockwise moments at both ends

Solving Eq. (6-31) for w and differentiating it with respect to x gives:

$$w' = \frac{-EI_i \psi'' + \frac{M_{n(i)} + M_{f(i)} + P\Delta_i}{L_i}}{P} \quad (6-32)$$

The shear force perpendicular to the deformed axis arises by differentiating Eq. (6-31) once and is equal to:

$$Q = -EI_i \psi'' = Pw' - \frac{M_{n(i)} + M_{f(i)} + P\Delta_i}{L_i} \quad (6-33)$$

The shear deformation according to Hooke's law is equal to:

$$\gamma = \frac{Q}{S_{v(i)}} \quad (6-34)$$

Based on Eq. (6-33), Eq. (6-34) becomes:

$$\gamma = \frac{-E I_i \psi''}{S_{v(i)}} \quad (6-35)$$

As also described in Chapter 2, the total rotation w' consists of the rotation ψ due to bending only and of the shear deformation γ :

$$w' = \psi + \gamma \quad (6-36)$$

Making use of Eq. (6-32) and Eq. (6-35), Eq. (6-36) yields the following differential equation that controls the problem:

$$E I_i \psi'' \left(1 - \frac{P}{S_{v(i)}} \right) + P \psi = \frac{M_{n(i)} + M_{f(i)} + P \Delta_i}{L_i} \quad (6-37)$$

The solution of the differential Eq. (6-37) is:

$$\psi(x) = B_{1(i)} \sin(\alpha_i x) + B_{2(i)} \cos(\alpha_i x) + B_{3(i)} x + \frac{M_{n(i)} + M_{f(i)} + P \Delta_i}{P L_i} \quad (6-38)$$

where B parameters are integration constants,

$$\alpha_i^2 = \frac{P}{E I_i \beta_i} \quad (6-39)$$

$$\beta_i = \left(1 - \frac{P}{S_{v(i)}} \right) \quad (6-40)$$

Differentiating Eq. (6-35) once gives:

$$\gamma' = \frac{-E I_i \psi'''}{S_{v(i)}} \quad (6-41)$$

Solving Eq. (6-31) for ψ' gives:

$$\psi' = \frac{-M_{n(i)} + \left(M_{n(i)} + M_{f(i)} + P \Delta_i \right) \frac{x}{L_i} - P w}{E I_i} \quad (6-42)$$

Differentiating Eq. (6-36) once and making use of Eq. (6-41) and Eq. (6-42), the following differential equation is obtained:

$$E I_i w'' \left(1 - \frac{P}{S_{v(i)}} \right) + P w = -M_{n(i)} + \left(M_{n(i)} + M_{f(i)} + P \Delta_i \right) \frac{x}{L_i} \quad (6-43)$$

Eq. (6-43) is the second differential equation that controls the problem. Its solution is:

$$w(x) = A_{1(i)} \sin(\alpha_i x) + A_{2(i)} \cos(\alpha_i x) + A_{3(i)} x + \frac{M_{n(i)} + M_{f(i)} + P\Delta_i}{P} \frac{x}{L_i} - \frac{M_{n(i)}}{P} \quad (6-44)$$

The parameters B can be expressed in terms of the parameters A by making use of Eq. (6-36) and Eq. (6-41), transforming Eq. (6-38) into:

$$\psi(x) = -\alpha_i \beta_i A_{2(i)} \sin(\alpha_i x) + \alpha_i \beta_i A_{1(i)} \cos(\alpha_i x) + \frac{M_{n(i)} + M_{f(i)} + P\Delta_i}{PL_i} \quad (6-45)$$

The boundary conditions are:

$$w(0) = 0 \quad (6-46)$$

$$w(L_i) = \Delta_i \quad (6-47)$$

$$\psi(0) = \psi_{n(i)} \quad (6-48)$$

$$\psi(L_i) = \psi_{f(i)} \quad (6-49)$$

Applying the expressions of Eq. (6-44) and Eq. (6-45) to the boundary conditions the rotations due to bending are obtained:

$$\psi_{n(i)} = \frac{\sin(\alpha_i L_i) - \alpha_i \beta_i L_i \cos(\alpha_i L_i)}{\alpha_i^2 \beta_i L_i \sin(\alpha_i L_i)} \left(\frac{M_{n(i)}}{EI_i} \right) + \frac{-\alpha_i \beta_i L_i + \sin(\alpha_i L_i)}{\alpha_i^2 \beta_i L_i \sin(\alpha_i L_i)} \left(\frac{M_{f(i)}}{EI_i} \right) + \frac{\Delta_i}{L_i} \quad (6-50)$$

$$\psi_{f(i)} = \frac{\sin(\alpha_i L_i) - \alpha_i \beta_i L_i \cos(\alpha_i L_i)}{\alpha_i^2 \beta_i L_i \sin(\alpha_i L_i)} \left(\frac{M_{f(i)}}{EI_i} \right) + \frac{-\alpha_i \beta_i L_i + \sin(\alpha_i L_i)}{\alpha_i^2 \beta_i L_i \sin(\alpha_i L_i)} \left(\frac{M_{n(i)}}{EI_i} \right) + \frac{\Delta_i}{L_i} \quad (6-51)$$

Setting $\phi_i = \alpha_i L_i$ in the previous equations the rotations due to bending at points N and F are obtained. The bending rotations at points N' and F' can be obtained by including the effect of the semi-rigid connections as:

$$\theta_{n(i)} = \psi_{n(i)} + \frac{M_{n(i)}}{C_{n(i)}} \quad (6-52)$$

$$\theta_{f(i)} = \psi_{f(i)} + \frac{M_{f(i)}}{C_{f(i)}} \quad (6-53)$$

By making use of Eq. (6-50), (6-51), (6-52) and (6-53) and rearranging appropriately the terms, the slope-deflection equations for shear-weak members with semi-rigid connections at their ends can be obtained as:

$$M_{n(i)} = \frac{EI_i}{L_i} A_{11(i)} \left(\theta_{n(i)} - \frac{\Delta_i}{L_i} \right) + \frac{EI_i}{L_i} A_{12(i)} \left(\theta_{f(i)} - \frac{\Delta_i}{L_i} \right) \quad (6-54)$$

$$M_{f(i)} = \frac{E_i I_i}{L_i} A_{21(i)} \left(\theta_{n(i)} - \frac{\Delta_i}{L_i} \right) + \frac{E_i I_i}{L_i} A_{22(i)} \left(\theta_{f(i)} - \frac{\Delta_i}{L_i} \right) \quad (6-55)$$

The stiffness coefficients are summarised in Table 6-23. In their derivation the distribution factors used for the elastic critical buckling load are also inserted:

$$z_{n(i)} = \frac{c_{m(i)}}{c_{m(i)} + c_{n(i)}}, \quad z_{f(i)} = \frac{c_{m(i)}}{c_{m(i)} + c_{f(i)}} \quad (6-56)$$

where

$$c_{m(i)} = \frac{4E_i I_i}{L_i} \quad (6-57)$$

Table 6-23: Stiffness coefficients for axially loaded Timoshenko member with semi-rigid connections

$A_{11(i)} = \frac{(1-z_{n(i)})(1-z_{f(i)}) \left(1 - \frac{\beta_i \varphi_i}{\tan \varphi_i} \right) + \frac{1}{4} (1-z_{n(i)}) z_{f(i)} \beta_i \varphi_i^2}{(1-z_{n(i)})(1-z_{f(i)}) \left(\frac{2 \tan(0.5 \varphi_i)}{\varphi_i} - \beta_i \right) + \frac{1}{4} ((1-z_{n(i)}) z_{f(i)} + (1-z_{f(i)}) z_{n(i)}) \left(1 - \frac{\beta_i \varphi_i}{\tan \varphi_i} \right) + \frac{1}{16} z_{n(i)} z_{f(i)} \beta_i \varphi_i^2}$
$A_{12(i)} = A_{21(i)} = \frac{(1-z_{n(i)})(1-z_{f(i)}) \left(\frac{\beta_i \varphi_i}{\sin \varphi_i} - 1 \right)}{(1-z_{n(i)})(1-z_{f(i)}) \left(\frac{2 \tan(0.5 \varphi_i)}{\varphi_i} - \beta_i \right) + \frac{1}{4} ((1-z_{n(i)}) z_{f(i)} + (1-z_{f(i)}) z_{n(i)}) \left(1 - \frac{\beta_i \varphi_i}{\tan \varphi_i} \right) + \frac{1}{16} z_{n(i)} z_{f(i)} \beta_i \varphi_i^2}$
$A_{22(i)} = \frac{(1-z_{n(i)})(1-z_{f(i)}) \left(1 - \frac{\beta_i \varphi_i}{\tan \varphi_i} \right) + \frac{1}{4} (1-z_{f(i)}) z_{n(i)} \beta_i \varphi_i^2}{(1-z_{n(i)})(1-z_{f(i)}) \left(\frac{2 \tan(0.5 \varphi_i)}{\varphi_i} - \beta_i \right) + \frac{1}{4} ((1-z_{n(i)}) z_{f(i)} + (1-z_{f(i)}) z_{n(i)}) \left(1 - \frac{\beta_i \varphi_i}{\tan \varphi_i} \right) + \frac{1}{16} z_{n(i)} z_{f(i)} \beta_i \varphi_i^2}$

6.3.1.2 First-order analysis

For the case without axial force the procedure is similar if P is set equal to zero and 3rd and 2nd order polynomial functions are used for the total lateral deflection $w(x)$ and rotation $\psi(x)$ due to bending only, respectively.

For zero axial force P Eq. (6-37) becomes:

$$E_i I_i \psi'' = \frac{M_{n(i)} + M_{f(i)}}{L_i} \quad (6-58)$$

For zero axial force P Eq. (6-43) becomes:

$$E_i I_i w'' = -M_{n(i)} + (M_{n(i)} + M_{f(i)}) \frac{x}{L_i} \quad (6-59)$$

Applying the boundary conditions of Eqs. (6-46)-(6-49), the integration constants of the polynomial solutions can be obtained resulting in the following closed-form solutions for rotations ψ due to bending only:

$$\psi_{n(i)} = \left(\frac{1}{3} + \mu_i\right) \left(\frac{M_{n(i)} L_i}{E I_i}\right) + \left(-\frac{1}{6} + \mu_i\right) \left(\frac{M_{f(i)} L_i}{E I_i}\right) + \frac{\Delta_i}{L_i} \quad (6-60)$$

$$\psi_{f(i)} = \left(\frac{1}{3} + \mu_i\right) \left(\frac{M_{f(i)} L_i}{E I_i}\right) + \left(-\frac{1}{6} + \mu_i\right) \left(\frac{M_{n(i)} L_i}{E I_i}\right) + \frac{\Delta_i}{L_i} \quad (6-61)$$

The dimensionless shear parameter μ_i can be obtained by:

$$\mu_i = \frac{E I_i}{S_{v(i)} L_i^2} \quad (6-62)$$

Rearranging the terms and making use of Eq. (6-52) and Eq. (6-53) leads to the following expressions for the first-order slope deflection equations for Timoshenko members with semi-rigid connections:

$$M_{n(i)} = \frac{E I_i}{L_i} A'_{11(i)} \left(\theta_{n(i)} - \frac{\Delta_i}{L_i}\right) + \frac{E I_i}{L_i} A'_{12(i)} \left(\theta_{f(i)} - \frac{\Delta_i}{L_i}\right) \quad (6-63)$$

$$M_{f(i)} = \frac{E I_i}{L_i} A'_{21(i)} \left(\theta_{n(i)} - \frac{\Delta_i}{L_i}\right) + \frac{E I_i}{L_i} A'_{22(i)} \left(\theta_{f(i)} - \frac{\Delta_i}{L_i}\right) \quad (6-64)$$

The stiffness coefficients are summarised in Table 6-24.

Table 6-24: Stiffness coefficients for non-axially loaded Timoshenko member with semi-rigid connections

$A'_{11(i)} = \frac{4(4+12\mu_i)(1-z_{n(i)})(1-z_{f(i)}) + 12(1-z_{n(i)})z_{f(i)}}{4(1+12\mu_i)(1-z_{n(i)})(1-z_{f(i)}) + (4+12\mu_i)((1-z_{n(i)})z_{f(i)} + (1-z_{f(i)})z_{n(i)}) + 3z_{n(i)}z_{f(i)}}$
$A'_{12(i)} = A'_{21(i)} = \frac{4(2-12\mu_i)(1-z_{n(i)})(1-z_{f(i)})}{4(1+12\mu_i)(1-z_{n(i)})(1-z_{f(i)}) + (4+12\mu_i)((1-z_{n(i)})z_{f(i)} + (1-z_{f(i)})z_{n(i)}) + 3z_{n(i)}z_{f(i)}}$
$A'_{22(i)} = \frac{4(4+12\mu_i)(1-z_{n(i)})(1-z_{f(i)}) + 12(1-z_{f(i)})z_{n(i)}}{4(1+12\mu_i)(1-z_{n(i)})(1-z_{f(i)}) + (4+12\mu_i)((1-z_{n(i)})z_{f(i)} + (1-z_{f(i)})z_{n(i)}) + 3z_{n(i)}z_{f(i)}}$

6.3.2 Rigid connections at the ends

Rotationally very stiff connections are characterised as rigid connections. The rotational stiffness of these connections approaches infinity. In this section slope-deflection equations for Timoshenko members with rigid connections are presented.

6.3.2.1 Second-order analysis

In order to account for rigid connections at the ends of the Timoshenko member, the distribution factors in the second-order coefficients for semi-rigid connections should be set equal to zero. In such a case the slope-deflection equations for axially loaded Timoshenko member become:

$$M_{n(i)} = \frac{E_i I_i}{L_i} S_{11(i)} \left(\psi_{n(i)} - \frac{\Delta_i}{L_i} \right) + \frac{E_i I_i}{L_i} S_{12(i)} \left(\psi_{f(i)} - \frac{\Delta_i}{L_i} \right) \quad (6-65)$$

$$M_{f(i)} = \frac{E_i I_i}{L_i} S_{21(i)} \left(\psi_{n(i)} - \frac{\Delta_i}{L_i} \right) + \frac{E_i I_i}{L_i} S_{22(i)} \left(\psi_{f(i)} - \frac{\Delta_i}{L_i} \right) \quad (6-66)$$

The distribution factors are summarised in Table 6-25. They were initially derived by Absi [6-6].

Table 6-25: Stiffness coefficients for axially loaded Timoshenko member with rigid connections

$S_{11(i)} = S_{22(i)} = \frac{\varphi_i \sin \varphi_i - \beta_i \varphi_i^2 \cos \varphi_i}{-2 \cos \varphi_i - \beta_i \varphi_i \sin \varphi_i + 2}$
$S_{12(i)} = S_{21(i)} = \frac{\beta_i \varphi_i^2 - \varphi_i \sin \varphi_i}{-2 \cos \varphi_i - \beta_i \varphi_i \sin \varphi_i + 2}$

6.3.2.2 First-order analysis

In order to account for rigid connections at the ends of the Timoshenko member, the distribution factors in the first-order coefficients for semi-rigid connections should be set equal to zero. The slope-deflection equations for non-axially loaded Timoshenko member become:

$$M_{n(i)} = \frac{E_i I_i}{L_i} S'_{11(i)} \left(\psi_{n(i)} - \frac{\Delta_i}{L_i} \right) + \frac{E_i I_i}{L_i} S'_{12(i)} \left(\psi_{f(i)} - \frac{\Delta_i}{L_i} \right) \quad (6-67)$$

$$M_{f(i)} = \frac{E_i I_i}{L_i} S'_{21(i)} \left(\psi_{n(i)} - \frac{\Delta_i}{L_i} \right) + \frac{E_i I_i}{L_i} S'_{22(i)} \left(\psi_{f(i)} - \frac{\Delta_i}{L_i} \right) \quad (6-68)$$

Table 6-26: Stiffness coefficients for non-axially loaded Timoshenko member with rigid connections

$S'_{11(i)} = S'_{22(i)} = \frac{4 + 12\mu_i}{1 + 12\mu_i}$
$S'_{12(i)} = S'_{21(i)} = \frac{2 - 12\mu_i}{1 + 12\mu_i}$

6.4 ROTATIONAL STIFFNESSES

As explained before, the members that converge to the top and bottom node of a column, offer resistance to rotation that can be modelled as an equivalent spring at each end. The resistance that a converging member offers can be evaluated by considering the slope-deflection equations. The derivation of the rotational stiffness of the springs for three specific cases is described in detail next.

6.4.1 Fixed support at the far end and a semi-rigid connection at the near end, without axial force

Consider a member i of length L_i , bending rigidity $E_i I_i$ and shear rigidity $S_{v(i)}$, extending from near end N to far end F . The member has a fixed support at its far end F , while the flexibility of the beam-column connection at its near end N is modelled by means of a rotational spring of stiffness $c_{n(i)}$ (Figure 6-27).

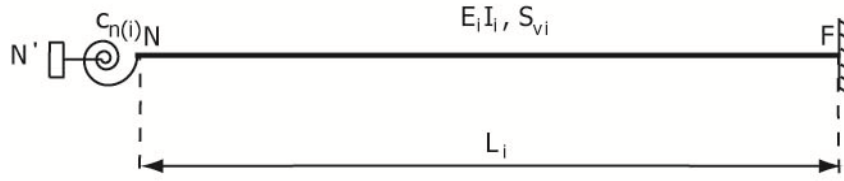


Figure 6-27: Shear-weak member with semi-rigid connection at the near end and fixed support at the far end

The bending rotation at the far end and the differential transverse displacement are equal to zero:

$$\theta_{f(i)} = 0 \quad (6-69)$$

$$\Delta_i = 0 \quad (6-70)$$

Making use of Eq. (6-63) the following expression arises:

$$M_{n(i)} = \frac{E_i I_i}{L_i} A'_{11(i)} \theta_{n(i)} \quad (6-71)$$

The rotational stiffness for this case is equal to the multiplier of $\theta_{n(i)}$. As the connection at the far end is rigid, $z_{f(i)} = 0$ should be substituted in $A'_{11(i)}$.

6.4.2 Rotationally fixed support at the far end and a rigid connection at the near end, with axial force

Consider a member NF of length L_i , bending rigidity $E_i I_i$ and shear rigidity S_{vi} . The member (Figure 6-28) has a rotationally fixed support ($\theta_{f(i)} = 0$) at the far end and the presence of axial force leads to the appearance of second-order effects. The connection at the close end is rigid ($c_{n(i)} = \infty$).

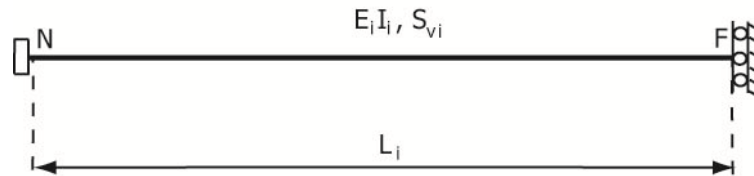


Figure 6-28: Shear-weak member with rigid connection at the near end and rotationally fixed support at the far end

The bending moment at the near end N according to Eq. (6-54) is equal to:

$$M_{n(i)} = \frac{E_i I_i}{L_i} \left[A_{11(i)} \theta_{n(i)} - (A_{11(i)} + A_{12(i)}) \frac{\Delta_i}{L_i} \right] \quad (6-72)$$

Considering that the connection at the near end is also rigid, Eq. (6-72) becomes:

$$M_{n(i)} = \frac{E_i I_i}{L_i} \left[S_{11(i)} \psi_{n(i)} - (S_{11(i)} + S_{12(i)}) \frac{\Delta_i}{L_i} \right] \quad (6-73)$$

The bending moment at the far end F is equal to:

$$M_{f(i)} = \frac{E_i I_i}{L_i} \left[S_{12(i)} \left(\psi_{n(i)} - \frac{\Delta_i}{L_i} \right) - S_{11(i)} \frac{\Delta_i}{L_i} \right] \quad (6-74)$$

By considering the moment equilibrium of the member, the relative lateral deflection between the points N and F is calculated:

$$M_{n(i)} + M_{f(i)} + P \Delta_i = 0 \Rightarrow \Delta_i = \psi_{n(i)} \left(\frac{2}{L_i} - \frac{P L_i}{E_i I_i (S_{11(i)} + S_{12(i)})} \right)^{-1} \quad (6-75)$$

Resubstituting Eq. (6-75) into Eq. (6-73), the rotational stiffness of the member is obtained:

$$c_i = \frac{E_i I_i}{L_i} \left[S_{11(i)} - \frac{(S_{11(i)} + S_{12(i)})}{\left(2 - \frac{P L_i^2}{E_i I_i (S_{11(i)} + S_{12(i)})} \right)} \right] \quad (6-76)$$

6.4.3 Rotational and translational spring at the far end and a rigid connection at the near end, with axial force

Consider a member NF of length L_i , bending rigidity $E_i I_i$ and shear rigidity S_{vi} . The member (Figure 6-29) has a rotational and a translational spring at the far end and the presence of axial force leads to the appearance of second-order effects. The connection at the close end is rigid ($c_{n(i)} = \infty$).

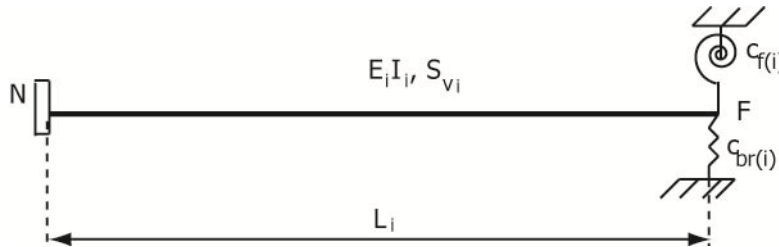


Figure 6-29: Shear-weak member with rigid connection at the near end and a rotational and a translational spring at the far end

The bending moment at the far end F according to Eq. (6-55) is equal to:

$$M_{f(i)} = \frac{E_i I_i}{L_i} A_{21(i)} \left(\theta_{n(i)} - \frac{\Delta_i}{L_i} \right) + \frac{E_i I_i}{L_i} A_{22(i)} \left(\theta_{f(i)} - \frac{\Delta_i}{L_i} \right) \quad (6-77)$$

Considering that the connection at the near end is also rigid, Eq. (6-77) becomes:

$$M_{f(i)} = \frac{E_i I_i}{L_i} S_{21(i)} \left(\psi_{n(i)} - \frac{\Delta_i}{L_i} \right) + \frac{E_i I_i}{L_i} S_{22(i)} \left(\psi_{f(i)} - \frac{\Delta_i}{L_i} \right) \quad (6-78)$$

The bending moment at the far end F is also equal to:

$$M_{f(i)} = -c_{f(i)} \psi_{f(i)} \quad (6-79)$$

By setting Eq. (6-78) and Eq. (6-79) equal, the following expression for the bending rotation at the far end is obtained:

$$\psi_{f(i)} = \frac{S_{21(i)} \psi_{n(i)} - (S_{11(i)} + S_{12(i)}) \frac{\Delta_i}{L_i}}{-c_{f(i)} - S_{11(i)}} \quad (6-80)$$

The vertical equilibrium of the shear force with the translational spring's reaction at the far end F gives the following equation:

$$\frac{\Delta_i}{L_i} = \frac{\left(1 - \frac{S_{12(i)}}{c_{f(i)} + S_{11(i)}}\right) \psi_{n(i)}}{2 - \frac{S_{11(i)} + S_{12(i)}}{c_{f(i)} + S_{11(i)}} + \frac{c_{br(i)} L_i^2 - \frac{P L_i^2}{E_i I_i}}{S_{11(i)} + S_{12(i)}}} \quad (6-81)$$

The bending moment at the near end N is equal to:

$$M_{n(i)} = \frac{E_i I_i}{L_i} S_{11(i)} \left(\psi_{n(i)} - \frac{\Delta_i}{L_i} \right) + \frac{E_i I_i}{L_i} S_{12(i)} \left(\psi_{f(i)} - \frac{\Delta_i}{L_i} \right) \quad (6-82)$$

Substituting Eq. (6-80) and Eq. (6-81) into Eq. (6-82) the rotational stiffness can be calculated as the factor of the bending rotation at the near end N:

$$c_i = \frac{E_i I_i}{L_i} \left[S_{11(i)} - \frac{S_{12(i)}^2}{c_{f(i)} + S_{11(i)}} - \frac{(S_{11(i)} + S_{12(i)}) \left(\frac{S_{12(i)}}{c_{f(i)} + S_{11(i)}} - 1 \right)^2}{\left(2 - \frac{S_{11(i)} + S_{12(i)}}{c_{f(i)} + S_{11(i)}} + \frac{c_{br(i)} L_i^2 - \frac{P L_i^2}{E_i I_i}}{S_{11(i)} + S_{12(i)}} \right)} \right] \quad (6-83)$$

where the value of $c^{\#}$ is given for both the rotational and translational springs as:

$$c^{\#} = \frac{c L_i}{E_i I_i} \quad (6-84)$$

6.4.4 Members with other boundary conditions at the far end

The above approach has been used to derive rotational stiffnesses for all possible boundary conditions at the far end of the converging members, whether they are axially loaded or not, with semi-rigid or rigid connection at the near end. The results are presented in Table 6-27 and Table 6-28 for the case of semi-rigid connections and in Table 6-29 and Table 6-30 for the case of members with rigid connections. The rotational stiffnesses converge to those of Euler-Bernoulli beam-columns, reported by Gantes and Mageirou [6-1], [6-2], as the shear rigidity approaches infinity.

Table 6-27: Rotational stiffnesses for non-axially loaded members with semi-rigid connection at the near end (N) on the left

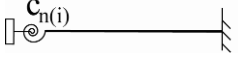
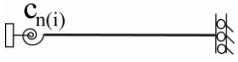
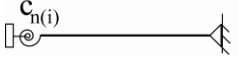

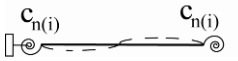

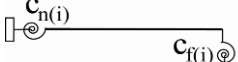
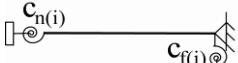
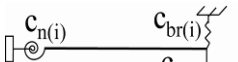
Support at far end	Member i	Rotational stiffness	Distribution factors
Fixed support		$c_i = \frac{E_i I_i}{L_i} A'_{11(i)}$	$z_{n(i)} = \frac{c_{m(i)}}{c_{m(i)} + c_{n(i)}}$ $z_{f(i)} = 0$
Roller fixed support		$c_i = \frac{E_i I_i}{L_i} \left(\frac{A'_{11(i)} A'_{22(i)} - A'^2_{12(i)}}{A'_{11(i)} + 2A'_{12(i)} + A'_{22(i)}} \right)$	$z_{n(i)} = \frac{c_{m(i)}}{c_{m(i)} + c_{n(i)}}$ $z_{f(i)} = 0$
Pinned support		$c_i = \frac{E_i I_i}{L_i} \left(A'_{11(i)} - \frac{A'^2_{12(i)}}{A'_{22(i)}} \right)$	$z_{n(i)} = \frac{c_{m(i)}}{c_{m(i)} + c_{n(i)}}$ $z_{f(i)} = 0$
Simple curvature		$c_i = \frac{E_i I_i}{L_i} \left(A'_{11(i)} - A'_{12(i)} \right)$	$z_{n(i)} = \frac{c_{m(i)}}{c_{m(i)} + c_{n(i)}}$ $z_{f(i)} = \frac{c_{m(i)}}{c_{m(i)} + c_{n(i)}}$
Double curvature		$c_i = \frac{E_i I_i}{L_i} \left(A'_{11(i)} + A'_{12(i)} \right)$	$z_{n(i)} = \frac{c_{m(i)}}{c_{m(i)} + c_{n(i)}}$ $z_{f(i)} = \frac{c_{m(i)}}{c_{m(i)} + c_{n(i)}}$
Roller support		$c_i = 0$	-
Rotational spring support		$c_i = \frac{E_i I_i}{L_i} \left(A'_{11(i)} - \frac{(A'_{11(i)} + A'_{12(i)})^2}{A'_{11(i)} + 2A'_{12(i)} + A'_{22(i)}} \right)$	$z_{n(i)} = \frac{c_{m(i)}}{c_{m(i)} + c_{n(i)}}$ $z_{f(i)} = \frac{c_{m(i)}}{c_{m(i)} + c_{f(i)}}$
Pinned and rotational spring support		$c_i = \frac{E_i I_i}{L_i} A'_{11(i)}$	$z_{n(i)} = \frac{c_{m(i)}}{c_{m(i)} + c_{n(i)}}$ $z_{f(i)} = \frac{c_{m(i)}}{c_{m(i)} + c_{f(i)}}$
Rotational and translational spring support		$c_i = \frac{E_i I_i}{L_i} \left(A'_{11(i)} - \frac{(A'_{11(i)} + A'_{12(i)})^2}{A'_{11(i)} + 2A'_{12(i)} + A'_{22(i)} + c_{br(i)}} \right)$	$z_{n(i)} = \frac{c_{m(i)}}{c_{m(i)} + c_{n(i)}}$ $z_{f(i)} = \frac{c_{m(i)}}{c_{m(i)} + c_{f(i)}}$

Table 6-28: Rotational stiffnesses for axially loaded members with semi-rigid connection at the near end (N) on the left

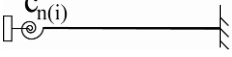

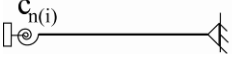

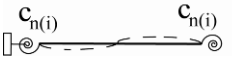

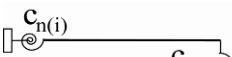


Support at the far end	Member i	Rotational stiffness	Distribution factors
Fixed support		$c_i = \frac{E_i I_i}{L_i} A_{11(i)}$	$Z_{n(i)} = \frac{C_{m(i)}}{C_{m(i)} + C_{n(i)}}$ $Z_{f(i)} = 0$
Roller fixed support		$c_i = \frac{E_i I_i}{L_i} \left[A_{11(i)} - \frac{(A_{11(i)} + A_{12(i)})^2}{A_{11(i)} + 2A_{12(i)} + A_{22(i)} - \frac{P_i L_i^2}{E_i I_i}} \right]$	$Z_{n(i)} = \frac{C_{m(i)}}{C_{m(i)} + C_{n(i)}}$ $Z_{f(i)} = 0$
Pinned support		$c_i = \frac{E_i I_i}{L_i} \left(A_{11(i)} - \frac{A_{12(i)}^2}{A_{22(i)}} \right)$	$Z_{n(i)} = \frac{C_{m(i)}}{C_{m(i)} + C_{n(i)}}$ $Z_{f(i)} = 0$
Simple curvature		$c_i = \frac{E_i I_i}{L_i} (A_{11(i)} - A_{12(i)})$	$Z_{n(i)} = \frac{C_{m(i)}}{C_{m(i)} + C_{n(i)}}$ $Z_{f(i)} = \frac{C_{m(i)}}{C_{m(i)} + C_{n(i)}}$
Double curvature		$c_i = \frac{E_i I_i}{L_i} (A_{11(i)} + A_{12(i)})$	$Z_{n(i)} = \frac{C_{m(i)}}{C_{m(i)} + C_{n(i)}}$ $Z_{f(i)} = \frac{C_{m(i)}}{C_{m(i)} + C_{n(i)}}$
Roller support		$c_i = -\frac{E_i I_i}{L_i} \left[\left(A_{11(i)} - \frac{A_{12(i)}^2}{A_{22(i)}} \right) \frac{P_i L_i}{\left(\frac{E_i I_i}{L_i} \right) \left(A_{11(i)} - \frac{A_{12(i)}^2}{A_{22(i)}} \right) - P_i L_i} \right]$	$Z_{n(i)} = \frac{C_{m(i)}}{C_{m(i)} + C_{n(i)}}$ $Z_{f(i)} = 0$
Rotational spring support		$c_i = \frac{E_i I_i}{L_i} \left[A_{11(i)} - \frac{(A_{11(i)} + A_{12(i)})^2}{A_{11(i)} + 2A_{12(i)} + A_{22(i)} - \frac{P_i L_i^2}{E_i I_i}} \right]$	$Z_{n(i)} = \frac{C_{m(i)}}{C_{m(i)} + C_{n(i)}}$ $Z_{f(i)} = \frac{C_{m(i)}}{C_{m(i)} + C_{f(i)}}$
Pinned and rotational spring support		$c_i = \frac{E_i I_i}{L_i} A_{11(i)}$	$Z_{n(i)} = \frac{C_{m(i)}}{C_{m(i)} + C_{n(i)}}$ $Z_{f(i)} = \frac{C_{m(i)}}{C_{m(i)} + C_{f(i)}}$
Rotational and translational spring support		$c_i = \frac{E_i I_i}{L_i} \left[A_{11(i)} - \frac{(A_{11(i)} + A_{12(i)})^2}{A_{11(i)} + 2A_{12(i)} + A_{22(i)} + C_{br(i)} - \frac{P_i L_i^2}{E_i I_i}} \right]$	$Z_{n(i)} = \frac{C_{m(i)}}{C_{m(i)} + C_{n(i)}}$ $Z_{f(i)} = \frac{C_{m(i)}}{C_{m(i)} + C_{f(i)}}$

Table 6-29: Rotational stiffnesses for non-axially loaded members with rigid connection at the near end (N) on the left

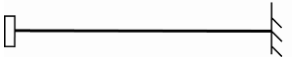
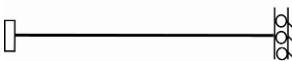
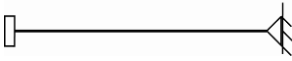
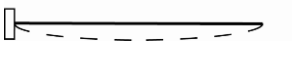
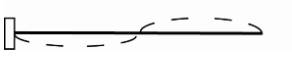
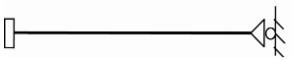

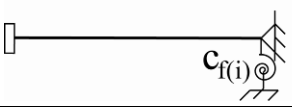
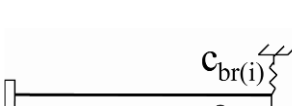
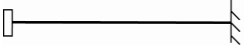
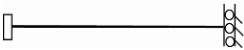
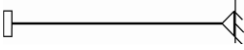
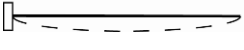
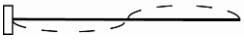

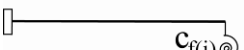
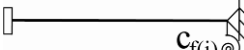
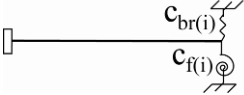
Support at the far end	Member i	Rotational stiffness
Fixed support		$c_i = \frac{E_i I_i}{L_i} S'_{11(i)}$
Roller fixed support		$c_i = \frac{0.5 E_i I_i}{L_i} (S'_{11(i)} - S'_{12(i)})$
Pinned support		$c_i = \frac{E_i I_i}{L_i} \left(\frac{S'_{11(i)}^2 - S'_{12(i)}^2}{S'_{11(i)}} \right)$
Simple curvature		$c_i = \frac{E_i I_i}{L_i} (S'_{11(i)} - S'_{12(i)})$
Double curvature		$c_i = \frac{E_i I_i}{L_i} (S'_{11(i)} + S'_{12(i)})$
Roller support		$c_i = 0$
Rotational spring support		$c_i = \frac{E_i I_i}{L_i} c_{f(i)}^{\#} \left(\frac{S'_{11(i)} (c_{f(i)}^{\#} + S'_{11(i)} - S'_{12(i)}) - S'_{12(i)} c_{f(i)}^{\#}}{(-c_{f(i)}^{\#} - S'_{11(i)}) (-2c_{f(i)}^{\#} - S'_{11(i)} + S'_{12(i)})} \right)$
Pinned and rotational spring support		$c_i = \frac{E_i I_i}{L_i} \left(S'_{11(i)} - \frac{S'_{12(i)}^2}{c_{f(i)}^{\#} + S'_{11(i)}} \right)$
Rotational and translational spring support		$c_i = \frac{E_i I_i}{L_i} \left(S'_{11(i)} - \frac{S'_{12(i)}^2}{c_{f(i)}^{\#} + S'_{11(i)}} - \frac{(S'_{11(i)} + S'_{12(i)}) \left(1 - \frac{S'_{12(i)}}{S'_{11(i)} + c_{f(i)}^{\#}} \right)^2}{2 - \frac{S'_{11(i)} + S'_{12(i)}}{c_{f(i)}^{\#} + S'_{11(i)}} + \frac{c_{br(i)}^{\#} L_i^2}{S'_{11(i)} + S'_{12(i)}}} \right)$

Table 6-30: Rotational stiffnesses for axially loaded members with rigid connection at the near end (N) on the left

Support at the far end	Member i	Rotational stiffness
Fixed support		$c_i = \frac{E_i I_i}{L_i} S_{11(i)}$
Roller fixed support		$c_i = \frac{E_i I_i}{L_i} \left(S_{11(i)} - \frac{S_{11(i)} + S_{12(i)}}{2 - \frac{P L_i^2}{E_i I_i (S_{11(i)} + S_{12(i)})}} \right)$
Pinned support		$c_i = \frac{E_i I_i}{L_i} \left(\frac{S_{11(i)}^2 - S_{12(i)}^2}{S_{11(i)}} \right)$
Simple curvature		$c_i = \frac{E_i I_i}{L_i} (S_{11(i)} - S_{12(i)})$
Double curvature		$c_i = \frac{E_i I_i}{L_i} (S_{11(i)} + S_{12(i)})$
Roller support		$c_i = -\frac{E_i I_i}{L_i} \left[\left(\frac{S_{11(i)}^2 - S_{12(i)}^2}{S_{11(i)}} \right) \frac{P L_i}{\left(\frac{E_i I_i}{L_i} \right) \left(\frac{S_{11(i)}^2 - S_{12(i)}^2}{S_{11(i)}} \right) - P L_i} \right]$
Rotational spring support		$c_i = \frac{E_i I_i}{L_i} \left[\left(S_{11(i)} - \frac{S_{12(i)}^2}{c_{f(i)}^{\#} + S_{11(i)}} \right) - \frac{(-c_{f(i)}^{\#} - S_{11(i)} + S_{12(i)}) \left(S_{11(i)} - \frac{S_{12(i)}^2 - c_{f(i)}^{\#} S_{12(i)}}{c_{f(i)}^{\#} + S_{11(i)}} \right)}{(-2c_{f(i)}^{\#} - S_{11(i)} + S_{12(i)}) + \frac{P L_i^2}{E_i I_i} \left(\frac{c_{f(i)}^{\#} + S_{11(i)}}{S_{11(i)} + S_{12(i)}} \right)} \right]$
Pinned and rotational spring support		$c_i = \frac{E_i I_i}{L_i} \left(S_{11(i)} - \frac{S_{12(i)}^2}{c_{f(i)}^{\#} + S_{11(i)}} \right)$
Rotational and translational spring support		$c_i = \frac{E_i I_i}{L_i} \left[S_{11(i)} - \frac{S_{12(i)}^2}{c_{f(i)}^{\#} + S_{11(i)}} - \frac{(S_{11(i)} + S_{12(i)}) \left(\frac{S_{12(i)}}{c_{f(i)}^{\#} + S_{11(i)}} - 1 \right)^2}{2 - \frac{S_{11(i)} + S_{12(i)}}{c_{f(i)}^{\#} + S_{11(i)}} + \frac{c_{br(i)}^{\#} L_i^2 - \frac{P L_i^2}{E_i I_i}}{S_{11(i)} + S_{12(i)}}} \right]$

6.5 EXAMPLES

The approximate analytical method proposed for Euler-Bernoulli members by Gantes and Mageirou [6-1], [6-2] was validated with the use of a large amount of examples thoroughly presented by Mageirou [6-11]. They concluded that the procedure gives very accurate results for the buckling loads of multi-story frames when compared with Linearised Buckling Analysis (LBA) performed with finite element software.

Among a wide range of numerical examples that have been solved in order to verify the proposed approach, five are reported here. They refer to a three-story braced frame with rigid connections, a three-story unbraced frame with semi-rigid connections, a three-story braced frame with asymmetrically applied loads, a partially braced asymmetric frame and a symmetric one-story frame consisting of laced built-up members. For all frames the proposed method is used and the results obtained for the elastic buckling loads are compared with the ones obtained by a Linearised Buckling Analysis performed with the use of the finite element software ADINA [6-12], in order to verify the correctness of the proposed rotational stiffness coefficients. The members are modelled with the use of a sufficient number of Hermitian beam elements, and the results of the finite element model are considered as an appropriate basis for comparison. The shear deformations are incorporated in the FEM analyses by assigning appropriate values of the shear area factors when solid cross-sections are used.

6.5.1 Example 1

Consider the three-story braced frame of Figure 6-30(a) with a span of $L=20\text{m}$ and story height of $h=10\text{m}$. Both columns and beams are susceptible to shear deformations. The columns' cross-section has a moment of inertia $I=0.0004319\text{m}^4$ and a value of $\mu=0.02$, which could correspond to a battened built-up column. The beams' cross-section has a moment of inertia $I=0.0002313\text{m}^4$ and a value of $\mu=0.0044$, which could correspond to a laced built-up member. The frame is made of steel with Young's modulus equal to $E=210000000\text{kN/m}^2$ and Poisson ratio $\nu=0.3$. The columns are considered to be pinned at the base while the loads are concentrated at the beam-column joints and equal to $P/3$. The connections between the beam and the column are considered to be rigid.

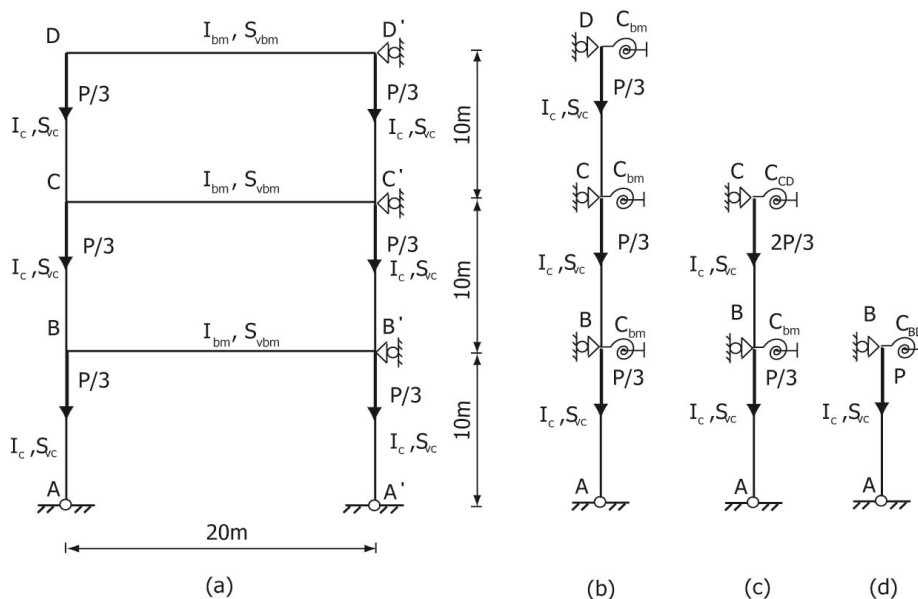


Figure 6-30: (a) Example 1: Three-story braced frame with rigid beam-column connections, (b) Model "a", (c) Model "b" and (d) Model "c"

In the beginning, the frame is analysed by carrying out LBA using the finite element software ADINA. The mesh is sufficiently dense to obtain converging results for the frame's buckling load. The first buckling mode shown in Figure 6-31 is related to a critical load equal to 9180kN. Afterwards, the frame is replaced by successive equivalent models that are used to test the correctness of the proposed stiffness coefficients.

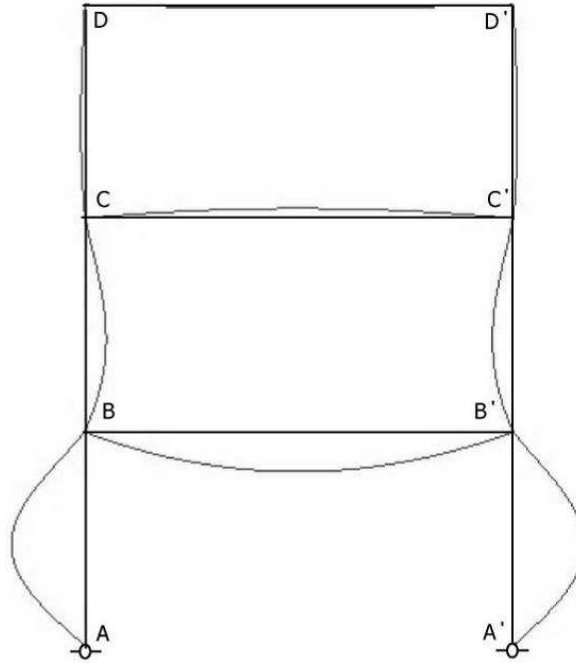


Figure 6-31: First buckling mode of frame of example 1

The first of them is called model "a" and contains the replacement of the beams with equivalent rotational springs (Figure 6-30(b)). At this stage, it is assumed that in the first buckling mode the beams deform in single curvature and are not axially loaded. Then, from Table 6-29 the stiffness of each equivalent rotational spring is equal to:

$$c_{bm} = \frac{E_{bm} I_{bm}}{L_{bm}} (S'_{11(bm)} - S'_{12(bm)}) = 4857.3 \text{ kNm} \quad (6-85)$$

If the formula that corresponds to single curvature for axially loaded members (Table 6-30) is used and a very small value of the axial load is incorporated, the same result will be obtained for c_{bm} . The buckling load of the first mode of model "a" obtained with ADINA is equal to 9191.2kN.

The second equivalent model is called "b" and is obtained from "a" by replacing column CD with a spring of equivalent rotational stiffness (Figure 6-30(c)). Based on Table 6-30 for axially loaded members, the stiffness of the equivalent spring is:

$$c'_{CD} = \frac{E_{CD} I_{CD}}{h_{CD}} \left(S_{11(CD)} - \frac{S_{12(CD)}^2}{c^{\#} + S_{11(CD)}} \right) = 20167.84 \text{ kNm} \quad (6-86)$$

using $P = 9180 \text{ kN} / 3 = 3060 \text{ kN}$ and

$$c^{\#} = \frac{c_{bm}}{E_{CD} I_{CD} / h_{CD}} \quad (6-87)$$

The total rotational stiffness of the spring at point C is:

$$c_{CD} = c'_{CD} + c_{bm} = 20167.84 \text{ kNm} + 4857.3 \text{ kNm} = 25025.14 \text{ kNm} \quad (6-88)$$

The buckling load of the first mode of model "b" according to ADINA is equal to 9191.8 kN.

The third equivalent model is called "c" and results from "b" by replacing column BC with a spring of equivalent rotational stiffness (Figure 6-30(d)). As for column CD, it is calculated that:

$$c'_{BC} = \frac{E_{BC} I_{BC}}{h_{BC}} \left(S_{11(BC)} - \frac{S_{12(BC)}^2}{c^{\#} + S_{11(BC)}} \right) = 15196.15 \text{ kNm} \quad (6-89)$$

using $P = 2 \cdot 9180 \text{ kN} / 3 = 6120 \text{ kN}$ and

$$c^{\#} = \frac{c_{CD}}{E_{BC} I_{BC} / h_{BC}} \quad (6-90)$$

The total rotational stiffness of the spring at point B is:

$$c_{BD} = c_{BC} = c'_{BC} + c_{bm} = 15196.15 \text{ kNm} + 4857.3 \text{ kNm} = 20053.45 \text{ kNm} \quad (6-91)$$

The buckling load of the first mode of model "c" is now calculated from ADINA equal to 9213.2 kN. In Table 6-31 the results obtained for the original frame and for the successive simpler models are summarised. The differences are very small, thus verifying the correctness of the rotational stiffnesses used for creating models "a", "b" and "c". It is noted that the value of buckling load of the frame used to calculate the rotational stiffnesses of the upper columns will not be known in prior. A reasonable value of P should be assumed for the calculations, commonly taken as the design value of the column's axial force due to vertical loading. The closer the assumed value is to the critical load of the frame, the smaller the final error will be, but this influence is relatively small in any case.

Table 6-31: Summary of the results for the frame of Example 1 consisting of members susceptible to shear deformations

Method / Model		Critical load (kN)	Error (%)
FEM (ADINA)	Actual frame	9180	0
	"a"	9191.2	-0.12
	"b"	9191.8	-0.13
	"c"	9213.2	-0.36
Proposed analytical method		9304	-1.35

Moreover, the value of critical buckling load obtained for original model "c" using Eq. (6-30) is equal to 9304 kN, differing by only 1.35% from the buckling load of the frame as obtained from finite element analysis. Thus it was shown that very satisfactory accuracy is possible by applying the proposed analytical approach and without any numerical analysis.

It should also be mentioned that the finite element analysis of the structure under uniformly distributed load along the beams results in an elastic critical load $P_{cr} = 9318 \text{ kN}$ which is very close to the one obtained previously. Finally, it is noted that the critical buckling load of the same frame without shear deformations is $P_{cr} = 11778 \text{ kN}$, which is indicative of the significant influence of shear deformations for high values of the dimensionless shear parameter μ .

6.5.2 Example 2

The three-story frame of Figure 6-32 has the same geometry and cross-sections as the one analysed in example 1, but it is now unbraced and the beam to column joints are considered to be semi-rigid with a rotational stiffness of $c_{sr}=3000\text{kNm}$. In the beginning, the frame is analysed by performing LBA using ADINA. The mesh is sufficiently dense to obtain accurate results as far as the frame's buckling load is concerned. The first buckling mode shown in Figure 6-33 is related to a critical load equal to 302kN.

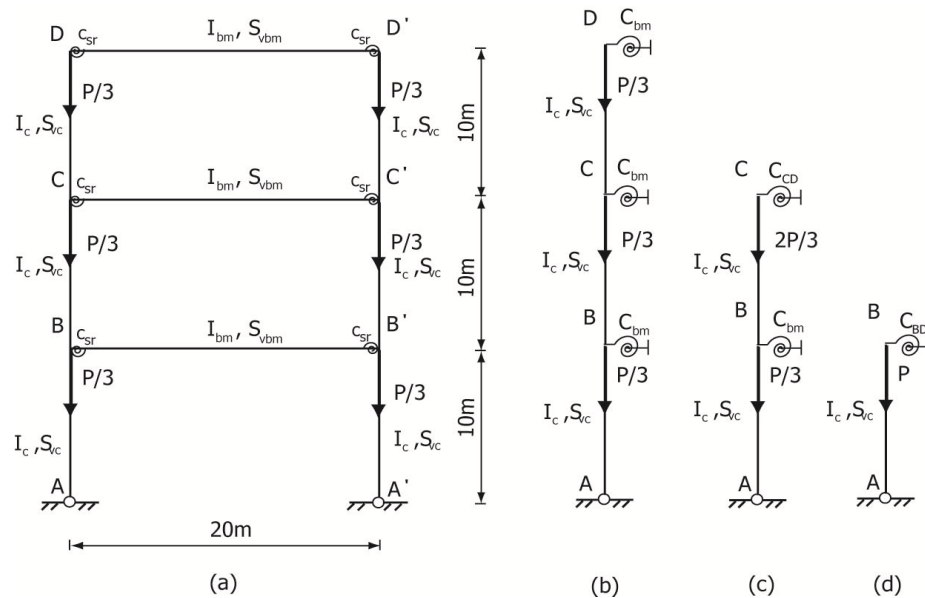


Figure 6-32: (a) Example 2: Three-story unbraced frame with semi-rigid beam-column connections, (b) Model "a", (c) Model "b" and (d) Model "c"

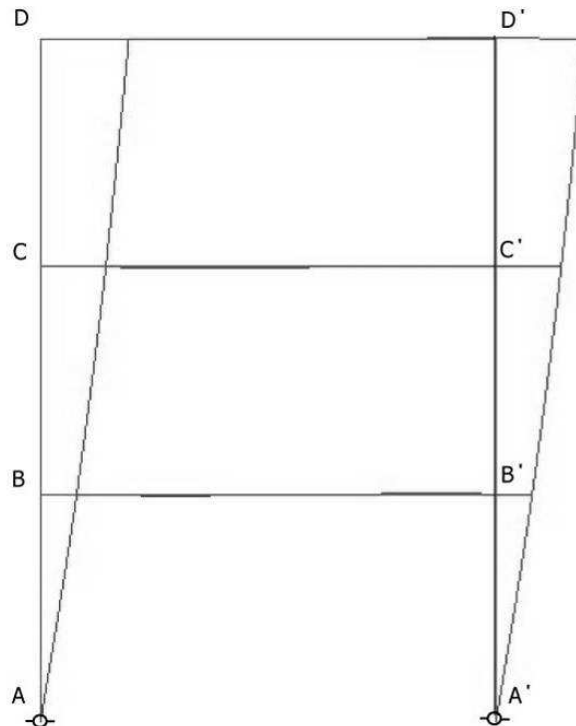


Figure 6-33: First buckling mode of frame of example 2

Working in the same manner as for the previous example, but using now the stiffness expressions for the case of semi-rigid beam to column connections and taking into account the fact that the frame buckles in sway mode, thus the beams deform in double curvature, the results listed in Table 6-32 are obtained, leading to the same conclusions. The buckling load calculated from Eq. (6-29) is equal to 302.2kN, differing by only 0.07% from the buckling load of the original frame obtained with finite element analysis. It is also noted that the finite element analysis of the structure under uniformly distributed load along the beams results in elastic critical buckling load $P_{cr}=303.6\text{kN}$, which is very close to the one obtained for concentrated loads.

Table 6-32: Summary of the results for the frame of Example 2 consisting of members susceptible to shear deformations

Method / Model		Critical load (kN)	Error (%)
FEM (ADINA)	Actual frame	302.0	0
	"a"	301.9	0.03
	"b"	301.9	0.03
	"c"	300.5	0.49
Proposed analytical method		302.2	-0.07

6.5.3 Example 3

The three-story braced frame of Figure 6-34(a) has the same geometry and cross-sections as the ones analyzed in the previous examples. The only difference from example 1 is the fact that the loads applied are not symmetrical. From the loads' distribution it can be concluded that column AB of the frame will buckle first, contrary to the previously examined cases where both columns AB and A'B' buckled at the same time. This is also shown in Figure 6-34(b) where the 1st mode obtained by a LBA is shown. The finite element analysis gives an elastic critical load $P_{cr}=9408.19\text{kN}$, slightly higher than in the case of symmetrical loading, which is compatible with the fact that the beams rotate less at the far end, thus they resist more against buckling of the loaded column. If the procedure of example 1 (assuming conservatively that the frame is loaded symmetrically) is followed, the error is approximately equal to 1.15%.

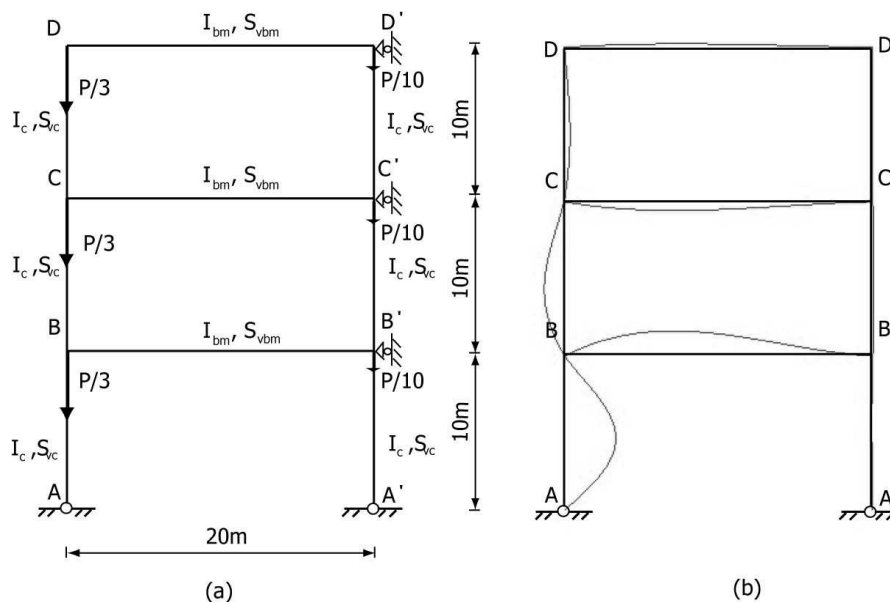


Figure 6-34: (a) Example 3: Three-story braced frame with rigid beam-column connections and non-symmetrical loading and (b) first buckling mode of frame of example 3

6.5.4 Example 4

The frame of Figure 6-35(a) consists of a beam of span $L=20\text{m}$ and a column of height $h=10\text{m}$, which are both susceptible to shear deformations. The structural elements' cross-sections and shear rigidities are the same as the ones presented in example 1. Lateral displacements of the beam are resisted by a horizontal translational spring with axial stiffness. c_{br} is equal to 1000kN/m . The connection between the beam and the column is considered to be rigid.

The first buckling mode obtained with ADINA is shown in Figure 6-35(b) and corresponds to a critical load $P_{cr}=8012.72\text{kN}$. The analytical procedure gives a result of $P_{cr}=8074.98\text{kN}$ leading to an error of 0.78% .

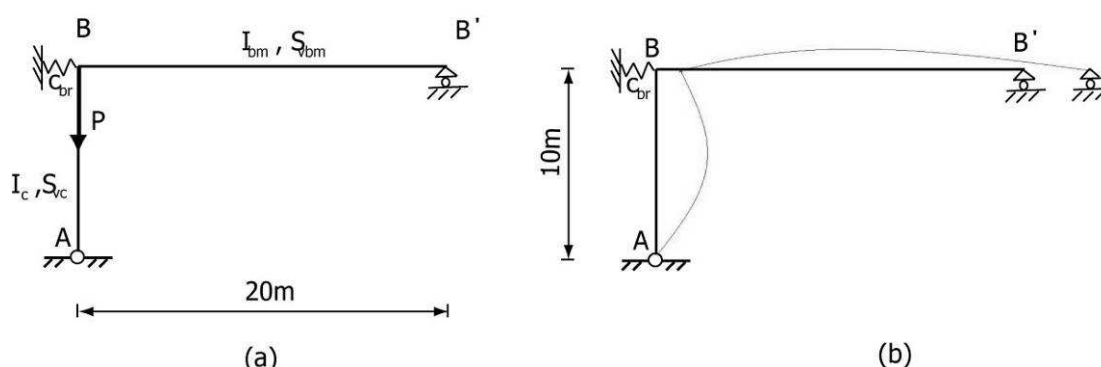


Figure 6-35: (a) Example 4: (a) Single-story partially-braced frame with rigid beam-column connection and (b) first buckling mode of frame of example 4

Assuming that instead of a concentrated load applied directly on column AB, a uniformly distributed load along beam BB' is applied, the previous result is conservative. Finite element analysis resulted in a total critical load $P_{cr}=13622\text{kN}$. In this case a simple elastic analysis with small displacements can be employed for calculating approximately the amount of vertical loading that is transferred to the column. For the specific example this amount is approximately 60% of the totally applied uniformly distributed load and this leads to the conclusion that an approximate elastic critical load of the frame calculated analytically is $P_{cr}=13458.3\text{kN}$ ($=8074.98\text{kN}/0.6$) which is very close to the numerical result.

6.5.5 Example 5

A frame that consists of laced built-up columns hinged at their base and a truss beam is examined, in order to focus on a structure commonly met in industry, for which shear deformations are of importance. The columns have a height of 18.7m and the beam a length of 31.7m . Both the laced built-up columns and the truss beam can be considered as Timoshenko members with approximate equivalent bending and shear rigidities provided in many structural textbooks and EC3 [6-3] for such structures, while the beam-column joint is considered to be rigid. In this specific example, the equivalent bending rigidities of the columns and the beam are equal to 0.031501m^4 and 0.1156m^4 , respectively. The equivalent shear rigidities of the columns and the beam are equal to 246313kN and 824284kN , respectively. The elastic buckling load obtained with ADINA [6-12] is equal to 33740kN and the sway buckling mode is shown in Figure 6-36. The result obtained with the proposed method considering a double curvature deformation of the truss beam is equal to 33179kN . If shear deformations are neglected, the elastic critical buckling load predicted by EC3 [6-3] is equal to 40270kN , highlighting the significance of shear deformation in such frames. The error of neglecting shear deformations for this specific case reaches a magnitude of 20% on the unsafe side.

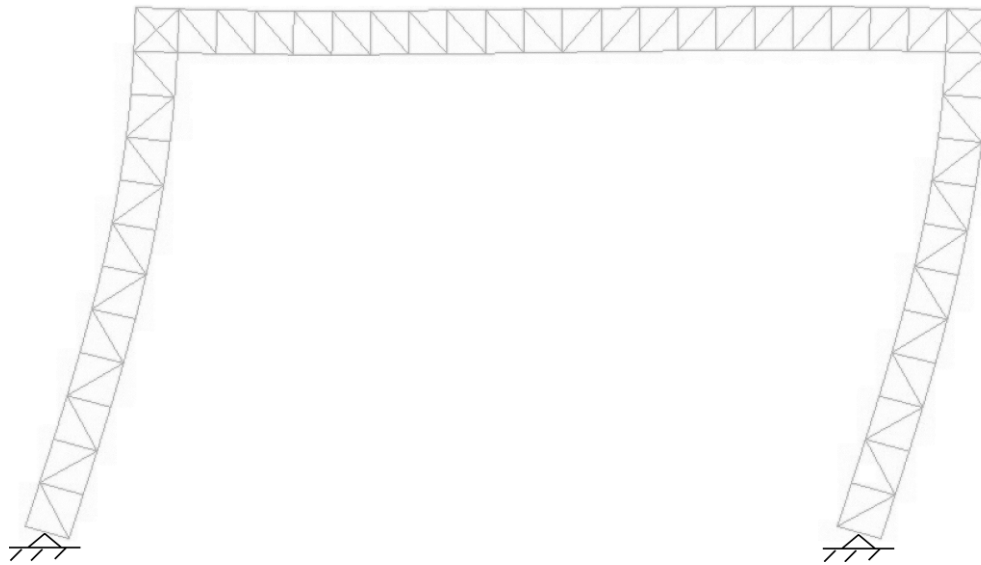


Figure 6-36: Single-story sway frame with laced built-up columns and truss beam

6.6 CONCLUSIONS

An approximate analytical methodology has been proposed for the evaluation of the elastic critical buckling load of frames consisting of members that are susceptible to transverse shear deformations based on Engesser's approach. To that effect, critical columns in the frame are modelled individually, while the rotational restraints offered to the end nodes by adjacent members are modelled by means of rotational springs. The resistance to relative transverse displacements of the ends is simulated with a translational spring for the general case of partially braced frames. The stiffness of this spring becomes zero for unbraced frames and approaches infinity for fully braced frames.

For the analytical evaluation of the critical buckling load a stability matrix has been formulated and three general equations of stability have been derived for the cases of unbraced, partially braced and braced frames. Indicative graphical solutions of the stability equations for the previously mentioned cases have been plotted and detailed tables have been given for facilitating the procedure. Then, in the second part of this chapter, slope-deflection equations for shear-weak members with semi-rigid connections based on Engesser's theory have been derived and used for the presentation of a complete set of rotational stiffness coefficients, which can be used for the replacement of members converging at the bottom and top ends of the column in question by equivalent springs. All possible rotational and translational boundary conditions at the far end of these members, as well as the eventual presence of axial force, have been taken into consideration. The method can be readily adapted to frames without shear deformable members by assuming that their shear rigidity approaches infinity.

Five verification examples have been presented, of which the first two deal with three-story braced or unbraced frames with rigid and semi-rigid beam to column connections, the third with a three-story frame with non-symmetrically applied load, the fourth with a partially braced frame and the fifth with a frame consisting of laced built-up columns. The proposed approach for the elastic critical buckling load for Timoshenko members with arbitrary supports and for multi-story frames consisting of Timoshenko members was found to be in excellent agreement with finite element results.

6.7 REFERENCES

- [6-1] Gantes C.J., Mageirou G.E. "Improved stiffness distribution factors for evaluation of effective buckling lengths in multi-story sway frames", *Engineering Structures*, Vol. 27, No. 7, pp. 1113-1124, 2005
- [6-2] Mageirou G.E., Gantes C.J. "Buckling strength of multi-story sway, non-sway and partially sway frames with semi-rigid connections", *Journal of Constructional Steel Research*, Vol. 62, pp. 893-905, 2006
- [6-3] Eurocode 3: Design of Steel Structures. Part 1.1: General structural rules. CEN-European Committee for Standardisation, Brussels, EN1993-1-1, 2005
- [6-4] Maney G.A., Wilson W.M. "Slope-deflection method", University of Illinois Engineering Experiment Station, Bulletin 80, 1915
- [6-5] Salmon C.G., Johnson J.E. "Steel Structures: Design and Behaviour", 4th edition, Harper Collins College Publishers, 1996
- [6-6] Absi, E. "Equations intrinseques d'une poutre droite a section constant", *Annales de l'Institut Technique du Batiment et des Travaux Publics*, Vol. 21(229), pp. 151-167, 1967
- [6-7] Lin, F.J., Glauser, E.C., Johnston, B.G., "Behaviour of laced and battened structural members", *Journal of the Structural Division, American Society of Civil Engineers (A.S.C.E.)*, Vol. 96, No. ST7, pp. 1377-1401, 1970
- [6-8] Aristizabal-Ochoa, J.D. "Slope-deflection equations for stability and second-order analysis of Timoshenko beam-column structures with semi-rigid connections", *Journal of Engineering Structures*, Vol. 30, pp. 2517-2527, 2008
- [6-9] Banerjee, J.R., Williams, F.W. "The effect of shear deformation on the critical buckling of columns", *Journal of Sound and Vibration*, Vol. 174, No. 5, pp. 607-616, 1994
- [6-10] MATLAB, Version 7 (R14), Copyright 1984-2004, The Mathworks Inc
- [6-11] Mageirou, G.E. "Contribution to the design of multi-story steel frames against flexural buckling", Doctoral thesis, National Technical University of Athens, Greece, 2011
- [6-12] ADINA System 8.5, Release Notes. ADINA R & D Inc., 71 Elton Avenue, Watertown, MA 02472, USA, 2008

7 SECOND-ORDER ELASTIC ANALYSIS OF IMPERFECT TIMOSHENKO BEAM-COLUMNS WITH ARBITRARY SUPPORTS

7.1 INTRODUCTION

In Chapter 5 it was concluded that laced built-up columns can be modelled as equivalent Timoshenko members. For this reason in Chapter 6, an analytical procedure for the calculation of the elastic critical buckling loads of Timoshenko columns with arbitrary boundary conditions and of multi-story frames consisting of Timoshenko members was proposed. The elastic buckling load for a structure is an upper bound of its capacity, while second-order analysis results in the calculation of deflections, bending moments and shear forces along the structure's members. Many researchers have worked on second-order analysis of Timoshenko members and frames developing slope-deflection equations [7-1], [7-2], [7-3] and iterative procedures [7-4], which require extensive calculations and in many cases computer programming. But the second-order analysis of Timoshenko members with arbitrary supports in a form that offers straight-forward solutions has not been addressed in the literature, where focus is mainly on simply-supported columns and cantilevers.

In this chapter second-order analysis of imperfect Timoshenko beam-columns with arbitrary supports will be presented in the form of closed-form solutions that facilitate the calculations and do not require iterative procedures. Straight-forward solutions capturing both $P-\Delta$ and $P-\delta$ effects can be a useful tool for engineers of practice. To that effect, an approximate analytical procedure for the calculation of the second-order bending moment and shear force along such members is proposed here. The procedure is verified by means of geometrically nonlinear numerical analyses with the use of shear deformable beam elements.

7.2 IMPERFECT TIMOSHENKO MEMBERS

Initial imperfections are considered in modern codes of practice in order to account for geometrical out-of-straightness and thermally induced residual stresses. It is also common design practice to consider the first buckling mode as a geometrical shape of the imperfections. For simplicity the effect of initial imperfections on the bending moment, shear force and deflections of the column is taken into

account with the use of the magnification factor initially proposed by Young [7-5]. Eurocode 3 [7-6] uses an appropriately modified magnification factor for simply-supported Timoshenko columns, in order to incorporate in the analysis shear deformations. In reality, the initial imperfections' pattern is not known and it is common practice that buckling mode shapes are used for its incorporation in structural analysis. In columns, the effect of the first buckling mode is much more important than that of other buckling modes and dominates the response. As a result, a satisfactory approximation is to use only the first buckling mode shape as an initial imperfection pattern ignoring higher-order buckling modes.

Additionally, 2nd-order elastic analysis leads to inaccuracies as the applied axial load approaches the elastic critical buckling load of the column and deflections become very large, as it is based on small deflection theory. Nevertheless, it is very satisfactory for practical purposes, as material nonlinearity does not allow for very large deformations. In addition, serviceability limit checks do not permit the excess of specific deformation limits in structures. As a result, at ultimate limit state where the loads are approximately 1.5 times larger than the ones corresponding to serviceability limit state, very large deformations cannot occur.

In the present section, the approximate second-order analysis of imperfect Timoshenko members under axial loading based on Engesser's method will be presented, based only on the first buckling mode. Initially, the procedure will be thoroughly illustrated for the simply-supported case, so that the concept behind the formulation is explained. Then, it will be expanded to the more general case of arbitrary boundary conditions. For verification Geometrically Nonlinear Imperfection Analyses (GNIA) will be used in shear deformable imperfect columns with the use of finite element software ADINA [7-7].

7.2.1 Simply-supported case

Consider a simply-supported member of length L , bending rigidity EI and shear rigidity S_v as depicted in Figure 7-1. An initial imperfection $w_0(x)$ based on the first buckling mode is considered, having a sinusoidal shape with maximum value w_0 in the middle of the member.

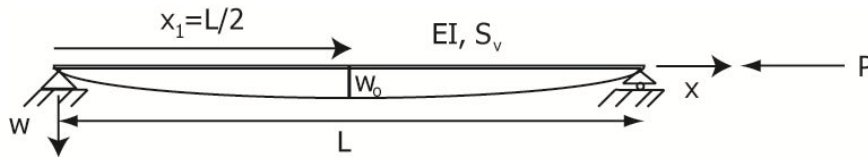


Figure 7-1: Imperfect simply-supported Timoshenko column

The application of a compressive axial force P amplifies the initial imperfection and causes second-order bending moments along the member. The bending moment along the member can be expressed as

$$M(x) = -EI w_B''(x) \quad (7-1)$$

where $w_B(x)$ is the deflection along the member due to bending only and prime denotes differentiation with respect to longitudinal coordinate x . The external bending moment along the beam can be expressed as

$$M(x) = P(w(x) + w_0(x)) \quad (7-2)$$

where $w(x)$ is the total additional deflection of the member consisting of the deflections due to bending deformation $w_B(x)$ and those due to shear deformation $w_S(x)$, as shown in Eq. (7-3):

$$w(x) = w_B(x) + w_S(x) \quad (7-3)$$

The shear deformation is equal to the shear force (first derivative of bending moment) divided by the shear rigidity S_v :

$$w'_S(x) = -\frac{EI w''_B}{S_v} \quad (7-4)$$

By integrating Eq. (7-4) the deflection due to shear deformation is obtained:

$$w_S(x) = -\frac{EI w''_B}{S_v} x + c \quad (7-5)$$

where c is an integration constant, which for the simply-supported case is equal to zero.

By equating the internal and external moments of Eqs. (7-1) and Eq. (7-2) and based on Eq. (7-3) and Eq. (7-5) the differential Eq. (7-6) arises:

$$w''_B(x) + a^2 w_B(x) = -a^2 w_0(x) \quad (7-6)$$

where

$$a^2 = \frac{P}{EI\beta} \quad (7-7)$$

and

$$\beta = 1 - \frac{P}{S_v} \quad (7-8)$$

The 1st buckling mode shape of a Timoshenko simply-supported member can be obtained by substituting its boundary conditions into Eq. (6-8) and Eq. (6-9). The solution obtained has the well-known sinusoidal shape. For this reason, the initial imperfection can be written in the sinusoidal form of the first buckling mode of the simply-supported member:

$$w_0(x) = w_0 \sin(a_{cr} x) \quad (7-9)$$

where a_{cr} is the value of a corresponding to the elastic critical buckling load P_{cr} :

$$a_{cr}^2 = \frac{P_{cr}}{EI\beta_{cr}} \quad (7-10)$$

If a sinusoidal shape is also assumed for $w_B(x)$, then the solution of Eq. (7-6) is obtained and $w_B(x)$ can be expressed approximately in terms of the maximum initial imperfection w_0 as shown in Eq. (7-11).

$$w_B(x) = \frac{w_0}{\left(\frac{a_{cr}^2}{a^2} - 1\right)} \sin(a_{cr} x) \quad (7-11)$$

Based on Eq. (7-5) and Eq. (7-11) the deflection due to shear deformation can be evaluated in terms of the initial imperfection:

$$w_s(x) = \frac{EI}{S_v} \frac{a_{cr}^2 w_o}{\left(\frac{a_{cr}^2}{a^2} - 1\right)} \sin(a_{cr}x) \quad (7-12)$$

Making use of Eq. (7-3), Eq. (7-11) and Eq. (7-12) the total additional deflection in terms of initial imperfection can be calculated:

$$w(x) = \frac{w_o}{\beta_{cr} \left(\frac{a_{cr}^2}{a^2} - 1\right)} \sin(a_{cr}x) \quad (7-13)$$

Substituting Eq. (7-11) in Eq. (7-1) the bending moment along the imperfect member in terms of the maximum value of imperfection can be found according to Eq. (7-14).

$$M(x) = \frac{Pw_o}{\left(1 - \frac{P}{P_{cr}}\right)} \sin(a_{cr}x) \quad (7-14)$$

The 2nd order shear force arises by differentiating Eq. (7-14):

$$Q(x) = \frac{Pa_{cr}w_o}{\left(1 - \frac{P}{P_{cr}}\right)} \cos(a_{cr}x) \quad (7-15)$$

The effect of shear deformation is incorporated in the calculation of the elastic critical load. It should also be noted that the total deflection, consisting of the total additional deflection and the initial imperfection, is:

$$w_T(x) = w(x) + w_o(x) \quad (7-16)$$

Substituting Eq. (7-9) and Eq. (7-13) in Eq. (7-16) it becomes:

$$w_T(x) = \left(\frac{1}{\beta_{cr} \left(\frac{a_{cr}^2}{a^2} - 1\right)} + 1 \right) w_o \sin(a_{cr}x) \quad (7-17)$$

After some calculations Eq. (7-17) becomes:

$$w_T(x) = \left(\frac{1}{1 - \frac{P}{P_{cr}}} \right) w_o \sin(a_{cr}x) \quad (7-18)$$

At the middle of the column where the maximum deflection appears, Eq. (7-18) gives:

$$w_T\left(\frac{L}{2}\right) = \frac{w_o}{1 - \frac{P}{P_{cr}}} \quad (7-19)$$

Eq. (7-19) yields the maximum total deflection at the middle based on the well-known approximate magnification factor. Note that if Eq. (7-19) is substituted in Eq. (7-2) the maximum bending moment along an imperfect simply-supported column is obtained. The result is exactly the same as the one found by maximising Eq. (7-14).

7.2.2 Arbitrary boundary conditions

Consider now a member of length L , bending rigidity EI , shear rigidity S_v and arbitrary boundary conditions, as shown in Figure 7-2. The member has an initial imperfection $w_o(x)$ based on its first mode of buckling, which has a maximum value w_o , and is loaded axially by a compressive force P .

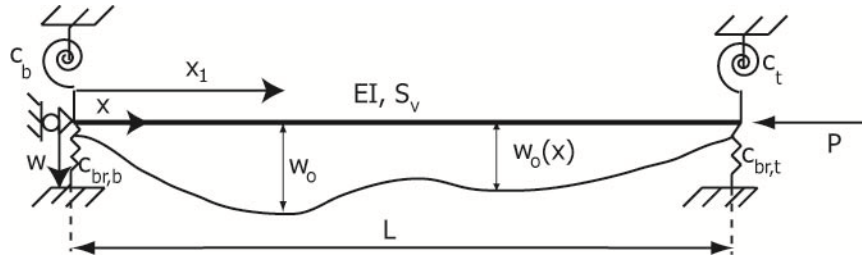


Figure 7-2: Axially loaded imperfect Timoshenko member with arbitrary boundary conditions

For the simply-supported case, it was shown that the magnification factor can be obtained by incorporating the Timoshenko buckling load into the formula initially proposed by Young [7-5]. Similarly to Eq. (7-13), in the case of arbitrary boundary conditions the total additional deflection can be approximately obtained from the 1st buckling mode shape $w_o(x)$ as:

$$w(x) = \frac{w_o(x)}{\beta_{cr} \left(\frac{a_{cr}^2}{a^2} - 1 \right)} \quad (7-20)$$

The value of a_{cr} can be obtained for sway, partially-sway or non-sway members from the nonlinear equations given for Timoshenko members as proposed in Chapter 6.

By differentiating Eq. (6-8) twice and Eq. (6-9) once, the second derivatives of the total additional deflection and of the deflection due to bending only can be obtained. The relation between the two can be expressed as:

$$w_B''(x) = \beta_{cr} w''(x) \quad (7-21)$$

As for the simply-supported column, the initial imperfection in terms of the 1st buckling mode shape of the column with arbitrary supports depicted in Figure 7-2 can be written as:

$$w_o(x) = \frac{w_o(f_1 \sin(a_{cr}x) + \cos(a_{cr}x) + f_2x + f_3)}{f_1 \sin(a_{cr}x_1) + \cos(a_{cr}x_1) + f_2x_1 + f_3} \quad (7-22)$$

where

$$f_1 = \frac{\frac{a_{cr}^4 \beta_{cr}^2}{c_b^*} \left(\frac{1}{c_{br,b}^*} + \frac{1}{c_{br,t}^*} \right) - \frac{a_{cr}^2 \beta_{cr} L}{c_b^*} + \cos(a_{cr}L) - 1}{a_{cr} \beta_{cr} L \sin(a_{cr}L) - a_{cr}^3 \beta_{cr}^2 \left(\frac{1}{c_{br,b}^*} + \frac{1}{c_{br,t}^*} \right)} \quad (7-23)$$

$$f_2 = -a_{cr} \beta_{cr} \left(\frac{a_{cr}}{c_b^*} + f_1 \right) \quad (7-24)$$

$$f_3 = -\frac{a_{cr}^2 \beta_{cr} f_2}{c_{br,b}^*} - 1 \quad (7-25)$$

$$c_i^* = \frac{c_i}{EI} \quad (7-26)$$

The numerator corresponds to the 1st buckling mode shape while the denominator gives the maximum value of the 1st buckling mode shape. The value of x_1 corresponds to the location of the maximum deflection. Dividing the buckling mode function by its maximum value ensures that the result is normalised to the maximum value w_o . The value of x_1 can be obtained by maximising the quantity in the brackets in Eq. (7-27), which corresponds to the mode shape of the 1st buckling mode.

$$\max(|f_1 \sin(a_{cr}x_1) + \cos(a_{cr}x_1) + f_2x_1 + f_3|) \quad (7-27)$$

Based on Eqs. (7-20) and (7-21) the second derivative of the deflection due to bending only is calculated:

$$w_B''(x) = \frac{w_o''(x)}{\frac{a_{cr}^2}{a^2} - 1} \quad (7-28)$$

Substituting Eq. (7-22) in Eq. (7-28) the following expression is obtained:

$$w_B''(x) = \frac{-a_{cr}^2 w_o(f_1 \sin(a_{cr}x) + \cos(a_{cr}x))}{\left(\frac{a_{cr}^2}{a^2} - 1 \right) (f_1 \sin(a_{cr}x_1) + \cos(a_{cr}x_1) + f_2x_1 + f_3)} \quad (7-29)$$

Substituting Eq. (7-29) in Eq. (7-1), the bending moment along an imperfect Timoshenko member can be expressed as:

$$M_{\text{imp}}(x) = \frac{Pw_o}{1 - \frac{P}{P_{\text{cr}}}} f \quad (7-30)$$

where P_{cr} is the elastic critical load of the member and f is given by Eq. (7-31).

$$f = \frac{f_1 \sin(a_{\text{cr}} x) + \cos(a_{\text{cr}} x)}{f_1 \sin(a_{\text{cr}} x_1) + \cos(a_{\text{cr}} x_1) + f_2 x_1 + f_3} \quad (7-31)$$

The numerator of Eq. (7-31) corresponds to the bending moment function along the imperfect member. The shear force along the member is obtained by differentiating Eq. (7-30) with respect to x .

$$Q_{\text{imp}}(x) = \frac{a_{\text{cr}} Pw_o}{1 - \frac{P}{P_{\text{cr}}}} f' \quad (7-32)$$

where f' is defined in Eq. (7-34).

$$f' = \frac{f_1 \cos(a_{\text{cr}} x) - \sin(a_{\text{cr}} x)}{f_1 \sin(a_{\text{cr}} x_1) + \cos(a_{\text{cr}} x_1) + f_2 x_1 + f_3} \quad (7-33)$$

For the case of a simply-supported member f and f' can be calculated by substituting very large ($\rightarrow \infty$) and very small values ($\rightarrow 0$) for the translational and rotational springs' constants, respectively. In this case both these factors take the value of 1, as expected.

The total deflection is given by Eq. (7-16) and by making use of Eq. (7-22) it becomes for a member with arbitrary boundary conditions:

$$w_T(x) = \left(\frac{1}{1 - \frac{P}{P_{\text{cr}}}} \right) w_o(x) = \left(\frac{1}{1 - \frac{P}{P_{\text{cr}}}} \right) \frac{w_o (f_1 \sin(a_{\text{cr}} x) + \cos(a_{\text{cr}} x) + f_2 x + f_3)}{f_1 \sin(a_{\text{cr}} x_1) + \cos(a_{\text{cr}} x_1) + f_2 x_1 + f_3} \quad (7-34)$$

7.2.3 Numerical verification in imperfect Timoshenko members

The results obtained with the described procedure were verified with geometrically nonlinear static analysis of several examples in the finite element software ADINA [7-7], using shear deformable beam elements. Three cases for non-sway, partially-sway and sway members are presented here. In all three cases the member is made of steel (elastic modulus $E=210\text{GPa}$ and Poisson's ratio $\nu=0.3$), has a length $L=3\text{m}$ and a cross-section with shear rigidity $S_v=16154\text{kN}$ and moment of inertia $I=8.33\text{e-}6\text{m}^4$. The non-dimensional parameter μ described in Chapter 6, which measures the sensitivity of a member to shear deformation, is equal to 0.012 and could correspond to a laced built-up column. The maximum initial imperfection's magnitude is assumed to be equal to $w_o=L/500=0.006\text{m}$.

The results are presented with the use of equilibrium paths (load-displacement curves), bending moment and shear force diagrams for specific axial forces and graphs in which the value of the applied axial force is plotted on the horizontal axis and the ratio of the maximum numerically calculated values for the bending moment and the shear force to the corresponding maximum values found analytically with the use of the proposed formulas on the vertical axis. The maximum analytical

values are calculated by maximising the function of the bending moment and shear force along the imperfect Timoshenko column, as given by Eq. (7-30) and Eq. (7-32), respectively. The lateral displacement at a given location is calculated with the use of Eq. (7-34).

7.2.3.1 Non-sway member

The non-sway column considered has one rotationally fixed end and one hinged end. The non-sway column's first buckling load is equal to 3072kN according to LBA with the use of finite element software ADINA. The first buckling mode shape of the non-sway member is shown in Figure 7-3. The use of the proposed method presented in Chapter 6 (nonlinear equation for braced members) results in a buckling load equal to 3098kN, very close to the numerical one. The equilibrium path based on the displacement at the maximum initial imperfection's location is presented in Figure 7-4. It can be observed that the deflection is sufficiently predicted by the proposed analytical calculations. Loss of accuracy is only observed at load levels very close to the elastic critical buckling load.

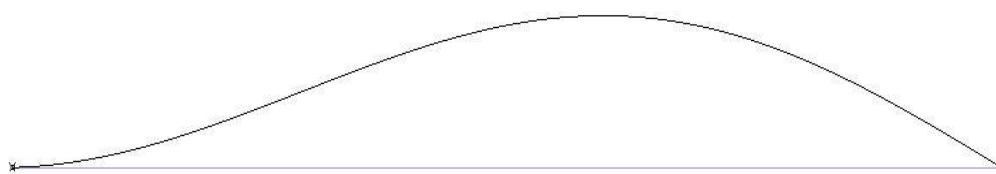


Figure 7-3: Buckling mode shape of non-sway member

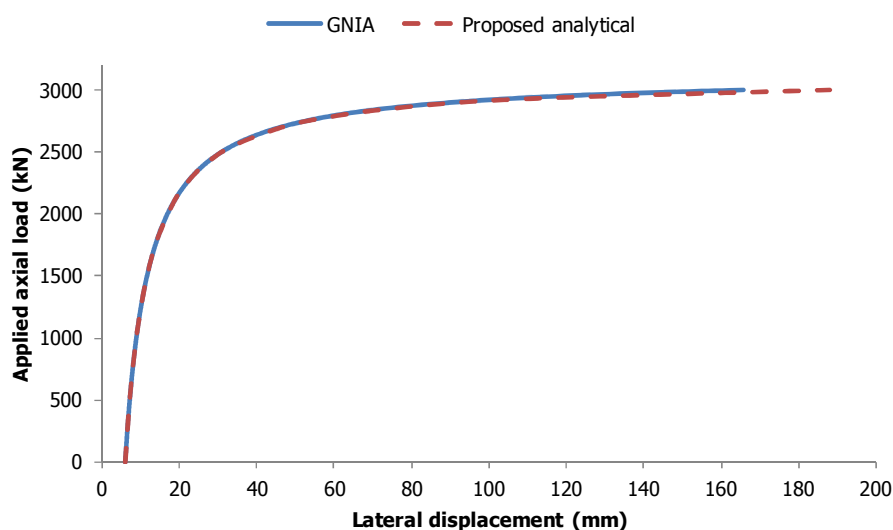


Figure 7-4: Equilibrium path for the imperfect non-sway member

The bending moment and shear force diagrams along the column for a load equal to $0.8P_{cr}$ are shown in Figure 7-5 and Figure 7-6, respectively. A very satisfactory comparison between the results obtained with the use of GNIA and the analytical predictions is observed. The ratio of the numerical and analytical maximum bending moments and shear forces for different levels of axial force is presented in Figure 7-7. It can be seen that it is close to 1 for a large range of axial forces, while it diverts from this value as the axial force approaches the elastic critical buckling load of the column.

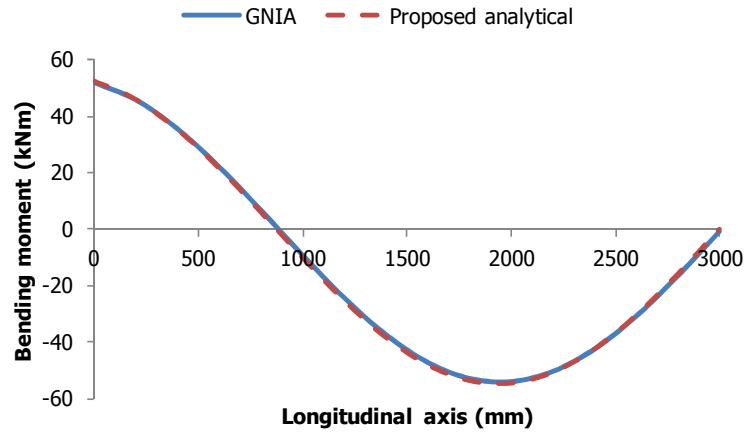
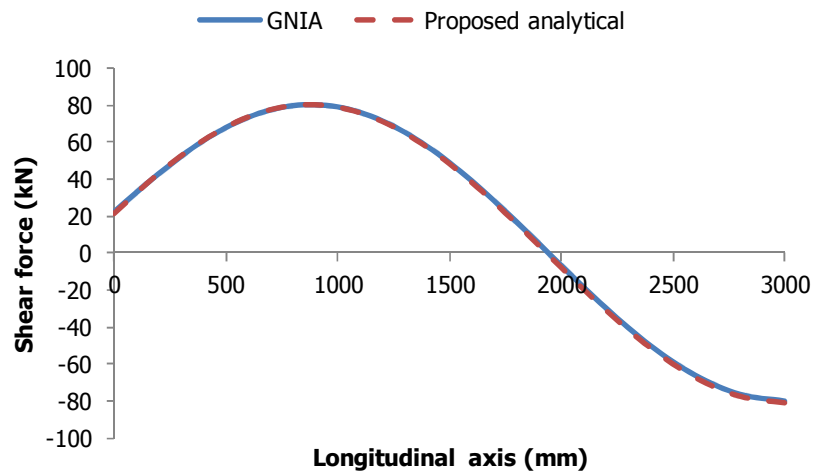
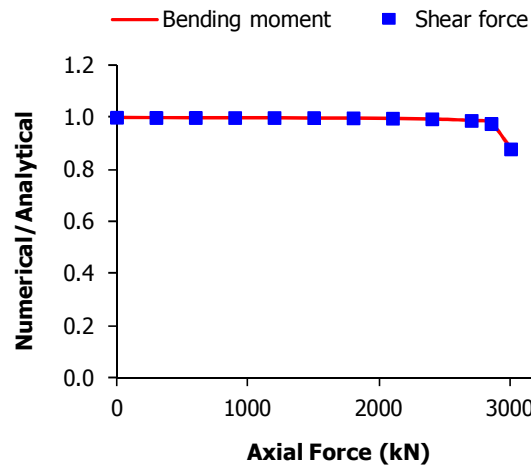
Figure 7-5: Bending moment diagram at load level $0.8P_{cr}$ for the imperfect non-sway memberFigure 7-6: Shear force diagram at load level $0.8P_{cr}$ for the imperfect non-sway member

Figure 7-7: Comparison of numerically and analytically obtained maximum bending moments and shear forces for various levels of axial load for the imperfect non-sway Timoshenko column

7.2.3.2 Partially sway member

The partially sway member has springs $c_b=2000\text{kNm}$, $c_{br,b}\rightarrow\infty$, $c_t\rightarrow\infty$ and $c_{br,t}=1000\text{kN/m}$ at its ends. The partially sway column's first buckling load is equal to 3438kN according to LBA with the use of

finite element software ADINA. The first buckling mode shape of the partially sway member is shown in Figure 7-8. The use of the proposed method presented in Chapter 6 (nonlinear equation for partially braced members) results in a buckling load equal to 3454kN, very close to the numerical one. The equilibrium path is presented in Figure 7-9, revealing that loss of accuracy is observed at load levels very close to the elastic critical buckling load, while the deflections are sufficiently predicted by the proposed procedure for smaller axial load levels.

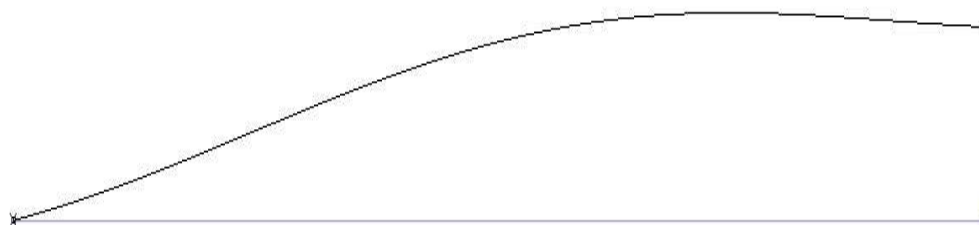


Figure 7-8: Buckling mode shape of partially sway member

The bending moment and shear force diagrams along the column for a load equal to $0.8P_{cr}$ are shown in Figure 7-10 and Figure 7-11, respectively. A very satisfactory comparison between the results obtained with the use of GNIA and the analytical predictions is observed. The ratio of the numerical and analytical maximum bending moments and shear forces for different levels of axial force is presented in Figure 7-12. It can be seen that it is equal to 1 for a large range of axial forces while loss of accuracy is observed only at high levels of axial load.

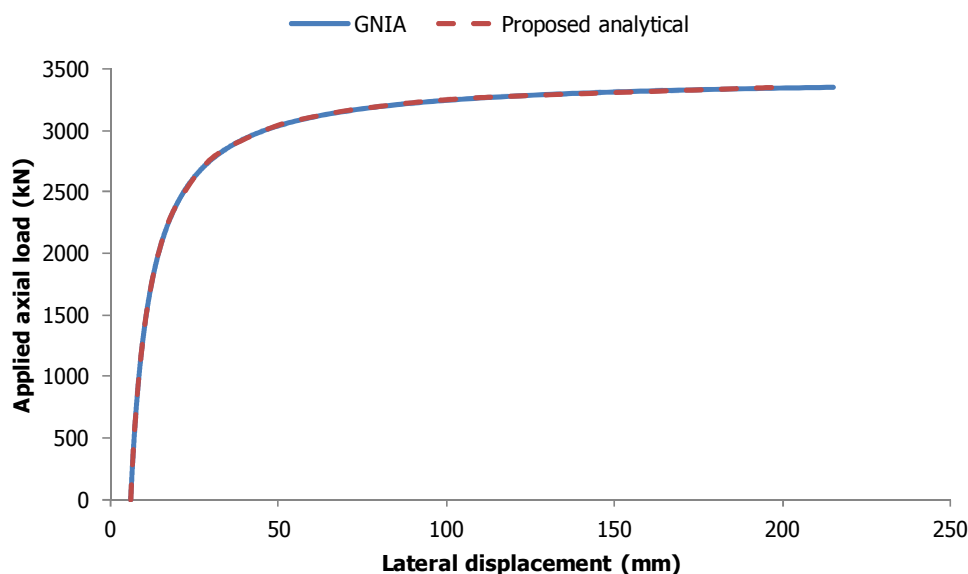


Figure 7-9: Equilibrium path for the imperfect partially sway member

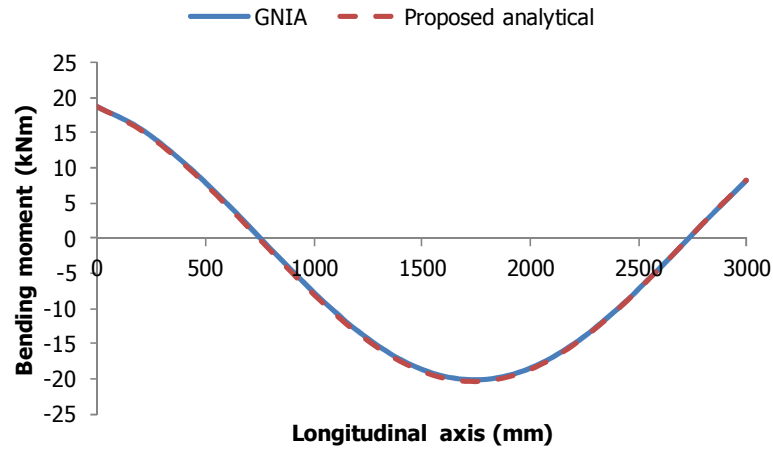


Figure 7-10: Bending moment diagram at load level $0.8P_{cr}$ for the imperfect partially sway member

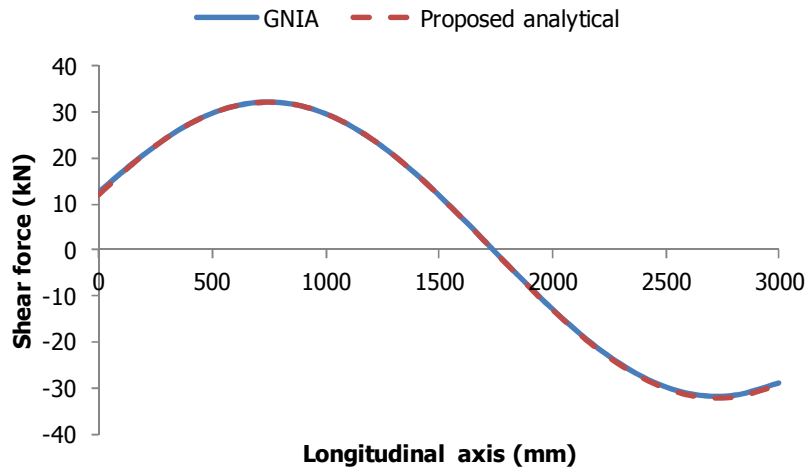


Figure 7-11: Shear force diagram at load level $0.8P_{cr}$ for the imperfect partially sway member

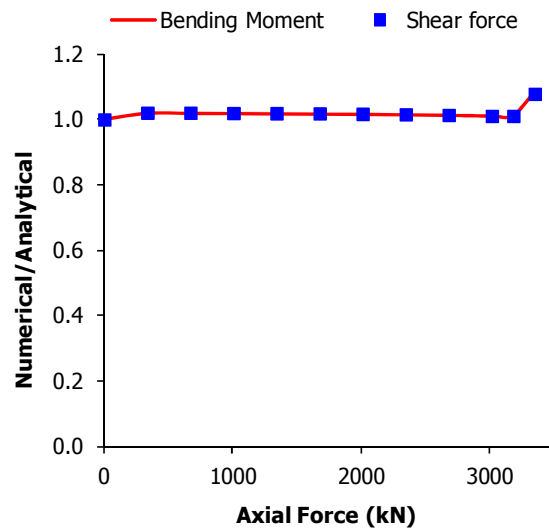


Figure 7-12: Comparison of numerically and analytically obtained maximum bending moments and shear forces for various levels of axial load for the imperfect partially sway Timoshenko column

7.2.3.3 Sway member

The sway member has springs $c_b \rightarrow \infty$, $c_{br,b} \rightarrow \infty$, $c_t = 2000 \text{ kNm}$ and $c_{br,t} \rightarrow 0$ at its ends. The sway column's first buckling load is equal to 1137 kN according to LBA with the use of finite element software ADINA. The first buckling mode shape of the sway member is shown in Figure 7-13. The use of the proposed method presented in Chapter 6 (nonlinear equation for unbraced members) results in a buckling load equal to 1138 kN, very close to the numerical one. The equilibrium path is presented in Figure 7-14, revealing that loss of accuracy is observed at load levels very close to the elastic critical buckling load, while the deflections are sufficiently predicted by the proposed procedure for smaller axial load levels.

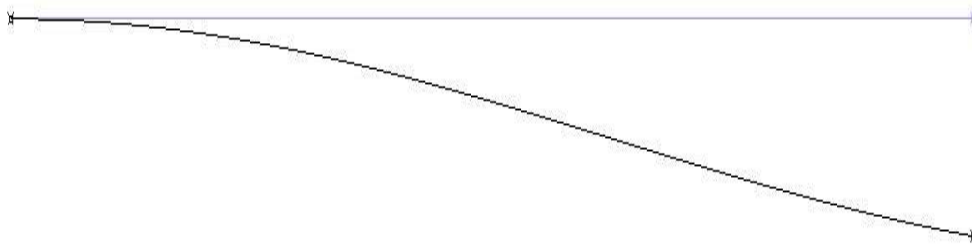


Figure 7-13: Buckling mode shape of sway member

The bending moment and shear force diagrams along the column for a load equal to $0.8P_{cr}$ are shown in Figure 7-15 and Figure 7-16, respectively. A very satisfactory comparison between the results obtained with the use of GNIA and the analytical predictions is observed. The ratio of the numerical and analytical maximum bending moments and shear forces for different levels of axial force is presented in Figure 7-17. It can be seen that it is close to 1 for a large range of axial forces while loss of accuracy is observed only at high levels of axial load.

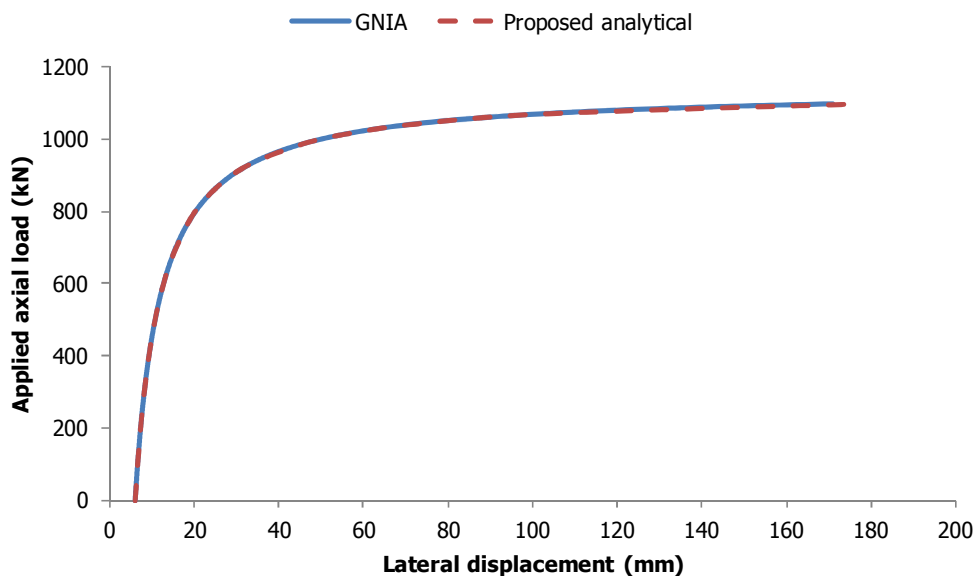


Figure 7-14: Equilibrium path for the imperfect sway column

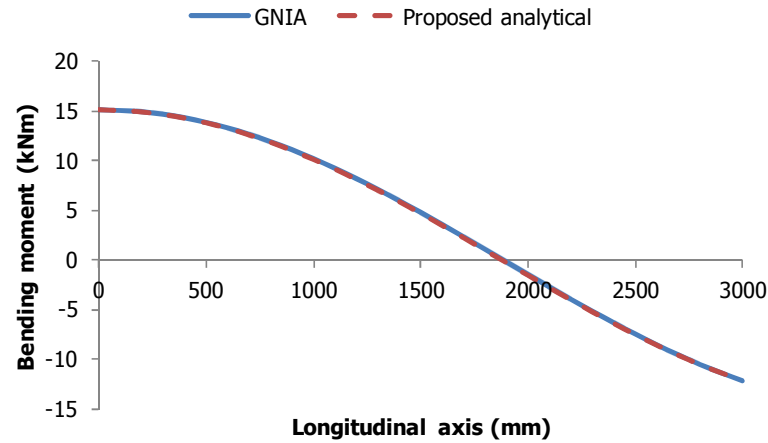


Figure 7-15: Bending moment diagram at load level $0.8P_{cr}$ for the imperfect sway member

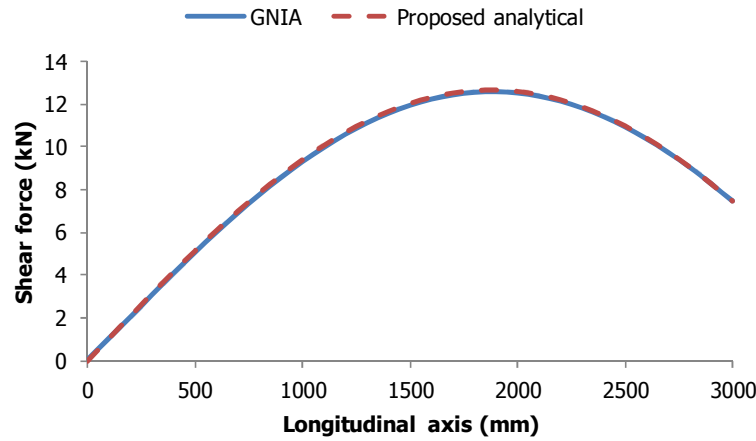


Figure 7-16: Shear force diagram at load level $0.8P_{cr}$ for the imperfect sway member

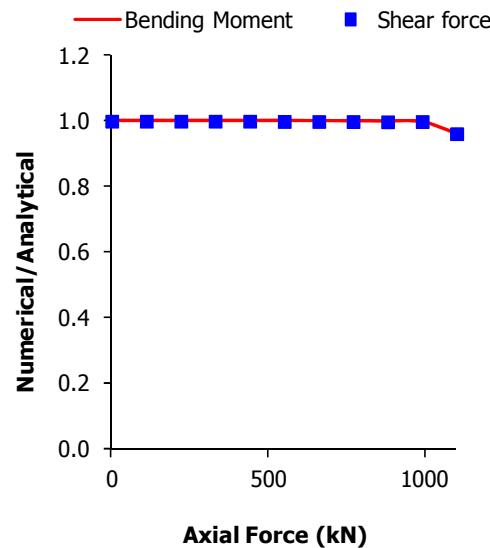


Figure 7-17: Comparison of numerically and analytically obtained maximum bending moments and shear forces for various levels of axial load for the imperfect sway Timoshenko column

7.3 LATERALLY LOADED TIMOSHENKO MEMBERS

Members belong to structures that are subjected to both vertical and horizontal loads. As a result they are usually subjected to both axial and lateral loads and they are characterised as beam-columns. The presence of axial force affects the behaviour of laterally loaded members and should be taken into account. In such cases, the deformed shape is considered for equilibrium and both the internal forces and deflections are affected. In this section, Timoshenko beam-columns with arbitrary supports under axial and lateral loads are examined. Three common cases of external lateral loading are considered: uniformly distributed transverse load, concentrated moments at both ends and concentrated forces at both ends.

The derivations of the bending moment, shear force and deflection functions for each case separately are presented in the following subsections. They are based on 2nd-order analysis with the use of the 2nd-order slope-deflection equations for Timoshenko members according to Engesser's method that were presented in Chapter 6. The results are given as closed-form solutions so that their use is straight-forward without the need for additional calculations and iterations. The procedure is described in detail for the lateral uniformly distributed load and only the results are presented for the other lateral load types considered.

7.3.1 Lateral uniformly distributed load

Consider the Timoshenko beam-column with arbitrary boundary conditions shown in Figure 7-18, which is subjected to an axial compressive load P and a uniformly distributed transverse load q . The deformed shape is also shown in Figure 7-18, while clockwise rotations and bending moments are considered to be positive.

The reactions and shear forces perpendicular to the undeformed axis for this specific lateral type of loading at the two ends of the member can be described as a function of the deflections at these ends:

$$V_{AB(q)} = c_{br,b} \delta_q = 0.5qL - \frac{M_{AB(q)} + M_{BA(q)} + P\Delta_q}{L} \quad (7-35)$$

$$V_{BA(q)} = c_{br,t} (\delta_q + \Delta_q) = 0.5qL + \frac{M_{AB(q)} + M_{BA(q)} + P\Delta_q}{L} \quad (7-36)$$

where δ_q and $\delta_q + \Delta_q$ are the deflections at ends A and B, respectively.

The bending moments at the ends A and B can be expressed by using the slope-deflection equations for shear-weak members as:

$$M_{AB(q)} = \frac{EI}{L} S_{11} \left(\psi_{A(q)} - \frac{\Delta_q}{L} \right) + \frac{EI}{L} S_{12} \left(\psi_{B(q)} - \frac{\Delta_q}{L} \right) - M_F = -c_b \psi_{A(q)} \quad (7-37)$$

$$M_{BA(q)} = \frac{EI}{L} S_{12} \left(\psi_{A(q)} - \frac{\Delta_q}{L} \right) + \frac{EI}{L} S_{11} \left(\psi_{B(q)} - \frac{\Delta_q}{L} \right) + M_F = -c_t \psi_{B(q)} \quad (7-38)$$

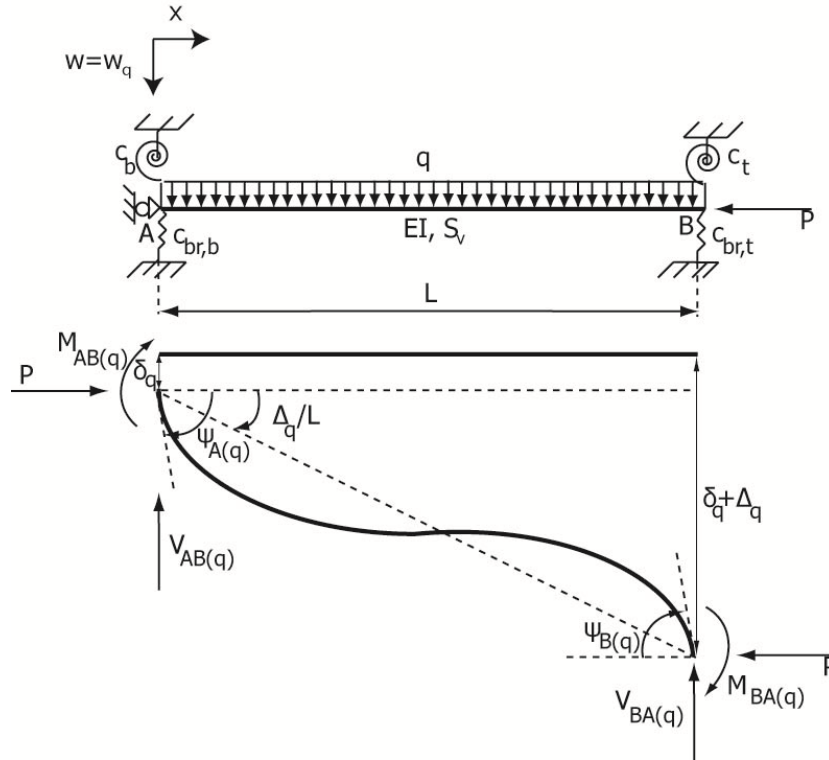


Figure 7-18: Timoshenko member with arbitrary boundary conditions subjected to an axial compressive load and uniformly distributed transverse load

In these equations $\psi_{A(q)}$ and $\psi_{B(q)}$ are the rotations due to bending only at points A and B, respectively, and Δ_q/L is the total member rotation due to relative transverse translation Δ_q of its ends A and B. The coefficients S_{kj} have been derived in Chapter 6 and depend on the applied axial load P . The term M_F denotes the fixed end bending moments at the ends of a Timoshenko member according to Engesser's approach and should be inserted in the slope-deflection equations in order to account for the uniformly distributed load q . For its derivation consider the Timoshenko member with fixed ends described by Horne and Merchant [7-8], who investigated Euler-Bernoulli beam-columns, which is loaded axially by a compressive force P and laterally by uniformly distributed load q . The bending moment along the member is given by:

$$M(x) = -EI\psi_q'(x) = -M_F + Pw_q(x) + 0.5qx(L-x) \quad (7-39)$$

The differential equations that control the problem are:

$$EI\left(1 - \frac{P}{S_v}\right)\psi_q''(x) + P\psi_q(x) = -0.5q(L-2x) \quad (7-40)$$

$$EI\left(1 - \frac{P}{S_v}\right)w_q''(x) + Pw_q(x) = M_F - 0.5qx(L-x) - \frac{EI}{S_v}q \quad (7-41)$$

The solutions of Eq. (7-40) and Eq. (7-41) are:

$$\psi_q(x) = -a\beta A_2 \sin ax + a\beta A_1 \cos ax - 0.5q \frac{(L-2x)}{P} \quad (7-42)$$

$$w_q(x) = A_1 \sin ax + A_2 \cos ax + \frac{M_F - q \left(\frac{1}{a^2} + 0.5x(L-x) + \frac{EI}{S_v} \right)}{P} \quad (7-43)$$

where A_1 and A_2 are integration constants and all other parameters have been defined previously.

Applying the boundary conditions $w_q(0) = \psi_q(0) = 0$, the constants A_1, A_2 can be evaluated. Substituting them in the boundary condition $w_q(L) = 0$ and solving for the bending moment at the fixed ends, the latter can be calculated:

$$M_F = \frac{q}{a^2} \left[1 - \frac{La}{2\beta} \cot \left(\frac{aL}{2} \right) \right] + \frac{EI}{S_v} q \quad (7-44)$$

From Eq. (7-35) the deflection at end A can be calculated:

$$\delta_q = \frac{0.5qL - \frac{M_{AB(q)} + M_{BA(q)} + P\Delta_q}{L}}{c_{br,b}} \quad (7-45)$$

Alternatively, the deflection at end A can be expressed as:

$$\delta_q = \frac{qL - c_{br,t} \Delta_q}{c_{br,b} + c_{br,t}} \quad (7-46)$$

By making use of Eqs. (7-35)-(7-38) and Eq. (7-45), Eq. (7-47) giving the deflection at end B arises:

$$\frac{\Delta_q}{L} = \frac{\rho_1 (-c_b \psi_{A(q)} - c_t \psi_{B(q)}) + \chi_q}{\omega} \quad (7-47)$$

where $\rho_1 = 1 + c_{br,t}/c_{br,b}$, $\rho_2 = 1 - c_{br,t}/c_{br,b}$, $\chi_q = 0.5qp_2L^2$ and

$$\omega = L^2 \left(c_{br,t} - \rho_1 \frac{P}{L} \right) \quad (7-48)$$

Based on Eq. (7-37), Eq. (7-38), Eq. (7-44) and Eq. (7-47), the rotations due to bending only can be calculated at the two ends:

$$\psi_{B(q)} = \frac{\chi_q S + \frac{\omega M_F L}{EI} - (\omega(S_{11} + c_b^\#) + S\rho_1 c_b) \psi_{A(q)}}{\omega S_{12} + S\rho_1 c_t} \quad (7-49)$$

$$\psi_{A(q)} = \frac{(\omega S_{12} + S\rho_1 c_t) \left(\frac{-\omega M_F L}{EI} + S\chi_q \right) - (\omega S_{11} + \omega c_t^\# + S\rho_1 c_t) \left(\frac{\omega M_F L}{EI} + S\chi_q \right)}{(\omega S_{12} + S\rho_1 c_b)(\omega S_{12} + S\rho_1 c_t) - (\omega S_{11} + \omega c_t^\# + S\rho_1 c_t)(\omega S_{11} + \omega c_b^\# + S\rho_1 c_b)} \quad (7-50)$$

where $S = S_{11} + S_{12}$ and

$$c_i^\# = \frac{c_i L}{EI} \quad (7-51)$$

The bending moment along the member due to the axial compressive load and the uniformly distributed transverse load is:

$$M_q(x) = -EI\psi_q'(x) = M_{AB(q)} + V_{AB(q)}x + P(w_q(x) - \delta_q) - 0.5qx^2 \quad (7-52)$$

The 2nd-order shear force is found by differentiating Eq. (7-52):

$$Q_q(x) = -EI\psi_q''(x) = V_{AB(q)} + Pw_q'(x) - qx \quad (7-53)$$

Solving Eq. (7-52) for ψ_q' Eq. (7-54) is obtained:

$$\psi_q'(x) = -\frac{M_{AB(q)} + V_{AB(q)}x + P(w_q(x) - \delta_q) - 0.5qx^2}{EI} \quad (7-54)$$

The first derivative of shear deformation is given by:

$$V_q'(x) = \frac{Pw_q''(x) - q}{S_v} \quad (7-55)$$

If the relationship between total rotation, rotation due to bending only and shear deformation is differentiated with respect to x , Eq. (7-56) arises:

$$w_q''(x) = \psi_q'(x) + V_q'(x) \quad (7-56)$$

By substituting Eq. (7-54) and Eq. (7-55) into Eq. (7-56) the differential equation describing the problem arises and its trigonometric solution for boundary conditions $w_q(0) = \delta_q$ and $w_q(L) = \delta_q + \Delta_q$ is:

$$w_q(x) = \frac{\frac{1}{P} \left(- \left(M_{AB(q)} + q \left(\frac{1}{a^2} + \frac{EI}{S_v} \right) \right) \cos aL + M_{AB(q)} + V_{AB(q)}L + q \left(\frac{1}{a^2} + \frac{EI}{S_v} - 0.5L^2 \right) \right) + \Delta_q}{\sin aL} \sin ax + \frac{1}{P} \left(M_{AB(q)} + q \left(\frac{1}{a^2} + \frac{EI}{S_v} \right) \right) \cos ax + \frac{1}{P} \left(-M_{AB(q)} - V_{AB(q)}x + P\delta_q + q \left(-\frac{1}{a^2} - \frac{EI}{S_v} + 0.5x^2 \right) \right) \quad (7-57)$$

The derivative of Eq. (7-57) with respect to x is equal to:

$$w_q'(x) = a \frac{\frac{1}{P} \left(- \left(M_{AB(q)} + q \left(\frac{1}{a^2} + \frac{EI}{S_v} \right) \right) \cos aL + M_{AB(q)} + V_{AB(q)}L + q \left(\frac{1}{a^2} + \frac{EI}{S_v} - 0.5L^2 \right) \right) + \Delta_q}{\sin aL} \cos ax - \frac{a}{P} \left(M_{AB(q)} + q \left(\frac{1}{a^2} + \frac{EI}{S_v} \right) \right) \sin ax + \frac{1}{P} \left(-V_{AB(q)} + qx \right) \quad (7-58)$$

Incorporating Eq. (7-57) into Eq. (7-52) and Eq. (7-58) into Eq. (7-53) the second-order bending moment and shear force due to laterally distributed load q , respectively, along the member can be calculated.

7.3.2 Concentrated moments at the ends

Consider the Timoshenko beam-column with arbitrary boundary conditions shown in Figure 7-19, which is subjected to an axial compressive load P and concentrated moments M_1 and M_2 at its ends,

considered as positive when clockwise. The same procedure is followed as in the previous section for the laterally distributed load q . The deformed shape is also shown in Figure 7-19, while clockwise rotations and bending moments are considered to be positive.

The reactions and shear forces perpendicular to the undeformed axis for this specific lateral type of loading at the two ends of the member can be described as a function of the deflections at these ends:

$$V_{AB(M)} = c_{br,b} \delta_M = - \frac{M_{AB(M)} + M_{BA(M)} + P \Delta_M}{L} \quad (7-59)$$

$$V_{BA(M)} = c_{br,t} (\delta_M + \Delta_M) = \frac{M_{AB(M)} + M_{BA(M)} + P \Delta_M}{L} \quad (7-60)$$

where δ_M and $\delta_M + \Delta_M$ are the deflections at ends A and B, respectively.

The bending moments at the ends A and B can be expressed by using the slope-deflection equations for shear-weak members as:

$$M_{AB(M)} = \frac{EI}{L} S_{11} \left(\psi_{A(M)} - \frac{\Delta_M}{L} \right) + \frac{EI}{L} S_{12} \left(\psi_{B(M)} - \frac{\Delta_M}{L} \right) = -c_b \psi_{A(M)} + M_1 \quad (7-61)$$

$$M_{BA(M)} = \frac{EI}{L} S_{12} \left(\psi_{A(M)} - \frac{\Delta_M}{L} \right) + \frac{EI}{L} S_{11} \left(\psi_{B(M)} - \frac{\Delta_M}{L} \right) = -c_t \psi_{B(M)} + M_2 \quad (7-62)$$

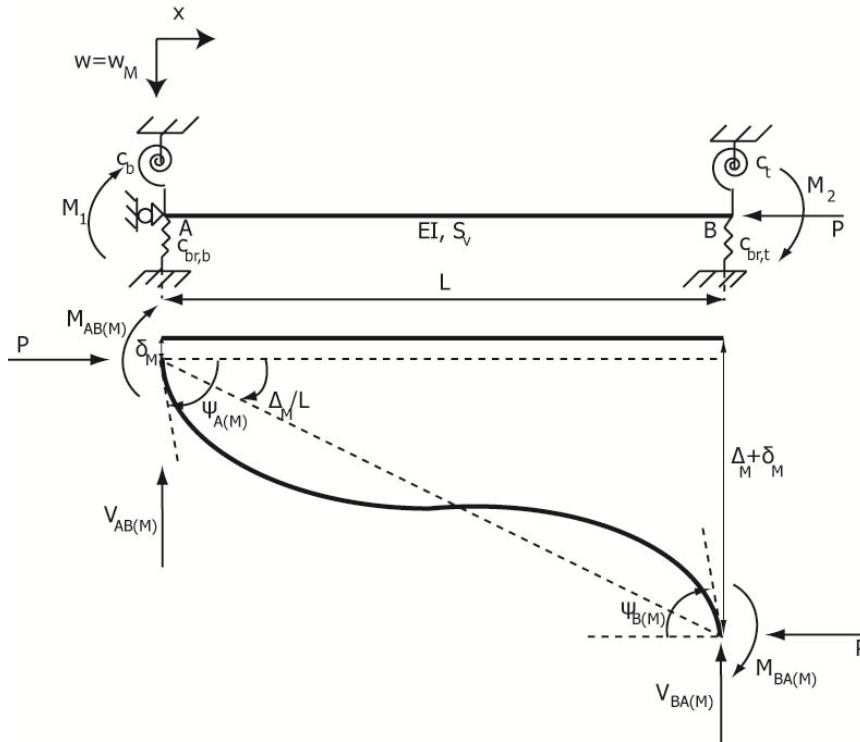


Figure 7-19: Timoshenko member with arbitrary boundary conditions subjected to an axial compressive load and concentrated moments at its ends

Making use of Eqs. (7-59)-(7-62) the deflections, rotations, bending moment and shear forces can be calculated allowing evaluation of the structural behaviour of the Timoshenko beam-column under concentrated end moments. The results are summarised in Table 7-1.

Table 7-1: Summary of results for the case of concentrated moments at the ends

$\delta_M = -\frac{c_{br,t}\Delta_M}{c_{br,b} + c_{br,t}}$
$\frac{\Delta_M}{L} = \frac{\rho_1 \left(-c_b \psi_{A(M)} - c_t \psi_{B(M)} \right) + \chi_M}{\omega}, \text{ where } \chi_M = (M_1 + M_2)\rho_1$
$M_{AB(M)} = \frac{EI}{L} S_{11} \left(\psi_{A(M)} - \frac{\Delta_M}{L} \right) + \frac{EI}{L} S_{12} \left(\psi_{B(M)} - \frac{\Delta_M}{L} \right)$ $M_{BA(M)} = \frac{EI}{L} S_{12} \left(\psi_{A(M)} - \frac{\Delta_M}{L} \right) + \frac{EI}{L} S_{11} \left(\psi_{B(M)} - \frac{\Delta_M}{L} \right)$
$V_{AB(M)} = -V_{BA(M)} = -\frac{M_{AB(M)} + M_{BA(M)} + P\Delta_M}{L}$
$\psi_{B(M)} = \frac{\chi_M S + \frac{\omega M_1 L}{EI} - \left(\omega (S_{11} + c_b^\#) + S\rho_1 c_b \right) \psi_{A(M)}}{\omega S_{12} + S\rho_1 c_t}, \text{ where } S = S_{11} + S_{12}.$
$\psi_{A(M)} = \frac{(\omega S_{12} + S\rho_1 c_t) \left(\frac{\omega M_2 L}{EI} + S\chi_M \right) + (\omega S_{11} + \omega c_t^\# + S\rho_1 c_t) \left(\frac{-\omega M_1 L}{EI} - S\chi_M \right)}{(\omega S_{12} + S\rho_1 c_b)(\omega S_{12} + S\rho_1 c_t) - (\omega S_{11} + \omega c_t^\# + S\rho_1 c_t)(\omega S_{11} + \omega c_b^\# + S\rho_1 c_b)}$
$w_M(x) = \frac{\frac{M_{AB(M)}}{P}(1 - \cos \alpha L) + \frac{V_{AB(M)}L}{P} + \Delta_M}{\sin \alpha L} \sin \alpha x + \frac{M_{AB(M)}}{P} \cos \alpha x + \frac{1}{P} \left(-M_{AB(M)} - V_{AB(M)}x + P\delta_M \right)$
$w'_M(x) = \alpha \frac{\frac{M_{AB(M)}}{P}(1 - \cos \alpha L) + \frac{V_{AB(M)}L}{P} + \Delta_M}{\sin \alpha L} \cos \alpha x - \alpha \frac{M_{AB(M)}}{P} \sin \alpha x - \frac{V_{AB(M)}}{P}$
$M_M(x) = M_{AB(M)} + V_{AB(M)}x + P(w_M(x) - \delta_M)$
$Q_M(x) = V_{AB(M)} + Pw'_M(x)$

7.3.3 Concentrated forces at the ends

Consider the Timoshenko beam-column with arbitrary boundary conditions shown in Figure 7-20, which is subjected to an axial compressive load P and concentrated forces H_1 and H_2 at its ends, considered as positive when oriented towards the positive w axis. The same procedure is followed as in the previous section for the laterally distributed load q . The deformed shape is also shown in Figure 7-20, while clockwise rotations and bending moments are considered to be positive.

The shear forces perpendicular to the undeformed axis at the two ends of the member can be described as a function of the deflections at these ends:

$$V_{AB(H)} = c_{br,b} \delta_H - H_1 = -\frac{M_{AB(H)} + M_{BA(H)} + P\Delta_H}{L} \quad (7-63)$$

$$V_{BA(H)} = c_{br,t} (\delta_H + \Delta_H) - H_2 = \frac{M_{AB(H)} + M_{BA(H)} + P\Delta_H}{L} \quad (7-64)$$

where δ_H and $\delta_H + \Delta_H$ are the deflections at ends A and B, respectively.

The bending moments at the ends A and B can be expressed by using the slope-deflection equations for shear-weak members as:

$$M_{AB(H)} = \frac{EI}{L} S_{11} \left(\psi_{A(H)} - \frac{\Delta_H}{L} \right) + \frac{EI}{L} S_{12} \left(\psi_{B(H)} - \frac{\Delta_H}{L} \right) = -c_b \psi_{A(H)} \quad (7-65)$$

$$M_{BA(H)} = \frac{EI}{L} S_{12} \left(\psi_{A(H)} - \frac{\Delta_H}{L} \right) + \frac{EI}{L} S_{11} \left(\psi_{B(H)} - \frac{\Delta_H}{L} \right) = -c_t \psi_{B(H)} \quad (7-66)$$

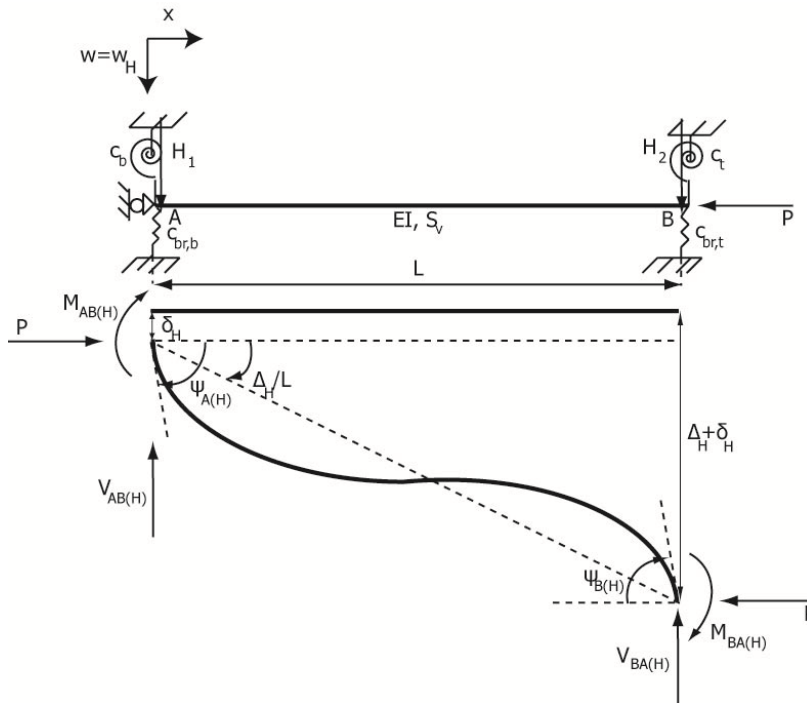


Figure 7-20: Timoshenko member with arbitrary boundary conditions subjected to an axial compressive load and lateral concentrated loads at its ends

Making use of Eqs. (7-63)-(7-66) the deflections, rotations, bending moment and shear forces can be calculated leading to the specification of the structural behaviour of the Timoshenko beam-column under end concentrated lateral forces. The results are summarised in Table 7-2.

Table 7-2: Summary of results for the case of concentrated loads at the ends

$\delta_H = \frac{H_1 + H_2 - c_{br,t} \Delta_H}{c_{br,b} + c_{br,t}}$
$\frac{\Delta_H}{L} = \frac{\rho_1 \left(-c_b \psi_{A(H)} - c_t \psi_{B(H)} \right) + \chi_H}{\omega}, \text{ where } \chi_H = L(H_2 - H_1 c_{br,t} / c_{br,b})$
$M_{AB(H)} = \frac{EI}{L} S_{11} \left(\psi_{A(H)} - \frac{\Delta_H}{L} \right) + \frac{EI}{L} S_{12} \left(\psi_{B(H)} - \frac{\Delta_H}{L} \right)$ $M_{BA(H)} = \frac{EI}{L} S_{12} \left(\psi_{A(H)} - \frac{\Delta_H}{L} \right) + \frac{EI}{L} S_{11} \left(\psi_{B(H)} - \frac{\Delta_H}{L} \right)$
$V_{AB(H)} = -V_{BA(H)} = -\frac{M_{AB(H)} + M_{BA(H)} + P\Delta_H}{L}$
$\psi_{B(H)} = \frac{\chi_H S - (\omega(S_{11} + c_b^\#) + S\rho_1 c_b) \psi_{A(H)}}{\omega S_{12} + S\rho_1 c_t}, \text{ where } S = S_{11} + S_{12}.$
$\psi_{A(H)} = \frac{(\omega S_{12} - \omega S_{11} - \omega c_t^\#)(S\chi_H)}{(\omega S_{12} + S\rho_1 c_b)(\omega S_{12} + S\rho_1 c_t) - (\omega S_{11} + \omega c_t^\# + S\rho_1 c_t)(\omega S_{11} + \omega c_b^\# + S\rho_1 c_b)}$
$w_H(x) = \frac{\frac{M_{AB(H)}}{P}(1 - \cos \alpha L) + \frac{V_{AB(H)}L}{P} + \Delta_H}{\sin \alpha L} \sin \alpha x + \frac{M_{AB(H)}}{P} \cos \alpha x + \frac{1}{P} \left(-M_{AB(H)} - V_{AB(H)}x + P\delta_H \right)$
$w_H'(x) = \alpha \frac{\frac{M_{AB(H)}}{P}(1 - \cos \alpha L) + \frac{V_{AB(H)}L}{P} + \Delta_H}{\sin \alpha L} \cos \alpha x - \alpha \frac{M_{AB(H)}}{P} \sin \alpha x - \frac{V_{AB(H)}}{P}$
$M_H(x) = M_{AB(H)} + V_{AB(H)}x + P(w_H(x) - \delta_H)$
$Q_H(x) = V_{AB(H)} + Pw_H'(x)$

7.3.4 Combination of the above load conditions

Each of the lateral load cases examined above addresses one type of transverse load acting in parallel with an applied axial force. For the same axial force P , the principle of superposition can be applied for different lateral loading conditions along the pre-buckling loading path, as long as the material behaviour remains in the elastic range. Therefore, the response to combined lateral loading and imperfection can be found by summing up the corresponding values. An approximate calculation of bending moment and shear force along the member's length under the same axial force P is equal to:

$$M(x) = M_{imp}(x) + M_q(x) + M_M(x) + M_H(x) \quad (7-67)$$

$$Q(x) = Q_{imp}(x) + Q_q(x) + Q_M(x) + Q_H(x) \quad (7-68)$$

It should be noted that the closed-form solutions correspond to second-order analysis and are based on trigonometrical functions for the deflections and rotations, differing in this way from the polynomial functions that are used for first-order analysis. Therefore, the use of small values of the applied axial force P is expected to give results very close to the ones that would be obtained from first-order analysis of Timoshenko members but the limiting case of P equal to zero leads to numerical difficulties. A general theory for Euler-Bernoulli members was formulated by Rubin [7-9] overcoming

the inconsistency between first-order and second-order analysis for zero axial force P . It should also be noted that the use of either very large or very small values for the springs' stiffness (for modelling either fixed or free degrees of freedom) may lead to numerical difficulties and should be treated with care. Finally, it should be mentioned that, as second-order analysis is associated with an engineering problem, any numerical difficulties observed in very rare and specific cases resulting in indeterminate results are attributed to the approximate nature of the second-order analysis presented.

7.4 NUMERICAL VERIFICATION OF THE PROPOSED EQUATIONS

The results obtained with the described procedure were verified for several examples by means of geometrically nonlinear imperfection analysis (GNIA) in finite element software ADINA [7-7] with the use of Hermitian shear deformable beam elements. A large number of numerical examples was used for the numerical verification of the proposed closed-form solutions and three cases for non-sway, partially-sway and sway members are presented here. The three cases presented here have the same material and cross-sectional characteristics as the ones examined above considering only initial imperfections. The non-dimensional parameter $\mu = EI/S_v L^2$ which defines the sensitivity of the member to shear deformation is equal to 0.012, which is a realistic value for a laced built-up column. The initial imperfection is assumed to be equal to $w_0 = L/500 = 0.006\text{m}$ and is based on the first buckling mode of the member. The lateral distributed load q , the concentrated moments M_1 and M_2 and the concentrated loads H_1 and H_2 are equal to 10kN/m, 50kNm, -100kNm, 50kN and 10kN, respectively.

The results are presented with the use of equilibrium paths (load-displacement curves), indicative bending moment and shear force diagrams for axial force equal to $0.8P_{cr}$ and graphs in which the applied axial force is plotted on the horizontal axis and the ratio of the maximum numerically calculated values for the bending moment and the shear force found with the use of GNIA (large deflection theory) to the corresponding maximum values found analytically on the vertical axis.

The maximum analytical values are calculated by maximising the function of the bending moment and shear force along the imperfect Timoshenko column as given by Eq. (7-67) and Eq. (7-68), respectively. The lateral displacement at a given location is calculated with the use of Eq. (7-34) and the deflections $w_q(x)$, $w_M(x)$ and $w_H(x)$. Based on these results, the efficiency of the proposed analytical method is checked as far as both internal forces and deflections are concerned.

7.4.1.1 Non-sway member

The non-sway column considered has one rotationally fixed end and one hinged end and is the same as the one examined previously considering only the existence of axial force and initial imperfection. The lateral load is directly applied at the first step while the axial force is gradually applied until it takes its maximum value. The equilibrium path based on the displacement at the maximum initial imperfection's location is presented in Figure 7-21. It can be observed that the deflection is sufficiently predicted by the proposed analytical calculations. Loss of accuracy is only observed at load levels very close to the elastic critical buckling load. At these load levels, small deflection theory is inadequate but it can be observed that the deflection for a 3 metre long member exceeds 300mm, a value unacceptable for structural engineering applications.

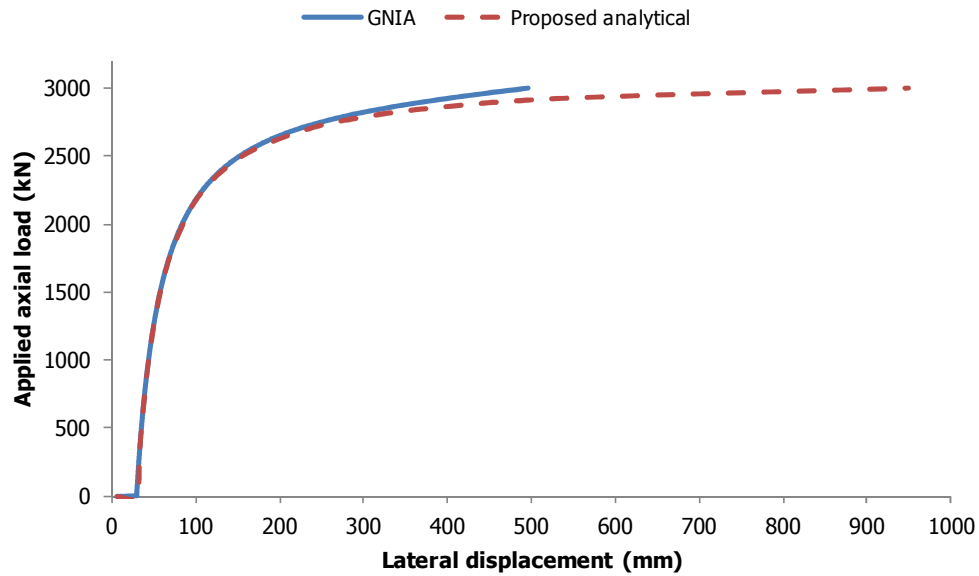


Figure 7-21: Equilibrium path for the imperfect non-sway member under lateral load directly applied at the first step

The bending moment and shear force diagrams along the column for a load equal to $0.8P_{cr}$ are shown in Figure 7-22 and Figure 7-23, respectively. A very satisfactory comparison between the results obtained with the use of GNIA and the analytical predictions is observed. The ratio of the numerical and analytical maximum bending moments and shear forces for different levels of axial force is presented in Figure 7-24. It can be seen that it is close to 1 for a large range of axial forces while it diverts from this value as the axial force approaches the elastic critical buckling load of the member.

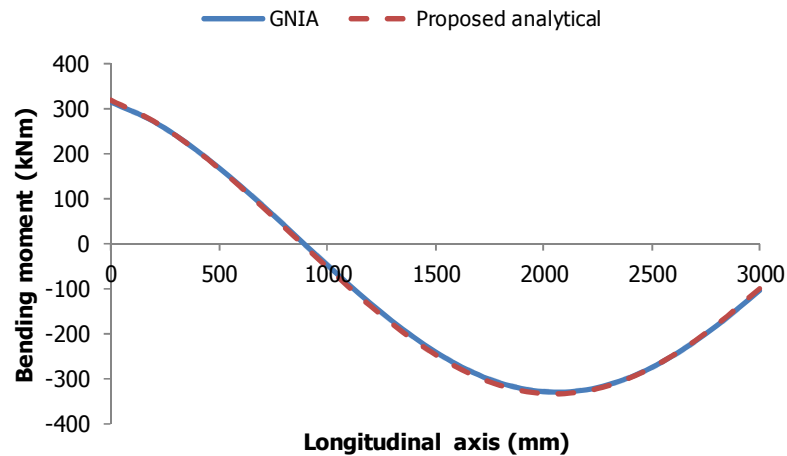


Figure 7-22: Bending moment diagram at load level $0.8P_{cr}$ for the imperfect non-sway member under lateral load

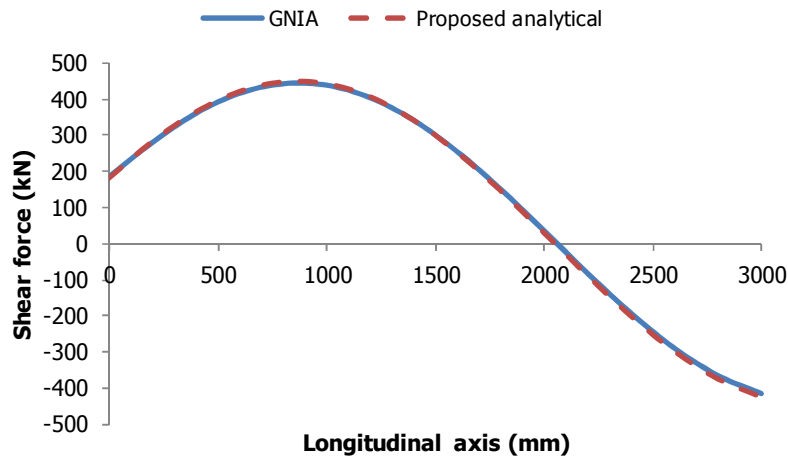


Figure 7-23: Shear force diagram at load level $0.8P_{cr}$ for the imperfect non-sway member under lateral load

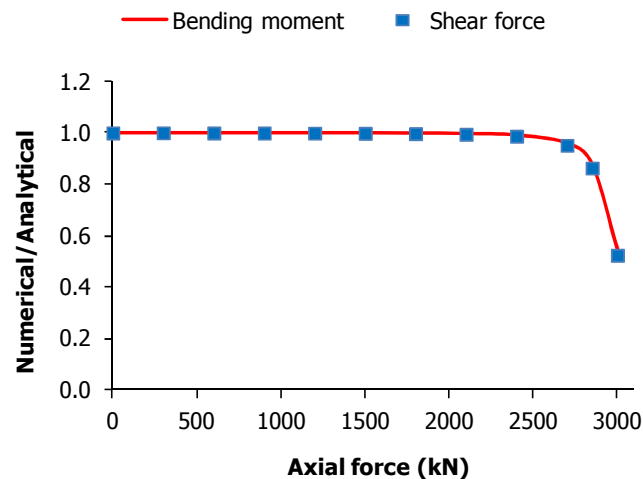


Figure 7-24: Comparison of analytically and numerically obtained maximum bending moments and shear forces for various levels of axial load for the non-sway imperfect Timoshenko member under lateral load

If both the lateral and axial loads are gradually applied until they reach their prescribed maximum value the equilibrium path will be different. The results obtained analytically and numerically with gradual application of the loads are shown for the non-sway member in Figure 7-25. It can be concluded that the proposed analytical method is sufficient for a wide range of axial forces as it is for the case that the lateral loads are directly applied at the beginning of the analysis.

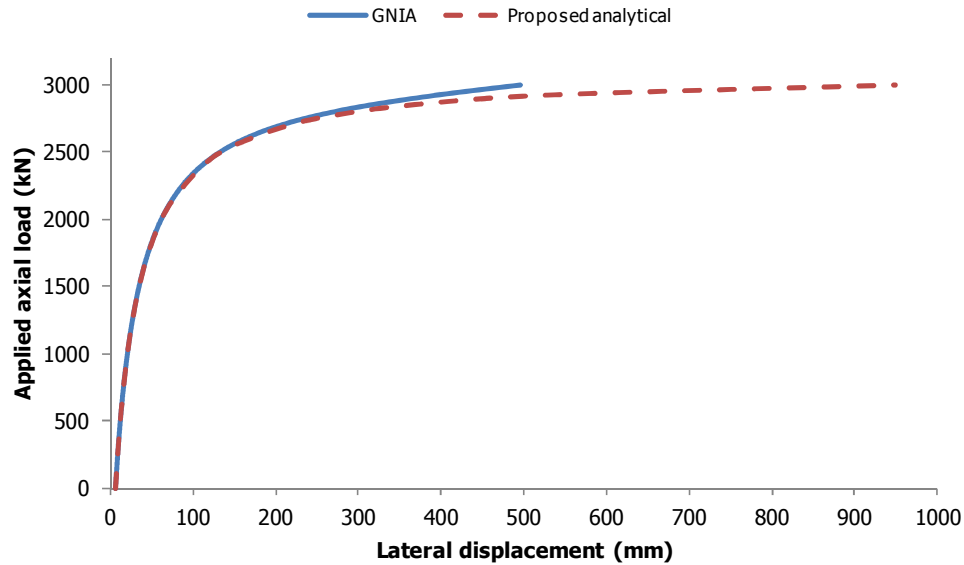


Figure 7-25: Equilibrium path for the imperfect non-sway member under lateral load gradually applied

7.4.1.2 Partially sway member

The partially sway member has springs $c_b=2000\text{kNm}$, $c_{br,b}\rightarrow\infty$, $c_t\rightarrow\infty$ and $c_{br,t}=1000\text{kN/m}$ at its ends and is the same as the one examined previously considering only the existence of axial load and initial imperfection. The lateral load is applied directly at the first step while the axial force is gradually applied. The equilibrium path based on the displacement at the maximum initial imperfection's location is presented in Figure 7-26. It can be observed that the deflection is sufficiently predicted by the proposed analytical calculations. Loss of accuracy is only observed at load levels very close to the elastic critical buckling load. Similar conclusions to the previously mentioned case can be drawn for this case, too.

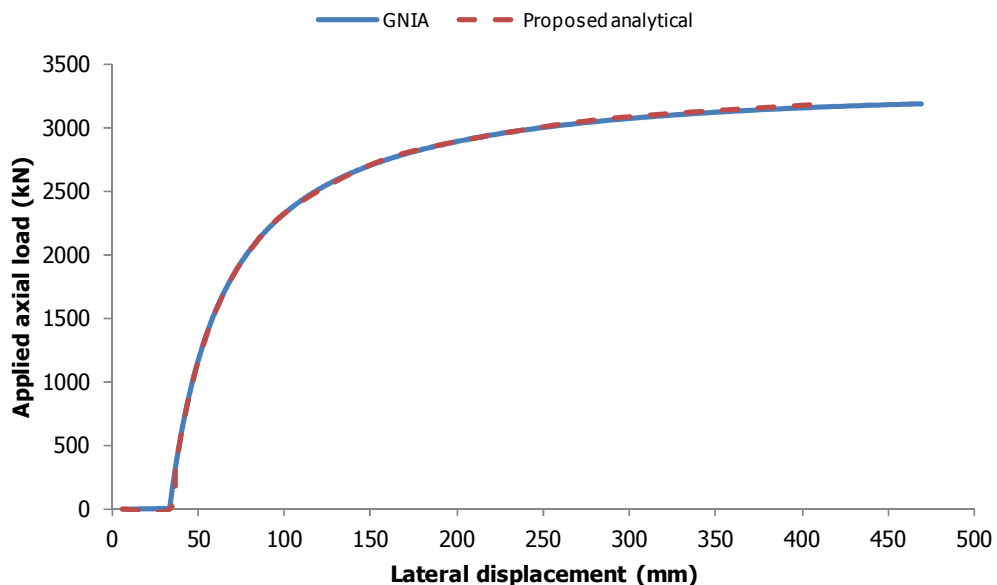


Figure 7-26: Equilibrium path for the imperfect partially sway member under lateral load directly applied at the first step

The bending moment and shear force diagrams along the column for a load equal to $0.8P_{cr}$ are shown in Figure 7-27 and Figure 7-28, respectively. A very satisfactory comparison between the results

obtained with the use of GNIA and the analytical predictions is observed. The proposed method cannot only predict the maximum values of the bending moment and shear forces in a satisfactory way but also their variation along the examined member. The ratio of the numerical and analytical maximum bending moments and shear forces for different levels of axial force is presented in Figure 7-29. It can be seen that it is close to 1 for a large range of axial forces while it diverts from this value as the axial force approaches the elastic critical buckling load of the column.

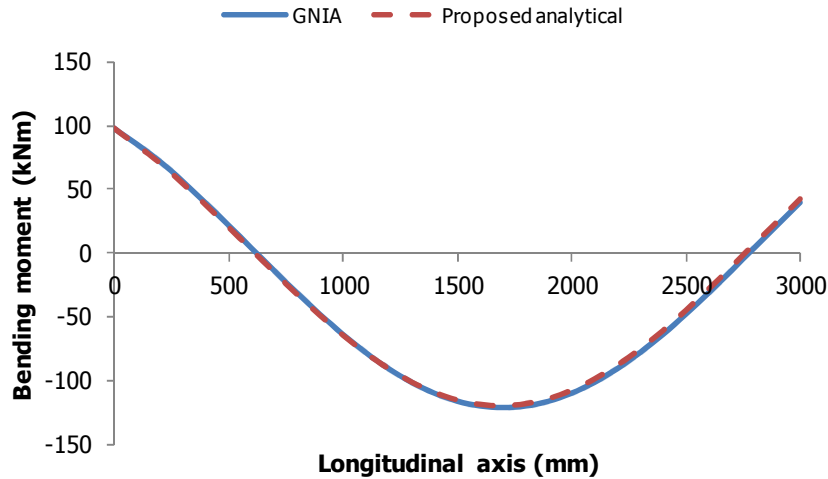


Figure 7-27: Bending moment diagram at load level $0.8P_{cr}$ for the imperfect partially sway member under lateral load

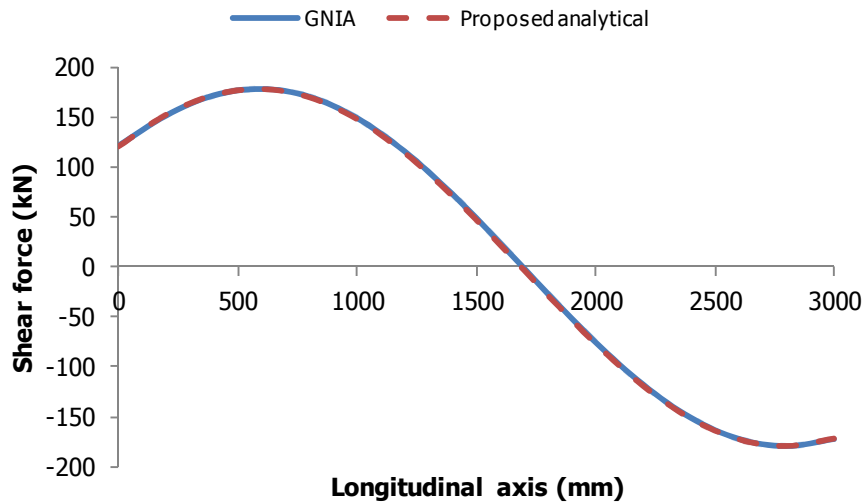


Figure 7-28: Shear force diagram at load level $0.8P_{cr}$ for the imperfect partially sway member under lateral load

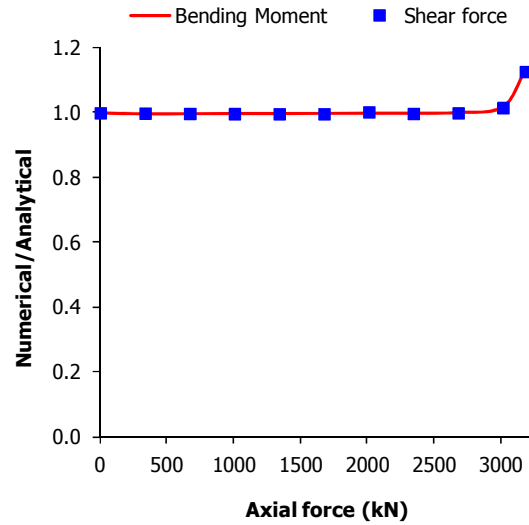


Figure 7-29: Comparison of analytically and numerically obtained maximum bending moments and shear forces for various levels of axial load for the partially sway imperfect Timoshenko member under lateral load

If both the lateral and axial loads are gradually applied the equilibrium path will be different from the case that the lateral loads are applied at the beginning of the analyses. The results obtained analytically and numerically with gradual application of the loads are shown for the partially sway member in Figure 7-30.

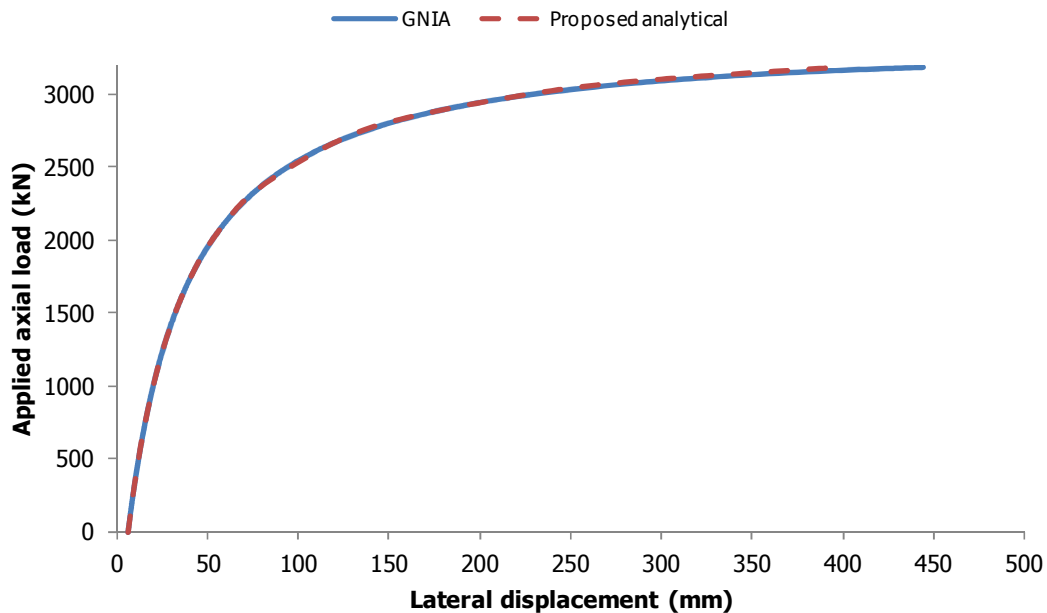


Figure 7-30: Equilibrium path for the imperfect partially sway member under lateral load gradually applied

7.4.1.3 Sway member

The sway member has springs $c_b \rightarrow \infty$, $c_{br,b} \rightarrow \infty$, $c_t = 2000 \text{ kNm}$ and $c_{br,t} \rightarrow 0$ at its ends and is the same as the one examined previously considering only the existence of axial force and initial imperfection. The lateral load is applied directly at the first step while the axial force is gradually applied. The equilibrium path based on the displacement at the maximum initial imperfection's location is presented in Figure 7-31. It can be observed that the deflection is sufficiently predicted by the proposed

analytical calculations. Loss of accuracy is only observed at load levels very close to the elastic critical buckling load.

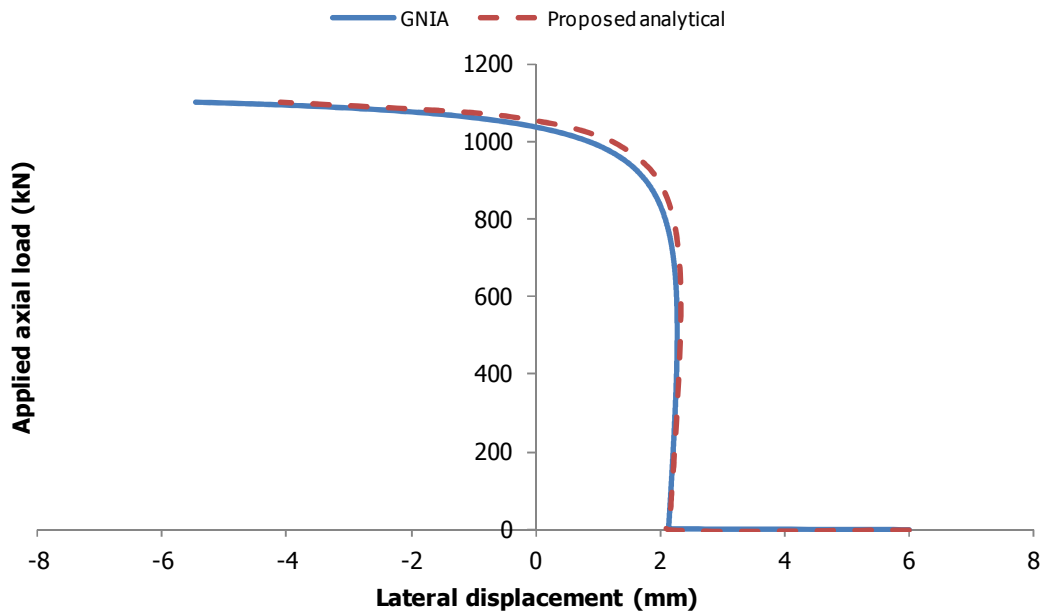


Figure 7-31: Equilibrium path for the imperfect sway member under lateral load directly applied at the first step

The bending moment and shear force diagrams along the column for a load equal to $0.8P_{cr}$ are shown in Figure 7-32 and Figure 7-33, respectively. A very satisfactory comparison between the results obtained with the use of GNIA and the analytical predictions is observed. The ratio of the numerical and analytical maximum bending moments and shear forces for different levels of axial force is presented in Figure 7-34. It can be seen that it is close to 1 for a large range of axial forces while it diverts from this value as the axial force approaches the elastic critical buckling load of the column.

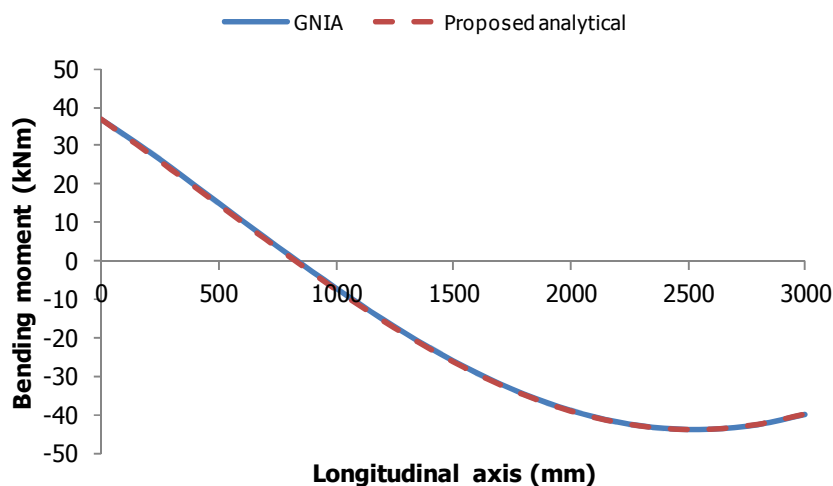


Figure 7-32: Bending moment diagram at load level $0.8P_{cr}$ for the imperfect sway member under lateral load

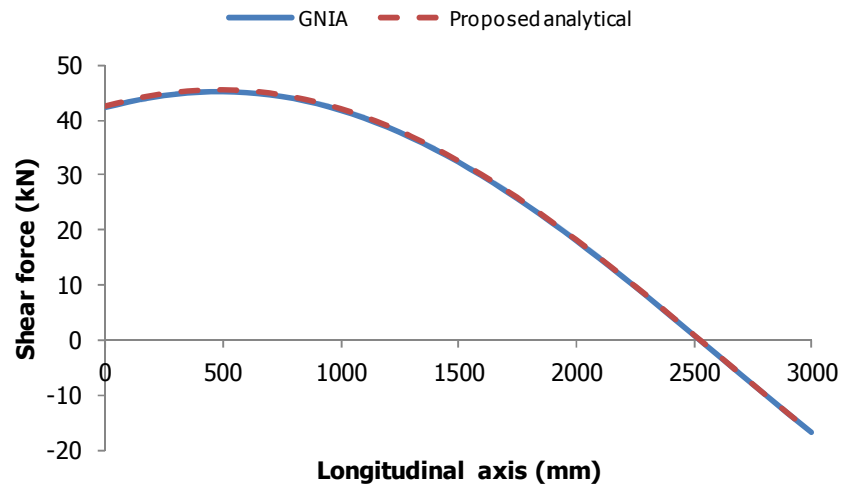


Figure 7-33: Shear force diagram at load level $0.8P_{cr}$ for the imperfect sway member under lateral load

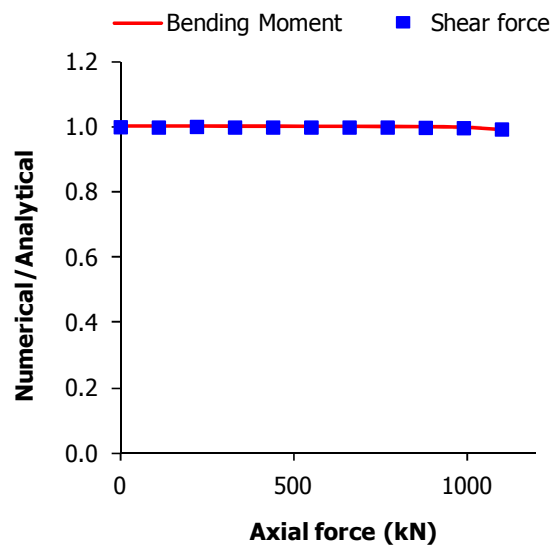


Figure 7-34: Comparison of analytically and numerically obtained maximum bending moments and shear forces for various levels of axial load for the sway imperfect Timoshenko member under lateral load

If both the lateral and axial loads are gradually applied the equilibrium path will be different. The results obtained analytically and numerically with gradual application of the loads are shown for the sway member in Figure 7-35.

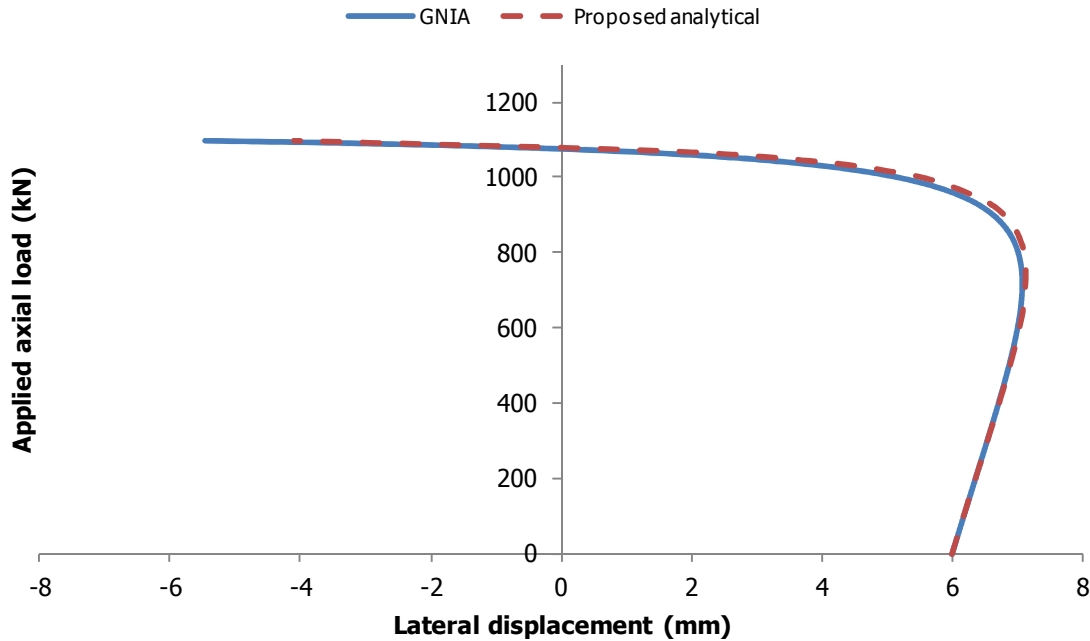


Figure 7-35: Equilibrium path for the imperfect sway member under lateral load gradually applied

7.5 CONCLUSIONS

An approximate analytical methodology has been proposed for the evaluation of the 2nd-order elastic response of members with arbitrary boundary conditions that are susceptible to transverse shear deformations based on Engesser's approach. The members are considered to be loaded axially by a compressive force, to have an initial imperfection according to their first buckling mode shape only and to be subjected to uniformly distributed load along their length, concentrated end moments and concentrated end lateral forces. For the axially compressed Timoshenko member with arbitrary supports, the existence of initial imperfection and each lateral load case are considered separately. Finally, at specific axial load levels, the principle of superposition is applied for obtaining their combined effect.

The incorporation of initial imperfection's effect is achieved with the use of the approximate magnification factor accounting only for the first buckling mode and for Engesser's method for the incorporation of shear deformations. The closed-form solutions for the lateral load cases of uniformly distributed load, concentrated end moments and concentrated end forces are formulated with the use of 2nd-order slope-deflection equations according to Engesser's method for the incorporation of shear deformations as they were presented in Chapter 6. The deflection, bending moment and shear force along the member can be evaluated with the use of the proposed method.

Verification examples dealing with imperfect Timoshenko columns and beam-columns have been presented considering non-sway, partially-sway and sway translational behaviour. The comparison included deflections and internal forces (bending moment and shear forces) leading to the conclusion that the proposed closed-form solutions result in very satisfactory accuracy. Divergence between the analytical and numerical results was observed only at very large axial load levels (close to the elastic critical buckling load) at which small deflection theory is inaccurate. The proposed analytical results can be used for performing straight-forward 2nd-order analysis of Timoshenko and Euler-Bernoulli members (if shear deformations are neglected by considering very large shear rigidity).

7.6 REFERENCES

- [7-1] Absi, E. "Equations intrinseques d'une poutre droite a section constant", Annales de l'Institut Technique du Batiment et des Travaux Publics, Vol. 21(229), pp. 151-167, 1967
- [7-2] Lin, F.J., Glauser, E.C., Johnston, B.G. "Behaviour of laced and battened structural members", Journal of the Structural Division, American Society of Civil Engineers (A.S.C.E.), Vol. 96, No. ST7, pp. 1377-1401, 1970
- [7-3] Aristizabal-Ochoa, J.D. "Slope-deflection equations for stability and second-order analysis of Timoshenko beam-column structures with semi-rigid connections", Journal of Engineering Structures, Vol. 30, pp. 2517-2527, 2008
- [7-4] Marinetti, A., Oliveto, G. "Second order analysis of elastic frames with Timoshenko members", Engineering Analysis, Vol. 1, No. 2, pp. 92-98, 1984
- [7-5] Young, T. "A course of lectures on Natural Philosophy and the Mechanical arts" Reprint of 1807 edition, Thoemmes Press, Bristol, 2002
- [7-6] Eurocode 3: Design of Steel Structures. Part 1.1: General structural rules. CEN-European Committee for Standardisation, Brussels, EN1993-1-1, 2005
- [7-7] ADINA System 8.5, Release Notes. ADINA R & D Inc., 71 Elton Avenue, Watertown, MA 02472; USA. 2008
- [7-8] Horne, M.R., Merchant, W. "The stability of frames", Pergamon Press, Oxford, England, 1965
- [7-9] Rubin, H. "Uniform formulae of first- and second-order theory for skeletal structures", Journal of Engineering Structures, Vol. 19, No. 11, pp. 903-909, 1997

8 BEHAVIOUR OF LACED BEAM-COLUMNS WITH ARBITRARY SUPPORTS

8.1 INTRODUCTION

In Chapter 5, a simple method was proposed for the second-order elastic analysis of laced columns modelled as equivalent Timoshenko members and for the calculation of the collapse load based on an interaction equation. The method was verified numerically and the conclusion that laced built-up columns mainly fail in practice due to local elastoplastic failure of a critical panel was drawn.

In order to expand these conclusions to cases of imperfect laced built-up members under axial and transverse loading, with the use of the results obtained in Chapter 6 for the elastic critical buckling load of Timoshenko members and frames, in Chapter 7, the second-order elastic analysis of imperfect Timoshenko beam-columns with arbitrary supports was proposed in the form of closed-form solutions. These analytical results are useful for elastic geometrically nonlinear analysis of Timoshenko members, from which bending moments and shear forces along the members can be obtained.

In general, the collapse load can be calculated if an appropriate interaction equation accounting for structural failure is used for “terminating” the second-order analysis. In the present chapter, by making the assumption that axially and laterally loaded imperfect laced built-up members fail when local elastoplastic failure of the critical panel takes place, as in imperfect laced built-up columns described in Chapter 5, an interaction equation for the collapse load of such members will be presented. Then, interaction diagrams will be used for comparing different methods for the calculation of the collapse load of a large variety of laced built-up members. The results obtained with the proposed method will be compared with the ones obtained numerically with Geometrically and Materially Nonlinear Imperfection Analyses (GMNIA), and with the use of first-order and second-order elastic analyses in commercial software.

8.2 INTERACTION EQUATION FOR COLLAPSE LOAD OF LACED MEMBERS

In the analysis and design of structures, it is common practice that they are analysed elastically and appropriate interaction equations are used for “terminating” the analysis when structural failure takes place. Initially, Allowable Stress Design was the basic design method for many decades, computing stresses based on principles of mechanics and then checking against the allowable stress depending

on the material. This design concept is relatively conservative as it does not account for plastic hinge formation and plastic reserve due to redistribution of stresses in indeterminate structures. Modern codes are based on the Ultimate Strength Design, according to which the structure should withstand the applied loads without collapse. In this section interaction equations for “terminating” the second-order analysis at a load level for which the internal forces, as obtained from the closed-form solutions of Chapter 7, marginally become equal to the member’s strength will be presented.

8.2.1 Interaction equation

The procedure for evaluating the behaviour of a laced member is based on the assumption that it is considered as a Timoshenko member with equivalent bending and shear rigidity. In this way, the degrees of freedom of the indeterminate structure are significantly reduced and it can be easily analysed. The 2nd-order analysis of the equivalent Timoshenko member results in obtaining internal forces along its length, as it was presented in Chapter 7. These internal forces can be used for the approximate calculation of the internal forces of the laced member’s components. Thus, the performance of checks according to the Ultimate Strength Design is possible.

Laced built-up members are truss-like structural systems and therefore their primary stresses in the chords are due to axial forces and the secondary ones due to local bending moments, usually about the weak axis of the chords. The local bending moments develop due to initial local imperfections and due to the continuity of the chords in elevation. In the proposed interaction equations, only the axial forces and the local bending moments due to initial local imperfections are taken into account. The reason for neglecting the local bending moments due to continuity of the chords will be thoroughly presented in the next section.

In laced built-up columns both global (w_o) and local (z_o) imperfections should be considered, based on the buckling mode shapes, as explained in Chapter 5. In the same chapter it was concluded numerically that a laced built-up column can fail either due to local elastoplastic failure of a critical panel (usually under compression) or due to elastic failure of the whole column. In the first case, the effect of global imperfections should be taken into account in the global response, while for reasonable magnitudes of local imperfections, their effect can be incorporated in the inelastic capacity of the critical panel, as yielding of the material limits their effect on the global response. In the second case both global and local imperfections play an important role in the global response of the structure. In most practical cases the reason leading to collapse is the first one. By setting the force in the more compressed chord equal to the local buckling resistance N_L of a panel, interaction Eq. (8-1) is derived:

$$\frac{P}{2} + \frac{|M_{\max}|}{h_o} = N_L \quad (8-1)$$

where P is the applied axial load and M_{\max} is the maximum value of the global bending moment along the equivalent Timoshenko member (by maximising Eq. (7-67)). Eq. (8-1) can be modified for the case that the maximum bending moment appears at a built-up member’s support (at $x=0$ or L) and a diagonal lacing bar converges at the end of the critical panel, accounting for the fact that a small part of the axial force caused by the maximum moment is sustained by the lacing bar (either in tension or in compression depending on the direction of the shear force Q). The shear force Q can be evaluated with the use of Eq. (7-68).

In this case Eq. (8-1) becomes, for the case of X-lacing and X-lacing with transverse bars that were presented in Chapter 2:

$$\frac{P}{2} + \frac{|M_{\max}(0;L)|}{h_o} \pm \frac{|Q(0;L)| \tan \phi_l}{2} = N_L \quad (8-2)$$

In the case of N-lacing, V-lacing and Z-lacing types that were presented in Chapter 2, Eq. (8-2) becomes:

$$\frac{P}{2} + \frac{|M_{\max}(0;L)|}{h_o} \pm |Q(0;L)| \tan \phi_l = N_L \quad (8-3)$$

The unknown parameters in Eq. (8-1) to Eq. (8-3) are both the location of the maximum bending moment and the collapse load P and for this reason an iterative procedure should be performed for their solution. These interaction equations are valid only if failure of the diagonal bars is avoided, being in accordance with common practice in which lacing bars are designed with sufficient overstrength. The local capacity N_L takes into account the existence of local imperfections and material yielding. The critical panel can be considered in most cases as simply-supported at failure and this approximation is justified by the following observations:

- Adjacent panels to the critical one are usually loaded by axial forces of similar magnitude to it. It was shown in Chapter 6 that the rotational stiffness offered by the converging members at the top and bottom nodes of the column in question, depends on the magnitude of the compressive axial force. The larger the axial force the smaller the rotational restraint provided. Additionally, material yielding may also appear along adjacent panels reducing their stiffness. As a result, the rotational restraint that adjacent panels can offer to the critical one at its ends is rather limited.
- The non-dimensional slenderness of the panels (local non-dimensional slenderness) is usually in practice relatively small and in such cases the boundary conditions play little role, as the capacity is governed by yielding.

This approximation is convenient due to its simplicity but it is not always sufficient, as will be illustrated in the examples of the present chapter. The local capacity can be calculated either based on the first yield of the cross-section or by accounting for its plastic reserve, too.

8.2.1.1 Local capacity based on first yield

The local capacity of a simply-supported imperfect panel based on the first yield of the cross-section at mid-height, by making use of Eq. (6.47) of Eurocode 3 [8-1], is equal to:

$$N_L = N_{ch,Rd} = \frac{\chi_z A_{ch} f_y}{\gamma_{M1}} \quad (8-4)$$

where χ_z is a reduction coefficient corresponding to the magnitude of the local imperfections and the slenderness of the member and γ_{M1} is the partial safety factor. The calculation of the reduction coefficient is based on the well-known Ayrton-Perry formula [8-2] and is a lower bound of the actual capacity, as it is associated with the first yield of the concave side of the member. Eurocode 3 [8-1] provisions are based on five different magnitudes of imperfections, distinguished by different values of the imperfection factor η' that varies from 0.13 to 0.76. The magnitude of the imperfection is given by:

$$z_o = \eta' (\lambda_{ch,z} - 0.2) \frac{W_{el,z,ch}}{A_{ch}} \quad (8-5)$$

where η' is the imperfection factor, $\lambda_{ch,z}$ is the local non-dimensional slenderness of the panel about the weak axis z-z, $W_{el,z,ch}$ the elastic modulus of the chord's cross-section about axis z-z and A_{ch} the chord's cross-sectional area.

8.2.1.2 Local capacity accounting for plastic reserve

In practice, imperfect columns do not fail when the material yield stress is reached in the more compressed fibre as shown in Figure 8-1(a), even if elastic-perfectly plastic material behaviour is considered. Consider an imperfect simply-supported column under axial load N . N_y is considered to be the axial load N at which the more stressed fibre yields. N_u is the maximum axial load N that the column can carry. The load increases and becomes larger than N_y , reaching a magnitude of N_u at failure. The plastic reserve allows for this increase, as plasticity expands in the cross-section and extends over a region close to the location where the onset of yielding took place (Figure 8-1(b)). The case shown in Figure 8-1(b) refers to a relatively small imperfection that permits the appearance of plastified regions on the convex side of the column, too. For larger magnitudes of imperfection, plasticity gathers only on the concave side of the column.

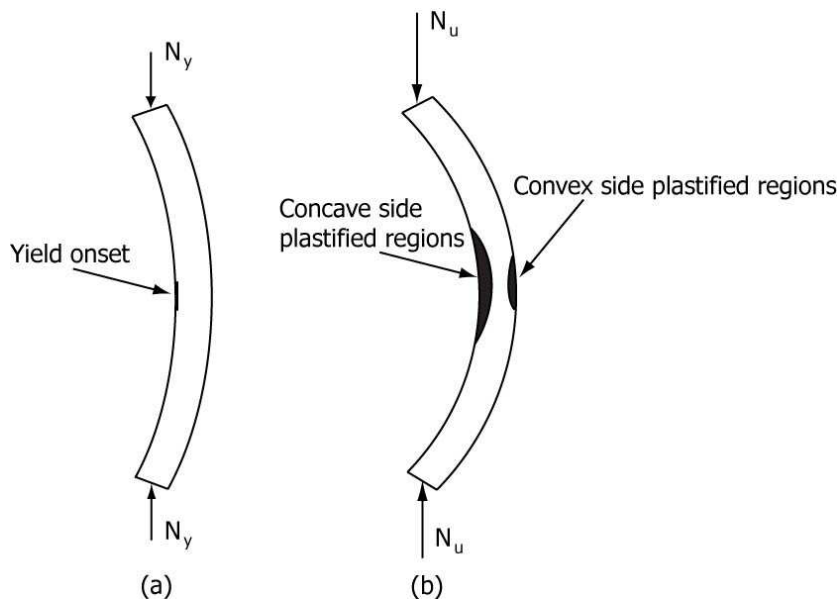


Figure 8-1: Imperfect simply-supported column (small imperfection) at (a) first yield and (b) ultimate load

The plastic strength reserve and therefore the expected increase in the ultimate strength in comparison to the first yield load depend on the following factors:

- The magnitude of the external bending moment due to eccentricity of the axial load
- The stress-strain relationship of the material
- The cross-sectional shape

A simple method to calculate the compressive strength of a column is the ultimate strength curve method. In this procedure the ultimate compressive strength N_u is obtained from the intersection of the plastic strength curve (Axial force N -Bending Moment M interaction diagram) with the elastic second-order curve (Axial force N -Bending Moment M) as obtained from the analysis (Figure 8-2). One of the main assumptions made in this procedure is that at failure the critical cross-section is entirely plasticised. This is not accurate as only a part of the critical cross-section is plasticised at failure, and for this reason the ultimate strength curve method is expected to be an upper bound of the capacity of the column.

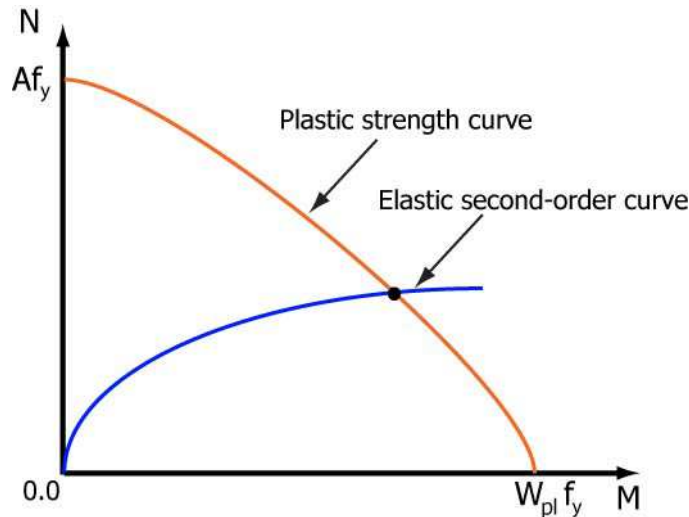


Figure 8-2: Application of Ultimate Strength Curve Method

Rankine [8-3] proposed a formula for the approximation of the collapse load of imperfect columns that requires the elastic critical buckling load of the column and the collapse load that leads to the plastic moment of resistance of the critical cross-section with the use of second-order stereoplastic analysis [8-4]. This procedure is also unconservative, as it is based on the full plastic moment of resistance of the critical cross-section, which cannot be attained under the presence of both axial force and bending moment.

In the present doctoral thesis, the local capacity accounting for the plastic reserve, used in the proposed interaction equations, will be obtained with the use of GMNIA of individual imperfect simply-supported axially loaded panels in finite element software ADINA [8-5]. In this way a very accurate prediction of the local capacity will be achieved and no additional errors will be incorporated in the proposed equations. Nevertheless, the approximate analytical methods existing in literature and described previously are expected to be sufficient for practical use.

8.2.2 Effect of local moments on failure

As it was foretold, laced built-up members are truss-like structural systems and for this reason their primary type of stress in the chords is attributed to axial forces and the secondary one to local bending moments, usually about the weak axis of the chords. The local bending moments appear due to initial local imperfections and due to the continuity of the chords in elevation. Their magnitude is relatively small but, as they are usually applied about the weak axis, their effect on the local capacity of the member may be of importance. Their existence was verified experimentally in the specimens tested in the context of the present doctoral thesis, as presented in Chapter 3.

The first type of local bending moments appears due to the axial compression of the panels and the local out-of-straightness. Therefore, such bending moments become larger with increase of the axial force in the chord and/or with increase of the magnitude of initial imperfections. In stocky panels, their magnitude is expected to be very small, while in slender panels the opposite happens. This type of local bending moments is incorporated in the local capacity of the proposed interaction equations, as described in the section 8.2.1.1 with the conservative assumptions that each panel can be assumed to be simply-supported at failure (thus neglecting any rotational stiffness offered by the adjacent panels and the continuity of the chords).

The second type of local bending moments appears due to the continuity of the chords in elevation, whether the lacing bars' connections to chords are considered as hinged or not. It highly depends on

the external type of loading and is not required for global equilibrium. Bonab and Hashemi [8-6] in their experimental and numerical investigation of the cyclic behaviour of laced built-up columns under constant axial load, measured the local bending moments that appeared along the chords. They concluded that their magnitude was small but the normal stresses due to them were large. Similar conclusions were drawn for the diagonal bars. For this reason, they proposed that local bending moments should be taken into account in the design process of laced members.

By considering that the local non-dimensional slenderness of the specimens tested by Bonab and Hashemi [8-6] was very small (small effect of initial local imperfections), it can be concluded that they could only be associated with the continuity of the chords in elevation. Therefore, an issue which one should look into is the fact that the stresses were probably measured while the material was still elastic. Numerical analyses performed in the context of the present doctoral thesis showed that the plasticity of the material leads to reduction of the local bending moments, allowing in this way for an increase of the applied axial force, which can be explained if one looks into the plastic interaction surfaces of the cross-section [8-7], [8-8].

The numerical explanation of this phenomenon is briefly described here: when the stress state at any cross-section along the beam element reaches the full plastic surface and strain-hardening is not taken into account, the internal forces can be modified, as long as they do not violate the plastic strength surface requirement. As a result, if the axial force of the member increases in the next numerical iteration (this is the case in laced built-up columns as their primary type of stress is related to axial forces) a corresponding decrease of the moment should take place as it is depicted in Figure 8-3 with the stress state movement from Q to R. Exactly, the opposite would happen in the case that the bending moment would increase in the next numerical iteration.

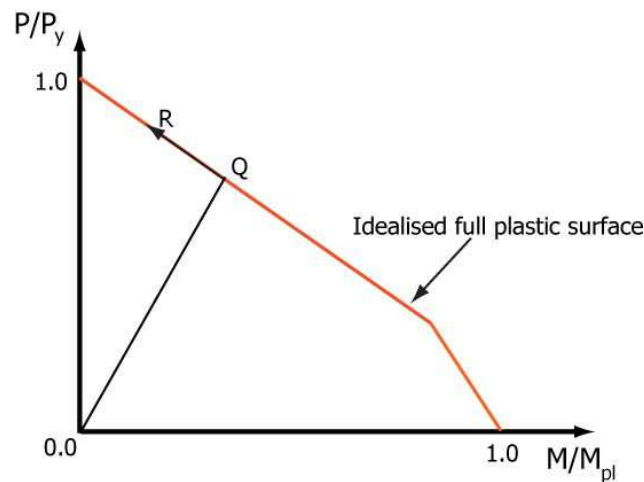


Figure 8-3: Force-point movement along the idealised full plastic surface of a cross-section

8.3 DESIGN OF LACING BARS

The lacing consists of bars considered to be simply-supported in different configurations that are loaded axially by the compressive load P due to the continuity of the flanges and the second-order shear force that appears along the imperfect laterally loaded laced built-up column. Therefore, it can be concluded that a satisfactory approximation of the maximum force of the diagonals can be found by

$$D_{\max} = D_1 + D_2 \quad (8-6)$$

where D_1 and D_2 are the maximum forces in the diagonals due to axial load P and second-order shear force, respectively. The maximum 2nd-order shear force can be calculated from the closed-form solutions provided in Chapter 7 and can then be suitably applied on the diagonals for the evaluation of D_2 , as described by Ramm and Uhlmann [8-9] and repeated here for completeness.

For V-lacing, N-lacing and Z-lacing and for two lacing planes, the design force of the diagonal bars should be taken equal to:

$$D_2 = \frac{Q_{\max}}{2\cos\varphi_l} \quad (8-7)$$

For X-lacing and X-lacing with transverse bars and for two lacing planes, the design force of the diagonal bars should be equal to:

$$D_2 = \frac{Q_{\max}}{4\cos\varphi_l} \quad (8-8)$$

The maximum force in the transverse bars of Z-lacing type and for two lacing planes is equal to:

$$D_2 = \frac{Q_{\max}}{2} \quad (8-9)$$

It can be concluded that the transverse bars have a smaller axial force and larger buckling strength due to their smaller buckling length when compared with the diagonal bars. For this reason, the use of the same cross-section for the transverse bars as for the diagonal ones is sufficient.

Force D_1 can be obtained approximately by considering a first-order elastic analysis of the column under the collapse load. It is expected that force D_1 is important for X-lacing and X-lacing with transverse bars and in other cases that transverse bars are used. The reason for this is that transverse bars prohibit the extension of the distance between the chords when the built-up member is subjected to external loading. This restriction leads to an increase of the axial force of the lacing bars and of the local bending moments due to continuity.

8.4 VERIFICATION WITH NUMERICAL RESULTS

The proposed design method of imperfect laced built-up beam-columns is verified in this section against results obtained with the use of finite element software ADINA [8-5]. The numerical analyses performed for the calculation of the collapse load are geometrically and materially nonlinear. The shapes of global and local imperfections are based on the global and local buckling modes, respectively. The global imperfection has a magnitude of $L/500$ while the local one is either the EC3's specified value according to the corresponding buckling curves or $a/500$. Local imperfections are directed so that they lead to the lowest collapse load. The steel used in all cases is S355 and its stress-strain relationship is assumed to be bilinear without strain hardening. The diagonal bars in all cases are designed with sufficient overstrength and are excluded from possible failure modes, as this is in accordance with common practice. The approaches used are summarised as:

- GMNIA: The laced built-up members are modelled with the use of finite element software. The collapse load is considered to be the maximum load value of the equilibrium path obtained with GMNIA (Geometrically and Materially Nonlinear Imperfection Analyses), using either 2-node Hermitian beam elements or 4-node shell elements. The chords are modelled as continuous members while the lacing bars have both ends rotationally free. The numerical models were calibrated against the experimental work presented in the context of the present doctoral thesis.

For this reason, this procedure is considered to result in a very accurate prediction of the collapse load and will be the basis for comparison.

- Proposed-A method (Pr.-A): The collapse load is obtained by making use of Eqs. (8-2)-(8-3) depending on the lacing configuration and incorporating the local capacity associated with the first yield as described in Eq. (8-4). Eq. (7-67) and Eq. (7-68) are used for the calculation of the maximum bending moment and corresponding shear force along the equivalent Timoshenko member. This calculation is the lower bound of the proposed procedure.
- Proposed-B method (Pr.-B): The collapse load is obtained by making use of Eqs. (8-2)-(8-3) depending on the lacing configuration and incorporating the local capacity associated with the full plastic reserve of the cross-section. The local capacity is obtained with the use of GMNIA in an imperfect (local imperfection) simply-supported panel. Eq. (7-67) and Eq. (7-68) are used for the calculation of the maximum bending moment and corresponding shear force along the equivalent Timoshenko member.
- C.S. 1st order and 2nd order: Use of Commercial Software (C.S.) for the performance of 1st-order analyses and 2nd-order elastic analyses including P-Δ effects. The numerical models are created with the use of beam elements. The commercial software cannot capture P-δ effects and cannot incorporate initial imperfections. The collapse loads calculated with these two procedures are the ones leading to marginal satisfaction of the interaction check at any cross-section of the chords:

$$\frac{N}{\chi_z A_{ch} f_y} + k_{zz} \frac{M_z}{M_{z,pl,Rd}} \leq 1 \quad (8-10)$$

where N and M_z are the applied axial force and bending moment at the examined cross-section, χ_z the reduction coefficient for flexural buckling about the weak axis, k_{zz} the interaction factor as defined by Method 2 of EC3 [8-1] and $M_{z,pl,Rd}$ is the plastic moment of resistance of the cross-section about the axis of bending (z -axis).

The symbols for the geometrical and inertial parameters presented in previous chapters and for the external loads shown in Chapter 7 are used in this parametric study, too. Additionally, the laced members considered follow the notations of sections 7.3.1, 7.3.2 and 7.3.3 as far as the boundary conditions and external loads are concerned. The bottom node of each vertical laced member is considered to be end A and the top node, end B.

8.4.1 Modelling with beam elements

In this section, analyses performed with the use of 2-noded Hermitian beam elements will be presented. The chords are modelled as continuous members, while the diagonal bars have rotationally free ends. The chords have either rectangular cross-sections (for which ADINA [8-5] offers elastoplastic analysis options) or I-sections for which moment-curvature relationships for different levels of axial force are calculated and inserted in the software. The diagonal bars have hinges at their ends and no transverse loading, which means that only their area is of importance in the structural analysis. The finite element mesh is sufficiently dense in order to obtain accurate results. The results are presented in interaction diagrams, with the axial capacity plotted on the vertical axis and the magnitude of the lateral loads on the horizontal axis.

The results on the vertical axis correspond to column behaviour (zero lateral loading), while the ones on the horizontal axis apply to beam behaviour (zero axial loading). Intermediate results are associated with beam-column behaviour (both axial and lateral loading) and normally correspond to the most common cases encountered in practice.

8.4.1.1 Rectangular sections

Initially, rectangular sections are used for the chords, as ADINA [8-5] is capable of performing elastoplastic analysis for this cross-sectional shape. This type of cross-section is not commonly used for laced columns' chords, but its use is not expected to lead to significant deviations as far as the behaviour and collapse load of laced columns are concerned. This is attributed to the fact that laced members behave almost elastically until failure and for this reason elastic properties play the most important role.

Example 1 – Partially sway member

The geometrical, inertial and boundary characteristics of the first laced member are summarised in Table 8-1. X-lacing is used for the shear system of the laced beam-column. The global and local buckling loads are equal to 1712kN and 5969kN, respectively. The local non-dimensional slenderness is equal to 0.55. The squash load is equal to 1775kN. In these analyses the local imperfection is taken equal to $a/500$.

Table 8-1: Geometrical, inertial and boundary characteristics of Example 1

L (m)	h_o (cm)	a (cm)	A_{ch} (cm ²)	$I_{ch,z}$ (cm ⁴)	A_d (cm ²)	C_b (Nm)	$C_{br,b}$ (N/m)	C_t (Nm)	$C_{br,t}$ (N/m)
12	50	60	25	52	4	$8 \cdot 10^6$	$\rightarrow \infty$	$1 \cdot 10^6$	$1 \cdot 10^5$

The results for the lateral load case of uniformly distributed load q applied on the non-critical (less compressed) and critical (more compressed) chord are shown in Figure 8-4 and Figure 8-5, respectively. A very satisfactory correlation between the proposed methods (especially Proposed-B method) and GMNIA is observed. The use of first-order analysis with commercial software is unable to predict the collapse load accurately and safely. The use of second-order analysis with commercial software gives satisfactory results, on the safe side.

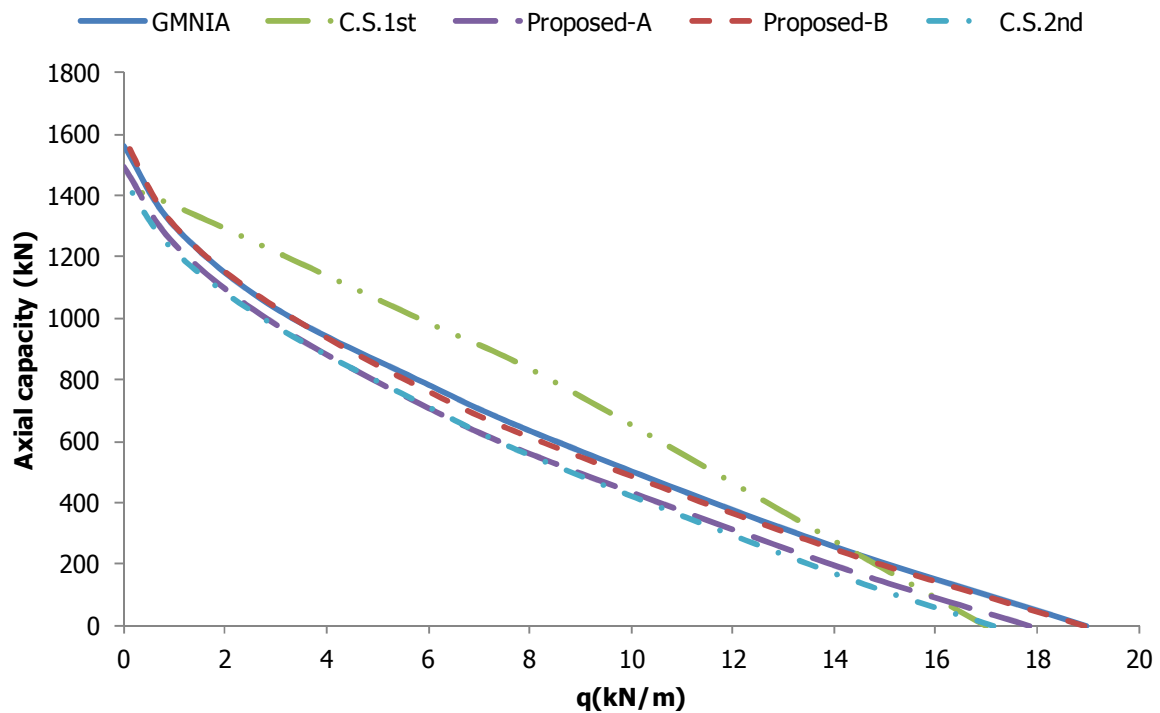


Figure 8-4: Interaction diagram of Example 1 for uniformly distributed load q along the non-critical (less compressed) chord

The results for the lateral load case of constant moment $M_1=300\text{kNm}$ at end A and varying moment M_2 at end B are depicted in the interaction diagram of Figure 8-6. In these analyses the local imperfection is taken equal to $a/500$. Proposed-B method is in excellent agreement with GMNIA while slightly more conservative results are obtained with Proposed-A method. The first-order analysis with commercial software cannot capture satisfactorily the collapse loads while the use of second-order analysis improves the results that remain slightly below the ones obtained with Proposed-A method.

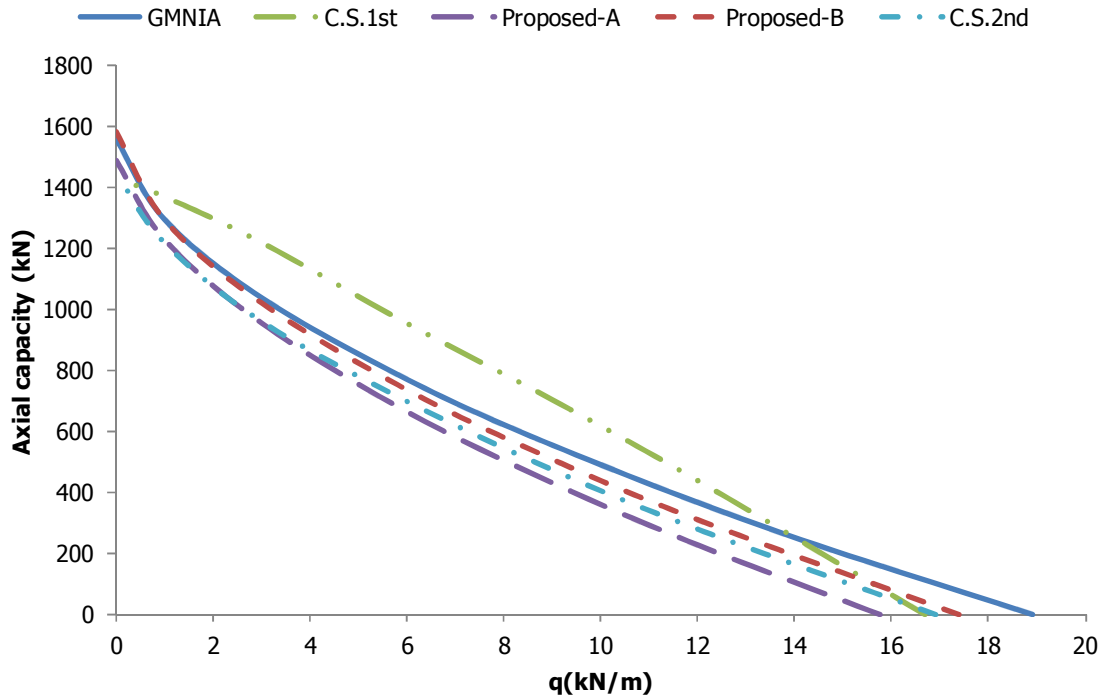


Figure 8-5: Interaction diagram of Example 1 for uniformly distributed load q along the critical (more compressed) chord

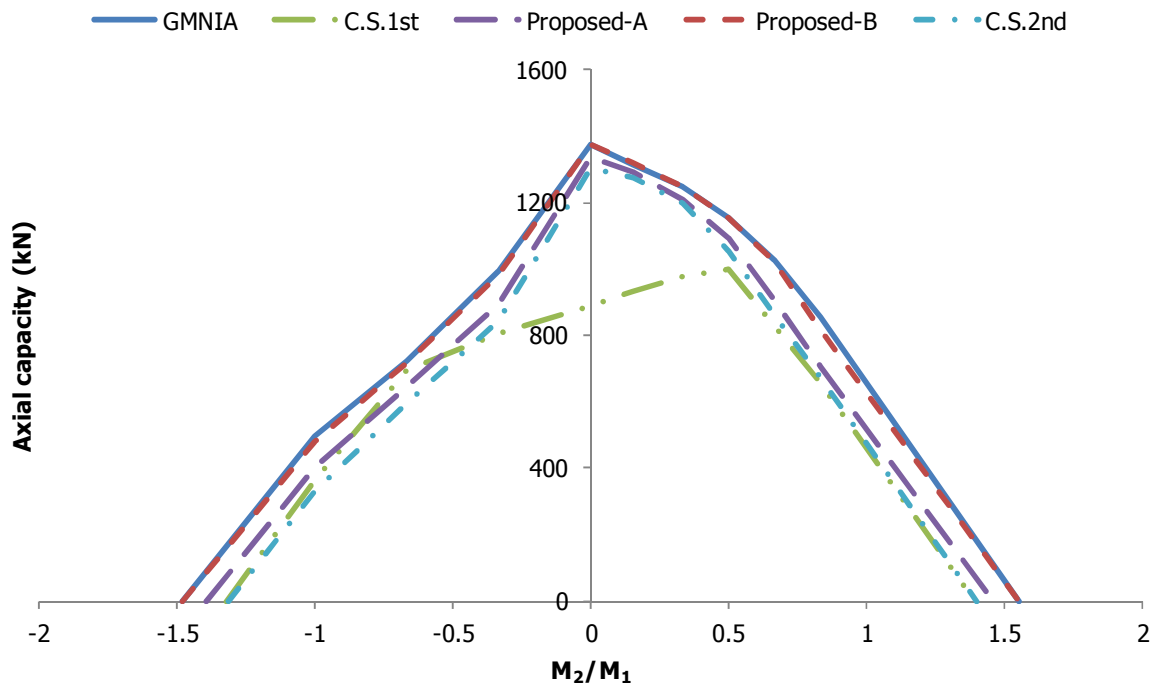


Figure 8-6: Interaction diagram of Example 1 for constant moment M_1 at end A and varying moment M_2 at end B

The results for the lateral load case of concentrated load H_2 at end B are depicted in the interaction diagram of Figure 8-7. In these analyses the local imperfection is taken equal to $a/500$. Proposed-B method is in very good agreement with GMNIA while slightly more conservative results are obtained with Proposed-A method and commercial software with second-order analysis. The first-order analysis with commercial software cannot capture satisfactorily the collapse loads especially for beam-column behaviour for which it becomes significantly unsafe and should be avoided.

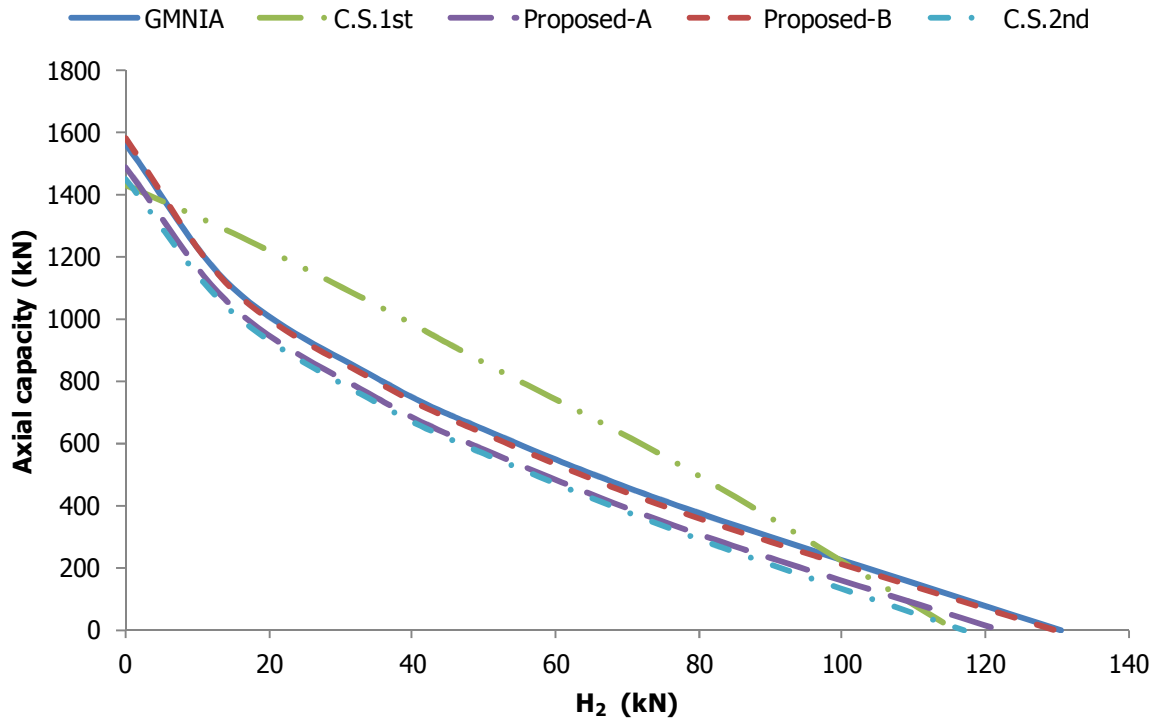


Figure 8-7: Interaction diagram of Example 1 for a concentrated load H_2 at end B

In the last lateral load case for Example 1, the laced member is loaded by uniformly distributed load $q=2\text{kN/m}$, concentrated moment $M_1=20\text{kNm}$ at end A, concentrated moment $M_2=10\text{kNm}$ at end B and concentrated load $H_2=2\text{kN}$ at end B. Different magnitudes depending on a factor multiplying the lateral external loads are examined and the results are presented in Figure 8-8. Similar conclusions to the previous cases can be drawn for this load combination, too. Ignoring second-order effects leads to very unsafe results for beam-column behaviour. The undeformed and deformed configurations of the laced member under combined lateral loads are depicted in Figure 8-9(a). In Figure 8-9(b) the axial force diagram is also shown from which it can be concluded that the panel with the largest axial force is the one at the bottom for this specific case. For this reason, as it is assumed that all panels have the same buckling strength, this panel's failure is expected to lead to overall collapse.

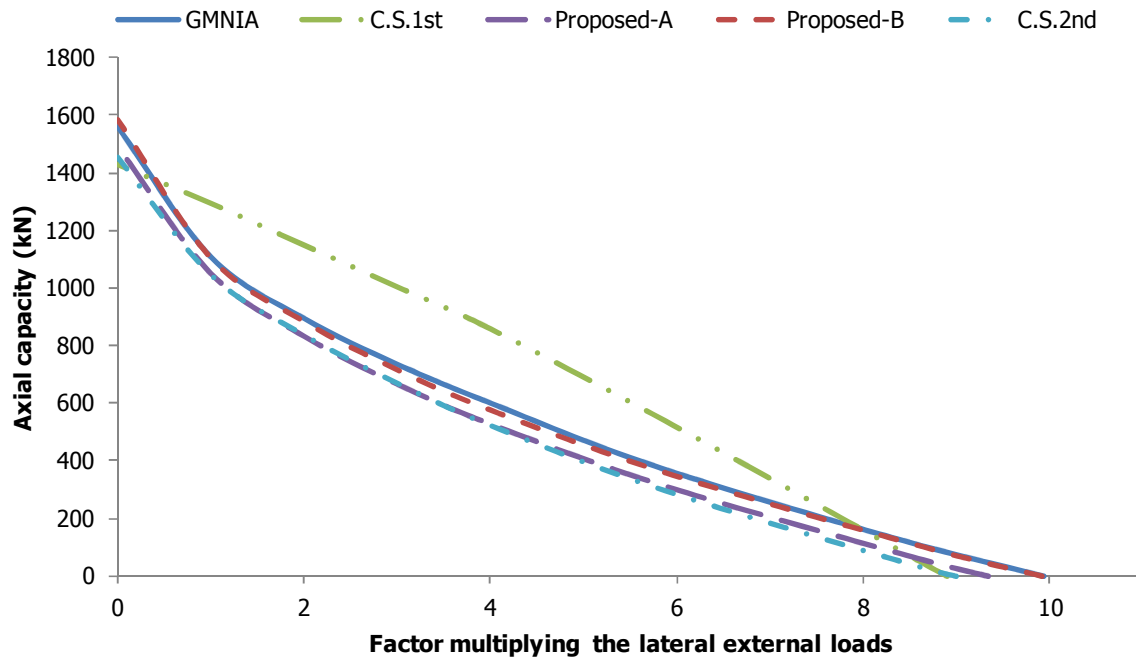


Figure 8-8: Interaction diagram of Example 1 for combined lateral external loads

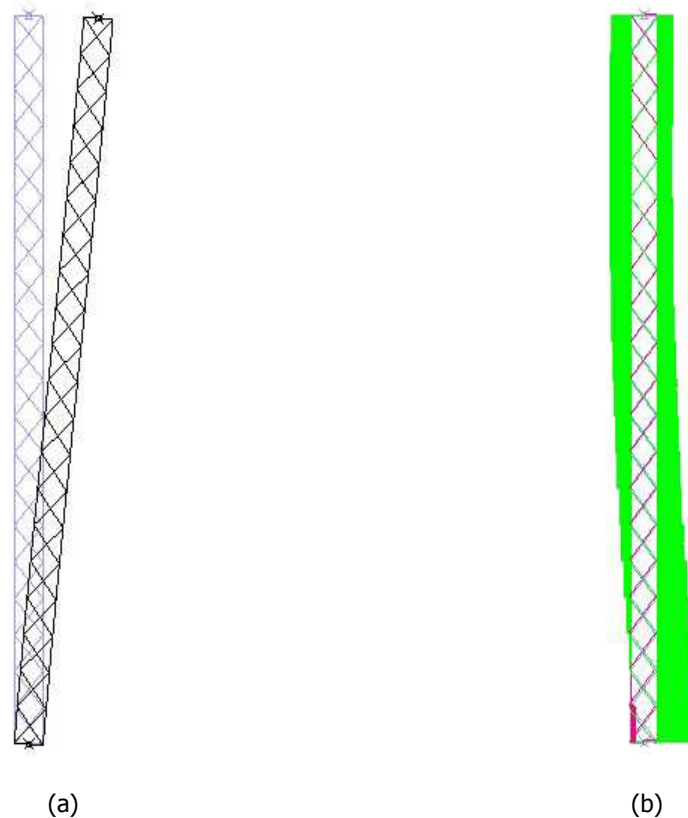


Figure 8-9: (a) Undeformed and deformed shape and (b) axial force diagram of laced member of Example 1 under axial load and combined lateral external loads at failure

Example 2 - Non-sway member

The geometrical, inertial and boundary characteristics of the second laced member are summarised in Table 8-2. X-lacing is used for the shear system of the laced beam-column. The global buckling load

and local buckling load are equal to 16790kN and 11940kN, respectively. The squash load is equal to 3550kN. The local non-dimensional slenderness is equal to 0.55. A global imperfection equal to $L/500$ based on the first global buckling mode shape is considered. The local imperfection is taken according to buckling curve "b" of Eurocode 3 [8-1].

Table 8-2: Geometrical, inertial and boundary characteristics of Example 2

L (m)	h_o (cm)	a (cm)	A_{ch} (cm ²)	$I_{ch,z}$ (cm ⁴)	A_d (cm ²)	C_b (Nm)	$C_{br,b}$ (N/m)	C_t (Nm)	$C_{br,t}$ (N/m)
12	50	60	50	104	16	$\rightarrow \infty$	$\rightarrow \infty$	$\rightarrow 0$	$\rightarrow \infty$

The laced member of Example 2 is loaded by $-M_2$ at the end B and by uniformly distributed load q along its length. The results are given graphically in the interaction diagrams presented in Figure 8-10 and Figure 8-11, respectively. In both examined load cases, very good correlation between GMNIA and Proposed-B method is observed. Proposed-A method gives results very close to the ones obtained with elastic second-order analysis and commercial software. The use of commercial software and first-order analysis gives also satisfactory results, highlighting that the restriction of translation at the two ends reduced significantly the second-order effects.

The undeformed and deformed shapes of the imperfect laced member under uniformly distributed load q are depicted in Figure 8-12(a). In Figure 8-12(b) the axial force diagram is also shown from which it can be concluded that the panel with the largest axial force is the one at the bottom for this specific case. Therefore, it is expected that this panel initially fails and leads to overall collapse.

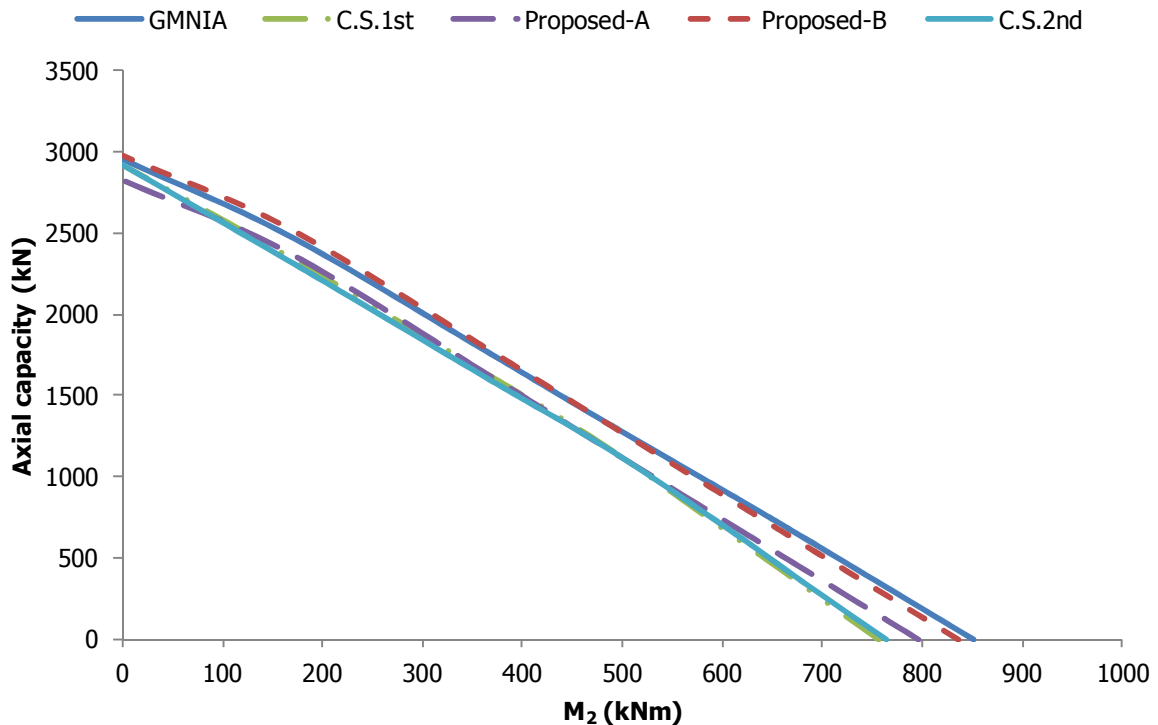


Figure 8-10: Interaction diagram of Example 2 for concentrated $-M_2$ at end B

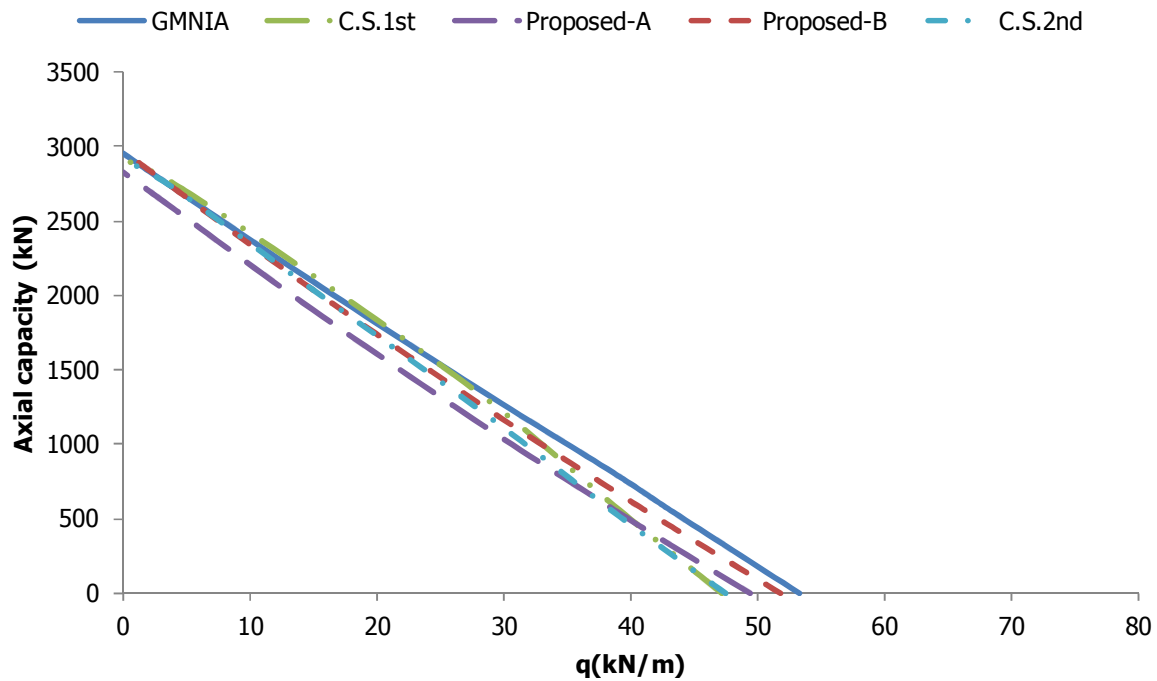


Figure 8-11: Interaction diagram of Example 2 for uniformly distributed load q along the member

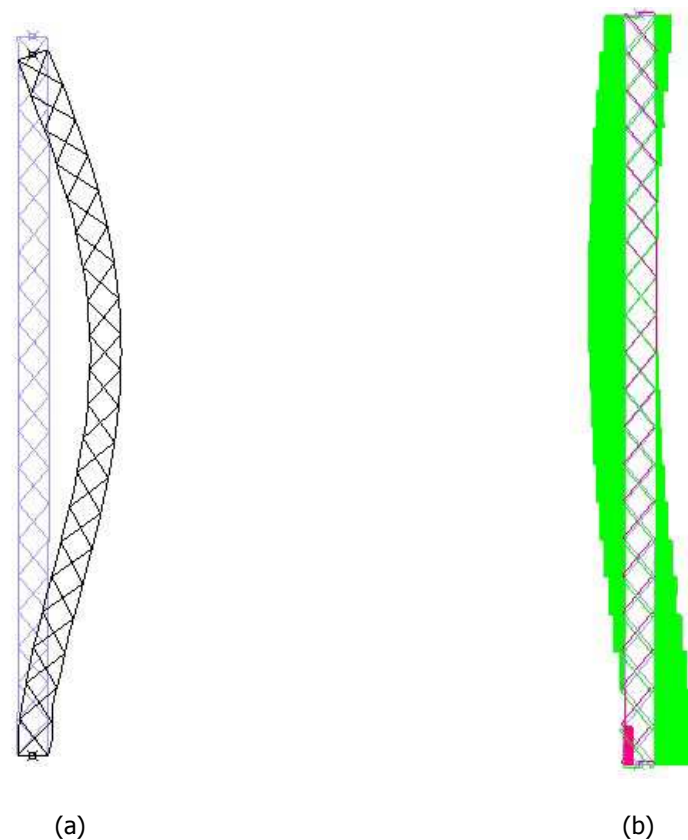


Figure 8-12: (a) Undeformed and deformed shape and (b) axial force diagram of the laced member of Example 2 under axial load and uniformly distributed load q at failure

Example 3 - Arbitrary boundary conditions

The geometrical, inertial and boundary characteristics of the third laced member are summarized in Table 8-3. N-lacing is used for the shear system of the laced beam-column. The global and local buckling loads are equal to 1738kN and 3752kN, respectively. The squash load is equal to 3479kN. A global imperfection equal to $L/500$ based on the first global buckling mode shape is considered. The local imperfection is taken according to buckling curve "c" of Eurocode 3 [8-1].

Table 8-3: Geometrical, inertial and boundary characteristics of Example 3

L (m)	h_o (cm)	a (cm)	A_{ch} (cm ²)	$I_{ch,z}$ (cm ⁴)	A_d (cm ²)	C_b (Nm)	$C_{br,b}$ (N/m)	C_t (Nm)	$C_{br,t}$ (N/m)
13.5	40	150	49	200	12.25	$8 \cdot 10^6$	$2 \cdot 10^4$	$5 \cdot 10^7$	10^5

The laced member of Example 3 is loaded by $-M_1=50\text{kNm}$ at the end B, by uniformly distributed load $q=2\text{kN/m}$ along its length and by $H_2=2\text{kN}$ at the end B. Different magnitudes depending on a factor multiplying the lateral external loads are examined and the results are presented in Figure 8-13. A satisfactory correlation between GMNIA and Proposed-B method is observed. The accuracy is somewhat reduced for large lateral loads and this is due to the fact that in such cases the shear force perpendicular to the deformed axis Q (first derivative of bending moment M) is relatively large. This means that the axial force of adjacent panels to the critical one may differ more than usual. In this way, adjacent panels may offer rotational stiffness to the critical panel's ends and the assumption that the latter behaves as a simply-supported local column may be conservative. Additionally, in this specific case, the non-dimensional local slenderness is equal to 0.96 (relatively large for panels), and therefore the effect of the boundary conditions of the panel is more important than in previous examples. Proposed-A method gives more conservative results, while commercial software with the use of second-order analysis is unsafe for small lateral loads due to the non-incorporation of initial imperfection and conservative for large lateral loads. The use of commercial software and first-order analysis gives unsatisfactory results.

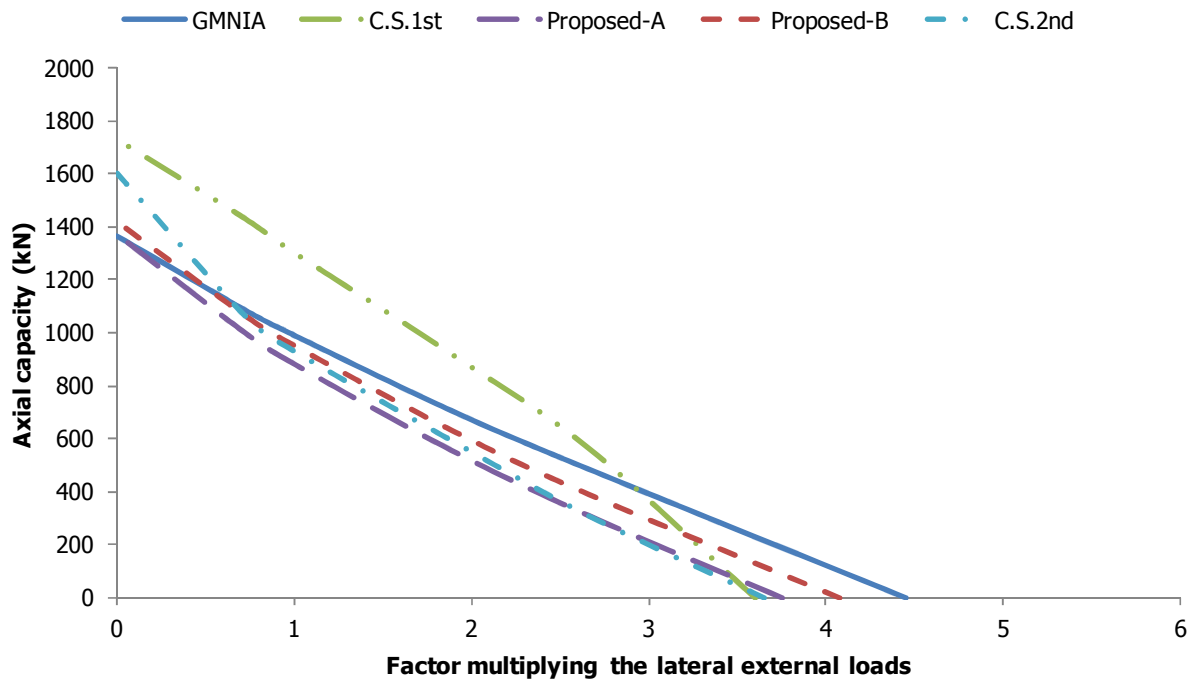


Figure 8-13: Interaction diagram of Example 3 for combined lateral loads including concentrated moment $-M_1$, uniformly distributed load q and concentrated force H_2

The undeformed and deformed shape of the laced member under combined lateral loads is depicted in Figure 8-14(a). In Figure 8-14(b) the axial force diagram is also shown from which it can be concluded that the panel with the largest axial compressive force is the one at the top for this specific case. Therefore, it is expected that this panel initially fails and leads to overall collapse. It can also be seen that the axial force of the critical panel differs significantly from the axial force of the adjacent one.

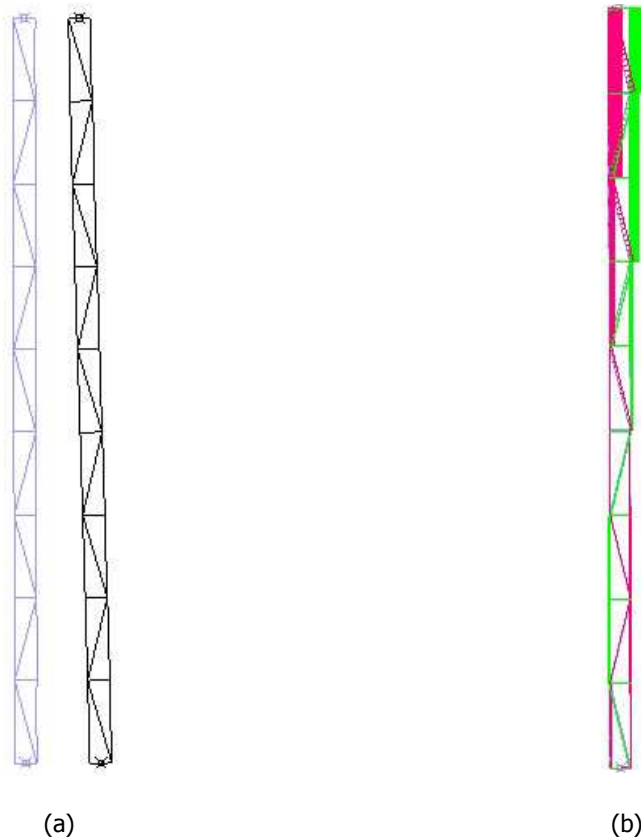


Figure 8-14: (a) Undeformed and deformed shape and (b) axial force diagram of the laced member of Example 3 under concentrated moment $-M_1$, concentrated load H_2 and uniformly distributed load q at failure

The laced member of Example 3 is also loaded by $-M_1=50\text{kNm}$ at the end B and by $H_2=2\text{kN}$ at the end B. Different magnitudes depending on a factor multiplying the lateral external loads are examined and the results are presented in Figure 8-15. A very satisfactory correlation between GMNIA and Proposed-B method is observed. In this case, the shear force is much smaller than in the previous load combination of Example 3 and the prediction of Proposed-B method is accurate for all the range from column to beam behaviour. Proposed-A method is more conservative but more accurate than C.S.2nd, while the use of C.S.1st gives inaccurate and against safety results.

The undeformed and deformed shape of the laced member under combined lateral loads is depicted in Figure 8-16(a). In Figure 8-16(b) the axial force diagram is also shown, from which it can be concluded that the panel that has the largest axial compressive force is the one at the bottom for this specific case. Therefore, it is expected that it is the one that initially fails and leads to overall collapse. It can also be seen that the axial force of the critical panel is slightly larger than the axial force of the adjacent one. For this reason, the adjacent panel does not offer rotational stiffness to the critical panel and the simply-supported assumption is sufficiently accurate.

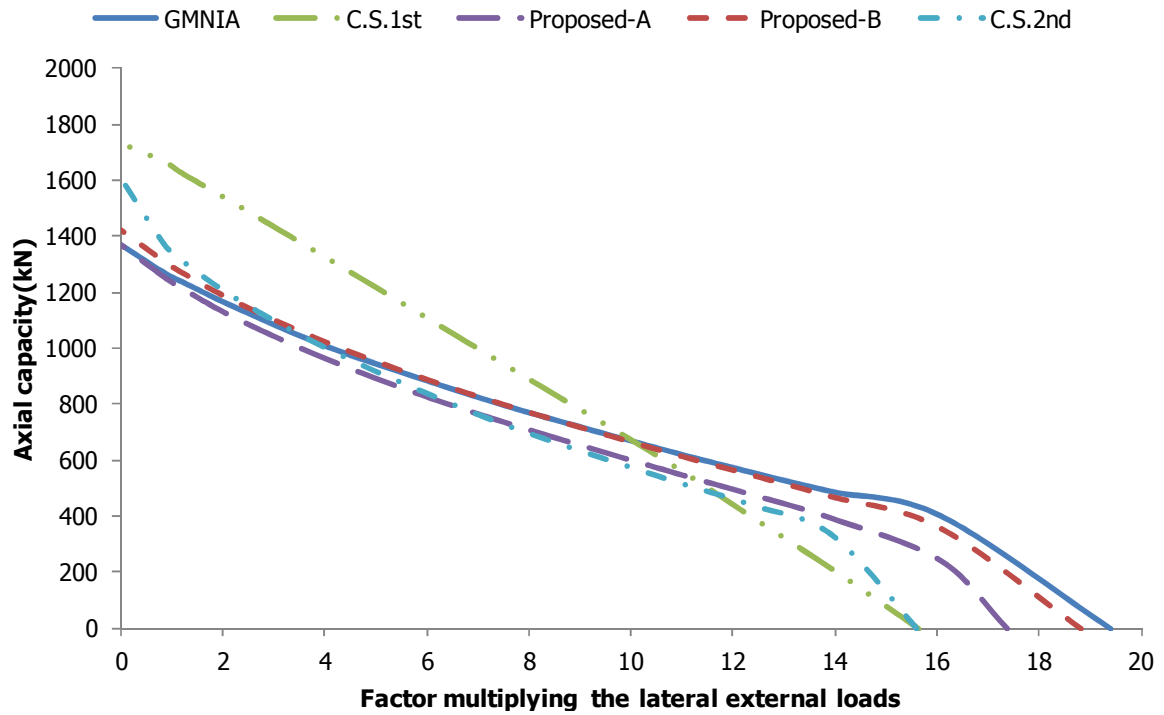


Figure 8-15: Interaction diagram of Example 3 for combined lateral loads including concentrated moment $-M_1$ and concentrated force H_2

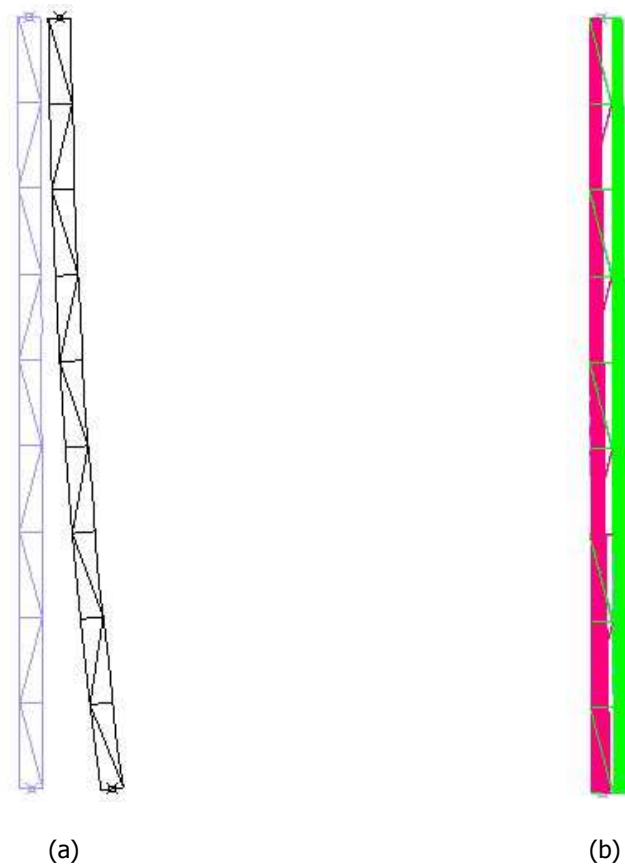


Figure 8-16: (a) Undeformed and deformed shape and (b) axial force diagram of the laced member of Example 3 under concentrated moment $-M_1$ and concentrated load H_2 at failure

8.4.1.2 I-sections

The examples presented for rectangular sections for the chords are repeated with the use of equivalent I-sections (having approximately the same areas as the rectangular ones) for the chords. The load cases investigated are exactly the same as the ones considered for the rectangular cross-sections of the chords. The behaviour of the I-sections under axial force and bending moment about z-z axis is modelled with the use of moment-curvature relationships for different levels of axial force. This procedure was reported in the literature by many researchers such as Chen and Atsuta [8-10] and Baptista and Muzeau [8-11]. The moment-curvature relationships for bending about the weak axis z-z are finally obtained with the use of XTRACT [8-12] software for the analysis of cross-sections. GMNIA results are compared with Proposed-A and Proposed-B methods.

Example 1-Partially sway member

The geometrical and boundary characteristics are the same as the ones presented for the partially sway member of the rectangular cross-section. The only difference is that an IPE180 cross-section is used for the flanges. The global and local buckling loads are equal to 1699kN and 11490kN, respectively. The local non-dimensional slenderness is equal to 0.38. The squash load is equal to 1651kN. In these analyses the local imperfection is taken equal to $a/500$. The results for the load cases examined are shown in Figure 8-17-Figure 8-21. A very satisfactory correlation between the proposed methods (especially Proposed-B method) and GMNIA is observed. It is also interesting to note that the interaction curves obtained with GMNIA for the rectangular cross-sections are close to the ones found for I-sections with similar areas.

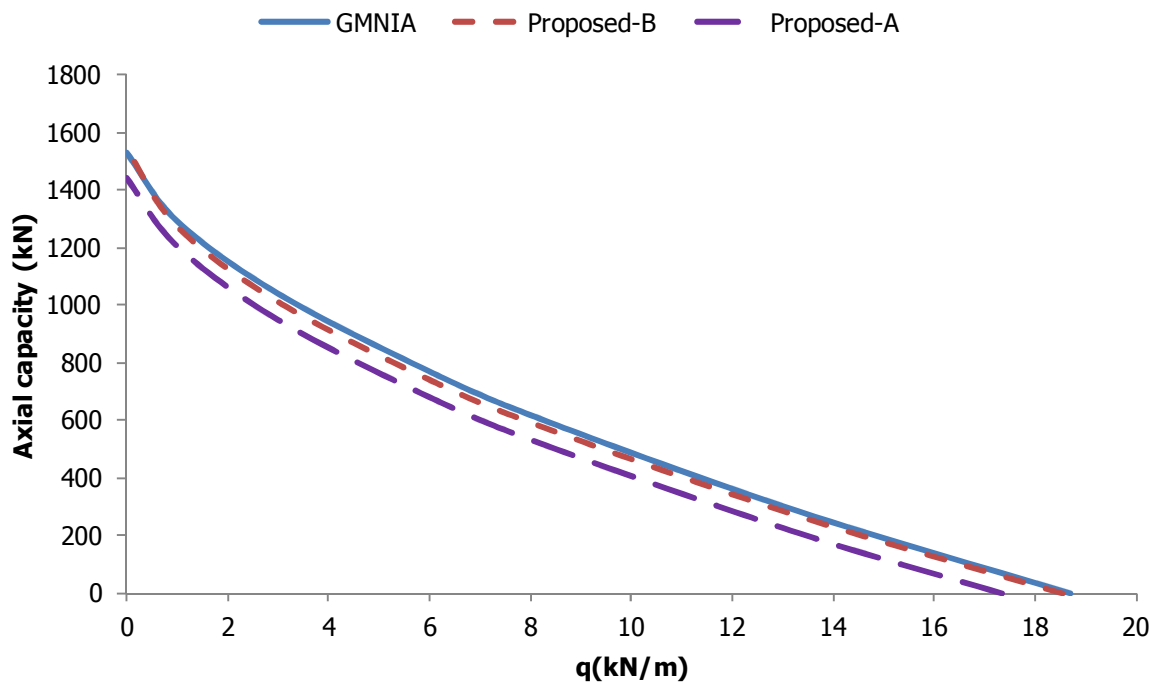


Figure 8-17: Interaction diagram of Example 1 with IPE180 chords' cross-section for uniformly distributed load q along the non-critical (less compressed) chord

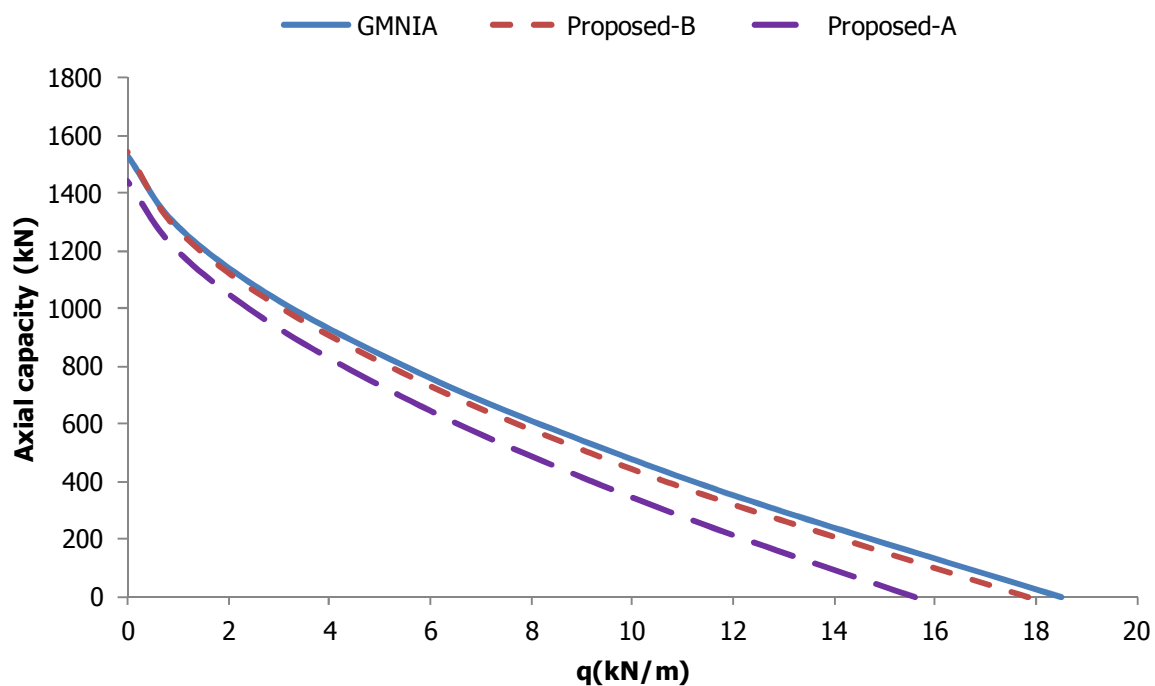


Figure 8-18: Interaction diagram of Example 1 with IPE180 chords' cross-section for uniformly distributed load q along the critical (more compressed) chord

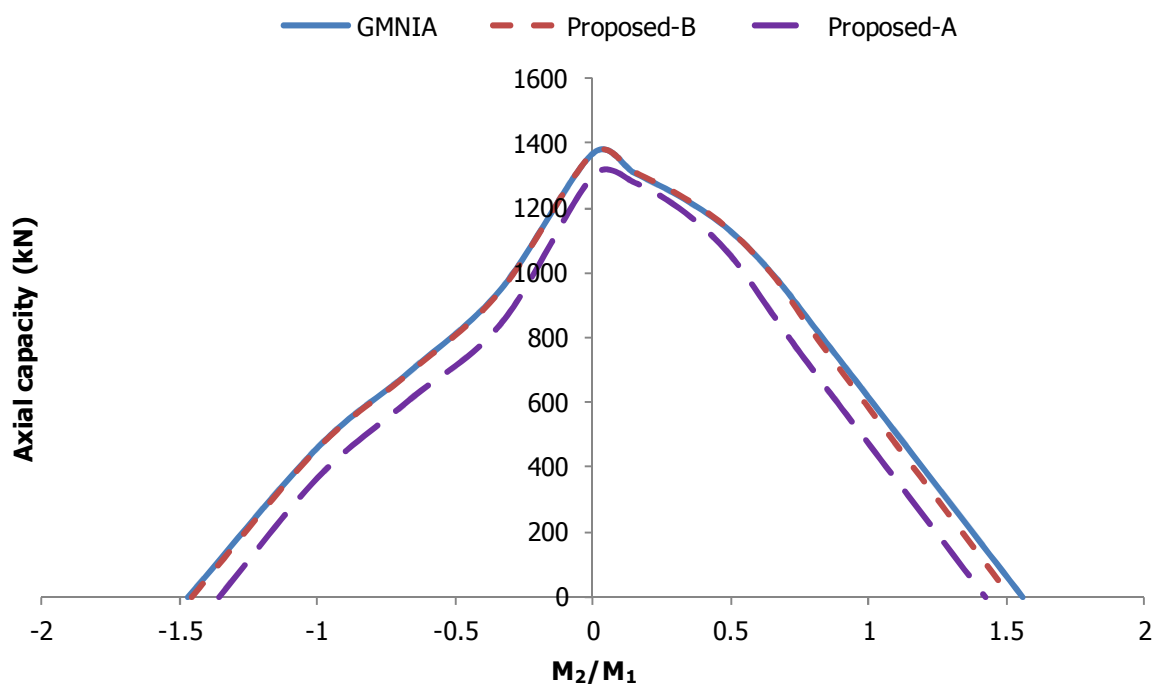


Figure 8-19: Interaction diagram of Example 1 with IPE180 chords' cross-section for constant moment M_1 at end A and varying moment M_2 at end B

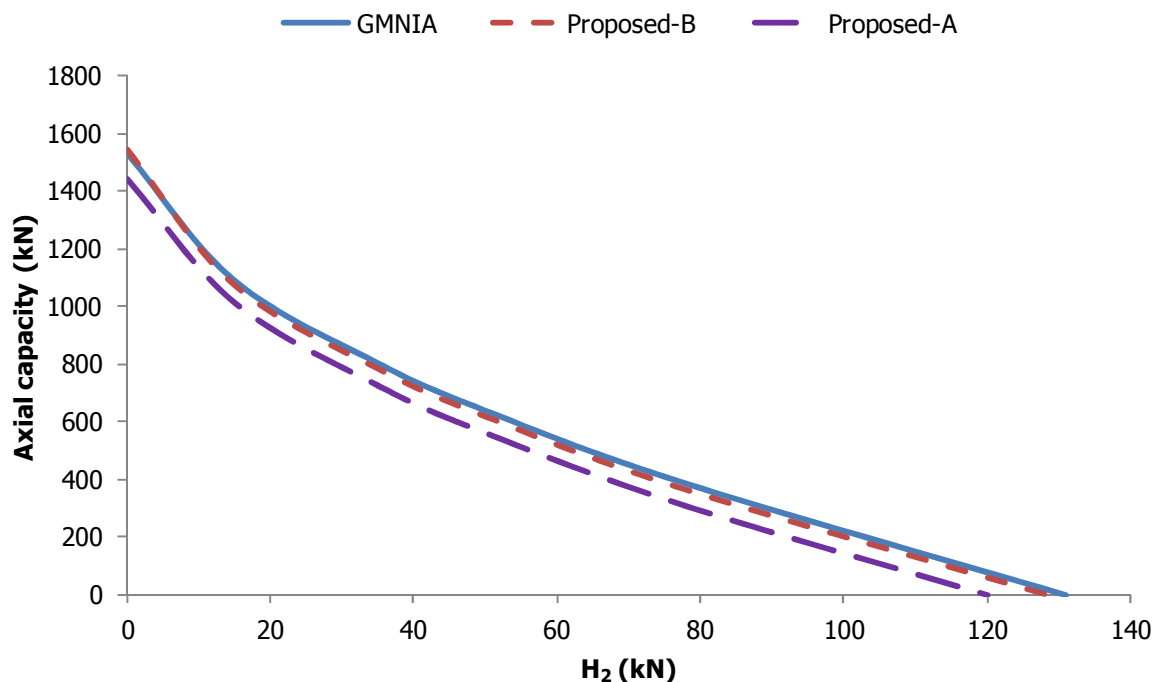


Figure 8-20: Interaction diagram of Example 1 with IPE180 chords' cross-section for varying load H_2 at end B

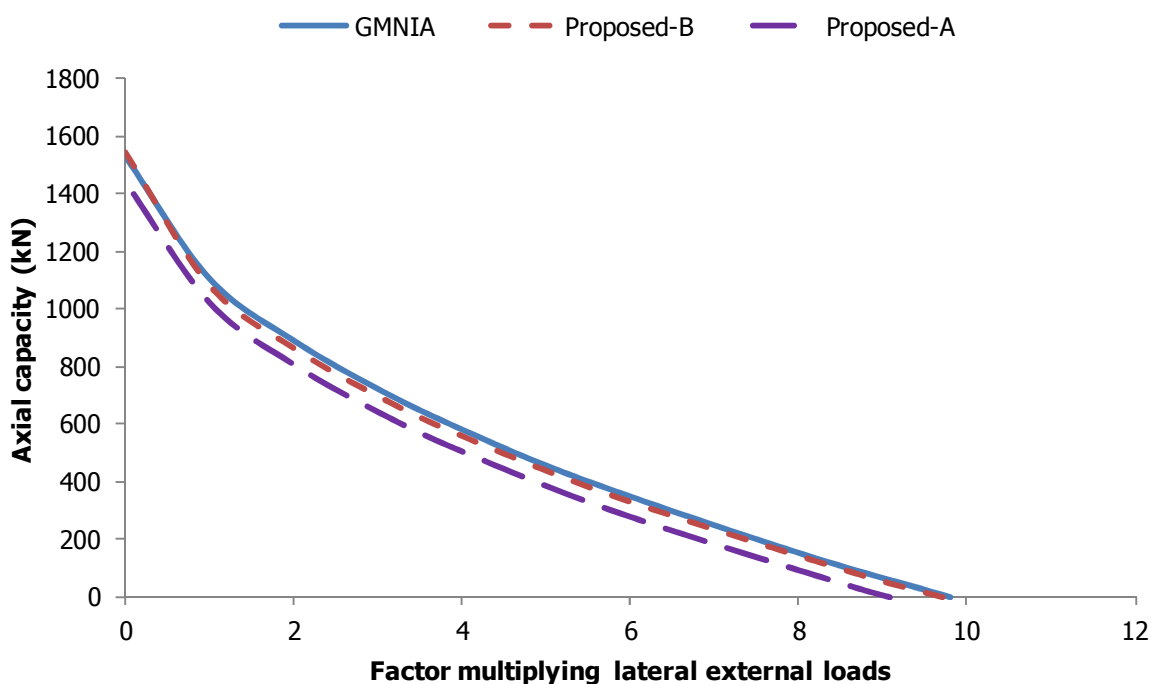


Figure 8-21: Interaction diagram of Example 1 with IPE180 chords' cross-section for combined lateral external loads

Example 2 - Non-sway member

The geometrical and boundary characteristics of the second laced member are the same as for the case of the rectangular cross-sections while the only difference is that IPE270 is used for the chords. The global and local buckling loads are equal to 15200kN and 47150kN, respectively. The squash load is equal to 3125kN. The local non-dimensional slenderness is equal to 0.26. A global imperfection equal to $L/500$ based on the first global buckling mode shape is considered. The local imperfection is

taken according to buckling curve “b” of Eurocode 3 [8-1]. The results for the load cases investigated are shown in Figure 8-22 and Figure 8-23 for the application of $-M_2$ at end B and q , respectively. A very satisfactory correlation between the proposed methods (especially Proposed-B method) and GMNIA is observed. It is also interesting to note that the interaction curves obtained with GMNIA for the rectangular cross-sections are close to the ones found for I-sections with similar areas.

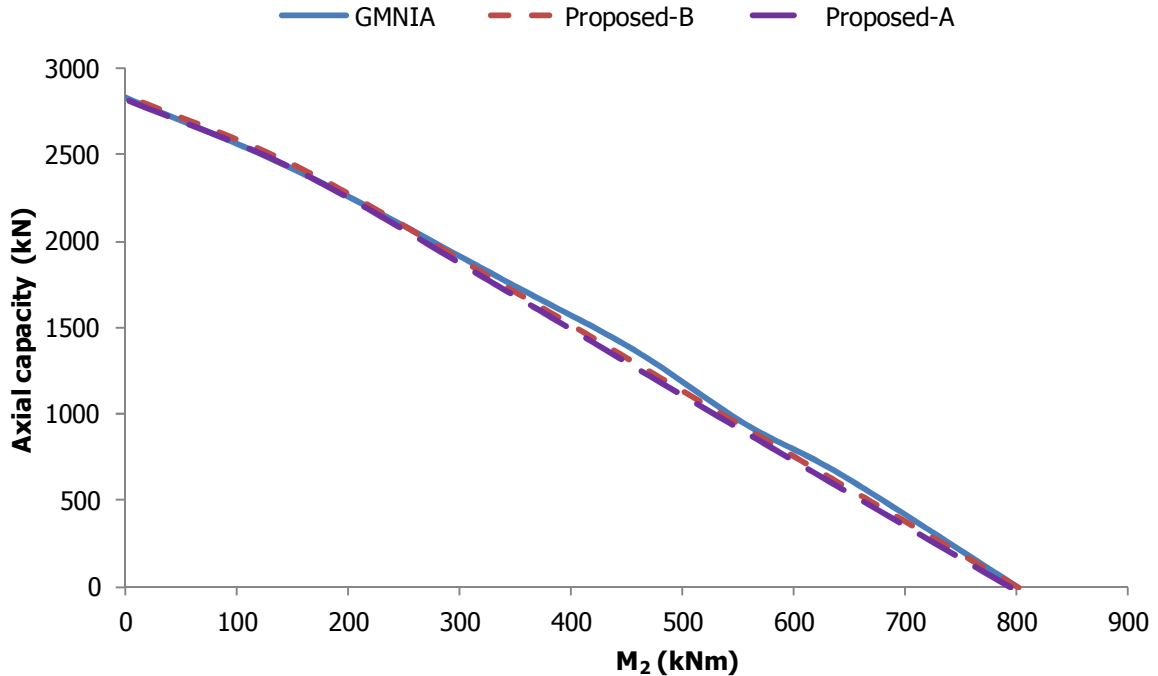


Figure 8-22: Interaction diagram of Example 2 with IPE270 chords' cross-section for varying moment $-M_2$ at end B

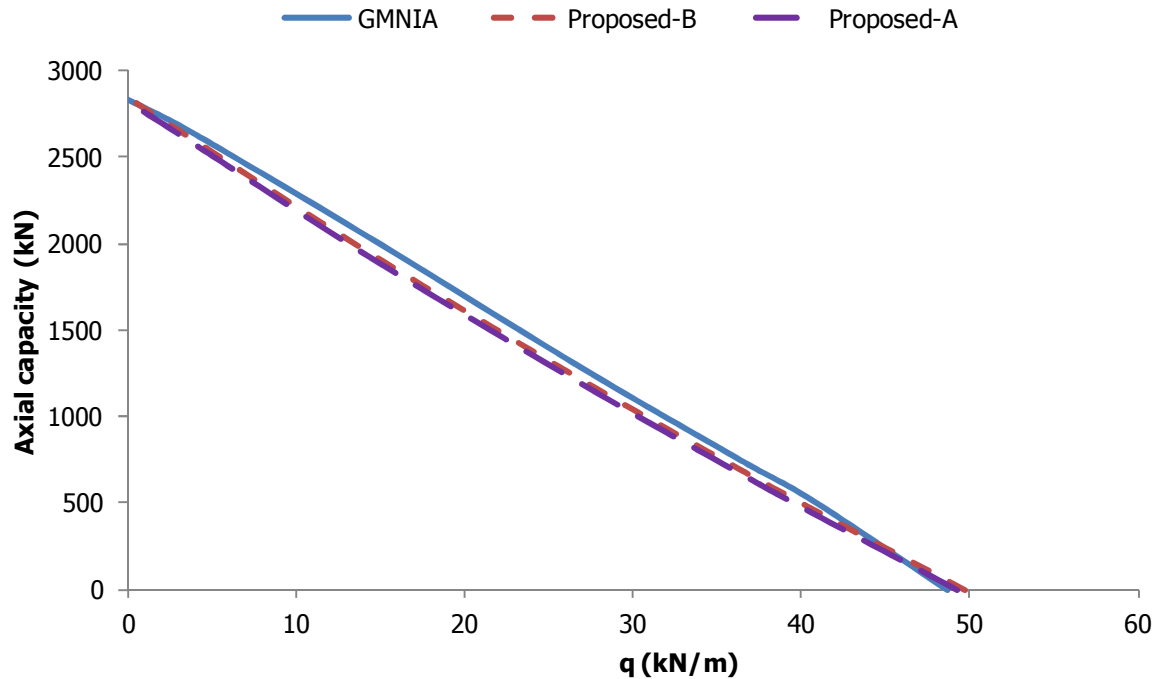


Figure 8-23: Interaction diagram of Example 2 with IPE270 chords' cross-section for varying uniformly distributed load q

Example 3- Arbitrary boundary conditions

The geometrical and boundary characteristics of the third laced member are the same as the ones used for rectangular cross-sections while the only difference is that IPE270 is used for the chords. The global and local buckling loads are equal to 1677kN and 7500kN, respectively. The squash load is equal to 3125kN. The local non-dimensional slenderness is equal to 0.66. A global imperfection equal to $L/500$ based on the first global buckling mode shape is considered. The local imperfection is taken according to buckling curve "c" of Eurocode 3 [8-1]. The results for the load cases investigated are shown in Figure 8-24 and Figure 8-25, respectively. A very satisfactory correlation between the proposed methods (especially Proposed-B method) and GMNIA is observed. It is also interesting to note that the interaction curves obtained with GMNIA for the rectangular cross-sections are close to the ones found for I-sections with similar areas.

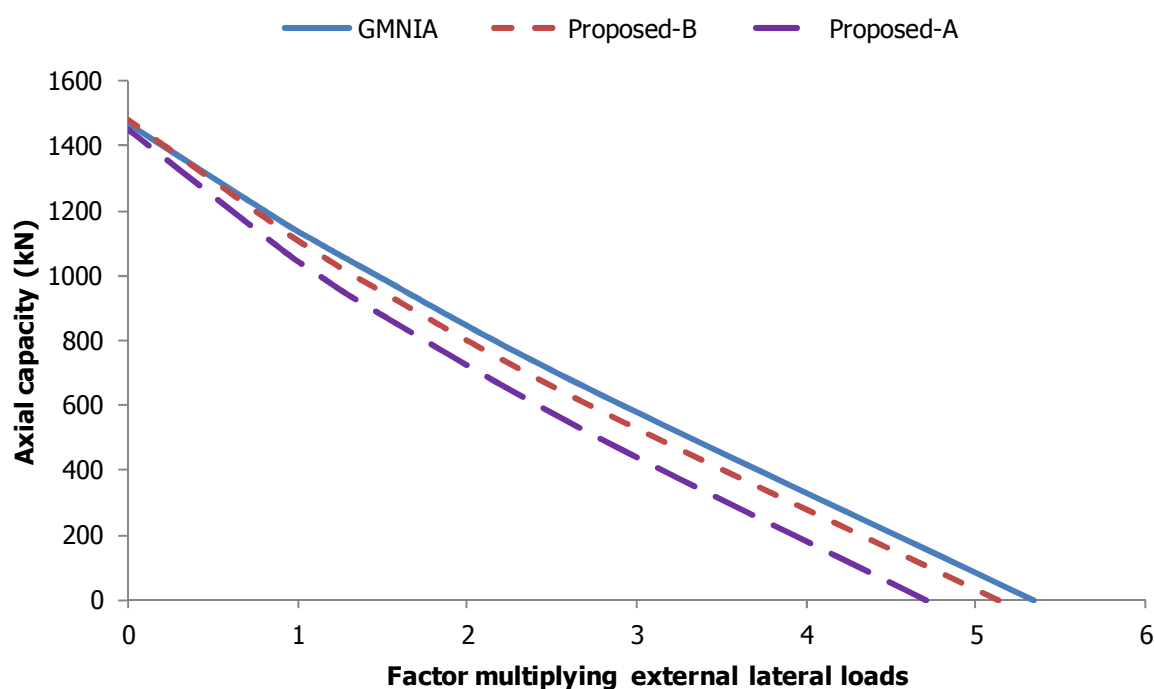


Figure 8-24: Interaction diagram of Example 3 with IPE270 chords' cross-section for combined lateral loads including uniformly distributed load q , concentrated moment $-M_1$ and concentrated force H_2

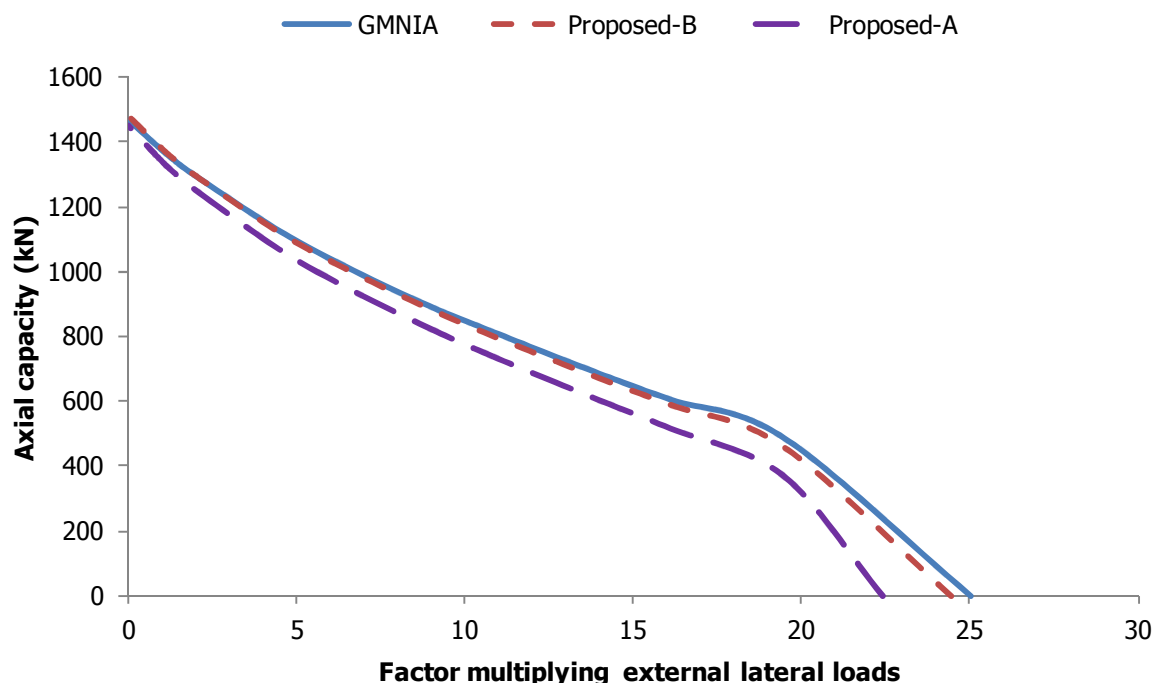


Figure 8-25: Interaction diagram of Example 3 with IPE270 chords' cross-section for combined lateral loads including concentrated moment $-M_1$ and concentrated force H_2

8.4.2 Modelling with shell elements

The use of shell elements is mandatory mainly in cases that the structure is prone to local plate buckling. Despite that fact, a wide range of analyses are also performed modelling the chords of the built-up column with 4-node shell elements, in order to observe more accurately the spread of plastification in the flanges. All laced beam-columns have an initial global imperfection equal to $L/500$, a local imperfection according to EC3 buckling curves and the material is S355. In addition to the collapse loads, the maximum force in the diagonals is also given.

Example 1 - Partially sway member

The geometrical, inertial and boundary characteristics of Example 1 with shell elements are summarised in Table 8-4. An X-lacing shear system is used while load combinations including concentrated moment M_2 at end B and concentrated load H_2 at end B are analysed. The global and local buckling loads are equal to 1289kN and 4855kN, respectively. The squash load is equal to 1427kN. The local non-dimensional slenderness is equal to 0.54.

Table 8-4: Geometrical, inertial and boundary characteristics of Example 1 with shell elements

L (m)	h_o (cm)	a (cm)	Flange cross-section	C_b (Nm)	$C_{br,b}$ (N/m)	C_t (Nm)	$C_{br,t}$ (N/m)
8.25	45	75	IPE160	$5 \cdot 10^6$	$\rightarrow \infty$	$5 \cdot 10^6$	$3 \cdot 10^4$

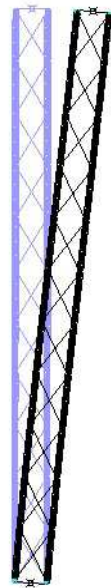
The results are shown in Table 8-5 and Table 8-6 for example 1 with shell elements for both collapse loads (c.l.) and maximum diagonal forces (d.f.) as obtained with the use of GMNIA, Proposed-B (Pr.-B), Proposed-A (Pr.-A), and commercial software 1st order (C.S.1st) and 2nd order (C.S.2nd) analyses. It can be seen that Proposed-B method gives results very close to the numerical ones while Proposed-A is always more conservative. The use of 1st-order analysis with commercial software is in general inaccurate while the use of 2nd-order analysis with commercial software improves the results remaining on the safe side. The undeformed shape, deformed configuration and plastified zones (red colour) in the critical panel at failure are depicted in Figure 8-26.

Table 8-5: Collapse loads of Example 1 with shell elements

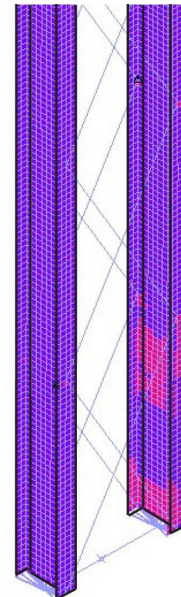
Lateral loads	GMNIA collapse load (kN)	Proposed-B collapse load (kN)	Proposed-A collapse load (kN)	Commercial software 1 st order collapse load (kN)	Commercial software 2 nd order collapse load (kN)
$M_2=0\text{kNm}$, $H_2=0\text{kN}$	1125	1124	1090	1152	1152
$M_2=353\text{kNm}$, $H_2=0\text{kN}$	565	555	520	532	480
$M_2=325\text{kNm}$, $H_2=6.5\text{kN}$	521	515	480	660	447
$M_2=202\text{kNm}$, $H_2=40.5\text{kN}$	324	311	275	470	260
$M_2=143\text{kNm}$, $H_2=57\text{kN}$	230	221	185	314	155

Table 8-6: Maximum diagonal forces of Example 1 with shell elements

Lateral loads	GMNIA diagonal forces (kN)	Proposed diagonal forces (kN)	Commercial software 1 st order diagonal forces (kN)	Commercial software 2 nd order diagonal forces (kN)
$M_2=0\text{kNm}$, $H_2=0\text{kN}$	21	26	20	18
$M_2=353\text{kNm}$, $H_2=0\text{kN}$	20	22	14	20
$M_2=325\text{kNm}$, $H_2=6.5\text{kN}$	21	23	11	21
$M_2=202\text{kNm}$, $H_2=40.5\text{kN}$	29	29	21	29
$M_2=143\text{kNm}$, $H_2=57\text{kN}$	33	32	27	33



(a)



(b)

Figure 8-26: (a) Undeformed and deformed shape and (b) plastified zones (red colour) of laced member of Example 1 with shell elements under axial load, concentrated moment M_2 and concentrated load H_2 at failure

Example 2 - Partially sway member

The geometrical, inertial and boundary characteristics of Example 2 with shell elements are summarised in Table 8-7. An X-lacing shear system is used while load combinations including concentrated moment M_1 at end A, concentrated moment M_2 at end B and concentrated load H_2 at end B are analysed. The global buckling load and squash load are equal to 17000kN and 8378kN, respectively. The local buckling is much larger and therefore the local non-dimensional slenderness is less than 0.2. For this reason, no local imperfections are used.

Table 8-7: Geometrical, inertial and boundary characteristics of Example 2 with shell elements

L (m)	h_o (cm)	a (cm)	Flange cross- section	C_b (Nm)	$C_{br,b}$ (N/m)	C_t (Nm)	$C_{br,t}$ (N/m)
13.2	75	132	HEB260	$\rightarrow 0$	$\rightarrow \infty$	$1 \cdot 10^8$	$1 \cdot 10^6$

The results are shown in Table 8-8 and Table 8-9 for Example 2 with shell elements for both collapse loads (c.l.) and maximum diagonal forces (d.f.) as obtained with the use of GMNIA, Proposed-B (Pr.-B), Proposed-A (Pr.-A), and commercial software 1st order (C.S.1st) and 2nd order (C.S.2nd) analyses. It can be seen that Proposed-B method gives results very close to the numerical ones while Proposed-A is always more conservative. The use of 1st-order analysis with commercial software is in general inaccurate while the use of 2nd-order analysis with commercial software improves the results remaining on the safe side. The concentration of plastification (red colour) in the critical panel at failure is depicted in Figure 8-27.

Table 8-8: Collapse loads of Example 2 with shell elements

Lateral loads	GMNIA collapse load (kN)	Pr.-B collapse load (kN)	Pr.-A collapse load (kN)	C.S. 1 st order collapse load (kN)	C.S. 2 nd order collapse load (kN)
$M_2=0\text{kNm}$, $H_2=0\text{kN}$, $M_1=0\text{kNm}$	7849	7812.0	7640	7355	7350
$M_2=-427.3\text{kNm}$, $H_2=427.3\text{kN}$ $M_1=2137\text{kNm}$	2137	2006	1875	1315	1125
$M_2=0\text{kNm}$, $H_2=560.9\text{kN}$ $M_2=0\text{kNm}$	2704	2661	2472	3125	2300

Table 8-9: Maximum diagonal forces of Example 2 with shell elements

Lateral loads	GMNIA diagonal forces (kN)	Proposed diagonal forces (kN)	C.S. 1 st order diagonal forces (kN)	C.S. 2 nd order diagonal forces (kN)
$M_2=0\text{kNm}$, $H_2=0\text{kN}$, $M_1=0\text{kNm}$	51	83	85	81
$M_2=-427.3\text{kNm}$, $H_2=427.3\text{kN}$ $M_1=2137\text{kNm}$	33	46	60	36
$M_2=0\text{kNm}$, $H_2=560.9\text{kN}$ $M_2=0\text{kNm}$	117	126	121	124

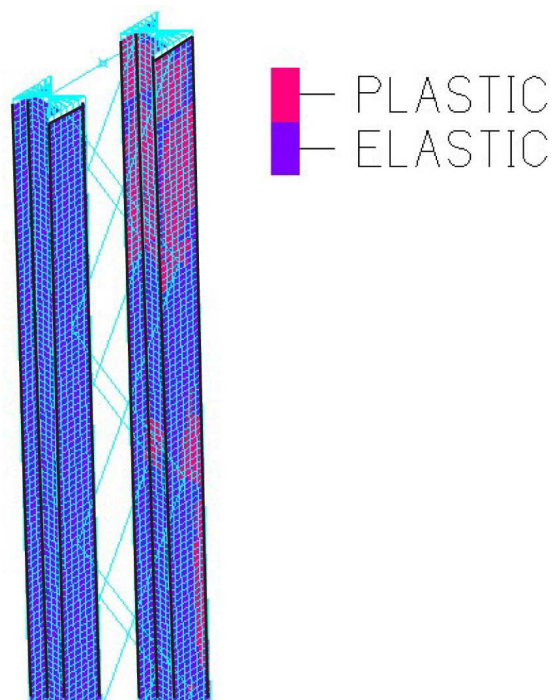


Figure 8-27: Plastified zones (red colour) of laced member of Example 2 with shell elements under axial load and concentrated load H_2 at failure

A very good correlation of the equilibrium paths obtained with GMNIA and Proposed-B method is shown in Figure 8-28. It can be seen that both the lateral deflections until failure and the collapse load are sufficiently captured by Proposed-B method. GMNIA revealed that the laced member behaves elastically until failure at which stiffness is almost equal to zero.

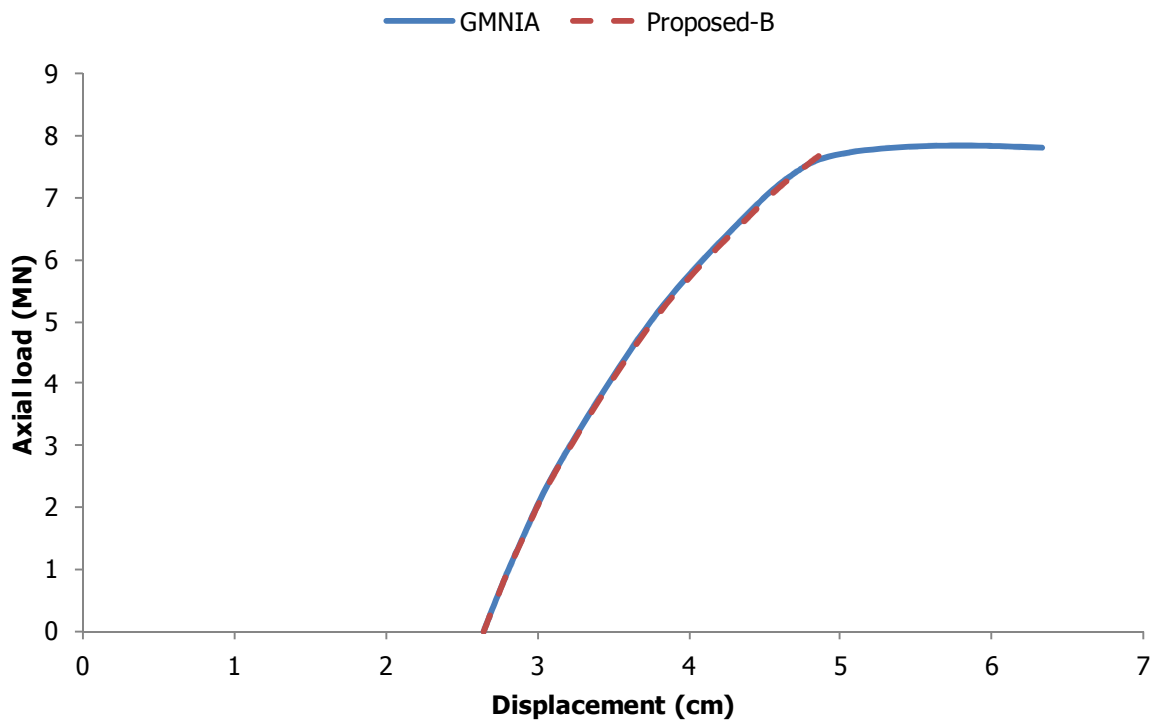


Figure 8-28: Equilibrium paths of the laced member of Example 2 with shell elements under axial load obtained with the use of GMNIA and Proposed-B method

8.5 VERIFICATION WITH EXPERIMENTAL RESULTS

The proposed design method of imperfect laced built-up beam-columns is verified in this section against experimental and corresponding numerical results. The test results are associated with the 43 ones reported by Klöppel and Ramm [8-13] and with the 10 laced beam-columns tested in the context of the present doctoral thesis (five groups of similar specimens). The numerical results are obtained with the use of GMNIA in shell element models. In the proposed and numerical methods, the global imperfection has a magnitude of $L/500$, while the local one is EC3's specified value according to the corresponding buckling curves, as initial imperfections were not measured in the tests. In all cases the material properties obtained with tensile tests performed on appropriately manufactured coupons are used. The approaches are summarised as:

- Experimental results: The maximum load that the specimens sustained in the tests.
- GMNIA: The laced built-up members are modelled with the use of finite element software. The collapse load is considered to be the maximum load value of the equilibrium path obtained with GMNIA, using 4-node shell elements. The chords are modelled as continuous members while the lacing bars are modelled with the use of Hermitian beam elements. Conservatively, global imperfections are directed so that they lead to the lowest collapse load in all cases. Local imperfections are directed so that they lead to the lowest collapse load in the literature experimental results (the exact direction of the critical panel is not reported) and so that they are in accordance with the direction of the critical panel observed in the present doctoral thesis's experimental tests.
- Proposed-A method: The collapse load is obtained by making use of Eq. (8-1) and incorporating the local capacity related to first yield as described in Eq. (8-4). Eq. (7-67) and Eq. (7-68) are used for the calculation of the maximum bending moment and corresponding shear force. This calculation is the lower bound of the proposed procedure and gives the same result as EC3 as all tests refer to simply-supported columns with relatively small lateral loads.
- Proposed-B method: The collapse load is obtained by making use of Eq. (8-1) and incorporating the local capacity associated with the full plastic reserve of the cross-section. The local capacity is obtained with the use of GMNIA in an imperfect (local imperfection) simply-supported panel with the appropriate direction of local imperfection so that the minimum local capacity is obtained. Eq. (7-67) and Eq. (7-68) are used for the calculation of the maximum bending moment and corresponding shear force.

The results are presented in graphs in which on both the vertical and the horizontal axes the collapse loads obtained with the use of the procedures presented in this section are plotted. The comparison between the collapse loads obtained with the procedure of the vertical axis with the ones obtained with the procedure of the horizontal axis for each specimen is illustrated by plotting a point in the two-dimensional graph. If the two collapse loads coincide, the corresponding point lies on the 45 degrees line.

8.5.1 Klöppel and Ramm experimental results

Klöppel and Ramm [8-13] tested 43 different laced columns under combined axial loading and concentrated bending moments at the ends due to small eccentricity of the load. The small eccentricities caused single curvature deformation. The comparison of the ultimate strength obtained numerically (GMNIA) and experimentally is presented in Figure 8-29 in which a satisfactory correlation can be noticed. A more accurate prediction of the ultimate strength is not possible as initial imperfections (either geometrical or material) were not measured in the tests.

Similar conclusions can be drawn from the comparison between Proposed-B method and experimental collapse loads depicted in Figure 8-30. The comparison between GMNIA and Proposed-B method is shown in Figure 8-31 and a remarkable accuracy is observed as the initial imperfections' magnitude and direction are in accordance in the two procedures. Proposed-A method that is based on first yield (in these cases it is close to Eurocode 3 predictions as it refers to simply-supported members) gives more conservative results when compared with GMNIA in Figure 8-32. The improvement with the use of the full local capacity in Proposed-B method is obvious.

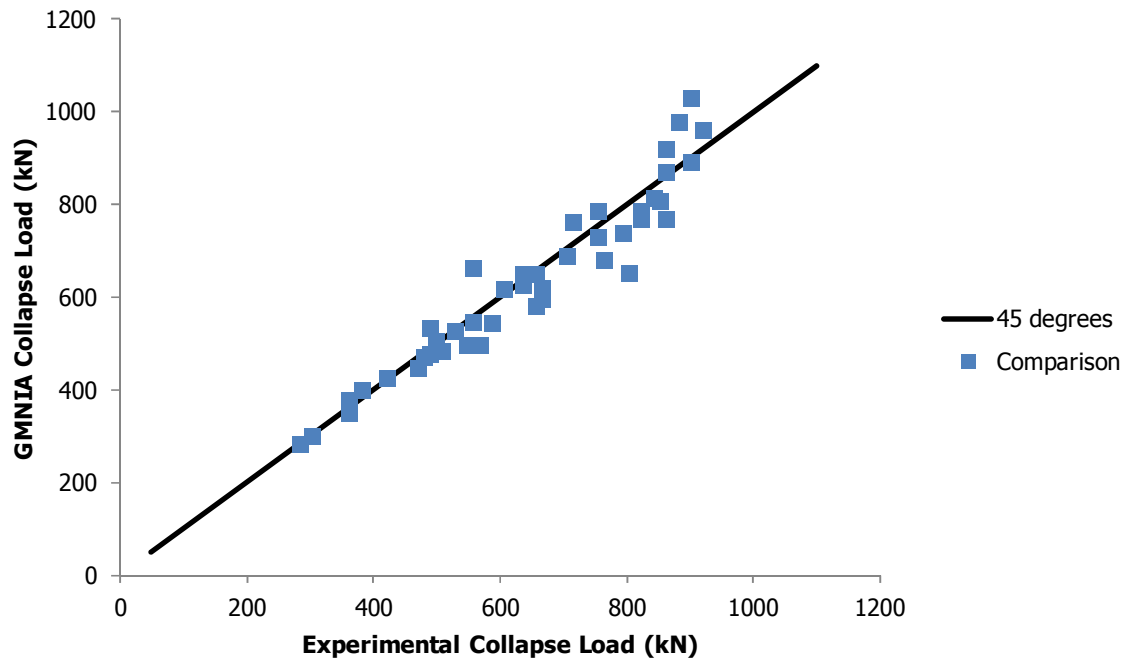


Figure 8-29: Comparison between numerical (GMNIA) and experimental collapse loads for Klöppel and Ramm tests

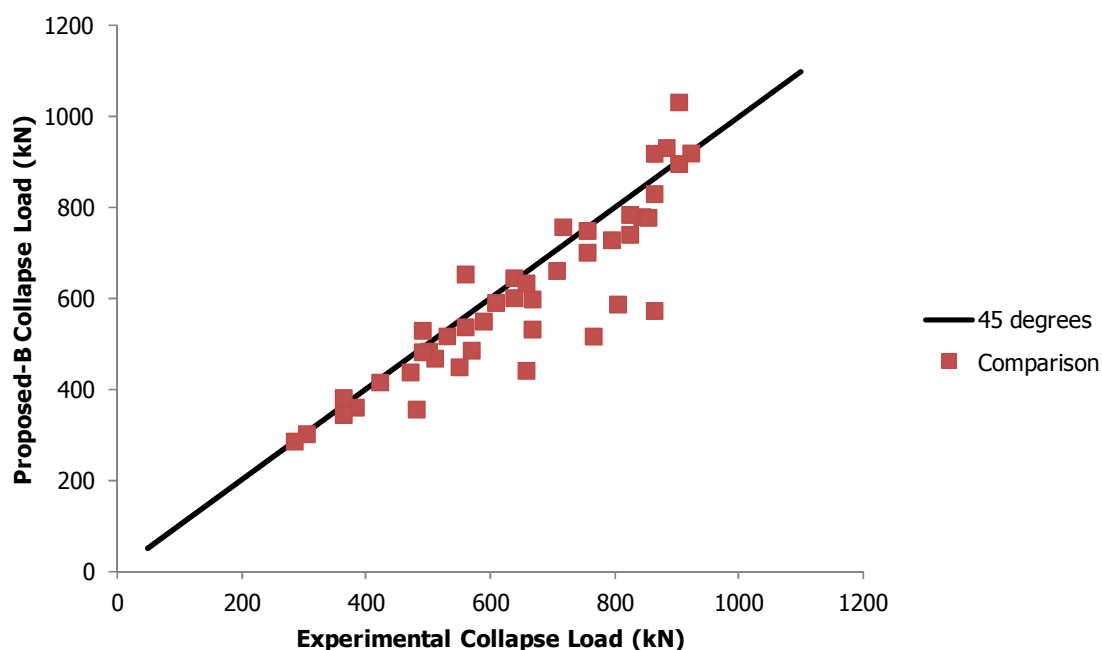


Figure 8-30: Comparison between Proposed-B method and experimental collapse loads for Klöppel and Ramm tests

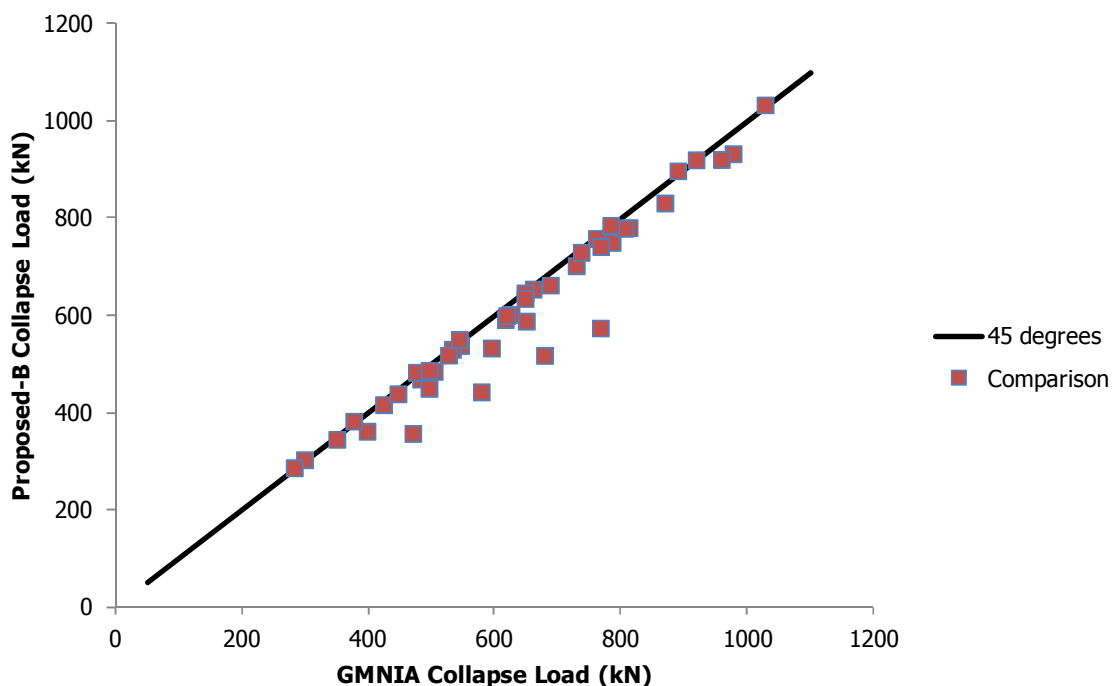


Figure 8-31: Comparison between Proposed-B method and numerical (GMNIA) collapse loads for Klöppel and Ramm tests

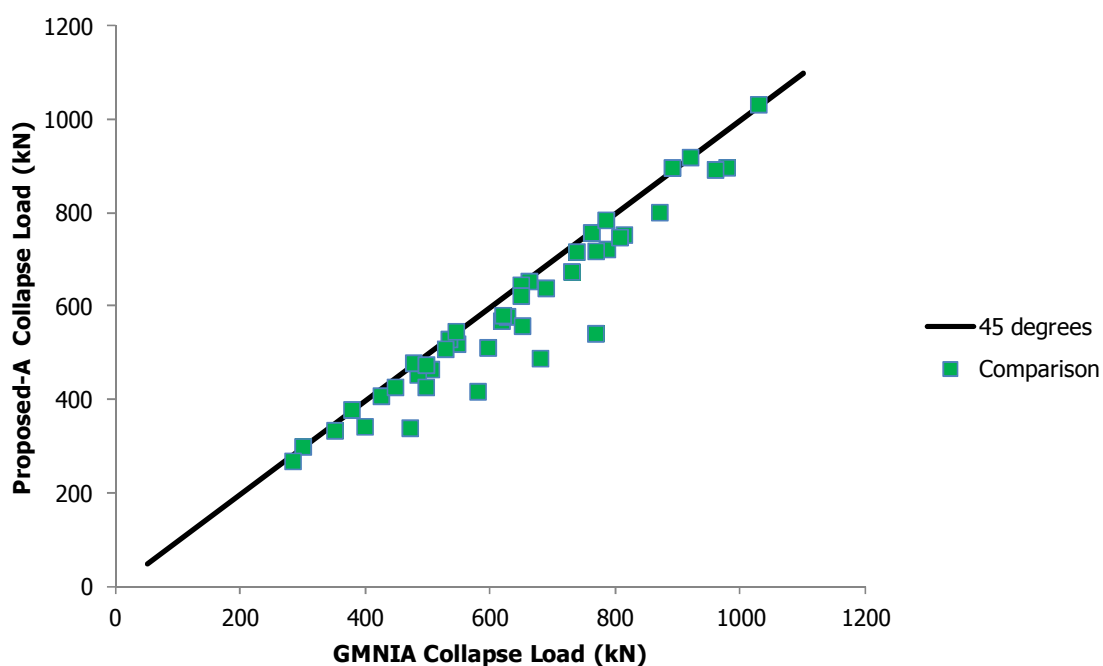


Figure 8-32: Comparison between Proposed-A method and numerical (GMNIA) collapse loads for Klöppel and Ramm tests

When comparing the different methods with the experimental results the mean and absolute errors for GMNIA, Proposed-B method and Proposed-A method (close to EC3 for this specific case) are approximately equal to 6%, 9% and 11%, respectively.

Also, it should be noted that the four cases that are much more conservative than the others as shown in Figure 8-31 and Figure 8-32, refer to a laced specimen that had 3 panels, fewer than the

minimum number of panels (four) required for satisfactory modelling of the laced member as an equivalent Timoshenko one with constant bending and shear rigidities along its length.

8.5.2 Present doctoral thesis's experimental results

In the context of the present doctoral thesis ten simply-supported laced built-up columns were tested and the results obtained experimentally and numerically with the use of GMNIA were presented in detail in Chapter 3 and Chapter 4, respectively. The specimens were subjected to compressive loads with end eccentricities causing either single or double curvature deformation. A graphic comparison between GMNIA and experimental collapse loads is shown in Figure 8-33 revealing the conclusion drawn in Chapter 4 that the numerical models capture the collapse mechanism sufficiently. It is possible that better accuracy could be achieved if initial imperfections were measured and used in the numerical analyses instead of the code specified values.

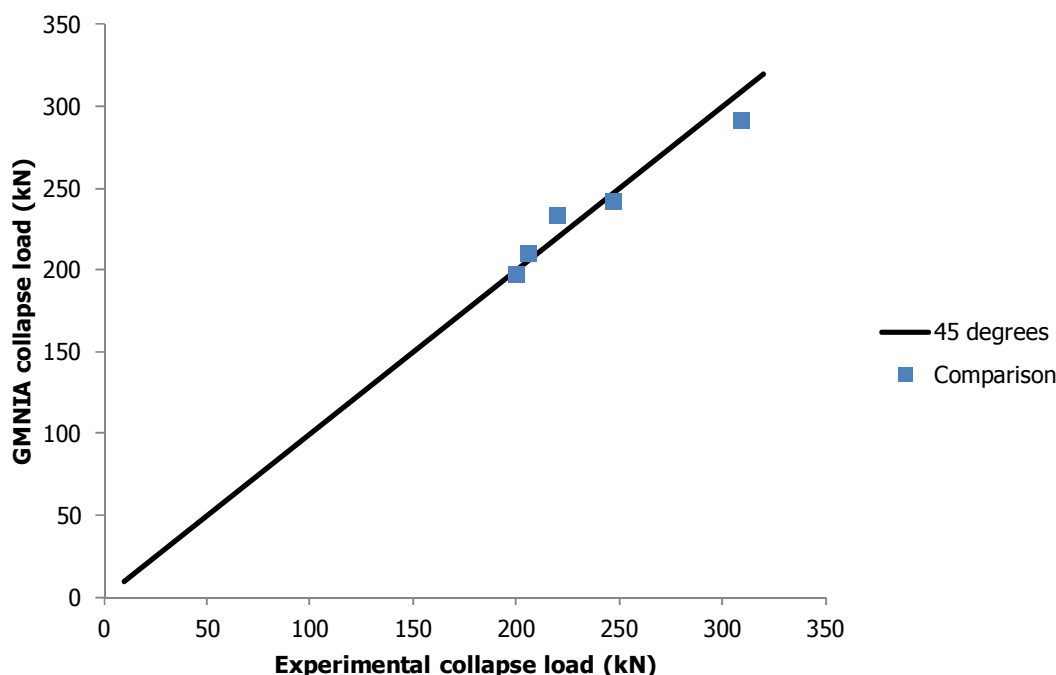


Figure 8-33: Comparison between numerical (GMNIA) and experimental collapse loads for present doctoral thesis's tests

In Figure 8-34 and Figure 8-35 the results obtained with the two proposed procedures are depicted and compared with experimental collapse loads. Both of them are conservative especially Proposed-A method. Proposed-B method has also a safe margin and appears to be not as accurate as for the literature's tests presented in subsection 8.5.1. The reason behind this divergence lies in the important difference between the unrestricted and restricted panels' lengths as described in Chapter 4, explaining the differences in the collapse load between beam and shell element models. As in the numerical models with beam elements, the proposed analytical methods consider the local buckling length to be equal to the theoretical distance between adjacent connections. Nevertheless, for the specific specimens tested, the unrestricted length of the panels was approximately equal to 75% of the theoretical one which means that the local buckling load was much larger (approximately 1.8 times larger).

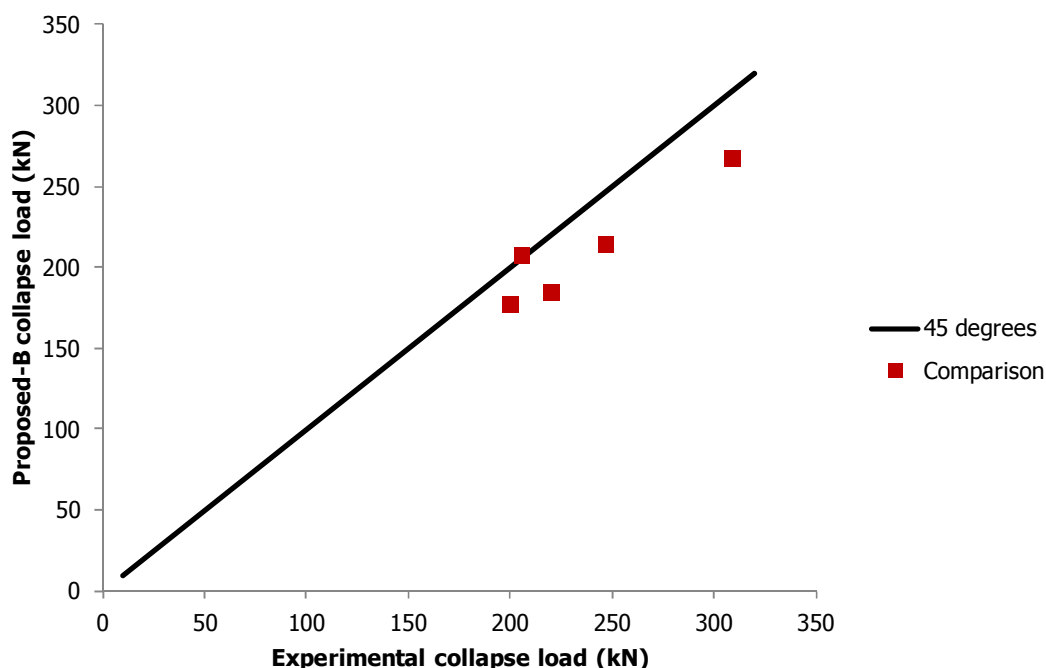


Figure 8-34: Comparison between Proposed-B method and experimental collapse loads for present doctoral thesis's tests

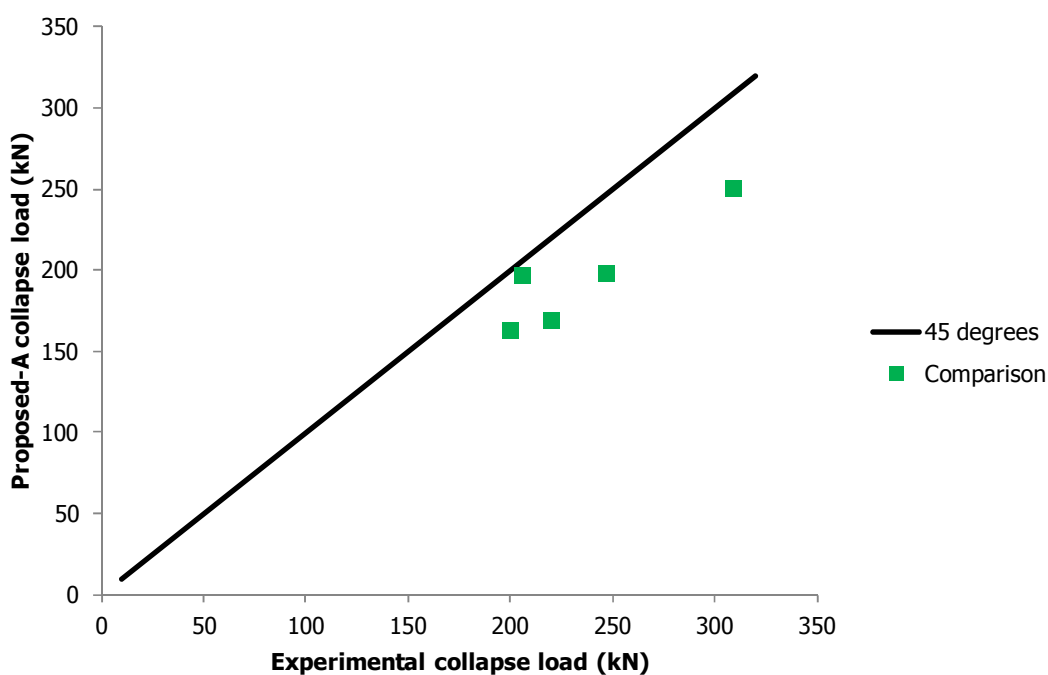


Figure 8-35: Comparison between Proposed-A method and experimental collapse loads for present doctoral thesis's tests

The results of the two proposed methods with the use of the unrestricted length for the critical panel's buckling length are given in Figure 8-36 and Figure 8-37. It can be concluded that the results are significantly improved when the unrestricted length is used as the local buckling length. Of course the results remain on the safe side due to the fact that conservative initial imperfections based on code's provisions are used while the existing imperfections in the specimens were not measured. Another reason behind the safety margin is that initial local imperfections are directed so that the minimum

collapse load of the critical panel is obtained for all five cases, being in accordance with the result that the engineer of practice would obtain.

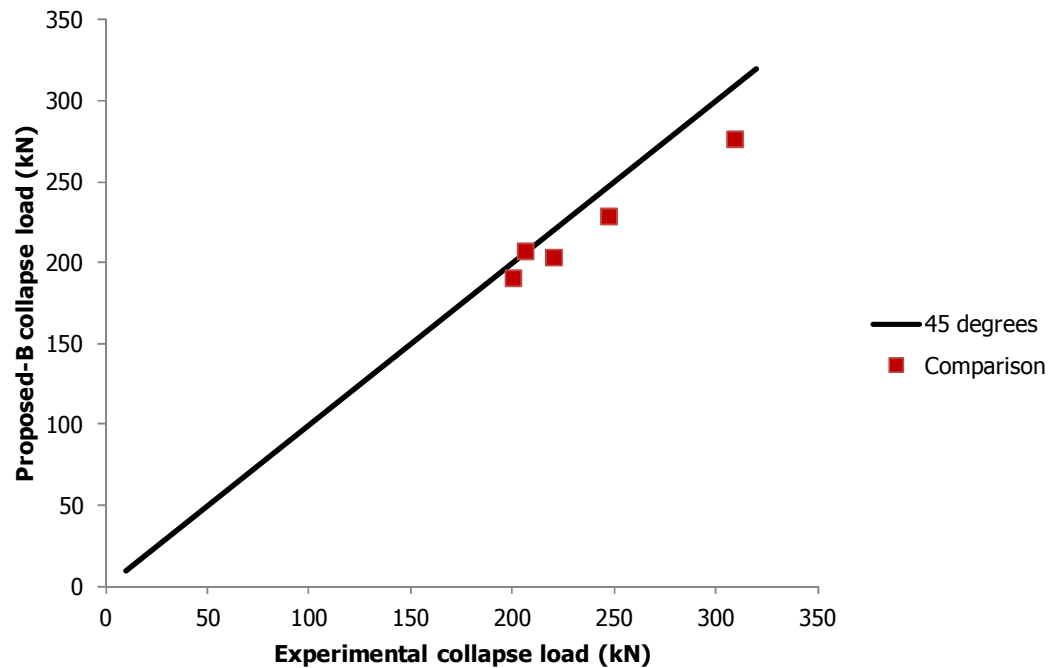


Figure 8-36: Comparison between Proposed-B method (unrestricted length used) and experimental collapse loads for present doctoral thesis's tests

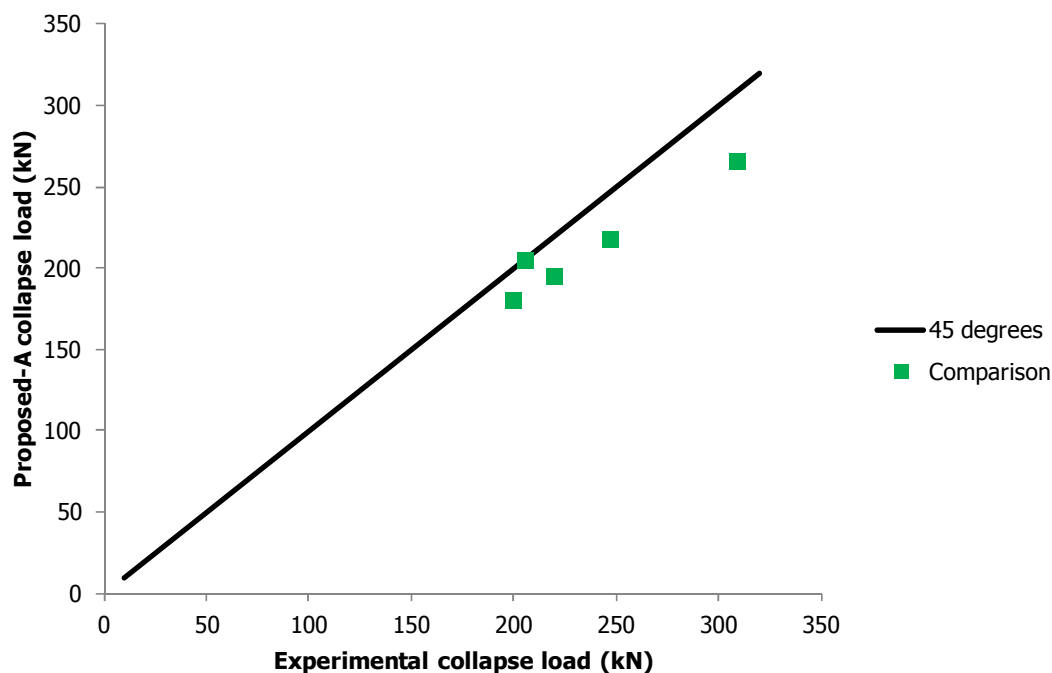


Figure 8-37: Comparison between Proposed-A method (unrestricted length used) and experimental collapse loads for present doctoral thesis's tests

The comparison between the results obtained with Proposed-B method and GMNIA is depicted in Figure 8-38. When comparing the different methods with the experimental results the mean and absolute errors for GMNIA, Proposed-B method and Proposed-A method (close to EC3 for this specific case) are equal to 3.4%, 6.1% and 9.7%, respectively.

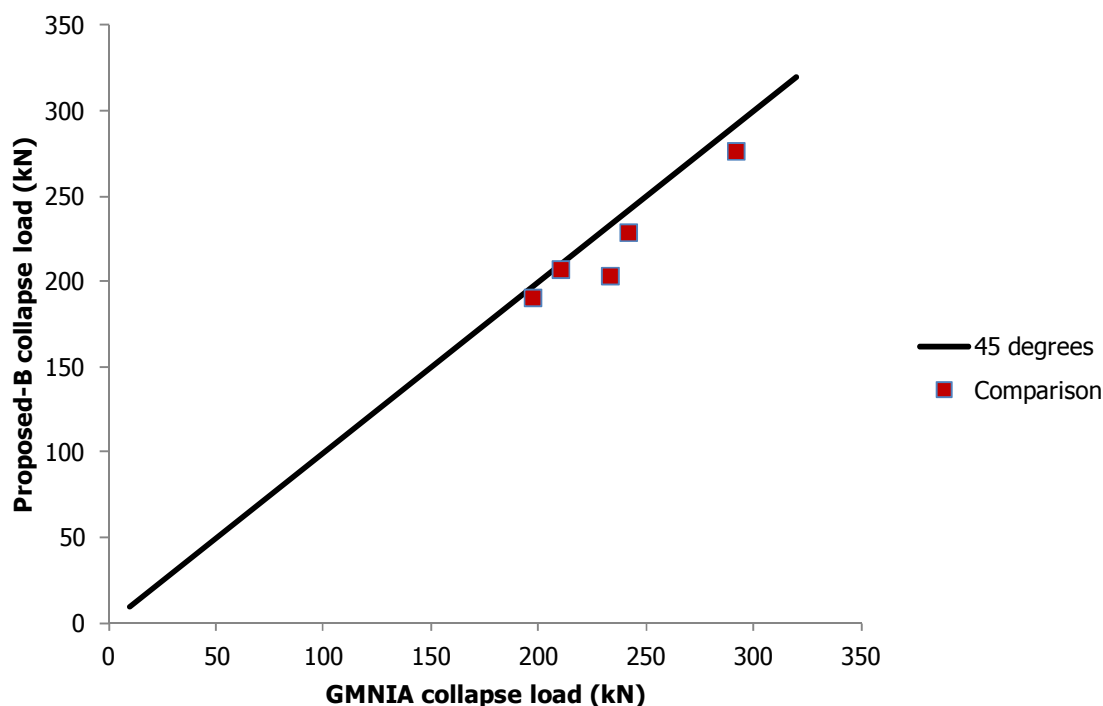


Figure 8-38: Comparison between Proposed-B method (unrestricted length used) and numerical (GMNIA) collapse loads for present doctoral thesis's tests

8.6 CONCLUSIONS

A general interaction equation for laced built-up beam-columns with arbitrary boundary conditions was presented. Based on the analytical procedures proposed in the previous chapters for the second-order elastic analysis of imperfect Timoshenko beam-columns with arbitrary supports and on the general interaction equation, two methods were presented: Proposed-A and Proposed-B that differ only in the local capacity of the critical panel. In the first case, the local capacity is associated with the 1st yield, while in the latter one the spread of plasticity in the cross-section is taken into account, thus requiring a slightly larger computational effort.

Both procedures gave very satisfactory results when compared with GMNIA results for a wide range of laced members that were analysed using beam and shell elements. Proposed-A was more conservative while Proposed-B method resulted in very good accuracy. Both methods were in general more accurate than using 1st-order and 2nd-order elastic analyses with commercial software and checking according to the Method 2 interaction equations of Eurocode 3 [8-1]. To be more specific, the use of 1st-order analysis proved to be unsafe in many cases and should be avoided. The use of 2nd-order analysis and checking based on the interaction equations of Eurocode 3 is much more sufficient than using 1st-order analysis but results in less accurate results when compared with the proposed methods. The reason is that it accounts for elastic local bending moments that will probably be reduced due to material yielding.

The proposed methods were also validated against experimental results for simply-supported laced columns with small lateral loads obtained from literature and from the present doctoral thesis's experimental effort. The results of Proposed-A method were close to the ones found when using Eurocode 3 and were sufficiently safe. The results obtained with the use of Proposed-B method were also very accurate and closer to the ones obtained numerically.

The proposed methods are sufficiently accurate and offer a useful tool in the hands of structural engineers. Therefore, it can be concluded that in practice the following procedures can be used:

- Proposed-A method for preliminary design and/or for checking the results obtained with commercial software.
- Proposed-B method for preliminary design and/or for checking the results obtained with commercial software, being confident that very accurate results (compared with GMNIA) will be obtained as far as the behaviour and collapse load are concerned.
- Use of an equivalent Timoshenko beam-column for the elastic second-order analysis and application of the internal forces in the interaction Eq. (8-1) to Eq. (8-3) depending on the lacing system.

8.7 REFERENCES

- [8-1] Eurocode 3: Design of Steel Structures. Part 1.1: General structural rules. CEN-European Committee for Standardisation, Brussels, EN1993-1-1, 2005
- [8-2] Ayrton, W.E., Perry, J. "On struts", *The Engineer*, pp. 464-513, 1886
- [8-3] Rankine, W.J.M. "Useful rules and tables", 1866
- [8-4] Vayas, J. "Steel Structures: Analysis and Design", Kleidarithmos Press, Athens, Greece, 2003 (in Greek)
- [8-5] ADINA System 8.5, "Release Notes", ADINA R & D Inc., 71 Elton Avenue, Watertown, MA 02472; USA, 2008
- [8-6] Bonab, A.P., Hashemi, B.H. "Analytical investigation of cyclic behaviour of laced built-up columns", *Journal of Constructional Steel Research*, Vol. 73, pp. 128-138, 2012
- [8-7] Chiorean, C.G. "A computer method for nonlinear inelastic analysis of 3D semi-rigid steel frameworks", *Journal of Engineering Structures*, Vol. 31, pp. 3016-3033, 2009
- [8-8] Chen W.F., Kim, S.E., Choi, S.H. "Practical second-order inelastic analysis for three-dimensional steel frames", *Steel Structures*, Vol. 1, pp. 213-223, 2001
- [8-9] Ramm, W., Uhlmann W. "Zur Anpassung des Stabilitätsnachweises für mehrteilige Druckstäbe an das europäische Nachweiskonzept", *Der Stahlbau*, Vol. 50, pp. 161-172, 1981
- [8-10] Chen, W.F., Atsuta T. "Theory of beam-columns", McGraw-Hill, New York, 1976
- [8-11] Baptista, A.M., Muzeau, J.P. "Analytical formulation of the elastic-plastic behaviour of bi-symmetrical steel shapes", *Journal of Constructional Steel Research*, Vol. 62, pp. 872-884, 2006
- [8-12] XTRACT v3.0.1, "Release Notes", Imbsen Software Systems, 9912 Business Park Drive, Suite 130, Sacramento, CA 95827; USA, 2004
- [8-13] Klöppel, K. Ramm, W. "Versuche und Berechnung zur Bestimmung der Traglast mehrteiliger Gitterstäbe unter aussermittiger Belastung", *Der Stahlbau*, Vol. 37 p. 164 and 236, 1968

9 BEHAVIOUR OF INDUSTRIAL FRAMES

9.1 INTRODUCTION

The structural behaviour and ultimate strength of laced built-up beam-columns was thoroughly presented in the previous chapters. The proposed methods were applied to laced built-up beam-columns with arbitrary supports. Usually these members are part of the supporting system in one-story industrial buildings that consist of successive planar vertical frames. Indicative photos of such structures were presented in Chapter 1. Literature regarding industrial frames with built-up members is very limited, including mainly the work of Richard et al. [9-1] who performed elastic time-history analyses on planar single-story moment-resisting frames with fixed base supports at their laced built-up columns' ends.

Industrial frames usually consist of successive planar frames having a beam (usually a truss beam) and two laced columns. In many cases they carry crane bridges and are designed for heavy loads. The beam-column connections are in principle rigid. The laced members can have either a constant cross-section (continuous in elevation) or a significantly smaller cross-section close to the beam-column connection (discontinuous in elevation) for the proper support of the crane bridge that runs along the structure. Both types are investigated in the present chapter as far as their behaviour and collapse loads are concerned, with emphasis on the first one.

The application of the proposed methods and of existing analysis and design procedures is investigated. Frames with realistic geometry, cross-sections and external loadings are used. Each frame is free to sway and consists of a truss beam and two laced built-up columns that are either continuous or discontinuous in elevation. Results obtained with the application of the proposed methods and existing analysis and design procedures are compared with GMNIA results obtained with finite element software ADINA [9-2]. Useful conclusions are drawn that lead to the presentation of practical design guidelines.

9.2 METHODS OF ANALYSIS AND DESIGN FOR LACED MEMBERS

The advance in computer science resulted in the appearance of significant tools in the hands of the structural engineer for modelling, analysing and designing structures. The possible procedures that one can use for obtaining the structural response and ultimate capacity of laced built-up members in

frames are summarised in the next subchapters, covering separately modelling procedures, types of analysis and design checks. The merits and disadvantages of each method are also discussed.

9.2.1 Modelling procedures

The main types of modelling include the use of either beam elements or shell elements or a combination of the two. Both of them are acceptable for laced members while each one has its merits and drawbacks, presented in this subchapter.

9.2.1.1 Euler- Bernoulli beam elements

The use of Euler-Bernoulli beam elements with equivalent characteristics for modelling laced members is not acceptable, as such elements take into account only bending deformations ignoring shear effects. It was shown that shear deformations play an important role in the behaviour of laced members resulting in larger deflections and smaller buckling and collapse loads when compared with the case that they are ignored. Therefore, the use of Euler-Bernoulli beam elements is expected to lead to unsafe and inaccurate results.

9.2.1.2 Timoshenko beam elements

The use of Timoshenko beam elements with equivalent characteristics for modelling laced members is acceptable, as both bending and shear deformations are taken into account. Therefore, their use leads to a sufficient evaluation of deflections and internal forces. Finite element software, in general, use a formulation that is close to Engesser's method for incorporating shear deformation in beam elements. Additionally, parametric studies presented in this doctoral thesis show that using Timoshenko members with equivalent bending and shear rigidities (described in many structural textbooks) for modelling laced members leads to very satisfactory results.

The use of a single beam element for modelling a laced member facilitates the analysis, as the number of degrees of freedom is significantly reduced, but this does not come without any cost. First of all, the internal forces refer to an equivalent structural model and should be appropriately used in order to refer to the laced member, something for which no specific guidance exists. Additionally, errors may be induced in the modelling, mainly attributed to the validity of the assumptions made, regarding equivalent characteristics, boundary conditions, loads and connections between chords and lacing bars. It is clear that when modelling a structure and a connection of finite dimensions as a single beam and node, respectively, it is possible to ignore some parameters. Nevertheless, as was shown in previous chapters and will be investigated in the present one, the importance of these parameters is expected to be small.

9.2.1.3 Full laced member with the use of Euler-Bernoulli beam elements

Modelling the full laced member with all its structural components as Euler-Bernoulli beam elements is very common in practice and is considered to be a very sufficient approximation of the real response. Analysis of full laced members results in the calculation of internal forces of each structural component, which can be used for their design. Chords are modelled as continuous components while lacing bars usually have moment releases at their ends.

The main shortcoming of such modelling is that welded connections between lacing bars and chords are considered to be nodal. In the previous chapters, it was concluded that this is expected to play a somewhat important role only if the finite dimensions of the connections are a significant part of the panels' length as in the tests performed in the context of the present doctoral thesis. In practice, this will not be the case as connections' dimensions are only a small part of the panel's length.

Additionally, in riveted connections this assumption is very close to reality, while some commercial software are capable of taking this effect into account.

9.2.1.4 Full laced member with the use of shell elements

Modelling the full laced member with all its structural components as shell elements is the most accurate type of modelling as it accounts for the finite dimensions and rigidity of the connections and for local plate buckling. Nevertheless, it requires extensive computational effort, especially for modelling large scale structures. Connecting shell elements between each other, applying boundary conditions and applying external loads demand very careful modelling in order to avoid undesirable local stress concentrations that may be far from real behaviour. Use of shell elements should be selected only if local behaviour, not sufficiently captured by beam elements, is expected to play a significant role.

9.2.2 Types of analysis

There are many possible types of analysis that differ between each other in the assumptions they include, and therefore in the computational effort required. In this section many types of analysis are briefly presented, starting from the simpler one and ending with the most sophisticated and accurate one.

9.2.2.1 Linear analysis (LA)

Linear analysis is the most commonly used type of structural analysis and is based on 1st-order theory. Equilibrium is considered in the undeformed configuration. Material is assumed to be elastic. As a result the least computational effort is required. Deflections and internal forces are obtained and it may be an acceptable type of analysis in case of relatively stiff structures when the undeformed and deformed configurations do not differ significantly.

9.2.2.2 Linearised Buckling Analysis (LBA)

Linearised Buckling Analysis results in the evaluation of the elastic critical buckling loads of the structure and of the corresponding buckling mode shapes. The elastic critical buckling loads are an upper bound of the capacity. The main usefulness of LBA is that the buckling mode shapes can be used as initial imperfection patterns for the performance of nonlinear analyses.

9.2.2.3 Nonlinear analysis P- Δ

Nonlinear analysis P- Δ includes the global geometrical nonlinearity dealing with differential deflections between the ends of a sway member. These effects are very important in slender and flexible structures and this type of analysis is expected to be more conservative than LA. Equilibrium is based on the deformed configuration and deflections and internal forces are also obtained. No material nonlinearity is considered and for this reason the collapse load cannot be directly calculated.

9.2.2.4 Nonlinear analysis P- δ

Nonlinear analysis P- δ includes the local geometrical nonlinearity dealing with the deflections between the ends of a non-sway member. These effects are usually small but may play an important role in slender and flexible structures. Additionally, they are expected to be less important than P- Δ effects. Equilibrium is based on the deformed configuration and deflections and internal forces are also obtained. No material nonlinearity is considered and for this reason the direct evaluation of the collapse load is not possible.

9.2.2.5 Geometrically Nonlinear Analysis - Geometrically Nonlinear Imperfection Analysis

This type of analysis includes both P- Δ and P- δ effects, either with the use of initial imperfections or not. It should be used in cases that structures are slender and flexible, which means that the deformed configuration differs significantly from the undeformed one. As in the previously mentioned nonlinear analyses, GNA and GNIA result in the calculation of deflections and internal forces. The material is considered to be elastic and the collapse load cannot be directly calculated by this type of analysis.

9.2.2.6 Geometrically and Materially Nonlinear and Geometrically and Materially Nonlinear Imperfection Analyses

This type of analysis includes both geometrical and material nonlinearity either with the use of initial imperfections or not. The spread of plasticity in the structure is taken into account and this type of analysis results in a very accurate prediction of the response of the structure and of the collapse load. The computational effort required is much larger than the ones for the previously mentioned analysis methods.

9.2.2.7 Proposed analytical second-order approach including initial imperfections

This type of analysis includes P- Δ and P- δ effects including member's initial out-of-straightness. It is based on small deflection theory which can be used for the reliable calculation of deflections and internal forces in realistic structures in which excessive deformations are undesirable. The closed-form solutions provided in Chapter 7 are based on these assumptions.

9.2.3 Design checks

The capacity of structural components can be calculated with the use of an appropriate failure criterion. In modern code provisions, extensive guidance is given on the failure criteria and design checks that should be used by structural engineers. For laced built-up members, one of the following design checks can be applied.

9.2.3.1 Allowable Stress Design

The elastic calculation of the stresses based on internal forces obtained from the analysis can be used for checking the capacity of the structure. Stress check for steel can be based on the von Mises yield criterion incorporating in this way the effect of both normal and shear stresses:

$$\sigma_{vM} \leq f_y \quad (9-1)$$

where σ_{vM} is the von Mises stress and f_y the yield stress of the material. In laced columns mainly normal stresses appear along the chords simplifying the calculations. The use of stress checks for evaluating the ultimate strength of a laced member is expected to be conservative.

9.2.3.2 Interaction equation of Eurocode 3

The interaction equation of Eurocode 3 for buckling about the weak axis z-z can be used for checking the capacity of the critical panel of a laced member:

$$\frac{N}{\chi_z A_{ch} f_y} + k_{zz} \frac{M_z}{M_{z,pl,Rd}} \leq 1 \quad (9-2)$$

where N and M_z are the applied axial force and bending moment at the examined cross-section, χ_z the reduction coefficient for flexural buckling about the weak axis, k_{zz} the interaction factor as defined by

Method 2 of EC3 [9-3] and $M_{z,pl,Rd}$ is the plastic moment of resistance about the axis of bending (z-axis).

9.2.3.3 Proposed interaction equation

The interaction equation for laced built-up beam-columns with arbitrary supports proposed in Chapter 8 (Eqs. (8-1), (8-2) or (8-3) for different types of lacing) can be used for calculating the ultimate strength of a laced built-up column. Parametric studies, some of which are included in Chapter 8, showed that the proposed interaction equation results in a satisfactory estimation of the collapse load for any type of loading and boundary conditions.

9.3 EXISTING ANALYSIS AND DESIGN PROCEDURES FOR FRAMES

In the previous section possible methods for modelling, analysing and designing laced built-up members were presented but not all of them can be used and combined for obtaining sufficiently acceptable results for laced members. The combinations that can be used in practice are summarised in the present section. They are also to be used in the numerical studies of industrial frames that follow.

9.3.1 Linear elastic analysis and design of the full frame (C.S.1st)

Modelling: Euler-Bernoulli beam elements for modelling the full frame (presented in section 9.2.1.3)

Type of analysis: Linear elastic analysis (presented in section 9.2.2.1)

Design check: Interaction Eq. (9-2) (presented in section 9.2.3.2)

In this case, beam elements are used for the modelling of the full laced member with all its structural components. Linear elastic analysis of the laced member is employed with the use of commercial software for obtaining the internal forces and deflections. The elastic analysis is terminated with the use of either stress checks or the interaction Eq. (9-2) with the second one primarily used in practice. First-order elastic analysis and design with commercial software was also presented as C.S.1st in the parametric study of laced beam-columns with arbitrary supports in Chapter 8. This type of analysis and design is very commonly used in modern design practice as it can be easily performed by all structural commercial software. It is acceptable in cases of small deflections but unsafe in flexible and slender structures with highly nonlinear geometrically response.

9.3.2 Nonlinear elastic analysis and design of the full frame (C.S.2nd)

Modelling: Euler-Bernoulli beam elements for modelling the full frame (presented in section 9.2.1.3)

Type of analysis: Nonlinear elastic analysis (presented in section 9.2.2.5)

Design check: Interaction Eq. (9-2) (presented in section 9.2.3.2)

The only difference from linear elastic analysis and design of the full laced member is that it accounts for geometrical nonlinearity. Nonlinear elastic analysis and design with commercial software was also presented as C.S.2nd in the parametric study of laced beam-columns with arbitrary supports in Chapter 8. Some commercial software can perform this type of analysis accounting for geometrical nonlinearity. It should be used for both flexible and slender structures.

9.3.3 Geometrically and Materially Nonlinear Imperfection Analysis of the full frame (GMNIA)

Modelling: Euler-Bernoulli beam elements for modelling the full frame (presented in section 9.2.1.3)

Type of analysis: Nonlinear analysis with elastoplastic material (presented in section 9.2.2.6)

Design check: No additional design check is required as the collapse load is directly calculated by GMNIA.

As it was previously mentioned, this type of analysis is the most sophisticated one as it accounts for both types of nonlinearity and results in the calculation of both the deflections and collapse load. It incorporates plasticity criteria without requiring by the user the definition of any additional design checks. Spread of plasticity inside the structural components is taken into account leading to an accurate evaluation of both elastic and elastoplastic response. In case that arc-length method is used, the post-buckling response can also be identified. This type of analysis is not commonly used as only advanced finite element software can perform it. In addition, even with the use of them, the computational effort is relatively large. Nevertheless, it is expected that further progress of computer science will lead to an extensive use of GMNIA.

9.4 APPLICATION OF PROPOSED METHOD TO FRAMES

9.4.1 Analytical proposed method applied to frames

Modelling: Timoshenko members with equivalent characteristics (presented in section 9.2.1.2)

Type of analysis: Analytical closed-form solutions for 2nd-order elastic analysis (presented in section 9.2.2.7)

Design check: Proposed interaction equation (presented in section 9.2.3.3)

The proposed method (with alternatives A and B) can be applied to single imperfect laced beam-columns with arbitrary supports. Therefore it is clear that its application to an industrial frame, such as the one described in the introduction, should be based on appropriate and reasonable assumptions that transform the frame into a sufficiently approximate equivalent member in which the proposed methods can be used. In order to be conservative, this equivalent member should deal with the more compressed one of the two frame's columns, as it is the one that leads to overall failure.

Initially, the truss beam and the laced built-up columns are modelled as Timoshenko members with equivalent bending and shear rigidity (Figure 9-1). The calculation of the latter is based on Eurocode3 provisions [9-3]. The connections between the beam and the columns are considered to be nodal and rigid. In this way, the degrees of freedom of the model are significantly reduced.

Afterwards, the most unfavourable column (usually the more compressed one) is considered and the truss beam is replaced with an equivalent rotational spring based on either double curvature or single curvature deformation according to Chapter 6 accounting for shear deformations of the truss beam (Figure 9-1). Double curvature deformation (based on sway mode with anti-symmetrical deformation) is used in the cases of horizontal loads and initial global imperfection and the rotational spring at the top of the more compressed laced member is called $c_{t,d}$. Single curvature deformation (based on a non-sway mode with symmetrical deformation) is considered when the loads are symmetrically applied on the frame, as there is no horizontal perturbation for triggering a sway type of deformation. The rotational spring at the top of the more compressed laced member in this case is called $c_{t,s}$. When a uniformly distributed load is considered along the truss beam, apart from the rotational spring $c_{t,s}$ an equivalent load and moment should be also transferred to the tip of each laced built-up column. The equivalent load is equal to $gL_b/2$ while the equivalent moment is equal to $g(L_b)^2/12$ where g is the lateral distributed load along the beam and L_b is the length of the beam. It should be mentioned that the assumption of double curvature deformation for sway behaviour under lateral horizontal loading is conservative as it does not account for the fact that the less compressed column will provide lateral

support to the more compressed one and as a result the beam will not deform exactly in a double curvature configuration.

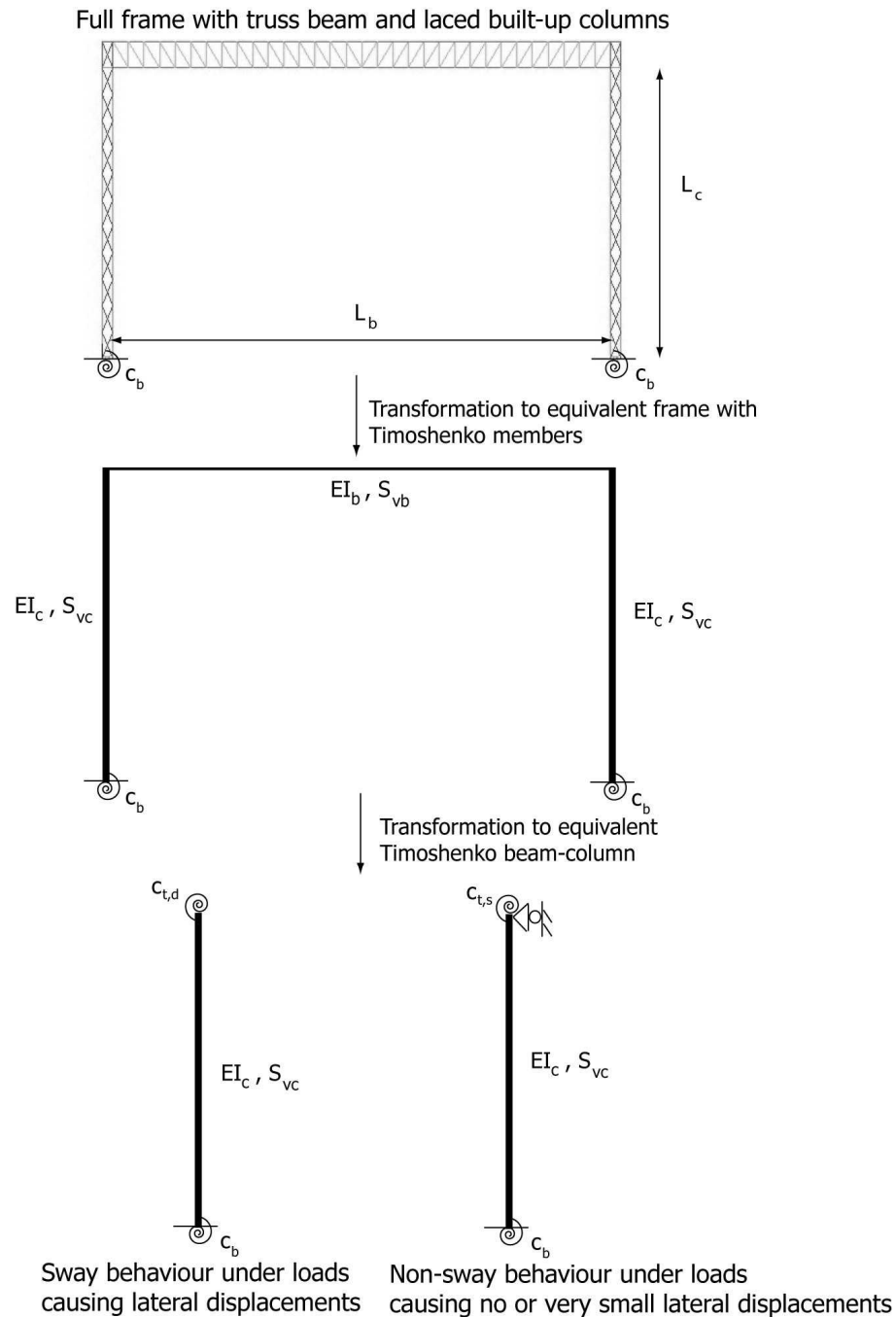


Figure 9-1: Gradual transformation of full frame to equivalent Timoshenko member

The axial force that is applied to the more compressed column is associated with half of the vertical loads (the other half is carried by the other column) and with the compressive force caused due to horizontal loads (a tensile force is caused to the other column). The most unfavourable column under this axial force is considered separately for each type of deformation. The first type of deformation considers a sway column (Figure 9-1) with rotational spring $c_{t,d}$ under loads that lead to sway deformation (horizontal loads and initial global imperfections). The second one considers a non-sway column (Figure 9-1) with rotational spring $c_{t,s}$ under loads that lead to non-sway deformation

(symmetrical vertical loads and loads causing symmetrical deformation). As the axial force is the same for the two types of deformation the principle of superposition is then applied in order to evaluate their combined effect on lateral deflections and internal forces.

The gradual transformation of a typical full frame with arbitrary rotational supports at the bottom that is free to move transversely at the top, into an equivalent Timoshenko beam-column depicted in Figure 9-1, highlights the significant simplification of the initial model. Finally, the most unfavourable laced built-up column is considered alone allowing for the use of the proposed methods presented in Chapters 6, 7 and 8. To be more specific, the work presented in Chapter 6 can be used for evaluating the rotational stiffness that the truss beam offers to the more compressed columns and for the calculation of the column's (and subsequently the frame's) elastic critical buckling load. The closed-form solutions in Chapter 7 can be used for analytically performing the 2nd-order elastic analysis of the column (and subsequently of the frame) in order to obtain lateral deflections and internal forces to be used for the design. Finally, the interaction equation described in Chapter 8 can be used for the calculation of the column's ultimate strength (and subsequently the full frame's capacity).

It should be noted that the application of the proposed method is approximate and may be inaccurate in some cases. Nevertheless, it is expected to be sufficient for practical industrial frames with laced members. Additionally, the proposed methods are applicable only to symmetrical and/or anti-symmetrical load patterns. It is clear that this way of applying external loads is an idealised confrontation of much more complex load distributions that usually take place in practice. Despite that fact, the purpose of this study is to provide engineers with a tool that can predict the behaviour of such frames in typical cases without the use of finite element software and/or can be used for checking results already obtained with analysis and design commercial software.

9.4.2 Equivalent Timoshenko frame with GNIA

Modelling: Timoshenko members with equivalent characteristics (presented in section 9.2.1.2)

Type of analysis: Nonlinear elastic analysis (presented in section 9.2.2.5)

Design check: Proposed interaction equation (presented in section 9.2.3.3)

In case that finite element software is available, the use of a frame consisting of equivalent Timoshenko members can be feasible. The performance of GNIA can result in the evaluation of deflections and internal forces along the laced members. The evaluated internal forces can then be used in the proposed interaction equation (Eqs. (8-1), (8-2) or (8-3) depending on the type of lacing and location of failure) for the evaluation of the ultimate strength of the laced member, and in consequence of the full frame.

9.5 NUMERICAL VERIFICATION IN FRAMES WITH UNIFORM LACED MEMBERS

In this section, the applicability of the existing design procedures (described in section 9.3) and of the proposed analytical method (described in section 9.4) for predicting the structural behaviour of frames with uniform in elevation laced beam-columns is investigated. In such frames, the laced members are continuous in elevation and a rigid connection between the beam and the columns is constructed. When crane bridges need to run along the structure, corbels (short cantilevers) at an intermediate point of the laced built-up columns' interior chord are used. Full cooperation between them is guaranteed by the rigid beam-column connection. It should be noted that failures of the truss beam or of the truss beam-laced column connection are excluded from the presented numerical verification, as the latter focuses on the behaviour and collapse of laced members only.

The comparison basis is associated with the use of finite element software ADINA [9-2] that is employed for the performance of LBA and GMNIA on the full frame. Two-noded Hermitian beam elements are used for all structural components. Bending moment end releases are used for the lacing bars' ends. LB Analyses are used for the numerical calculation of elastic critical buckling loads and for obtaining the global and local buckling mode shapes that will be used as initial global and local imperfection patterns, respectively. GMNI Analyses are used for the numerical evaluation of the frames' ultimate strength and deflections.

The investigated procedures are summarised as:

- Commercial Software linear analysis (C.S.1st): Application of the linear analysis with commercial software, as presented in section 9.3.1. The full frame is modelled and interaction equation (9-2) is used. The results appear in both tables and equilibrium paths.
- Commercial Software nonlinear analysis (C.S.2nd): Application of the geometrically nonlinear analysis with commercial software, as presented in section 9.3.2. The full frame is modelled and interaction equation (9-2) is used. The results appear in both tables and equilibrium paths.
- Geometrically and Materially Nonlinear Imperfection Analysis (Numerical): GMNIA is used for obtaining the deflections and capacity of the frame, as presented in section 9.3.3. It is considered to be the comparison standard and the results are presented in both tables and equilibrium paths.
- Proposed-A (Pr.-A): Application of the Proposed-A method, as presented section 9.4.1. The results appear only in the tables as the elastic analysis coincides with Proposed-B method.
- Proposed-B (Pr.-B): Application of the Proposed-B method, as presented in section 9.4.1. The results appear in both tables and equilibrium paths.
- GNIA Timoshenko frame: Based on deflections and internal forces obtained from the geometrically nonlinear analysis of an equivalent Timoshenko frame modelled with finite element software, as presented in section 9.4.2. Application of the interaction equation (8-1), (8-2) or (8-3) depending on the lacing type leads to calculation of the collapse load. The results appear only in the equilibrium paths.

9.5.1 Load cases

Three different load cases are considered that are idealised load patterns of the ones used by engineers of practice. All of them are either symmetrical or anti-symmetrical load patterns, being consistent with the basic assumption of the application of the proposed analytical method to frames. They include both vertical and horizontal loads and are categorised in three cases. Load case-A consists mainly of vertical loads, Load case-B of vertical and horizontal loads that could be attributed to seismic actions, while Load case-C is associated with vertical loads and horizontal loads that could be related to wind actions.

9.5.1.1 Load case-A

Load case-A consists of vertical loads and initial imperfections. The vertical loads include uniformly distributed load $g=30\text{kN/m}$ along the beam due to dead and snow loads and concentrated loads $P=500\text{kN}$ due to crane bridge applied directly on the interior chord of the laced columns as shown in Figure 9-2 obtained from finite element software ADINA. The equivalent Timoshenko frame is depicted in Figure 9-3 and due to the eccentricity of load P , a concentrated moment M at the top of each column appears. Global imperfections $w_0=L_d/500$ based on the first global buckling mode shape (sway mode) and local imperfections z_0 based on the local buckling mode shape (depending on the laced built-up member used) are also considered. The distributed load g and concentrated moments M

cause a non-sway single curvature deformation, while the initial global imperfections w_0 result in a sway double curvature deformation. The total axial force applied to the more compressed laced member includes one half of the vertical loads.

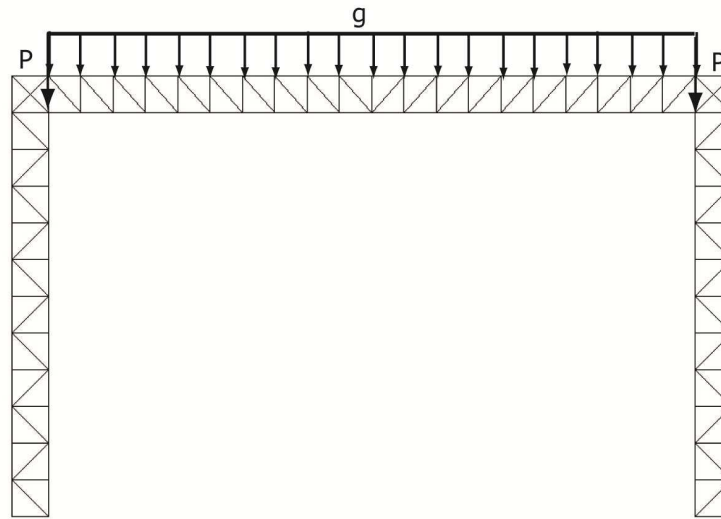


Figure 9-2: Load case-A applied to full frame with laced members

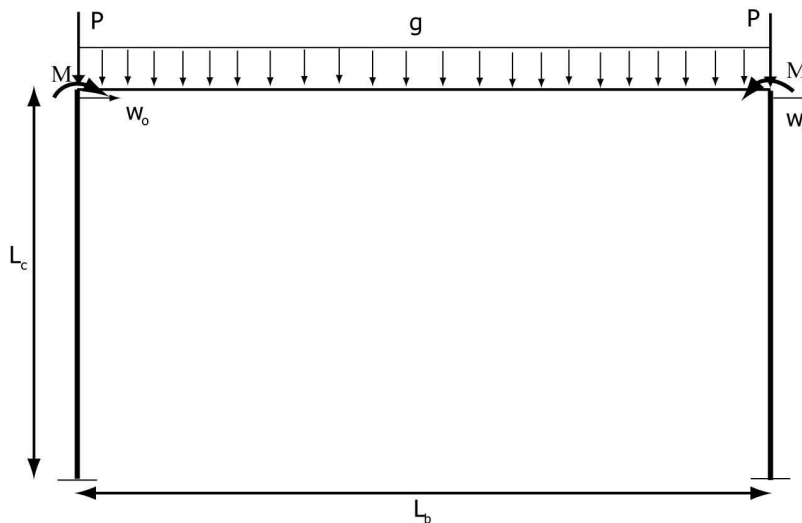


Figure 9-3: Load case-A applied to equivalent Timoshenko frame

9.5.1.2 Load case-B

Load case-B consists of vertical loads, horizontal loads and initial imperfections. The vertical loads include uniformly distributed load $g=12\text{kN/m}$ along the beam due to dead and snow loads and concentrated loads $P=500\text{kN}$ due to crane bridge applied directly on the interior chord of the laced columns as shown in Figure 9-4 obtained from finite element software ADINA. The horizontal loads include the seismic loading $H=450\text{kN}$ applied at the tops of the built-up columns considering that the seismic mass of the structure is concentrated on the roof (Figure 9-4). The equivalent Timoshenko frame is depicted in Figure 9-5 and due to the eccentricity of load P , a concentrated moment M at the top of each column appears. The initial imperfections include global imperfection $w_0=L_c/500$ based on the first global buckling mode shape (sway mode) and local imperfection z_0 based on the local buckling mode shape (depending on the laced built-up member used). The distributed load g and

concentrated moments M cause a non-sway single curvature deformation while the initial global imperfection w_0 and horizontal loads H result in a sway double curvature deformation. The total axial force applied to the more compressed laced member includes one half of the vertical loads and the vertical reaction caused by the appearance of the horizontal load $2H$ on the roof. Conservatively, the vertical reaction due to horizontal load $2H$ is taken equal to:

$$V_H = \frac{2HL_c}{L_b} \quad (9-3)$$

where all parameters have been previously defined. This value corresponds to the vertical reactions of a single-story frame with hinged bases under total lateral load $2H$ at the top of the columns. For base supports with rotational stiffness other than zero this value is conservative and for this reason it will be used for any type of base boundary conditions.

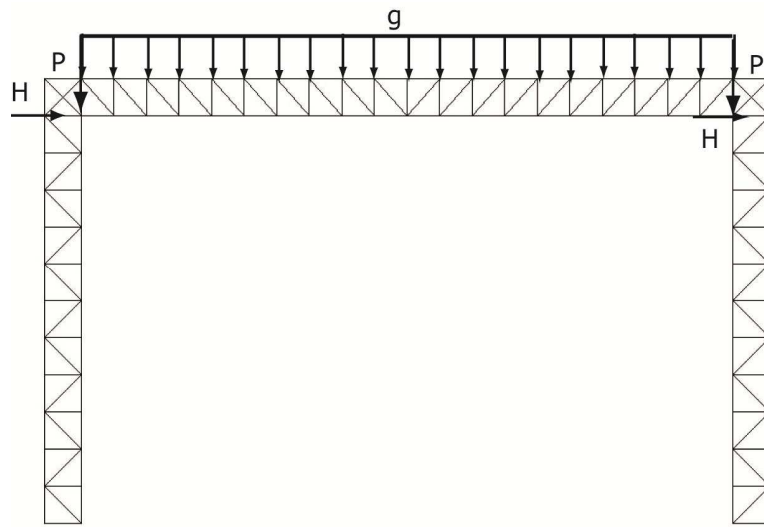


Figure 9-4: Load case-B applied to full frame with laced members

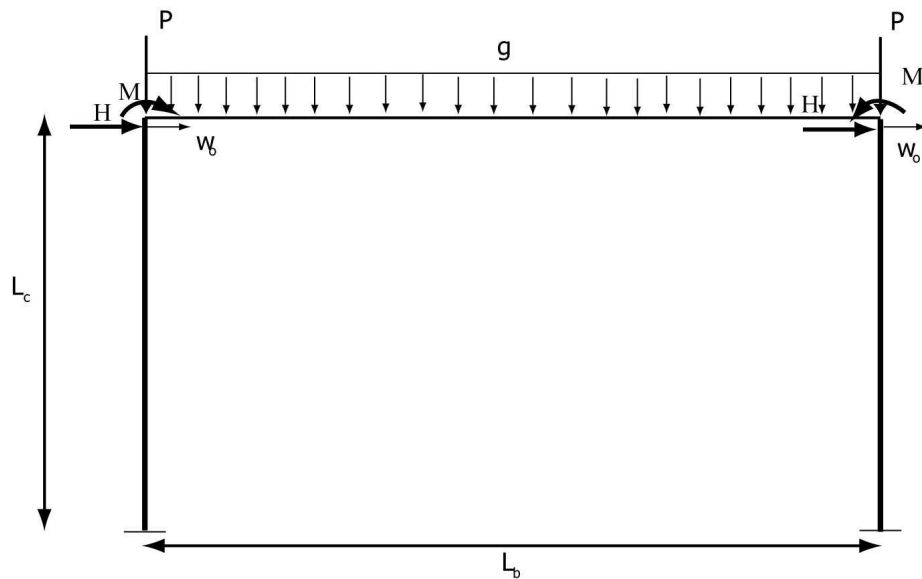


Figure 9-5: Load case-B applied to equivalent Timoshenko frame

9.5.1.3 Load case-C

Load case-C consists of vertical loads, horizontal loads and initial imperfections. The vertical loads include uniformly distributed load $g=25\text{kN/m}$ along the beam due to dead and snow loads and concentrated loads $P=500\text{kN}$ due to crane bridge applied directly on the interior chord of the laced columns, as shown in Figure 9-6 obtained from finite element software ADINA. The horizontal loads consist of the wind loading $q=12\text{kN/m}$ applied along the exterior chords of the built-up columns, by assuming that exterior cladding is attached to the exterior chords of the industrial structure (Figure 9-6). The equivalent Timoshenko frame is depicted in Figure 9-7 and due to the eccentricity of load P , a concentrated moment M at the top of each column appears. The initial imperfections include global imperfection $w_0=L_c/500$ based on the first global buckling mode shape (sway mode) and local imperfection z_0 based on the local buckling mode shape (depending on the laced built-up member used). The distributed load g and concentrated moments M cause a non-sway single curvature deformation while the initial global imperfection w_0 and horizontal loads q result in a sway double curvature deformation. The total axial force applied to the more compressed laced member includes one half of the vertical loads and the vertical reaction caused by the horizontal load $2q$. Conservatively, the vertical reaction due to horizontal load $2q$ is taken equal to:

$$V_H = q \frac{L_c^2}{L_b} \quad (9-4)$$

where all parameters have been previously defined. This value corresponds to the vertical reactions of a single-story frame with hinged bases under total lateral load $2q$ along the columns. For base supports with rotational stiffness other than zero this value is conservative and for this reason it will be used for any type of base boundary conditions.

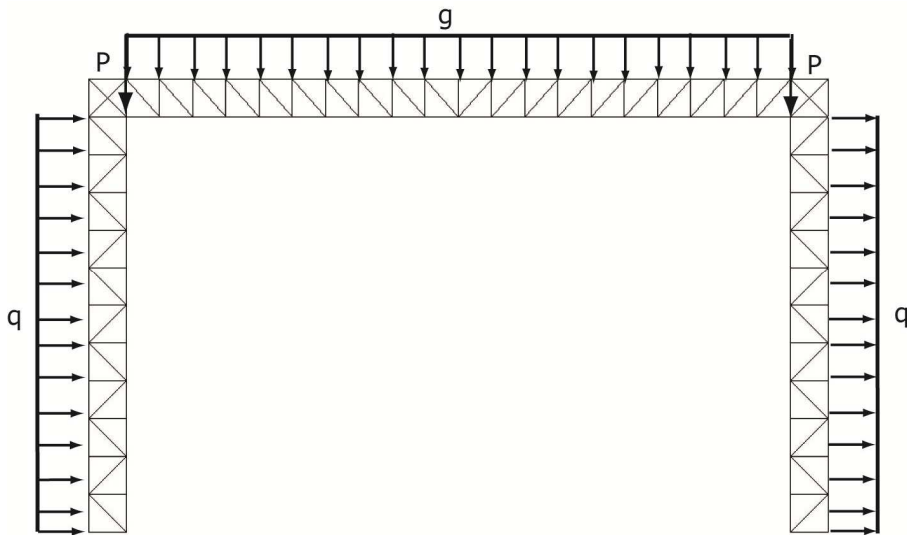


Figure 9-6: Load case-C applied to full frame with laced members

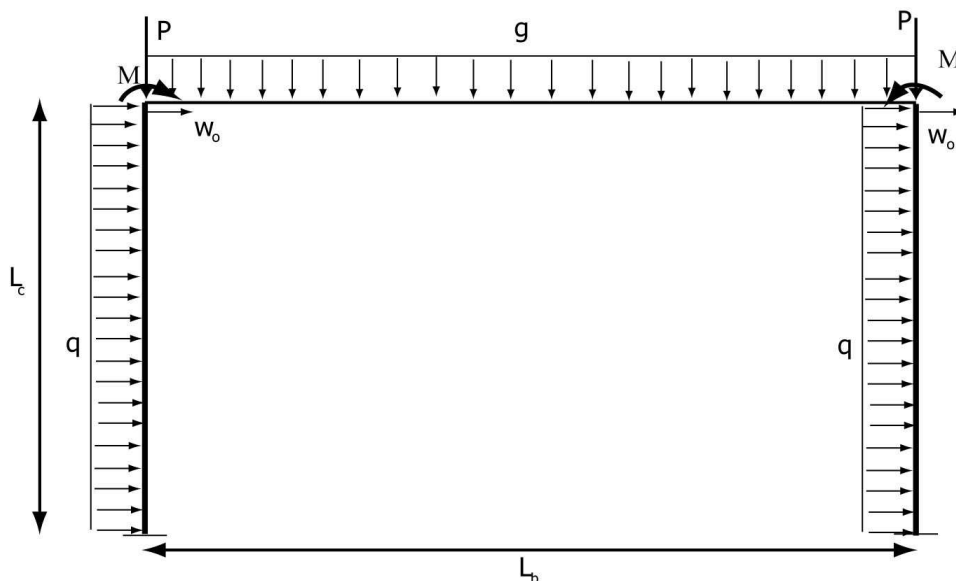


Figure 9-7: Load case-C applied to equivalent Timoshenko frame

9.5.2 Examples

In the following examples realistic single-story industrial frames are investigated from a structural point of view. The design loads presented in the previous section are applied and the load factor is calculated with the methods previously described. The numerical method GMNIA will be considered as the comparison basis as it is based on the use of the most sophisticated modelling, analysis and checking procedures. The equilibrium paths provide an overall view of the stiffness and collapse load that each method predicts. In the tables the load factor of each method and the maximum deflection Δ_{\max} for Load Case-B and Load Case-C at a numerical load level (load equal to the collapse load obtained numerically for comparison reasons) is given. For the case that the load factor is equal to unity, the design loads lead to marginal collapse of the frame. For the case that the load factor is larger than 1, the structure is safe for the specific design loads while the opposite happens for load factor less than 1. Unsafe predictions of the results are identified in the tables with the use of red colour. Except for the graphs, in the text the term load factor is used for the collapse load factor (maximum load factor along an equilibrium path).

I-sections are used for the chords of the laced built-up columns. Their numerical modelling capturing elastoplastic behaviour is accomplished with the use of moment-curvature relationships about the weak axis of bending z - z for different levels of axial force as described in Chapter 8 ([9-4], [9-5] and [9-6]). The steel grade considered for the material properties is S355 without strain hardening and with 21000 kN/cm^2 elastic modulus.

9.5.2.1 Example 1

The first example's geometrical characteristics for both laced built-up columns and truss beam are summarised in Table 9-1. Additionally, the equivalent bending and shear rigidities for the structural components are also presented. Both hinged and fixed supports are examined for the load cases described previously. The frame's global and local buckling mode shapes as obtained with LBA are shown in Figure 9-8 and Figure 9-9, respectively. It should be noted that the local buckling mode shape shown deals with buckling of the internal chords while at the same load level the external chords buckle, too. The local buckling mode shape of the external chords is not given, as it is similar to the internal chords' local buckling mode shape.

Table 9-1: Geometrical characteristics and equivalent bending and shear rigidities of Example 1

Member	L (m)	h_o (cm)	a (cm)	Chord cross-section	A_d (cm ²)	I_{eff} (cm ⁴)	S_v (kN)
Columns	23.8	170	170	HEB450	65.3	3150100	484805
Truss	43.0	300	295	HEA400	100	7155000	549407

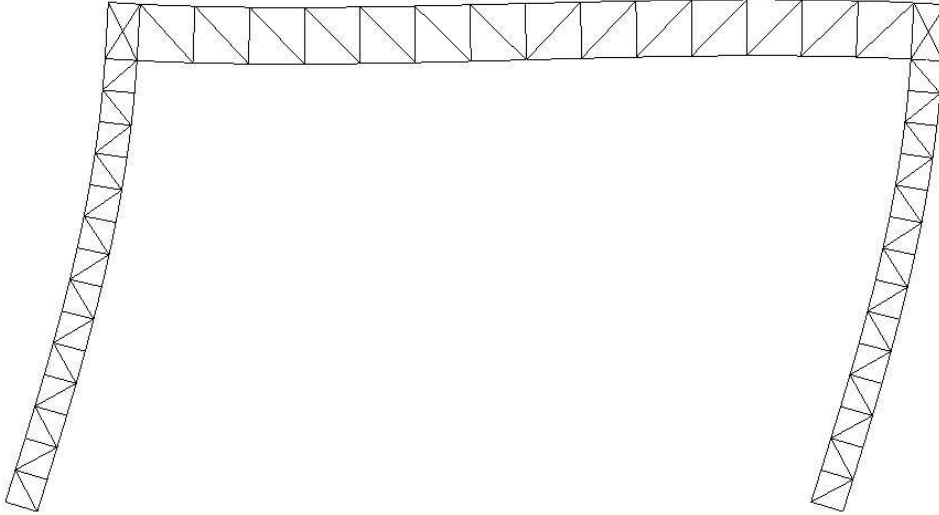


Figure 9-8: Global buckling mode shape of frame of Example 1 with hinged supports

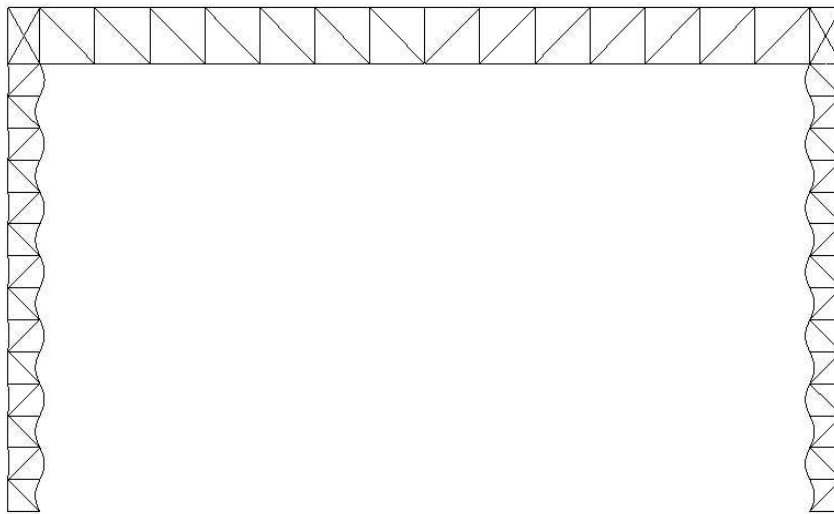


Figure 9-9: Local buckling mode shape of frame of Example 1 with hinged supports

The rotational stiffness that can be used to replace the truss beam corresponding to the non-sway mode is approximately equal to 700000kNm (single curvature beam deformation), while for the sway mode it is approximately equal to 1780000kNm (double curvature beam deformation). The local capacity of the simply-supported critical panel is equal to 7451kN and 7515kN for the case of 1st yield failure and of accounting for plastic reserve, respectively.

The equilibrium paths obtained with each procedure for Load Case-B are presented in Figure 9-10. The use of GNIA in Timoshenko frame leads to the most sufficient prediction of the collapse load. Proposed-B method is also very close to GMNIA results and always on the safe side. The use of C.S.2nd results in an accurate prediction of the stiffness and in a conservative evaluation of the collapse load. C.S.1st leads to an unsafe prediction of deflections but to a conservative calculation of the ultimate strength of the frame.

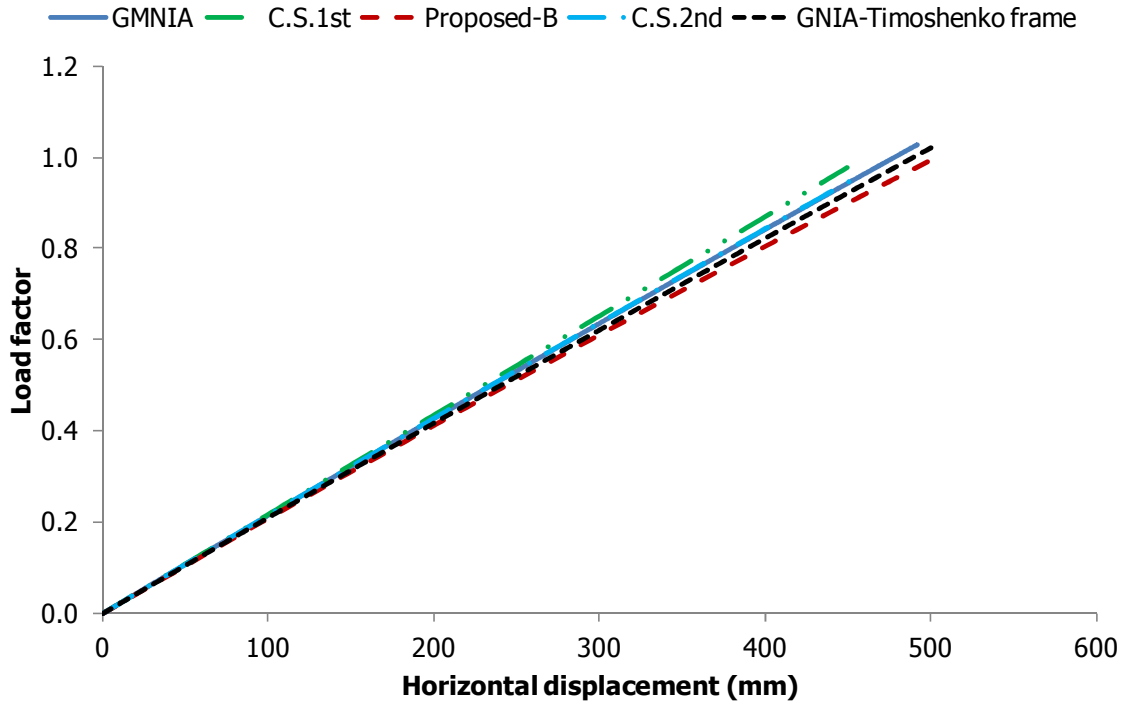


Figure 9-10: Equilibrium paths for Example 1 with hinged supports under Load Case-B

The equilibrium paths obtained for Load Case-C are presented in Figure 9-11. The Proposed-B method predicts sufficiently the behaviour and collapse of the frame being very close to GMNIA and GNIA with equivalent Timoshenko frame. C.S.2nd predicts satisfactorily the stiffness of the frame but is more conservative as far as the collapse load is concerned. Finally, C.S.1st is unconservative in the calculation of the lateral deflections.

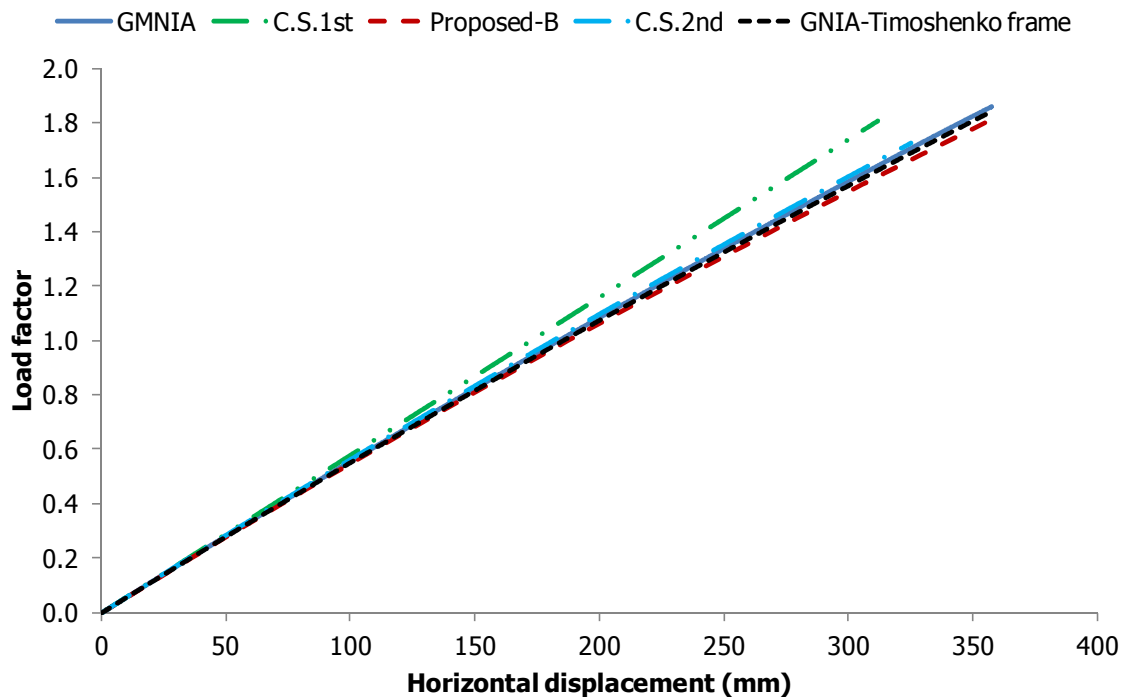


Figure 9-11: Equilibrium paths for Example 1 with hinged supports under Load Case-C

The results for the frame of Example 1 with hinged supports are given in Table 9-2. A very good comparison between the numerical results and the proposed methods is achieved for the load factors and maximum deflections. GNA using commercial software (C.S. 2nd) gives satisfactory results but less accurate than the ones obtained with the proposed methods. The use of linear analysis without including geometrical nonlinearity leads to less accurate results, especially as far as the deflections are concerned.

Table 9-2: Summary of results for Example 1 frame with hinged supports

	Method					Absolute Error (%)			
	GMNIA	C.S. 2 nd	C.S. 1 st	Pr.-B	Pr.-A	C.S. 2 nd	C.S. 1 st	Pr.-B	Pr.-A
Global buckling load (kN)	21230	-	-	20720		-	-	2.40	
Local buckling load (kN)	169957	-	-	168104		-	-	1.09	
Squash load (kN)	15478	-	-	15478		-	-	0.00	
L.F. Load Case -A	3.654	3.424	3.424	3.645	3.615	6.29	6.29	0.25	1.07
L.F. Load Case -B	1.027	0.952	0.975	0.998	0.990	7.30	5.06	2.82	3.60
L.F. Load Case -C	1.860	1.732	1.812	1.830	1.815	6.88	2.58	1.61	2.42
Δ_{\max} Load Case-C (mm)	357.9	352.7	320.6	367.9		1.45	10.42	2.79	
Δ_{\max} Load Case-B (mm)	491.5	489.8	472.1	518.5		0.35	3.95	5.49	

The axial force diagram for Load Case-B as obtained with GMNIA is depicted in Figure 9-12. The critical panel is the top one in the right column. At the base, the axial forces are very small as the hinged supports do not restrict rotation and no bending moments appear. It is also interesting to note that for the specific load case, the main deformation of the truss beam is related to double curvature. This can be understood if one observes the axial force distribution in the truss beam's chords. They are large at the ends and approach zero at the middle (double curvature deformation).

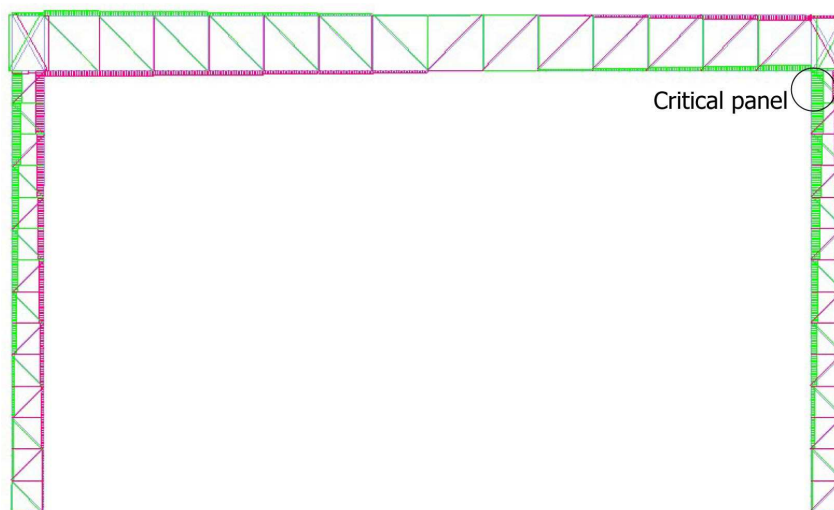


Figure 9-12: Axial force diagram of frame of Example 1 with hinged supports under Load Case-B (green colour corresponds to compression)

The bending moment diagram only along the chords of the laced built-up members with hinged supports is depicted in Figure 9-13. It can be seen that an approximately trapezoidal bending moment distribution appears along the critical panel at the top of the right column. The corresponding bending moment diagram at collapse is shown in Figure 9-14 at which the critical panel's bending moment distribution has a parabolic shape and a smaller maximum value. It can therefore be seen that the bending moment distribution changed along the critical panel and to be more specific reduced

allowing for an increase of its internal axial force. This phenomenon is more obvious in relatively stocky panels in which initial local imperfections do not play an important role and bending moments appear mainly due to continuity of the chords.

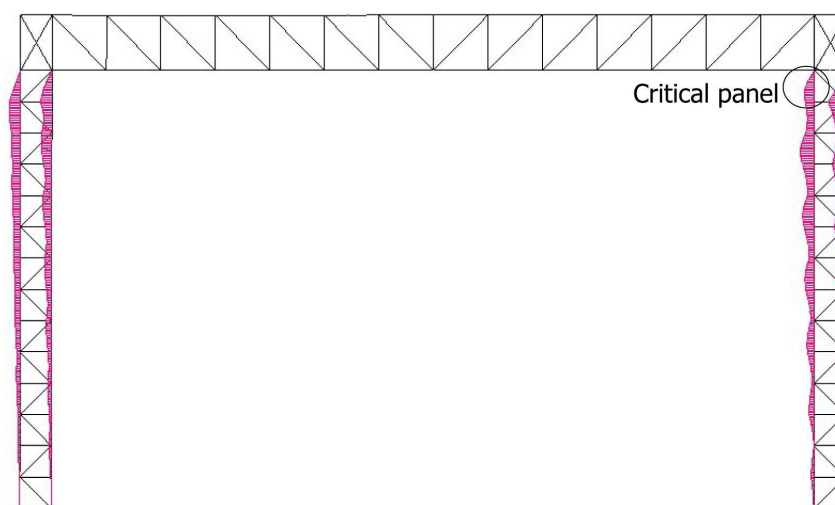


Figure 9-13: Bending moment diagram of laced members' chords of Example 1 with hinged supports under Load Case-B at an elastic state before collapse

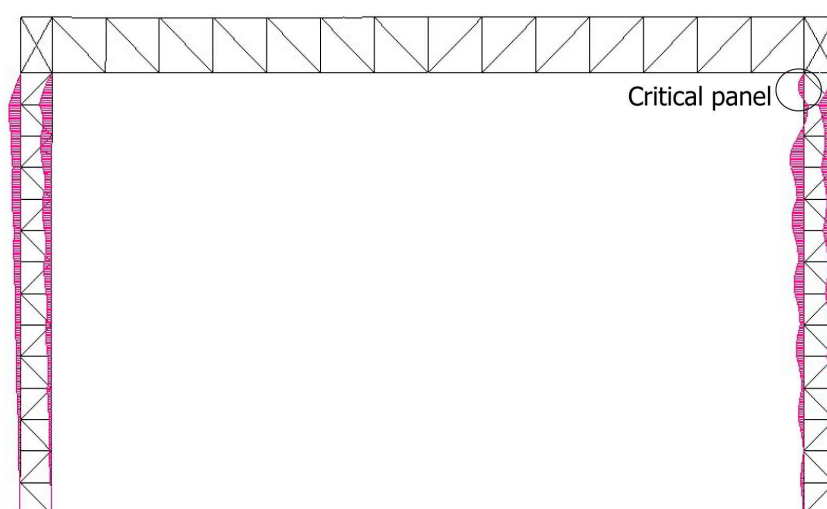


Figure 9-14: Bending moment diagram of laced members' chords of Example 1 with hinged supports under Load Case-B at collapse

The global buckling mode shape of the frame of Example 1 with fixed supports is provided in Figure 9-15 while the results are given in Table 9-3. It should be noted that the rotational springs for the substitution of the truss beam in the case of single and double curvature deformation are the same as the ones presented for the hinged supports. The local buckling mode shape is exactly the same as the one presented for the hinged supports as the boundary conditions at the base affect only the global response and not the local one.

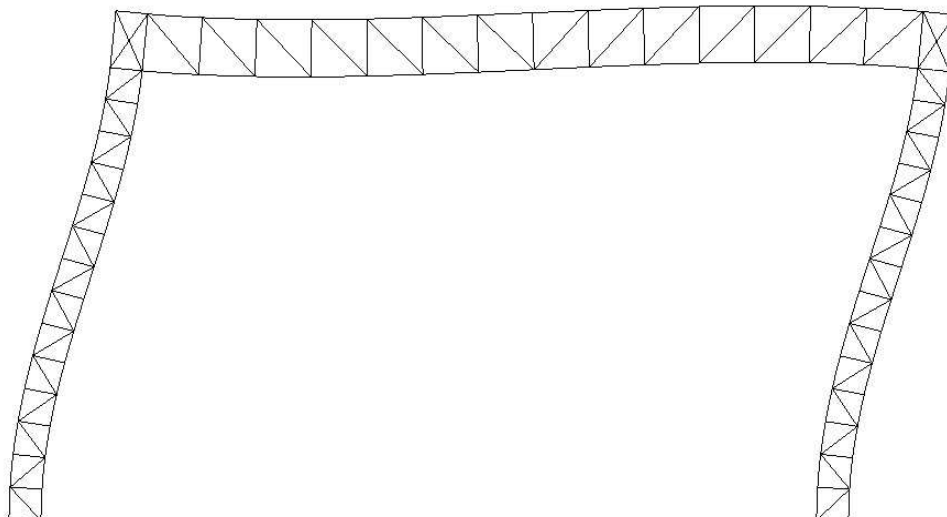


Figure 9-15: Global buckling mode shape of frame of Example 1 with fixed supports

The equilibrium paths obtained with each procedure for Load Case-B are presented in Figure 9-16. All procedures predict in a satisfactory way the stiffness of the frame, while the use of GNIA in Timoshenko frame leads to the most sufficient prediction of the collapse load. Proposed-B method is also very close to GMNIA results and always on the safe side. The use of C.S.1st is more efficient than in the case of hinged base supports for Load Case-B, as fixed supports lead to a significant reduction of the lateral deflections' magnitude, allowing in this way for the use of linear analysis.

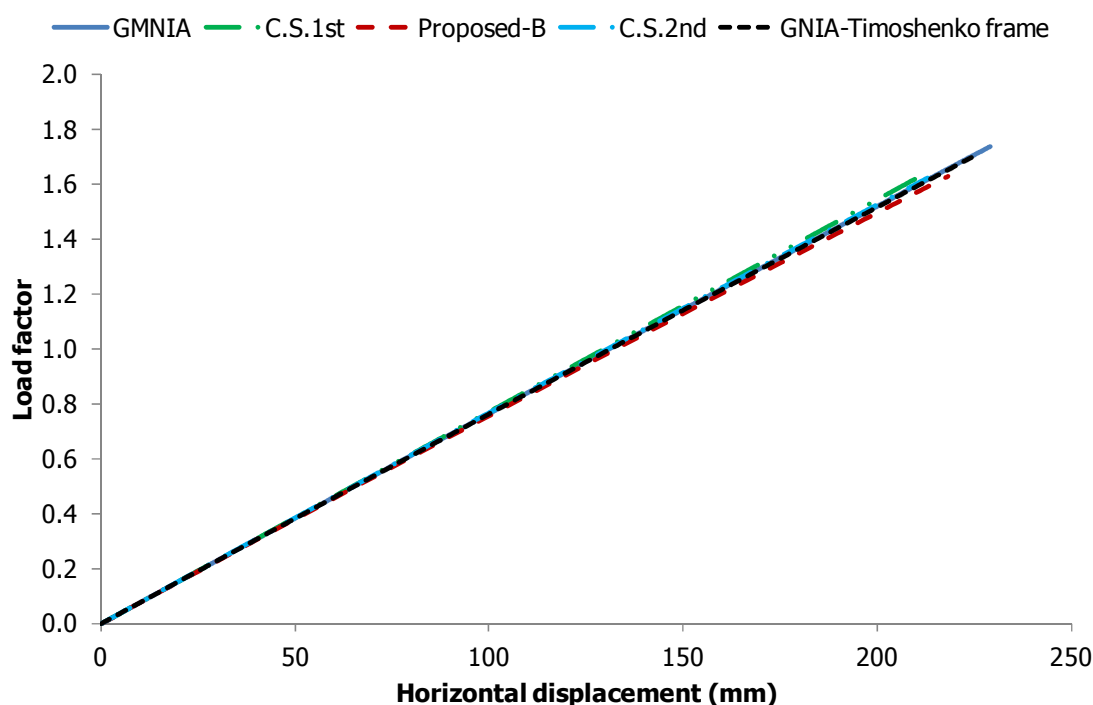


Figure 9-16: Equilibrium paths for Example 1 with fixed supports under Load Case-B

The equilibrium paths obtained for Load Case-C are presented in Figure 9-17. All procedures result in a slightly unconservative prediction of the overall stiffness but in a safe calculation of the ultimate strength. The larger stiffness predicted by the proposed procedure and GNIA with frame consisting of equivalent Timoshenko members is attributed to the fact that the beam-column connection is considered to be nodal while in reality it has finite dimensions. Therefore, even under only vertical

loads, the rotation of the laced member at its top results in small transverse displacements at the location that the horizontal displacement is measured. This difference is expected to become more prominent in the case of fixed supports that the deflections are rather small and in the case that the dimensions of the beam-column connection are large.

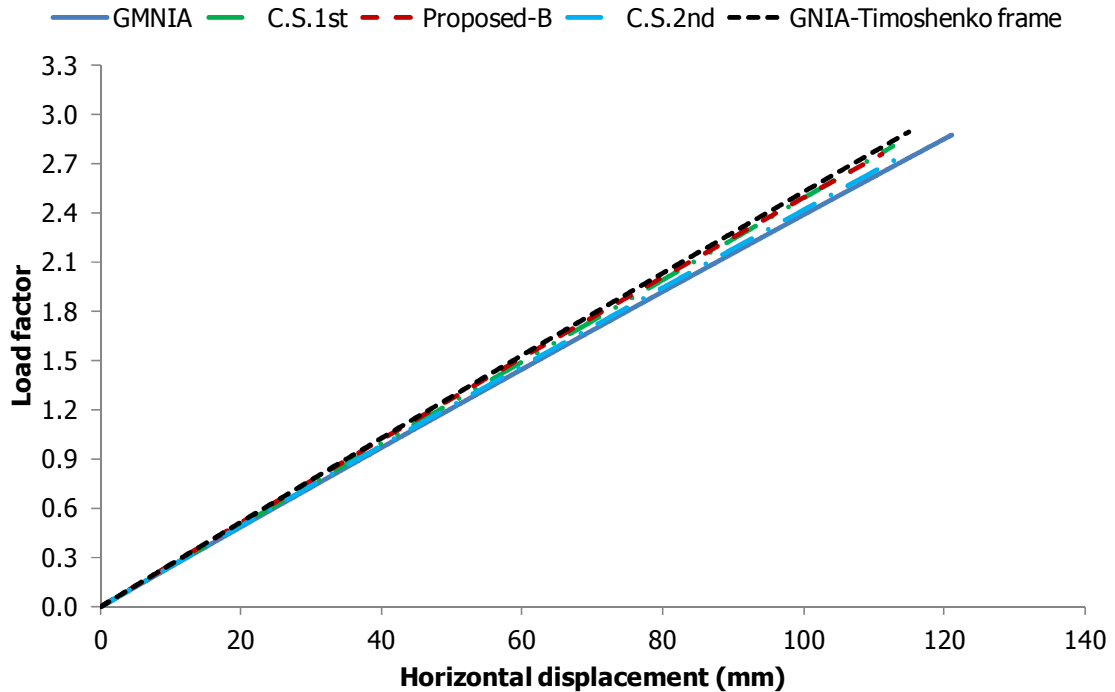


Figure 9-17: Equilibrium paths for Example 1 with fixed supports under Load Case-C

A satisfactory comparison between the numerical results and the proposed methods is achieved for the load factors and maximum deflections in this case, too, as presented in Table 9-3. The fixed supports lead to an increase of the strength and reduction of horizontal deflections in the case that significant lateral loads exist. The accuracy of the GNA with commercial software is also satisfactory but always less than the one found for the proposed procedures. The use of linear analysis with commercial software is also acceptable as the overall deflections are small and geometrical nonlinearity plays a smaller role in this case when compared with the one associated with hinged supports.

Table 9-3: Summary of results for Example 1 frame with fixed supports

	Method					Absolute error (%)			
	GMNIA	C.S. 2 nd	C.S. 1 st	Pr.-B	Pr.-A	C.S. 2 nd	C.S. 1 st	Pr.-B	Pr.-A
Global buckling load (kN)	74790	-	-	74145kN		-	-	0.86	
Local buckling load (kN)	170200	-	-	168104kN		-	-	1.23	
Squash load (kN)	15478	-	-	15478kN		-	-	0.00	
L.F. Load Case -A	3.612	3.344	3.344	3.560	3.525	7.42	7.42	1.44	2.41
L.F. Load Case -B	1.718	1.624	1.640	1.629	1.615	5.47	4.54	5.18	6.00
L.F. Load Case -C	2.869	2.766	2.814	2.760	2.670	3.59	1.92	3.80	6.94
Δ_{\max} Load Case-C (mm)	121.1	119.1	115.3	115.8		1.65	4.79	4.38	
Δ_{\max} Load Case-B (mm)	229.3	226.7	223.0	230.4		1.13	2.75	0.48	

The axial force diagram for Load Case-B as obtained with GMNIA is depicted in Figure 9-18. The critical panel is the bottom one in the right column. At the base, the axial forces are larger due to the restriction of rotation and appearance of bending moments. It is also interesting to note that for the specific load case, the main deformation of the truss beam is related to double curvature. This can be understood if one observes the axial force distribution in the truss beam's chords. They are large at the ends and approach zero at the middle (double curvature deformation).

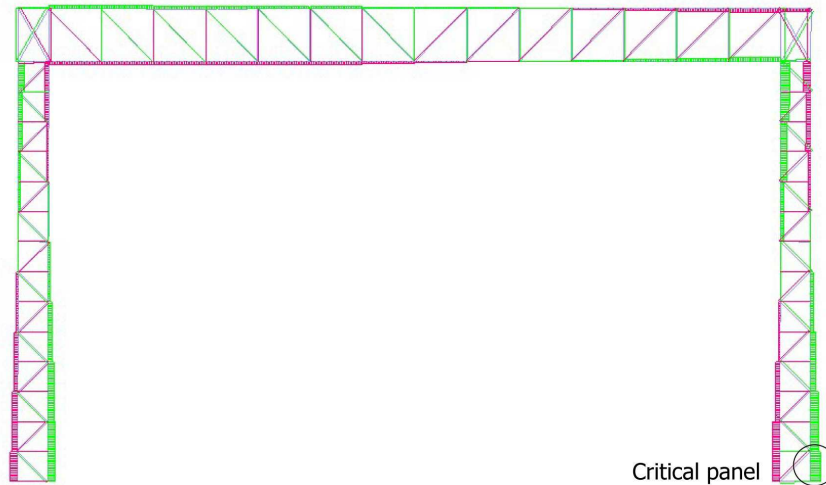


Figure 9-18: Axial force diagram of frame of Example 1 with fixed supports under Load Case-B (green colour corresponds to compression)

The bending moment diagram only along the chords of the laced built-up members with fixed supports is depicted in Figure 9-19. It can be seen that an approximately trapezoidal bending moment distribution appears along the critical panel at the bottom of the right column. The corresponding bending moment diagram at collapse is shown in Figure 9-20 at which the critical panel's bending moment distribution has a parabolic shape and a smaller maximum value. As for the hinged supports, the local bending moment maximum value reduced along the critical panel and allowed for an increase of its internal axial force.

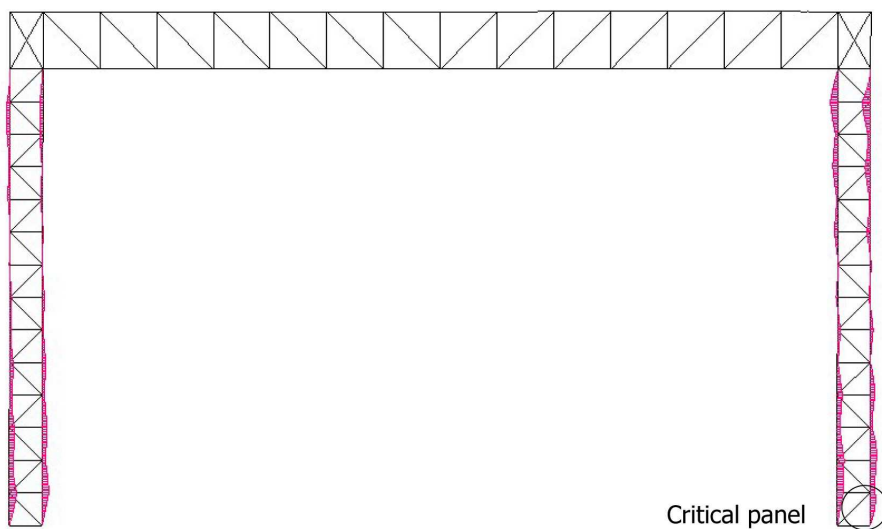


Figure 9-19: Bending moment diagram of laced members' chords of Example 1 with fixed supports under Load Case-B at an elastic state before collapse

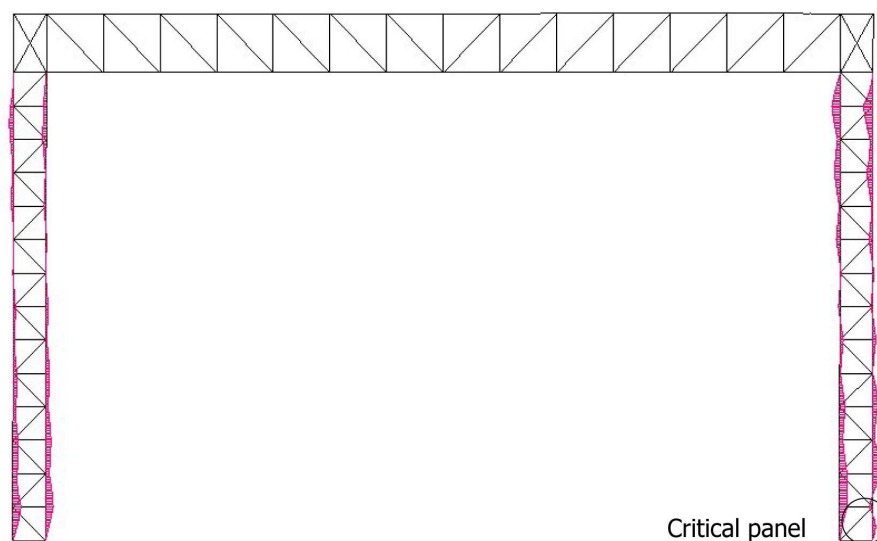


Figure 9-20: Bending moment diagram of laced members' chords of Example 1 with fixed supports under Load Case-B at collapse

9.5.2.2 Example 2

The second example deals with X-lacing laced built-up members and its geometrical characteristics for both laced built-up columns and truss beam are summarised in Table 9-4. Additionally, the equivalent bending and shear rigidities for the structural components are also presented. Both hinged and fixed supports are examined for the load cases described previously. The frame's global buckling mode shape as obtained with LBA for the hinged supports is shown in Figure 9-21. The local buckling mode shape and load are the same as the ones obtained with the use of LBA for Example 1, as no changes are made at a local level.

Table 9-4: Geometrical characteristics and equivalent bending and shear rigidities of Example 2

Member	L (m)	h_o (cm)	a (cm)	Chord cross-section	A_d (cm ²)	I_{eff} (cm ⁴)	S_v (kN)
Columns	18.7	70	170	HEB450	65.3	557540	367648
Truss	32.7	170	100	HEA400	100	2297550	482230

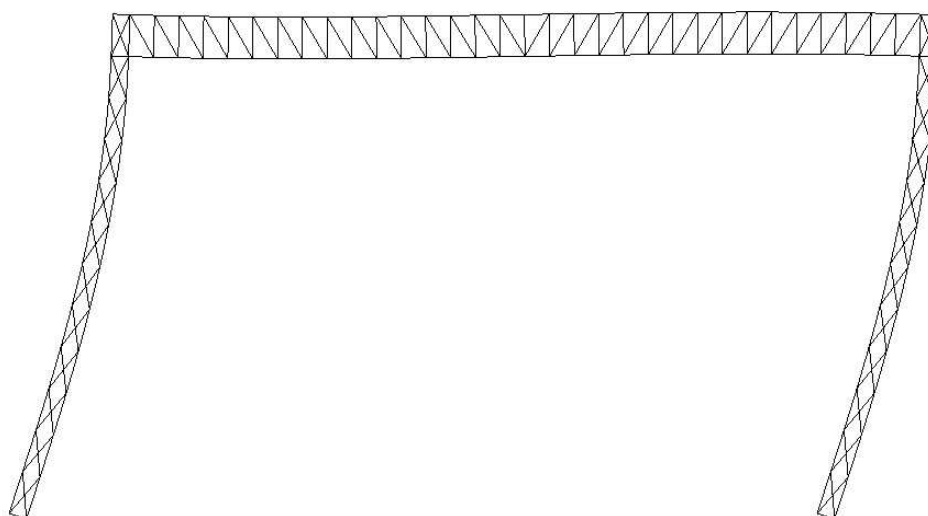


Figure 9-21: Global buckling mode shape of frame of Example 2 with hinged supports

The rotational stiffness that can be used to replace the truss beam corresponding to the non-sway mode is approximately equal to 295000kNm (single curvature beam deformation), while for the sway mode it is approximately equal to 796000kNm (double curvature beam deformation). The local capacity of the simply-supported critical panel is equal to 7451kN and 7515kN for the case of 1st yield failure and of accounting for plastic reserve, respectively.

The equilibrium paths obtained with each procedure for Load Case-B are presented in Figure 9-22. The use of GNIA in Timoshenko frame leads to the most sufficient prediction of the stiffness and collapse load. Proposed-B method is also very close to GMNIA results and always on the safe side. The use of C.S.2nd leads to a satisfactory and relatively safe calculation of the deflections and collapse load. C.S.1st results in a stiffer response but in a smaller collapse load when compared with GMNIA predictions. Therefore, it is highlighted that geometrical nonlinearity should be taken into account.

The equilibrium paths obtained for Load Case-C are presented in Figure 9-23. It can be seen that the GMNIA equilibrium path is more nonlinear when compared with the one presented in Figure 9-22, as the total axial force applied to the more compressed column is larger. Similar conclusions, as far as the deflections and collapse loads are concerned, are drawn for all cases except for C.S.1st. In this case, a much stiffer response is predicted and C.S.1st doesn't capture the nonlinearity of the equilibrium path that corresponds to GMNIA. Nevertheless, the collapse load is safely predicted by this method, too.

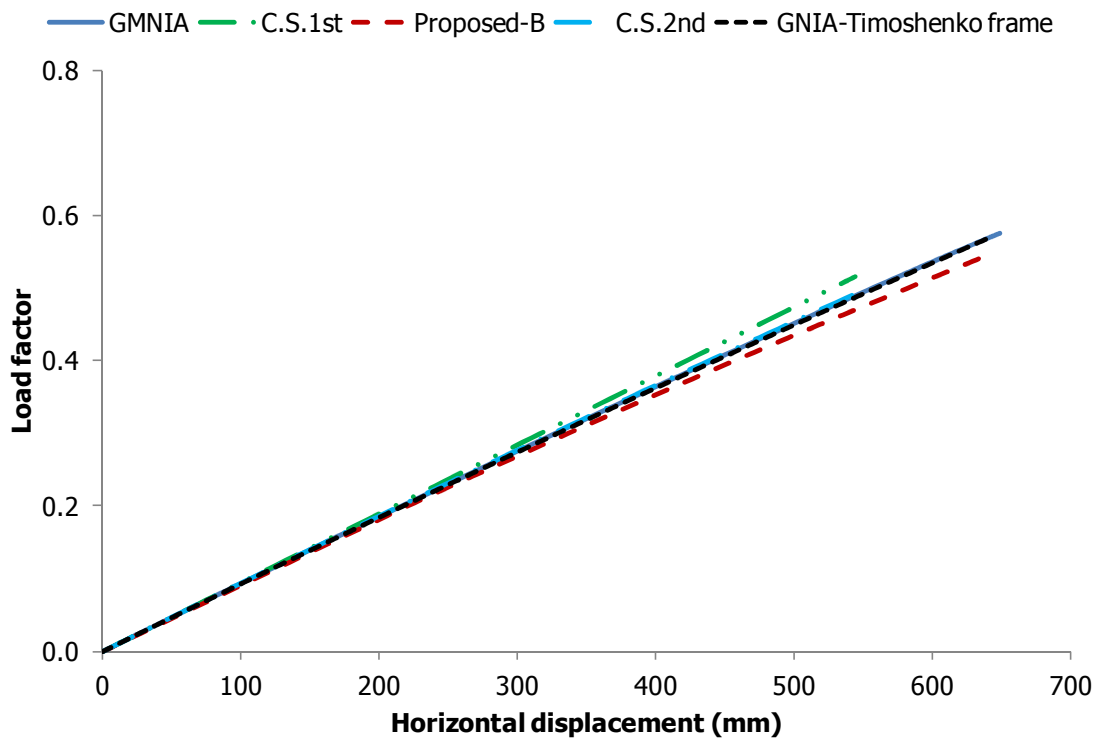


Figure 9-22: Equilibrium paths for Example 2 with hinged supports under Load Case-B

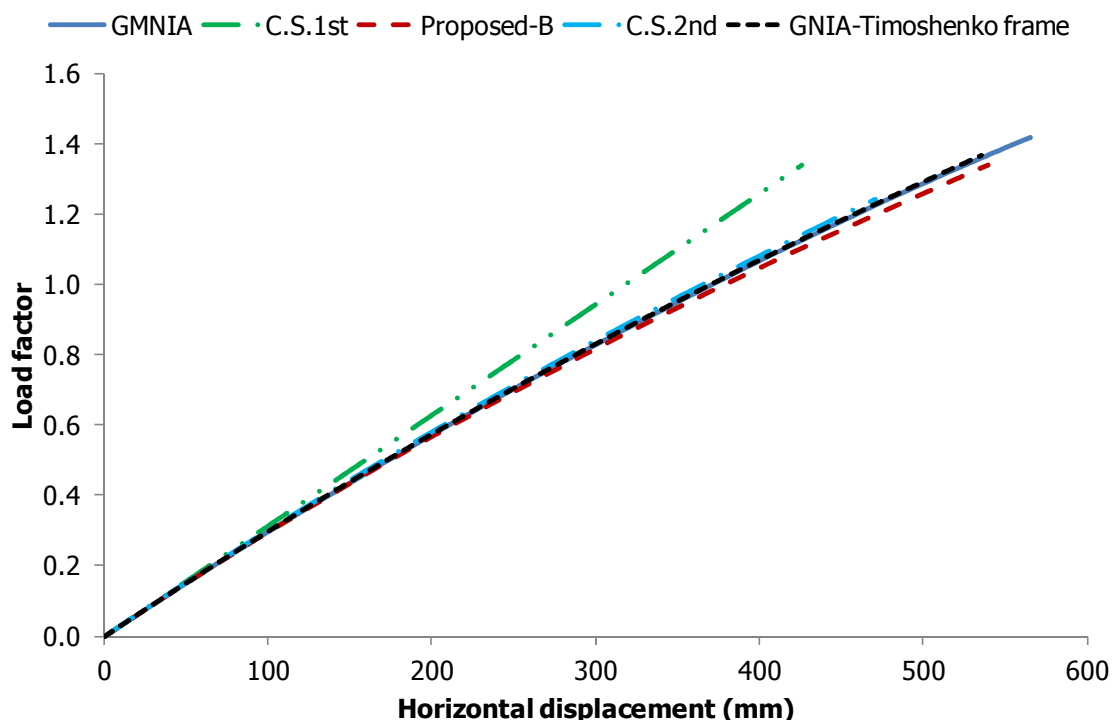


Figure 9-23: Equilibrium paths for Example 2 with hinged supports under Load Case-C

The results for the frame of Example 2 with hinged supports are given in Table 9-5. A very good comparison between the numerical results and the proposed methods is achieved for the load factors and maximum deflections. The use of GNA with commercial software gives satisfactory results but always less accurate than the ones obtained with the proposed methods. The use of linear elastic analysis results in satisfactory comparison of the load factors but not of the lateral deflections which it predicts unsafely.

Table 9-5: Summary of results for Example 2 frame with hinged supports

	Method					Absolute error (%)			
	GMNIA	C.S. 2 nd	C.S. 1 st	Pr.-B	Pr.-A	C.S. 2 nd	C.S. 1 st	Pr.-B	Pr.-A
Global buckling load (kN)	7058	-	-	6970		-	-	1.25	
Local buckling load (kN)	169957	-	-	168104		-	-	1.09	
Squash load (kN)	15478	-	-	15478		-	-	0.00	
L.F. Load Case -A	3.780	3.608	3.504	3.670	3.635	4.55	7.30	2.91	3.84
L.F. Load Case -B	0.577	0.500	0.516	0.542	0.537	13.34	10.57	6.06	6.93
L.F. Load Case -C	1.418	1.248	1.335	1.341	1.331	12.00	5.85	5.43	6.13
Δ_{\max} Load Case-C (mm)	565.5	553.5	451.6	578.8		2.12	20.14	2.35	
Δ_{\max} Load Case-B (mm)	649.5	645.6	609.3	681.9		0.60	6.19	4.99	

The deformed configuration of the frame of Example 2 with hinged connections under the application of Load Case-C is presented in Figure 9-24 magnified for better graphical representation. The truss beam's deformation is a superposition of the single curvature and double curvature deformations, something that is reflected in the axial force diagram shown in Figure 9-25, too.

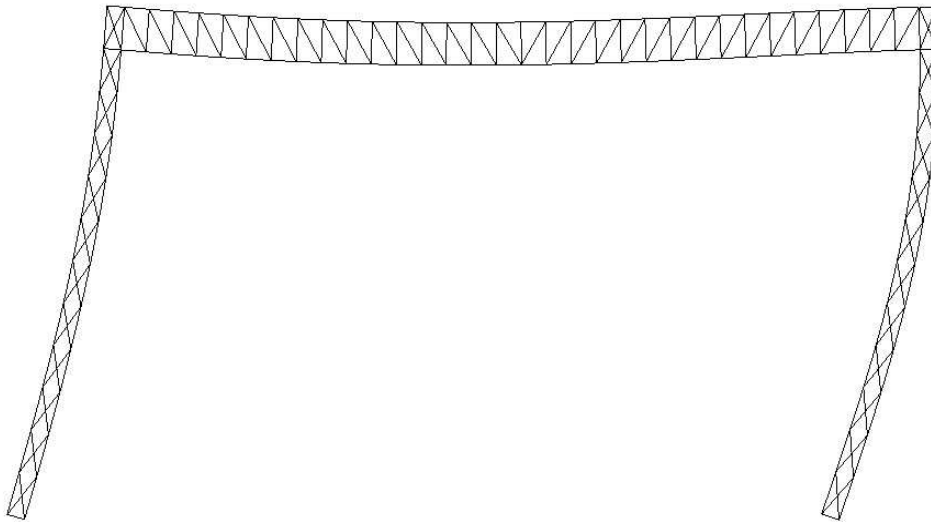


Figure 9-24: Deformed configuration of frame of Example 2 with hinged supports under the application of Load Case-C

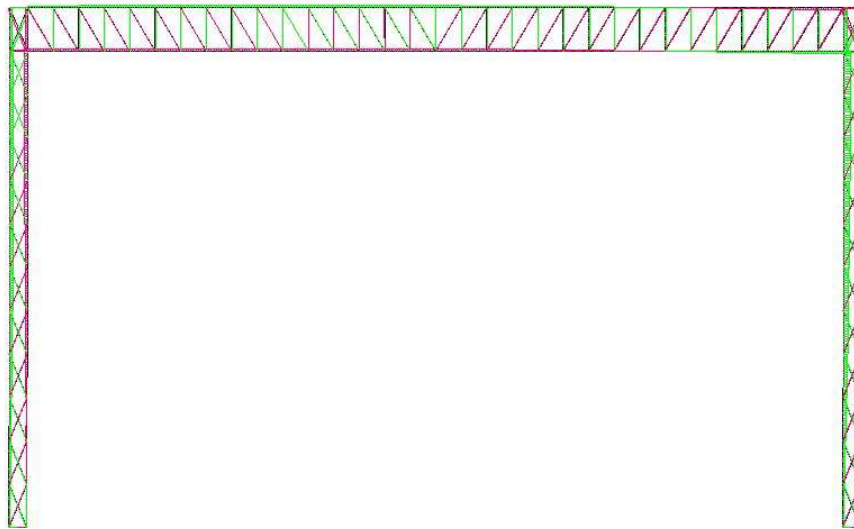


Figure 9-25: Axial force diagram of frame of Example 2 with hinged supports under Load Case-C (green colour corresponds to compression)

The global buckling mode shape of the frame of Example 2 with fixed supports is provided in Figure 9-26. The double curvature deformation of the truss beam in the global buckling mode is obvious. It should be noted that the rotational springs for the substitution of the truss beam in the case of single and double curvature deformation are the same as the ones presented for the hinged supports.

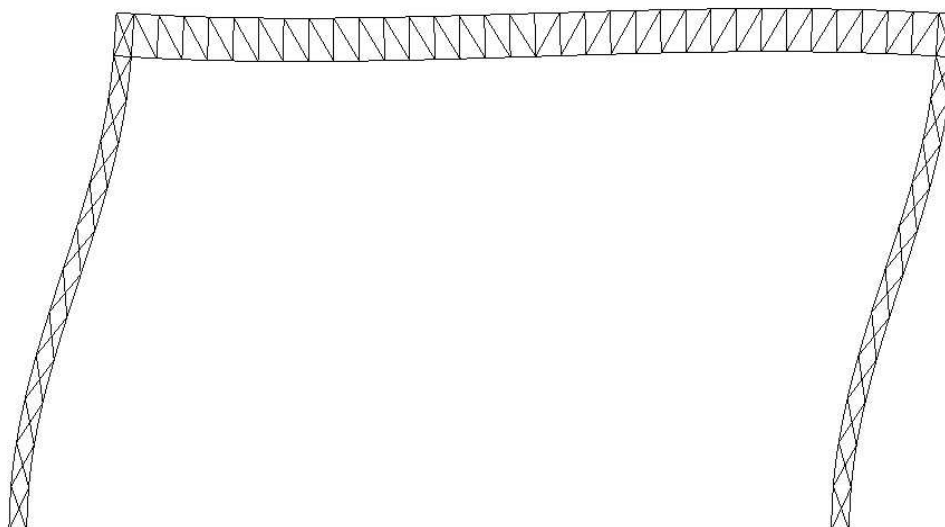


Figure 9-26: Global buckling mode shape of frame of Example 2 with fixed supports

The equilibrium paths obtained with each procedure for Load Case-B are presented in Figure 9-27. The use of GNIA in Timoshenko frame leads to the most sufficient prediction of the stiffness and collapse load. The use of C.S.2nd leads to a satisfactory and relatively safe calculation of the deflections and collapse load. C.S.1st results in a slightly stiffer response but in a smaller collapse load when compared with GMNIA predictions. Proposed-B method is also very close to GMNIA results and always on the safe side. It results in a better estimation of the collapse load when compared with C.S.1st and C.S.2nd.

The equilibrium paths obtained for Load Case-C are presented in Figure 9-28. It can be seen that the GMNIA equilibrium path is more nonlinear when compared with the one presented in Figure 9-27, as the total axial force applied to the more compressed column is larger. The response of all cases is slightly stiffer, especially the one corresponding to C.S.1st. The collapse load is safely predicted by all procedures. Proposed-B method results in better approximation of the ultimate strength when compared with the use of commercial software C.S.1st and C.S.2nd.

The larger stiffness predicted by the proposed procedure and GNIA with frame consisting of equivalent Timoshenko members is attributed to the fact that the beam-column connection is considered to be nodal while in reality it has finite dimensions. Therefore, even under only vertical loads, the rotation of the laced member at its top results in small transverse displacements at the location that the horizontal displacement is measured. This difference is expected to become more prominent in the case of fixed supports that the deflections are rather small and in the case that the dimensions of the beam-column connection are large.

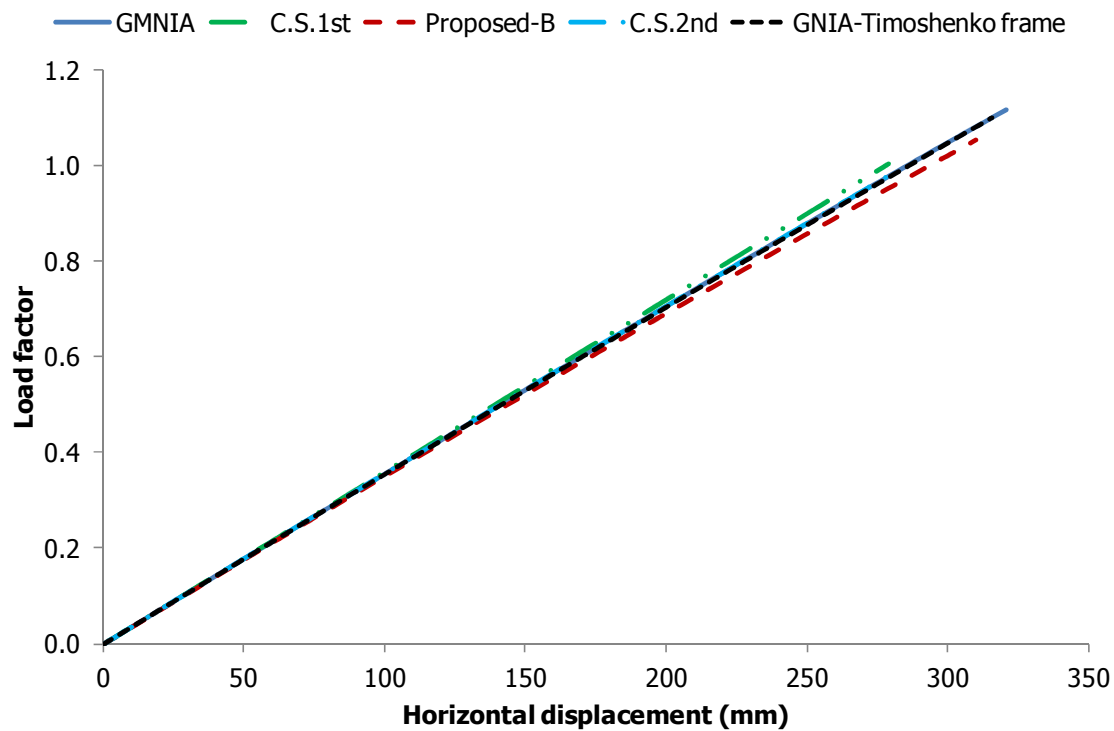


Figure 9-27: Equilibrium paths for Example 2 with fixed supports under Load Case-B

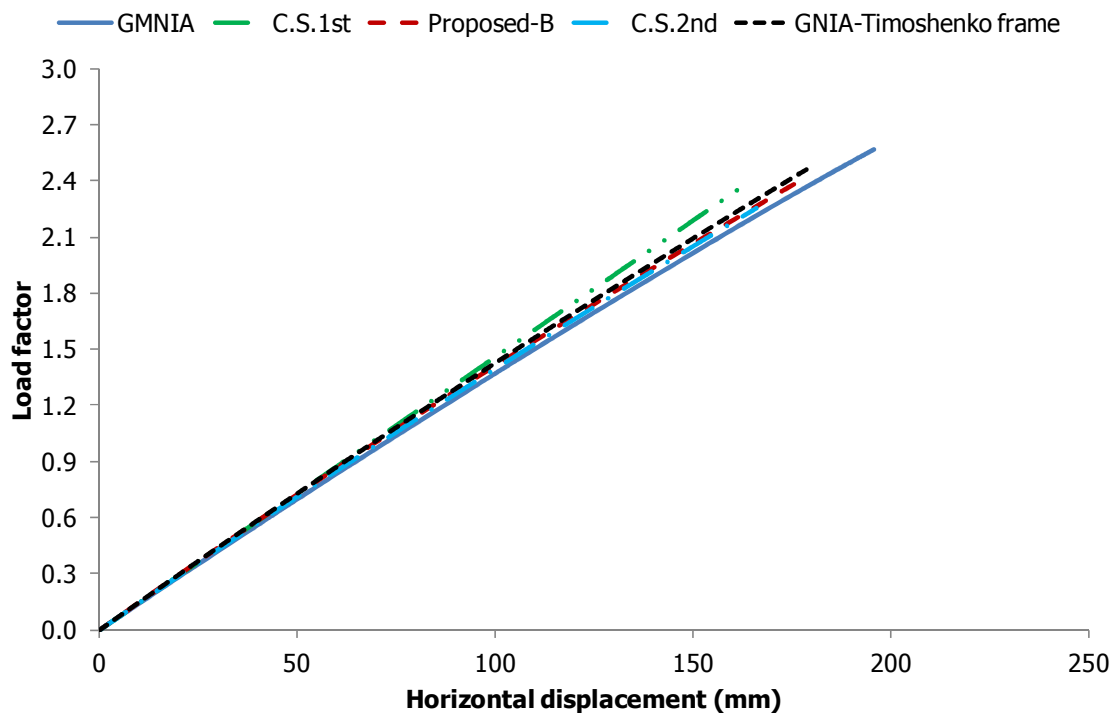


Figure 9-28: Equilibrium paths for Example 2 with fixed supports under Load Case-C

The results for Example 2 with fixed base supports are summarised in Table 9-6. A very good comparison between the numerical results and the proposed methods is achieved for the load factors and maximum deflections in this case, too. The fixed supports lead to an increase of the strength and reduction of horizontal deflections in the case that significant lateral loads exist. The use of GNA with commercial software is more conservative for load factors in all cases. The use of linear elastic

analysis results in even more conservative results as far as the load factor is concerned but in smaller deflections.

Table 9-6: Summary of results for Example 2 frame with fixed supports

	Method					Absolute error (%)			
	GMNIA	C.S. 2 nd	C.S. 1 st	Pr.-B	Pr.-A	C.S. 2 nd	C.S. 1 st	Pr.-B	Pr.-A
Global buckling load (kN)	26950	-	-	26425		-	-	1.94	
Local buckling load (kN)	169957	-	-	168104		-	-	1.09	
Squash load (kN)	15478	-	-	15478		-	-	0.00	
L.F. Load Case -A	3.630	3.240	3.200	3.442	3.415	10.74	11.85	5.18	5.92
L.F. Load Case -B	1.115	0.987	1.002	1.055	1.046	11.48	10.13	5.38	6.19
L.F. Load Case -C	2.573	2.262	2.352	2.420	2.401	12.10	8.59	5.95	6.68
Δ_{\max} Load Case-C (mm)	195.6	191.3	176.5	191.2		2.20	9.76	2.25	
Δ_{\max} Load Case-B (mm)	321.1	319.4	310.5	328.5		0.53	3.30	2.30	

The deformed configuration of the frame of Example 2 with fixed connections under the application of Load Case-A is presented in Figure 9-29 magnified for better graphical representation. Load Case-A is mainly related to symmetrical loads and for this reason the truss beam's deformation is mainly associated with single curvature deformation, something that is reflected in the axial force diagram shown in Figure 9-30, too. In this case, the axial force diagram takes its maximum value at the middle of the truss beam as expected.

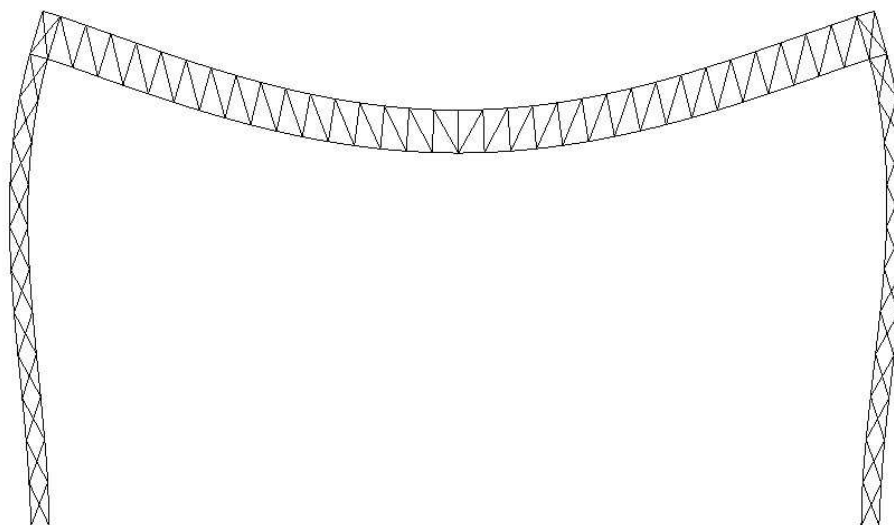


Figure 9-29: Deformed configuration of frame of Example 2 with fixed supports under the application of Load Case-A

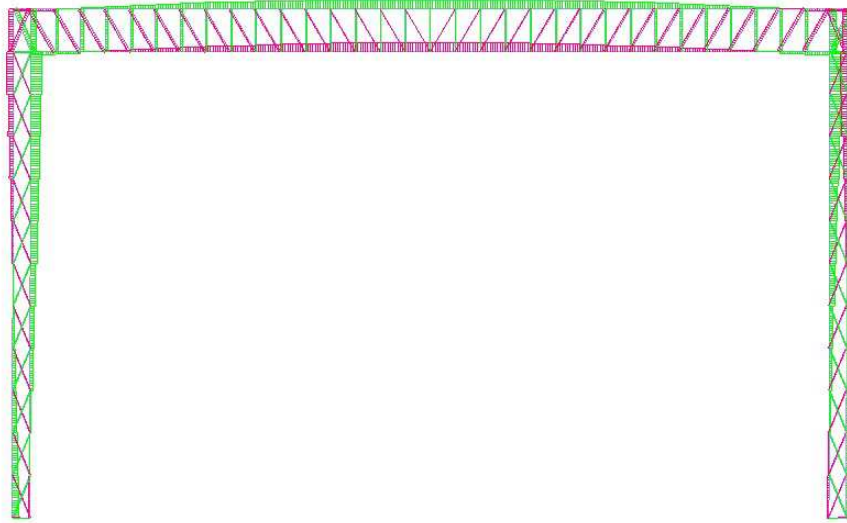


Figure 9-30: Axial force diagram of frame of Example 2 with fixed supports under Load Case-A (green colour corresponds to compression)

9.5.2.3 Example 3

The third example's geometrical characteristics for both laced built-up columns and truss beam are summarised in Table 9-7. Additionally, the equivalent bending and shear rigidities for the structural components are also presented. Both hinged and fixed supports are examined for the load cases described previously. The frame's global and local buckling mode shapes as obtained with LBA are shown in Figure 9-31 and Figure 9-32, respectively. It should be noted that the local buckling mode shape shown is related to buckling of the internal chords while at the same load level the external chords buckle, too. The local buckling mode shape of the external chords is not given as it is similar to the internal chords' local buckling mode shape.

Table 9-7: Geometrical characteristics and equivalent bending and shear rigidities of Example 3

Member	L (m)	h_o (cm)	a (cm)	Chord cross-section	A_d (cm ²)	I_{eff} (cm ⁴)	S_v (kN)
Columns	23.8	170	170	HEB160	10.0	784635	74242
Truss	43.0	300	295	HEA400	100	7155000	549407

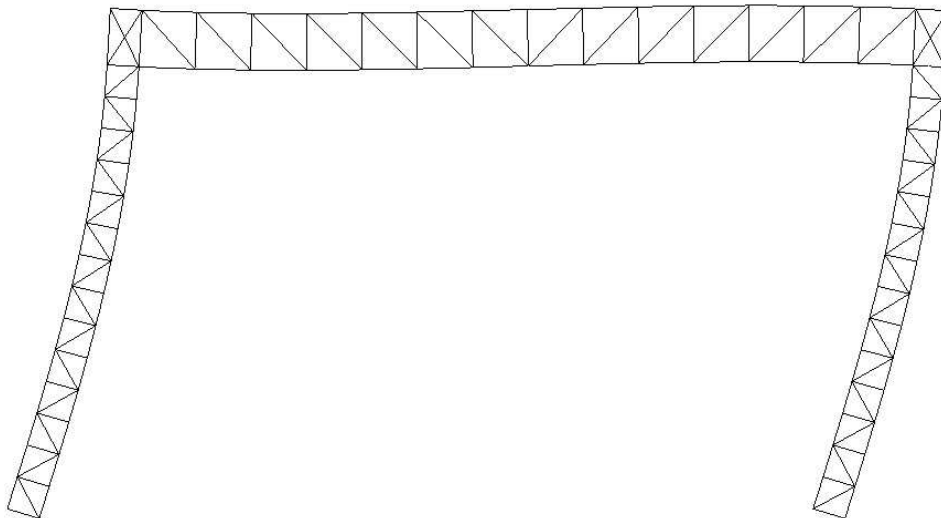


Figure 9-31: Global buckling mode shape of frame of Example 3 with hinged supports

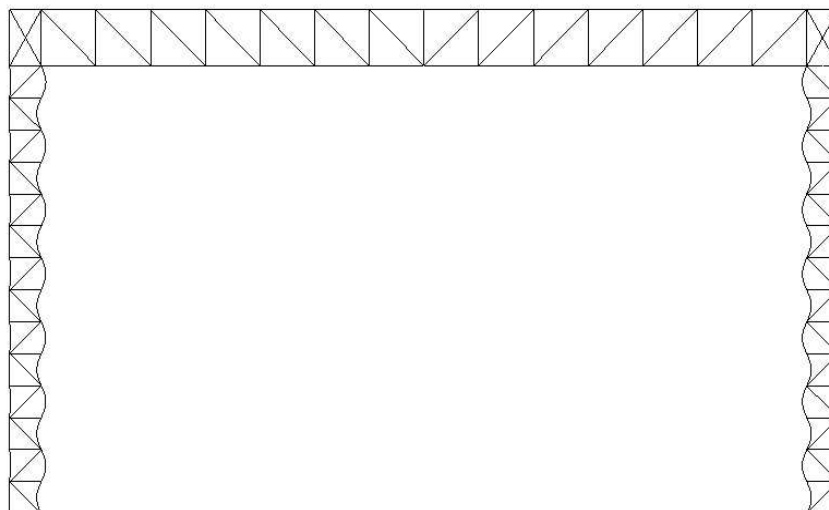


Figure 9-32: Local buckling mode shape of frame of Example 3 with hinged supports

The rotational stiffness that can be used to replace the truss beam corresponding to the non-sway mode is approximately equal to 700000kNm (single curvature beam deformation), while for the sway mode it is approximately equal to 1780000kNm (double curvature beam deformation). The local capacity of the simply-supported critical panel is equal to 1570.35kN and 1702.5kN for the case of 1st yield failure and of accounting for plastic reserve, respectively.

The equilibrium paths obtained with each procedure for Load Case-B are presented in Figure 9-33. The use of GNIA in Timoshenko frame leads to the most sufficient prediction of the stiffness and collapse load. Proposed-B method is also very close to GMNIA results and always on the safe side. The use of C.S.2nd leads to a satisfactory and relatively safe calculation of the deflections and collapse load. C.S.1st results in a slightly stiffer response but in a smaller collapse load when compared with GMNIA predictions.

The equilibrium paths obtained for Load Case-C are presented in Figure 9-34. It can be seen that the GMNIA equilibrium path is more nonlinear when compared with the one presented in Figure 9-33, as the total axial force applied to the more compressed column is larger. Similar conclusions, as far as the deflections and collapse loads are concerned, are drawn for all cases except for C.S.1st. In this case, a much stiffer response is predicted and C.S.1st doesn't capture the nonlinearity of the equilibrium path that corresponds to GMNIA. Nevertheless, the collapse load is safely predicted by this method, too.

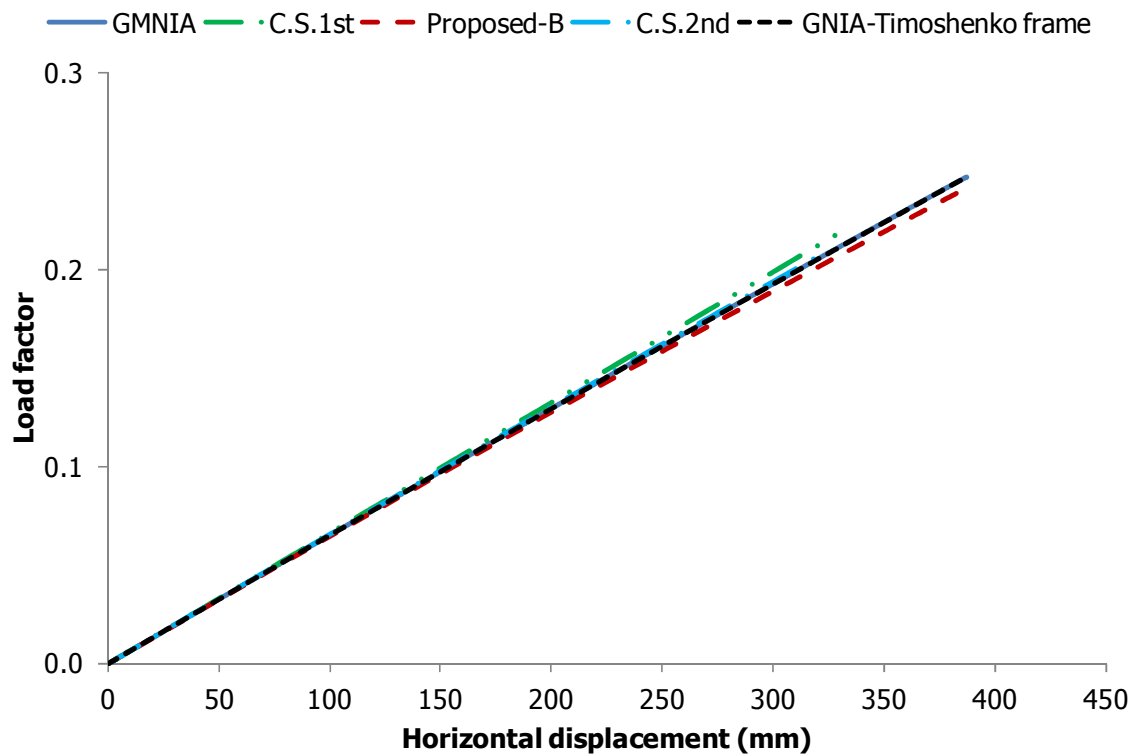


Figure 9-33: Equilibrium paths for Example 3 with hinged supports under Load Case-B

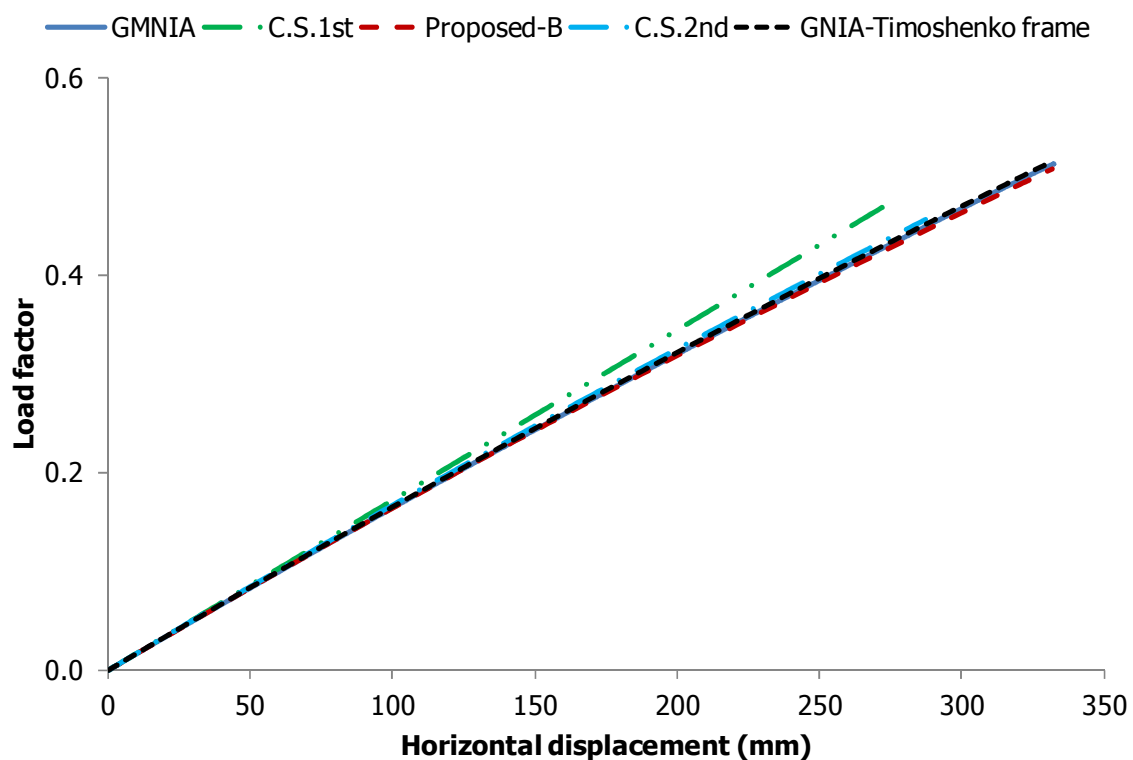


Figure 9-34: Equilibrium paths for Example 3 with hinged supports under Load Case-C

The results for the frame of Example 3 with hinged supports are given in Table 9-8. A very good comparison between the numerical results and the proposed methods is achieved for the load factors and maximum deflections. The use of GNA with commercial software leads to errors close to or larger

than 10% being on the conservative side in all cases for load factors. The use of C.S.2nd is slightly unsafe for the prediction of the lateral deflections. C.S.1st is also on the safe side for load factors but unconservative for the deflections, especially for Load Case-C.

Table 9-8: Summary of results for Example 3 frame with hinged supports

	Method					Absolute error (%)			
	GMNIA	C.S. 2 nd	C.S. 1 st	Pr.-B	Pr.-A	C.S. 2 nd	C.S. 1 st	Pr.-B	Pr.-A
Global buckling load (kN)	6115	-	-	6104kN		-	-	0.18	
Local buckling load (kN)	12800	-	-	12751kN		-	-	0.38	
Squash load (kN)	3855	-	-	3855kN		-	-	0.00	
L.F. Load Case -A	1.410	1.272	1.260	1.435	1.323	9.79	10.64	1.77	6.17
L.F. Load Case -B	0.247	0.210	0.22	0.241	0.223	14.98	10.93	2.43	9.72
L.F. Load Case -C	0.512	0.456	0.478	0.508	0.471	10.94	6.64	0.78	8.00
Δ_{\max} Load Case-C (mm)	332.2	326.1	297.8	334.5		1.84	10.36	0.69	
Δ_{\max} Load Case-B (mm)	387.5	386.2	374.7	396.2		0.34	3.30	2.25	

The deformed shape of the frame of Example 3 with hinged supports under Load Case-C is shown in Figure 9-35. Despite the fact that the frame deflects laterally the deformation of the truss is mainly associated with single curvature deformation due to the uniformly distributed load applied along it, something that is verified by the axial force diagram as obtained with GMNIA and depicted in Figure 9-36. The critical panel is the top one in the right column.

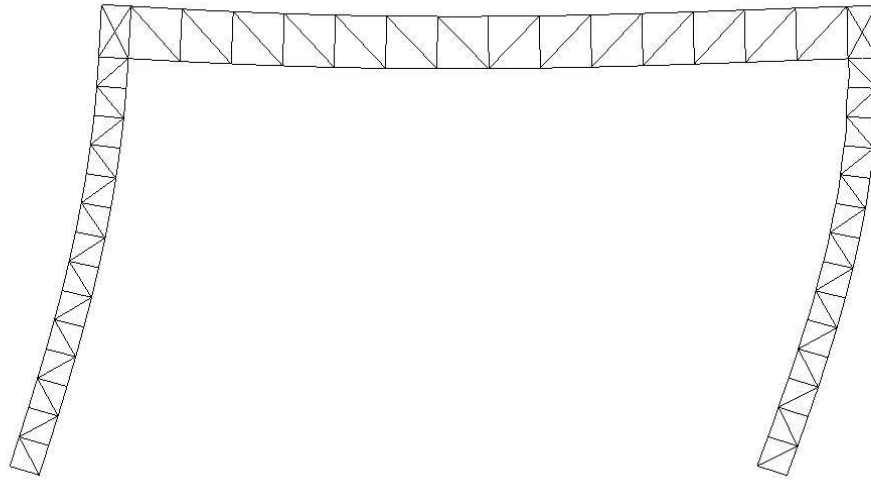


Figure 9-35: Deformed shape of frame of Example 3 with hinged supports under Load Case-C

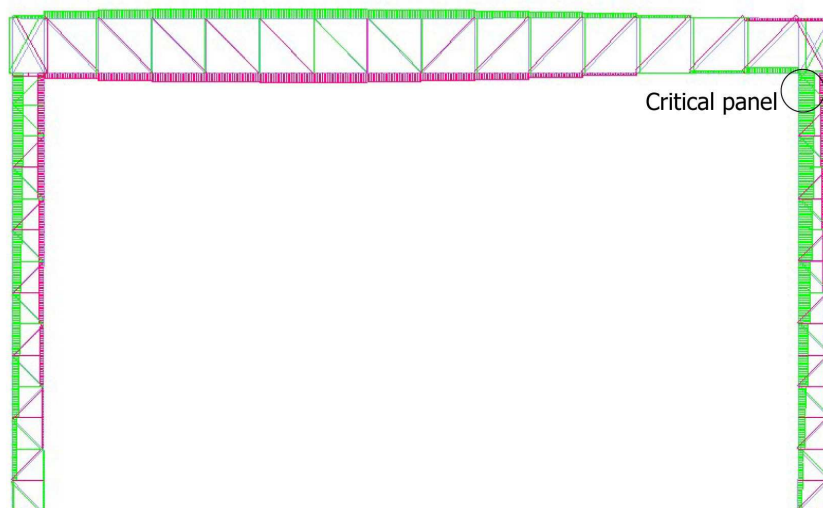


Figure 9-36: Axial force diagram of frame of Example 3 with hinged supports under Load Case-C (green colour corresponds to compression)

The bending moment diagram only along the chords of the laced built-up members with hinged supports is depicted in Figure 9-37. It can be seen that the bending moment distribution along the critical panel at the top of the right column follows the local imperfection shape (local buckling mode shape). The corresponding bending moment diagram at collapse is shown in Figure 9-38 at which the critical panel's bending moment distribution has a very similar shape and no reduction is observed in the magnitude. This happens because the local non-dimensional slenderness of the panels is relatively large and initial local imperfections play an important role and internal bending moments along the chords appear mainly due to their effect. Therefore, contrary to the phenomenon observed in Examples 1 and 2, internal bending moments along the critical panel in this case do not reduce due to plastification of the material and are taken into account in the proposed procedures.

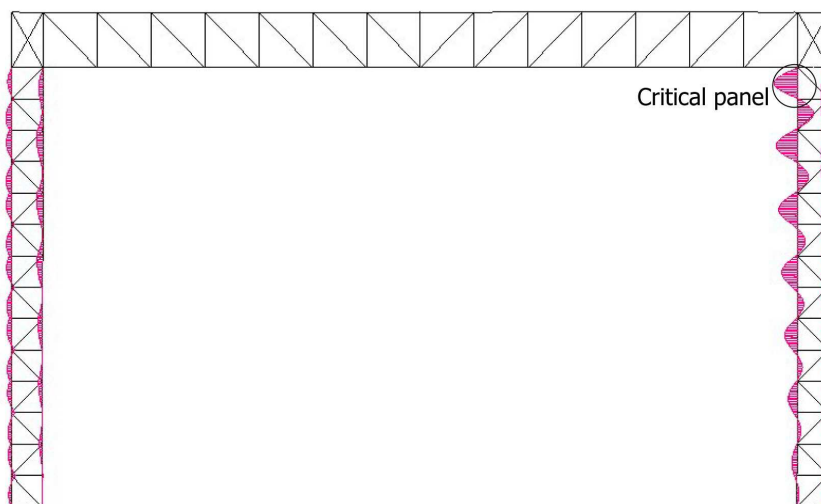


Figure 9-37: Bending moment diagram of laced members' chords of Example 3 with hinged supports under Load Case-C at an elastic state before collapse

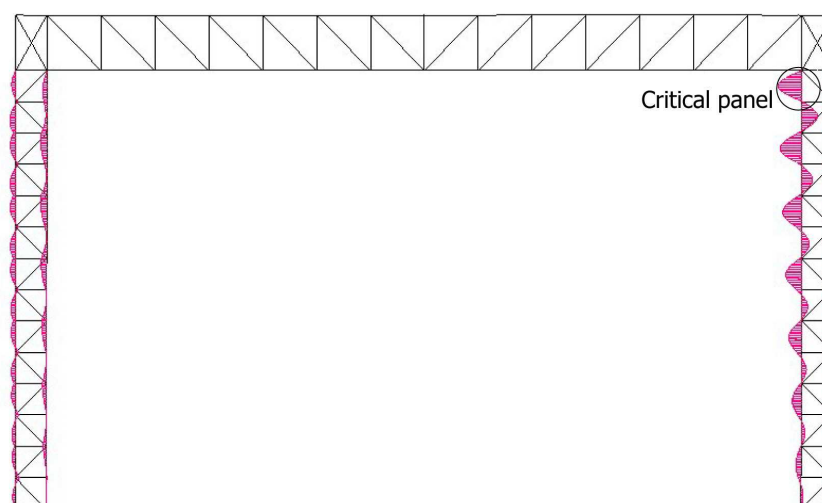


Figure 9-38: Bending moment diagram of laced members' chords of Example 3 with hinged supports under Load Case-C at collapse

The global buckling mode shape of the frame of Example 3 with fixed supports is provided in Figure 9-39. It should be noted that the rotational springs for the substitution of the truss beam in the case of single and double curvature deformation are the same as the ones presented for the hinged supports. The local buckling mode shape is exactly the same as the one presented for the hinged supports as they affect only the global response and not the local one.

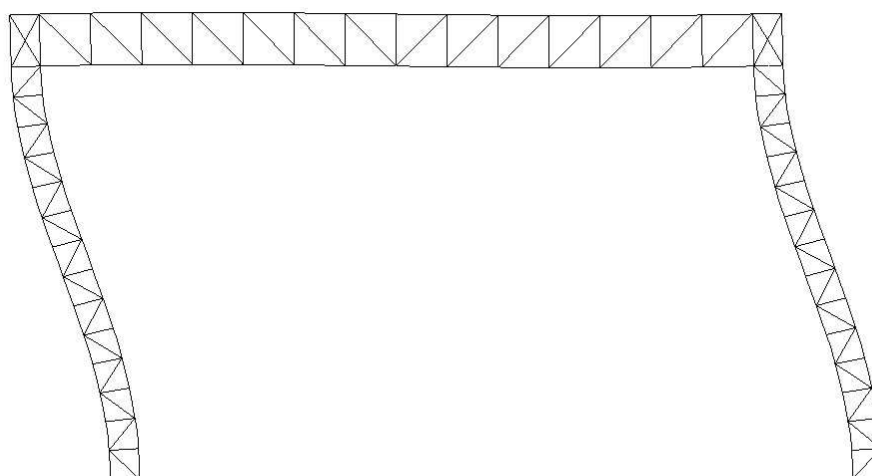


Figure 9-39: Global buckling mode shape of frame of Example 3 with fixed supports

The equilibrium paths obtained with each procedure for Load Case-B are presented in Figure 9-40. All procedures predict in a satisfactory way the stiffness of the frame, while the use of GNIA in Timoshenko frame leads to the most sufficient prediction of the collapse load. Proposed-B method is also very close to GMNIA results and always on the safe side. The use of C.S.1st is more efficient than in the case of hinged base supports for Load Case-B, as fixed supports lead to a significant reduction of the lateral deflections' magnitude, allowing in this way for the use of linear analysis.

The equilibrium paths obtained for Load Case-C are presented in Figure 9-41. All procedures result in an unconservative prediction of the overall stiffness but in a safe calculation of the ultimate strength. The larger stiffness predicted by the proposed procedure and GNIA with frame consisting of equivalent Timoshenko members is attributed to the fact that the beam-column connection is

considered to be nodal while in reality it has finite dimensions. Therefore, even under only vertical loads, the rotation of the laced member at its top results in small transverse displacements at the location that the horizontal displacement is measured.

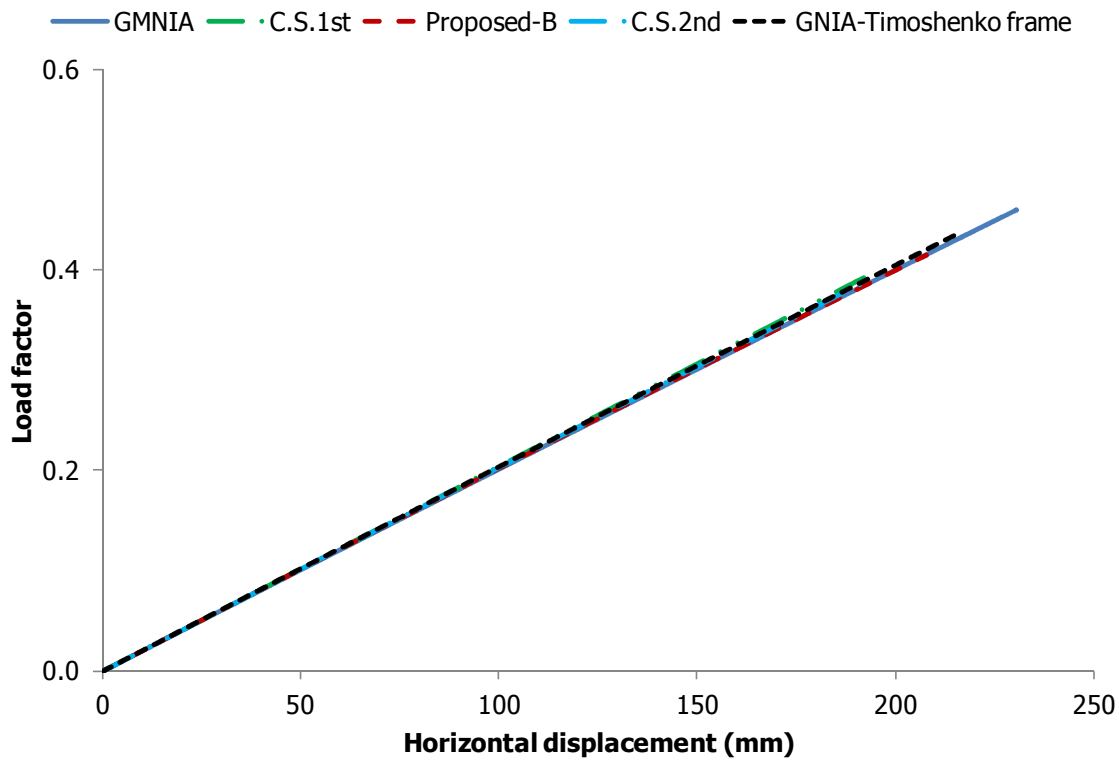


Figure 9-40: Equilibrium paths for Example 3 with fixed supports under Load Case-B

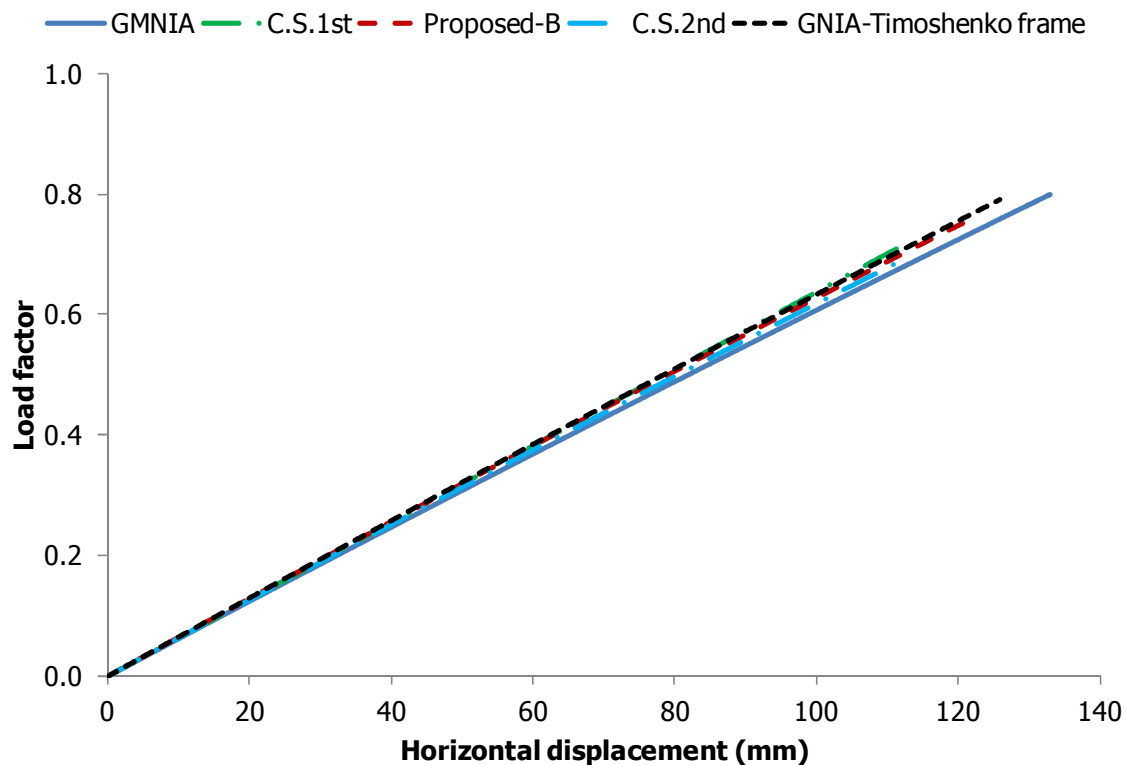


Figure 9-41: Equilibrium paths for Example 3 with fixed supports under Load Case-C

The results for Example 3 with fixed base supports are summarised in Table 9-9. A very good comparison between the numerical results and the proposed methods is achieved for the load factors. The fixed supports lead to an increase of the strength and reduction of horizontal deflections in the case that significant lateral loads exist. The use of GNA and commercial software leads to conservative errors that exceed 10% in all cases. The predictions of the proposed methods, C.S.1st and C.S.2nd for the lateral deflections are slightly unsafe when compared with GMNIA results. The axial force diagram for Load Case-C as obtained with GMNIA is depicted in Figure 9-42. The critical panel is the bottom one in the right column. At the base, the axial forces are larger due to the restriction of rotation and appearance of bending moments. The distribution of the axial forces along the truss beam's chords reveals that single curvature deformation is the dominant one.

Table 9-9: Summary of results for Example 3 frame with fixed supports

	Method					Absolute error (%)			
	GMNIA	C.S. 2 nd	C.S. 1 st	Pr.-B	Pr.-A	C.S. 2 nd	C.S. 1 st	Pr.-B	Pr.-A
Global buckling load (kN)	19400	-	-	19589		-	-	0.97	
Local buckling load (kN)	12800	-	-	12751		-	-	0.38	
Squash load (kN)	3855	-	-	3855		-	-	0.00	
L.F. Load Case -A	1.390	1.227	1.218	1.410	1.300	11.73	12.37	1.44	6.47
L.F. Load Case -B	0.460	0.390	0.392	0.415	0.384	15.20	14.78	9.78	16.52
L.F. Load Case -C	0.800	0.690	0.710	0.764	0.707	13.75	11.25	4.50	11.63
Δ_{\max} Load Case-C (mm)	132.9	130.6	125.6	128.7		1.73	5.49	3.16	
Δ_{\max} Load Case-B (mm)	230.5	229.2	225.4	231.3		0.56	2.21	0.35	

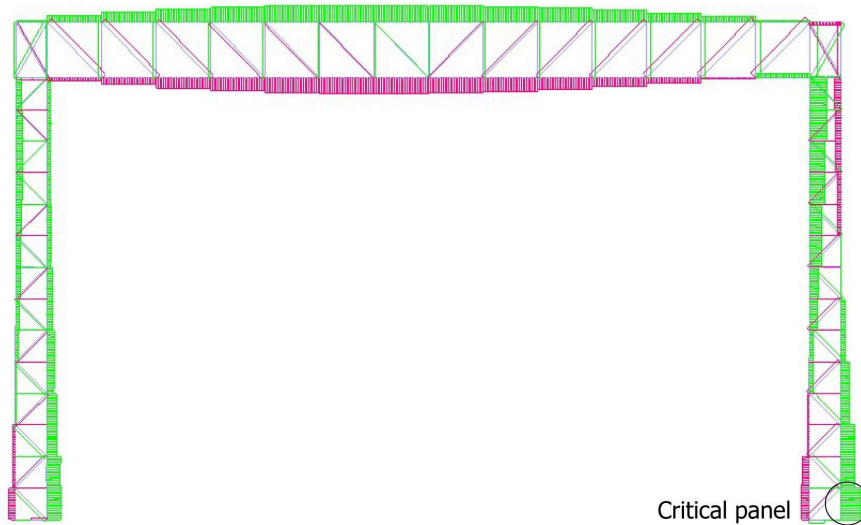


Figure 9-42: Axial force diagram of frame of Example 3 with fixed supports under Load Case-C (green colour corresponds to compression)

The bending moment diagram only along the chords of the laced built-up members with fixed supports before collapse is depicted in Figure 9-43 and follows the shape of the local imperfections. The corresponding bending moment diagram at collapse is shown in Figure 9-44 at which the critical panel's bending moment distribution is very similar to the elastic case despite the fact that the material is plastified. The same conclusions as for the hinged case of Example 3 are drawn.

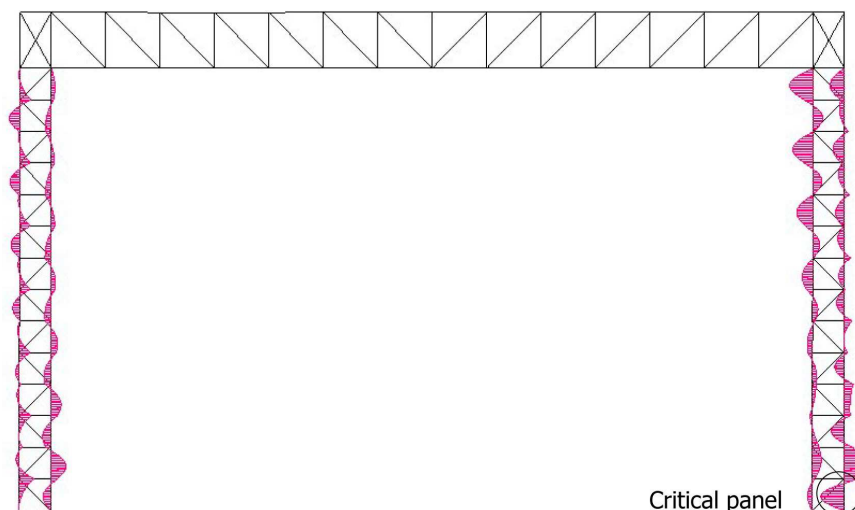


Figure 9-43: Bending moment diagram of laced members' chords of Example 3 with fixed supports under Load Case-C at an elastic state before collapse

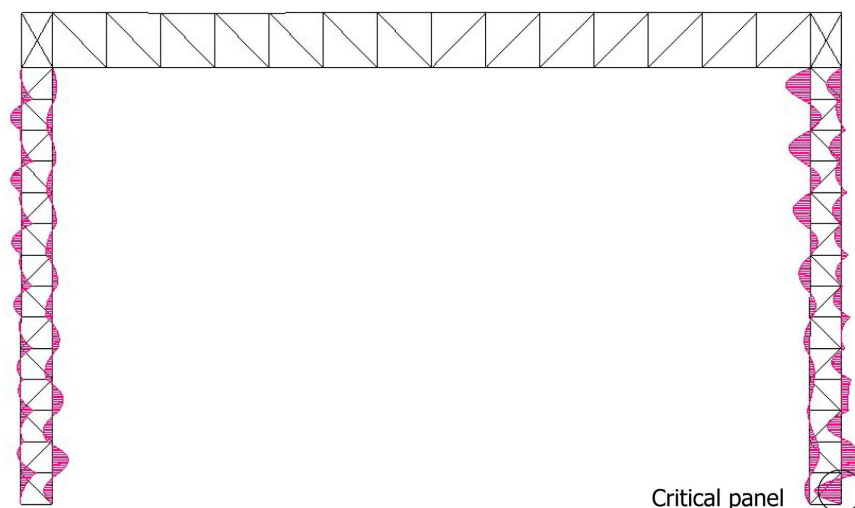


Figure 9-44: Bending moment diagram of laced members' chords of Example 3 with fixed supports under Load Case-C at collapse

9.5.2.4 Example 4

The fourth example's geometrical characteristics for both laced built-up columns and truss beam are summarised in Table 9-10. Additionally, the equivalent bending and shear rigidities for the structural components are also presented. Both hinged and fixed supports are examined for the load cases described previously. The frame's global and local buckling mode shapes as obtained with LBA are similar to the ones obtained for Example 2.

Table 9-10: Geometrical characteristics and equivalent bending and shear rigidities of Example 4

Member	L (m)	h_o (cm)	a (cm)	Chord cross-section	A_d (cm ²)	I_{eff} (cm ⁴)	S_v (kN)
Columns	18.7	70	170	HEB160	10.0	134813	56301
Truss	32.7	170	100	HEA400	100	2297550	482230

The rotational stiffness that can be used to replace the truss beam corresponding to the non-sway mode is approximately equal to 295000kNm (single curvature beam deformation), while for the sway mode it is approximately equal to 796000kNm (double curvature beam deformation). The local

capacity of the simply-supported critical panel is equal to 1570.35kN and 1702.5kN for the case of 1st yield failure and of accounting for plastic reserve, respectively.

The equilibrium paths obtained with each procedure for Load Case-B are presented in Figure 9-45. The use of GMNIA in Timoshenko frame leads to the most sufficient prediction of the stiffness and collapse load. Proposed-B method is also very close to GMNIA results and always on the safe side. The use of C.S.2nd leads to a satisfactory calculation of the deflections and to a very conservative prediction of the collapse load. C.S.1st results in a slightly stiffer response but in a much smaller collapse load when compared with GMNIA predictions.

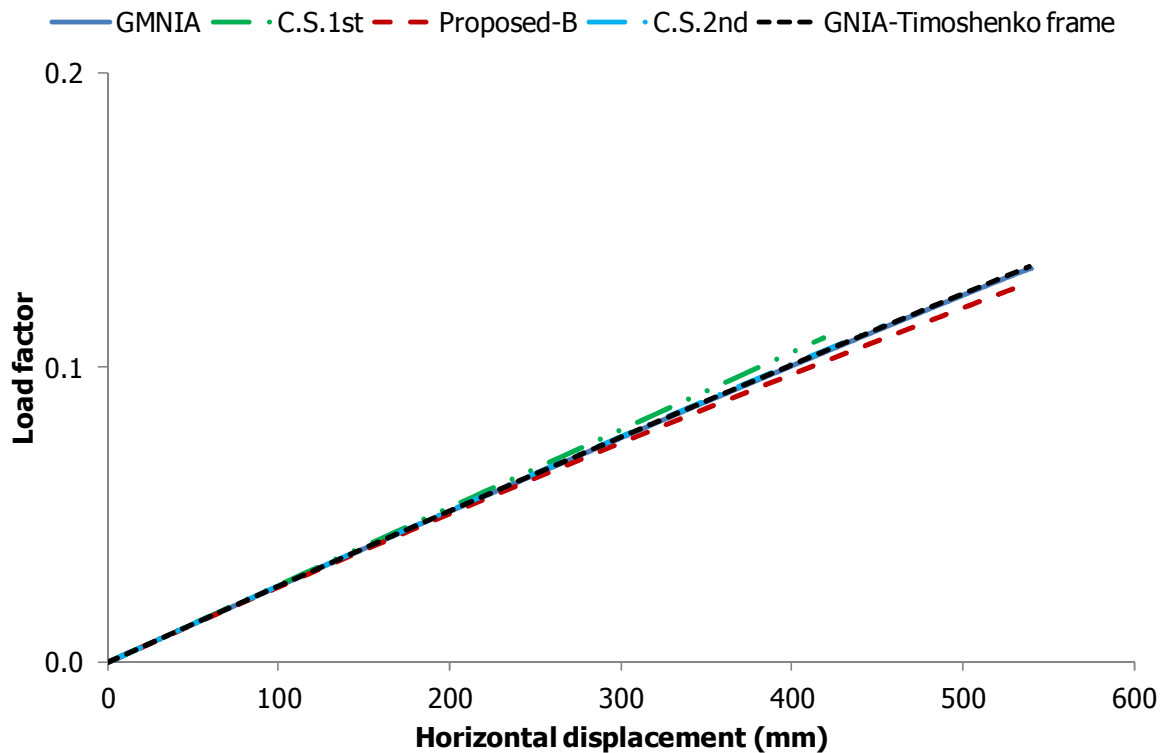


Figure 9-45: Equilibrium paths for Example 4 with hinged supports under Load Case-B

The equilibrium paths obtained for Load Case-C are presented in Figure 9-46. It can be seen that the GMNIA equilibrium path is more nonlinear when compared with the one presented in Figure 9-45, as the total axial force applied to the more compressed column is larger. Similar conclusions, as far as the deflections and collapse loads are concerned, are drawn for all cases except for C.S.1st. In this case, a much stiffer response is predicted and C.S.1st doesn't capture the nonlinearity of the equilibrium path that corresponds to GMNIA. Nevertheless, the collapse load is safely predicted by this method despite the fact that the conservatism in its calculation is significant.

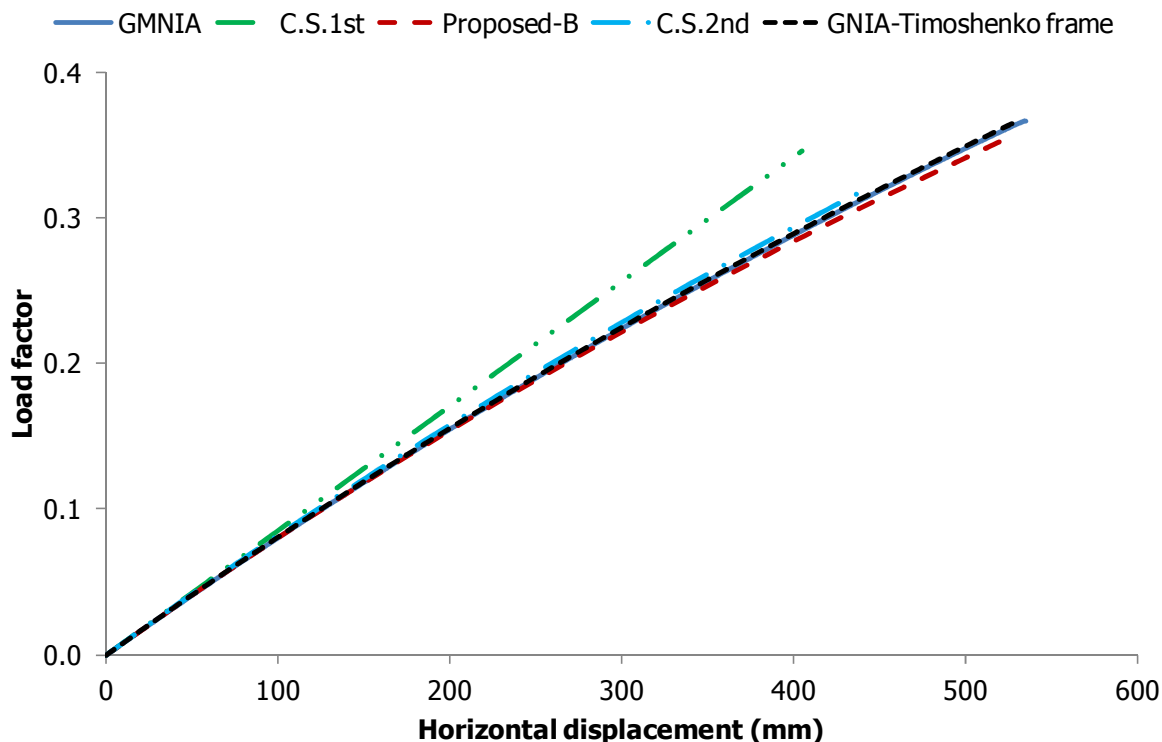


Figure 9-46: Equilibrium paths for Example 4 with hinged supports under Load Case-C

The results for the frame of Example 4 with hinged supports are given in Table 9-11. A very good comparison between the numerical results and the proposed methods is achieved for the load factors and maximum deflections.

Table 9-11: Summary of results for Example 4 frame with hinged supports

	Method					Absolute error (%)			
	GMNIA	C.S. 2 nd	C.S. 1 st	Pr.-B	Pr.-A	C.S. 2 nd	C.S. 1 st	Pr.-B	Pr.-A
Global buckling load (kN)	1882	-	-	1860		-	-	1.17	
Local buckling load (kN)	12780	-	-	12751		-	-	0.23	
Squash load (kN)	3855	-	-	3855		-	-	0.00	
L.F. Load Case -A	1.450	1.552	1.544	1.445	1.365	7.00	6.48	0.34	5.86
L.F. Load Case -B	0.133	0.113	0.109	0.128	0.119	15.04	18.05	3.76	10.53
L.F. Load Case -C	0.367	0.322	0.346	0.357	0.334	12.26	5.72	2.72	8.99
Δ_{\max} Load Case-C (mm)	534.6	523.8	430.4	548.3		2.02	19.49	2.56	
Δ_{\max} Load Case-B (mm)	539.3	536.3	510.1	557.7		0.56	5.41	3.41	

The deformed shape of the frame of Example 4 with hinged supports under Load Case-B is shown in Figure 9-47. The truss is mainly related to double curvature deformation, something that is verified by the axial force diagram as obtained with GMNIA and depicted in Figure 9-48. The critical panel is the top one in the right column.

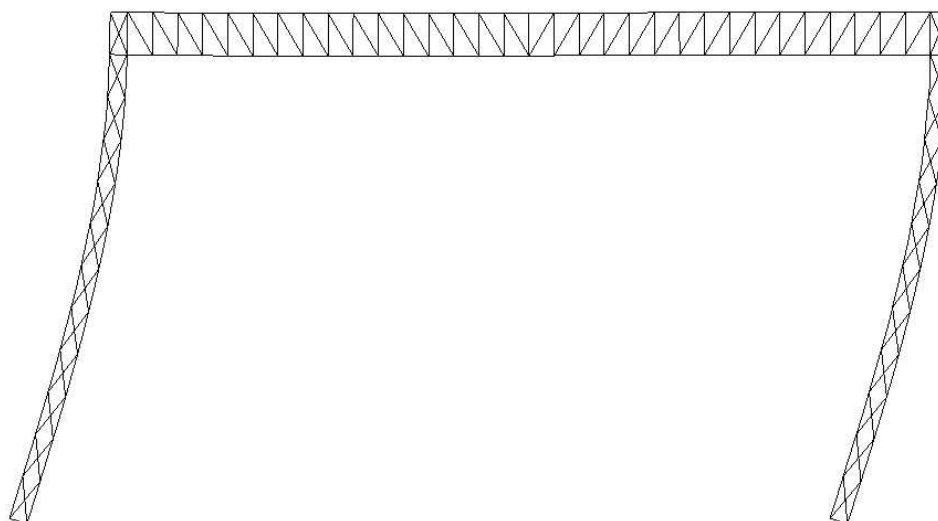


Figure 9-47: Deformed shape of frame of Example 4 with hinged supports under Load Case-B

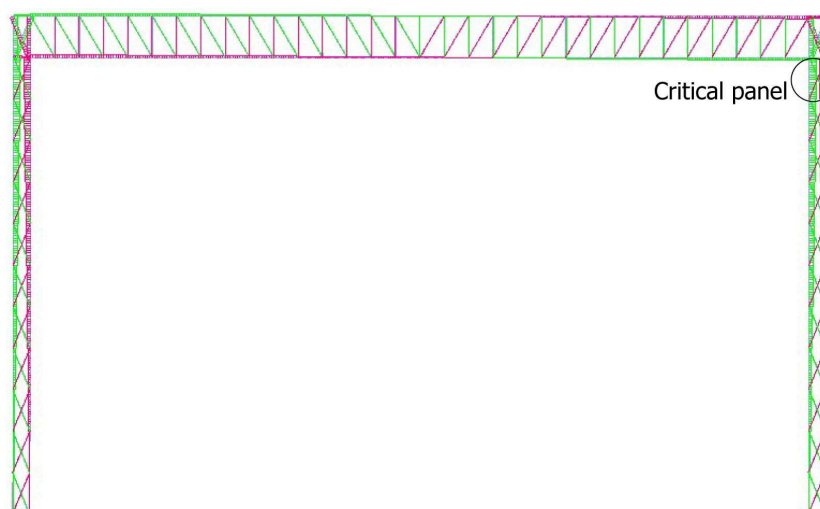


Figure 9-48: Axial force diagram of frame of Example 4 with hinged supports under Load Case-B (green colour corresponds to compression)

The bending moment diagram only along the chords of the laced built-up members with hinged supports is depicted in Figure 9-49. It can be seen that the bending moment distribution along the critical panel at the top of the right column follows the local imperfection shape (local buckling mode shape). The corresponding bending moment diagram at collapse is shown in Figure 9-50 at which the critical panel's bending moment distribution has a very similar shape and no reduction is observed in the magnitude. The same conclusions drawn for Example 3 with hinged supports apply in this case, too.

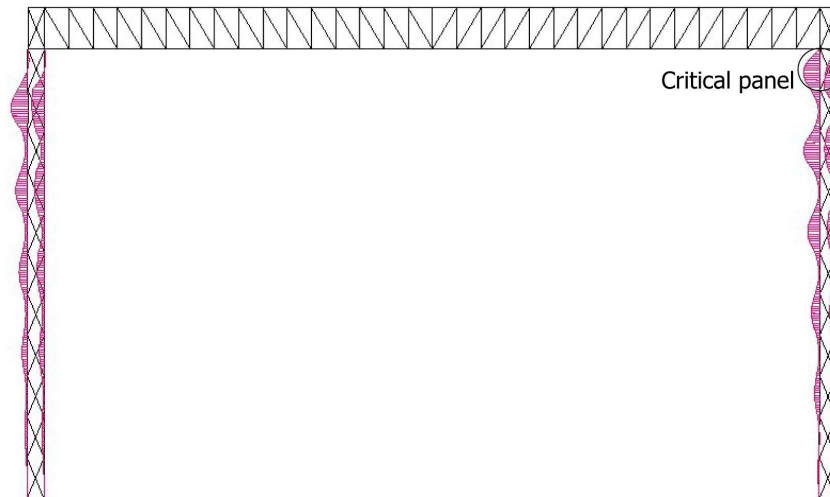


Figure 9-49: Bending moment diagram of laced members' chords of Example 4 with hinged supports under Load Case-B at an elastic state before collapse

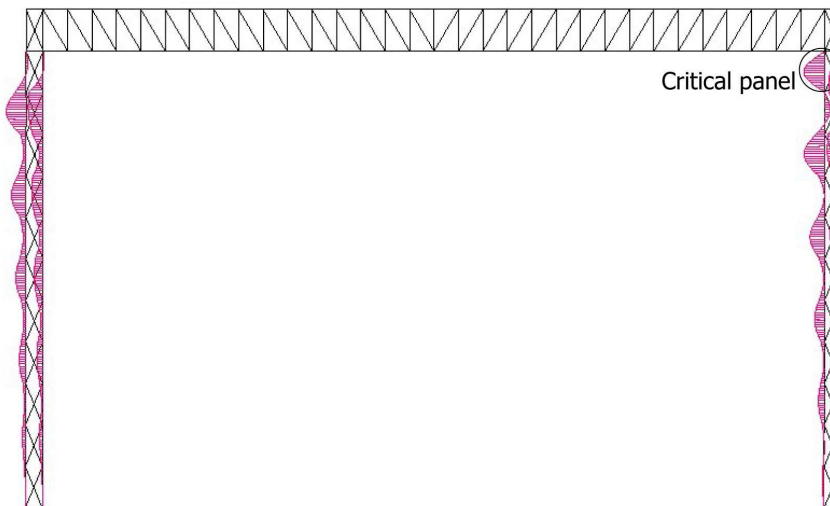


Figure 9-50: Bending moment diagram of laced members' chords of Example 4 with hinged supports under Load Case-B at collapse

The global buckling mode shape of the frame of Example 4 with fixed supports is provided in Figure 9-51. It should be noted that the rotational springs for the substitution of the truss beam in the case of single and double curvature deformation are the same as the ones presented for the hinged supports. The local buckling mode shape is exactly the same as the one presented for the hinged supports as the boundary conditions at the base affect only the global response and not the local one.

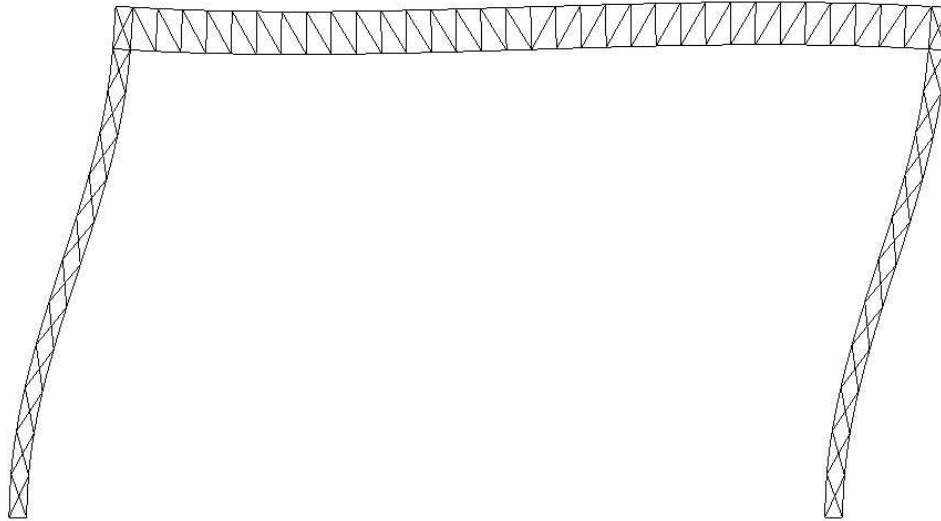


Figure 9-51: Global buckling mode shape of frame of Example 4 with fixed supports

The equilibrium paths obtained with each procedure for Load Case-B are presented in Figure 9-52. The use of GMNIA in Timoshenko frame leads to the most sufficient prediction of the stiffness and collapse load. Proposed-B method is also very close to GMNIA results and always on the safe side. The use of C.S.2nd leads to a satisfactory calculation of the deflections and a very conservative prediction of the collapse load. C.S.1st results in a slightly stiffer response but in a very conservative calculation of the collapse load when compared with GMNIA predictions.

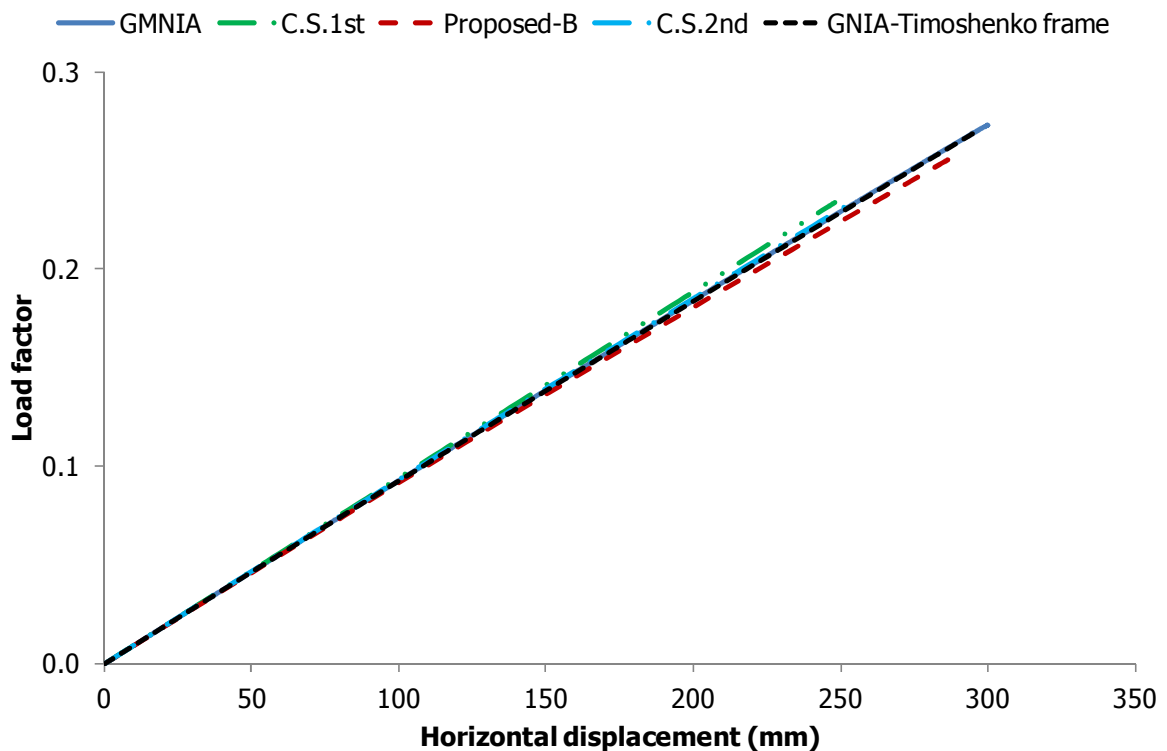


Figure 9-52: Equilibrium paths for Example 4 with fixed supports under Load Case-B

The equilibrium paths obtained for Load Case-C are presented in Figure 9-53. It can be seen that the GMNIA equilibrium path is more nonlinear when compared with the one presented in Figure 9-52, as the total axial force applied to the more compressed column is larger. The use of the equivalent

Timoshenko frame and of the proposed method leads to a very accurate prediction of the deflections and a relatively conservative calculation of the ultimate strength of the frame. The use of C.S.2nd results in a slightly stiffer response but in a very conservative prediction of the collapse load. The use of C.S.1st results in much smaller deflections and in a safe magnitude for the ultimate load.

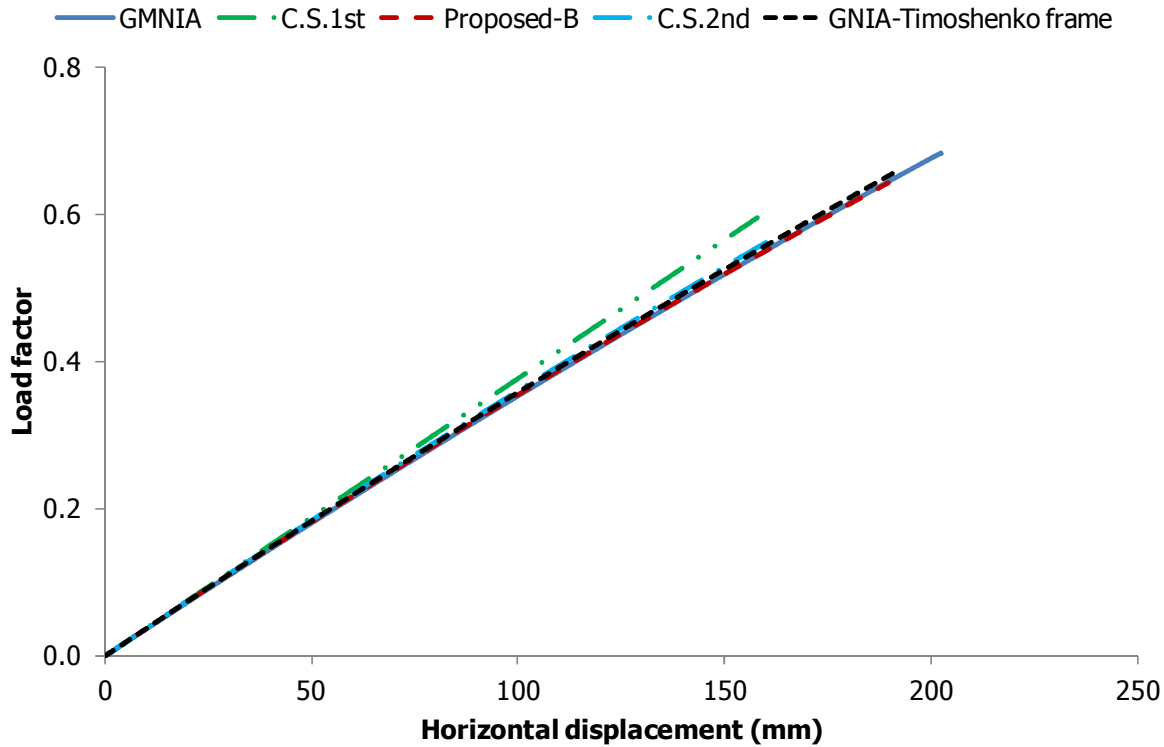


Figure 9-53: Equilibrium paths for Example 4 with fixed supports under Load Case-C

The results for Example 4 with fixed base supports are summarised in Table 9-12. A very good comparison between the numerical results and the proposed methods is achieved for the load factors and maximum deflections in this case, too. The fixed supports lead to an increase of the strength and reduction of horizontal deflections in the case that significant lateral loads exist. The use of analyses with commercial software leads to safe prediction of collapse loads but unconservative calculation of deflections.

Table 9-12: Summary of results for Example 4 frame with fixed supports

	Method					Absolute error (%)			
	GMNIA	C.S. 2 nd	C.S. 1 st	Pr.-B	Pr.-A	C.S. 2 nd	C.S. 1 st	Pr.-B	Pr.-A
Global buckling load (kN)	6871	-	-	6770		-	-	1.47	
Local buckling load (kN)	12780	-	-	12751		-	-	0.23	
Squash load (kN)	3855	-	-	3855		-	-	0.00	
L.F. Load Case –A	1.591	1.448	1.413	1.560	1.433	8.99	11.19	1.95	9.93
L.F. Load Case –B	0.273	0.232	0.234	0.259	0.240	15.02	14.29	5.13	12.09
L.F. Load Case –C	0.684	0.570	0.596	0.642	0.596	16.67	12.87	6.14	12.87
Δ_{\max} Load Case-C (mm)	202.6	198.1	181.5	203.3		2.22	10.41	0.35	
Δ_{\max} Load Case-B (mm)	300.0	298.6	290.6	306.9		0.47	3.13	2.30	

The axial force diagram for Load Case-A as obtained with GMNIA is depicted in Figure 9-54. The critical panel is the top one in the right column while at the base, the axial forces are slightly smaller.

The distribution of the axial forces along the truss beam's chords reveals that single curvature deformation is the dominant one.

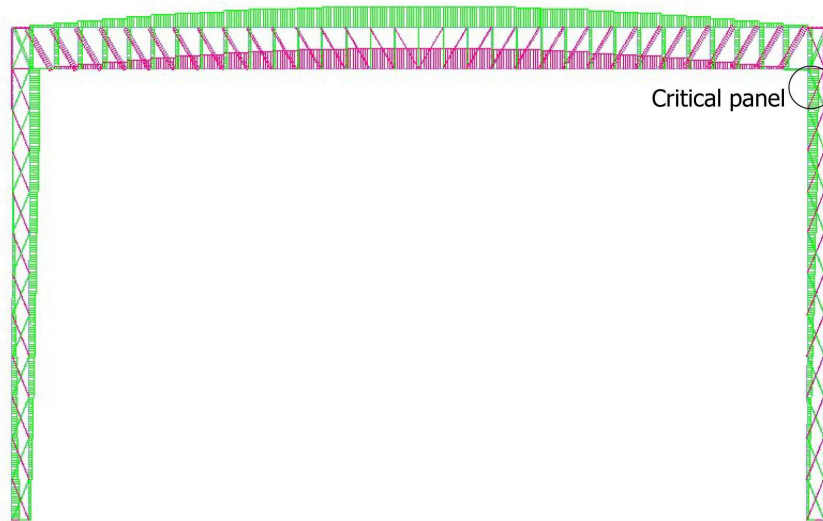


Figure 9-54: Axial force diagram of frame of Example 4 with fixed supports under Load Case-A (green colour corresponds to compression)

The bending moment diagram only along the chords of the laced built-up members with fixed supports before collapse is depicted in Figure 9-55 and follows the shape of the local imperfections. The corresponding bending moment diagram at collapse is shown in Figure 9-56 at which the critical panel's bending moment distribution is very similar to the elastic case despite the fact that the material is plastified. The same conclusions as for the hinged case of Example 4 are drawn.

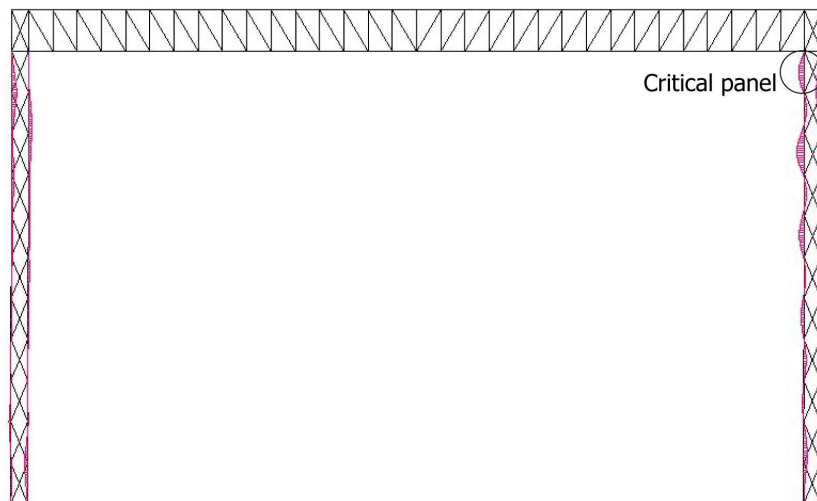


Figure 9-55: Bending moment diagram of laced members' chords of Example 4 with fixed supports under Load Case-A at an elastic state before collapse

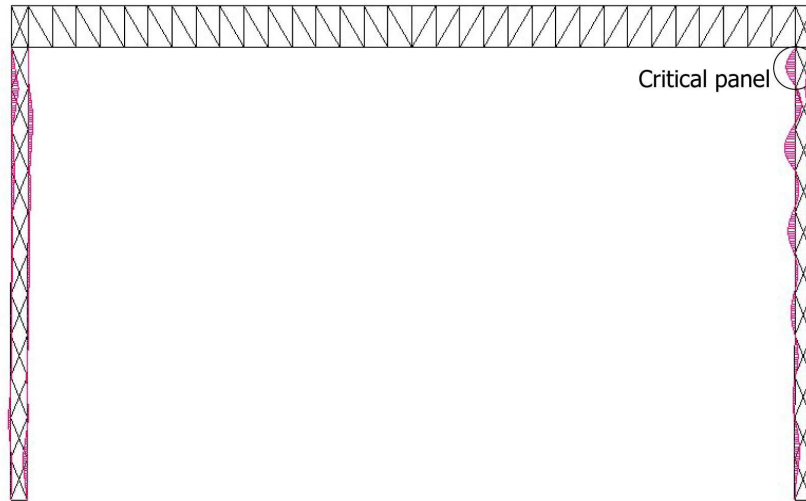


Figure 9-56: Bending moment diagram of laced members' chords of Example 4 with fixed supports under Load Case-A at collapse

9.5.2.5 Example 5

Example 5 is related to the single-story frame with fixed supports presented in Example 29 by Vayas et al. [9-7] in which the two laced columns are axially loaded. The frame is free to sway laterally and initial global and local imperfections are taken into account. The beam's cross-section has a second moment of inertia about the axis of bending equal to 73800cm^4 and its length is equal to 17.0m . The geometrical and inertial characteristics of the laced columns are summarised in Table 9-13. The Proposed-B method, GMNIA results and the procedure used in the structural textbook are compared.

Table 9-13: Geometrical characteristics and equivalent bending and shear rigidities of Example 5

Member	L (m)	h_o (cm)	a (cm)	Chord cross-section	A_d (cm^2)	I_{eff} (cm^4)	S_v (kN)
Columns	8.5	34.6	69.2	UPN300	4.8	35197	71284

According to the procedure described in the structural textbook the collapse load of the frame is equal to 2297kN . The Proposed-B method and GMNIA result in collapse loads equal to 2528.5kN and 2530kN , respectively. The Proposed-B method gives a more accurate prediction of both the internal forces and the local capacity of the critical panel and in this way predicts the collapse load with an error equal to 0.06% . The error of the procedure in the structural textbook reaches a magnitude of 9.20% . The undeformed and deformed shapes of the frame of Example 5 are depicted magnified in Figure 9-57.



Figure 9-57: Undeformed and deformed shapes at collapse load of frame of Example 5

9.6 FRAMES WITH NON-UNIFORM LACED MEMBERS

In many industrial buildings, laced built-up columns are not continuous in elevation due to the fact that the crane bridge often carried by such structures is designed to be supported by the inner chord of the laced members. A typical industrial frame with truss beam and discontinuous in elevation laced members is depicted in Figure 9-58. The frame is exactly the same as the ones with uniform laced members in elevation with the only difference that a member with a much smaller bending rigidity intervenes between the laced members and the truss beam. This member usually is the continuation of the outer chord of the laced column. This discontinuity facilitates the movement of the crane bridge but from a structural point of view reduces dramatically the rotational stiffness that the truss beam offers to the top of the laced members.

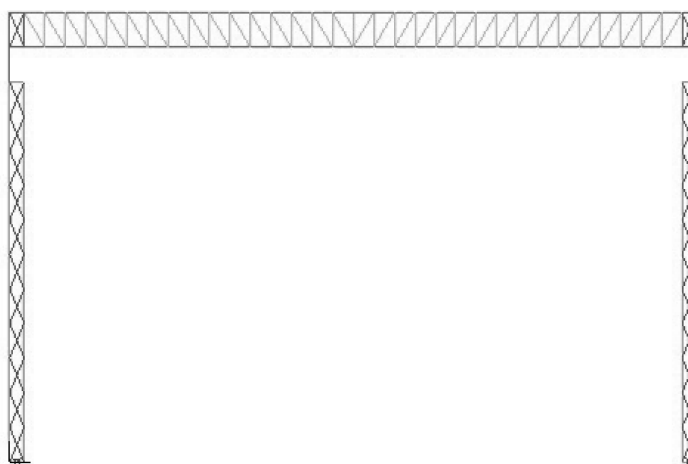


Figure 9-58: Typical industrial frame with truss beam and discontinuous in elevation laced members

A comparison between the frame of Example 2 with fixed supports and with uniform and non-uniform laced members is presented. In the structure with the non-uniform laced members the outer chord connects the truss beam with the laced members and the length of the discontinuity is equal to 170cm. The structures are subjected to the same loads but an absolute comparison between the two cannot take place as the vertical loads along the truss beam cause different direction of moments at the top of the laced members for the two cases as in the uniform case they are transferred through the rigid connection while in the non-uniform case they are transferred through the outer chord of the laced members. The global buckling mode shape of the structure is depicted in Figure 9-59. The numerical results are summarised in Table 9-14.

It can be concluded that the global buckling load is significantly reduced due to the interposition of the lower stiffness member, revealing that the global response is affected. The local behaviour of the laced members is not modified and the local buckling load and squash loads of the laced members remain the same. The load factor for Load Case-A is much larger for the non-uniform laced members due to the fact that the vertical loads along the truss beam are transferred through the outer chord to the laced members relieving the inner critical chord that is loaded by the crane bridge. This is not the case in uniform laced members in which the inner chord is loaded by both the crane bridge and the vertical loads along the truss beam.

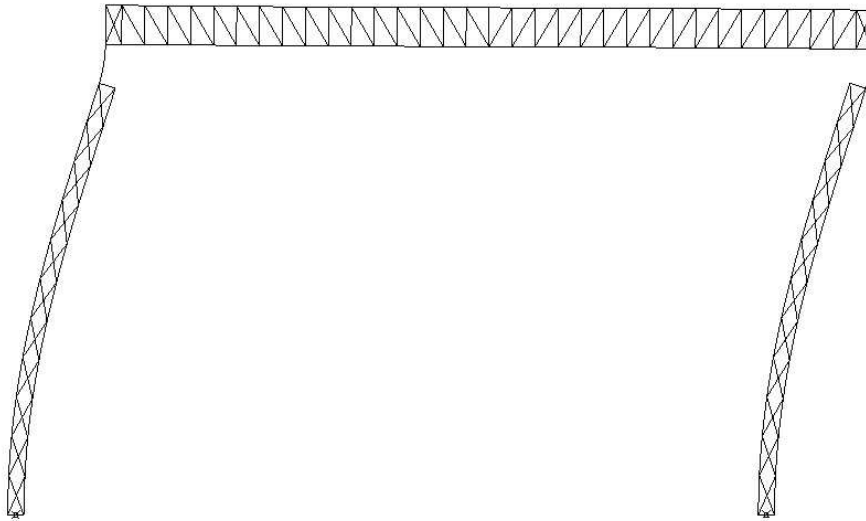


Figure 9-59: Global buckling mode shape of frame of Example 2 with fixed supports and discontinuous laced members

In Load Case-B and Load Case-C that the horizontal loads play an important role and the effect of the vertical loads along the truss beam becomes smaller, the load factors for the non-uniform laced members are significantly smaller than the ones for the uniform laced members. Additionally, the deflections at their top are much larger even for smaller loads highlighting that the lateral stiffness of the structures is dramatically reduced as the truss beam is “isolated” from the columns.

Table 9-14: Comparison between numerical results for the frame of Example 2 with uniform and non-uniform laced members

	Numerical results for uniform laced members	Numerical results for non-uniform laced members
Global buckling load	26950kN	9511kN
Local buckling load	169957kN	169957kN
Squash load	15478kN	15478kN
Load factor for Load Case –A	3.630	7.169
Load factor for Load Case –B	1.115	0.656
Load factor for Load Case –C	2.573	2.068

The proposed methods cannot be used in industrial buildings with discontinuous laced columns in elevation as they are based on the second-order elastic analysis of Timoshenko members with constant cross-section along their length. Therefore, it is recommended that in discontinuous laced members the whole frame is modelled with equivalent Timoshenko members and then the proposed interaction equations are used based on the analysis’s output for the internal forces.

The equilibrium paths obtained with GMNIA for the case of uniform and non-uniform laced members in elevation are presented for Load Case-B and Load Case-C in Figure 9-60 and Figure 9-61, respectively. Based on the comparison between the two, it is recommended that the second type of construction should be avoided. The reason behind this recommendation lies on the fact that it usually leads to small exploitation of the beam’s stiffness, to smaller collapse loads and to larger lateral deflections. It is therefore clear, that the use of discontinuous laced members in elevation leads to more expensive structures in terms of material and financial cost.

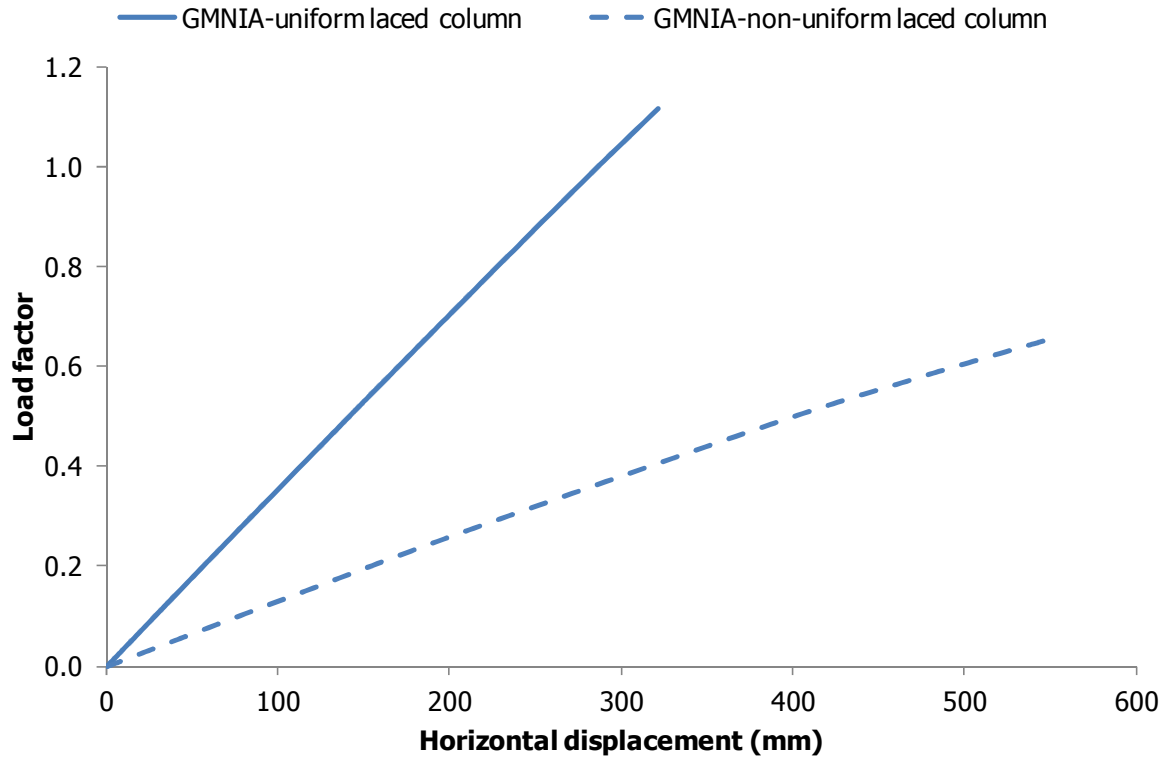


Figure 9-60: Equilibrium paths obtained with GMNIA for the frame of Example 2 with fixed supports and with either uniform or non-uniform laced column under the application of Load Case-B

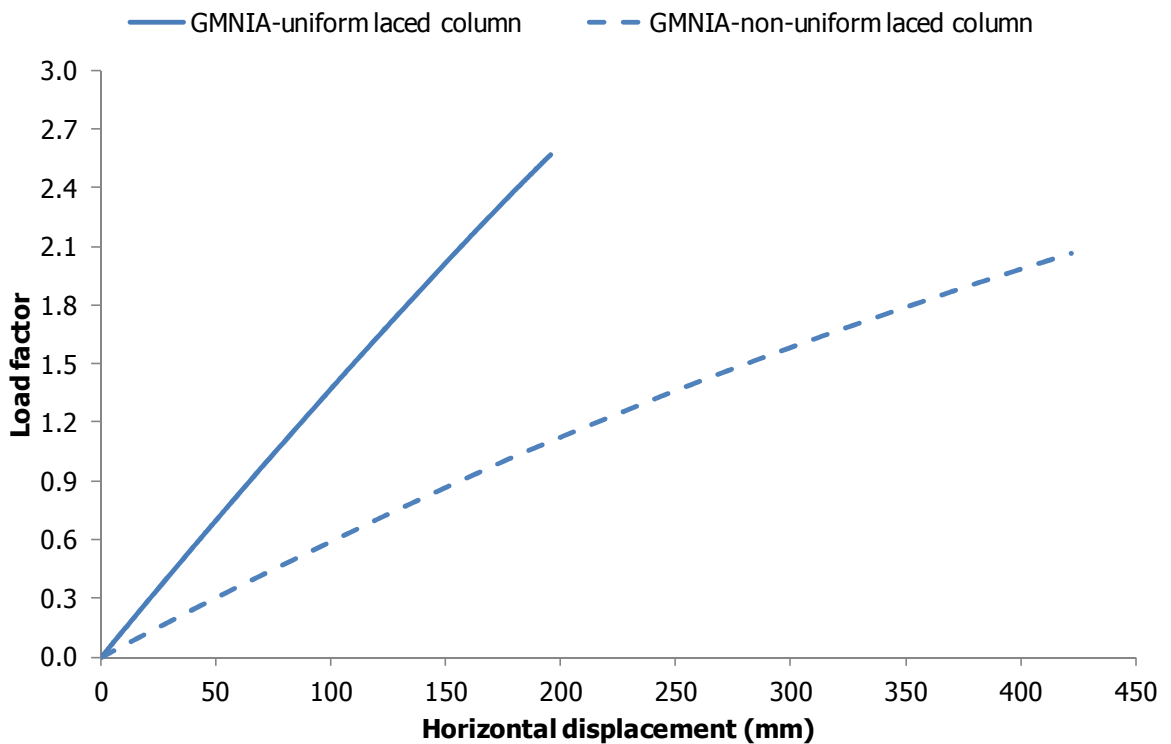


Figure 9-61: Equilibrium paths obtained with GMNIA for the frame of Example 2 with fixed supports and with either uniform or non-uniform laced column under the application of Load Case-C

9.7 GUIDELINES FOR PRACTICAL USE

In practice many different ways can be used for the analysis and design of industrial frames that consist of laced built-up columns, as discussed at the beginning of the present chapter. Each procedure has merits and drawbacks and the selection of a suitable method should be based on the availability of tools and time. In this section, based on the qualitative and quantitative conclusions drawn by the present doctoral thesis, all possible types of analysis and design will be summarised so that guidelines for practical use can be drawn.

9.7.1 Linear elastic analysis and design of full frame (C.S.1st)

In this type of analysis and design the detailed modelling of the full frame with the use of beam elements is required. Using LA in full frames and checking according to interaction formula Eq. (9-2) as provided by Eurocode 3 proved to be conservative for the prediction of the collapse load in the examples presented in this chapter. Nevertheless, in some cases of relatively slender frames the deflections predicted by C.S.1st were not on the safe side.

One of the advantages of this procedure is that limitless load patterns and frames' geometries can be analysed. Engineering software, commonly used, can easily perform linear elastic analysis and design checks with little computational effort.

The main disadvantage deals with the fact that geometrical nonlinearity is not taken into account. As was observed in the presented examples, this may lead to very unsafe prediction of the response and deflections of the frame.

In conclusion, this type of analysis is recommended in cases that the planar behaviour of the frame is expected to be very stiff and geometrical nonlinearity is not anticipated to play a significant role in the overall behaviour. The critical panel can be checked only against local buckling by ignoring the existence of internal local bending moments and by accounting for plastic reserve.

9.7.2 Nonlinear elastic analysis and design of the full frame (C.S.2nd)

In this type of analysis and design the detailed modelling of the frame with the use of beam elements is required. Using GNA in full frames and checking according to interaction formula Eq. (9-2) as provided by Eurocode 3 proved to be conservative and satisfactory in the previously presented examples.

The main advantage of this procedure is that limitless load patterns and frames' geometries can be analysed. The results are expected to be on the safe side while geometrical nonlinearity is taken into account. This type of analysis requires slightly larger computational effort than linear elastic analysis but not prohibitive in any case for use in practical cases. The main disadvantage of GNA of full frame is that not many engineering software can perform nonlinear elastic analysis accounting for P- Δ effects.

In conclusion, this type of analysis is recommended in cases that the planar behaviour of the frame is either stiff or more flexible, as geometrical nonlinearity is taken into account. The critical panel can be checked only against local buckling by ignoring the existence of internal local bending moments and by accounting for plastic reserve, leading in this way to more accurate results.

9.7.3 GNIA of equivalent Timoshenko frame

In GNIA of equivalent Timoshenko frame as described previously, the full frame is replaced by an equivalent frame that consists of Timoshenko members with equivalent characteristics. Boundary conditions and load patterns are also appropriately modified. The internal forces (axial force, bending

moment and shear force perpendicular to the deformed axis) can be used in the proposed interaction Eqs. (8-1), (8-2) or (8-3) for checking the efficiency of the structural components.

The main advantage of GNIA of equivalent frame is the same as the one of GNA of full frame with the addition that modelling becomes less demanding. This procedure proved to be the most sufficient for the prediction of structural behaviour and collapse load in the examples investigated previously.

The main disadvantage is that the design checks are not automatically performed by commercial software but require their appropriate incorporation in the interaction formula proposed in the present doctoral thesis. Additionally, it requires the calculation of the members' equivalent characteristics and loads that is somewhat time-consuming. Also, the procedure of replacing the full frame with an equivalent one induces some errors as this simplification does not come without a cost. These errors proved to be trivial for the examples examined previously.

In conclusion, this type of analysis may be appropriate in cases that the planar behaviour of the frame is either stiff or not, as geometrical nonlinearity is taken into account. It can be of usefulness for preliminary design and/or for checking the numerical results obtained with GNA of full frame.

9.7.4 Proposed procedure

As validated in the present doctoral thesis, the proposed procedure (Proposed-A and Proposed-B alternatives) can be used for the calculation of the global elastic critical buckling load and the second-order elastic analysis of imperfect industrial frames under symmetrical and anti-symmetrical axial and lateral loads. The use of the calculated internal forces (axial force, bending moment and shear force perpendicular to the deformed axis) can be used in the proposed interaction Eqs. (8-1), (8-2) or (8-3) for calculating the collapse load of the structure with sufficient accuracy.

The main advantage of the proposed procedure is that calculations are based on closed-form solutions that facilitate its use. Therefore, the proposed method can be used for an accurate prediction of the collapse load especially for preliminary design purposes and/or for checking the numerical results obtained with the use of finite element software. Additionally, it can be proved useful in performing parametric studies by varying the geometrical and cross-sectional characteristics of the frame.

The main drawback is that this analytical procedure requires manual programming by the designer, so that its use becomes easy. Additionally, the proposed method deals with symmetrical and anti-symmetrical load patterns and it cannot account for discontinuities of the laced members in elevation. Finally, the procedure of using an equivalent Timoshenko column instead of analysing the full frame induces some shortcomings.

9.7.5 GMNIA of full frame

GMNIA is a type of analysis that was used for the numerical verification of the experimental tests and analytical procedures in the present doctoral thesis and is one of the most accurate available numerical methods for the calculation of a structure's capacity. It accounts for large displacements and elastoplastic material leading to the direct calculation of the ultimate strength of the structure. A LBA is initially used for obtaining the global and local elastic buckling mode shapes for the incorporation of initial global and local imperfections, respectively. It requires the detailed modelling of the chords, lacing bars and connections in the frame with the use of either beam or shell elements.

The main advantages of this procedure are the high level of accuracy, the limitless load patterns that can be used and the limitless geometries (symmetrical or non-symmetrical, continuous or discontinuous laced members) that can be analysed. The structural engineer is not required to perform additional design checks.

The main drawback is associated with the requirement for the use of special finite element software as commonly used engineering software cannot perform this type of analysis. Another disadvantage deals with the time required for the complete modelling of the frame especially if shell elements are selected for this purpose and for the elastoplastic analysis that usually needs a large number of iterations.

9.8 CONCLUSIONS

In the present chapter, the application of the proposed methods for the calculation of the collapse load of industrial buildings was described. The proposed procedures were validated against the use of GMNIA in industrial frames with realistic dimensions and cross-sections with both hinged and fixed supports. The frames were subjected to realistic types and magnitudes of external loads. The correlation between the numerical and analytical results was very satisfactory as far as the global buckling load, collapse load factor and deflections were concerned. Therefore, it was concluded that the use of the proposed method can sufficiently lead to reliable evaluation of the behaviour of industrial frames in terms of both deflections and collapse loads. The accuracy of using GNA with commercial software and checking the critical panels according to the interaction formula of Eurocode 3 described in Eq. (9-2) was less than the one of the proposed procedures but usually on the safe side. The use of LA with commercial software proved to be sufficient only in cases that the in-plane behaviour of the frames was sufficiently stiff.

Industrial buildings with appropriate discontinuity in elevation for the support of the crane bridge were also discussed and an example was presented in order to quantitatively observe the effect of the interposition of a lower stiffness member between the top of the laced members and the truss beam. It is concluded that the ultimate strength and lateral stiffness are significantly reduced. For this reason, it is recommended that alternative designs should be investigated. Although not investigated in the context of the present doctoral thesis, a possible method for carrying the bridge could be the use of appropriate short cantilevers instead of "isolating" the truss beam from the laced columns.

Finally, guidelines for the analysis and design of industrial frames were given describing the merits and disadvantages that each procedure has. It is concluded that the use of GNIA in equivalent frames and the application of the calculated internal forces in the proposed interaction equations can lead to a sufficient calculation of the strength and stiffness of industrial buildings with laced columns without any limitations regarding geometry and load patterns. The proposed procedure offers the advantage of closed-form solutions without the need of iterations for obtaining internal forces and deflections. Nevertheless, it requires to be programmed so that it can be of practical use for the structural engineer. Another disadvantage is that it deals with symmetrical uniform frames and with symmetrical and anti-symmetrical load patterns. Nevertheless, its use can be a useful tool for the engineer in preliminary design, in checking the numerical results obtained with the use of finite element software and in performing extensive parametric studies.

9.9 REFERENCES

- [9-1] Richard, J., Tremblay, R., Koboevic, S., MacCrimmon, R.A. "Seismic analysis and design approaches for crane-supporting steel structures", *Proceedings of the Behaviour of Steel Structures in Seismic Areas*, pp. 511-517, Philadelphia, United States, 2009
- [9-2] ADINA System 8.5, "Release Notes", ADINA R & D Inc., 71 Elton Avenue, Watertown, MA 02472; USA, 2008

- [9-3] Eurocode 3: Design of Steel Structures. Part 1.1: General structural rules. CEN-European Committee for Standardisation, Brussels, EN1993-1-1, 2005
- [9-4] Chen, W.F., Atsuta T. "Theory of beam-columns", McGraw-Hill, New York, 1976
- [9-5] Baptista, A.M., Muzeau, J.P. "Analytical formulation of the elastic-plastic behaviour of bi-symmetrical steel shapes", Journal of Constructional Steel Research, Vol. 62, pp. 872-884, 2006
- [9-6] XTRACT v3.0.1, "Release Notes" Imbsen Software Systems, 9912 Business Park Drive, Suite 130, Sacramento, CA 95827; USA, 2004
- [9-7] Vayas, J., Ermopoulos, J., Ioannidis, G. "Steel Structures: Examples of application of Eurocode 3", Kleidarithmos Press, Athens, Greece, 1997 (in Greek)

10 SUMMARY AND CONCLUSIONS

10.1 SUMMARY

During the last decades the structural response of built-up columns has been thoroughly investigated by many researchers. Analytical investigations, experimental tests and a limited number of numerical analyses are included in the literature. Their common characteristic is that they are mainly related to simply-supported built-up members, either under only axial load or under combined axial and small lateral loads, usually due to the eccentricity of the applied axial load. Nevertheless, one can hardly find a reliable solution process for the nonlinear problem concerning imperfect laced built-up members with arbitrary boundary conditions and subjected to combined axial and lateral loads. This shortage is reflected in modern design guidelines that focus on simply-supported columns only.

Additionally, according to modern design practice laced built-up members are modelled in commercial software using beam elements for both chords and lacing bars. By means of elastic analysis, either linear or nonlinear (including usually only $P-\Delta$ effects), internal forces are obtained, which are then used for the design of the laced members' components. The design process includes both cross-sectional and member checks. Nevertheless, it does not account for global and local buckling interaction and its effect on deflections and internal forces.

The aim of the present research is to investigate the response of imperfect laced built-up beam-columns with arbitrary boundary conditions, taking into consideration both geometrical and material nonlinearity. To that effect the present study consists of experimental tests, analytical procedures and numerical analyses, combining in this way the three available research approaches in modern structural engineering.

Initially, the design and testing of a series of experimental specimens took place. Tests were conducted on ten simply-supported laced columns (5 groups of similar columns for repeatability reasons) with realistic global and local slendernesses. The specimens were subjected to axial compressive loads and concentrated end moments due to eccentricity of the applied axial loads. Group 1 was the basis of the experimental tests, having laced columns with chords' cross-section UNP60, panels' length equal to 40cm and end eccentricities equal to 10cm resulting in single curvature deformation. Each one of the other groups differed from the first one only in one parameter, so that the effect of the differing parameter could be separately examined. The specimens of Group 2 had panels with half length, while Group 3's had IPE80 chords' cross-section. The 4th Group was related to

end concentrated moments of the same direction causing double curvature deformation, while in Group 5 the eccentricity of the applied axial forces was half. The steel's constitutive behaviour for each specimen was extracted through tensile testing of appropriately constructed coupons. The experimental tests differ from the ones in the literature, as they had larger end eccentricities (and therefore larger lateral loads) and included deflection measurements, indicative of global response, as well as local measurements, facilitating in this way the understanding of the specimens' local response. The results for each specimen were presented with characteristic photographs at different load levels, equilibrium paths in the form of load-lateral displacement diagrams and load-strain graphs at characteristic locations.

The satisfactory agreement between the results for specimens of the same group at both global and local level shows that the experimental results can be considered as reliable. The behaviour of all specimens was initially elastic, while for larger load levels a gradual decrease of the stiffness was observed. The stiffness's gradual decrease was attributed to the existence of thermally induced residual stresses in the chords' cross-sections that led to premature yielding in the critical cross-sections. The load corresponding to zero stiffness was considered to be the collapse load, while after its attainment a descending post-buckling branch followed. It was concluded that in all groups, local elastoplastic failure of a critical panel resulted in overall collapse without any allowance for redistribution of internal forces, despite the indeterminate nature of laced columns. In many cases, specimens of the same group failed in different panels, highlighting the effect of local imperfections. Additionally, the existence of internal bending moments due to the continuity of the chords was verified, as inwards deflection of the critical panels was observed regardless of whether single or double symmetrical cross-sections were used. Finally, no significant effect of residual stresses due to welding was observed in specimens with a large number of welds between chords and lacing bars.

Afterwards, numerical modelling of the experimental tests took place, aiming at calibration of the numerical models, so that they can be considered as sufficiently accurate and reliable. Shell elements were used for the numerical modelling of both chords and lacing bars. The existence of thermally induced residual stresses was taken into account and their modelling relied on discretising the cross-section of the chords (UNP60 and IPE80) in sufficiently small shell elements and on using appropriate material yield strengths in each element group, so that the residual stress distribution would be correctly applied. The material yield strength of each element group depended on whether it belonged to a location with tensile or compressive residual stresses and on the yield strength measured through tensile tests. Global and local imperfections were incorporated in the analyses according to the global and local buckling modes, respectively. Their magnitude was based on Eurocode 3 provisions, as actual imperfections of the specimens were not measured.

Based on the numerical analyses, it was concluded that the use of Geometrically and Material Nonlinear Analysis with Imperfections (GMNIA) in combination with modelling thermally induced residual stresses led to very good agreement between the numerical and experimental results. The agreement was satisfactory at both global and local level. In the case that initial geometrical imperfections and residual stresses were neglected, the numerical collapse loads obtained were larger than the experimental ones and the gradual decrease of the stiffness at high load levels could not be predicted. Moreover, the use of numerical models with beam elements led to the conclusion that they can predict the behaviour of laced built-up members in a satisfactory manner, with significantly smaller computational effort as compared to numerical models with shell elements.

Taking advantage of the conclusion that using beam elements for numerical modelling is sufficient, an extensive parametric study has been performed to investigate the response of globally and locally imperfect laced built-up columns (simply-supported and cantilevers). It was concluded that overall collapse takes place usually when local elastoplastic failure of a critical panel appears or, more rarely,

when global elastic instability takes place. In the second case, interaction between global and local buckling is important and should be taken into account, while in the first one it can be indirectly included in the local capacity of the critical panel. The largest reduction of the collapse load of the imperfect structure with respect to the perfect one occurs if the global buckling, local buckling and squash loads coincide. The effect of imperfections is the smallest if the global buckling load is smaller than the local buckling load.

The use of Eurocode 3 cannot safely predict the collapse load in the second case, as it does not account for the interaction between global and local buckling. This drawback was the motivation for the derivation of an approximate analytical procedure that predicts sufficiently the behaviour of laced built-up columns in both types of failure. In the proposed procedure, laced built-up columns are modelled as Timoshenko members with equivalent bending and shear rigidity according to Engesser's method. The bending rigidity is appropriately modified in order to incorporate the effect of local imperfections on the global response. Elastic analysis is terminated when the stiffness of the structure becomes zero, either without yielding (elastic failure), or when the critical panel reaches its local capacity (local elastoplastic failure). The required computational effort of the proposed procedure is slightly heavier than the one of Eurocode 3. For laced columns the proposed procedure and Eurocode 3 led to similar results to the ones obtained from GMNIA in the case of local elastoplastic failure. Nevertheless, in the case of elastic failure, the proposed method remained satisfactorily accurate and on the safe side, while the opposite happened with Eurocode 3. Despite that fact, the most common type of failure is the local elastoplastic one, due to the use of members with small and moderate global and local non-dimensional slendernesses and due to the existence of significant lateral loads. For this reason, the subsequent research activities were based on the concept of Eurocode 3.

Afterwards, after concluding previously that laced members can be sufficiently modelled as Timoshenko members based on Engesser's method, the present research focused on the prediction of the elastic critical buckling load of Timoshenko columns with arbitrary boundary conditions and of multi-story frames consisting of Timoshenko members. To that effect a 3x3 stability matrix was proposed based on Engesser's method, that leads to three nonlinear equations for non-sway, partially sway and sway members. Additionally, slope-deflection equations based on Engesser's method were proposed for Timoshenko members with semi-rigid connections at their ends. Based on them, a complete set of rotational stiffness coefficients was presented, which were then used for the replacement of members converging at the bottom and top ends of the column in question by equivalent springs. All possible rotational and translational boundary conditions at the far end of these members, as well as the eventual presence of axial force, were considered. The final goal was the use of the nonlinear equations for the calculation of the elastic critical buckling load of multi-story frames consisting of Timoshenko and laced built-up members. A very satisfactory agreement between the proposed analytical procedure for the elastic critical buckling load and numerical procedures was observed.

Subsequently, the 2nd-order response of imperfect Timoshenko members with arbitrary boundary conditions under commonly used lateral loads was investigated, in order to propose closed-form solutions for the calculation of the internal forces and deflections along them. To that effect, each loading was considered separately and then the principle of superposition was applied. The incorporation of initial global imperfection based on the 1st buckling mode shape was achieved with the use of the approximate magnification factor, which is commonly employed by code provisions, by using the elastic critical buckling load of Timoshenko members mentioned in the previous paragraph. The lateral loads included uniformly distributed load, end concentrated moments and end concentrated forces and the analysis under their effect was based on slope-deflection equations according to Engesser's method for Timoshenko members. When compared with existing methods,

the proposed one considers the effect of initial imperfection based on the 1st buckling mode, while the closed-form solutions facilitate their use for obtaining internal forces and deflections without requiring iterative procedures or further treatment. The comparison of the proposed method for the 2nd-order analysis of imperfect Timoshenko beam-columns with the performance of GNIA on numerical models constructed with beam elements resulted in very satisfactory agreement.

The 2nd-order elastic analysis of a Timoshenko member results in the calculation of internal forces and the termination of the analysis for the calculation of the collapse load of the laced member requires a suitable failure criterion. For this reason, and based on the conclusion drawn from both experimental and numerical investigation that laced members collapse due to local elastoplastic failure, a simple interaction equation was proposed that is in accordance with the philosophy of code provisions. Thus, the proposed method for evaluating the strength of a laced built-up beam-column consists of a 2nd-order elastic analysis of an equivalent Timoshenko member and of its termination for the calculation of the collapse load based on the interaction equation. The use of the proposed procedure for the evaluation of the deflections and collapse loads of a large number of laced built-up beam-columns was found to be in very good agreement with results obtained with GMNIA of numerical models. It was also observed that the approach prevailing in modern design practice led to less accurate results in comparison with the proposed method, as it accounts for local internal bending moments along the chords due to their continuity. These bending moments exist but are drastically reduced due to yielding as the member approaches collapse, therefore they do not affect significantly the collapse load. In addition, the approach adopted in modern design practice does not account for the effect of the spread of yielding on the local capacity of the critical panel, and consequently on the collapse load.

The proposed procedure was also applied to single-story industrial frames consisting of laced built-up columns under symmetrical and anti-symmetrical load patterns. In each case, the frame's girder is replaced by rotational springs corresponding to either single or double curvature deformation, as they were obtained for the calculation of the elastic critical buckling load of multi-story frames consisting of Timoshenko members, depending on whether the load pattern causes single (non-sway behaviour) or double (sway behaviour) curvature deformation. Subsequently, the critical laced member is examined separately, both symmetrical and non-symmetrical load patterns are applied, the principle of superposition is used and the procedure described in the previous paragraph for laced beam-columns with arbitrary supports is followed. The comparison of the analytical results with the ones obtained with GMNIA performed on single-story frames consisting of laced members was found to be very satisfactory. As observed for laced members, the use of the modern design practice led to less accurate results than the ones found with the proposed procedure. Finally, based on the observations made during the experimental, numerical and analytical research, guidelines for the analysis and design of laced members in practice were provided. Their aim is to improve the reliability of laced members' design in everyday engineering practice.

10.2 CONCLUDING REMARKS

The experimental, numerical and analytical approaches used for the investigation of the response of laced built-up columns lead to the following conclusions:

- Laced built-up columns behave almost elastically until failure, without any significant allowance for redistribution of internal forces, despite the fact that they are characterised by high static indeterminacy. Collapse in all experimental specimens was attributed to local elastoplastic failure of the more stressed panel.

- Local imperfections influence the collapse of laced members and their appearance was experimentally verified due to the fact that in some cases specimens of the same group failed in different panels. Internal bending moments also develop along the chords due to their continuity, verified experimentally by the inwards deflection of critical panels in all cases.
- Very good agreement between numerical models consisting of shell elements and experimental results was observed at both global (lateral deflections) and local (strains) level. Therefore, such models can be a reliable tool for the prediction of the behaviour of laced members. The use of numerical models consisting of beam elements also leads to satisfactory results in terms of deflections and collapse loads. The much smaller computational effort associated with the second type of numerical modelling makes such models attractive for the analysis and design of laced members.
- Initial global and local imperfections should be taken into account in the analysis and design of laced members as they affect both the global response and the collapse load. Eurocode 3 provisions for imperfections of laced members proved to be relatively conservative for the experimental specimens, leading to results on the safe side.
- Numerical modelling of thermally induced residual stresses based on the simple concept of modifying the yield strength of appropriate regions based on the residual stress distribution in the cross-section leads to effective capturing of the gradual yielding of columns. The concept can be used only if the primary type of stress is known in advance. Its main advantage is that it can be employed in any finite element software whether elastoplastic analysis with the existence of initial strains/stresses is supported or not.
- Interaction between global and local buckling plays an important role in the response of laced built-up columns. The coexistence of global and local imperfections increases the lateral deflections and decreases the collapse load of the laced member when compared with the case that only global imperfections are taken into account. The largest reduction of capacity due to initial imperfections takes place when global buckling, local buckling and squash loads coincide. The decrease of the collapse load of an imperfect structure when compared with a perfect one may reach magnitudes in the order of 50% in some cases.
- The failure modes of imperfect laced built-up columns are distinguished into global elastic failure and local elastoplastic failure. It was concluded, that for reasonable magnitudes of imperfections, in the first case the interaction between buckling modes should be taken into account directly in the global response, while in the second one it can be inserted indirectly through the local capacity of the critical panel. The most common type of failure is the second one, as global and local non-dimensional slendernesses in practice are relatively small, leading to material yielding.
- Eurocode 3 results in satisfactory estimation of collapse loads in the case of the second type of failure but not of the first one. For this reason, a method was proposed that predicts both types of failure in a satisfactory manner and yields collapse loads on the safe side. The proposed method is based on modelling the laced column as equivalent Timoshenko member with modified bending stiffness in order to account for the effect of local imperfections on the global behaviour. The results are satisfactory for both deflections and collapse loads.
- Built-up columns are subjected to significant shear deformations due to the fact that they are characterised by large bending rigidity and relatively small shear rigidity. For this reason, it is necessary that they are modelled according to Timoshenko beam theory accounting in this way for both bending and shear deformations. The existence of Engesser's and Haringx's theories for the incorporation of shear deformations in structural analysis is still on debate. Nevertheless, it was

concluded that laced built-up members should be modelled according to Engesser's theory when the shear rigidities provided in structural textbooks and code provisions are used.

- The elastic 2nd-order analysis of imperfect Timoshenko beam-columns according to Engesser's theory can predict in a satisfactory manner the internal forces along an imperfect laced built-up beam-column. As laced members behave elastically almost until failure, these internal forces can be inserted in an appropriate interaction equation for the calculation of the collapse load.
- The interaction equation contains the axial forces applied to the more compressed panel on the left hand-side while the local capacity of the imperfect critical panel considered as simply-supported is included in the right-hand side. The assumption that the critical panel of the chord is simply-supported at failure is convenient, facilitates the calculations and approximates in most cases the actual behaviour. In cases of large shear forces, adjacent panels to the critical one may offer rotational stiffness to its ends, thus increasing its buckling strength. Commonly, the local non-dimensional slenderness of the panels is small or moderate and, as a result, boundary conditions do not play a very important role. Additionally, if the local capacity of the critical panel is obtained by accounting for the spread of yielding over the entire cross-section, the calculated collapse loads are improved compared to the ones obtained if the local capacity is associated with the first yield.
- Local bending moments appear due to both local imperfections and continuity of the chords. In slender panels the first ones are, in general, more significant, while the opposite happens in stocky panels. Both of them are not important for global equilibrium. The increase of the axial force in a chord leads to higher local bending moments due to local imperfections and this is more prominent in slender panels. For this reason, local bending moments due to local imperfections should be taken into account in the calculation of local capacity. On the contrary, in stocky panels that fail mainly due to material yielding, local bending moments due to continuity of the chords are reduced due to yielding, allowing for an increase of the corresponding axial force. As a result, elastic calculation of local bending moments due to continuity of the chords and incorporation of them in interaction equations is conservative.
- The proposed analytical procedures result in satisfactory approximation of the behaviour and collapse loads of imperfect laced built-up beam-columns with arbitrary boundary conditions and of single-story industrial frames consisting of laced members. The commonly used design practice of using linear elastic analysis and Eurocode 3 provisions for the capacity of the panels yields less accurate results. These results are in some cases very unsafe for the prediction of deflections. The use of geometrically nonlinear elastic analysis improves significantly the results.

10.3 RESEARCH CONTRIBUTION AND INNOVATION

The present doctoral thesis deals with the analysis and design of laced built-up members with arbitrary boundary conditions under both axial and lateral loads. It consists of experimental, numerical and analytical research and offers both scientific and practical contribution. The scientific originality is mainly achieved by proposed analytical methods, procedures of numerical modelling and experimental works that are not available in the literature and offer improved qualitative understanding of structural behaviour as well as quantitative evaluation of response and strength of such members. Objective of this thesis was to take advantage of scientific originality, in order to contribute also to structural engineering practice. For that purpose, guidelines for numerical simulation, analysis and design have also been formulated. The achieved innovation of the thesis, both scientific and practical, is presented next.

10.3.1 Contribution to the advancement of engineering science

The innovations that contribute to the advancement of engineering science can be summarised as:

- Original experimental tests of built-up specimens with realistic global and local non-dimensional slenderness were performed, including both global and local measurements for the better qualitative understanding and quantitative evaluation of the response ([10-1], [10-2]).
- Geometrically and Materially Nonlinear Imperfection Analyses, including the effect of thermally induced residual stresses based on a simple concept of appropriately modifying the material's strength in specific cross-sectional regions, were performed for the calibration of numerical models based on the experimental results. It is noted that the numerical modelling of experimental tests of this type is not commonly encountered in the existing literature. Therefore, the numerical features and details presented in the present doctoral thesis can prove beneficial for other researchers ([10-1], [10-2]).
- Extensive numerical parametric studies were performed and led to the observation that the overall collapse of an imperfect laced column can be attributed either to global elastic failure or to local elastoplastic failure, with the second one being more common in practice. An analytical procedure that can sufficiently capture both types of failure was proposed. Due to the lack of existing analytical methods for capturing both failure modes, the only alternative is by means of nonlinear numerical analyses, which requires much heavier computational effort ([10-3]).
- An analytical procedure for the calculation of the elastic critical buckling load of multi-story frames consisting of Timoshenko members based on Engesser's method was proposed, by expanding an existing method for multi-story frames consisting of Euler-Bernoulli members. To that effect, a stability matrix, slope-deflection equations for shear-weak members with semi-rigid connections based on Engesser's method and a complete set of rotational stiffness coefficients for the replacement of members converging at the bottom and top ends of the column in question by equivalent springs were proposed ([10-4]).
- Closed-form solutions for the direct calculation of internal forces and deflections as obtained from the 2nd-order analysis of imperfect Timoshenko members with arbitrary boundary conditions under both axial and lateral loading were proposed. The incorporation of shear deformations was based on Engesser's theory. The lateral loads include uniformly distributed line load, end concentrated moments and end concentrated forces ([10-5], [10-6], [10-7]).
- Using the results of the two previous paragraphs and a proposed simple interaction formula for the termination of the 2nd-order elastic analysis, the collapse load of locally and globally imperfect laced built-up beam-columns either with arbitrary boundary conditions or as part of single-story frames under symmetrical and anti-symmetrical load patterns can be evaluated ([10-5], [10-6], [10-7]).

10.3.2 Contribution to the advancement of engineering practice

Previous research on built-up members dealt mainly with simply-supported columns, while in practice such members are usually part of larger frames. For this reason, the existing analytical predictions cannot be applied to more complex cases and require appropriate modifications. The main contributions of the present doctoral thesis to practical engineering design can be summarised as:

- The proposed method, based on the analytical calculations and interaction equation, can be used for the analysis and design of laced built-up members, regardless of whether they are parts of frames or not, without requiring any iterative solution process. This facilitates its direct use from engineers of practice. The proposed procedure can be used for calculating internal forces and deflections at any load level. Moreover, the maximum load factor which can be sustained by the

laced member can be sufficiently predicted with the use of the proposed interaction equation. The method's accuracy was checked against results obtained with the use of GMNIA and proved to be sufficient for practical purposes.

- As the proposed procedure does not require the use of commercial software, it is suitable for preliminary design purposes, offering sufficient accuracy with low computational demands. The analytical nature of the proposed method also facilitates its easy incorporation in software. Thus, it can prove beneficial for the performance of extensive parametric studies by the design engineer, towards the preliminary selection of appropriate geometrical and cross-sectional characteristics for a laced built-up member. In addition, it can be a useful tool for qualitative checking of the numerical results obtained with commercial software.
- Useful conclusions were drawn for the analysis and design methods that are commonly used in design practice, by comparing their results with the ones obtained with GMNIA. The use of linear elastic analysis proved to be sufficient only in cases that the lateral behaviour of the laced members and frames is expected to be very stiff, thus leading to negligible geometrically nonlinear effects. In more slender frames the use of linear analysis proved to be sufficient for the calculation of the ultimate strength but unsafe for the prediction of the lateral deflections. The use of geometrically nonlinear elastic analysis proved to be satisfactory and on the safe side for any case of laced members and industrial frames for the calculation of both deflections and collapse loads. It can be improved if the interaction equation for buckling about the weak axis z - z of the chords includes only the term associated with the axial force.
- Modelling the full frame using equivalent Timoshenko members and performing GNIA proved to be of sufficient accuracy for predicting the structural response of the industrial frames. The use of the proposed interaction equation based on the internal forces obtained from GNIA of equivalent Timoshenko frames leads to satisfactory prediction of the ultimate strength of the frames. This procedure is fast for analysing and designing single-story industrial frames with laced members without detailed modelling of the laced members. Thus, it can be used for preliminary design and for qualitative checking of the numerical results obtained based on full modelling of the frame with commercial software.
- Non-uniformity of laced columns in elevation, for example employed commonly in order to support a crane runway beam on the inner chord, should be avoided. Such non-uniformity causes lack of full cooperation between the laced column and the frame girder, leading to much larger lateral deflections and to smaller collapse loads. The use of a short cantilever for the support of the crane beam may be preferable.

10.4 SUGGESTIONS FOR FUTURE RESEARCH

The topic of built-up beam-columns is broad and cannot be fully covered only in the context of a doctoral thesis. Some suggestions for future research are summarised next:

- The present work focuses on the in-plane behaviour of laced built-up beam-columns, examining two-dimensional frames. For this reason, the analytical solutions for imperfect Timoshenko beam-columns also deal only with planar response. Usually, out-of-plane behaviour of laced members does not include any lateral forces due to the existence of bracing systems. Nevertheless, the proposed method cannot be directly applied in cases of three-dimensional response and both numerical and experimental studies should be performed in order to understand the modifications required in such cases.

- The derived analytical solutions deal with laced columns with constant cross-section in elevation. In many cases, non-uniform members in elevation are used in single-story industrial frames, such as the ones presented in Chapter 9. In order to facilitate calculations, analytical solutions for the 2nd-order analysis of non-uniform imperfect Timoshenko beam-columns should be derived.
- In the present doctoral thesis only statically applied external loads are considered. Wind and seismic actions are approximately applied on the studied frames as equivalent static loads according to code provisions. Despite the fact that the behaviour of laced members under dynamic loading is not expected to differ significantly from that under static loading as far as collapse load is concerned, it is interesting to investigate the behaviour of laced members under cyclic loading in terms of stiffness, energy dissipation and ductility. Realistic frames should be analysed under dynamic loading and the case of arbitrary supports should be considered.
- Battened built-up members are not investigated in the present doctoral thesis. In many existing structures, they are used either as columns or as beam-columns in moment-resisting frames. For this reason, it is suggested that their behaviour under static and dynamic loads is investigated, aiming at checking their adequacy and proposing retrofitting methods.

10.5 REFERENCES

- [10-1] Kalochairetis, K.E., Gantes, C.J. "Experimental and Numerical Investigation of Collapse Load of Laced Built-up Columns", International Association for Shell and Spatial Structures (IASS) Symposium 2013 "Beyond the Limits of Man", J.B. Obrebski and R. Tarczewski (eds.), Wroclaw University of Technology, Poland, 23-27 Sep. 2013
- [10-2] Kalochairetis, K.E., Gantes, C.J., Lignos, X.A. "Experimental and Numerical Investigation of Eccentrically Loaded Laced Built-up Steel Columns", (submitted for possible publication in scientific journal)
- [10-3] Kalochairetis, K.E., Gantes, C.J. "Numerical and Analytical Investigation of Collapse Loads of Laced Built-up Columns", Computers & Structures, Vol. 89, pp. 1166-1176, June 2011
- [10-4] Kalochairetis, K.E., Gantes, C.J. "Elastic Buckling Load of Multi-Story Frames Consisting of Timoshenko Members", Journal of Constructional Steel Research, Vol. 71, pp. 231-244, April 2012
- [10-5] Kalochairetis, K.E., Gantes, C.J. "Second Order Analysis of Imperfect Timoshenko Members: Arbitrary Boundary Conditions and Application to Laced Built-up Columns", 6th European Conference on Steel and Composite Structures, Budapest, Hungary, August 31-September 2, 2011
- [10-6] Gantes, C.J., Kalochairetis, K.E. "Nonlinear Analysis of Imperfect Timoshenko Members under Lateral Loading and its Application to Laced Built-up Columns", 7th National Conference on Steel Structures, Volos, Greece, September 29-30, 2011, (in Greek)
- [10-7] Gantes, C.J., Kalochairetis, K.E. "Axially and Transversely Loaded Timoshenko and Laced Built-up Columns with Arbitrary Supports", Journal of Constructional Steel Research, Vol. 77, pp. 95-106, October 2012

